

Third Edition

Internal Combustion Engines

Applied
Thermosciences



Colin R. Ferguson and Allan T. Kirkpatrick



WILEY

WILEY END USER LICENSE AGREEMENT

Go to www.wiley.com/go/eula to access Wiley's ebook EULA.

Internal Combustion Engines

Internal Combustion Engines

Applied Thermosciences

Third Edition

Colin R. Ferguson
Allan T. Kirkpatrick

*Mechanical Engineering Department
Colorado State University, USA*

WILEY

This edition first published 2016
© 2016, John Wiley & Sons, Ltd

First Edition published in 2014

Registered office

John Wiley & Sons Ltd, The Atrium, Southern Gate, Chichester, West Sussex, PO19 8SQ,
United Kingdom

For details of our global editorial offices, for customer services and for information about
how to apply for permission to reuse the copyright material in this book please see our
website at www.wiley.com.

The right of the author to be identified as the author of this work has been asserted in
accordance with the Copyright, Designs and Patents Act 1988.

All rights reserved. No part of this publication may be reproduced, stored in a retrieval
system, or transmitted, in any form or by any means, electronic, mechanical, photocopying,
recording or otherwise, except as permitted by the UK Copyright, Designs and Patents Act
1988, without the prior permission of the publisher.

Wiley also publishes its books in a variety of electronic formats. Some content that appears
in print may not be available in electronic books.

Designations used by companies to distinguish their products are often claimed as
trademarks. All brand names and product names used in this book are trade names, service
marks, trademarks or registered trademarks of their respective owners. The publisher is
not associated with any product or vendor mentioned in this book

Limit of Liability/Disclaimer of Warranty: While the publisher and author have used their
best efforts in preparing this book, they make no representations or warranties with respect
to the accuracy or completeness of the contents of this book and specifically disclaim
any implied warranties of merchantability or fitness for a particular purpose. It is sold
on the understanding that the publisher is not engaged in rendering professional services
and neither the publisher nor the author shall be liable for damages arising herefrom. If
professional advice or other expert assistance is required, the services of a competent
professional should be sought.

Library of Congress Cataloging-in-Publication Data

Ferguson, Colin R.

Internal combustion engines : applied thermosciences / Colin R. Ferguson,
Allan T. Kirkpatrick. – Third edition.

pages cm

Includes bibliographical references and index.

ISBN 978-1-118-53331-4 (hardback)

1. Internal combustion engines. 2. Thermodynamics. I. Ferguson, Colin, R.
II. Kirkpatrick, Allan T. III. Title.

TJ756.F47 2015

621.43–dc23

2015016357

A catalogue record for this book is available from the British Library.

Set in 10/12pt TimesLTStd-Roman by Thomson Digital, Noida, India

Contents

Preface xi

Acknowledgments xiii

1. Introduction to Internal Combustion Engines 1

- 1.1 Introduction 1
- 1.2 Historical Background 4
- 1.3 Engine Cycles 5
- 1.4 Engine Performance Parameters 9
- 1.5 Engine Configurations 16
- 1.6 Examples of Internal Combustion Engines 23
- 1.7 Alternative Power Plants 26
- 1.8 References 29
- 1.9 Homework 30

2. Heat Engine Cycles 32

- 2.1 Introduction 32
- 2.2 Constant Volume Heat Addition 33
- 2.3 Constant Pressure Heat Addition 36
- 2.4 Limited Pressure Cycle 37
- 2.5 Miller Cycle 39
- 2.6 Finite Energy Release 41
- 2.7 Ideal Four-Stroke Process and Residual Fraction 54
- 2.8 Discussion of Gas Cycle Models 62
- 2.9 References 63
- 2.10 Homework 64

3. Fuel, Air, and Combustion Thermodynamics 66

- 3.1 Introduction 66
- 3.2 Thermodynamic Properties of Ideal Gas Mixtures 66
- 3.3 Liquid–Vapor–Gas Mixtures 72
- 3.4 Stoichiometry 76
- 3.5 Low-Temperature Combustion Modeling 79
- 3.6 General Chemical Equilibrium 84
- 3.7 Chemical Equilibrium using Equilibrium Constants 89
- 3.8 References 94
- 3.9 Homework 94

4. Fuel–Air Combustion Processes 97

- 4.1 Introduction 97
- 4.2 Combustion and the First Law 97

4.3	Maximum Work and the Second Law	103
4.4	Fuel–Air Otto Cycle	108
4.5	Four-Stroke Fuel–Air Otto Cycle	113
4.6	Homogeneous Two-Zone Finite Heat Release Cycle	116
4.7	Comparison of Fuel–Air Cycles with Actual Spark Ignition Cycles	123
4.8	Limited Pressure Fuel–Air Cycle	125
4.9	Comparison of Limited Pressure Fuel–Air Cycles with Actual Compression Ignition Cycles	128
4.10	References	129
4.11	Homework	129

5. Intake and Exhaust Flow 131

5.1	Introduction	131
5.2	Valve Flow	131
5.3	Intake and Exhaust Flow	147
5.4	Superchargers and Turbochargers	150
5.5	Effect of Ambient Conditions on Engine and Compressor Mass Flow	158
5.6	References	159
5.7	Homework	160

6. Fuel and Airflow in the Cylinder 163

6.1	Introduction	163
6.2	Carburetion	163
6.3	Fuel Injection–Spark Ignition	166
6.4	Fuel Injection–Compression Ignition	168
6.5	Large-Scale in-Cylinder Flow	174
6.6	In-Cylinder Turbulence	180
6.7	Airflow in Two-Stroke Engines	185
6.8	References	193
6.9	Homework	195

7. Combustion Processes in Engines 197

7.1	Introduction	197
7.2	Combustion in Spark Ignition Engines	198
7.3	Abnormal Combustion (Knock) in Spark Ignition Engines	206
7.4	Combustion in Compression Ignition Engines	214
7.5	Low-Temperature Combustion	225
7.6	References	229
7.7	Homework	231

8. Emissions 234

8.1	Introduction	234
8.2	Nitrogen Oxides	235
8.3	Carbon Monoxide	243
8.4	Hydrocarbons	245
8.5	Particulates	249

8.6	Emissions Regulation and Control	251
8.7	References	258
8.8	Homework	259

9. Fuels 262

9.1	Introduction	262
9.2	Hydrocarbon Chemistry	263
9.3	Refining	266
9.4	Fuel Properties	267
9.5	Gasoline Fuels	269
9.6	Alternative Fuels for Spark Ignition Engines	274
9.7	Hydrogen	281
9.8	Diesel Fuels	282
9.9	References	286
9.10	Homework	287

10. Friction and Lubrication 288

10.1	Introduction	288
10.2	Friction Coefficient	288
10.3	Friction Mean Effective Pressure	291
10.4	Friction Measurements	291
10.5	Friction Modeling	294
10.6	Journal Bearing Friction	295
10.7	Piston and Ring Friction	298
10.8	Valve Train Friction	306
10.9	Accessory Friction	308
10.10	Pumping Mean Effective Pressure	310
10.11	Overall Engine Friction Mean Effective Pressure	311
10.12	Lubrication	312
10.13	References	315
10.14	Homework	316

11. Heat and Mass Transfer 318

11.1	Introduction	318
11.2	Engine Cooling Systems	319
11.3	Engine Energy Balance	320
11.4	Cylinder Heat Transfer	324
11.5	Heat Transfer Modeling	326
11.6	Heat Transfer Correlations	330
11.7	Heat Transfer in the Exhaust System	338
11.8	Radiation Heat Transfer	339
11.9	Mass Loss or Blowby	340
11.10	References	342
11.11	Homework	344

12. Engine Testing and Control 346

12.1	Introduction	346
12.2	Instrumentation	347

12.3	Combustion Analysis	354
12.4	Exhaust Gas Analysis	358
12.5	Control Systems in Engines	366
12.6	Vehicle Emissions Testing	369
12.7	References	370
12.8	Homework	370

13. Overall Engine Performance 372

13.1	Introduction	372
13.2	Effect of Engine and Piston Speed	372
13.3	Effect of Air–Fuel Ratio and Load	373
13.4	Engine Performance Maps	376
13.5	Effect of Engine Size	379
13.6	Effect of Ignition and Injection Timing	380
13.7	Effect of Compression Ratio	383
13.8	Vehicle Performance Simulation	383
13.9	References	384
13.10	Homework	385

Appendices 387

A	Physical Properties of Air	387
B	Thermodynamic Property Tables for Various Ideal Gases	389
C	Curve-Fit Coefficients for Thermodynamic Properties of Various Fuels and Ideal Gases	397
D	Conversion Factors and Physical Constants	401
E	Thermodynamic Analysis of Mixtures	403
E.1	Thermodynamic Derivatives	403
E.2	Numerical Solution of Equilibrium Combustion Equations	405
E.3	Isentropic Compression/Expansion with Known ΔP	408
E.4	Isentropic Compression/Expansion with Known Δv	409
E.5	Constant Volume Combustion	410
E.6	Quality of Exhaust Products	411
E.7	References	412
F	Computer Programs	413
F.1	Volume.m	414
F.2	Velocity.m	414
F.3	BurnFraction.m	414
F.4	FiniteHeatRelease.m	415
F.5	FiniteHeatMassLoss.m	417
F.6	FourStrokeOtto.m	420
F.7	RunFarg.m	421
F.8	farg.m	422
F.9	fuel.m	425
F.10	RunEcp.m	426
F.11	ecp.m	427
F.12	AdiabaticFlameTemp.m	437
F.13	OttoFuel.m	438

- F.14 FourStrokeFuelAir.m 440
- F.15 Homogeneous.m 444
- F.16 Friction.m 450
- F.17 WoschniHeatTransfer.m 451

Index 455

Preface

This textbook presents a modern approach to the study of internal combustion engines. Internal combustion engines have been, and will remain for the foreseeable future, a vital and active area of engineering education and research. The purpose of this book is to apply the principles of thermodynamics, fluid mechanics, and heat transfer to the analysis of internal combustion engines. This book is intended first to demonstrate to the student the application of engineering sciences, especially the thermal sciences, and second, it is a book about internal combustion engines. Considerable effort is expended making the requisite thermodynamics accessible to students. This is because most students have little, if any, experience applying the first law to unsteady processes in open systems or in differential form to closed systems, and have experience with only the simplest of reacting gas mixtures.

The text is designed for a one-semester course in internal combustion engines at the senior undergraduate level. At Colorado State University, this text is used for a single term class in internal combustion engines. The class meets for a lecture two times per week and a recitation/laboratory once a week, for a term of 15 weeks.

This third edition builds upon the foundation of the second edition. The major changes are the adoption of the programming software MATLAB® for the examples, and chapter reorganization for a greater emphasis on combustion. The content changes include additional topics on heat and mass loss in finite heat release models, thermodynamic properties of reacting mixtures, two-zone burn models for homogeneous mixtures, exhaust blowdown modeling, diesel fuel injection, NO_x concentration using finite rate chemistry, homogeneous charge compression ignition, and alternative fuels. The homework problems have increased in number and topics covered.

Acknowledgments

The approach and style of this text reflects our experiences as students at the Massachusetts Institute of Technology. In particular, we learned a great deal from MIT Professors John B. Heywood, Warren M. Rohsenow, Ascher Shapiro, and Jean F. Louis.

Many thanks to the editorial staff at John Wiley & Sons for their work on the third edition. Mr. Paul Petralia, Mr. Clive Lawson, Ms. Sandra Grayson, and Ms. Shikha Pahuja deserve special acknowledgement for their editorial assistance with this project. This edition also benefited from technical discussions with Professors Anthony Marchese, Daniel Olsen, and Brian Willson. Mr. Aron Dobos, a CSU ME graduate student, deserves thanks for converting many of the computer programs in the first and second editions to a Matlab® form. Mr. Tyler Schott helped produce and format the solutions to the homework problems.

Finally, Allan Kirkpatrick would like to thank his family: Susan, Anne, Matt, Rob, and Kristin for their unflagging support while this third edition was being written.

*Dr. Allan T. Kirkpatrick (allan@engr.colostate.edu)
Fort Collins, Colorado*

Chapter 1

Introduction to Internal Combustion Engines

1.1 INTRODUCTION

The main focus of this text is on the application of the engineering sciences, especially the thermal sciences, to internal combustion engines. The goals of the text are to familiarize the reader with engine nomenclature, describe how internal combustion engines work, and provide insight into how engine performance can be modeled and analyzed. An internal combustion engine is defined as an engine in which the chemical energy of the fuel is released inside the engine and used directly for mechanical work, as opposed to an external combustion engine in which a separate combustor is used to burn the fuel.

In this chapter, we discuss the engineering parameters that are used to characterize the overall performance of internal combustion engines. Major engine cycles, configurations, and geometries are covered. The following chapters will apply the principles of thermodynamics, combustion, fluid flow, friction, and heat transfer to determine an internal combustion engine's temperature and pressure profiles, work, thermal efficiency, and exhaust emissions.

An aspect upon which we have put considerable emphasis is the process of constructing idealized models to represent actual physical situations in an engine. Throughout the text, we will calculate the values of the various thermal and mechanical parameters that characterize internal combustion engine operation.

With the advent of high-speed computers and advanced measurement techniques, today's internal combustion engine design process has evolved from being purely empirical to a rigorous semiempirical process in which computer-based engineering software is used to evaluate the performance of a proposed engine design even before the engine is built and tested. The development of a successful engine requires knowledge of methods and analyses introduced in the text which are used to parameterize and correlate experiments, and to calculate the performance of a proposed engine design.

The internal combustion engine was invented and successfully developed in the late 1860s. It is considered as one of the most significant inventions of the last century, and has had a significant impact on society, especially human mobility. The internal combustion engine has been the foundation for the successful development of many commercial technologies. For example, consider how the internal combustion engine has transformed the transportation industry, allowing the invention and improvement of automobiles, trucks, airplanes, and trains. The adoption and continued use of the internal combustion engine



Figure 1.1 Piston and connecting rod.
(Courtesy Mahle, Inc.)

in different application areas has resulted from its relatively low cost, favorable power to weight ratio, high efficiency, and relatively simple and robust operating characteristics.

The reciprocating piston–cylinder geometry is the primary geometry that has been used in internal combustion engines, and is shown in Figure 1.1. As indicated in the figure, a piston oscillates back and forth in a cyclic pattern in a cylinder, transmitting power to a drive shaft through a connecting rod and crankshaft mechanism. Valves or ports are used to control the flow of gas into and out of the engine. This configuration of a reciprocating internal combustion engine, with an engine block, pistons, valves, crankshaft, and connecting rod, has remained basically unchanged since the late 1800s.

The main differences between a modern-day engine and one built 100 years ago can be seen by comparison of their reliability, thermal efficiency, and emissions level. For many years, internal combustion engine research was aimed at improving thermal efficiency and reducing noise and vibration. As a consequence, the thermal efficiency has increased from about 10–20% at the beginning of the 20th century to values as high as 50% today.

Internal combustion engine efficiency continues to increase, driven both by legislation and the need to reduce operating costs. The primary United States vehicle mileage standard is the federal corporate average fuel economy (CAFE) standard. The CAFE standard for passenger vehicles and light duty trucks was 27.5 miles per gallon (mpg) for a 20 year period from 1990 to 2010. The CAFE standards have risen in the last few years, and will reach 35.5 mpg in 2016, and 54.5 mpg by 2025. This doubling of vehicle mileage requirements will require increased use of techniques such as electronic control, engine downsizing, turbocharging, supercharging, variable valve timing, low temperature combustion, and electric motors and transmissions.

Internal combustion engines have become the dominant prime mover technology in several areas. For example, in 1900 most automobiles were steam or electrically powered, but by 1920 most automobiles were powered by gasoline engines. As of the year 2010, in the United States alone there are about 220 million motor vehicles powered by internal combustion engines. In 1900, steam engines were used to power ships and railroad locomotives; today two- and four-stroke diesel engines are used. Prior to 1950, aircraft relied



Figure 1.2 Automobile engine. (Courtesy Mercedes-Benz Photo Library.)

almost exclusively on piston engines. Today gas turbines are the power plant used in large planes, and piston engines continue to dominate the market in small planes.

Internal combustion engines have been designed and built to deliver power in the range from 0.01 to 20×10^3 kW, depending on their displacement. They compete in the market place with electric motors, gas turbines, and steam engines. The major applications are in the vehicular (see Figure 1.2), railroad, marine (see Figure 1.3), aircraft, stationary power, and home use areas. The vast majority of internal combustion engines are produced for vehicular applications, requiring a power output on the order of 100 kW.

Since 1970, with the recognition of the importance of environmental issues such as the impact of air quality on health, there has also been a great deal of work devoted to reducing the various emissions from engines. The emissions level of current internal combustion engines has decreased to about 5% of the emissions levels 40 years ago. Currently, meeting emission requirements is one of the major factors in the design and operation of internal combustion engines. The major emissions from internal combustion engines include

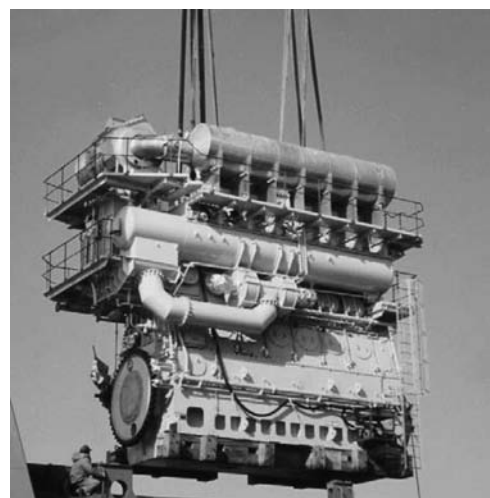


Figure 1.3 Marine engine. (Courtesy MAN B&W Diesel.)

nitrogen oxides (NO_x), carbon monoxide (CO), hydrocarbons (HC), particulates (PM), and aldehydes. These combustion products are a significant source of air pollution, as the internal combustion engine is the source of about half of the NO_x , CO, and HC pollutants in the air. Carbon dioxide (CO_2), a primary gaseous combustion product of internal combustion engines is also a greenhouse gas, and is in the process of being regulated as well.

1.2 HISTORICAL BACKGROUND

In this section, we briefly discuss a few of the major figures in the invention and development of the internal combustion engine. The ingenuity and creativity demonstrated by these early engineers in producing these successful inventions is truly inspiring to today's engine designers. In 1858, J. Léonard (1822–1900), a Belgian engineer, developed a two-stroke engine that developed 6 hp with an efficiency of about 5%. During the intake stroke, a gas-air mixture at atmospheric pressure was drawn into the engine, and ignited by a spark, causing the cylinder pressure to increase during the latter half of the stroke, producing work. The return stroke was used to remove the combustion products through an exhaust valve. The Léonard engine was primarily used in stationary power applications.

In 1872, George Brayton (1830–1892), an American mechanical engineer, patented and commercialized a constant pressure internal combustion engine, "Brayton's Ready Engine". The engine used two reciprocating piston-driven cylinders, a compression cylinder, and an expansion cylinder. This cycle was also called the "flame cycle", as ignition of the gas-air mixture was by a pilot flame, and the mixture was ignited and burned at constant pressure as it was pumped from the compression cylinder to the expansion cylinder. The Brayton piston engine was used on the first automobile in 1878. The Brayton cycle is the thermodynamic cycle now used by gas turbines, which use rotating fan blades to compress and expand the gas flowing through the turbine.

Nikolaus Otto (1832–1891), a German engineer, developed the "Otto Silent Engine", the first practical four-stroke engine with in-cylinder compression in 1876. With a compression ratio of 2.5, the gas engine produced 2 hp at 160 rpm, and had a brake efficiency of 14%. Nikolaus Otto is considered the inventor of the modern internal combustion engine, and the founder of the internal combustion engine industry. The concept of a four-stroke engine had been conceived and patented by A. de Rochas in 1861, however Otto is recognized as the first person to build and commercialize a working flame ignition engine. Otto had no formal engineering schooling, and was self-taught. He devoted his entire career to the advancement of the internal combustion engine. In 1872, he founded the first internal combustion engine manufacturing company, N. A. Otto and Cie, and hired Gottlieb Daimler and Wilhelm Maybach, who would go on to start the first automobile company, the Daimler Motor Company in 1890. Otto's son Gustav founded the automotive company now known as BMW.

The first practical two-stroke engine was invented and built by Sir Dugald Clerk (1854–1932), a Scottish mechanical engineer, in 1878. Clerk graduated from Yorkshire College in 1876, and patented his two-stroke engine in 1881. He is well known for his career-long contributions to improvement of combustion processes in large-bore two-stroke engines. Clerk's engine was made of two cylinders—one a working cylinder to produce power, and the other a pumping cylinder to compress and transfer the intake air and fuel mixture to the working cylinder. Poppet valves were used for intake flow, and a cylinder port uncovered by the piston on the expansion stroke was used to exhaust the combustion gases.

Many of these early internal combustion engines, such as the Léonard, Brayton, and Otto engines, were powered by coal gas, a mixture of methane, hydrogen, carbon monoxide, and

other gases produced by the partial pyrolysis of coal. In the 1880s, crude oil refineries began producing gasoline and kerosene in quantities sufficient to create a market for liquid-fueled internal combustion engines.

Gottlieb Daimler (1834–1900), a German engineer, is recognized as one of the founders of the automotive industry. He developed a high-speed four-stroke gasoline-fueled engine in 1883. The liquid fuel was vaporized and mixed with the intake air in a carburetor before being drawn into the combustion chamber. The fuel air mixture was ignited by a flame tube. In 1886, he built the first four-wheeled automobile, and founded the Daimler Motor Company in 1890.

Karl Benz (1844–1929), a German engineer, successfully developed a 3.5 hp liquid-fueled two-stroke engine with a carburetor and spark ignition in 1885. The ignition system consisted of an electrical induction coil with a rotary breaker driven by the engine and a removable spark plug fitted into the cylinder head, similar to what is found in today's engines. The engine was installed on a three-wheeled vehicle in 1886, the first “horseless carriage”. The transmission was a two-chain arrangement that connected the engine to the rear axle.

In 1897, Rudolph Diesel (1858–1913), a German engineer, developed the first practical four-stroke engine using direct injection of liquid fuel into the combustion chamber. The high compression ratio of the engine resulted in autoignition and combustion of the fuel air mixture. Diesel graduated from Munich Polytechnic in 1880, and worked with his former professor, Carl von Linde, initially on ammonia Rankine cycle refrigeration, then worked with the MAN company to develop compression ignition engines. He designed his engines to follow Carnot's thermodynamic principles as closely as possible. Accordingly, his initial objective was to have constant temperature combustion, however, this was not realized in practice, and he adopted the strategy of constant pressure combustion.

Rudolph Diesel's single-cylinder engine had a bore of 250 mm, stroke of 400 mm, for a 20 L displacement. The diesel fuel was atomized using air injection, a technique where compressed air entrained diesel fuel in the injector and carried it into the cylinder. The engine operated at a speed of 170 rpm, and produced 18 hp, with an efficiency of 27% at full load. This is a much greater efficiency than the steam engines and spark ignition engines in use at that time.

Sir Harry Ricardo (1885–1974), a mechanical engineering graduate of Cambridge, and a prominent English engineer, patented the use of a spherical prechamber, the Ricardo “Comet”, to greatly increase the fuel–air mixing rate, allowing diesel engines to be used in high-speed, 2000 rpm and higher, engine vehicular applications. The first multi-cylinder diesel engines for trucks were available by 1924, and the first diesel-powered automobiles were available by 1936. During his career, Ricardo also contributed to greater understanding of the role of turbulence, swirl and squish in enhancing flame speed in both spark and diesel engines, commercialized sleeve valves for aircraft engines, developed an octane rating system for quantifying knock in spark engines, and founded what is now the Ricardo Consulting Engineers Company.

These early engines were air cooled, since they produced relatively low power. Natural-convection water-cooling using the thermosyphon principle, and forced convection cooling using water pumps was adopted after about 1910 for higher horsepower engines. For example, Henry Ford's Model T engine of 1908, and the Wright Brother's Flyer engine of 1903 used natural convection water cooling.

1.3 ENGINE CYCLES

The two major cycles currently used in internal combustion engines are termed Otto and Diesel, named after the two men credited with their invention. The Otto cycle is also

known as a constant volume combustion or spark ignition cycle, and the Diesel cycle is also known as a constant pressure combustion or compression ignition cycle. These cycles can be configured as either a two-stroke cycle in which the piston produces power on every downward stroke, or a four-stroke cycle in which the piston produces power every other downward stroke.

Otto Cycle

As shown in Figure 1.4, the four-stroke Otto cycle has the following sequence of operations:

1. An intake stroke that draws a combustible mixture of fuel and air past the throttle and the intake valve into the cylinder.
2. A compression stroke with the valves closed that raises the temperature of the mixture. A spark ignites the mixture toward the end of the compression stroke.
3. An expansion or power stroke resulting from combustion of the fuel–air mixture.
4. An exhaust stroke that pushes out the burned gases past the exhaust valve.

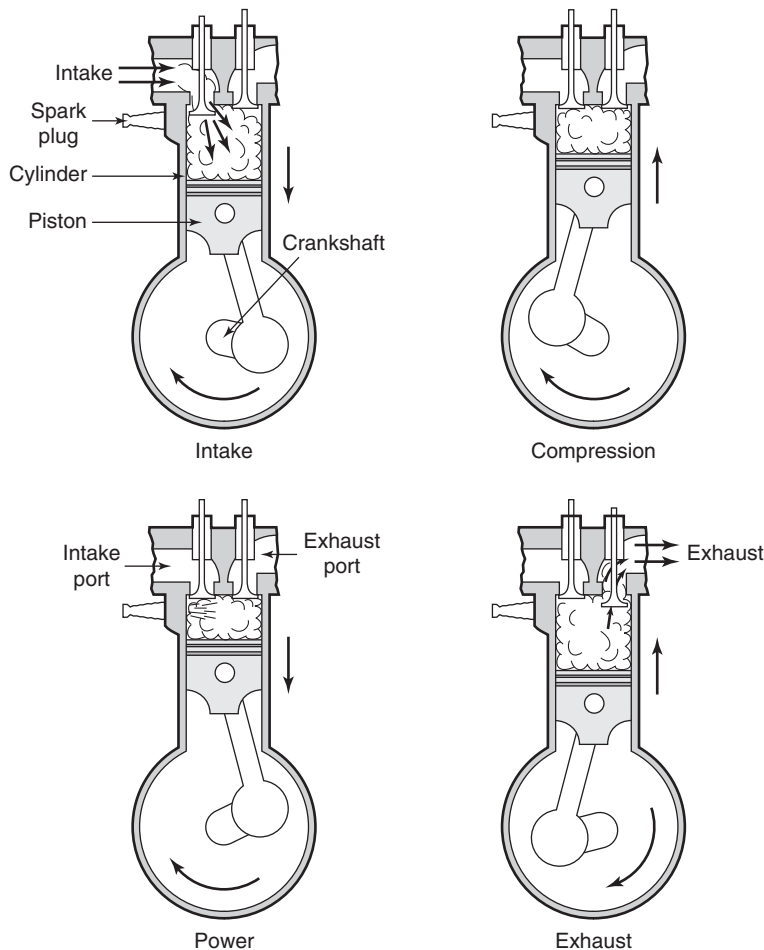


Figure 1.4 Four-stroke spark ignition cycle.

Air enters the engine through the intake manifold, a bundle of passages that evenly distribute the air mixture to individual cylinders. The fuel, typically gasoline, is mixed with the inlet air using a fuel injector or carburetor in the intake manifold, intake port, or directly injected into the cylinder, resulting in the cylinder filling with a homogeneous mixture. When the mixture is ignited by a spark, a turbulent flame develops and propagates through the mixture, raising the cylinder temperature and pressure. The flame is extinguished when it reaches the cylinder walls. If the initial pressure is too high, the compressed gases ahead of the flame will autoignite, causing a problem called knock. The occurrence of knock limits the maximum compression ratio and thus the efficiency of Otto cycle engines. The burned gases exit the engine past the exhaust valves through the exhaust manifold. The exhaust manifold channels the exhaust from individual cylinders into a central exhaust pipe.

In the Otto cycle, a throttle is used to control the amount of air inducted. As the throttle is closed, the amount of air entering the cylinder is reduced, causing a proportional reduction in the cylinder pressure. Since the fuel flow is metered in proportion to the airflow, the throttle in an Otto cycle, in essence, controls the power.

Diesel Cycle

The four-stroke Diesel cycle has the following sequence:

1. An intake stroke that draws inlet air past the intake valve into the cylinder.
2. A compression stroke that raises the air temperature above the autoignition temperature of the fuel. Diesel fuel is sprayed into the cylinder near the end of the compression stroke.
3. Evaporation, mixing, ignition, and combustion of the diesel fuel during the later stages of the compression stroke and the expansion stroke.
4. An exhaust stroke that pushes out the burned gases past the exhaust valve.

There are two types of diesel combustion systems, direct injection (DI) into the main cylinder, and indirect injection (IDI) into a prechamber connected to the main cylinder. With indirect injection, air is compressed into a prechamber during the compression stroke, producing a highly turbulent flow field, and thus high mixing rates when the diesel fuel is sprayed into the prechamber toward the end of the compression stroke. The combustion process is initiated in the prechamber, raising the pressure in the prechamber above that of the main chamber, which forces the combusting mixture of burning gases, fuel, and air back into the main chamber, resulting in the propagation of a highly turbulent swirling flame into the main chamber. Indirect injection engines tend to be used where the engine is expected to perform over a wide range of speeds and loads such as in an automobile. When the operating range of the engine is less broad such as in ships, trucks, locomotives, or electric power generation, direct injection engines predominate.

The inlet air in the diesel engine is unthrottled, and the combustion is lean. The power is controlled by the amount of fuel injected and the subsequent mixing of the fuel spray with the inlet air. The injection duration is proportional to the engine load. In order to ignite the fuel-air mixture, diesel engines are required to operate at a higher compression ratio, compared to spark ignition (SI) engines, with typical values in the range of 15–20, resulting in a greater theoretical efficiency. Since the diesel fuel is mixed with cylinder air just before combustion is to commence, the knock limitation that occurs in SI engines is greatly reduced.

Diesel engine performance is limited by the time required to mix the fuel and air, as incomplete mixing and combustion results in decreased power, increased unburned hydrocarbon emissions, and visible smoke. As we shall see, many different diesel combustion chamber designs have been invented to achieve adequate mixing. Since the mixing time is inversely proportional to the engine speed, diesel engines are classified into three classes, high-speed, medium speed, and low speed. High-speed diesels are designed to operate at speeds of 1000 rpm or higher, have up to a 300 mm bore, and use high-quality distillate fuels. Medium-speed diesels operate at speeds ranging from 375 to 1000 rpm, have a medium bore typically between 200 and 600 mm, and can operate with a range of fuels. The low-speed class of diesel engines operate at speeds less than 375 rpm, are typically large-bore (> 600 mm) two-stroke cycle engines, and use residual fuel oil. Each engine manufacturer has worked to optimize the design for a particular application, and that each manufacturer has produced an engine with unique characteristics illustrates that the optimum design is highly dependent on the specific application.

Two-Stroke Cycle

As the name implies, two-stroke engines need only two-strokes of the piston or one revolution to complete a cycle. There is a power stroke every revolution instead of every two revolutions as for four-stroke engines. Two-stroke engines are mechanically simpler than four-stroke engines, and have a higher specific power, the power to weight ratio. They can use either spark or compression ignition cycles. One of the performance limitations of two-stroke engines is the scavenging process, simultaneously exhausting the burnt mixture and introducing the fresh fuel-air mixture into the cylinder. As we shall see, a wide variety of two-stroke engines have been invented to ensure an acceptable level of scavenging.

The principle of operation of a crankcase-scavenged two-stroke engine, developed by Joseph Day (1855–1946), is illustrated in Figure 1.5. During compression of the crankcase-scavenged two-stroke cycle, a subatmospheric pressure is created in the crankcase. In the example shown, this opens a reed valve letting air rush into the crankcase. Once the piston reverses direction during combustion and expansion begins, the air in the crankcase closes

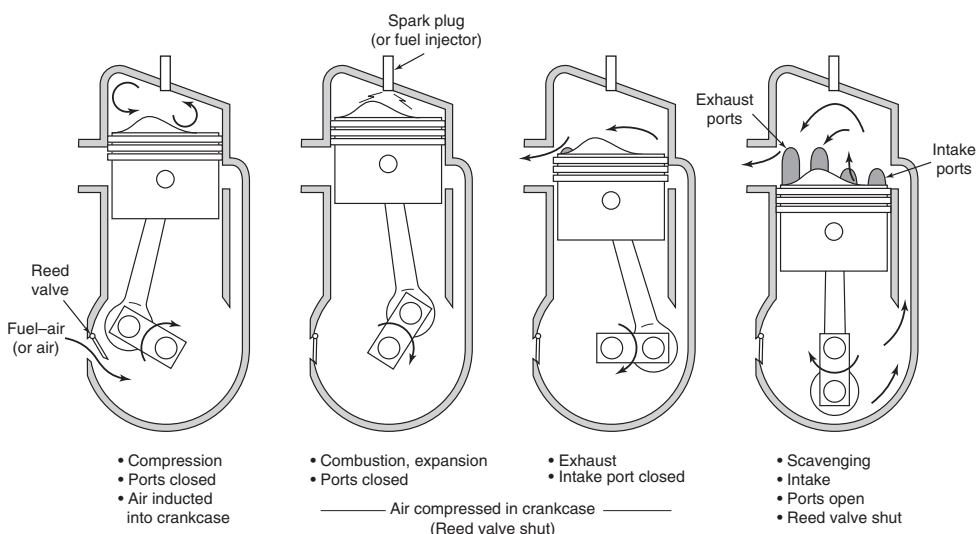


Figure 1.5 A cross-scavenged two-stroke cycle.

the reed valve so that the air is compressed. As the piston travels further, it uncovers holes or exhaust ports, and exhaust gases begin to leave, rapidly dropping the cylinder pressure to that of the atmosphere. Then the intake ports are opened and compressed air from the crankcase flows into the cylinder pushing out the remaining exhaust gases. This pushing out of exhaust by the incoming air is called scavenging.

Herein lies one problem with two-stroke engines: the scavenging is not perfect; some of the air will go straight through the cylinder and out the exhaust port, a process called short-circuiting. Some of the air will also mix with exhaust gases and the remaining incoming air will push out a portion of this mixture. The magnitude of the problem is strongly dependent on the port designs and the shape of the piston top.

Less than perfect scavenging is of particular concern if the engine is a carbureted gasoline engine, for instead of air being in the crankcase there is a fuel-air mixture. Some of this fuel-air mixture will short circuit and appear in the exhaust, wasting fuel and increasing the hydrocarbon emissions. Carbureted two-stroke engines are used where efficiency is not of primary concern and advantage can be taken of the engine's simplicity; this translates into lower cost and higher power per unit weight. Familiar examples include motorcycles, chain saws, outboard motors, and model airplane engines. However, use in motorcycles is decreasing because they have poor emission characteristics. Two-stroke industrial engines are mostly diesel, and typically supercharged. With a two-stroke diesel or fuel injected gasoline engine, air only is used for scavenging, so loss of fuel through short-circuiting or mixing with exhaust gases is not a problem.

1.4 ENGINE PERFORMANCE PARAMETERS

Engine Geometry

For any one cylinder, the crankshaft, connecting rod, piston, and head assembly can be represented by the mechanism shown in Figure 1.6. Of particular interest are the following geometric parameters: bore, b ; connecting rod length, l ; crank radius, a ; stroke, s ; and crank angle, θ . The crank radius is one-half of the stroke. The top dead center (tdc) of an engine

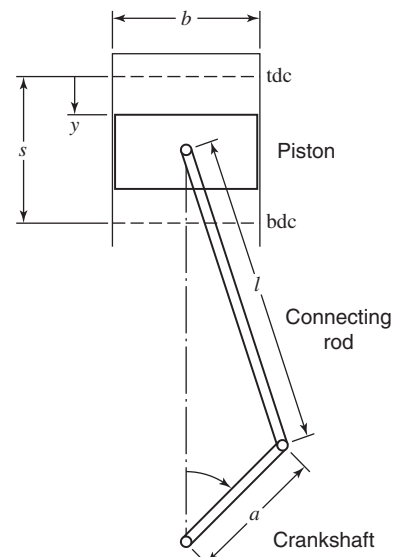


Figure 1.6 Engine slider–crank geometry.

refers to the crankshaft being in a position such that $\theta = 0^\circ$. The cylinder volume in this position is minimum and is also called the clearance volume, V_c . Bottom dead center (bdc) refers to the crankshaft being at $\theta = 180^\circ$. The cylinder volume at bottom dead center V_1 is maximum.

The compression ratio, r , is defined as the ratio of the maximum to minimum volume.

$$r = \frac{V_{\text{bdc}}}{V_{\text{tdc}}} = \frac{V_1}{V_c} \quad (1.1)$$

The displacement volume, V_d , is the difference between the maximum and minimum volume; for a single cylinder,

$$V_d = V_1 - V_c = \frac{\pi}{4} b^2 s \quad (1.2)$$

A useful expression relating V_d and V_{bdc} is

$$V_1 = V_{\text{bdc}} = \frac{r}{r-1} V_d \quad (1.3)$$

For multicylinder engines, the total displacement volume is the product of the number of cylinders, n_c , and the volume of a single cylinder.

$$V_d = n_c \frac{\pi}{4} b^2 s \quad (1.4)$$

The mean piston speed \bar{U}_p is an important parameter in engine design since stresses and other factors scale with piston speed rather than with engine speed. Since the piston travels a distance of twice the stroke per revolution, it should be clear that

$$\bar{U}_p = 2Ns \quad (1.5)$$

The engine speed, N , refers to the rotational speed of the crankshaft and is expressed in revolutions per minute. The engine frequency, ω , also refers to the rotation rate of the crankshaft but in units of radians per second.

Power, Torque, and Efficiency

The brake power, \dot{W}_b , is the rate at which work is done; and the engine torque, τ , is a measure of the work done per unit rotation (radians) of the crank. The brake power is the power output of the engine, and measured by a dynamometer. Early dynamometers were simple brake mechanisms. The brake power is less than the boundary rate of work done by the gas, called indicated power, partly because of friction. As we shall see when discussing dynamometers in Chapter 10, the brake power and torque are related by

$$\dot{W}_b = 2\pi\tau N \quad (1.6)$$

The net power is from the complete engine, whereas gross power is from an engine without the cooling fan, muffler, and tail pipe.

The indicated work W_i is the net work transferred from the gas to the piston during a cycle, which is the integral of the pressure over the cylinder volume:

$$W_i = \int P dV \quad (1.7)$$

and the indicated power \dot{W}_i , for an engine with n_c cylinders, is

$$\dot{W}_i = n_c W_i N / 2 \quad (\text{four stroke engine}) \quad (1.8)$$

$$\dot{W}_i = n_c W_i N \quad (\text{two stroke engine}) \quad (1.9)$$

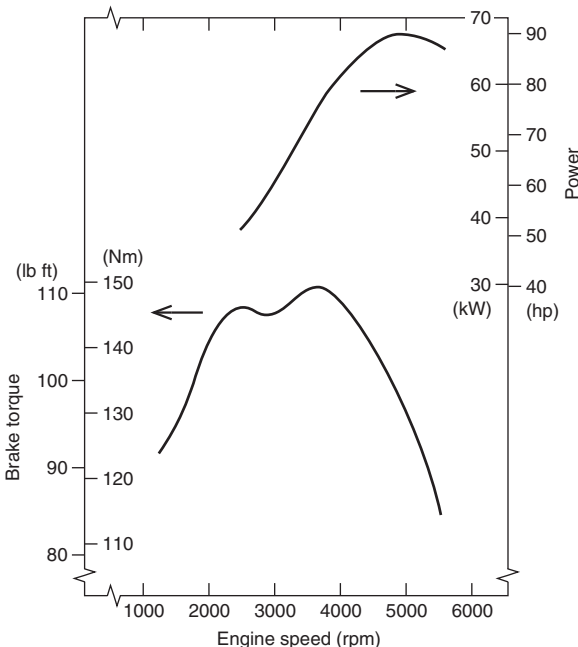


Figure 1.7 Wide open throttle (WOT) performance of an automotive four-stroke engine.

since the four-stroke engine has two revolutions per power stroke and the two-stroke engine has one revolution per power stroke.

The brake power is less than the indicated power due to engine mechanical friction, pumping losses in the intake and exhaust, and accessory power needs, which are grouped as a friction power loss, \dot{W}_f

$$\dot{W}_f = \dot{W}_i - \dot{W}_b \quad (1.10)$$

The ratio of the brake power to the indicated power is the mechanical efficiency, η_m :

$$\eta_m = \dot{W}_b / \dot{W}_i = 1 - \dot{W}_f / \dot{W}_i \quad (1.11)$$

The wide open throttle performance of a 2.0 L automotive four-stroke engine is plotted in Figure 1.7. As with most engines, the torque and power both exhibit maxima with engine speed. Viscous friction effects increase quadratically with engine speed, causing the torque curve to decrease at high engine speeds. The maximum torque occurs at lower speed than maximum power, since power is the product of torque and speed. Notice that the torque curve is rippled. This is due to both inlet and exhaust airflow dynamics and mechanical friction, discussed later.

Mean Effective Pressure

The mean effective pressure (mep) is the work done per unit displacement volume, and has units of force/area. It is the average pressure that results in the same amount of work actually produced by the engine. The mean effective pressure is a very useful parameter as it scales out the effect of engine size, allowing performance comparison of engines of different displacement. There are three useful mean effective pressure parameters—mep, bmep, and fmep.

The indicated mean effective pressure (imep) is the net work per unit displacement volume done by the gas during compression and expansion. The name originates from the use of an “indicator” card used to plot measured pressure versus volume. The pressure in the cylinder initially increases during the expansion stroke due to the heat addition from the fuel, and then decreases due to the increase in cylinder volume.

The brake mean effective pressure (bmep) is the external shaft work per unit volume done by the engine. The name originates from the “brake” dynamometer used to measure the torque produced by the rotating shaft. Typical values of measured bmep for naturally aspirated automobile engines depend on the load, with maximum values of about 10 bar, and greater values of about 20 bar for turbo or supercharged engines.

Based on torque, the bmep is

$$\begin{aligned} \text{bmep} &= \frac{4\pi\tau}{V_d} \quad (\text{four stroke engine}) \\ &= \frac{2\pi\tau}{V_d} \quad (\text{two stroke engine}) \end{aligned} \quad (1.12)$$

and in terms of power the bmep is

$$\begin{aligned} \text{bmep} &= \frac{\dot{W}_b}{V_d N/2} \quad (\text{four stroke engine}) \\ &= \frac{\dot{W}_b}{V_d N} \quad (\text{two stroke engine}) \end{aligned} \quad (1.13)$$

The bmep can also be expressed in terms of piston area A_p , mean piston speed \bar{U}_p , and number of cylinders n_c :

$$\begin{aligned} \text{bmep} &= \frac{4\dot{W}_b}{n_c A_p \bar{U}_p} \quad (\text{four stroke engine}) \\ &= \frac{2\dot{W}_b}{n_c A_p \bar{U}_p} \quad (\text{two stroke engine}) \end{aligned} \quad (1.14)$$

The friction mean effective pressure (fmep) includes the mechanical engine friction, the pumping losses during the intake and exhaust strokes, and the work to run auxiliary components such as oil and water pumps. Accordingly, the friction mean effective pressure (fmep) is the difference between the imep and the bmep. Determination of the fmep is discussed further in Chapter 10.

$$\text{fmep} = \text{imep} - \text{bmep} \quad (1.15)$$

The bmep of two different displacement automobile engines at wide open throttle (WOT) is compared versus mean piston speed in Figure 1.8. Notice that when performance is scaled to be size independent, there is considerable similarity.

Volumetric Efficiency

A performance parameter of importance for four-stroke engines is the volumetric efficiency, e_v . It is defined as the mass of fuel and air inducted into the cylinder divided by the mass that would occupy the displaced volume at the density ρ_i in the intake manifold. The flow restrictions in the intake system, including the throttle, intake port, and valve, create a pressure drop in the inlet flow, which reduces the density and thus the mass of the gas in the

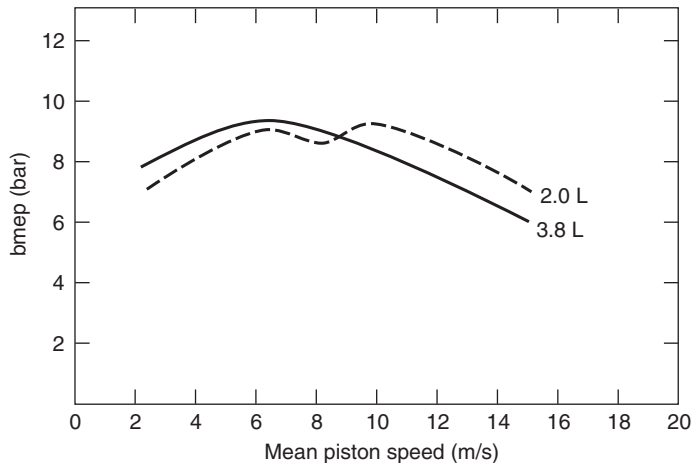


Figure 1.8 Brake mean effective pressure at WOT versus mean piston speed for two automotive engines.

cylinder. The volumetric efficiency is a mass ratio and not a volume ratio. The volumetric efficiency for an engine operating at a speed N is thus

$$e_v = \frac{\dot{m}_{in}}{\rho_i V_d N/2} \quad (1.16)$$

where

$$\dot{m}_{in} = \dot{m}_a + \dot{m}_f \quad (1.17)$$

In Equation 1.17, \dot{m}_f is the flow rate of the fuel inducted in the intake manifold. For a direct injection engine, $\dot{m}_f = 0$. The factor of 2 accounts for the two revolutions per cycle in a four-stroke engine. The intake manifold density is used as a reference condition instead of the standard atmosphere, so that supercharger performance is not included in the definition of volumetric efficiency. For two-stroke cycles, a parameter related to volumetric efficiency called the delivery ratio is defined in terms of the airflow only and the ambient air density instead of the intake manifold density.

A representative plot of volumetric efficiency versus engine speed of an automotive four-stroke engine is shown in Figure 1.9. The shape and location of the peaks of the volumetric efficiency curve are very sensitive to the engine speed as well as the manifold configuration. Some configurations produce a flat curve, others produce a very peaked and asymmetric curve. As we will see later, the volumetric efficiency is also influenced by the

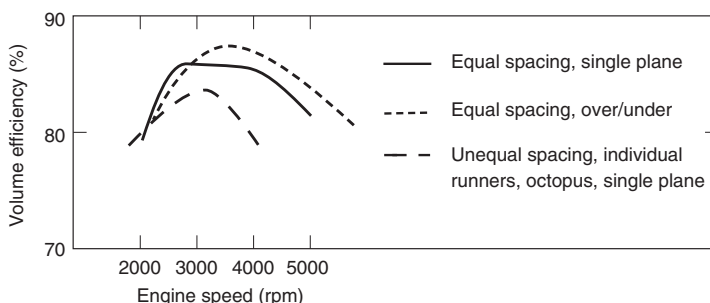


Figure 1.9 Effect of engine speed and intake manifold geometry on volumetric efficiency.
Adapted from Armstrong and Stirrat (1982).

valve size, valve lift, and valve timing. It is desirable to maximize the volumetric efficiency of an engine, since the amount of fuel that can be burned and power produced for a given engine displacement (hence size and weight) is maximized. Although it does not influence in any way the thermal efficiency of the engine, the volumetric efficiency will influence the overall thermal efficiency of the system in which it is installed. As Example 1.1 below indicates, the volumetric efficiency is useful for determination of the airflow rate of an engine of a given displacement and speed.

EXAMPLE 1.1 Volumetric efficiency

A four-stroke 2.5 L direct injection automobile engine is tested on a dynamometer at a speed of 2500 rpm. It produces a torque of 150 Nm, and its volumetric efficiency is measured to be 0.85. What is the brake power \dot{W}_b , and the mass airflow rate \dot{m}_a through the engine? The inlet air pressure and temperature are 75 kPa and 40°C.

SOLUTION The engine power \dot{W}_b is

$$\dot{W}_b = 2\pi\tau N = (2\pi)(150)(2500/60) = 39.3 \text{ kW}$$

The inlet air density is

$$\rho_i = P/RT_i = 75,000/(287 \times 313) = 0.835 \text{ kg/m}^3$$

and the mass airflow rate \dot{m}_a is

$$\dot{m}_a = \frac{1}{2}e_v\rho_iV_dN = \frac{1}{2}(0.85)(0.835)(2.5 \times 10^{-3})(2500/60) = 3.70 \times 10^{-2} \text{ kg/s}$$

Specific Fuel Consumption

The specific fuel consumption is a comparative metric for the efficiency of converting the chemical energy of the fuel into work produced by the engine. As with the mean effective pressure, there are two specific fuel consumption parameters, brake and indicated. The brake specific fuel consumption (bsfc) is the fuel flow rate \dot{m}_f , divided by the brake power \dot{W}_b . It has three terms that are standard measurements in an engine test: the fuel flow rate, the torque, and the engine speed:

$$\text{bsfc} = \frac{\dot{m}_f}{\dot{W}_b} = \frac{\dot{m}_f}{2\pi\tau N} \quad (1.18)$$

The indicated specific fuel consumption (isfc) is the ratio of the mass of fuel injected during a cycle to the indicated cylinder work, and is used to compare engine performance in computational simulations that do not include the engine friction.

$$\text{isfc} = \frac{\dot{m}_f}{W_i} \quad (1.19)$$

Typical values of measured bsfc for naturally aspirated automobile engines depend on the engine load, with values ranging from about 200 to 400 g/kWh.

The specific fuel consumption and engine efficiency are inversely related, so that the lower the specific fuel consumption, the greater the engine efficiency. Engineers use

bsfc rather than thermal efficiency primarily because a more or less universally accepted definition of thermal efficiency does not exist. We will explore the reasons why in Chapter 4. Note for now only that there is an issue with assigning a value to the energy content of the fuel. Let us call that energy the heat of combustion q_c ; the brake thermal efficiency is then

$$\eta = \frac{\dot{W}_b}{\dot{m}_f q_c} = \frac{1}{\text{bsfc } q_c} \quad (1.20)$$

Inspection of Equation 1.20 shows that bsfc is a valid measure of efficiency provided q_c is held constant. Thus, two different engines can be compared on a bsfc basis provided that they are operated with the same fuel.

EXAMPLE 1.2 Engine Parameters Calculation

A six-cylinder four-stroke automobile engine is being designed to produce 75 kW at 2000 rpm with a bsfc of 300 g/kWh and a bmepl of 12 bar. The engine is to have equal bore and stroke, and fueled with gasoline with a heat of combustion of 44,510 kJ/kg. (a) What should be the design displacement volume and bore? (b) What is the mean piston speed at the design point? (c) What is the fuel consumption per cycle per cylinder? (d) What is the brake thermal efficiency?

SOLUTION (a) The displacement volume V_d is

$$V_d = \frac{\dot{W}_b}{\text{bmepl } N/2} = \frac{75}{(1200)(2000/2)(1/60)} = 3.75 \times 10^{-3} \text{ m}^3 = 3.75 \text{ L}$$

$$b = \left(\frac{V_d}{n_c} \frac{4}{\pi} \right)^{1/3} = \left(\frac{3.75 \times 10^{-3}}{6} \frac{4}{\pi} \right)^{1/3} = 92.7 \text{ mm}$$

Most automobile engines have approximately a 90 mm bore and stroke.

(b) The mean piston speed is

$$\bar{U}_p = 2Ns = (2)(9.27 \times 10^{-2})(2000/60) = 6.18 \text{ m/s}$$

(c) The cycle average fuel consumption rate per cylinder is

$$\bar{m}_f = \text{bsfc} \times \dot{W}_b / n_c = 300 \times 75 / (6 \times 60) = 62.5 \text{ g/min}$$

so the mass of fuel injected per cylinder per cycle is

$$m_f = \bar{m}_f / (N/2) = 62.5 / (2000/2) = 6.25 \times 10^{-2} \text{ g}$$

(d) The brake thermal efficiency is

$$\eta = \frac{1}{\text{bsfc } q_c} = \frac{3600}{(0.3)(44,510)} = 0.27$$

Table 1.1 Performance Comparison of Three Different Four-Stroke Turbocharged Diesel Engines

Parameter	1.9 L Automobile	5.9 L Truck	7.2 L Military
# Cylinders	4	6	6
Bore (mm)	82	102	110
Stroke (mm)	90	120	127
Displacement per cylinder (L)	0.475	0.983	1.20
Power (kW)	110	242	222
Mass (kg)	200	522	647
Engine speed (rpm)	4000	3200	2400
Mean piston speed (m/s)	12.05	12.78	10.16
Bmep (bar)	17.3	15.4	15.4
Power/volume (kW/L)	57.9	41.0	30.8
Mass/volume (kg/L)	105	88	90
Power/mass (kW/kg)	0.55	0.46	0.35

Scaling of Engine Performance

The performance characteristics of three different diesel engines is compared in Table 1.1. The engines are a four-cylinder 1.9 L automobile engine, a six-cylinder 5.9 L truck engine, and a six-cylinder 7.2 L military engine. Comparison of the data in the Table indicates that the performance characteristics of piston engines are remarkably similar when scaled to be size independent. As Table 1.1 illustrates, the mean piston speed is about 12 m/s, the bmep is about 15 bar, the power/volume is about 40 kW/L, and the power/mass about 0.5 kW/kg for the three engines.

There is good reason for this; all engines tend to be made from similar materials. The small differences noted could be attributed to different service criteria for which the engine was designed. Since material stresses in an engine depend to a first order only on the bmep and mean piston speed, it follows that for the same stress limit imposed by the material, all engines should have the same bmep and mean piston speed. Finally, since the engines geometrically resemble one another independent of size, the mass per unit displacement volume is more or less independent of engine size.

1.5 ENGINE CONFIGURATIONS

Internal combustion engines can be built in many different configurations. For a given engine, using a four- or two-stroke Otto or Diesel cycle, the configurations are characterized by the piston–cylinder geometry, the inlet and exhaust valve geometry, the use of super or turbochargers, the type of fuel delivery system, and the type of cooling system.

The reciprocating piston–cylinder combination remains the dominant form of the internal combustion engine. Since the invention of the internal combustion engine, many different piston–cylinder geometries have been designed, as shown in Figure 1.10. The choice of a given arrangement depends on a number of factors and constraints, such as engine balancing and available volume. The in-line engine is the most prevalent as it is the simplest to manufacture and maintain. The V engine is formed from two in-line banks of cylinders set at an angle to each other, forming the letter V. A horizontally opposed or flat engine is a V engine with 180° offset piston banks. The W engine is formed from

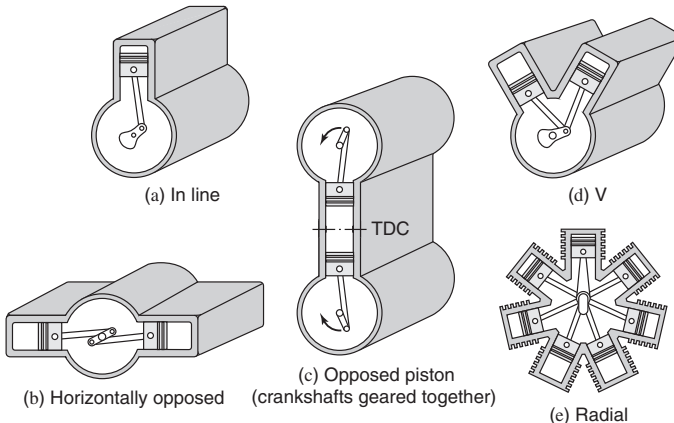


Figure 1.10 Various piston–cylinder geometries. Adapted from Obert (1950).

three in-line banks of cylinders set at an angle to each other, forming the letter W. A radial engine has all of the cylinders in one plane with equal spacing between cylinder axes. Radial engines are used in air-cooled aircraft applications, since each cylinder can be cooled equally. Since the cylinders are in a plane, a master connecting rod is used for one cylinder, and articulated rods are attached to the master rod. Alternatives to the reciprocating piston–cylinder arrangement have also been developed, such as the rotary Wankel engine, in which a triangular shaped rotor rotates eccentrically in a housing to achieve compression, ignition, and expansion of a fuel–air mixture.

Engine Kinematics

Assuming a flat piston top, the instantaneous cylinder volume, $V(\theta)$, at any crank angle is

$$V(\theta) = V_c + \frac{\pi}{4} b^2 y \quad (1.21)$$

where y is the instantaneous stroke distance from top dead center:

By reference to Figure 1.6

$$y = l + a - [(l^2 - a^2 \sin^2 \theta)^{1/2} + a \cos \theta] \quad (1.22)$$

The instantaneous volume $V(\theta)$ can be nondimensionalized by the clearance volume at top dead center, V_{tdc} , resulting in

$$\tilde{V}(\theta) = \frac{V(\theta)}{V_{tdc}} = 1 + (r - 1) \frac{y}{s} \quad (1.23)$$

We define a nondimensional parameter, ϵ , the ratio of the crankshaft radius a to the connecting rod length l , as

$$\epsilon = \frac{a}{l} = \frac{s}{2l} \quad (1.24)$$

The value of ϵ for the slider–crank geometries used in modern engines is of order 1/3.

Therefore, the nondimensional piston displacement y/s is

$$\frac{y}{s} = \frac{1}{2}(1 - \cos \theta) + \frac{1}{2\epsilon} [1 - (1 - \epsilon^2 \sin^2 \theta)^{1/2}] \quad (1.25)$$

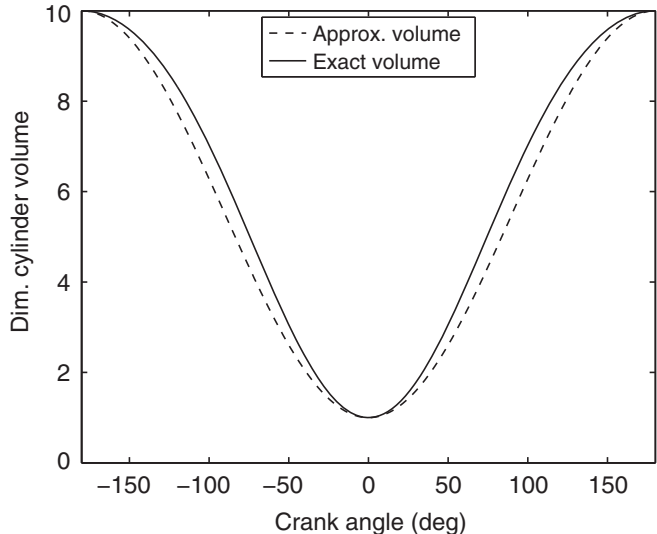


Figure 1.11 Cylinder volume versus crank angle for $r = 10$, $\epsilon = 1/3$ (Equations 1.26 and 1.29).

and the nondimensional cylinder volume $\tilde{V}(\theta)$ is

$$\tilde{V}(\theta) = 1 + \frac{(r-1)}{2}(1 - \cos \theta) + \frac{1}{2\epsilon} [1 - (1 - \epsilon^2 \sin^2 \theta)^{1/2}] \quad (1.26)$$

For $\epsilon < 1$, we can expand the $\sin^2 \theta$ term in a Taylor series,

$$(1 - \epsilon^2 \sin^2 \theta)^{1/2} \simeq \frac{1}{2}\epsilon^2 \sin^2 \theta + O(\epsilon^4) \quad (1.27)$$

so

$$\frac{y}{s} \simeq \frac{1}{2}(1 - \cos \theta) + \frac{\epsilon}{4} \sin^2 \theta \quad (1.28)$$

As $\epsilon \rightarrow 0$, the approximate volume $\tilde{V}(\theta)$ can then be expressed as a function only of the compression ratio r :

$$\tilde{V}(\theta) \simeq 1 + \frac{(r-1)}{2}(1 - \cos \theta) \quad (1.29)$$

The cylinder volumes predicted by Equations 1.26 and 1.29 are compared in Figure 1.11 for a value of $\epsilon = 1/3$, using the Matlab® program `Volume.m` listed in Appendix F.1. Both equations give identical results at bottom dead center and top dead center, and since the second term of the expansion is relatively small, the approximate volume relation under-predicts the exact cylinder volume only by about 10% in the middle of the stroke.

The instantaneous piston velocity U_p can be found by replacing θ with ωt and differentiating Equation 1.25 with respect to time t giving

$$U_p(\omega t) = \frac{dy}{dt} = \frac{\omega s \sin(\omega t)}{2} \left[1 + \frac{\epsilon \cos \omega t}{(1 - \epsilon^2 \sin^2 \omega t)^{1/2}} \right] \quad (1.30)$$

Equation 1.30 can be nondimensionalized by the mean piston speed \bar{U}_p , resulting in

$$\tilde{U}_p(\theta) = \frac{U_p}{\bar{U}_p} = \frac{\pi}{2} \sin \theta \left[1 + \frac{\epsilon \cos \theta}{(1 - \epsilon^2 \sin^2 \theta)^{1/2}} \right] \quad (1.31)$$

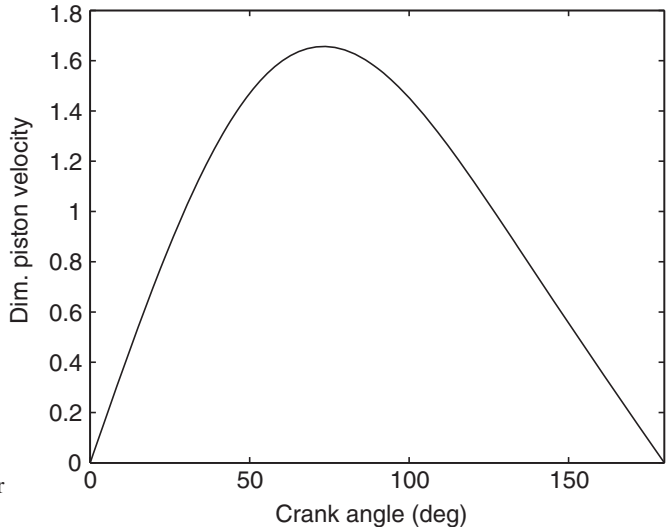


Figure 1.12 Nondimensional velocity versus crank angle for $\epsilon = 1/3$ (Equation 1.31).

Using the Matlab® program `Velocity.m` listed in the Appendix F.2, the nondimensional velocity $\tilde{U}_p(\theta)$ is plotted versus crank angle from top dead center (tdc) to bottom dead center (bdc) in Figure 1.12 for a value of $\epsilon = 1/3$. The piston velocity is zero at tdc and bdc. Due to the geometry of the slider–crank mechanism, the velocity profile is nonsymmetric, with the maximum nondimensional velocity of $\tilde{U}_p(\theta) = 1.65$ occurring at 72°atdc.

If we neglect terms of $O(\epsilon^2)$, and use the trigonometric identity $\sin^2 \omega t = (1 - \cos 2\omega t)/2$, the piston velocity can be approximated as

$$U_p = \frac{dy}{dt} \simeq \frac{\omega s}{2} \left[\sin \omega t + \frac{\epsilon}{2} \sin 2\omega t \right] \quad (1.32)$$

The acceleration a_p is found by differentiating Equation 1.32 with respect to time

$$a_p = \frac{d^2y}{dt^2} \simeq \frac{\omega^2 s}{2} [\cos \omega t + \epsilon \cos 2\omega t] \quad (1.33)$$

Note that the velocity and acceleration terms have two components, one varying with the same frequency ω as the crankshaft, known as the primary term, and the other varying at twice the crankshaft frequency 2ω , known as the secondary term. In the limit of an infinitely long connecting rod, i.e., $\epsilon \rightarrow 0$, the motion reduces to a simple harmonic at a frequency ω .

The reciprocating motion of the connecting rod and piston creates accelerations and thus inertial forces and moments that need to be considered in the choice of an engine configuration. In multicylinder engines, the cylinder arrangement and firing order are chosen to minimize the primary and secondary forces and moments. Complete cancellation is possible for the following four-stroke engines: in-line 6- and 8-cylinder engines; horizontally opposed 8- and 12-cylinder engines, and 12- and 16-cylinder V engines (Taylor, 1985).

Intake and Exhaust Valve Arrangement

Gases are admitted and expelled from the cylinders by valves that open and close at the proper times, or by ports that are uncovered or covered by the piston. There are many design variations for the intake and exhaust valve type and location.

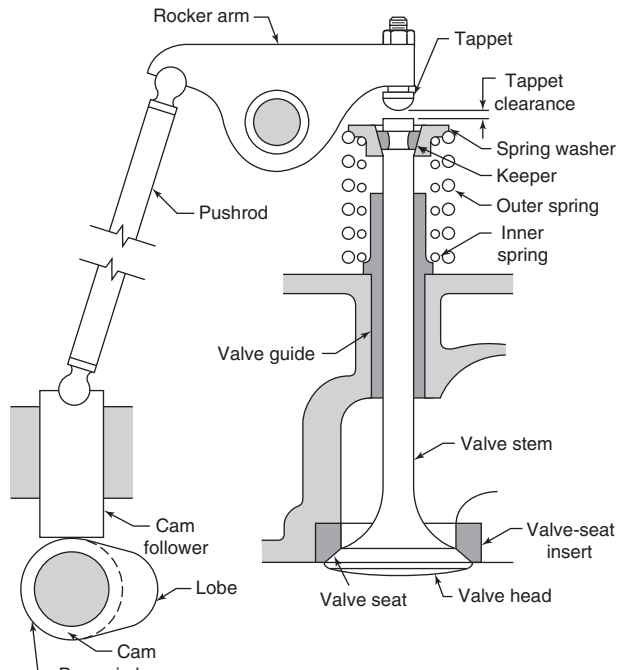


Figure 1.13 Poppet valve nomenclature (Taylor, 1985).

Poppet valves (see Figure 1.13) are the primary valve type used in internal combustion engines, since they have excellent sealing characteristics. Sleeve valves have also been used, but do not seal the combustion chamber as well as poppet valves. The poppet valves can be located either in the engine block or in the cylinder head, depending on manufacturing and cooling considerations. Older automobiles and small four-stroke engines have the valves located in the block, a configuration termed underhead or L-head. Currently, most engines use valves located in the cylinder head, an overhead or I-head configuration, as this configuration has good inlet and exhaust flow characteristics.

The valve timing is controlled by a camshaft that rotates at half the engine speed for four-stroke engine. A valve timing profile is shown in Figure 1.14. Lobes on the camshaft along with lifters, pushrods, and rocker arms control the valve motion. Some engines use an overhead camshaft to eliminate pushrods. The valve timing can be varied to increase volumetric efficiency through the use of advanced camshafts that have moveable lobes, or with electric valves. With a change in the load, the valve opening duration and timing can be adjusted.

Superchargers and Turbochargers

All the engines discussed so far are naturally aspirated, i.e., as the intake gas is drawn in by the downward motion of the piston. Engines can also be supercharged or turbocharged. Supercharging is mechanical compression of the inlet air to a pressure higher than standard atmosphere by a compressor powered by the crankshaft. The compressor increases the density of the intake air so that more fuel and air can be delivered to the cylinder to increase the power. The concept of turbocharging is illustrated in Figure 1.15. Exhaust gas leaving an engine is further expanded through a turbine that drives a compressor. The benefits are twofold: (1) the engine is more efficient because energy that

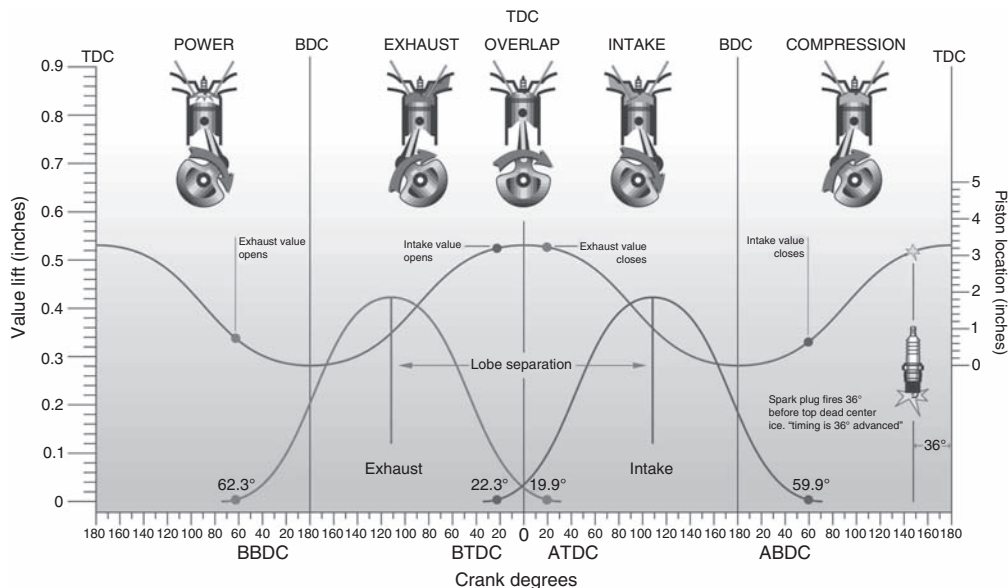


Figure 1.14 Poppet valve timing profile. (Courtesy of Competition Cams, Inc.)

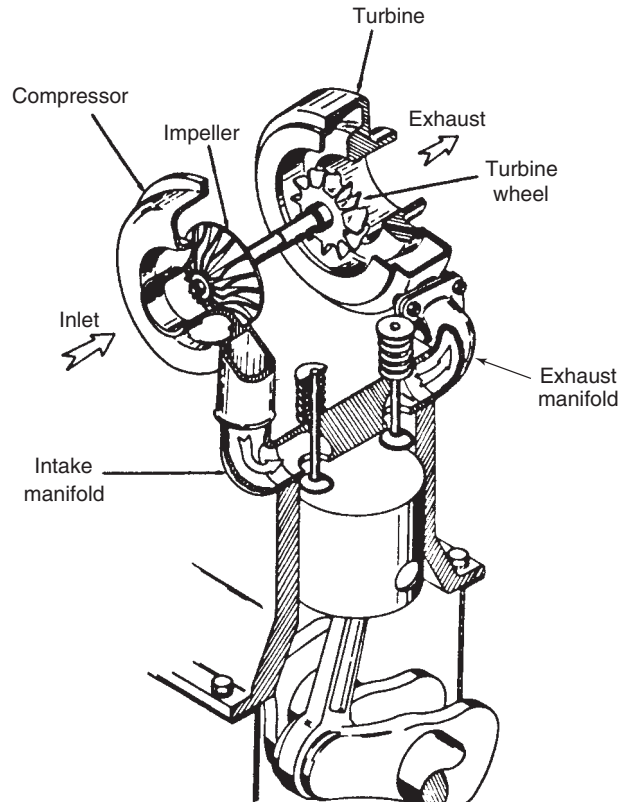


Figure 1.15 Turbocharger schematic. (Courtesy of Schwitzer.)

would have otherwise been wasted is recovered from the exhaust gas; and (2) a smaller engine can be constructed to produce a given power because it is more efficient and because the density of the incoming charge is greater. The power available to drive the compressor when turbocharging is a nonlinear function of engine speed such that at low speeds there is little, if any, boost (density increase), whereas at high speeds the boost is maximum. It is also low at part throttle and high at wide open throttle. These are desirable characteristics for an automotive engine since throttling or pumping losses are minimized. Most large- and medium-sized diesel engines are turbocharged to increase their efficiency.

Fuel Injectors and Carburetors

Revolutionary changes have taken place with computerized engine controls and fuel delivery systems in recent years and the progress continues. For example, the ignition and fuel injection is computer controlled in engines designed for vehicular applications. Conventional carburetors in automobiles were replaced by throttle body fuel injectors in the 1980s, which in turn were replaced by port fuel injectors in the 1990s. Port fuel injectors are located in the intake port of each cylinder just upstream of the intake valve, so there is an injector for each cylinder. The port injector does not need to maintain a continuous fuel spray, since the time lag for fuel delivery is much less than that of a throttle body injector.

Direct injection spark ignition engines are available on many production engines. With direct injection, the fuel is sprayed directly into the cylinder during the late stages of the compression stroke. Compared with port injection, direct injection engines can be operated at a higher compression ratio, and therefore will have a higher theoretical efficiency, since they will not be knock limited. They will also be unthrottled, so they will have a greater volumetric efficiency at part load. The evaporation of the injected fuel in the combustion chamber will have a charge cooling effect, which will also increase its volumetric efficiency.

Cooling Systems

Some type of cooling system is required to remove the approximately 30% of the fuel energy rejected as waste heat. Liquid and air cooling are the two main types of cooling systems. The liquid cooling system (see Figure 1.16) is usually a single loop where a water pump sends coolant to the engine block, and then to the head. Warm coolant flows through the intake manifold to warm it and thereby assist in vaporizing the fuel. The coolant will then flow to a radiator or heat exchanger, reject the waste heat to the atmosphere, and flow

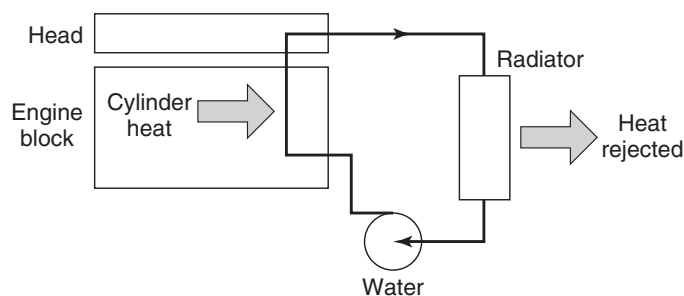


Figure 1.16 Liquid cooling system schematic.



Figure 1.17 Air cooling of model airplane engine. (Courtesy R. Schroeder.)

back to the pump. When the engine is cold, a thermostat prevents coolant from returning to the radiator, resulting in a more rapid warm-up of the engine. Liquid-cooled engines are quieter than air-cooled engines, but have leaking, boiling, and freezing problems. Engines with relatively low-power output, less than 20 kW, primarily use air cooling. Air cooling systems use fins to lower the air side surface temperature (see Figure 1.17). There are historical examples of combined water and air cooling. An early 1920s automobile, the Mors, had a finned air-cooled cylinder and water-cooled heads.

1.6 EXAMPLES OF INTERNAL COMBUSTION ENGINES

Automotive Spark Ignition Four-Stroke Engine

A photograph of a V-6 3.2 L automobile engine is shown as in Figure 1.18 and in cutaway view in Figure 1.19. The engine has a 89 mm bore and a stroke of 86 mm. The maximum power is 165 kW (225 hp) at 5550 rpm. The engine has a single overhead camshaft per



Figure 1.18 3.2 L V-6 automobile engine. (Courtesy of Honda Motor Co.)

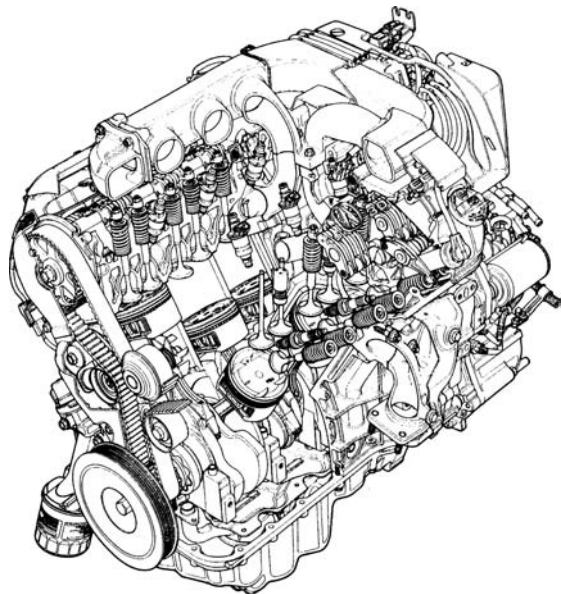


Figure 1.19 Cutaway view of 3.2 L V-6 automobile engine. (Courtesy of Honda Motor Co.)

piston bank with four valves per cylinder. The pistons are flat with notches for valve clearance. The fuel is mixed with the inlet air by spraying the fuel into the intake port at the Y-junction just above the intake valves.

As shown in Figure 1.20, the overhead camshaft acts on both the intake and exhaust valves via rocker arms. The engine has variable valve timing applied to the intake valves with a shift from low-lift short duration cam lobes to high-lift long duration cam lobes above

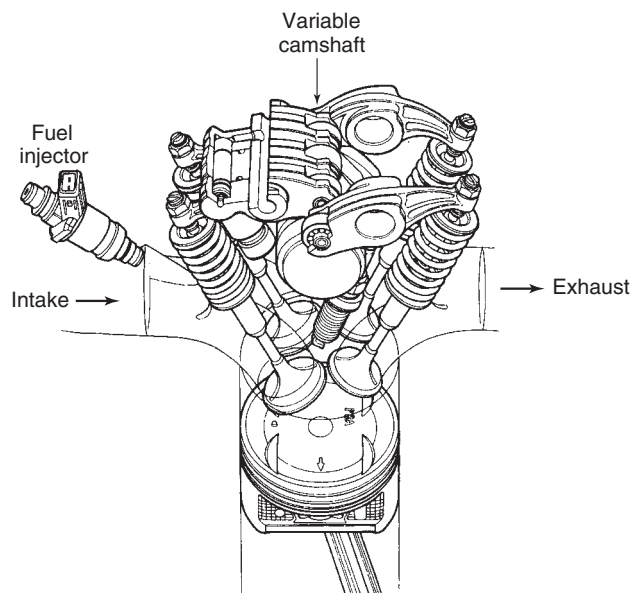


Figure 1.20 A variable valve timing mechanism. (Courtesy of Honda Motor Co.)



Figure 1.21 A 5.9 L L6 on-highway diesel engine. (Courtesy of PriceWebber.)

3500 rpm. In the low-lift short duration cam operation, the two intake valves have staggered timing that creates additional swirl to increase flame propagation and combustion stability. Roller bearings are used on the rocker arms to reduce friction. The clearance volume is formed by an angled pent roof in the cylinder head, with the valves also angled.

Heavy Duty Truck Diesel Engine

A heavy duty truck diesel engine is shown in Figures 1.21. This engine is an inline six-cylinder turbocharged diesel engine with a 137-mm bore and 165-mm stroke for a total displacement of 14.6 L. The rated engine power is 373 kW (500 hp). The compression ratio is 16.5 to 1. The engine has electronically controlled, mechanically actuated fuel injectors, and an overhead camshaft. Note that the cylinder head is flat, with the diesel fuel injector mounted in the center of the combustion chamber. The inlet ports impart a swirl to the air in the combustion chamber to improve mixing with the radial fuel spray.

The top of the piston has a Mexican hat-shaped crater bowl, so that the initial combustion will take place in the piston bowl. The injection nozzles have three to six holes through which the fuel sprays into the piston bowl. The pressure required to spray the diesel fuel into the combustion chamber is of the order of 1000 bar, for adequate spray penetration into the bowl and subsequent atomization of the diesel fuel. The fuel injection pressure is generated by a plunger driven by the camshaft rocker arm.

Stationary Gas Engine

A stationary natural gas engine is shown in Figures 1.22 and 1.23. Typical applications for stationary engines include cogeneration, powering gas compressors, and power generation. The engine shown in Figure 1.22 is an in-line eight-cylinder turbocharged engine, with rated power of 1200 kW, bore of 240 mm, and stroke of 260 mm for a total displacement of 94 L. The compression ratio is 10.9 to 1. This type of engine is designed to operate at a constant speed condition, typically 1200 rpm. Each cylinder has two intake and two exhaust valves. The piston has a combustion bowl with a deep dish concentrated near the center of the piston, so most of the clearance volume is in the piston bowl.

Since natural gas engines are operated lean to reduce nitrogen oxides (NO_x), prechambers are used to initiate a stable combustion process. Pressurized natural gas is injected into

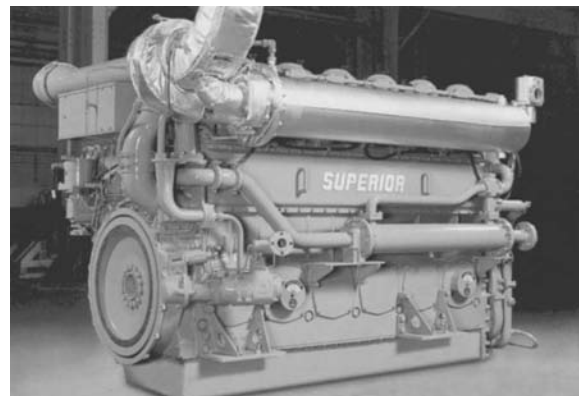


Figure 1.22 A 94 L L8 stationary natural gas engine. (Courtesy of Cooper Energy Services, Inc.)

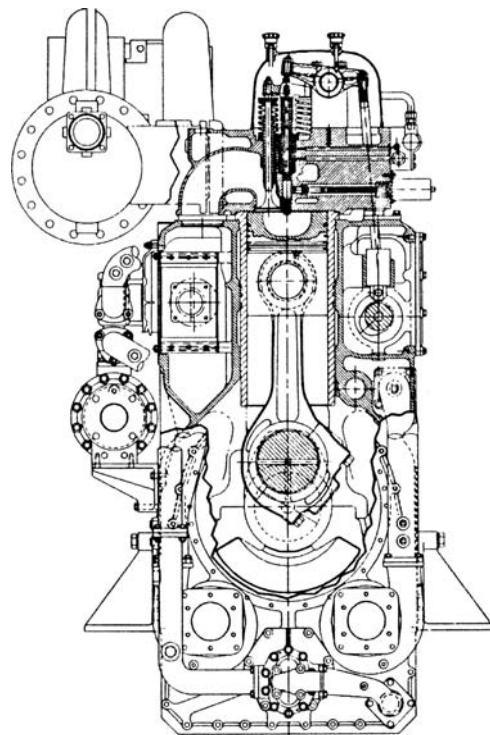


Figure 1.23 Cutaway view of 94 L L8 stationary natural gas engine. (Courtesy of Cooper Energy Services, Inc.)

a prechamber above the piston, and a spark plug in the prechamber is used to ignite the natural gas. The increase in pressure projects the burning mixture into the main combustion chamber, where the final stages of the combustion take place. Prechambers are also used in high-speed diesel engines to achieve acceptable mixing and more complete combustion.

1.7 ALTERNATIVE POWER PLANTS

In this section, alternative power plants will be discussed in terms of a particular application where they dominate the field by having some advantage over the internal combustion engine.

First, consider electric motors which compete in the range of powers less than about 500 kW. They are used, for example, in forklifts operated within a factory or warehouse. Internal combustion engines are not applied in this case because they would build up high levels of pollutants such as carbon monoxide or nitric oxide. Electric motors are found in a variety of applications, such as where the noise and vibration of a piston engine or the handling of a fuel are unacceptable. Other examples are easy to think of in both industrial and residential sectors. Electric motors will run in the absence of air, such as in outer space or under water; they are explosion proof; and they can operate at cryogenic temperatures. If one can generalize, one might state with respect to electric motors that internal combustion engines tend to be found in applications where mobility is a requirement or electricity is not available.

Proponents of electric vehicles point out that almost any fuel can be used to generate electricity, therefore we can reduce our dependence upon petroleum by switching to electric vehicles. There would be no exhaust emissions emitted throughout an urban environment. The emissions produced by the new electric generating stations could be localized geographically so as to minimize the effect. The main problem with electric vehicles is the batteries used for energy storage. The electric vehicles that have been built to date have a limited range of only 50–100 mi (80–160 km), on the order of one-fifth of what can be easily realized with a gasoline engine powered vehicle. It is generally recognized that a breakthrough in battery technology is required if electric vehicles are to become a significant part of the automotive fleet. Batteries have about 1% of the energy per unit mass of a typical vehicular fuel, and a life span of about 5 years.

Hybrid electric vehicles (HEV), which incorporate a small internal combustion engine with an electric motor and storage batteries, have been the subject of recent research, and as of the year 2015, have reached the production stage, primarily due to their low fuel consumption and emission levels. A hybrid electric vehicle has more promise than an electric vehicle, since the HEV has an internal combustion engine to provide the energy to meet vehicle range requirements. The battery then provides the additional power needed for acceleration and climbing hills. The fuels used in the HEV engines in current production include gasoline, diesel, and natural gas. Hybrid electric vehicles have a long history, as the first HEV, the Woods Dual Power automobile, was introduced in 1916.

As shown in Figure 1.24, the engine and electric motor are placed in either a series or parallel configuration. In a series configuration only the electric motor with power from the battery or generator is used to drive the wheels. The internal combustion engine is maintained at its most efficient and lowest emission operating points to run the generator and charge the storage batteries. With the parallel configuration, the engine and electric motor can be used separately or together to power the vehicle. The motors can be used as generators during braking to increase vehicle efficiency.

The fuel cell electric vehicle (FCEV) is currently in the development phase, and will be commercially available beginning in 2015. The chemical reaction in a fuel cell produces lower emissions relative to combustion in an internal combustion engine. Recent developments in proton exchange membrane (PEM) technology have been applied to vehicular fuel cells. Current PEM fuel cells are small enough to fit beneath a vehicle's floor next to storage batteries and deliver 50 kW to an electric motor. The PEM fuel cell requires a hydrogen fuel source to operate. Since there is presently no hydrogen fuel storage infrastructure, on-board reforming of methanol fuel to hydrogen and CO₂ is also required. The reforming efficiency is about 60%, so coupled with a fuel cell efficiency of 70%, and a motor efficiency of 90%, the overall fuel cell engine efficiency will be about 40%, about the same as high-efficiency internal combustion engines.

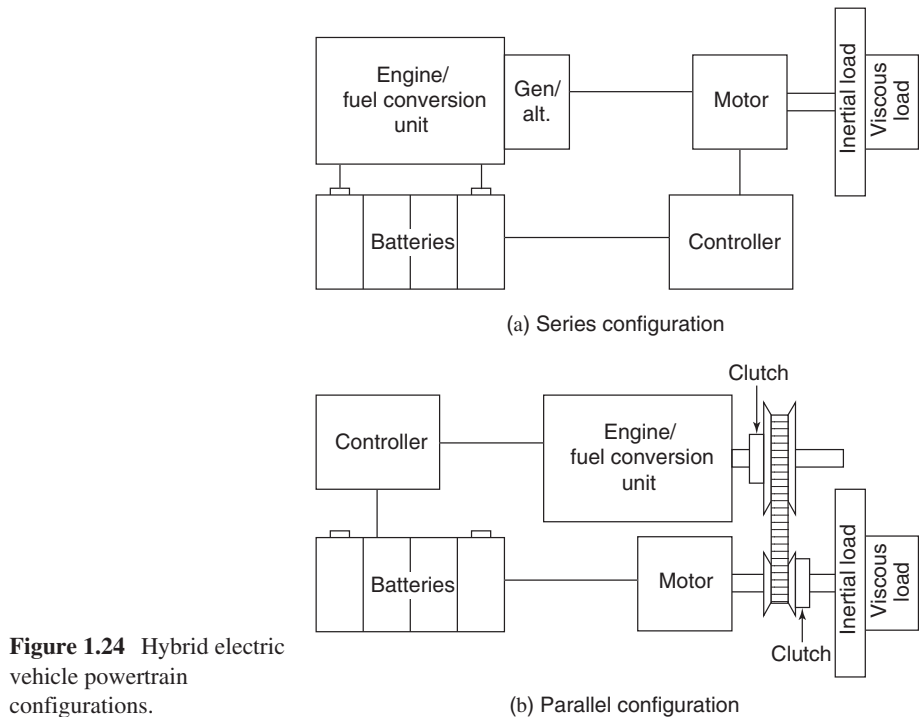


Figure 1.24 Hybrid electric vehicle powertrain configurations.

Gas turbine engines compete with internal combustion engines on the other end of the power spectrum, at powers greater than about 500 kW. The advantages offered depend on the application. Factors to consider are the efficiency and power per unit weight. A gas turbine consists basically of a compressor–burner–turbine combination that provides a supply of hot, high-pressure gas. This may then be expanded through a nozzle (turbojet), through a turbine, to drive a fan, and then through a nozzle (turbofan), through a turbine, to drive a propeller (turboprop), or through a turbine to spin a shaft in a stationary or vehicular application.

One advantage a gas turbine engine offers to the designer is that the hardware responsible for compression, combustion, and expansion are three different devices, whereas in a piston engine all these processes are done within the cylinder. The hardware for each process in a gas turbine engine can then be optimized separately; whereas in a piston engine compromises must be made with any given process, since the hardware is expected to do three tasks. However, it should be pointed out that turbochargers give the designer of conventional internal combustion engines some new degrees of freedom toward optimization.

With temperature limits imposed by materials, the reciprocating engine can have a greater peak cycle temperature than the gas turbine engine. In an internal combustion engine, the gases at any position within the engine vary periodically from hot to cold. Thus, the average temperature during the heat transfer to the walls is neither very hot nor cold. On the other hand, the gas temperature at any position in the gas turbine is steady, and the turbine inlet temperature is always very hot, thus tending to heat material at this point to a greater temperature than anywhere in a piston engine.

The thermal efficiency of a gas turbine engine is highly dependent upon the adiabatic efficiency of its components, which in turn is highly dependent upon their size and their operating conditions. Large gas turbines tend to be more efficient than small gas turbines.

That airliners are larger than automobiles is one reason gas turbines have displaced piston engines in airliners, but not in automobiles. Likewise gas turbines are beginning to penetrate the marine industry, though not as rapidly, as power per unit weight is not as important with ships as with airplanes.

Another factor favoring the use of gas turbines in airliners (and ships) is that the time the engine spends operating at part or full load is small compared to the time the engine spends cruising, therefore the engine can be optimized for maximum efficiency at cruise. It is a minor concern that at part load or at take-off conditions the engine's efficiency is compromised. Automobiles, on the other hand, are operated over a wide range of load and speed so a good efficiency at all conditions is better than a slightly better efficiency at the most probable operating condition and a poorer efficiency at all the rest.

Steam- or vapor-cycle engines are much less efficient than internal combustion engines, since their peak temperatures are about 800 K, much lower than the peak temperatures (\approx 2500 K) of an internal combustion engine. They are used today almost totally in stationary applications and where the energy source precludes the use of internal combustion engines. Such energy sources include coal, waste feed stocks, nuclear, solar, and waste heat in the exhaust gas of combustion devices including internal combustion engines.

In some applications, engine emission characteristics might be a controlling factor. In the 1970s, in fact, a great deal of development work was done toward producing an automotive steam engine when it was not known whether the emissions from the internal combustion engine could be reduced enough to meet the standards dictated by concern for public health. However, the development of catalytic converters, as discussed in Chapter 9, made it possible for the internal combustion engine to meet emission standards at that time, and remain a dominant prime mover technology.

The references of this introductory chapter contain a listing of both historical and current books that will provide additional information about internal combustion engine design, analysis, and performance. These books give the reader a deep appreciation of how much the technology of internal combustion engines has advanced in the last century. In chronological order, these books are Clerk (1910), Ricardo (1941), Benson and Whitehouse (1979), Heywood (1988), Cummins (1989), Arcoumanis (1998), Stone (1999), Lumley (1999), Pulkrabek (2003), Shi et al. (2011), Manning (2012), and Crolla et al. (2015).

1.8 REFERENCES

- ARCOUMANIS, C. (1988), *Internal Combustion Engines*, Academic Press, London, England.
- ARMSTRONG, D. and G. STIRRAT (1982), "Ford's 1982 3.8L V6 Engine," SAE paper 820112.
- BENSON, R. and N. WHITEHOUSE (1979), *Internal Combustion Engines*, Pergamon Press, New York.
- CLERK, D. (1910), *The Gas, Petrol, and Oil Engine*, Longmans, Green, and Co., London, England.
- CROLLA, D., Ed. (2015), *Encyclopedia of Automotive Engineering*, Wiley, New York.
- CUMMINS, L. (1989), *Internal Fire*, Society of Automotive Engineers, Warrendale, Pennsylvania.
- HEYWOOD, J. B. (1988), *Internal Combustion Engine Fundamentals*, McGraw-Hill, New York.
- LUMLEY, J. (1999), *Engines: An Introduction*, Cambridge University Press, Cambridge, England.
- MANNING, J. (2012), *Internal Combustion Engine Design*, Ricardo UK Limited, West Sussex, England.
- OBERT, E. (1950), *Internal Combustion Engines*, International Textbook Co., Scranton, Pennsylvania.
- PULKRABEK, W. (2003), *Engineering Fundamentals of the Internal Combustion Engine*, Prentice Hall, New York.
- RICARDO, H. R. (1941), *The High Speed Internal Combustion Engine*, Interscience Publishers, New York.
- SHI, Y., H. GE, and R. REITZ (2011), *Computational Optimization of Internal Combustion Engines*, Springer-Verlag, London, England.

Table 1.2 Engine Data for Homework Problems

Engine	Bore (mm)	Stroke (mm)	Cylinders	Speed (rpm)	Power (kW)
Marine	136	127	12	2600	1118
Truck	108	95	8	6400	447
Airplane	86	57	8	10,500	522

STONE, R. (1999), *Introduction to Internal Combustion Engines*, SAE International, Warrendale, Pennsylvania.

TAYLOR, C. (1985), *The Internal Combustion Engine in Theory and Practice*, Vols. 1 and 2, MIT Press, Cambridge, Massachusetts.

1.9 HOMEWORK

- 1.1 Compute the mean piston speed, bmepl (bar), torque (Nm), and the power per piston area for the engines listed in Table 1.2
- 1.2 A six-cylinder two-stroke engine with a compression ratio $r = 9$ produces a torque of 1100 Nm at a speed of 2100 rpm. It has a bore b of 123 mm and a stroke s of 127 mm. (a) What is the displacement volume and the clearance volume of a cylinder? (b) What is the engine bmepl, brake power, and mean piston speed?
- 1.3 A four-cylinder 2.5 L spark-ignited engine is mounted on a dyno and operated at a speed of $N = 3000$ rpm. The engine has a compression ratio of 10:1 and mass air–fuel ratio of 15:1. The inlet air manifold conditions are 80 kPa and 313 K. The engine produces a torque of 160 Nm and has a volumetric efficiency of 0.82. (a) What is the brake power \dot{W}_b (kW)? (b) What is the brake specific fuel consumption bsfc (g/kWh)?
- 1.4 The volumetric efficiency of the fuel injected marine engine in Table 1.2 is 0.80 and the inlet manifold density is 50% greater than the standard atmospheric density of $\rho_{amb} = 1.17 \text{ kg/m}^3$. If the engine speed is 2600 rpm, what is the air mass flow rate (kg/s)?
- 1.5 A 380 cc single-cylinder two-stroke motorcycle engine is operating at 5500 rpm. The engine has a bore of 82 mm and a stroke of 72 mm. Performance testing gives a bmepl = 6.81 bar, bsfc = 0.49 kg/kWh, and delivery ratio of 0.748. (a) What is the fuel to air ratio? (b) What is the air mass flow rate (kg/s)?
- 1.6 A 3.8 L four-stroke four-cylinder fuel-injected automobile engine has a power output of 88 kW at 4000 rpm and volumetric efficiency of 0.85. The bsfc is 0.35 kg/kW h. If the fuel has a heat of combustion of 42 MJ/kg, what are the bmepl, thermal efficiency, and air to fuel ratio? Assume atmospheric conditions of 298 K and 1 bar.
- 1.7 A 4.0 L six-cylinder engine is operating at 3000 rpm. The engine has a compression ratio of 10:1, and volumetric efficiency of 0.85. If the bore and stroke are equal, what is the stroke, the mean piston speed, cylinder clearance volume, and air mass flow rate into the engine? Assume standard inlet conditions.
- 1.8 Choose an automotive, marine, or aviation engine of interest, and compute the engine's mean piston speed, bmepl, power/volume, mass/volume, and power/mass. Compare your calculated values with those presented in Table 1.1.

- 1.9** Compare the approximate, Equation 1.29, and exact, Equation 1.26, dimensionless cylinder volume versus crank angle profiles for $r = 8$, $s = 100$ mm, and $l = 150$ mm. What is the maximum error and at what crank angle does it occur?
- 1.10** Plot the dimensionless piston velocity for an engine with a stroke $s = 100$ mm and connecting rod length $l = 150$ mm.
- 1.11** Assuming that the mean effective pressure, mean piston speed, power per unit piston area, and mass per unit displacement volume are all size independent, how will the power per unit weight of an engine depend upon the number of cylinders if the total displacement is constant? To make the analysis easier, assume that the bore and stroke are equal.

Chapter 2

Heat Engine Cycles

2.1 INTRODUCTION

Studying heat engine cycles as simplified models of internal combustion engine processes is very useful for illustrating the important parameters influencing engine performance. Heat engine cycle analysis treats the combustion process as an equivalent heat addition to an ideal gas. By modeling the combustion process as a heat addition, the analysis is simplified since the details of the physics and chemistry of combustion are not required. The various combustion processes are modeled as constant volume, constant pressure, or finite energy release processes.

The internal combustion engine is not a heat engine, since it relies on internal combustion processes to produce work. However, heat engine models are useful for introducing the idealized cycle parameters that are also used in more complex combustion cycle models, for example, the fuel–air cycle, to be introduced in Chapter 4. The fuel–air cycle accounts for the change in composition of the fuel–air mixture during the combustion process.

This chapter also provides a review of closed system and open system thermodynamics. This chapter first uses a first law closed system analysis to model the compression and expansion strokes and then incorporates open system control volume analysis of the intake and exhaust strokes. An important parameter in the open system analysis is the residual fraction of combustion gas, f , remaining in the cylinder at the end of the exhaust stroke.

The scientific theory of heat engine cycles was first developed by Sadi Carnot (1796–1832), a French engineer, in 1824. His theory has two main axioms. The first axiom is that in order to use a flow of energy to generate power, there must be two bodies at different temperatures, a hot body and a cold body. Work is extracted from the flow of energy from the hot body to the cold body or reservoir. The second axiom is that there must be at no point a useless flow of energy, so heat transfer at a constant temperature is needed. Carnot developed an ideal heat engine cycle, which is reversible; that is, if the balance of pressures is altered, the cycle of operation is reversed. The efficiency of this cycle, known as the Carnot cycle, is a function only of the reservoir temperatures, and the efficiency is increased as the temperature of the high-temperature reservoir is increased. The Carnot cycle, since it is reversible, is the most efficient possible, and is the standard to which all real engines are compared.

Let us assume, to keep our mathematics simple, that the gas cycles analyzed in this chapter use air with a constant specific heat as the working fluid. This assumption results in simple analytical expressions for the efficiency as a function of the compression ratio. A plot of the specific heat ratio, $\gamma = c_p/c_v$, of air as a function of temperature is given in Appendix A. Typical values of γ chosen for gas cycle calculations range from 1.3 to 1.4, to correspond with measured cylinder temperature data.

In performing a gas cycle computation, the heat addition Q_{in} (kJ) is required. It can be estimated from the heat of combustion, q_c (kJ/kg_{fuel}), of a fuel as follows:

$$Q_{\text{in}} = m_f q_c = mq_{\text{in}} \quad (2.1)$$

where m_f is the mass of fuel injected into the cylinder, m is the mass of the fuel-air gas mixture in the cylinder, and q_{in} is the heat addition per unit mass of fuel-air mixture (kJ/kg_{mix}). The mass of the fuel-air mixture can be determined using the ideal gas law with known cylinder volume, mixture molecular mass, inlet pressure, and temperature, as shown later in the text.

2.2 CONSTANT VOLUME HEAT ADDITION

This cycle is often referred to as the Otto cycle and considers the idealized case of an internal combustion engine whose combustion is so rapid that the piston does not move during the combustion process, and thus combustion is assumed to take place at constant volume. The Otto cycle is named after Nikolaus Otto (1832–1891) who developed a four-stroke engine in 1876. Otto is considered the inventor of the modern internal combustion engine, and founder of the internal combustion engine industry.

The Otto cycle engine is also called a spark ignition engine since a spark is needed to initiate the combustion process. As we shall see, the combustion in a spark ignition engine is not necessarily at constant volume. The working fluid in the Otto cycle is assumed to be an ideal gas. The constant volume heat addition Q_{in} is non dimensionalized by the initial pressure P_1 and volume V_1 . The Otto cycle example plotted in Figure 2.1 has a heat addition $Q_{\text{in}}/P_1 V_1 = 20$, a compression ratio $r = 8$, and a specific heat ratio $\gamma = 1.4$.

The state processes for the Otto cycle are plotted in Figure 2.1. The four basic processes are

- 1 to 2 isentropic compression
- 2 to 3 constant volume heat addition
- 3 to 4 isentropic expansion
- 4 to 1 constant volume heat rejection

The compression ratio of an engine is

$$r = \frac{V_1}{V_2} \quad (2.2)$$

The reader should be able to show that the following thermodynamic relations for the Otto cycle processes are valid:

Compression stroke

$$\frac{P_2}{P_1} = r^\gamma \quad \frac{T_2}{T_1} = r^{\gamma-1} \quad (2.3)$$

Constant volume heat addition

$$Q_{\text{in}} = mc_v(T_3 - T_2) \quad (2.4)$$

$$\frac{T_3}{T_2} = (\gamma - 1) \frac{Q_{\text{in}}}{P_1 V_1} r^{1-\gamma} + 1 \quad (2.5)$$

$$\frac{P_3}{P_2} = \frac{T_3}{T_2} \quad (2.6)$$

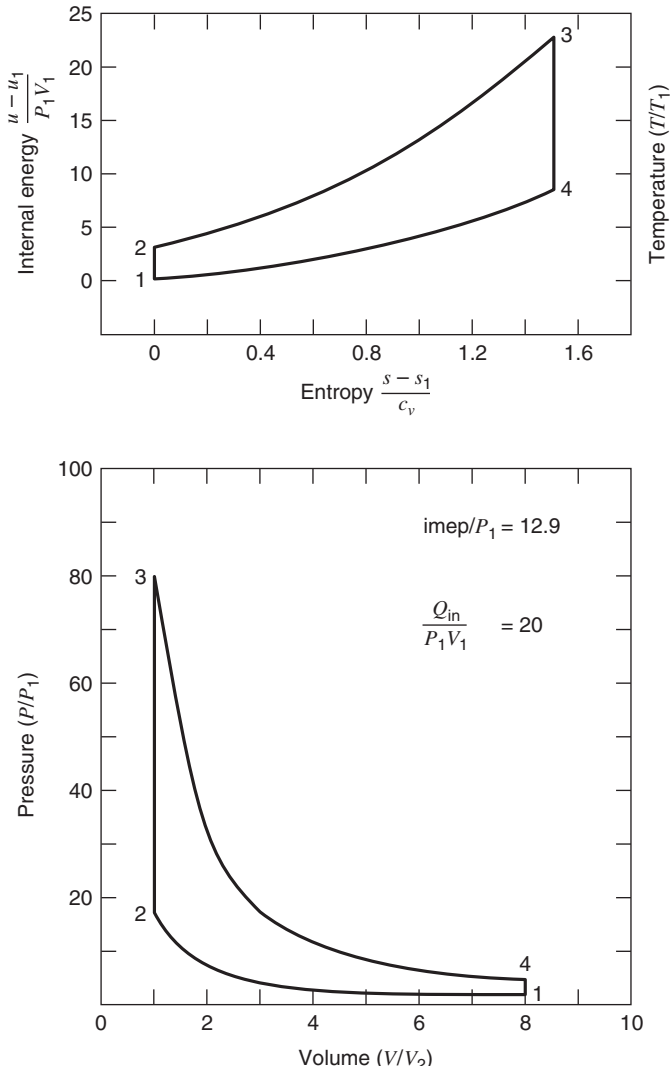


Figure 2.1 The Otto cycle ($\gamma = 1.40$, $r = 8$).

Expansion stroke

$$\frac{P_4}{P_3} = \left(\frac{1}{r}\right)^\gamma \quad \frac{T_4}{T_3} = \left(\frac{1}{r}\right)^{\gamma-1} \quad (2.7)$$

Heat rejection

$$Q_{\text{out}} = mc_v(T_4 - T_1) \quad (2.8)$$

where

m = mass of gas in the cylinder, $P_1 V_1 / RT_1$

c_v = constant volume specific heat

r = compression ratio

γ = specific heat ratio

The thermal efficiency is given by the usual definition:

$$\eta = \frac{W_{\text{out}}}{Q_{\text{in}}} = 1 - \frac{Q_{\text{out}}}{Q_{\text{in}}} \quad (2.9)$$

If we introduce the previously cited relations for Q_{in} , Equation 2.4, and Q_{out} , Equation 2.8, we get

$$\eta = 1 - \frac{(T_4 - T_1)}{(T_3 - T_2)} = 1 - \frac{1}{r^{\gamma-1}} \quad (2.10)$$

This cycle analysis indicates that the thermal efficiency η of the Otto cycle depends only on the specific heat ratio and the compression ratio. Figure 2.2 plots the thermal efficiency versus compression ratio for a range of specific heat ratios from 1.2 to 1.4. The efficiencies we have computed, for example, $\eta \sim 0.56$, for $r = 8$ and $\gamma = 1.40$, are about twice as large as those measured for actual engines. There are a number of reasons for this. We have not accounted for internal friction and the combustion of a fuel within the engine, and we have ignored heat transfer losses.

The indicated mean effective pressure (imep) is

$$\frac{\text{imep}}{P_1} = \eta \frac{Q_{\text{in}}}{P_1 V_1} \frac{r}{r-1} \quad (2.11)$$

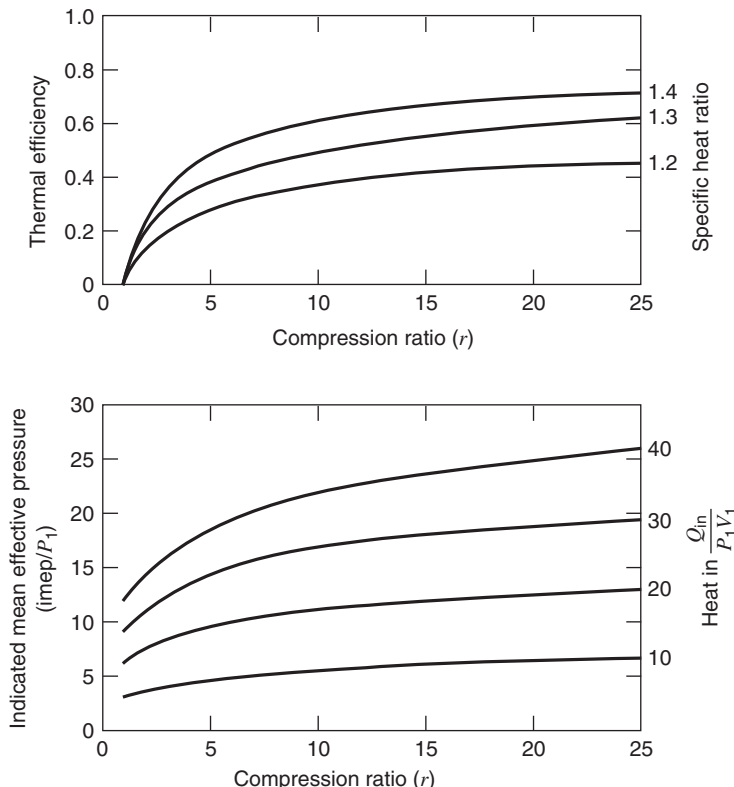


Figure 2.2 Otto cycle thermal efficiency and imep as a function of compression ratio and heat addition.

Note that the imep is nondimensionalized by the initial pressure P_1 . The indicated mean effective pressure is plotted versus compression ratio and heat addition in Figure 2.2 for $\gamma = 1.30$. As shown by Equation 2.11, the imep increases linearly with heat addition and to a lesser degree with compression ratio.

Compression ratios found in actual spark ignition engines typically range from 9 to 11. The compression ratio is limited by two practical considerations: material strength and engine knock. The maximum pressure, P_3 , of the cycle scales with compression ratio as r^γ . Engine heads and blocks have a design maximum stress, which should not be exceeded, thus limiting the compression ratio. In addition, the maximum temperature T_3 also scales with the compression ratio as r^γ . If T_3 exceeds the autoignition temperature of the air-fuel mixture, combustion will occur ahead of the flame, a condition termed knock. The pressure waves that are produced are damaging to the engine, and they reduce the combustion efficiency. The knock phenomenon is discussed further in Chapter 7.

2.3 CONSTANT PRESSURE HEAT ADDITION

This cycle is often referred to as the Diesel cycle and models a heat engine cycle in which energy is added at a constant pressure. The Diesel cycle is named after Rudolph Diesel (1858–1913), who in 1897 developed an engine designed for the direct injection, mixing, and autoignition of liquid fuel into the combustion chamber. The Diesel cycle engine is also called a compression ignition engine. As we will see, actual diesel engines do not have a constant pressure combustion process.

The cycle for analysis is shown in Figure 2.3. The four basic processes are

- 1 to 2 isentropic compression
- 2 to 3 constant pressure heat addition
- 3 to 4 isentropic expansion
- 4 to 1 constant volume heat rejection

Again assuming constant specific heats, the student should recognize the following equations:

Heat addition

$$Q_{\text{in}} = mc_p(T_3 - T_2) \quad (2.12)$$

Expansion stroke

$$\frac{P_4}{P_3} = \left(\frac{\beta}{r} \right)^\gamma \quad \frac{T_4}{T_3} = \left(\frac{\beta}{r} \right)^{\gamma-1} \quad (2.13)$$

where we have defined the parameter β , a measure of the combustion duration, as

$$\beta = \frac{V_3}{V_2} = \frac{T_3}{T_2} \quad (2.14)$$

In this case, the indicated efficiency is

$$\eta = 1 - \frac{1}{r^{\gamma-1}} \left[\frac{\beta^\gamma - 1}{\gamma(\beta - 1)} \right] \quad (2.15)$$

The term in brackets in Equation 2.15 is greater than 1, so that for the same compression ratio r , the efficiency of the Diesel cycle is less than that of the Otto cycle. However, since Diesel cycle engines are not knock limited, they operate at about twice the compression

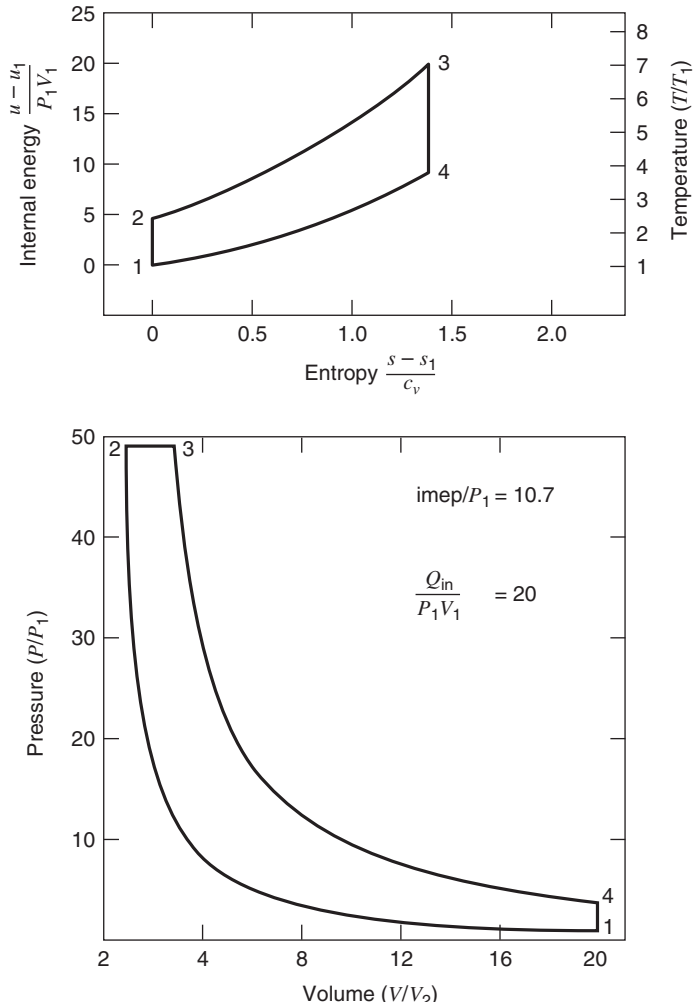


Figure 2.3 The Diesel cycle ($\gamma = 1.30, r = 20$).

ratio of Otto cycle engines. For the same maximum pressure, the efficiency of the Diesel cycle is greater than that of the Otto cycle. Diesel cycle efficiencies are shown in Figure 2.4 for a specific heat ratio of 1.30. They illustrate that high compression ratios are desirable and that the efficiency decreases as the heat input increases. As β approaches 1, the Diesel cycle efficiency approaches the Otto cycle efficiency.

Although Equation 2.15 is correct, its utility suffers somewhat in that β is not a natural choice of independent variable. Rather, in engine operation, we think more in terms of the heat transferred in. The two are related according to Equation 2.16.

$$\beta = 1 + \frac{\gamma - 1}{\gamma} \frac{Q_{in}}{P_1 V_1} \frac{1}{r^{\gamma-1}} \quad (2.16)$$

2.4 LIMITED PRESSURE CYCLE

Modern compression ignition engines resemble neither the constant volume nor the constant pressure cycle, but rather a cycle in which some of the heat is added at constant volume and

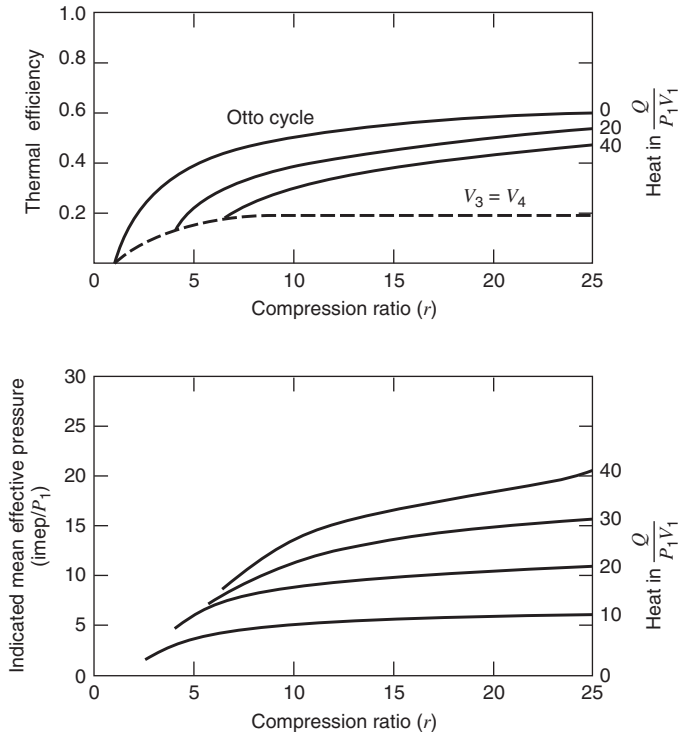


Figure 2.4 Diesel cycle characteristics as a function of compression ratio and heat addition ($\gamma = 1.30$).

then the remaining heat is added at constant pressure. This limited pressure or “dual” cycle is a gas cycle model that can be used to model combustion processes that are slower than constant volume, but more rapid than constant pressure. The limited pressure cycle can also provide algebraic equations for performance parameters such as the thermal efficiency and imep. The distribution of heat added in the two processes is something an engine designer can specify approximately by choice of fuel, the fuel injection system, and the engine geometry to limit the peak pressure in the cycle.

The cycle notation is illustrated in Figure 2.5. In this case, we have the following equation 2.17 for Q_{in} :

Heat addition

$$Q_{\text{in}} = mc_v(T_{2.5} - T_2) + mc_p(T_3 - T_{2.5}) \quad (2.17)$$

The expansion stroke is still described by Equation 2.14 provided we write $\beta = V_3/V_{2.5}$. If we let $\alpha = P_3/P_2$, a pressure rise parameter, it can be shown that

$$\eta = 1 - \frac{1}{r^{\gamma-1}} \frac{\alpha\beta^\gamma - 1}{\alpha - 1 + \alpha\gamma(\beta - 1)} \quad (2.18)$$

The constant volume and constant pressure cycles can be considered as special cases of the limited pressure cycle in which $\beta = 1$ and $\alpha = 1$, respectively. The use of the limited pressure cycle model requires information about either the fractions of constant volume and constant pressure heat addition or the maximum pressure, P_3 . A common assumption is to equally split the heat addition. Results for the case of $P_3/P_1 = 50$ and $\gamma = 1.3$ are shown in Figure 2.6, showing efficiencies and imep that are between the Otto and Diesel limits. For the same compression ratio, the Otto cycle has the largest net work, followed

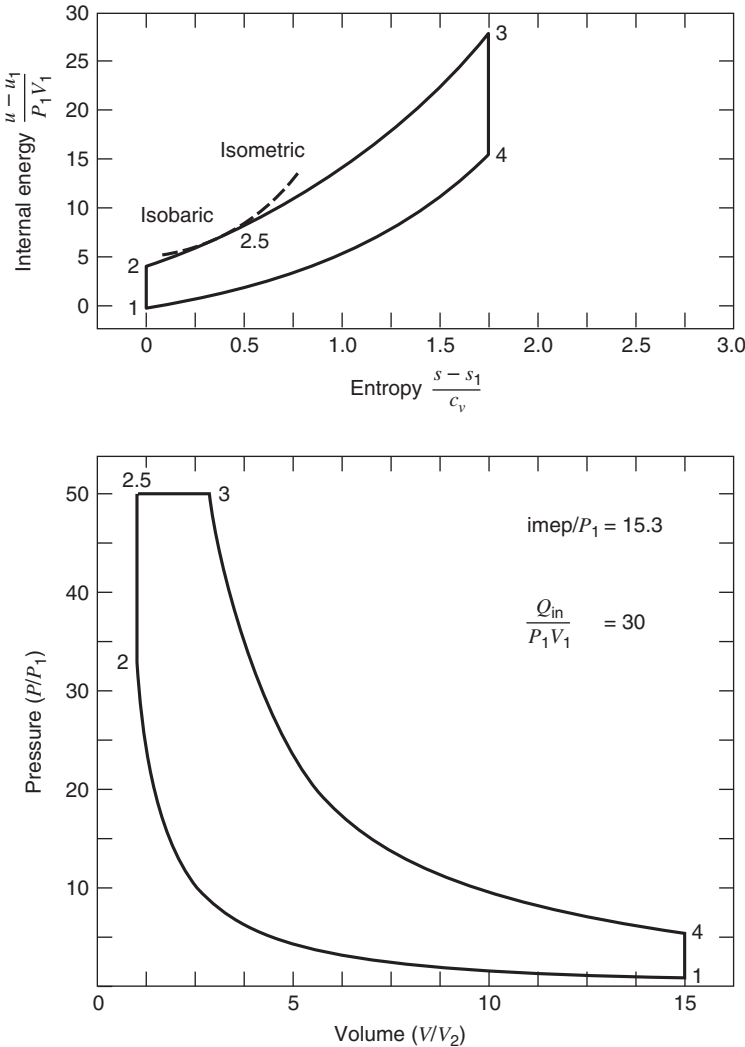


Figure 2.5 The limited pressure cycle ($\gamma = 1.30, r = 15$).

by the limited pressure and the Diesel. Transformation of β and α to more useful variables yields

$$\beta = 1 + \frac{\gamma - 1}{\alpha\gamma} \left[\frac{Q_{\text{in}}}{P_1 V_1} \frac{1}{r^{\gamma-1}} - \frac{\alpha - 1}{\gamma - 1} \right] \quad (2.19)$$

$$\alpha = \frac{1}{r^\gamma} \frac{P_3}{P_1} \quad (2.20)$$

2.5 MILLER CYCLE

The efficiency of an internal combustion engine will increase if the expansion ratio is larger than the compression ratio. There have been many mechanisms of varying degrees of complexity designed to produce different compression and expansion ratios, and thus

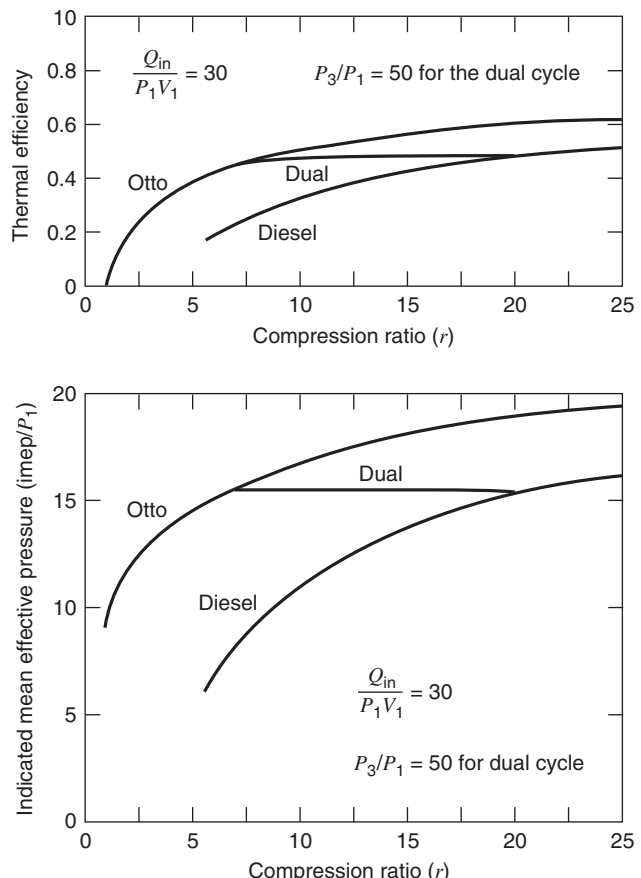


Figure 2.6 Comparison of limited pressure cycle with Otto and Diesel cycles ($\gamma = 1.30$).

greater efficiency. The Miller cycle (Miller, 1947), was patented by R. H. Miller (1890–1967), an American inventor, in 1957. It is a cycle that uses early or late inlet valve closing to decrease the effective compression ratio. This cycle has been used in ship diesel engines since the 1960s, and in the 1990s adopted by Mazda for use in vehicles. For example, a 2.3 L supercharged V6 Miller cycle engine was used as the replacement for a 3.3 L naturally aspirated V6 engine in the 1995 Mazda Millenia. This engine used late inlet valve closing at 30° after the start of the compression stroke.

A related cycle, the Atkinson cycle, is one in which the expansion stroke continues until the cylinder pressure at point 4 decreases to atmospheric pressure. This cycle is named after James Atkinson (1846–1914), an English engineer, who invented and built an engine he named the “cycle” engine in 1889. This engine had a two-bar linkage between the connecting rod and the crankshaft so that the piston traveled through four unequal strokes in every crankshaft revolution. The expansion to intake stroke ratio was 1.78:1.

The Miller gas cycle is shown in Figure 2.7. In this cycle, as the piston moves downward on the intake stroke, the cylinder pressure follows the constant pressure line from point 6 to point 1. For early inlet valve closing, the inlet valve is closed at point 1 and the cylinder pressure decreases during the expansion to point 7. As the piston moves upward on the compression stroke, the cylinder pressure retraces the path from point 7 through point 1 to point 2. The net work done along the two paths 1-7 and 7-1 cancel, so the effective compression ratio $r_c = V_1 / V_2$ is less than the expansion ratio $r_e = V_4 / V_3$.

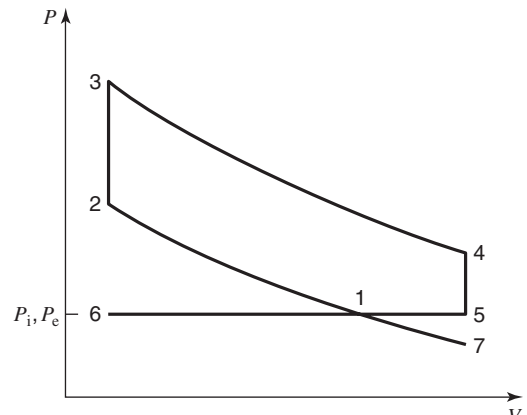


Figure 2.7 The Miller cycle.

For late inlet valve closing, a portion of the intake air is pushed back into the intake manifold before the intake valve closes at point 1. Once the inlet valve closes, there is less mixture to compress in the cylinder, and thus less compression work.

Performing a first law analysis of the Miller cycle, we first define the parameter λ , the ratio of the expansion ratio to the compression ratio:

$$\lambda = r_e / r_c \quad (2.21)$$

The heat rejection has two components:

$$Q_{\text{out}} = mc_v(T_4 - T_5) + mc_p(T_5 - T_1) \quad (2.22)$$

In this case, the thermal efficiency is

$$\eta = 1 - (\lambda r_c)^{1-\gamma} - \frac{\lambda^{1-\gamma} - \lambda(1-\gamma) - \gamma}{\gamma - 1} \frac{P_1 V_1}{Q_{\text{in}}} \quad (2.23)$$

Equation 2.23 reduces to the Otto cycle thermal efficiency as $\lambda \rightarrow 1$. The imep is:

$$\frac{\text{imep}}{P_1} = \eta \frac{Q_{\text{in}}}{P_1 V_1} \frac{r_c}{\lambda r_c - 1} \quad (2.24)$$

The thermal efficiency of the Miller cycle is not only a function of the compression ratio and specific heat ratio, but also a function of the expansion ratio and the load Q_{in} . The ratio of the Miller cycle thermal efficiency to an equivalent Otto cycle efficiency with the same compression ratio is plotted in Figure 2.8 for a range of compression ratios and λ values. For example, with $\lambda = 2$ and $r_c = 12$, the Miller cycle is about 20% more efficient than the Otto cycle. The ratio of the Miller/Otto cycle imep is plotted as a function of λ in Figure 2.9. As λ increases, the imep decreases significantly, since the fraction of the displacement volume V_d that is filled with the inlet fuel-air mixture decreases. This relative decrease in imep and engine power is a disadvantage of the Miller cycle, which is the reason supercharging of the inlet mixture is used to increase the imep.

2.6 FINITE ENERGY RELEASE

Energy Release Fraction

In the Otto and Diesel cycles, the fuel is assumed to burn at rates that result in constant volume top dead center combustion or constant pressure combustion, respectively. Actual

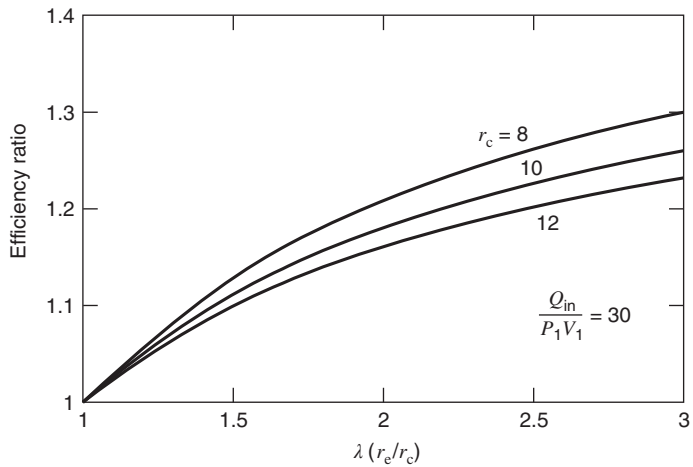


Figure 2.8 Ratio of Miller to Otto cycle thermal efficiency with same compression ratio, r_c ($\gamma = 1.30$).

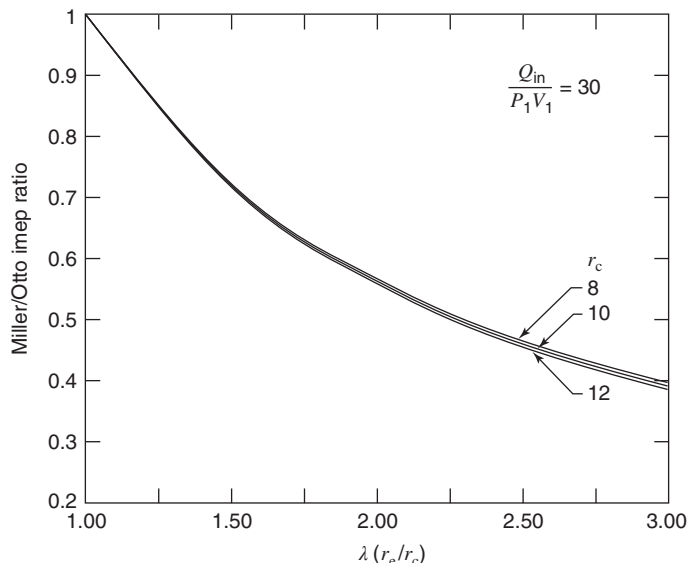


Figure 2.9 Ratio of Miller to Otto cycle imep with same compression ratio, r_c ($\gamma = 1.30$).

engine pressure and temperature profile data do not match these simple models, and more realistic modeling, such as a finite energy release model, is required. A finite energy release model is a differential equation model of an engine cycle in which the heat addition is specified as a function of the crank angle. It is also known as a “zero-dimensional” model, since it is a function only of crank angle, and not a function of the combustion chamber geometry.

Energy release models can address questions that the simple gas cycle models cannot. For example, if one wants to know about the effect of spark timing or heat and mass transfer on engine work and efficiency, an energy release model is required. Also if heat transfer is included, as is done in Chapter 11, then the state changes for the compression and expansion processes are no longer isentropic, and cannot be expressed as simple algebraic equations. For further information about energy release models, also known as zero-dimensional thermodynamic models since there is no engine spatial information used, the reader is referred to Foster (1985).

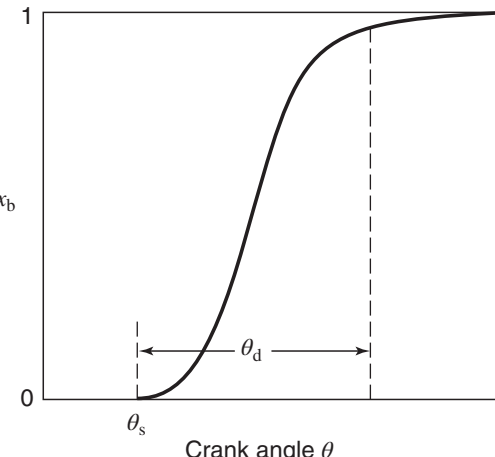


Figure 2.10 Cumulative energy release function.

A typical cumulative mass fraction burned, that is, fraction of fuel energy released, curve for a spark ignition engine is shown in Figure 2.10. The figure plots the cumulative mass fraction burned $x_b(\theta)$ versus the crank angle. The characteristic features of the mass fraction burned curve are an initial small slope region beginning with spark ignition and the start of energy release at θ_s , followed by a region of rapid growth and then a more gradual decay. The three regions correspond to the initial ignition development, a rapid burning region, and a burning completion region. This S-shaped curve can be represented analytically by a trigonometric function as indicated by Equation 2.25:

$$x_b(\theta) = \frac{1}{2} \left[1 - \cos \left(\frac{\pi(\theta - \theta_s)}{\theta_d} \right) \right] \quad (2.25)$$

or an exponential relation, known as a Wiebe function, as given in Equation 2.26:

$$x_b(\theta) = 1 - \exp \left[-a \left(\frac{\theta - \theta_s}{\theta_d} \right)^n \right] \quad (2.26)$$

where

x_b = fraction of energy release

θ = crank angle

θ_s = start of energy release

θ_d = duration of energy release

n = Wiebe form factor

a = Wiebe efficiency factor

The Wiebe function is named after Ivan Wiebe (1902–1969), a Russian engineer who developed an energy release model based on analysis of combustion chain reaction events (Ghojel, 2010). The Wiebe function can be used for modeling the energy release in a wide variety of combustion systems. For example, diesel engine combustion, which has a premixed phase and a diffusion phase, can be modeled using a combined double Wiebe function. The energy release curve for the diesel engine is double peaked due to the two combustion phases, and discussed in more detail later in the diesel combustion section of Chapter 7.

Since the cumulative energy release curve asymptotically approaches a value of 1, the end of combustion needs to be defined by an arbitrary limit, such as 90, 99, or 99.9% complete combustion; that is, $x_b = 0.90, 0.99, \text{ or } 0.999$, respectively. Corresponding values of the Wiebe efficiency factor a are 2.302, 4.605, and 6.908 respectively. The value of the efficiency factor $a = 6.908$ was used by Wiebe in his engine modeling calculations.

The values of the form factor n and burn duration θ_d depend on the particular type of engine, and to some degree on the engine load and speed. These parameters can be deduced using experimental burn rate data, which in turn are obtained from the cylinder pressure profile as a function of crank angle, discussed in more detail in the combustion analysis section of Chapter 12. Values of $a = 5$ and $n = 3$ have been reported to fit well with experimental data (Heywood, 1988).

The rate of energy release for the Wiebe function as a function of crank angle, Equation 2.27, is obtained by differentiation of the cumulative energy release function.

$$\begin{aligned}\frac{dQ}{d\theta} &= Q_{in} \frac{dx_b}{d\theta} \\ &= na \frac{Q_{in}}{\theta_d} (1 - x_b) \left(\frac{\theta - \theta_s}{\theta_d} \right)^{n-1}\end{aligned}\quad (2.27)$$

The computer program `BurnFraction.m` is listed in Appendix F, and can be used to plot the Wiebe function cumulative and rate of energy release for different engine conditions. The use of the program is detailed in the following example.

EXAMPLE 2.1 Energy Release Fractions

Using the Wiebe function, plot the cumulative and the rate of energy release for a combustion event with the start of energy release at $\theta_s = -20^\circ$ and the duration of energy release $\theta_d = 60^\circ$. Assume the Wiebe efficiency factor $a = 5$, that is, $x_b = 0.9933$, and the Wiebe form factor $n = 4$.

SOLUTION The above parameters are entered into the computer program `BurnFraction.m` as shown below, and the resulting plots are shown in Figures 2.11 and 2.12.

Comment: Note the asymmetry of the burn rate, as a result of the form factor value, and the peak value of the burn rate at 18° atdc. As discussed in more detail in the next example, optimal work from an engine usually occurs with a peak burn rate a few degrees after top dead center, so a significant fraction of the combustion will be occurring during the expansion process.

```
function [ ]=BurnFraction( )
This program computes and plots the cumulative burn fraction
and the instantaneous burn rate
a = 5;           Wiebe efficiency factor
n = 4;           Wiebe form factor
thetas = -20;    start of combustion
thetad = 60;    duration of combustion
....
```

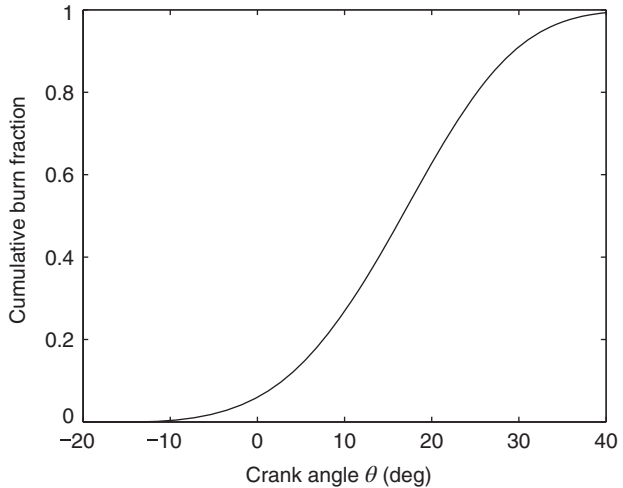


Figure 2.11 Cumulative energy release curve for Example 2.1.

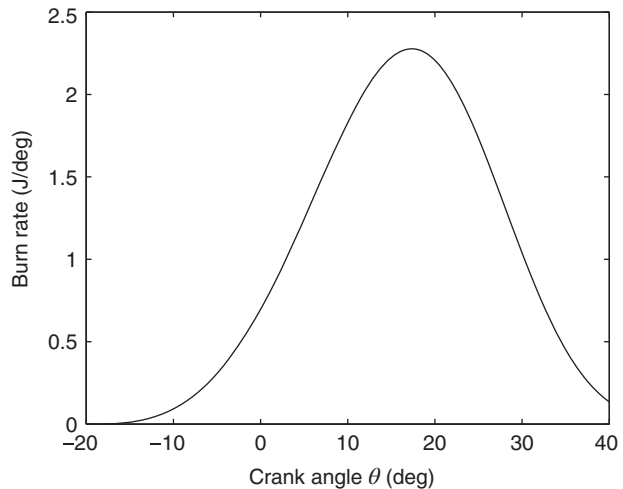


Figure 2.12 Rate of energy release curve for Example 2.1.

Energy Equation

We now develop a simple finite energy release model by incorporating the Wiebe function equation, Equation 2.27, into the differential energy equation. We assume that the energy release occurs for a given combustion duration θ_d during the compression and expansion strokes, and solve for the resulting cylinder pressure $P(\theta)$ as a function of crank angle. The simple model assumes the inlet and exhaust valves are closed at the start of integration at $\theta = -180^\circ$, so it does not account for flow into and out of the combustion chamber.

As shown in the following derivation, the differential form of the energy equation does not have a simple analytical solution due to the finite energy release term. It is integrated numerically, starting at bottom dead center, compressing to top dead center, and then expanding back to bottom dead center.

The closed system differential energy equation (note that work and heat interaction terms are not true differentials) for a small crank angle change, $d\theta$, is

$$\delta Q - \delta W = dU \quad (2.28)$$

since $\delta W = PdV$ and $dU = mc_v dT$,

$$\delta Q - PdV = mc_v dT \quad (2.29)$$

Assuming ideal gas behavior,

$$PV = mRT \quad (2.30)$$

which in differential form is

$$m dT = \frac{1}{R} (PdV + VdP) \quad (2.31)$$

The energy equation is therefore

$$\delta Q - PdV = \frac{c_v}{R} (PdV + VdP) \quad (2.32)$$

differentiating with respect to crank angle, and introducing $dQ = Q_{\text{in}}dx$,

$$Q_{\text{in}} \frac{dx}{d\theta} - P \frac{dV}{d\theta} = \frac{c_v}{R} \left(P \frac{dV}{d\theta} + V \frac{dP}{d\theta} \right) \quad (2.33)$$

Solving for the pressure P ,

$$\frac{dP}{d\theta} = -\gamma \frac{P}{V} \frac{dV}{d\theta} + (\gamma - 1) \frac{Q_{\text{in}}}{V} \frac{dx}{d\theta} \quad (2.34)$$

In practice, it is convenient to normalize the equation with the pressure P_1 and volume V_1 at bottom dead center:

$$\tilde{P} = P/P_1 \quad \tilde{V} = V/V_1 \quad \tilde{Q} = Q_{\text{in}}/P_1 V_1 \quad (2.35)$$

in which case we obtain

$$\frac{d\tilde{P}}{d\theta} = -\gamma \frac{\tilde{P}}{\tilde{V}} \frac{d\tilde{V}}{d\theta} + (\gamma - 1) \frac{\tilde{Q}}{\tilde{V}} \frac{dx}{d\theta} \quad (2.36)$$

The differential equation for the work is

$$\frac{d\tilde{W}}{d\theta} = \tilde{P} \frac{d\tilde{V}}{d\theta} \quad (2.37)$$

In order to integrate Equations 2.36 and 2.37, an equation for the cylinder volume \tilde{V} as a function of crank angle is needed. By reference to Chapter 1, the dimensionless cylinder volume $\tilde{V}(\theta) = V(\theta)/V_{\text{bdc}} = V(\theta)/V_1$ for $l \gg s$ is

$$\tilde{V}(\theta) = 1 + \frac{r-1}{2r}(1 - \cos \theta) \quad (2.38)$$

which upon differentiation gives

$$\frac{d\tilde{V}}{d\theta} = \frac{r-1}{2r} \sin \theta \quad (2.39)$$

Equations 2.36 and 2.37 are linear first-order differential equations of the form $d\tilde{Y}/d\theta = f(\theta, \tilde{Y})$, and easily solved by numerical integration. Solution yields $\tilde{P}(\theta)$ and $\tilde{W}(\theta)$, which once determined allow computation of the net work of the cycle, the thermal efficiency, and the indicated mean effective pressure. Note that in this analysis we have neglected heat and mass transfer losses, and will consider them in the next section.

The thermal efficiency is computed directly from its definition

$$\eta = \frac{\tilde{W}}{\tilde{Q}} \quad (2.40)$$

The imep is then computed using Equation 2.41

$$\frac{\text{imep}}{P_1} = \eta \tilde{Q} \left(\frac{r}{r-1} \right) \quad (2.41)$$

For the portions of the compression and expansion strokes before ignition and after combustion, that is, where $\theta < \theta_s$ and $\theta > \theta_s + \theta_d$, the energy release term $dQ/d\theta = 0$, allowing straightforward integration of the energy equation and recovery of the isentropic pressure–volume relation:

$$\frac{d\tilde{P}}{d\theta} = -\gamma \frac{\tilde{P}}{\tilde{V}} \frac{d\tilde{V}}{d\theta} \quad (2.42)$$

$$\frac{d\tilde{P}}{\tilde{P}} = -\gamma \frac{d\tilde{V}}{\tilde{V}} \quad (2.43)$$

$$\tilde{P}\tilde{V}^\gamma = \text{constant} \quad (2.44)$$

The differential energy equation, Equation 2.34, can also be used in reverse to compute energy release curves from experimental measurements of the cylinder pressure. This procedure is discussed in detail in Chapter 12. Commercial combustion analysis software is available to perform such analysis in real time during an experiment.

The computer program `FiniteHeatRelease.m` is listed in Appendix F, and can be used to compare the performance of two different engines with different combustion and geometric parameters. The program computes gas cycle performance by numerically integrating Equation 2.34 for the pressure as a function of crank angle. The integration starts at bottom dead center ($\theta = -180^\circ$), with initial inlet conditions P_1, V_1, T_1 , the gas molecular weight M , and specific heat ratio γ given. The integration proceeds degree by degree to top dead center ($\theta = 0^\circ$) and back to bottom dead center. Once the pressure is computed as a function of crank angle, the net work, thermal efficiency, and imep are also computed. The use of the program is detailed in the following example.

EXAMPLE 2.2 Finite Energy Release

A single-cylinder spark ignition cycle engine is operated at full throttle, and its performance is to be predicted using a Wiebe energy release analysis. The engine has a compression ratio of 10. The initial cylinder pressure, P_1 , at bottom dead center is 1 bar, with a temperature T_1 at bottom dead center of 300 K. The bore and stroke of the engine are $b = 100$ mm and $s = 100$ mm. The total heat addition $Q_{in} = 1764$ J and the combustion duration θ_d is constant at 40° . Assume that the ideal gas specific heat ratio γ is 1.4, the molecular mass of the gas mixture is 29 kg/kmol, and the Wiebe energy release parameters are $a = 5$ and $n = 3$.

- Compute the displacement volume V_d , the volume at bottom dead center V_1 , the dimensionless heat addition \tilde{Q} , and the mass of gas in the cylinder m .
- Plot the pressure and temperature profiles versus crank angle for $\theta_{s1} = -20^\circ$ (engine 1) and $\theta_{s2} = 0^\circ$ (engine 2).
- Determine the effect of changing the start of energy release from $\theta_s = -50^\circ$ to $\theta_s = +20^\circ$ atdc on the thermal efficiency, and imep of the engine.

SOLUTION (a) The displacement volume is

$$V_d = \frac{\pi}{4} b^2 s = 7.85 \times 10^{-4} \text{ m}^3$$

The volume at bottom dead center is

$$V_1 = \frac{V_d}{1 - 1/r} = \frac{7.85 \times 10^{-4}}{1 - 1/10} = 8.73 \times 10^{-4} \text{ m}^3$$

The dimensionless heat addition is

$$\tilde{Q} = Q_{\text{in}}/P_1 V_1 = 1764/[(101 \times 10^3)(8.73 \times 10^{-4})] = 20$$

The mass of gas in the cylinder is

$$m = \frac{P_1 V_1}{RT_1} = \frac{(101)(8.73 \times 10^{-4})}{(8.314/29)(300)} = 1.03 \times 10^{-3} \text{ kg}$$

(b) The above engine parameters are entered into the `FiniteHeatRelease.m` program as shown below. The start of energy release is $\theta_s = -20^\circ$ for engine 1 and $\theta_s = 0^\circ$ for engine 2, and all other parameters are the same for both engines.

```
function [ ] = FiniteHeatRelease( )
Gas cycle heat release code for two engines
Engine input parameters:
thetas(1,1) = -20;           Engine 1 start of heat release (deg)
thetas(2,1) = 0;             Engine 2 start of heat release (deg)
thetad(1,1) = 40;            Engine 1 duration of heat release (deg)
thetad(2,1) = 40;            Engine 2 duration of heat release (deg)
r = 10;                      Compression ratio
gamma = 1.4;                 Ideal gas const
Q = 20.4;                    Dimensionless total heat addition
a = 5;                       Wiebe efficiency factor a
n = 3;                       Wiebe exponent n
...}
```

The pressure profiles are compared in Figure 2.13. The pressure rise for engine 1 is more than double that of engine 2. The maximum pressure of about 8800 kPa occurs at 11° after top dead center for engine 1, and at about 25° after top dead center for engine 2. The temperature profiles are shown in Figure 2.14. Engine 1 has a peak temperature of about 2900 K, almost 400 K above that of engine 2.

(c) The start of heat release is varied from $\theta_s = -50^\circ$ to $\theta_s = 0^\circ$, as shown in Figures 2.15 and 2.16, and the resulting thermal efficiency η and imep are plotted.

Comment: The results indicate that there is an optimum crank angle for the start of energy release that will maximize the thermal efficiency and imep. For this computation, the optimum start of energy release is about $\theta_s = -20^\circ$, resulting in a maximum thermal efficiency of about 60% and imep/P_1 of about 13.2. At crank angles less than or greater than this optimal angle, the thermal efficiency and imep/P_1 decrease.

An explanation for the optimal crank angle is as follows. If the energy release begins too early during the compression stroke, the negative compression work will increase, since the piston is doing work against the increasing combustion gas pressure. Conversely, if the energy release begins too late, the energy release will occur in an increasing cylinder

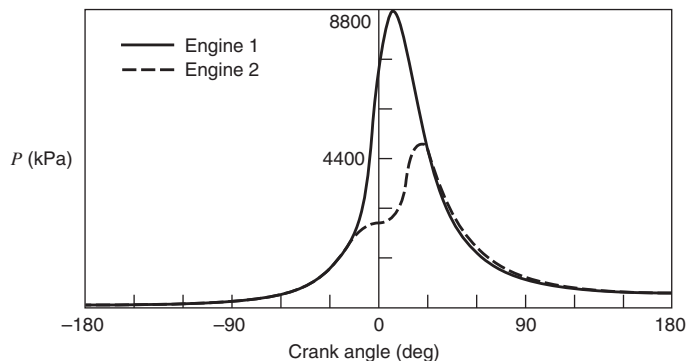


Figure 2.13 Pressure profiles for Example 2.2.

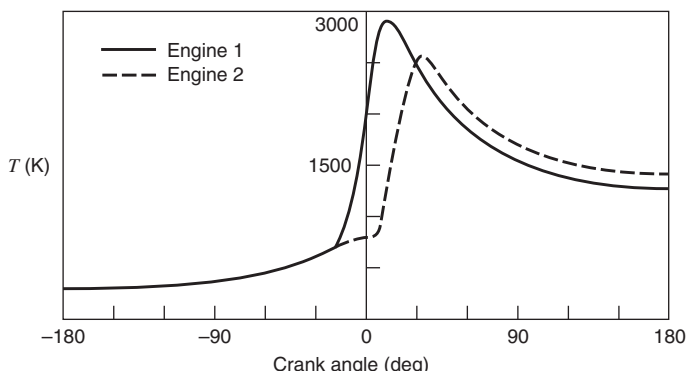


Figure 2.14 Temperature profiles for Example 2.2.

volume, resulting in lower combustion pressure, and lower net work. In practice, the optimum spark timing also depends on the engine load, and is in the range of $\theta_s = -30^\circ$ to $\theta_s = -5^\circ$. The resulting location of the peak combustion pressure is typically between 5° and 15° atdc.

Cylinder Heat and Mass Transfer Loss

In this section, we develop simple models of the heat transfer and the mass blowby process, and include them in the energy release analysis developed in the previous section. Engines are air or water cooled to keep the engine block temperatures within safe operating limits, so there is a significant amount of heat transfer from the combustion gas to the surrounding cylinder walls. Also, internal combustion engines do not operate on closed thermodynamic cycles, rather there is an induction of fresh charge and expulsion of combustion products, and there is leakage of combustion gases or blowby past the rings, since the rings do not provide a complete seal of the combustion chamber. The blowby can affect the indicated performance, the friction and wear, and the hydrocarbon emissions of the engine.

The heat transfer to the cylinder walls is represented by a Newtonian-type convection equation with a constant heat transfer coefficient h . More realistic models accounting for a variable h are presented in Chapter 11. The mass flow is assumed to be blowby past the rings from the combustion chamber at a rate proportional to the mass of the cylinder contents. A useful rule of thumb is that new engines will have a 0.5% blowby, then operate for most of their life at a typical level of 1% blowby, and gradually reach a maximum blowby of 2.5–3.0% at the end of their useful life.

The heat transfer to the walls can be included by expanding the energy release dQ term in the energy equation to include both heat addition and loss, as indicated in Equation 2.45:

$$dQ = Q_{\text{in}} dx - dQ_1 \quad (2.45)$$

The heat loss dQ_1 is

$$\frac{dQ_1}{dt} = hA(T - T_w) \quad (2.46)$$

where

h = heat transfer coefficient

A = cylinder surface area in contact with the gases

T_w = cylinder wall temperature

The combustion chamber area A is a function of crank angle θ , and is the sum of the combustion chamber area at top dead center A_o and the instantaneous cylinder wall area $A_w(\theta)$. The instantaneous combustion chamber area and volume are

$$A = A_o + \pi b y(\theta)$$

$$V = V_o + \frac{\pi b^2}{4} y(\theta)$$

or

$$A = (A_o - 4V_o/b) + 4V/b \quad (2.47)$$

where V_o is the cylinder volume at top dead center. When the parameters in the heat loss equation are normalized by the conditions at state 1, bottom dead center, they take the form

$$\tilde{Q} = \frac{Q_{\text{in}}}{P_1 V_1} \quad \tilde{T} = \frac{T}{T_1} \quad \tilde{Q}_1 = \frac{Q_1}{P_1 V_1} \quad (2.48)$$

and

$$\tilde{h} = \frac{4hT_1}{P_1 \omega \beta b} \quad \beta = \frac{4V_1}{b(A_o - 4V_o/b)} \quad (2.49)$$

The dimensionless heat loss is then

$$\frac{d\tilde{Q}_1}{d\theta} = \frac{hAT_1}{P_1 V_1 \omega} (\tilde{T} - \tilde{T}_w) = \tilde{h}(1 + \beta \tilde{V})(\tilde{P}\tilde{V} - \tilde{T}_w) \quad (2.50)$$

We can express the volume term β as a function of the compression ratio r . Since $r = V_1/V_o$,

$$\beta = \frac{4r}{b(A_o/V_o) - 4} \quad (2.51)$$

For example, for a square engine (bore b = stroke s) with a flat top piston and cylinder head geometry,

$$A_o/V_o = \frac{2(r - 1) + 4}{b} \quad (2.52)$$

and

$$\beta = \frac{2r}{r-1} \quad (2.53)$$

Note that when heat transfer losses are added, there are additional dependencies on the dimensionless wall temperature, heat transfer coefficient, and compression ratio.

If the mass in the cylinder is no longer constant due to blowby, the logarithmic derivative of the equation of state becomes

$$\frac{1}{P} \frac{dP}{d\theta} + \frac{1}{V} \frac{dV}{d\theta} = \frac{1}{m} \frac{dm}{d\theta} + \frac{1}{T} \frac{dT}{d\theta} \quad (2.54)$$

Similarly, the first law of thermodynamics in differential form applicable to an open system must be used.

$$\frac{dQ}{d\theta} - P \frac{dV}{d\theta} = mc_v \frac{dT}{d\theta} + c_v T \frac{dm}{d\theta} + \frac{\dot{m}_l h_l}{\omega} \quad (2.55)$$

The term \dot{m}_l is the instantaneous rate of leakage or blowby flow. The enthalpy of the blowby is assumed to be the same as that of the cylinder, so $h_l = c_p T$.

From the mass conservation equation applied to the cylinder,

$$\frac{dm}{d\theta} = -\frac{\dot{m}_l}{\omega} \quad (2.56)$$

Eliminating $dT/d\theta$ between Equations 2.54 and 2.55 yields the following:

$$\frac{dP}{d\theta} = -\gamma \frac{P}{V} \frac{dV}{d\theta} + \frac{(\gamma-1)}{V} \frac{dQ}{d\theta} - \frac{\gamma \dot{m}_l}{\omega m} P \quad (2.57)$$

Including heat transfer loss as per Equation 2.45 and defining the blowby coefficient C as

$$C = \frac{\dot{m}_l}{m} \quad (2.58)$$

results in the following four ordinary differential equations for pressure, work, heat loss, and cylinder mass as a function of crank angle:

$$\begin{aligned} \frac{d\tilde{P}}{d\theta} &= -\gamma \frac{\tilde{P}}{\tilde{V}} \frac{d\tilde{V}}{d\theta} + \frac{(\gamma-1)}{\tilde{V}} \left[\tilde{Q} \frac{dx}{d\theta} - \tilde{h}(1 + \beta \tilde{V})(\tilde{P}\tilde{V}/\tilde{m} - \tilde{T}_w) \right] - \frac{\gamma C \tilde{P}}{\omega} \\ \frac{d\tilde{W}}{d\theta} &= \tilde{P} \frac{d\tilde{V}}{d\theta} \\ \frac{d\tilde{Q}_l}{d\theta} &= \tilde{h}(1 + \beta \tilde{V})(\tilde{P}\tilde{V}/\tilde{m} - \tilde{T}_w) \\ \frac{d\tilde{m}}{d\theta} &= -C \frac{\tilde{m}}{\omega} \end{aligned} \quad (2.59)$$

The above four linear equations are solved numerically in the MATLAB® program `FiniteHeatMassLoss.m`, which is listed in Appendix F. The program is a finite energy release program that can be used to compute the performance of an engine and includes both heat and mass transfer. The engine performance is computed by numerically integrating Equation 2.59 for the pressure, work, heat loss, and cylinder gas mass as a function of crank angle. The integration starts at bottom dead center ($\theta = -180^\circ$), with initial inlet conditions given. The integration proceeds degree by degree to top dead center and back to bottom dead center. Once the pressure and other terms are computed as a function of crank angle, the overall cycle parameters of net work, thermal

efficiency, and imep are also computed. The use of the program is detailed in the following example.

EXAMPLE 2.3 Finite Energy Release with Heat and Mass Loss

For the same engine conditions as in Example 2.2, find the maximum imep and thermal efficiency when heat and mass loss is accounted for. Vary the start of energy release from $\theta_s = -50^\circ$ to $\theta_s = +20^\circ$ atdc. Assume the heat transfer coefficient $h = 500 \text{ W}(\text{m}^2\text{K})$, the cylinder wall temperature $T_w = 360 \text{ K}$, the top dead center area/volume ratio $A_o/V_o = 306.6 \text{ m}^{-1}$, and the mass transfer parameter $C = 0.08 \text{ s}^{-1}$, with engine speed $\omega = 200 \text{ rad/s}$.

SOLUTION The non dimensional parameters β , \tilde{h} , and \tilde{T}_w for this problem are

$$\beta = \frac{4r}{b(A_o/V_o) - 4} = \frac{(4)(10)}{(0.1)(306.6) - 4} = 1.50$$

$$\tilde{h} = \frac{4hT_1}{P_1\omega\beta b} = \frac{(4)(500)(300)}{(100,000)(200)(1.5)(0.1)} = 0.20$$

$$\tilde{T}_w = T_w/T_1 = 360/300 = 1.2$$

The above engine parameters are entered into the `FiniteHeatMassLoss.m` program as shown below.

```
function [ ] = FiniteHeatMassLoss( )
    Gas cycle heat release code with heat and mass transfer
    thetas = - 20;      start of heat release (deg)
    thetad = 40;       duration of heat release (deg)
    r = 10;            compression ratio
    gamma = 1.4;       ideal gas const
    Q = 20.;           dimensionless total heat release
    h = 0.2;           dimensionless heat transfer coeff.
    tw = 1.2;          dimensionless cylinder wall temp
    beta = 1.5;        dimensionless volume
    a = 5;             Wiebe parameter
    n = 3;             Wiebe exponent
    omega = 200.;      engine speed
    c = 0.8;           mass loss coefficient
    ...

```

The results are presented in Figures 2.15 and 2.16, and representative thermodynamic parameters are compared with the simple energy release computation with no heat or mass loss in Table 2.1. With the heat and mass transfer included, maximum efficiency is reduced from 0.60 to 0.52, and the maximum nondimensional imep is reduced from 13.24 to 11.55. The general dependence of the efficiency and imep on the start of energy release is very similar for both cases, as the optimum start of ignition remains at -20° and the peak pressure crank angle remains at $+11^\circ$.

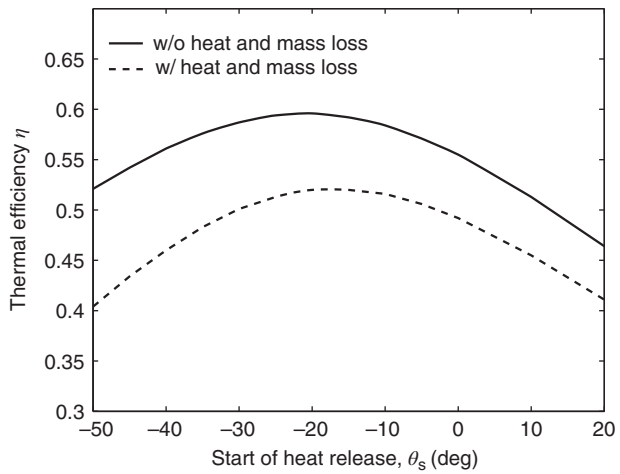


Figure 2.15 Thermal efficiency versus start of energy release for Examples 2.2 and 2.3.

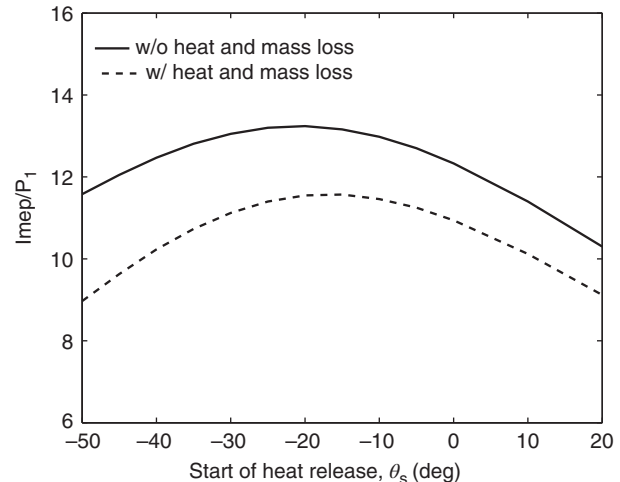


Figure 2.16 Imep versus start of energy release for Examples 2.2 and 2.3.

Table 2.1 Comparison of Energy Release Models With and Without Heat/Mass Transfer Loss at $\theta_s = -20^\circ$ and $\theta_d = 40^\circ$

	Without heat and mass loss	With heat and mass loss
P_{\max}/P_1	87.77	85.31
θ_{\max}	11.00	11.00
Net work/ $P_1 V_1$	11.91	10.39
Efficiency η	0.596	0.520
η/η_{Otto}	0.990	0.863
$Imep/P_1$	13.24	11.55

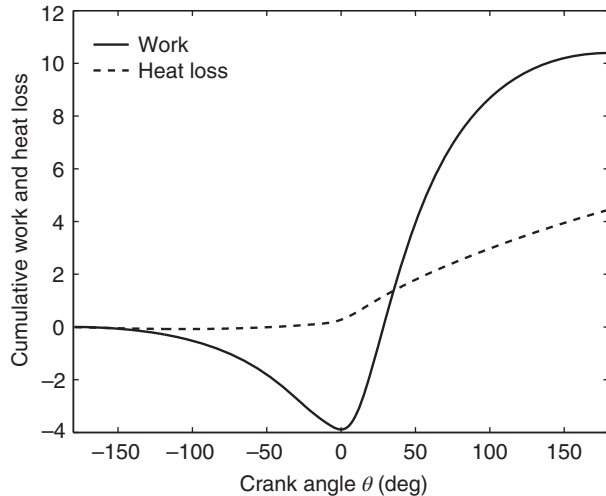


Figure 2.17 Cumulative work and heat/mass loss for Example 2.3.

The cumulative work and heat/mass transfer loss is plotted in Figure 2.17 as a function of crank angle for the optimum case of $\theta_s = -20^\circ$. The cumulative work is initially negative due to the piston compression and becomes positive on the expansion stroke. The heat transfer loss is very small during compression, indicating a nearly isentropic compression process, and is somewhat linear during the expansion process.

2.7 IDEAL FOUR-STROKE PROCESS AND RESIDUAL FRACTION

The simple gas cycle models assume that the heat rejection process occurs at constant volume, and neglect the gas flow that occurs when the intake and exhaust valves are opened and closed. In this section, we use the energy equation to model the exhaust and intake strokes, and determine the residual fraction of gas remaining in the cylinder.

At this level of modeling, we need to make some assumptions about the operation of the intake and exhaust valves. During the exhaust stroke, the exhaust valve is assumed to open instantaneously at bottom dead center and close instantaneously at top dead center. Similarly, during the intake stroke, the intake valve is assumed to open at top dead center and remain open until bottom dead center. The intake and exhaust valve overlap, that is, the time during which they are open simultaneously, is therefore assumed to be zero.

The intake and exhaust strokes are also assumed to occur adiabatically and at constant pressure. Constant pressure intake and exhaust processes occur only at low engine speeds. More realistic computations model the instantaneous pressure drop across the valves and furthermore would account for the heat transfer that is especially significant during the exhaust. Such considerations are deferred to Chapters 5 and 9.

Referring to Figure 2.18, the ideal intake and exhaust processes are as follows:

- 4 to 5a Constant cylinder volume blowdown
- 5a to 6 Constant pressure exhaustion
- 6 to 7 Constant cylinder volume reversion
- 7 to 1 Constant pressure induction

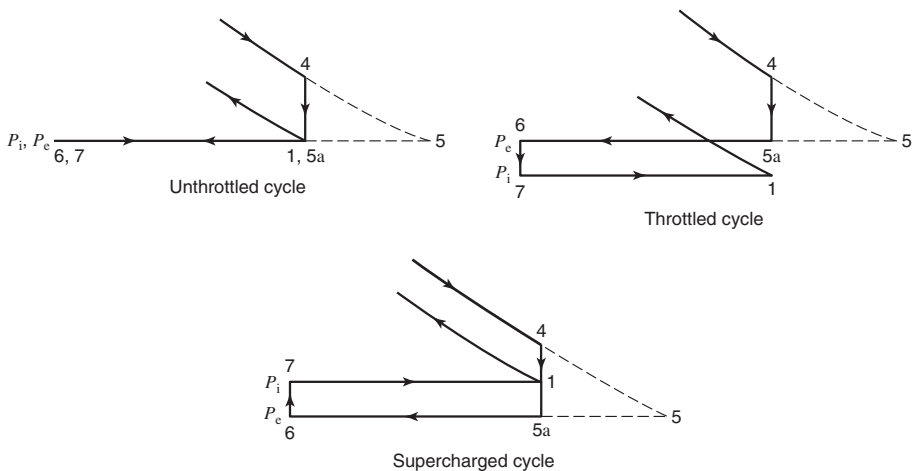


Figure 2.18 Four-stroke inlet and exhaust flow. P_i = inlet pressure; P_e = exhaust pressure.

Exhaust Stroke

The exhaust stroke has two processes: gas blowdown and gas displacement. At the end of the expansion stroke 3 to 4, the pressure in the cylinder is greater than the exhaust pressure. Hence, when the exhaust valve opens, gas will flow out of the cylinder even if the piston does not move. Typically, the pressure ratio, P_4/P_e , is large enough to produce sonic flow at the valve so that the pressure in the cylinder rapidly drops to the exhaust manifold pressure, P_e , and the constant volume approximation is justified. The remaining gas in the cylinder that has not flowed out through the exhaust valve undergoes an expansion process. If heat transfer is neglected, this unsteady expansion process can be modeled as isentropic. Note that both the closed valve expansion from 3 to 4 and the open valve expansion from 4 to 5 are modeled as isentropic processes.

Therefore, the temperature and pressure of the exhaust gases remaining in the cylinder are

$$T_5 = T_4 \left(\frac{P_5}{P_4} \right)^{(y-1)/y} \quad (2.60)$$

$$P_5 = P_e \quad (2.61)$$

As the piston moves upward from bottom dead center, it pushes the remaining cylinder gases out of the cylinder. The cylinder pressure is assumed to remain constant at $P_5 = P_6 = P_4$. Since internal combustion engines have a clearance volume, not all of the gases will be pushed out. There will be exhaust gas left in the clearance volume, called residual gas. This gas will mix with the incoming air or fuel-air mixture, depending on the location of the fuel injectors.

The state of the gas remaining in the cylinder during the exhaust stroke can be found by applying the closed system first law to the cylinder gas from state 5 to state 6 as shown in Figure 2.19. The closed system control volume will change in shape as the cylinder gases flow out of the exhaust port across the exhaust valve. Note that while the blowdown is assumed to occur at constant cylinder volume, the control mass is assumed to expand isentropically.

The energy equation is

$$Q_{5-6} - W_{5-6} = U_6 - U_5 \quad (2.62)$$

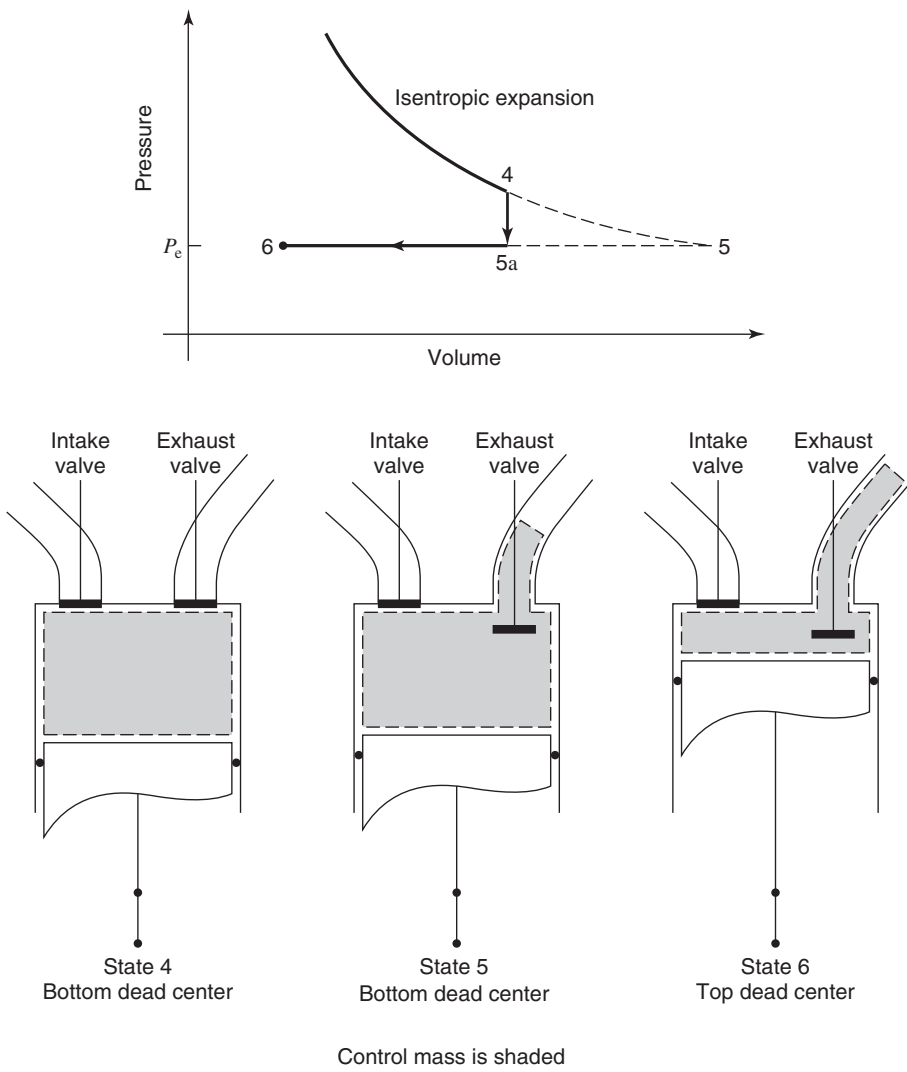


Figure 2.19 The exhaust stroke (4 to 5 to 6) illustrating residual mass.

The work term is

$$W_{5-6} = P_e(V_6 - V_5) \quad (2.63)$$

and if the flow is assumed to be adiabatic, the first law becomes

$$U_6 + P_e V_6 = U_5 + P_e V_5 \quad (2.64)$$

or

$$h_6 = h_5 \quad (2.65)$$

$$T_e = T_6 = T_5 \quad (2.66)$$

Therefore, during an adiabatic exhaust stroke, the enthalpy and temperature of the exhaust gases remain constant as they leave the cylinder, and the enthalpy of the residual gas left in the cylinder clearance volume is constant. The residual gas fraction, f , is the

ratio of the residual gas mass, $m_r = m_6$, in the cylinder at the end of the exhaust stroke (state 6) to the mass, $m = m_1 = m_4$, of the fuel-air mixture:

$$f = \frac{V_6/v_6}{V_4/v_4} = \frac{1}{r} \frac{v_4}{v_6} = \frac{1}{r} \frac{T_4}{T_e} \frac{P_e}{P_4} \quad (2.67)$$

Since

$$T_e = T_4 \left(\frac{P_e}{P_4} \right)^{(\gamma-1)/\gamma} \quad (2.68)$$

the residual fraction is

$$f = \frac{1}{r} \left(\frac{P_e}{P_4} \right)^{1/\gamma} \quad (2.69)$$

For example, for a compression ratio of $r = 9$, $P_e = 101$ kPa, $P_4 = 500$ kPa, and $\gamma = 1.3$, $f = 1/9(101/450)^{1/1.3} = 0.035$. Typical values of the residual gas fraction, f , are in the 0.03–0.12 range. The residual gas fraction is lower in Diesel cycle engines than in Otto cycle engines, due to the higher compression ratio in Diesel cycles.

Intake Stroke

When the intake valve is opened, the intake gas mixes with the residual gas. Since the intake gas temperature is usually less than the residual gas temperature, the cylinder gas temperature at the end of the intake stroke will be greater than the intake temperature. In addition, if heat transfer is neglected, the flow across the intake valve, either from the intake manifold to the cylinder or the reverse, is at constant enthalpy.

There are three different flow situations for the intake stroke, depending on the ratio of inlet to exhaust pressure. If the inlet pressure is less than the exhaust pressure, the engine is throttled. In this case, there is flow from the cylinder into the intake port when the intake valve opens. In the initial portion of the intake stroke, the induced gas is primarily composed of combustion products that have previously flowed into the intake port. In the latter portion of the stroke, the mixture flowing in is fresh charge, undiluted by any combustion products.

If the inlet pressure is greater than the exhaust pressure, the engine is said to be supercharged (turbocharging is a special case of supercharging in which a compressor driven by an exhaust turbine raises the pressure of atmospheric air delivered to an engine). In this case, there is flow from the intake port into the engine until the pressure equilibrates. In actual engines, because of valve overlap, there may be a flow of fresh mixture from the inlet to the exhaust port, which can waste fuel and be a source of hydrocarbon exhaust emissions. The third case is when inlet and exhaust pressures are equal; the engine is then said to be unthrottled.

The unsteady open system mass and energy equations can be used to determine the state of the fuel-air mixture and residual gas combination at state 1, the end of the intake stroke. The initial state of the gas in the system at the beginning of the intake process is at state 6.

As discussed above, there is a flow of a gas mixture into or out of the cylinder when the intake valve is opened, depending on the relative pressure difference. The net gas flow into the cylinder control volume has mass m_i , enthalpy h_i , and pressure P_i . As the piston moves downward, it is assumed that the cylinder pressure remains constant at the inlet pressure P_i , which is consistent with experimental observations. For the overall process from state

6 to state 1 with the inlet flow at state “i”, the conservation of mass equation is

$$m_i = m_1 - m_6 \quad (2.70)$$

The unsteady energy equation is

$$Q_{6-1} - W_{6-1} = -m_i h_i + m_1 u_1 - m_6 u_6 \quad (2.71)$$

If heat transfer is neglected, $Q_{6-1} = 0$, and the work done by the gas is $W_{6-1} = P_1(V_1 - V_6)$, so

$$-P_i(V_1 - V_6) = -(m_1 - m_6)h_i + m_1 u_1 - m_6 u_6 \quad (2.72)$$

Since $u_1 = h_1 - P_1 v_1$ and $u_6 = h_6 - P_e v_6$, we can write the energy equation in terms of enthalpy:

$$(P_i - P_e)m_6 v_6 = -(m_1 - m_6)h_i + m_1 h_1 - m_6 h_6 \quad (2.73)$$

Solving for h_1 ,

$$h_1 = \frac{m_6}{m_1} \left[h_6 + \left(\frac{m_1}{m_6} - 1 \right) h_i + (P_i - P_e)v_6 \right] \quad (2.74)$$

Therefore, the enthalpy at the end of the intake stroke is not just the average of the initial and intake enthalpies, as would be the case for a steady flow situation, but also includes the flow work term.

The equation for the enthalpy at the end of the intake stroke, Equation 2.74, can also be expressed in terms of the residual gas fraction, f . From Equation 2.67,

$$m_6 = m_1 f \quad \text{and} \quad m_1 - m_6 = m_1(1 - f) \quad (2.75)$$

so

$$m_i = m(1 - f) \quad (2.76)$$

and from the ideal gas law,

$$P_e v_6 = R T_6 \quad (2.77)$$

Upon substitution of Equations 2.76 and 2.77 into Equation 2.74,

$$h_1 = (1 - f)h_i + f h_e - \left(1 - \frac{P_i}{P_e} \right) f R T_e \quad (2.78)$$

If the reference enthalpy is chosen so that $h_i = c_p T_i$, then

$$T_1 = (1 - f)T_i + f \left[1 - \left(\frac{\gamma - 1}{\gamma} \right) \left(1 - \frac{P_i}{P_e} \right) \right] T_e \quad (2.79)$$

For example, if $f = 0.05$, $P_i/P_e = 0.5$, $\gamma = 1.35$, $T_i = 320$ K, and $T_e = 1400$ K, then $T_1 = 365$ K.

The volumetric efficiency of the inlet stroke for a gas cycle is given by

$$\epsilon_v = \frac{m_i}{\rho_i V_d} = 1 - \frac{P_e/P_i - 1}{\gamma(r - 1)} \quad (2.80)$$

During the intake process, the gas within the control volume does work since the piston is expanding the cylinder volume. During exhaust, work is done on the gas. The net effect during the intake and exhaust strokes is

$$W_{5a-1} = (P_i - P_e)V_d \quad (2.81)$$

The negative of that work is called pumping work since it is a loss of useful work for the throttled engine. The pumping mean effective pressure is defined as the pumping work per unit displacement volume:

$$p_{mep} = P_e - P_i \quad (2.82)$$

The indicated mean effective pressure (imep) is defined as the work per unit displacement volume done by the gas during the compression and expansion strokes. The work per unit displacement volume required to pump the working fluid into and out of the engine during the intake and exhaust strokes is termed the pumping mean effective pressure (pme). It is the sum of the pressure drops across flow restrictions during the intake and exhaust strokes, including intake system, valves, and the exhaust system.

The following relations should be clear:

$$(imep)_{net} = imep - p_{mep} \quad (2.83)$$

$$\eta_{net} = \eta \left(1 - \frac{imep}{p_{mep}} \right) \quad (2.84)$$

Four-Stroke Otto Gas Cycle Analysis

When we include the exhaust and intake strokes, we have two additional equations for the gas cycle analysis, the exhaust energy equation, and the intake energy equation. The two unknown parameters in these equations are the residual gas fraction, f , and the gas temperature at the end of the intake stroke, T_1 . When the residual gas fraction f is taken into account, the heat addition, Q_{in} , is

$$Q_{in} = m_i q_{in} = m(1 - f)q_{in} \quad (2.85)$$

where q_{in} is the heat addition per unit mass of gas inducted.

The cycle input parameters in this four-stroke gas cycle analysis are summarized in Table 2.2. Since it is difficult to solve these two equations algebraically, the solution is found by iteration, as shown in this section. Since T_1 is dependent on the residual gas fraction f and the residual gas temperature T_e , we first need to estimate the values of f and T_e , and then iterate through the cycle calculation repeatedly to get converged values of f and T_e .

6, i -1: Intake stroke

$$T_1 = (1 - f)T_i + f \left[1 - \left(\frac{\gamma - 1}{\gamma} \right) \left(1 - \frac{P_i}{P_e} \right) \right] T_e$$

Table 2.2 Input Parameters for Four-Stroke Gas Cycle

Parameter	Description
T_i	Inlet air or mixture temperature
r	Compression ratio
P_e	Exhaust pressure
P_i	Inlet pressure
γ	Ideal gas specific heat ratio
q_n	Heat added per unit mass of gas induced

$$P_1 = P_i$$

1-2: Isentropic compression stroke

$$P_2 = P_1(V_1/V_2)^\gamma = P_1 r^\gamma$$

$$T_2 = T_1 r^{\gamma-1}$$

2-3: Constant volume heat addition

$$T_3 = T_2 + q_{in}(1-f)/c_v$$

$$P_3 = P_2(T_3/T_2)$$

3-4: Isentropic expansion stroke

$$P_4 = P_3(1/r)^\gamma$$

$$T_4 = T_3(1/r)^{\gamma-1}$$

4-5: Isentropic blowdown

$$T_5 = T_4(P_4/P_e)^{(1-\gamma)/\gamma}$$

$$P_5 = P_e$$

5-6: Constant pressure adiabatic exhaust stroke

$$T_e = T_5$$

$$P_6 = P_5 = P_e$$

$$f = 1/r(P_6/P_4)^{1/\gamma}$$

Appendix F contains a listing of the program `FourStrokeOtto.m` that iterates through the above four-stroke Otto gas cycle equations to determine the cycle pressures, temperatures, and the overall thermal parameters.

EXAMPLE 2.4 *Four-Stroke Otto Cycle*

Compute the volumetric efficiency, net thermal efficiency, residual fraction, intake stroke temperature rise, $T_1 - T_i$, and the exhaust stroke temperature decrease, $T_4 - T_e$, of an engine that operates on the ideal four-stroke Otto cycle. The engine is throttled with an inlet pressure of $P_i = 50$ kPa and has an inlet temperature of $T_i = 300$ K. The exhaust pressure is $P_e = 100$ kPa. The compression ratio $r = 10$. Assume a heat input of $q_{in} = 2500$ kJ/kg and $\gamma = 1.3$. Plot the volumetric efficiency, net thermal efficiency, and residual fraction as a function of the intake/exhaust pressure ratio for $0.3 < P_i/P_e < 1.5$.

SOLUTION

The program input portion of `FourStrokeOtto.m` is shown below.

```

Four-stroke Otto cycle model
Input parameters:
Ti = 300;      inlet temperature (K)
Pi = 50;       inlet pressure (kPa)
Pe = 100;      exhaust pressure (kPa)
r = 10;        compression ratio
qin = 2500;    heat input, kJ/kg(gas)
R = 0.287;     gas constant (kJ/kg K)
f = 0.05;      guess value of residual fraction f
Tr = 1000;     guess value of exhaust temp (K)
tol = 0.001;   convergence tolerance
....
```

For the above conditions, as shown in Tables 2.3 and 2.4, the computation indicates that the intake stroke temperature rise, $T_1 - T_i$, is about 45 K and the exhaust blowdown temperature decrease, $T_4 - T_e$, is about 280 K. The volumetric efficiency $e_v = 0.91$, the net thermal efficiency $\eta = 0.46$, and the residual fraction $f = 0.053$.

The volumetric efficiency, Equation 2.80, the residual fraction, Equation 2.69, and the net thermal efficiency, Equation 2.84, are plotted in Figures 2.20, 2.21, and 2.22, respectively, as a function of the intake/exhaust pressure ratio.

Comment: As the pressure ratio increases, the volumetric efficiency and thermal efficiency increase, and the residual fraction decreases. The dependence of the volumetric efficiency e_v on compression ratio is reversed for the throttled and supercharged conditions. In addition, the residual gas fraction increases. The increase in residual fraction is due to the decrease in the intake mass relative to the residual mass as the intake pressure is decreased.

Table 2.3 State Variables for Four-Stroke Gas Cycle Example 2.4

State	1	2	3	4
Pressure (kPa)	50.0	997.6	4582.6	229.7
Temperature (K)	345.3	688.9	3164.3	1585.9

Table 2.4 Cycle Parameters for Four-Stroke Gas Cycle Example 2.4

Residual fraction f	0.053
Net imep (kPa)	612.0
Ideal thermal efficiency η	0.499
Net thermal efficiency η_{net}	0.461
Exhaust temperature (K)	1309
Volumetric efficiency e_v	0.91

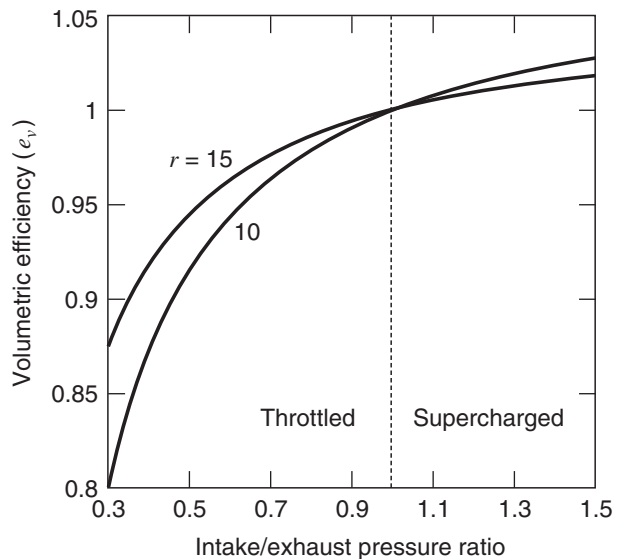


Figure 2.20 Volumetric efficiency for Example 2.3.

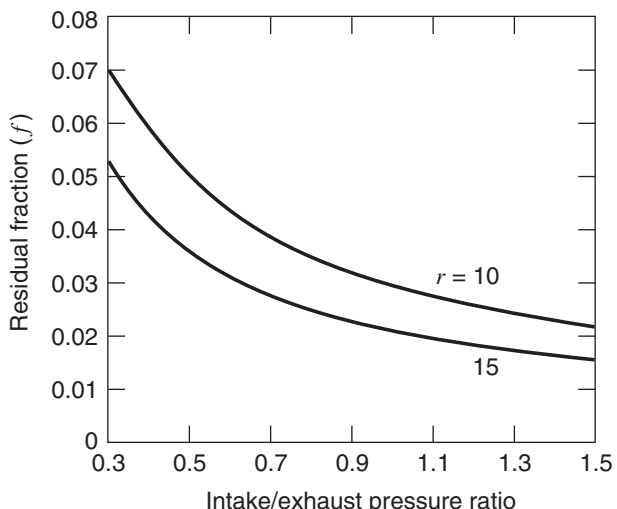


Figure 2.21 Residual fraction for Example 2.3.

2.8 DISCUSSION OF GAS CYCLE MODELS

Maximizing the mean effective pressure is important in engine design so that one can build a smaller, lighter engine to produce a given amount of work. As shown in Equation 2.11, there are evidently two ways to do this: (1) by increasing the compression ratio r and (2) by increasing the heat input Q_{in} . However, there are practical limitations to these approaches. For spark ignition engines of conventional design, the compression ratio must be low enough to avoid engine knock, whereas for diesel engines increasing engine friction limits the utility of increasing compression ratio. Other more complicated factors influence the selection of compression ratio, especially constraints imposed by emission standards and, for some diesel engines, problems of startability.

One might expect that we can increase Q_{in} by increasing the fuel flow rate delivered to an engine. As we shall see in our studies of fuel-air cycles in Chapter 4, this is not always

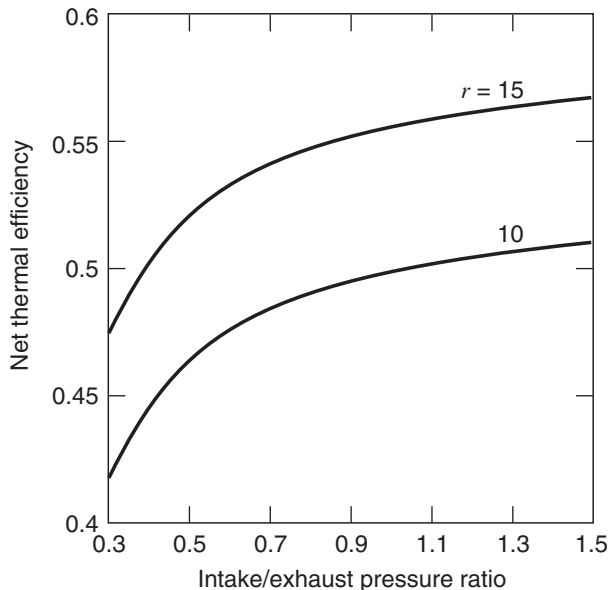


Figure 2.22 Net thermal efficiency for Example 2.3.

correct. With fuel-rich mixtures not all of the fuel energy is used, since there is not enough oxygen to burn the carbon monoxide to carbon dioxide nor the hydrogen to water. The fuel–air cycle predicts that the efficiency decreases as the mixture is made richer beyond stoichiometric.

According to the gas cycles, and the fuel–air cycles to be discussed later, the efficiency is greatest if heat can be added at constant volume:

$$\eta_{\text{Otto}} > \eta_{\text{dual}} > \eta_{\text{Diesel}} \quad (2.86)$$

Why then do we build engines that resemble constant pressure heat addition when we recognize that constant volume heat addition would be better? To illustrate how difficult that question is let us ask the following: Suppose that the maximum pressure in the cycle must be less than some value P_{\max} . How should the heat be added to produce the required work? The answer is now

$$\eta_{\text{Diesel}} > \eta_{\text{dual}} > \eta_{\text{Otto}} \quad (2.87)$$

This can be demonstrated with the aid of a temperature–entropy diagram. If the Otto cycle and the Diesel cycle are drawn on such a diagram so that the work done in each cycle is the same, it can then be shown (as per the homework problem at the end of the chapter) that the Diesel cycle is rejecting less heat and must therefore be the most efficient.

2.9 REFERENCES

- GHOJEL, J. (2010), “Review of the Development and Applications of the Wiebe Function,” *Int. J. Eng. Res.*, Vol. 11, pp. 297–312.
- FOSTER, D. (1985), “An Overview of Zero-Dimensional Thermodynamic Models for IC Engine Data Analysis,” SAE Technical Paper 852070.
- HEYWOOD, J. B. (1988), *Internal Combustion Engine Fundamentals*, McGraw-Hill, New York.
- MILLER, R. H. (1947), “Supercharging and Internal Cooling Cycle for High Output,” *ASME Trans.*, Vol. 69, pp. 453–464.

2.10 HOMEWORK

- 2.1** An engine cylinder contains 7×10^{-5} kg of fuel with a heat of combustion, q_c , of 45,000 kJ/kg. The volume V_1 at top dead center is 0.15×10^{-3} m³, and the volume V_2 at bottom dead center is 1.50×10^{-3} m³. The air-fuel ratio is 16:1, and the mixture temperature T_1 at the start of compression is 300 K. Modeling the compression and combustion as an ideal gas ($\gamma = 1.4$, $c_v = 0.87$ kJ/(kg K)) Otto cycle, (a) what is the maximum temperature T_3 and pressure P_3 ? and (b) what is the pressure P_1 at the start of compression?
- 2.2** The Lenoir air cycle is composed of three processes: 1-2 constant volume heat addition, 2-3 isentropic expansion, and 3-1 constant pressure heat rejection. This cycle is named after Jean Lenoir (1822–1900), a Belgian engineer who developed an internal combustion engine in 1858. It is a cycle in which combustion occurs without compression of the mixture. (a) Draw the Lenoir cycle on p - V and T - s diagrams. (b) Assuming the working fluid is an ideal gas with constant properties, derive an expression for the thermal efficiency of the Lenoir air cycle. (c) Compare the Lenoir cycle thermal efficiency to the Otto cycle efficiency for the standard inlet conditions, $Q_{in} = 1000$ J, $r = 8$, $m = 1.0$ g, and $\gamma = 1.4$.
- 2.3** (a) Show for an Otto cycle that $T_3/T_2 = T_4/T_1$.
 (b) Derive the Otto cycle efficiency equation, Equation 2.10.
- 2.4** Derive the Otto and Diesel cycle imep equation, Equation 2.11.
- 2.5** For equal maximum temperature and heat input, which cycle will be more efficient, the Diesel or Otto? Prove your answer by comparing the two cycles on the T - s diagram. The two cycles should have a common state corresponding to the start of compression.
- 2.6** (a) Show that for a Diesel cycle $(T_3/T_2)^\gamma = T_4/T_1$.
 (b) Derive Equations 2.15 and 2.16.
- 2.7** What does the compression ratio of a Diesel cycle need to be to have the same thermal efficiency of an Otto cycle engine that has a compression ratio $r = 9$? Assume the specific heat ratio $\gamma = 1.3$ and $Q_{in}/P_1 V_1 = 30$.
- 2.8** A Diesel cycle has a compression ratio of 20, and the heat input q_{in} to the working fluid is 1600 kJ/kg. The Diesel cycle is unthrottled, so at the start of compression $P_1 = 101$ kPa and $T_1 = 298$ K. Assuming the working fluid is air with constant properties, what is the maximum pressure and temperature in the cycle, the cycle efficiency, and imep?
- 2.9** Show that for the Otto cycle as $r \rightarrow 1$, $imep/P_1 \rightarrow Q_{in}(\gamma - 1)/P_1 V_1$ (use l'Hopital's rule).
- 2.10** A engine is modeled with a limited pressure cycle. The maximum pressure is to be 8000 kPa. The compression ratio is 17:1, the inlet conditions are 101 kPa and 320 K, and the nondimensional heat input $Q_{in}/P_1 V_1 = 30$. Find the thermal efficiency and the values of α and β . Assume $\gamma = 1.3$.
- 2.11** (a) Derive the equation for the Miller cycle efficiency, Equation 2.23.
 (b) Derive the equation for the Miller cycle imep, Equation 2.24.
- 2.12** For Otto and Miller cycles that have equal compression ratios ($r_c = 10$), what are the respective thermal efficiencies and non dimensional imeps? Assume that the parameter λ is equal to 1.5 for the Miller cycle, the specific heat ratio $\gamma = 1.3$, and $Q_{in}/P_1 V_1 = 30$.

- 2.13** Develop a complete expansion cycle model in which the expansion stroke continues until the pressure is atmospheric. Derive an expression for the efficiency in terms of γ , $\alpha = V_4/V_3$, and $\beta = V_1/V_4$.
- 2.14** If a four-cylinder, four-stroke engine with a 0.1 m bore and a 0.08 m stroke operating at 2000 rpm has the same heat/mass loss parameters as Example 2.3, how much indicated power (kW) would it produce? What if it were a two-stroke engine?
- 2.15** Using the program `BurnFraction.m`, and assuming that $a = 5$, the beginning of heat addition is -10° , and the duration of heat addition is 40° , (a) plot the Wiebe heat release fraction curve for the following form factor values: $n = 2, 3$, and 4 . (b) At what crank angle is 0.10, 0.50, and 0.90 of the heat released?
- 2.16** Using the program `FiniteHeatRelease.m`, determine the effect of heat release duration on the net work, power, mean effective pressure, and thermal efficiency for a four-stroke engine with heat release durations of $40^\circ, 30^\circ, 20^\circ, 10^\circ$, and 5° . Assume that the total heat addition $Q_{in} = 2500$ J, the start of heat release θ_s remains constant at -10° atdc, $a = 5$, $n = 3$, and $\gamma = 1.4$. The engine bore and stroke are 0.095 m, the compression ratio is 9:1, and engine speed is 3000 rpm.
- 2.17** If a four-cylinder unthrottled Otto cycle engine is to generate 100 kW at an engine speed of 2500 rpm, what should its bore and stroke be? Assume a square block engine with equal bore and stroke and a compression ratio of 10:1. The total heat addition $Q_{in} = 2200$ J, the start of heat release θ_s remains constant at -15° atdc, the combustion duration is 40° , $a = 5$, $n = 3$, and $\gamma = 1.4$. Use the single-cylinder program `FiniteHeatRelease.m` and solve for a power output of 25 kW.
- 2.18** Develop a four-stroke Diesel cycle model (along the lines used in Example 2.4) with the following data: $r = 22$, $\gamma = 1.3$, $T_i = 300$ K, $P_i = 101$ kPa, $P_i/P_e = 0.98$, $M = 29$, and $q_{in} = 2090$ kJ/kg_{gas}.
- 2.19** Using the program `FourStrokeOtto.m`, plot the effect of inlet throttling from 100 to 25 kPa on the peak pressure, P_3 , and the volumetric efficiency η_v . Assume the following conditions: $T_i = 300$ K, $r = 9$, $\gamma = 1.3$, and $q_{in} = 2400$ kJ/kg_{gas}.
- 2.20** In Example 2.3, T_e is the exhaust temperature during the constant pressure exhaust stroke. It is not the same as the average temperature of the gases exhausted. Explain.

Chapter 3

Fuel, Air, and Combustion Thermodynamics

3.1 INTRODUCTION

It has already been mentioned that an understanding of internal combustion engines will require a better thermodynamic model than the ideal gas models used in Chapter 2. In this chapter, we review the thermodynamics of combustion and develop models suitable for application to internal combustion engines. The chapter begins with multicomponent ideal gas property models, followed by stoichiometry, and then computation of equilibrium combustion components and properties. We will develop equations for the thermodynamic properties of fuel–air–residual gas mixtures as a function of the pressure, temperature, and the mole fractions of the component species, and introduce the equivalence ratio.

A few words about the atmosphere are in order. The properties of air vary geographically, with altitude, and with time. In this text, we will assume that air is 21% oxygen and 79% nitrogen by volume, that is for each mole of O₂, there are 3.76 moles of N₂. Selected physical properties of air, oxygen, and nitrogen are given in Appendices A and B. Extension of our analyses to different air mixtures encountered in practice is straightforward. The most frequent differences accounted for are the presence of water and argon in air.

3.2 THERMODYNAMIC PROPERTIES OF IDEAL GAS MIXTURES

In computing cycle parameters, thermal efficiency, and work produced by an engine, we need to compute the changes of state due to combustion, isentropic compression/expansion, and blowdown. In the analyses that follow, we model the fuel–air mixture and the products of combustion as ideal gas mixtures. For an ideal gas, the familiar relationships between pressure P , temperature T , and volume V are

$$\begin{aligned} PV &= N R_u T \\ PV &= m R T \\ Pv &= RT \end{aligned} \tag{3.1}$$

The mass, m (kg), of a gas mixture is the sum of the mass of all n components

$$m = \sum_{i=1}^n m_i \tag{3.2}$$

The mass fraction, x_i , of any given species is defined as

$$x_i = m_i/m \quad (3.3)$$

and it should be clear that

$$\sum_{i=1}^n x_i = 1 \quad (3.4)$$

The total number of moles, N , of a mixture is the sum of moles of all n components

$$N = \sum_{i=1}^n n_i \quad (3.5)$$

and the mole fraction y_i of any given species is the fraction of the total number of moles

$$y_i = \frac{n_i}{N} \quad (3.6)$$

We adopt capital letters for extensive variables and reserve lowercase letters for intensive, that is, specific (per unit mass or mole) variables. The molecular mass, M , of a mixture

$$M = \sum_{i=1}^n y_i M_i \quad (3.7)$$

is the conversion factor required between molar intensive and mass intensive units. For example, the mass intensive (specific) gas constant R is related to the molar intensive universal gas constant R_u by

$$R = \frac{R_u}{M} \quad (3.8)$$

where $R_u = 8.314 \text{ kJ/(kmol K)}$.

The internal energy U (kJ) of a mixture is the sum of the internal energy u_i of all n components

$$U = \sum_{i=1}^n m_i u_i \quad (3.9)$$

The specific internal energy u (kJ/kg) is

$$u = \sum_{i=1}^n x_i u_i \quad (3.10)$$

The internal energy U of a mixture can also be written on a molar basis as

$$U = \sum_{i=1}^n n_i \bar{u}_i \quad (3.11)$$

where the molar intensive properties are denoted with an overbar. The specific molar internal energy (kJ/kmol) is the mole fraction weighted sum of the component internal energies:

$$\bar{u} = \sum_{i=1}^n y_i \bar{u}_i \quad (3.12)$$

Analogous relations for the enthalpy H (kJ) and specific enthalpy h (kJ/kg) are

$$H = \sum_{i=1}^n m_i h_i \quad (3.13)$$

$$h = \sum_{i=1}^n x_i h_i \quad (3.14)$$

Note that the enthalpy h_i of a component is evaluated at the total pressure P

$$h_i = u_i + Pv_i$$

On a molar basis, the enthalpy is

$$H = \sum_{i=1}^n n_i \bar{h}_i \quad (3.15)$$

$$\bar{h} = \sum_{i=1}^n y_i \bar{h}_i \quad (3.16)$$

The enthalpy is defined using a standardized reference state, $T = 298.15$ K and $P_0 = 1$ bar. The standardized enthalpy has two parts, the enthalpy related to the chemical bond energy needed to form the substance from its elements, defined as the enthalpy of formation, \bar{h}_f^o , and the enthalpy related to the temperature T . Values of specific enthalpy at other states are determined relative to this standardized reference state, as shown by Equation 3.17.

$$\bar{h}_i(T) = \bar{h}_f^o + (\bar{h}_i(T) - \bar{h}_f^o) \quad (3.17)$$

Tabular molar specific enthalpy data for elemental gases and combustion products is given in Appendices B.3–B.8. The enthalpy of formation \bar{h}_f^o of the stable form of the elements such as hydrogen H₂, oxygen O₂, nitrogen N₂, and solid carbon C(s) is assigned a value of zero at the reference temperature $T = 298.15$ K. For compounds, the enthalpy of formation is the enthalpy required to form the compound from its elements in their stable state. The enthalpy of formation of CO₂ is $-393,522$ kJ/kmol = -8942 kJ/kg. Due to the difference in the bond energies, the enthalpy of CO₂ (-8942 kJ/kg) at the standard reference state is consequently less than the enthalpy of its elements C and O₂ (0 kJ/kg) at the same reference state. Similarly, the enthalpy of formation of H₂O vapor is $-241,826$ kJ/kmol = $-13,424$ kJ/kg.

The constant pressure and constant volume specific heats are defined as follows:

$$c_p = \left(\frac{\partial h}{\partial T} \right)_p \quad (3.18)$$

$$c_v = \left(\frac{\partial u}{\partial T} \right)_v \quad (3.19)$$

Useful relationships between ideal gas specific heats c_v , c_p and the gas constant R can be developed from the definition of enthalpy h :

$$\begin{aligned} h &= u + pv \\ &= u + RT \end{aligned} \quad (3.20)$$

in differential form,

$$\begin{aligned} dh &= du + RdT \\ c_p dT &= c_v dT + RdT \end{aligned} \quad (3.21)$$

so

$$\begin{aligned} R &= c_p - c_v \\ \frac{c_v}{R} &= \frac{1}{\gamma - 1} \\ \frac{c_p}{R} &= \frac{\gamma}{\gamma - 1} \end{aligned} \quad (3.22)$$

The entropy S (kJ/K) of a mixture is the sum of the entropy of each component

$$S = \sum_{i=1}^n m_i s_i = \sum_{i=1}^n n_i \bar{s}_i \quad (3.23)$$

From the Gibbs equations, the mass and molar specific entropy, s_i , (kJ/(kg K)) and \bar{s}_i (kJ/(kmol K)) of component i are

$$s_i(T, P) = s_i^0(T) - R_i \ln(P_i/P_0) \quad (3.24)$$

$$\bar{s}_i(T, P) = \bar{s}_i^0(T) - R_u \ln(P_i/P_0) \quad (3.25)$$

Note the entropy of a component is evaluated at its partial pressure, P_i , defined as

$$P_i = y_i P \quad (3.26)$$

following Dalton's rule of additive pressures for an ideal gas mixture, in which the partial pressure is the pressure that a component would exert if it occupied the entire volume at the given temperature.

A standardized reference state is also defined for entropy. The third law of thermodynamics, postulated by W. Nernst (1864–1941), sets the entropy of pure crystalline elements and compounds to zero at a temperature of 0 K, which has been chosen as the reference state for entropy. Values of the specific entropy at other states are determined relative to 0 K. The standard entropy terms s_i^0 and \bar{s}_i^0 depend only on temperature T , and are the mass and molar specific entropies of a component at the reference pressure P_0 , that is, $P_i = P_0 = 1$ bar. Tabular standard entropy data for ideal gases at $P_0 = 1$ bar is given in Appendices B.3–B.8. For example, at 298 K the molar standard entropy of carbon dioxide, CO₂, is 213.794 kJ/(kmol K).

Substitution of Equation 3.24 into Equation 3.23 yields convenient relations for the mixture mass (s) and molar (\bar{s}) specific entropies with separate pressure and temperature dependent terms:

$$s = -R \ln(P/P_0) + \sum_{i=1}^n x_i (s_i^0 - R_i \ln y_i) \quad (3.27)$$

$$\bar{s} = -R_u \ln(P/P_0) + \sum_{i=1}^n y_i (\bar{s}_i^0 - R_u \ln y_i) \quad (3.28)$$

The Gibbs free energy G of an ideal gas mixture is defined as

$$\begin{aligned} G = H - TS &= \sum_{i=1}^n n_i \bar{g}_i \\ &= \sum_{i=1}^n n_i (\bar{h}_i - T \bar{s}_i) \end{aligned} \quad (3.29)$$

EXAMPLE 3.1 Properties of Ideal Gas Mixtures

Compute the molecular mass M , mass specific enthalpy h (kJ/kg), mass specific entropy s (kJ/kg K), and mass specific Gibbs free energy g (kJ/kg) of a mixture of combustion products at $P = 2000$ kPa and $T = 1000$ K. The constituents and their mole fractions are

Species	y_i
CO_2	0.109
H_2O	0.121
N_2	0.694
CO	0.0283
H_2	0.0455

SOLUTION Using the tabular ideal gas data in Appendices B.3–B.8, the following table of component properties can be generated, and the mixture properties computed:

Species	y_i	M_i (kg/kmol)	\bar{h}_f° (kJ/kmol)	$\bar{h}_i - \bar{h}_f^\circ$ (kJ/kmol)	\bar{s}_i° (kJ/(kmol K))	$y_i (\bar{s}_i^\circ - R_u \ln y_i)$ (kJ/(kmol K))
CO_2	0.109	44.01	-393,522	33,397	269.30	31.36
H_2O	0.121	18.015	-241,826	26,000	232.74	30.28
N_2	0.694	28.013	0	21,463	228.17	160.05
CO	0.0283	28.01	-110,527	21,686	234.54	7.48
H_2	0.0455	2.016	0	20,663	166.22	8.73

1. Molecular mass: $M = \sum y_i M_i = 27.3$ kg/kmol
2. Molar specific enthalpy: $\bar{h} = \sum y_i \bar{h}_i = -52,047$ kJ/kmol
3. Molar specific entropy: $\bar{s} = -R_u \ln(P/P_0) + \sum y_i (\bar{s}_i^\circ - R_u \ln y_i) = 213.5$ kJ/(kmol K)
4. Molar specific Gibbs free energy: $\bar{g} = \bar{h} - T\bar{s} = -265,550$ kJ/kmol

Therefore,

$$h = \bar{h}/M = -1906 \text{ kJ/kg}$$

$$s = \bar{s}/M = 7.82 \text{ kJ/kg K}$$

$$g = \bar{g}/M = -9727.0 \text{ kJ/kg}$$

Comment: The entropy is calculated using the partial pressure, and the values of enthalpy and Gibbs free energy are relatively low, since this is a mixture of the products of combustion.

Specific Heat of Fuel–Air Mixtures

If the composition, that is, mole fractions, of the fuel–air–residual gas mixture are known, the thermodynamic properties h , u , s , and v of the mixture are found by application of the above property relations. The constant pressure specific heat of the fuel–air mixture, c_p , requires a more detailed analysis. The equilibrium constant pressure specific heat depends not only on the change in enthalpy but also on the change in mixture composition as a function of temperature. It is defined as

$$c_p = \left(\frac{\partial h}{\partial T} \right)_p \quad (3.30)$$

Since $h = \bar{h}/M$,

$$\frac{\partial h}{\partial T} = \frac{1}{M} \frac{\partial \bar{h}}{\partial T} + \bar{h} \frac{\partial}{\partial T} \left(\frac{1}{M} \right) \quad (3.31)$$

Differentiating the molar specific heat with respect to temperature,

$$\bar{h} = \sum_{i=1}^n y_i \bar{h}_i, \quad (3.32)$$

$$\frac{\partial \bar{h}}{\partial T} = \sum_{i=1}^n y_i \frac{\partial \bar{h}_i}{\partial T} + \sum_{i=1}^n \bar{h}_i \frac{\partial y_i}{\partial T} \quad (3.33)$$

results in

$$c_p = \frac{1}{M} \left[\sum_{i=1}^n y_i c_{pi} + \sum_{i=1}^n \bar{h}_i \frac{\partial y_i}{\partial T} \right] - \frac{\bar{h}}{M^2} \frac{\partial M}{\partial T} \quad (3.34)$$

The molecular mass is $M = \sum y_i M_i$, so upon substitution,

$$c_p = \frac{1}{M} \left[\sum_{i=1}^n y_i c_{pi} + \sum_{i=1}^n \bar{h}_i \frac{\partial y_i}{\partial T} - \frac{\bar{h}}{M} \sum_{i=1}^n M_i \frac{\partial y_i}{\partial T} \right] \quad (3.35)$$

The frozen specific heat, $c_{p,f}$ is computed holding the composition constant. It is defined as

$$c_{p,f} = \sum_{i=1}^n y_i c_{pi} \quad (3.36)$$

Note the important role that the changes in mole fraction with respect to pressure and temperature, $\partial y_i / \partial P$ and $\partial y_i / \partial T$, have in determination of the mixture specific heat.

For computer calculations it is awkward to deal with tabular data. For this reason, the specific heats of various species have been curve-fitted to polynomials by minimizing the least-squares error (Gordon and McBride, 1994). The function we will employ for any given species is

$$\frac{c_p}{R} = \frac{\bar{c}_p}{R_u} = a_1 + a_2 T + a_3 T^2 + a_4 T^3 + a_5 T^4 \quad (3.37)$$

Since for an ideal gas, $dh = c_p dT$ and $ds = (c_p/T) dT$, it follows that the enthalpy and standard entropy at atmospheric pressure are

$$\frac{h}{RT} = \frac{\bar{h}}{R_u T} = a_1 + \frac{a_2}{2} T + \frac{a_3}{3} T^2 + \frac{a_4}{4} T^3 + \frac{a_5}{5} T^4 + \frac{a_6}{T} \quad (3.38)$$

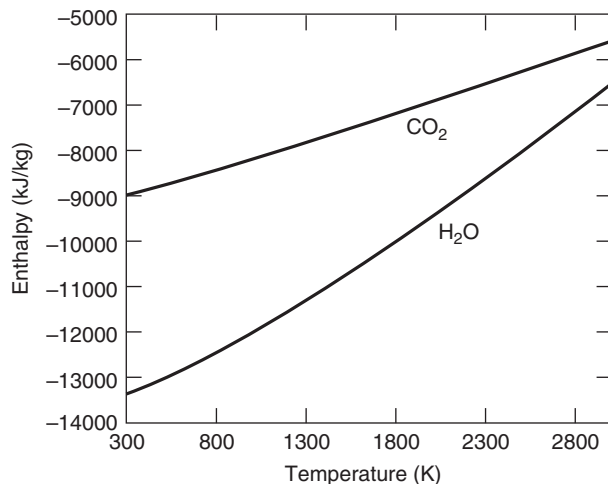


Figure 3.1 Enthalpy versus temperature curve fits for CO_2 and H_2O

$$\frac{s^{\circ}}{R} = \frac{\bar{s}^{\circ}}{R_u} = a_1 \ln T + a_2 T + \frac{a_3}{2} T^2 + \frac{a_4}{3} T^3 + \frac{a_5}{4} T^4 + a_7 \quad (3.39)$$

where a_6 and a_7 are constants of integration determined by matching the enthalpy and entropy to a zero datum at some reference temperature. As discussed above, the reference temperature for enthalpy is chosen to be 298.15 K with the enthalpy of H_2 , O_2 , N_2 , and C(s) set to zero.

Values of the curve-fit constants for several species of interest in combustion, CO_2 , H_2O , N_2 , O_2 , CO , H_2 , H , O , OH , and NO are given in Appendices C.2 and C.3 for the temperature ranges 300–1000 K and 1000–3000 K. Similar curve-fit coefficients for several fuels are also given in Appendix C.1.

The mass-specific enthalpies of CO_2 and H_2O given by Equation 3.38 are plotted versus temperature in Figure 3.1. At 298 K, the enthalpy of CO_2 is -8942 kJ/kg , and the enthalpy of H_2O vapor is $-13,424 \text{ kJ/kg}$, consistent with the definition of enthalpy of formation. Note that the slope of the H_2O curve is steeper than that of the CO_2 curve, as a result of the greater specific heat of the water vapor.

Thermodynamic data for elements, combustion products, and many pollutants are also available in a compilation published by the National Institute of Standards and Technology (NIST) called the JANAF Tables (Chase, 1998). For single-component fuels, the data presented by Stull et al. (1969) is in the same format as that of the JANAF Tables.

For several decades, S. Gordon and B. McBride at the NASA Glenn Research Center provided least-square coefficients of thermodynamic property data for use in computer programs. A representative listing of their publications, for example, McBride et al. (1993), Gordon and McBride (1994), and McBride et al. (2002), is given in the chapter references. In addition to these references, a compilation by Rossini (1953) is useful for hydrocarbon fuels at temperatures as high as 1500 K.

3.3 LIQUID-VAPOR-GAS MIXTURES

The thermodynamics involved with fuel injection and vaporization, water injection, and water condensation can be complicated, as the fuel-air mixtures are composed of more than one thermodynamic phase. Fortunately, we can make some simplifications that are quite accurate for our intended use.

First, let us consider a pure substance in terms of its compressed liquid, saturated liquid, saturated vapor, and superheated vapor states. The simplifications that we will introduce are

1. Compressed and saturated liquids are incompressible.
2. Saturated and superheated vapors are ideal gases.

For an incompressible substance, it can be shown that the internal energy and entropy depend only on temperature. Hence the approximation for compressed liquids can be

$$u = u_f(T) \quad (3.40)$$

$$s = s_f(T) \quad (3.41)$$

where the notation $u_f(T)$ and $s_f(T)$ denote the internal energy and entropy of saturated liquid at the temperature T . The enthalpy of a compressed liquid depends on pressure, and it is consistent with Equations 3.40 and 3.41 to assume that

$$h = h_f^0 + (h - h_{298}) + (P - P_{\text{atm}}) v \quad (3.42)$$

where $h_f^0(T)$ is the enthalpy of formation of the compressed liquid at standard atmospheric pressure (101.25 kPa) and temperature (298 K). The only property remaining to be prescribed is the specific volume v . Let us choose it to be the specific volume of compressed liquid at atmospheric pressure as these data are readily available.

$$v = v_0(T_1) \quad (3.43)$$

where T_1 is the initial temperature in the process being analyzed.

To introduce the enthalpy of vaporization into our equations of state for the liquids is convenient, since these data are usually easier to find than the saturated liquid data. We then have

$$h = h_g - h_{fg} + (P - P_{\text{atm}}) v \quad (3.44)$$

Unlike specific volume, data for the enthalpy of vaporization at saturation pressure are readily available. Hence we choose

$$h_{fg} = h_{fg}(T_1) \quad (3.45)$$

where, again, T_1 is the temperature at the start of the process being analyzed.

Typically

$$|P - P_{\text{atm}}|v \ll |h_{fg}| \quad \text{and} \quad |Pv| \ll |h| \quad (3.46)$$

so that in many cases we can write for liquids

$$h \approx h_g - h_{fg} = h_f^0 + (h - h_{298}) - h_{fg} \quad (3.47)$$

$$u \approx h \quad (3.48)$$

Table 3.1 gives the molar enthalpy of formation for the vapor and liquid state, molar enthalpy of vaporization, the saturation pressure, and the specific volume of compressed liquid, for several liquid fuels and water at $T = 298$ K. The entropy of vaporization is the difference between the enthalpies of formation of the liquid and the gaseous states. Table 3.2 gives most of the same information for octane but as a function of temperature. For example, at $T = 298$ K, the molar enthalpy \bar{h} of liquid octane is $h = \bar{h}_f^0 - \bar{h}_{fg} = -208.45 - 41.51 = -249.96$ kJ/mol.

Table 3.1 Ideal Gas Enthalpy of Formation, Enthalpy of Vaporization, Saturation Vapor Pressure, and Specific Volume of Some Liquid Fuels at $T = 298$ K

Formula	Name	$\bar{h}_{f,gas}^o$ (MJ/kmol)	$\bar{h}_{f,liquid}^o$ (MJ/kmol)	\bar{h}_{fg} (MJ/kmol)	P_{sat} (bar)	v_o (m ³ /kg)
CH ₃ NO ₂	Nitromethane	-74.73	-113.1	38.37	0.050	0.879×10^{-3}
CH ₄ O	Methanol	-201.17	-239.09	37.92	0.186	1.264×10^{-3}
C ₂ H ₆ O	Ethanol	-234.81	-277.15	42.34	0.084	1.267×10^{-3}
C ₄ H ₁₀ O	Ethyl ether	-252.21	-278.74	26.53	0.733	1.413×10^{-3}
C ₅ H ₁₂	Pentane	-146.00	-172.44	26.44	0.710	1.597×10^{-3}
C ₆ H ₁₄	Hexane	-167.19	-198.68	31.49	0.242	1.514×10^{-3}
C ₆ H ₆	Benzene	+82.93	+48.91	34.02	0.129	1.138×10^{-3}
C ₇ H ₁₇	Gasoline	-267.12	-305.63	38.51		1.449×10^{-3}
C ₈ H ₁₈	Octane	-208.45	-249.96	41.51	0.022	1.423×10^{-3}
C ₈ H ₁₈	Isooctane	-224.14	-259.25	35.11	0.071	1.445×10^{-3}
C ₈ H ₁₀	Ethylbenzene	+29.29	-12.72	42.01	0.013	1.153×10^{-3}
C ₁₂ H ₂₆	Dodecane	-290.87	-229.55	61.32	< 0.001	1.336×10^{-3}
C ₁₄ H ₃₀	Tetradecane	-332.13	-403.37	71.24	< 0.001	1.311×10^{-3}
C _{14.4} H _{24.9}	Diesel fuel	-100.00	-174.08	74.08		1.176×10^{-3}
C ₁₆ H ₃₄	Hexadecane (cetane)	-373.34	-454.48	81.14	< 0.001	1.293×10^{-3}
C ₁₉ H ₄₀	Nonadecane	-435.14	-530.17	95.03	< 0.001	1.286×10^{-3}
H ₂ O	Water	-241.83	-285.85	44.02	0.0317	1.000×10^{-3}

Source: P_{sat} and v_o are from the CRC Handbook of Chemistry and Physics (2012–2013); \bar{h}_{fg} is from Vargaftik (1975); and \bar{h}_f^o is from Stull et al. (1969).

Table 3.2 Enthalpy of Vaporization, Saturation Vapor Pressure, and Specific Volume of Octane, C₈H₁₈

T (K)	\bar{h}_{fg} (MJ/kmol)	P_{sat} (bar)	v_o (m ³ /kg)
298	41.51	0.018	1.432×10^{-3}
325	39.99	0.075	1.479×10^{-3}
350	38.22	0.211	1.527×10^{-3}
375	36.45	0.503	1.579×10^{-3}
400	34.46	1.058	1.639×10^{-3}
425	32.35	2.003	1.708×10^{-3}
450	30.07	3.500	1.789×10^{-3}
475	27.49	5.707	1.890×10^{-3}
500	24.32	8.837	2.022×10^{-3}
550	20.35	13.210	2.214×10^{-3}

Source: Vargaftik (1975).

The saturated vapor pressure is needed for calculations of fuel droplet evaporation. The Clausius–Clapeyron equation for the saturated vapor pressure as a function of temperature is

$$\frac{dP_{sat}}{dT} = \frac{h_{fg}}{Tv_{fg}} \quad (3.49)$$

Table 3.3 Curve-fit Coefficients for Antoine's Equation for Saturation Vapor Pressure P_{sat} (bar)

Formula	Name	a	b	c
CH_3NO_2	Nitromethane	4.1135	1229.6	-76.221
CH_4O	Methanol	5.1585	1569.6	-34.846
$\text{C}_2\text{H}_6\text{O}$	Ethanol	4.9253	1432.5	-61.819
C_8H_{18}	Octane	4.0487	1355.1	-63.633
$\text{C}_{12}\text{H}_{26}$	Dodecane	4.1055	1625.9	-92.839
$\text{C}_{14}\text{H}_{30}$	Tetradecane	4.1373	1739.6	-105.62
$\text{C}_{16}\text{H}_{34}$	Hexadecane (cetane)	4.1731	1845.7	-117.05
H_2O	Water	5.4022	1838.67	-31.737

Source: www.webbook.nist.gov

For conditions away from the critical point, we can assume ideal gas behavior $v_{\text{fg}} \approx v_g \approx RT/P_{\text{sat}}$, so Equation 3.49 becomes

$$\frac{dP_{\text{sat}}}{P_{\text{sat}}} = \frac{1}{R} \frac{h_{\text{fg}}(T)}{T^2} dT \quad (3.50)$$

The saturated vapor pressure is typically found from an integrated form of the Clausius–Clapeyron equation, called Antoine's equation. Antoine's Equation 3.51, has empirical coefficients, a , b , and c that are curve fits for a given fluid. Table 3.3 lists the curve fit coefficients for Antoine's equation for several liquid fuels and water, and temperature T in Kelvin.

$$\log_{10}(P_{\text{sat}}) = \left[a - \frac{b}{T + c} \right] \quad (3.51)$$

For example, Equation 3.51 predicts that the saturated vapor pressure P_{sat} of a cetane droplet at $T = 500$ K is 0.226 bar.

To integrate the Clausius–Clapeyron equation for the saturation pressure, one needs to know the temperature dependence of the enthalpy of vaporization, \bar{h}_{fg} . Equation 3.52 is a curve fit for the molar enthalpy of vaporization \bar{h}_{fg} as a function of the temperature ratio T/T_c , where T_c is defined as the temperature at the critical point where $\bar{h}_{\text{fg}} = 0$. Table 3.4 lists the curve-fit coefficients for Equation 3.52 for several liquid fuels.

$$\bar{h}_{\text{fg}} = A e^{(-\alpha T/T_c)} (1 - T/T_c)^\beta \quad (3.52)$$

Table 3.4 Curve-fit Coefficients for Enthalpy of Vaporization \bar{h}_{fg} (kJ/mole)

Formula	Name	A (MJ/kmol)	α	β	T_c (K)	P_c (bar)
CH_3NO_2	Nitromethane	53.33	0.2732	0.2732	588.0	58.7
CH_4O	Methanol	45.30	-0.3100	0.4241	512.6	81.0
$\text{C}_2\text{H}_6\text{O}$	Ethanol	50.43	-0.4475	0.4989	513.9	63.0
C_8H_{18}	Octane	58.46	0.1834	0.3324	568.8	24.9
$\text{C}_{14}\text{H}_{30}$	Tetradecane	95.66	0.2965	0.2965	694.0	14.4

Source: www.webbook.nist.gov

We will also deal with mixtures of gases in contact with a liquid phase. For example, the products of combustion can include water both in the vapor and in the liquid states. In these cases, we assume the following:

1. The liquid contains no dissolved gases.
2. The gases are ideal.
3. At equilibrium, the partial pressure of the water vapor is equal to the saturation pressure corresponding to the mixture temperature.

Note that the temperature of exhaust gases is usually high enough, so all of the water is in vapor form, except during engine warmup conditions. In that case, liquid water can be seen dripping from vehicle tail pipes, since the exhaust system temperature is below the dew point temperature.

Let χ denotes the quality of the condensable substance, that is, the ratio of the vapor mass or moles to the total liquid and vapor mass or moles. The quality χ has the same value on a mole or mass basis.

$$\chi = \frac{n_{\text{H}_2\text{O,g}}}{n_{\text{H}_2\text{O}}} = \frac{m_{\text{H}_2\text{O,g}}}{m_{\text{H}_2\text{O}}} \quad (3.53)$$

The enthalpy of the system is then

$$H = (1 - \chi) m_1 (h_{g,1} - h_{fg}) + \chi m_1 h_{g,1} + \sum_{i=2}^n m_i h_i \quad (3.54)$$

or

$$h = \sum_{i=1}^n x_i h_i - (1 - \chi)x_1 h_{fg} \quad (3.55)$$

The indexing is chosen so that $i = 1$ corresponds to the condensable substance and $i = 2, \dots, n$ corresponds to all other gases. Likewise, the system volume is

$$V = (1 - \chi) m_1 (v_{g,1} - v_{fg}) + \chi m_1 v_{g,1} + \sum_{i=2}^n m_i v_i \quad (3.56)$$

and the specific volume is

$$v = \sum_{i=1}^n x_i v_i - (1 - \chi)x_1 v_{fg} \quad (3.57)$$

where the v_i are computed at the total pressure P in accordance with the Amagat–Leduc Law of additive volumes.

3.4 STOICHIOMETRY

A stoichiometric reaction is defined such that the fuel burns completely and the only products are carbon dioxide and water. This reaction is used as a reference case, and we will treat a wider variety of combustion products in subsequent sections. The product composition resulting from fuel–air combustion depends on the stoichiometry. For example, if the reactants are fuel-rich, there is not enough oxygen to react completely with the fuel, resulting in the formation of additional products such as CO and H_2 , and if the mixture is fuel-lean, there is not enough fuel to consume the oxygen, so there will be unburned oxygen in the product mixture.

Let us represent the chemical formula of a fuel as $C_aH_bO_cN_d$ and assume the following stoichiometric reaction



and solve for a_s , the stoichiometric molar air-fuel ratio, and the moles n_i ($i = 1, 2, 3$) that describe the product composition. Note that the stoichiometric reaction is expressed per mole of fuel. We know that atoms are conserved, so using atomic species balance we can write

$$\begin{aligned} C : \quad a &= n_1 \\ H : \quad b &= 2n_2 \\ O : \quad c + 2a_s &= 2n_1 + n_2 \\ N : \quad d + 2 \times 3.76 \times a_s &= 2n_3 \end{aligned} \quad (3.59)$$

Solution of these four equations gives

$$\begin{aligned} a_s &= a + \frac{b}{4} - \frac{c}{2} \\ n_1 &= a \\ n_2 &= \frac{b}{2} \\ n_3 &= \frac{d}{2} + 3.76 \left(a + \frac{b}{4} - \frac{c}{2} \right) \end{aligned} \quad (3.60)$$

The stoichiometric mass air-fuel ratio AF_s can be determined from a_s and the fuel-air mixture molecular weights:

$$AF_s = \left(\frac{m_a}{m_f} \right)_s = \frac{28.85(4.76a_s)}{(12.01a + 1.008b + 16.00c + 14.01d)} \quad (3.61)$$

A dimensionless measure of the fuel-air ratio is the fuel-air equivalence ratio, ϕ , which is defined in Equation 3.62 as the actual fuel-air ratio, FA , divided by the stoichiometric fuel-air ratio, FA_s ,

$$\phi = \frac{FA}{FA_s} \quad (3.62)$$

The reciprocal of ϕ is λ , the air-fuel ratio, AF , divided by the stoichiometric air-fuel ratio, AF_s :

$$\lambda = \frac{AF}{AF_s} \quad (3.63)$$

The equivalence ratio has the same value on a mole or mass basis. If $\phi < 1$ the mixture is lean, if $\phi > 1$ the mixture is rich, and if $\phi = 1$ the mixture is stoichiometric.

Typical stoichiometric air-fuel ratio values of various fuels are given in Table 3.4. For hydrocarbons, that is ($c = d = 0$), the mass stoichiometric air-fuel ratio AF_s is approximately 15, and not a strong function of the number of carbon atoms. Table 3.4 also lists the molar stoichiometric air-fuel ratio, a_s , the CO_2 , and H_2O product mole fractions, and the last column in the table is the equilibrium product water quality, χ_{eq} , at a reference temperature of 298.15 K.

Table 3.5 Molecular Mass, Stoichiometric Air–Fuel Ratios, and Product Mole Fractions and Quality

Fuel		<i>M</i>	(kg/kmole)	<i>AF_s</i>	<i>a_s</i>	<i>y_{CO₂}</i>	<i>y_{H₂O}</i>	<i>χ_{eq}</i>
Hydrogen	H ₂	2.02	34.06	0.50	0.000	0.347	0.0061	
Methane	CH ₄	16.04	17.12	2.00	0.095	0.190	0.139	
Ammonia	NH ₃	17.03	6.05	0.75	0.000	0.311	0.0072	
Methanol	CH ₄ O	32.04	6.43	1.50	0.116	0.231	0.109	
Propane	C ₃ H ₈	44.09	15.57	5.00	0.116	0.155	0.178	
Ethanol	C ₂ H ₆ O	46.07	8.94	3.00	0.123	0.184	0.145	
Nitromethane	CH ₃ NO ₂	61.04	1.69	0.75	0.158	0.237	0.105	
Gasoline	C ₇ H ₁₇	101.21	15.27	11.25	0.121	0.147	0.201	
Octane	C ₈ H ₁₈	114.22	15.03	12.50	0.125	0.141	0.199	
Diesel	C _{14.4} H _{24.9}	198.04	14.30	20.63	0.138	0.119	0.242	
Tetradecane	C ₁₄ H ₃₀	198.39	14.54	21.50	0.127	0.110	0.207	
Hexadecane (Cetane)	C ₁₆ H ₃₄	226.44	14.56	24.5	0.128	0.136	0.208	

The mole and mass fractions of fuel in a stoichiometric fuel–air mixture are as follows:

$$y_s = \frac{n_f}{n_f + n_a} = \frac{1}{1 + 4.76 a_s} \quad (3.64)$$

$$x_s = \frac{m_f}{m_f + m_a} = \frac{1}{1 + AF_s} \quad (3.65)$$

EXAMPLE 3.2 Molecular Mass of Stoichiometric Fuel–Air Mixtures

- (a) What is the molecular mass M_{mix} (kg/kmole) of a stoichiometric mixture of octane (C_8H_{18}) and air? (b) If the mixture fills a automotive engine cylinder with a volume $V = 9.0 \times 10^{-4} \text{ m}^3$ at a pressure $P = 100 \text{ kPa}$ and temperature $T = 300 \text{ K}$, what is the mass of the fuel–air mixture in the cylinder?

SOLUTION (a) From Appendix B.1, the molecular mass of air is $M_a = 28.97 \text{ kg/kmol}$. From Table 3.5, the molecular mass M_f of octane is 114.22 kg/kmol , and the stoichiometric mass air–fuel ratio AF_s is 15.03. Therefore,

$$\begin{aligned} y_f &= \frac{n_f}{n_f + n_a} = \frac{m_f / M_f}{m_a / M_a + m_f / M_f} \\ &= \dots = 0.0166 \end{aligned}$$

$$y_a = 1 - y_f = 0.9834$$

$$M_{\text{mix}} = y_a M_a + y_f M_f = 30.89 \text{ kg/kmol}$$

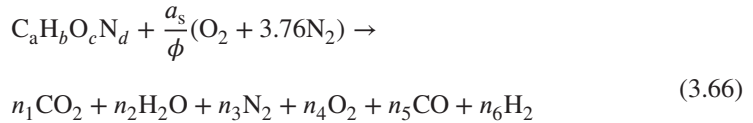
- (b) The mass of the mixture in the cylinder is

$$m_{\text{mix}} = \frac{PV M}{R_u T} = \frac{(100)(9.0 \times 10^{-4})(30.39)}{(8.314)(300)} = 1.097 \text{ g}$$

Comment For an automotive class engine, the molecular mass of the fuel–air mixture is of the order of 30 kg/kmol, and there is typically a gram of combustible mixture in a cylinder.

3.5 LOW-TEMPERATURE COMBUSTION MODELING

At low temperatures ($T < 1000$ K, such as in the product gases in the exhaust stream) and carbon to oxygen ratios less than one, the overall combustion reaction for any equivalence ratio can be written as



This equation assumes the dissociation of reactants is negligible, and a more general case including dissociation is treated later in this chapter. For reactant C/O ratios greater than one we would have to add solid carbon C(s) and several other species to the product list, as we shall see.

For lean ($\phi < 1$) combustion products at low temperature, we will assume no product CO and H₂, i.e., $n_5 = n_6 = 0$. In this case, atomic species balance equations are sufficient to determine the product composition, since there are four equations and four unknowns.

For rich ($\phi > 1$) combustion, we will assume that there is no product O₂, i.e., $n_4 = 0$. In this case, there are five unknowns, so we need an additional equation to supplement the four atom balance equations. Since we have incomplete products of combustion, we need to assume equilibrium conditions among the product species CO₂, H₂O, CO, and H₂ and no dissociation in order to determine the product composition. This equilibrium reaction is termed the water–gas shift reaction, given by Equation 3.67:



with the equilibrium constant $K(T)$ for the water–gas shift reaction providing the fifth equation:

$$K(T) = \frac{n_2 n_5}{n_1 n_6} \quad (3.68)$$

The equilibrium constant $K(T)$ equation, Equation 3.69, is a curve fit of JANAF Table data for $400 < T < 3200$:

$$\ln K(T) = 2.743 - \frac{1.761}{t} - \frac{1.611}{t^2} - \frac{0.2803}{t^3} \quad \left(t = \frac{T}{1000} \right) \quad (3.69)$$

Solutions for both rich and lean cases are given in Table 3.6. In the rich case, the number of moles of CO, n_5 , is given by the solution of the quadratic equation

$$n_5 = \frac{-b_1 + \sqrt{b_1^2 - 4a_1c_1}}{2a_1} \quad (3.70)$$

Table 3.6 Low-Temperature ($T < 1000$ K) Combustion Products

Species	n_i	$\phi \leq 1$	$\phi > 1$
CO_2	n_1	a	$a - n_5$
H_2O	n_2	$b/2$	$b/2 - d_1 + n_5$
N_2	n_3	$d/2 + 3.76a_s/\phi$	$d/2 + 3.76a_s/\phi$
O_2	n_4	$a_s(1/\phi - 1)$	0
CO	n_5	0	n_5
H_2	n_6	0	$d_1 - n_5$

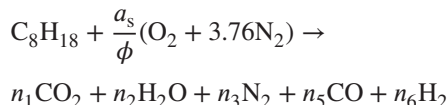
where the a_1 , b_1 , and c_1 coefficients are given by

$$\begin{aligned} a_1 &= 1 - K \\ b_1 &= b/2 + Ka - d_1(1 - K) \\ c_1 &= -ad_1K \\ d_1 &= 2a_s(1 - 1/\phi) \end{aligned} \tag{3.71}$$

EXAMPLE 3.3 Rich Octane Combustion

What are the mole fractions of CO_2 , H_2O , CO, N_2 , and H_2 produced when octane (C_8H_{18}) is burned in rich conditions at $\phi = 1.2$ and $T = 1000$ K?

SOLUTION Since the equivalence ratio of $\phi = 1.2$ is a rich combustion mixture, the product concentration of O_2 is assumed to be zero, that is, $n_4 = 0$. The combustion equation is



The calculation of the product mole fractions proceeds as follows:

$$\begin{aligned} a &= 8, b = 18, c = d = 0 \\ a_s &= a + b/4 - c/2 = 12.5 \\ d_1 &= 2a_s(1 - 1/\phi) = 4.167 \\ t &= T/1000 = 1 \\ \ln K &= 2.743 - 1.761/t - 1.611/t^2 + 0.2803/t^3 = -0.34 \\ a_1 &= 1 - K = 0.295 \\ b_1 &= b/2 + aK - d_1(1 - K) = 13.41 \\ c_1 &= -ad_1K = -23.50 \\ n_5 &= \left(-b_1 + \sqrt{b_1^2 - 4a_1c_1} \right) / 2a_1 = 1.690 \\ n_1 &= a - n_5 = 6.310 \end{aligned} \tag{3.72}$$

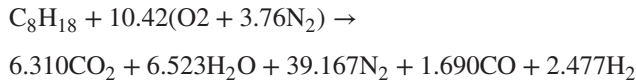
$$n_2 = b/2 - d + n_5 = 6.523$$

$$n_3 = d/2 + 3.76 a_s/\phi = 39.167$$

$$n_6 = d_1 - n_5 = 2.477$$

$$N = \sum n_i = 56.167$$

The combustion equation is therefore



so

$$y_{\text{CO}_2} = n_1/N = 0.112$$

$$y_{\text{H}_2\text{O}} = n_2/N = 0.116$$

$$y_{\text{N}_2} = n_3/N = 0.697$$

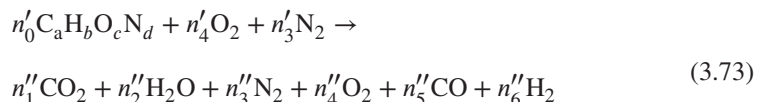
$$y_{\text{CO}} = n_5/N = 0.0301$$

$$y_{\text{H}_2} = n_6/N = 0.0441$$

Fuel–Air–Residual Gas

In reciprocating engines there is residual gas mixed with the fuel and air, since not all of the combustion gases leave the cylinder. We need to determine the composition of the fuel–air–residual gas mixture for analysis of the compression stroke and later for analysis of the unburned mixture ahead of the flame. The residual gas is assumed to be at a low enough temperature ($T < 1000$ K) so that the species relations in Table 3.6 specify its composition.

The fuel–air–residual gas mixture will contain both reactants and products. Let us rewrite the combustion equation as



where

n'_i = reactant coefficient for species i
 n''_i = product coefficient for species i

Adopting similar notation for other symbols, we can develop relations for the species mass and mole fractions for a mixture of residual gas (r) with residual fraction f and premixed fuel–air (fa).

The residual mole fraction y_r is

$$y_r = \frac{n_r}{n_{fa} + n_r} = \frac{1}{\frac{n_{fa}}{n_r} + 1}$$

Since $f = m_r/m$, we can write

$$\frac{m_{fa}}{m_r} = \frac{1}{f} - 1$$

and

$$\frac{n_{fa}}{n_r} = \frac{m_{fa}}{m_r} \frac{M_r}{M_{fa}} = \frac{m_{fa}}{m_r} \frac{M''}{M'}$$

Upon substitution, the residual mole fraction, y_r , is

$$y_r = \left[1 + \frac{M''}{M'} \left(\frac{1}{f} - 1 \right) \right]^{-1} \quad (3.74)$$

The species mole fractions y_i are

$$y_i = \frac{n_i}{N} = \frac{n_i}{n_{fa}} y_{fa} + \frac{n_i}{n_r} y_r$$

Since

$$y_{fa} = 1 - y_r$$

$$y'_i = \frac{n_i}{n_{fa}} \quad \text{and} \quad y''_i = \frac{n_i}{n_r}$$

The species mole fractions are

$$y_i = (1 - y_r) y'_i + y_r y''_i \quad i = 0, 6 \quad (3.75)$$

Similarly, the species mass fractions are

$$x_i = (1 - f) x'_i + f x''_i \quad i = 0, 6 \quad (3.76)$$

For a constant composition mixture, the equilibrium specific heat is identical to the frozen specific heat. However, for a reacting fuel, air, and residual gas mixture, the partial derivatives of the constituent mole fractions y_i with respect to temperature are required for determination of the equilibrium specific heat. Since neither the residual mole fraction y_r nor the reactant mole fractions y'_i depend on temperature, differentiation of Equation 3.75 with respect to temperature yields

$$\frac{\partial y_i}{\partial T} = y_r \frac{\partial y''_i}{\partial T} = y_r \frac{1}{N} \frac{\partial n_i}{\partial T} \quad (3.77)$$

Inspection of Table 3.6 indicates that for lean combustion, none of these six partial derivatives depend on temperature. For rich combustion, only those derivatives with n_5 (CO) depend on T , since the temperature-dependent equilibrium constant $K(T)$ appears in

the solution of the quadratic equation 3.70. Hence, we can write

$$\frac{\partial y_i}{\partial T} = 0 \quad (\text{lean})$$

$$\frac{\partial y_i}{\partial T} = y_r \frac{1}{N} \frac{\partial n_i}{\partial K} \frac{\partial n_5}{\partial K} \frac{\partial K}{\partial T} \quad (\text{rich}) \quad (3.78)$$

The terms $\partial n_i / \partial n_5$ in Equation 3.78 can be determined by differentiating the $\phi > 1$ column in Table 3.6 with respect to n_5 , resulting in: $\partial n_1 / \partial n_5 = -1$, $\partial n_2 / \partial n_5 = 1$, $\partial n_3 / \partial n_5 = 0$, $\partial n_4 / \partial n_5 = 0$, $\partial n_5 / \partial n_5 = 1$, and $\partial n_6 / \partial n_5 = -1$. Also, by differentiating Equation 3.69 with respect to T :

$$\begin{aligned} \frac{\partial K}{\partial T} &= \frac{\partial K}{\partial t} \frac{\partial t}{\partial T} \\ &= \left(\frac{1.761}{t^2} + \frac{3.222}{t^3} - \frac{0.8409}{t^4} \right) \frac{K}{1000} \end{aligned} \quad (3.79)$$

and finally,

$$\frac{\partial n_5}{\partial K} = -\frac{(\alpha - n_5)[n_5 + 2a_s(1/\phi - 1)]}{\beta/2 + n_5 + 2a_s(1/\phi - 1)} \quad (3.80)$$

The above equations are solved numerically in the Fuel–Air–Residual Gas program `farg.m`, which is listed in Appendix F.8. For temperatures between 300 and 1000 K, the program computes the properties of a fuel–air–residual gas mixture given the mixture pressure, temperature, the fuel–air equivalence ratio, and the residual mass fraction. With the mixture mole fraction composition known, the program then proceeds to compute the thermodynamic properties of the mixture: enthalpy, entropy, specific volume, internal energy, and equilibrium specific heat for the given conditions.

Five representative fuels are used in the program, and are identified with the following `fuel_id`, from 1–5:

1. Methane CH₄
2. Gasoline C₇H₁₇
3. Diesel C_{14.4}H_{24.9}
4. Methanol CH₃OH
5. Nitromethane CH₃NO₂

EXAMPLE 3.4 Fuel–Air–Residual Gas

What are the mole fractions and thermodynamic properties of a fuel–air–residual mixture of methane (`fuel_id = 1`) at a temperature T of 500 K, pressure P of 100 kPa, a fuel–air equivalence ratio ϕ of 0.8, and residual fraction f of 0.1?

SOLUTION The computation is performed using the Fuel–Air–Residual Gas program `RunFarg.m` input–output program with inputs T , P , ϕ , `fuel_id`, and f . As detailed in Appendix F.7, the program `RunFarg.m` calls the function `farg.m`, which in turn calls the function `fuel.m` for fuel properties, computes residual gas composition according to Table 3.6, computes residual mole fractions and molecular mass of the residual gas, then computes and outputs the fuel–air–residual gas mixture mole fractions, property values, and outputs the mole fractions and mixture properties.

```

Input parameters to farg:
T = 500;          % temperature (K)
P = 100;          % pressure (kPa)
phi = 0.8;        % equivalence ratio
f = 0.1;          % residual fraction
fuel_id = 1;      % methane identifier
% call function farg
function [y,h,u,s,v,R, Cp,MW,dvdt,dvdp] =
    farg(T, P, phi, fuel_id);
...

```

The resulting mole fractions and properties are listed below.

```

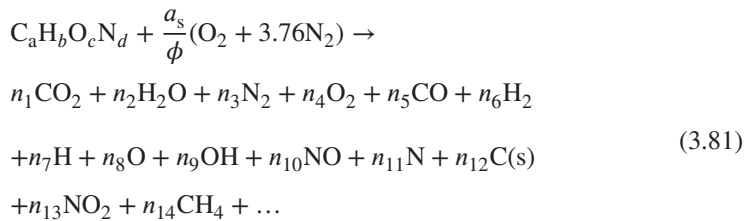
Fuel Air Residual Gas Output
Mole Fractions
CO2 = 0.0078
H2O = 0.0155
N2 = 0.7287
O2 = 0.1783
CO = 0.0000
H2 = 0.0000
H = 0.0000
O = 0.0000
OH = 0.0000
NO = 0.0000
Mixture Properties
h (kJ/kg) = -211.0
u (kJ/kg) = -360.3
s (kJ/Kg K) = 7.766
v (m3/kg) = 1.492
Cp (kJ/Kg K) = 1.122
Molecular Mass = 27.86
dvdt = 2.98e-03
dvdp = -1.49e-02

```

3.6 GENERAL CHEMICAL EQUILIBRIUM

In general, we often consider a combustion problem that has many product species. The fuel is initially mixed with air with an equivalence ratio ϕ . After combustion, the products of reaction are assumed to be in equilibrium at temperature T and pressure P . The composition and thermodynamic properties of the product mixture are to be determined. The overall

combustion reaction per mole of fuel is



The condition for equilibrium is usually stated in terms of thermodynamic functions such as the minimization of the Gibbs or Helmholtz free energy or the maximization of entropy. If temperature and pressure are used to specify a thermodynamic state, the Gibbs free energy is most easily minimized, since temperature and pressure are its fundamental variables. For a product mixture of n species, the Gibbs free energy G is

$$G = \sum_{j=1}^n n_j \mu_j \quad (3.82)$$

The chemical potential, μ_j , of species j represents the partial molal Gibbs free energy, i. e., the partial derivative of the Gibbs free energy with respect to the number of moles of component j holding T, P and the number of moles of the other components constant.

$$\mu_j = \left(\frac{\partial G}{\partial n_j} \right)_{T, P, n_{i \neq j}} \quad (3.83)$$

The equilibrium state can be determined by a Lagrangian multiplier approach, that is, minimizing the Gibbs free energy subject to constraints. In this case, the constraint is the conservation of the number of atoms of each reacting species, b'_i :

$$b'_i = \sum_{j=1}^n a_{ij} n_j \quad (3.84)$$

or

$$b_i - b'_i = 0 \quad (3.85)$$

where the index $i = 1, \dots, l$, the integer l is the number of atom types, a_{ij} is the number of atoms of element i in species j , b'_i is the number of atoms of element i in the reactants, and b_i is the number of atoms of element i in the products.

$$b_i = \sum_{j=1}^n a_{ij} n_j \quad (3.86)$$

is the number of atoms of element i in the products.

Using the Lagrangian optimization procedure, we first define the parameter B :

$$B = G + \sum_{i=1}^l \lambda_i (b_i - b'_i) \quad (3.87)$$

where the λ_i are the Lagrangian multipliers, one for each element. The variational condition, $\delta B = 0$, for equilibrium is

$$\delta B = \sum_{j=1}^n \left(\mu_j + \sum_{i=1}^l \lambda_i a_{ij} \right) \delta n_j + \sum_{i=1}^l (b_i - b'_i) \delta \lambda_i = 0 \quad (3.88)$$

Treating the variations δn_j and $\delta \lambda_i$ as independent

$$\mu_j + \sum_{i=1}^l \lambda_i a_{ij} = 0 \quad j = 1, \dots, n \quad (3.89)$$

For ideal gases the chemical potential μ_j is

$$\mu_j = \mu_j^0 + R_u T \ln(n_j/N) + R_u T \ln(P/P_o) \quad (3.90)$$

so that

$$\frac{\mu_j^0}{R_u T} + \ln(n_j/N) + \ln(P/P_o) + \sum_{i=1}^l \pi_i a_{ij} = 0 \quad j = 1, \dots, n \quad (3.91)$$

where the dimensionless Lagrange multiplier, π_i , is

$$\pi_i = \lambda_i / R_u T \quad (3.92)$$

To determine the equilibrium composition using the Lagrange multiplier approach, we have to solve a set of $n + l + 1$ equations. For a given temperature and pressure (T, P), Equation 3.91 is a set of n equations for the n unknowns n_j , l unknowns π_i , and N . Equation 3.85 provides an additional l equation and we close the set with

$$N = \sum_{j=1}^n n_j \quad (3.93)$$

Once the composition of the products has been determined, we can now compute the thermodynamic properties of the equilibrium mixture. Recall that any two of the independent properties T, P, H, S, U , and V specify the thermodynamic state. For example, for constant pressure combustion, the enthalpy is known instead of the temperature. For this case, we include an equation for the known enthalpy to our set of equations,

$$H = \sum_{j=1}^n n_j \bar{h}_j \quad (3.94)$$

For an isentropic compression or expansion, or expansion to a specified pressure, the entropy is given instead of enthalpy or temperature. In this case, we have

$$S = \sum_{j=1}^n n_j (\bar{s}_j^0 - R_u \ln(n_j/N) - R_u \ln(P/P_o)) \quad (3.95)$$

Finally, if in any case specific volume rather than pressure is known, then we have to minimize the Helmholtz free energy. In this case, a similar analysis (Gordon and McBride, 1994) shows that Equation 3.91 is replaced by

$$\frac{\mu_j^0}{R_u T} + \ln(n_j/N) + \ln(RT/P_o v) + \sum_{i=1}^l \pi_i a_{ij} = 0 \quad j = 1, \dots, n \quad (3.96)$$

For constant volume combustion, the internal energy is known, so we include

$$U = \sum_{j=1}^n n_j (\bar{h}_j - R_u T) \quad (3.97)$$

For an isentropic expansion or compression to a specified volume v , we include

$$S = \sum_{j=1}^n n_j (\bar{s}_j^0 - R_u \ln(n_j/N) - R_u \ln(RT/P_o v)) \quad (3.98)$$

Solution of these problems for practical application requires numerical iteration on a computer. Fortunately, there are now several computer programs available. Thermodynamic properties and equilibrium compositions can be computed using a classic NASA program called CEA (Chemical Equilibrium with Applications), Gordon and McBride (1994). This program uses the minimization of Gibbs free energy approach for computation of the equilibrium composition of reacting species.

Results illustrating composition shifts with temperature and equivalence ratio are given in Figures 3.2 and 3.3 for the combustion of C_8H_{18} at $P = 50$ bar. Composition as a function of temperature is shown in Figure 3.2. The largest mole fractions are N_2 , H_2O , and CO_2 . At this pressure, the composition predicted using Table 3.4 is a good approximation for

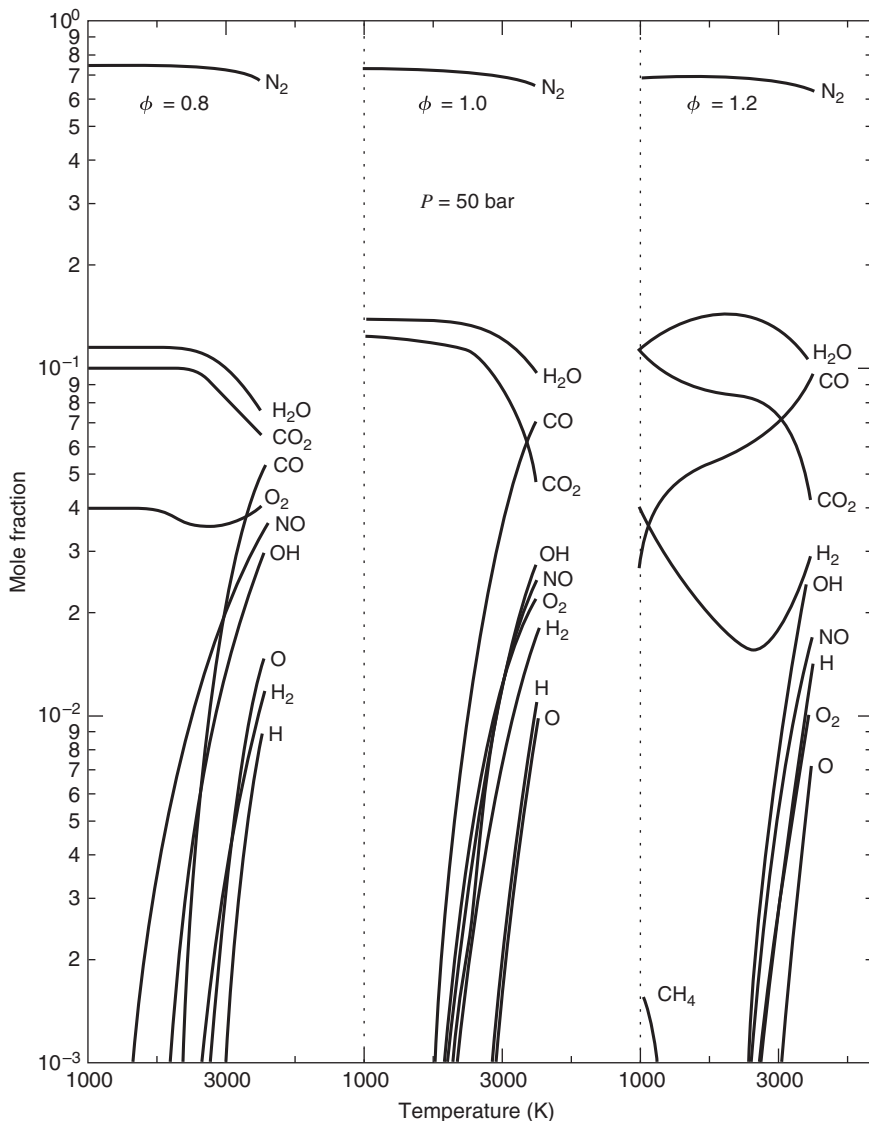


Figure 3.2 Equilibrium composition of octane (C_8H_{18})-air mixtures for different temperatures at $\phi = 0.8, 1.0$, and 1.2 .

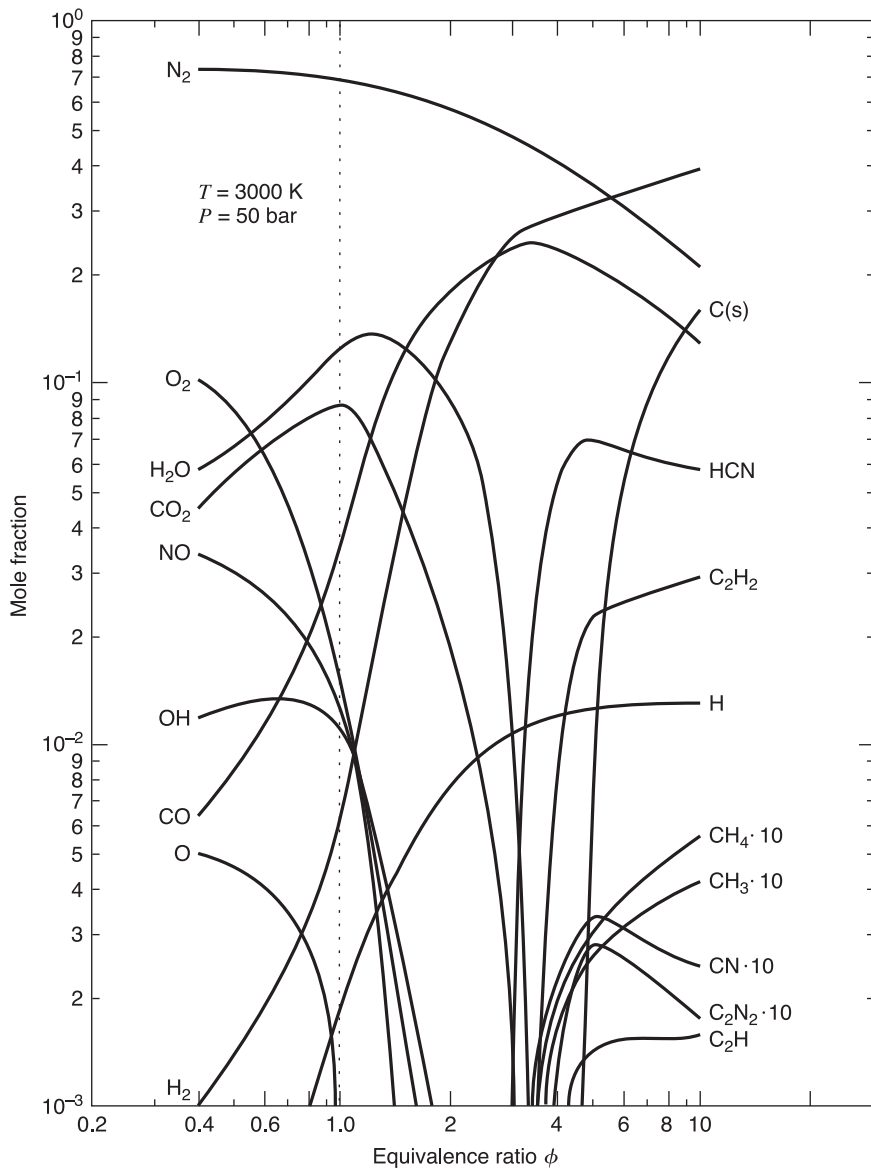


Figure 3.3 Equilibrium composition of octane (C_8H_{18})–air mixtures as a function of ϕ at $T = 3000\text{ K}$, and $P = 50\text{ bar}$.

temperatures less than about 2000 K. At lower pressures, dissociation is even greater, so that at atmospheric pressure, Table 3.6 is valid for temperatures less than about 1500 K. As the reaction temperature is increased above 1500 K, there is an exponential rise in product species such as CO, NO, OH, O_2 , O, H_2 , and H. For lean ($\phi < 1$) conditions, the O_2 fraction is relatively insensitive to temperature. For rich conditions, the H_2 mole fraction first decreases, then increases with increasing temperature.

Notice that at high temperatures there is a significant amount of nitric oxide (NO). If any gas in an engine cylinder is raised to these high temperatures, that gas will tend toward equilibrium at a rate determined by chemical kinetics. Since the chemistry for most

species that contribute to the thermodynamic properties is fast enough relative to engine time scales, in many cases local equilibrium may be assumed. Nitric oxide, however, is significant even though its concentrations are relatively low because it is an air pollutant. Unlike the species of thermodynamic importance, its chemistry is not fast enough to assume that it is in equilibrium concentrations. Likewise, once formed, its concentration “freezes” during the expansion stroke so that even in the low temperature exhaust gases nitric oxides are found. This will be discussed more fully when we deal with emissions.

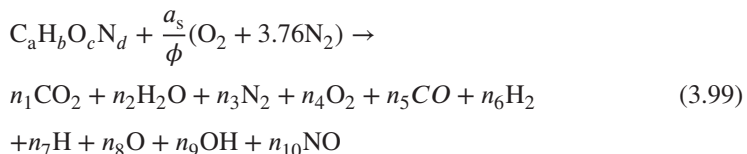
Composition as a function of equivalence ratio is illustrated in Figure 3.3. The mole fraction behavior relative to equivalence ratio is complex. The results show the general trends expected from Figure 3.4 and Table 3.6. The product species CO and H₂ generally increase with equivalence ratio, while the O₂, NO, OH, and O mole fractions decrease.

If the equivalence ratio ϕ is greater than about 4, the product species list becomes quite large and includes solid carbon, C(s); hydrogen cyanide, HCN; acetylene, C₂H₂; and methane, CH₄. Thus, if anywhere in the cylinder there are fuel air pockets where $\phi > 3$, such as in diesel or stratified charge engines, there will be a tendency for these species to form. Similar to nitric oxides, their concentration may freeze when mixed with leaner pockets or when the temperature drops, so these species can appear in the exhaust. For example, with diesel engines, even though the engine is running lean, the maximum power is limited by the appearance of solid carbon (smoke and soot) in the exhaust.

3.7 CHEMICAL EQUILIBRIUM USING EQUILIBRIUM CONSTANTS

This section presents a numerical solution for the properties of equilibrium combustion products based on an equilibrium constant method applied by Olikara and Borman (1975) to the gas phase products of combustion of hydrocarbon fuels. The use of equilibrium constants is also based on the minimization of the Gibbs free energy of the gas mixture; however, it is algebraically less complex than the Lagrange multiplier approach when considering restricted species lists. The equilibrium constant method does require however, that equilibrium reactions, such as the water–gas reaction given by Equation 3.67, be specified.

A more complete reaction calculation, such as done in the previous section, needs to be performed first to determine the significant product species to include in the equilibrium constant analysis. Inspection of Figures 3.2 and 3.3 shows that if $\phi < 3$, the only product species of importance resulting from dissociation are O, H, OH, and NO. Therefore, the species list in Equation 3.81 can be terminated at $i = 10$; that is, we need to consider only 10 species. Therefore, let us consider the following reaction:



Atom balancing yields the following four equations:

$$\begin{aligned} \text{C : } \quad a &= (y_1 + y_5) N \\ \text{H : } \quad b &= (2y_2 + 2y_6 + y_7 + y_9) N \\ \text{O : } \quad c + 2a_s/\phi &= (2y_1 + y_2 + 2y_4 + y_5 + y_8 + y_9 + y_{10}) N \\ \text{N : } \quad d + 7.52a_s/\phi &= (2y_3 + y_{10}) N \end{aligned} \quad (3.100)$$

where N is the total number of moles. By definition, the mole fractions sum to 1:

$$\sum_{i=1}^{10} y_i = 1 \quad (3.101)$$

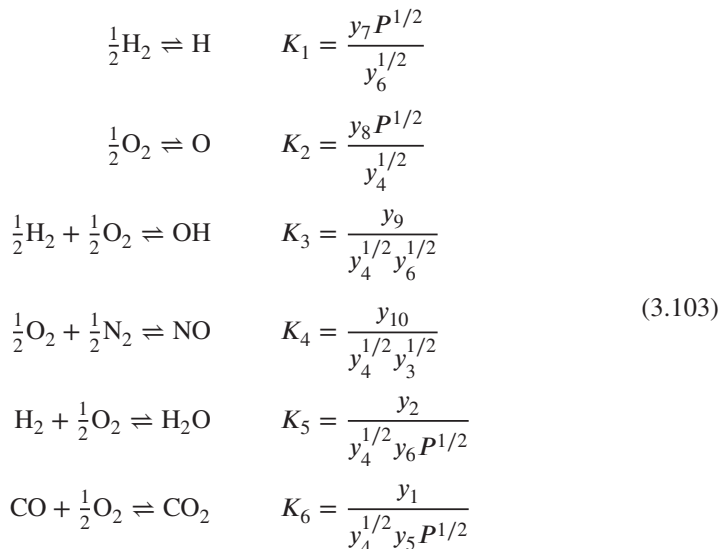
From these equations, three constants are defined:

$$\begin{aligned} d_1 &= \frac{b}{a} \\ d_2 &= \frac{c}{a} + 2 \frac{a_s}{\phi a} \\ d_3 &= \frac{d}{a} + \frac{7.52a_s}{\phi a} \end{aligned}$$

Upon substitution into the atom balance equations, and with some rearrangement,

$$\begin{aligned} 2y_2 + 2y_6 + y_7 + y_9 + d_1y_1 - d_1y_5 &= 0 \\ 2y_1 + y_2 + 2y_4 + y_5 + y_8 + y_9 + y_{10} - d_2y_1 - d_2y_5 &= 0 \\ 2y_3 + y_{10} - d_3y_1 - d_3y_5 &= 0 \\ \sum y_i &= 1 \end{aligned} \quad (3.102)$$

We now introduce six gas-phase equilibrium reactions. These reactions include the dissociation of hydrogen, oxygen, water, and carbon dioxide, and the formation of OH and NO:



The unit of pressure in the above six equations is in units of atmospheres (atm). Note that the water-gas shift reaction, given by Equation 3.67, is represented by the last two reaction equations for K_5 and K_6 . Olikara and Borman (1975) have curve fitted the equilibrium constants $K_i(T)$ to JANAF Table data for the temperature range $600 < T < 4000$ K. Their expressions are of the form

$$\log_{10} K_i(T) = A_i \ln(T/1000) + \frac{B_i}{T} + C_i + D_i T + E_i T^2 \quad (3.104)$$

Table 3.7 Equilibrium Constant K_i Curve-Fit Coefficients

K_i	A_i	B_i	C_i	D_i	E_i
K_1	+0.432168E + 00	-0.112464E + 05	+0.267269E + 01	-0.745744E - 04	+0.242484E - 08
K_2	+0.310805E + 00	-0.129540E + 05	+0.321779E + 01	-0.738336E - 04	+0.344645E - 08
K_3	-0.141784E + 00	-0.213308E + 04	+0.853461E + 00	+0.355015E - 04	-0.310227E - 08
K_4	+0.150879E - 01	-0.470959E + 04	+0.646096E + 00	+0.272805E - 05	-0.154444E - 08
K_5	-0.752364E + 00	+0.124210E + 05	-0.260286E + 01	+0.259556E - 03	-0.162687E - 07
K_6	-0.415302E - 02	+0.148627E + 05	-0.475746E + 01	+0.124699E - 03	-0.900227E - 08

where T is in Kelvin. The equilibrium constant K_i curve-fit coefficients are listed in Table 3.7. Given pressure P , temperature T , and equivalence ratio ϕ , Equations 3.100, 3.101, and 3.103 will yield eleven equations for the eleven unknowns: the ten unknown mole fractions y_i and the unknown total product moles N .

Substitution of the six individual equilibrium reaction equations into the atom balance equations results in four equations in four unknowns (y_3, y_4, y_5, y_6). These four equations are solved numerically in the Equilibrium Combustion Solver program `eCP.m`, which is listed in Appendix F.11. The program computes the product mole fractions and properties for five representative fuels given the mixture pressure, temperature, and the fuel-air equivalence ratio. The fuels are identified with the following `fuel_id`, from 1–5:

1. Methane CH_4
2. Gasoline C_7H_{17}
3. Diesel $\text{C}_{14.4}\text{H}_{24.9}$
4. Methanol CH_3OH
5. Nitromethane CH_3NO_2

With the mixture mole fraction composition known, one can then proceed to compute the thermodynamic properties of interest: enthalpy, entropy, specific volume, internal energy, and specific heat for the given conditions. A reacting mixture of ideal gases has an enthalpy dependent on temperature and pressure, and computing the mixture equilibrium specific heat c_p requires the change in mole fraction due to a change in temperature, so as discussed earlier in this chapter, the mole fraction partial derivatives $\partial y_i / \partial P$ and $\partial y_i / \partial T$ are also computed. The use of the program is detailed in the following example.

EXAMPLE 3.5 Equilibrium Combustion Mole Fraction

What are the mole fractions and mixture properties resulting from the combustion of a gasoline (`fuel_id = 2`) mixture at a temperature $T = 3000$ K, pressure $P = 5000$ kPa, and a fuel-air equivalence ratio $\phi = 0.8$?

SOLUTION The computation is performed using the Equilibrium Combustion Solver input–output program `RunEcp.m` with inputs T , P , ϕ , and `fuel.id`. As detailed in Appendix F.10, the program `RunEcp.m` calls the function `eCP.m`, which in turn calls the functions `fuel.m` for fuel properties and `farg.m` for initial guess values of mixture properties, then iterates for converged property values, and finally outputs the mole fractions and mixture properties.

```

Program RunEcp.m
Input parameters to ecp
T = 3000;      % temperature (K)
P = 5000;      % pressure (kPa)
phi = 0.8;      % equivalence ratio
fuel_id = 2;    % gasoline fuel identifier
% call function ecp
function [ierr,y,h,u,s,v,r, cp,mw,dvdt,dvdp] =
    ecp(T, P, phi, fuel_id);
...

```

The resulting mole fractions and properties are listed below. Note that the equilibrium mole fractions calculated with the equilibrium constant model compare well with the mole fractions of Figure 3.2 computed by the more general Lagrange multiplier method.

```

Equilibrium Combustion Solver Output
Mole Fractions
CO2 = 0.0775
H2O = 0.1064
N2 = 0.7203
O2 = 0.0359
CO = 0.0191
H2 = 0.0036
H = 0.0013
O = 0.0030
OH = 0.0133
NO = 0.0196

Mixture Properties
h(kJ/kg) = 1640.4
u(kJ/kg) = 751.5
s (kJ/Kg K) = 8.941
v (m3/kg) = 0.178
cp (kJ/Kg K) = 2.511
Molecular Mass = 28.06
dvdt = 6.81e-05
dvdp = -3.56e-05

```

The Equilibrium Combustion Solver program can be used to compute general trends for fuel-air combustion that are not immediately obvious. The effect of temperature on enthalpy of the combustion products for three different equivalence ratios is shown in Figure 3.4 for the combustion of gasoline at a pressure of 101.3 kPa. Note that the lowest value of enthalpy occurs at a stoichiometric equivalence ratio, and as the equivalence ratio is made lean or rich, below 2500 K, the enthalpy increases. The Equilibrium Combustion

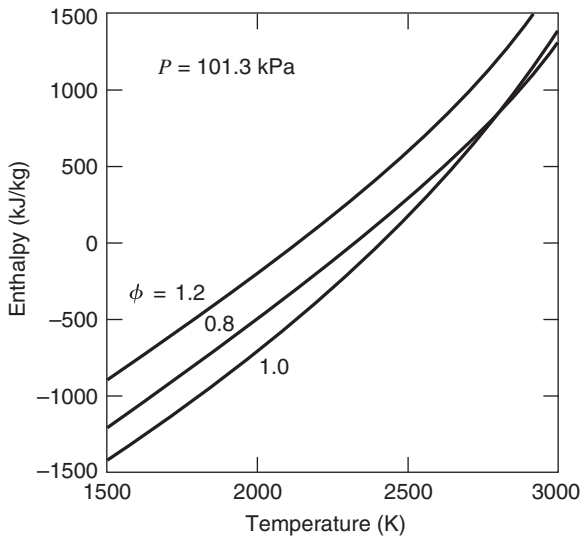


Figure 3.4 Enthalpy of combustion products for a gasoline–air equilibrium mixture for different temperatures at $P = 101.3$ kPa.

Solver program has been extended to include a wider variety of fuels, Buttsworth (2002).

This behavior is also shown in Figure 3.5, a plot of the enthalpy of the combustion products of methanol versus equivalence ratio at pressures of 101 kPa and 2000 kPa. The enthalpy is a minimum at near stoichiometric conditions, as on either side of stoichiometric, the combustion is incomplete. If the mixture is lean, there is an excess of unburnt oxygen. If the mixture is rich, there will be unburnt carbon monoxide. A minimal value of enthalpy implies that the specific heat of the combustion products is also a minimum, which will maximize the adiabatic flame temperature, discussed in Chapter 4.

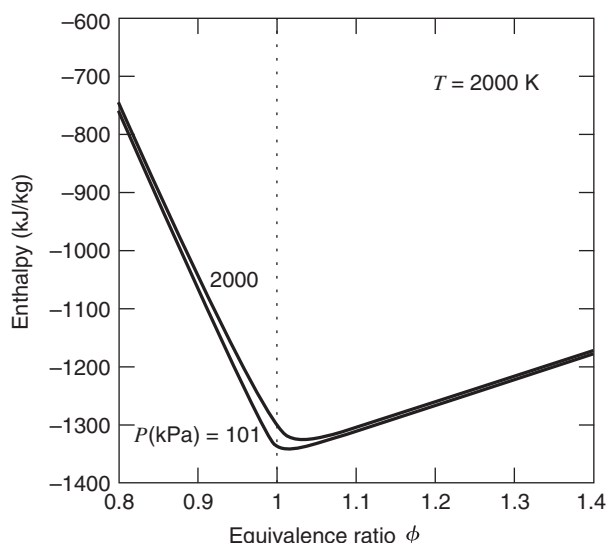


Figure 3.5 Enthalpy of combustion products of a methanol–air equilibrium mixture for different ϕ at $T = 2000$ K.

3.8 REFERENCES

- BUTTSWORTH, D. (2002), "Spark Ignition Internal Combustion Engine Modeling using Matlab," Report TR-2002-2, Univ. Southern Queensland, Toowoomba, Australia.
- CHASE, M. (1998), NIST - JANAF Thermochemical Tables, 4th edition, *J. Chemical and Physical Reference Data*, Monograph No. 9, NIST, Gaithersburg, Maryland, web: <http://www.kinetics.nist.gov/>.
- CRC Handbook of Chemistry and Physics (2012–2013), 93th ed., CRC Press, Cleveland, Ohio, web: <http://www.hbcpnetbase.com/>.
- GORDON, S. and B.J. MCBRIDE (1994), "Computer Program for Calculation of Complex Chemical Equilibrium Composition, and Applications," NASA RP-1311.
- MCBRIDE B., S. GORDON, and M.A. RENO (1993), "Coefficients for Calculating Thermodynamic and Transport Properties of Individual Species," NASA Report TM-4513.
- MCBRIDE B., M. ZEHE, and S. GORDON (2002), "NASA Glenn Coefficients for Calculating Thermodynamic Properties of Individual Species," NASA TP-2002-211556.
- OLIKARA, C. and G. L. BORMAN (1975), "A Computer Program for Calculating Properties of Equilibrium Combustion Products with Some Applications to I.C. Engines," SAE paper 750468.
- ROSSINI, E D. (1953), *Selected Values of Physical and Thermodynamic Properties of Hydrocarbons and Related Compounds*, Carnegie Press, Pittsburgh.
- STULL, D. R., E. F. WESTRUM, Jr., and G. C. Singe (1969), *The Chemical Thermodynamics of Organic Compounds*, Wiley, New York.
- VARGAFTIK, N. B. (1975), *Tables on the Thermophysical Properties of Liquids and Gases*, Wiley, New York.

3.9 HOMEWORK

- 3.1** What is the molecular weight, enthalpy (kJ/kg), and entropy (kJ/(kg K)) of a gas mixture at $P = 1000$ kPa and $T = 1000$ K, if the mixture contains the following species and mole fractions?

Species	y_i
CO_2	0.10
H_2O	0.15
N_2	0.70
CO	0.05

- 3.2** What is the enthalpy (kJ/kg) and entropy (kJ/(kg K)) of a mixture of 30% H_2 and 70% CO_2 by volume at a temperature of 3000 K and pressure of 2000 K?
- 3.3** Using the Gordon and McBride equations, Equations 3.38 and 3.39, calculate the enthalpy \bar{h} and standard entropy \bar{s}° of CO_2 and compare with the gas table values used in Example 3.1.
- 3.4** Using the program Fuel.m, at what temperature is the specific heat c_p of methane $\text{CH}_4 = 3.0$ kJ/(kg K)?
- 3.5** Why does Equation 3.27 contain y_i ?
- 3.6** A system whose composition is given below is in equilibrium at $P = 101$ kPa and $T = 298$ K. What is the enthalpy (kJ/kg), specific volume (m^3/kg), and quality χ of the mixture?

Species	y_i
CO ₂	0.125
H ₂ O	0.141
N ₂	0.734

- 3.7** A four-cylinder four-stroke 2.8 L port injected spark ignition engine is running at 2000 rpm on a lean ($\phi = 0.9$) mixture of octane and standard air (101 kPa, 298 K). If the octane flow rate is 2.5 g/s, what is the mass of fuel entering each cylinder per cycle and the volumetric efficiency?
- 3.8** An engine cylinder has a 90 mm bore and a 85 mm stroke, and contains air and residual gases at 350 K and 1 bar. If the engine is to operate on diesel fuel and run lean with an overall equivalence ratio of $\phi = 0.7$, what is the mass of diesel fuel that needs to be injected during the compression stroke? Assume $f = 0.015$, where f is the ratio of the residual mass m_r to the cylinder mass m prior to fuel injection, and the gas constant R of the air–residual gas mixture = 0.29 kJ/(kg K).
- 3.9** Using the low-temperature combustion equations, what are the composition, enthalpy, and entropy of the combustion products of methanol, CH₃OH, at $\phi = 1.1$, $T = 1200$ K, and $P = 101$ kPa? Compare with the results from the program ecp.m.
- 3.10** What are the mole fractions of CO₂, H₂O, CO, N₂, and H₂ produced when methane (CH₄) is burned in rich conditions at $\phi = 1.1$, $T = 1000$ K, and $P = 101$ kPa?
- 3.11** If a lean ($\phi = 0.8$) mixture of methane CH₄ is burned at a temperature of 1500 K and pressure of 500 kPa, what are the mole fractions of the products, and the product enthalpy, entropy, and specific heat? Use the program ecp.m.
- 3.12** (a) At what temperature is the saturation pressure P_{sat} of octane equal to 0.5 bar? At that temperature, what is the enthalpy of vaporization \bar{h}_{fg} ?
 (b) Repeat the calculations for tetradecane.
- 3.13** Compare the enthalpies of vaporization \bar{h}_{fg} (MJ/kg) of nitromethane, methanol, octane, and tetradecane at 400 K. What is an advantage of a high enthalpy of vaporization for an engine fuel?
- 3.14** A rich ($\phi = 1.1$) mixture of diesel fuel is burned at a temperature of 2000 K and pressure of 750 kPa. Using the program ecp.m, (a) What are the mole fractions of the products, and the product enthalpy, entropy, specific volume, and specific heat? (b) Repeat the calculation for $\phi = 1.25$. Discuss the effect of equivalence ratio.
- 3.15** Using the program ecp.m, plot the product equilibrium mole fractions as a function of equivalence ratio ($0.5 < \phi < 2$) resulting from the combustion of methane at 5000 kPa and 2500 K.
- 3.16** Derive Equations 3.74 and 3.75 for the species mole fractions of a mixture of air and residual gas.
- 3.17** At what equivalence ratio for octane–air mixtures does the carbon to oxygen ratio of the system equal one? Why is this of interest?
- 3.18** At what temperature is the concentration of H₂ a minimum for the combustion of gasoline and air at $\phi = 1.2$ and 4500 kPa? What is the minimum value of H₂?

- 3.19** At what equivalence ratio is the concentration of OH a maximum for the combustion of diesel and air at $T = 2500$ K and 4500 kPa? What is the maximum value of OH?
- 3.20** At what temperature does the mole fraction of NO reach 0.010 for the equilibrium products resulting from the combustion of gasoline and air at $\phi = 1.0$ and 5000 kPa?
- 3.21** At what temperature does the mole fraction of CO reach 0.080 for the equilibrium products resulting from the combustion of methane and air at $\phi = 1.1$ and 3000 kPa?
- 3.22** What is the equilibrium and the frozen specific heat c_p of the combustion products of gasoline at a pressure of 2000 kPa and temperature of 2000 K burned at (a) an equivalence ratio of 1.1, and (b) an equivalence ratio of 0.9?

Chapter 4

Fuel–Air Combustion Processes

4.1 INTRODUCTION

In this chapter, we apply the first law of thermodynamics to fuel–air combustion processes in a control volume, and compute the change in state, and the work and heat interactions between the fuel–air mixture and the environment. Using equilibrium combustion modeling, we are able to determine the product equilibrium state and thermodynamic properties that result from burning a fuel–air mixture as a function of initial conditions, such as pressure, temperature, equivalence ratio, and residual fraction. We introduce the heat of combustion, the adiabatic flame temperature, and then examine isentropic processes of a fuel–air mixture. A second law analysis is performed to introduce maximum work and exergy, and determine the first and second law efficiencies.

A set of fuel–air cycle computer models, including a closed system Otto cycle, a four-stroke open system Otto cycle, and a homogeneous two-zone finite energy release model are developed in this chapter. With these models, more realism is introduced into engine performance modeling, as the models are able to address the effects of parameters such as equivalence ratio, compression ratio, intake/exhaust pressure ratio, and residual fraction on net work, imep, and thermal efficiency.

4.2 COMBUSTION AND THE FIRST LAW

With chemical equilibrium modeling, we are able to predict the equilibrium state that results from burning a fuel–air mixture as a function of initial conditions, such as pressure, temperature, equivalence ratio, and residual fraction. In this and the next section, we apply the first law of thermodynamics to fuel–air combustion processes, and compute energy interactions between the fuel–air mixture and the environment. We discuss constant pressure and constant volume combustion to illustrate the principles, and introduce the heat of combustion and the adiabatic flame temperature.

Let us first consider the case in which combustion occurs at constant pressure. Suppose that the reactants consisting of fuel, air, and residual gases are premixed to a homogeneous state and burned in a combustion system. Application of the closed system first law to this combustion process leads to

$$Q - W = U_p - U_r \quad (4.1)$$

Since the process is constant pressure, $W = P\Delta V$, and since $H = U + PV$, we have

$$Q = H_p - H_r \quad (4.2)$$

where the subscript p represents products, and the subscript r represents reactants. The enthalpy of the products is equal to the enthalpy of the reactants minus any heat transferred out of the system.

For an open combustion system, we adopt a control volume approach. The control volume energy equation indicates that the enthalpy of the products is equal to the enthalpy of the reactants plus any heat transferred *into* the system, minus the shaft work *out* of the system.

Heat of Combustion

The heat of combustion or heating value, q_c , of a fuel is defined as the heat energy transferred out of a system per unit mass or mole of fuel when the initial and final states are at the reference temperature and pressure, $T_o = 298.15$ K and $P_o = 101$ kPa. The number of moles in the system is not constant during a combustion change of state. By convention, the heat transferred out of a system is negative, and the heat of combustion is a positive number, that is, $q_c = -Q$, so

$$q_c = H_r - H_p \quad (4.3)$$

An analogous discussion could be presented for constant volume combustion where $W = P\Delta V = 0$ and

$$q_c = U_r - U_p \quad (4.4)$$

However, as a rule of thumb, when the heat of combustion referred to without qualification, constant pressure combustion is implied.

Furthermore, the combustion is assumed to be complete, with the fuel burning to carbon dioxide and water. Since the products are at low temperature ($T_o < 1000$ K), the analyses that led to Table 3.6 for the lean or stoichiometric case can be used to compute the heat of combustion q_c . In this case, it can be shown that Equation 4.3 becomes

$$\begin{aligned} q_c &= \sum_i n_{r,i} \bar{h}_{r,i} - \sum_i n_{p,i} \bar{h}_{p,i} \\ &= 1 \times \bar{h}_{fuel} - n_{CO_2} \bar{h}_{CO_2} - n_{H_2O} [\bar{h}_{H_2O} - (1 - \chi) \bar{h}_{fg,H_2O}] \quad (\text{kJ/kmol}_{fuel}) \end{aligned} \quad (4.5)$$

since the enthalpies of oxygen O_2 and nitrogen N_2 are assigned to be zero at the reference temperature $T_o = 298.15$ K.

Two values of q_c are recognized (1) the lower heat of combustion q_{lhc} is defined as the state where all of the water in the products is vapor (the quality $\chi = 1$), and (2) the higher heat of combustion, q_{hhc} is defined as the state where all of the water in the products is liquid (the quality $\chi = 0$). If the water quality is not specified, one usually assumes that $q_c = q_{lhc}$.

The lower q_{lhc} and higher heat of combustion q_{hhc} of several gaseous and liquid fuels are given in Table 4.1. The heat of combustion is used primarily in two ways (1) in some cases, such as in the gas cycles of Chapter 2 or when solving reacting Navier–Stokes equations, it is desirable to relax the rigor of the thermodynamics by using the heat of combustion to define an equivalent energy release; and (2) for practical fuels, as discussed in Chapter 10, the enthalpy at $T_o = 298.15$ K can be determined inexpensively by measurement of the heat of combustion. Table 4.1 also lists \bar{h}_f^o , the enthalpy of

Table 4.1 Enthalpy of Formation, Entropy, Lower/Higher Heat of Combustion, and Maximum Available Energy of Combustion¹

Fuel		\bar{h}_f^o (MJ/kmol)	\bar{s}_{298}^o (kJ/(kmol K))	q_{lhc} (MJ/kg)	q_{hhc} (MJ/kg)	a_o (MJ/kg)
CH ₄ (g)	Methane	-74.9	186.2	50.01	55.5	52.42
C ₃ H ₈ (g)	Propane	-103.9	269.9	46.36	50.3	49.16
C ₇ H ₁₇ (l)	Gasoline ²	-305.6	345.8	44.51	47.87	
C ₈ H ₁₈ (l)	Octane	-249.96	360.8	44.43	47.9	47.67
C _{14.4} H _{24.9} (l)	Diesel ²	-174.0	525.9	42.94	45.73	
C ₁₅ H ₃₂ (l)	Pentadecane	-428.9	587.5	43.99	47.3	47.22
CH ₄ O (l)	Methanol	-239.1	126.8	19.91	22.7	22.68
C ₂ H ₆ O (l)	Ethanol	-277.2	160.7	26.82	29.7	29.71
CH ₃ NO ₂ (l)	Nitromethane	-113.1	171.8	10.54	11.6	12.43
H ₂ (g)	Hydrogen	0.0	130.6	119.95	141.6	119.52
C ₂ H ₂ (g)	Acetylene	226.7	200.8	48.22	49.9	48.58
C ₂ N ₂ (g)	Cyanogen	309.1	241.5	21.06	21.0	21.29
NH ₃ (g)	Ammonia	-45.7	192.6	18.61	22.5	20.29
C ₆ H ₆ (l)	Benzene	48.91	173.0	40.14		42.14
C ₁₀ H ₈ (s)	Naphthalene	78.1	166.9	38.86	40.3	40.84
C (s)	Graphite	0.0	5.7	32.76		33.70
C ₁₇₆ H ₁₄₄ O ₈ N ₃ (s)	Coal ²	-10,000.0	3000.0	31.57		33.57

¹Based on equilibrium water quality, lean combustion at $\phi = 0.01$, $T_o = 298$ K, $P_o = 1.013$ bar and unmixed reactants.

²Estimated for typical fuel.

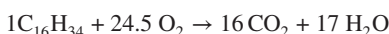
formation, \bar{s}_{298}^o , the absolute entropy at 298 K, and a_o , the maximum available energy of combustion.

EXAMPLE 4.1 Heat of Combustion

Compare the lower, q_{lhc} , and higher, q_{hhc} , heat of combustion of cetane C₁₆H₃₄ to the heat released q_{eq} with equilibrium water quality products.

SOLUTION Assume standard reference conditions $P = P_o = 1$ atm and $T_o = 298.15$ K for reactants and products, and the air and fuel enter unmixed. The molecular mass M of cetane is 226.4. As shown in Appendix E.6, the equilibrium water quality χ_{eq} for this reaction is 0.208. The nitrogen enthalpy is zero for both the reactants and products, and is not included in the energy equation computation.

The stoichiometric combustion equation per mole of cetane is



The first law, Equation 4.3, per kmol of fuel, is

$$\begin{aligned}\bar{q}_c &= \sum_i n_{r,i} \bar{h}_{r,i} - \sum_i n_{p,i} \bar{h}_{p,i} \\ &= 1 \times \bar{h}_{fuel} - n_{\text{CO}_2} \bar{h}_{\text{CO}_2} - n_{\text{H}_2\text{O}} [\bar{h}_{\text{H}_2\text{O}} - (1 - \chi) \bar{h}_{fg, \text{H}_2\text{O}}] \\ &= +1(-373.34) - 16(-393.52) - 17[(-241.83 - (1 - \chi)(43.99))]\end{aligned}$$

$$= +10,034 + (747.8)(1 - \chi) \text{ (MJ/kmol)}$$

Therefore,

$$q_{\text{lh}} = \frac{\bar{q}_c(\chi = 1)}{M} = 10,034/226.4 = 44.4 \text{ MJ/kg}$$

$$q_{\text{eq}} = \frac{\bar{q}_c(\chi = 0.208)}{M} = 10,624/226.4 = 47.0 \text{ MJ/kg}$$

$$q_{\text{hh}} = \frac{\bar{q}_c(\chi = 0)}{M} = 10,782/226.4 = 47.7 \text{ MJ/kg}$$

Adiabatic Flame Temperature

Another useful combustion parameter is the adiabatic flame temperature T_f . It is defined as the temperature of the combustion products when completely burned with no shaft work ($W = 0$) or heat transfer ($Q = 0$) to the surroundings. The adiabatic flame temperature represents the maximum temperature of a combustion process, since any heat transfer from the reaction and incomplete combustion will lower the temperature of the products.

For constant pressure combustion, the first law is

$$H_p = H_r \quad (4.6)$$

The initial state of the reactants is assumed to be at the reference temperature and pressure, $T_o = 298.15 \text{ K}$ and $P_o = 101 \text{ kPa}$. Since the product temperature is generally unknown in first law combustion calculations, iteration with an initial temperature estimate is required to determine the product mixture enthalpy. An assumption also needs to be made about the amount of dissociation in the combustion products. The adiabatic flame temperature with dissociation of the combustion products will be less than the computed value for combustion without dissociation.

For constant volume combustion, the first law of thermodynamics with no work ($W = 0$) or heat transfer ($Q = 0$) to the surroundings is

$$U_p = U_r \quad (4.7)$$

The constant volume adiabatic flame temperature is greater than the constant pressure adiabatic flame temperature since the pdV work is zero in a constant volume process. The stoichiometric adiabatic flame temperature of several fuels is listed in Table 4.2. The results tabulated assume reference conditions of $T_o = 298.15 \text{ K}$, $P_o = 101 \text{ kPa}$, $f = 0$, and $\phi = 1.0$. There is little dependence on fuel type among the hydrocarbons, which have adiabatic flame temperatures of about 2250 K. Note that operating engines will have a larger T_o , and a corresponding larger adiabatic flame temperature.

EXAMPLE 4.2 Adiabatic Flame Temperature

A stoichiometric mixture of gasoline C₇H₁₇, air, and residual gas is burned at constant pressure. Given that $T_1 = 298 \text{ K}$, $P_1 = 101.3 \text{ kPa}$, and $f = 0.10$, what is the constant pressure adiabatic flame temperature?

SOLUTION Appendix F.12 contains a listing of the program `AdiabaticFlameTemp.m` that computes the constant pressure adiabatic flame temperature. The program uses the fuel-air-residual gas routine `farg.m`, the equilibrium combustion routine `eCP.m` detailed in the previous chapter, and Newton-Raphson iteration for constant pressure, with inputs the

Table 4.2 Stoichiometric Adiabatic Flame Temperature of Various Fuels

Formula	Fuel	T_f (K)
CH_4 (g)	Methane	2227
C_3H_8 (g)	Propane	2268
C_8H_{18} (l)	Octane	2266
$\text{C}_{15}\text{H}_{32}$ (l)	Pentadecane	2269
$\text{C}_{20}\text{H}_{40}$ (g)	Eicosane	2291
CH_4O (l)	Methanol	2151
$\text{C}_2\text{H}_6\text{O}$ (l)	Ethanol	2197
CH_3NO_2 (l)	Nitromethane	2545
H_2 (g)	Hydrogen	2383
C_2N_2 (g)	Cyanogen	2596
NH_3 (g)	Ammonia	2076
C_2H_2 (g)	Acetylene	2540
C_{10}H_8 (s)	Naphthalene	2328

$P_0 = 1.0 \text{ atm}$, $T_0 = 298.15 \text{ K}$, $f = 0.0$

pressure P , initial temperature T , fuel–air equivalence ratio ϕ , and residual mass fraction f . The available fuel types are methane (CH_4), gasoline (C_7H_{17}), diesel ($\text{C}_{14.4}\text{H}_{24.9}$), methanol (CH_3OH), and nitromethane (CH_3NO_2).

The above information is entered into the program as shown below:

```
% Computes const pressure adiabatic flame temperature
% Inputs:
T1 = 298;% initial temperature (K)
P1 = 101.3; % initial pressure (kPa)
PHI = 1.1; % equivalence ratio
f = 0.1; % residual fraction
ifuel=2; % 1=Methane, 2=Gasoline, 3=Diesel, 4=Methanol, ...
5=Nitromethane
```

The resulting adiabatic flame temperature is $T = 2094 \text{ K}$.

The effect of equivalence ratio is plotted in Figure 4.1, which indicates that the adiabatic flame temperature is maximum near stoichiometric. This is consistent with the effect of equivalence ratio on enthalpy, as shown in the Chapter 3, since mixtures with a relatively lower specific heat will undergo a larger temperature change for a given energy release. Additional calculations show the adiabatic flame temperature decreases with increasing residual fraction, (see homework problem at end of chapter), and slightly increases with pressure. Note that of the fuels plotted, ethanol consistently has the lowest and nitromethane has the greatest adiabatic flame temperature.

Isentropic Processes

In internal combustion engine modeling, we need to determine the change in state due to an assumed isentropic compression or expansion to a specified pressure or specific volume. With a known change from an initial state 1 to a final state 2, the first law for an closed

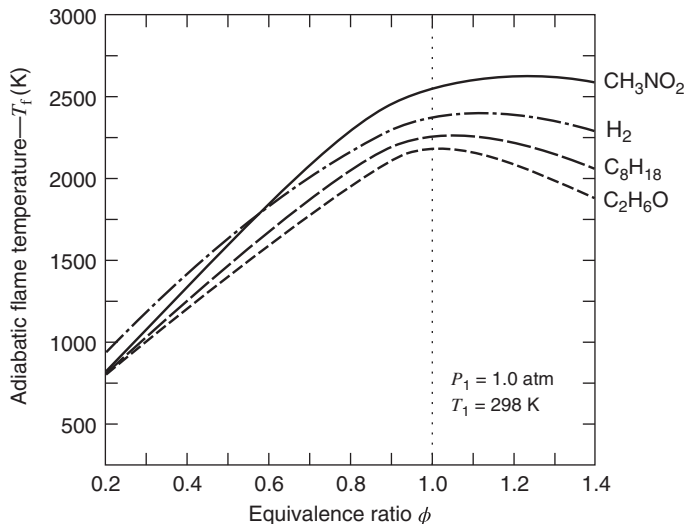


Figure 4.1 Adiabatic flame temperature of some fuels initially at atmospheric pressure and temperature, ($f = 0.0$).

system can be used to determine the work transfer W_{1-2} :

$$-W_{1-2} = U_2 - U_1 \quad (4.8)$$

and for an open system, the first law is

$$-W_{1-2} = H_2 - H_1 \quad (4.9)$$

For a mixture of ideal gases that chemically reacts to changing constraints, such as the volume and pressure relationship in an isentropic process, $pV^\gamma = \text{constant}$, simple algebraic relationships between the initial and final state cannot be derived, and computer solution is required. The equilibrium constant methodologies discussed in the previous sections allow the determination of the properties of mixture of gases given their temperature and pressure, so for an isentropic change of volume where the final temperature is unknown, iteration is required.

Given the heat transferred from a control volume, and the combustion pressure P , we can use Equation 4.2 to solve for the product enthalpy H_p . With two thermodynamic variables, P and H , known, the other properties such as the temperature T , specific volume v , and internal energy U of the products can also be computed. The equilibrium constant method of Section 3.6 is formulated with the assumption that the product pressure and temperature are known. Since the product temperature is generally unknown in first law combustion calculations, iteration with an initial temperature estimate is required.

EXAMPLE 4.3 Isentropic Fuel-Air Processes

A gasoline fuel-air mixture with $\phi = 0.8$ is initially at $T_1 = 300\text{ K}$, $P_1 = 101.3\text{ kPa}$. The mixture is compressed isentropically to state 2 to pressure $P_2 = 2020\text{ kPa}$. (a) What is the temperature T_2 and the work w_{1-2} ? (b) What is the compression ratio?

SOLUTION Since the engine cylinder volume is a closed system, the first law on a per unit mass of mixture basis for this isentropic process is

$$-w_{1-2} = u_2 - u_1 \quad (4.10)$$

Using the Equilibrium Combustion Solver program RunEcp.m, the mixture properties at state 1 at the beginning of compression are

$$T_1 = 300 \text{ K}$$

$$P_1 = 101.25 \text{ kPa}$$

$$h_1 = -2364 \text{ kJ/kg}$$

$$u_1 = -2451 \text{ kJ/kg}$$

$$s_1 = 7.040 \text{ kJ/kg K}$$

$$v_1 = 0.862 \text{ m}^3/\text{kg}$$

Since the compression is isentropic, $s_2 = s_1 = 7.040 \text{ kJ/(kg K)}$. The pressure at state 2 is known, but the temperature is not, so iteration of the temperature input to the program is needed, keeping entropy constant at $s_2 = s_1 = 7.040 \text{ kJ/(kg K)}$. This procedure results in $T_2 = 660.5 \text{ K}$, $u_2 = -2156 \text{ kJ/kg}$, and $v_2 = 0.095 \text{ m}^3/\text{kg}$. Therefore, the compression work $-w_{1-2}$ is equal to 295 kJ/kg, and the compression ratio r is 9.07.

4.3 MAXIMUM WORK AND THE SECOND LAW

For the purpose of defining engine efficiency with actual fuels, we will need to determine the maximum work that can be done by an engine system as it changes state. The following analysis derives both closed and open system maximum work in terms of the change in exergy.

For a closed system such as the compression stroke of a piston–cylinder system in communication with the environment at T_o , P_o , the first and second laws of thermodynamics for a change in state from 1 to 2 are

$$Q_{1-2} - W_{1-2} = U_2 - U_1 \quad (4.11)$$

$$Q_{1-2} \leq T_o(S_2 - S_1) \quad (4.12)$$

The total work transfer W_{1-2} can be therefore be expressed as

$$W_{1-2} \leq -[(U_2 - U_1) - T_o(S_2 - S_1)] \quad (4.13)$$

if we subtract the work done by the system against the atmosphere, $P_o(V_2 - V_1)$, we obtain the actual work

$$W_{\text{act},1-2} \leq -[(U_2 - U_1) + P_o(V_2 - V_1) - T_o(S_2 - S_1)] \quad (4.14)$$

We define the nonflow exergy A , a property of the system for a fixed T_o , P_o , as

$$A = U + P_oV - T_oS \quad (4.15)$$

and per unit mass,

$$a = u + P_o v - T_o s \quad (4.16)$$

so

$$W_{\text{act},1-2} \leq -(A_2 - A_1) \quad (4.17)$$

Therefore, the maximum work, $W_{\max,1-2}$, that can be done by the system as it changes state from 1 to 2 is the change in the exergy A :

$$W_{\max,1-2} = -(A_2 - A_1) = -[(U_2 - U_1) + P_o(V_2 - V_1) - T_o(S_2 - S_1)] \quad (4.18)$$

and per unit mass,

$$w_{\max,1-2} = -(a_2 - a_1) = -[(u_2 - u_1) + P_o(v_2 - v_1) - T_o(s_2 - s_1)] \quad (4.19)$$

For a compression process, the change in exergy will be positive, since work is performed on the system, for a exothermic combustion process the change in exergy will be negative, due to the change in chemical composition of the system, and for an expansion process, the change in exergy will be negative, since work is performed by the system.

If the system comes to thermal and mechanical equilibrium with the atmosphere during a change in state from 1 to 0, where the subscript 0 represents the final state in equilibrium with the atmosphere, then the maximum work is

$$W_{\max,1-0} = A_1 - A_0 \quad (4.20)$$

Exergy Change for an Isentropic Compression or Expansion

If a change in state for a closed system is isentropic, then Equation 4.19 reduces to

$$a_2 - a_1 = (u_2 - u_1) + P_o(v_2 - v_1) \quad (4.21)$$

For an ideal gas with constant properties, the change in state for an isentropic compression or expansion is

$$Pv^\gamma = \text{constant} \quad (4.22)$$

Using the definition of c_v , we can relate $u_2 - u_1$ to $T_2 - T_1$

$$u_2 - u_1 = c_v(T_2 - T_1) \quad (4.23)$$

and if $r = v_1/v_2$, and $v = RT/P$, then upon substitution into Equation 4.21, the exergy change for an ideal gas undergoing an isentropic compression from state 1 to state 2 is

$$a_2 - a_1 = c_v T_1 \left[(r^{\gamma-1} - 1) + \frac{P_o}{P_1} (\gamma - 1) \left(\frac{1}{r} - 1 \right) \right] \quad (4.24)$$

EXAMPLE 4.4 Isentropic Compression of a Fuel-Air Mixture

What is the exergy change for the isentropic fuel-air compression of Example 4.3?

SOLUTION Since the process is isentropic, $s_2 = s_1$, so

$$\begin{aligned} a_2 - a_1 &= (u_2 - u_1) + P_o(v_2 - v_1) \\ &= -2156 - (-2451) + (101.25)(0.095 - 0.862) \\ &= 217.3 \text{ kJ/kg}. \end{aligned} \quad (4.25)$$

Comment: The change in exergy is less than the isentropic compression work, since we have subtracted the work done against the atmosphere.

Available Energy of Combustion

The appropriate definition of efficiency for any of the gas cycles presented in Chapter 2 is clear, since the efficiency for a gas cycle is defined as the fraction of an “equivalent heat transfer” which is converted to work. When the analysis takes into account that the fuel is burned rather than heat being transferred to produce work, the first law efficiency for

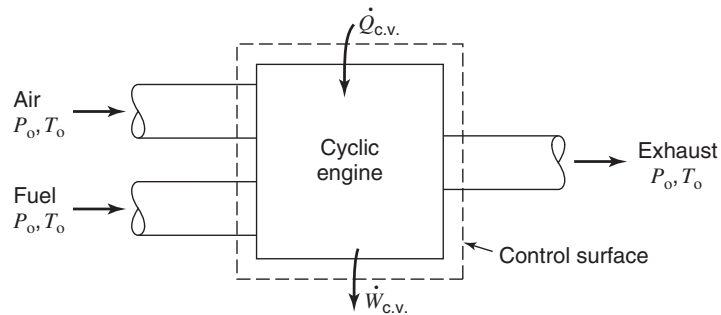


Figure 4.2 A control volume for analyzing the maximum work of a cyclic engine.

a control volume (c.v.) is defined as the ratio of the net work done per unit mass of fuel inducted into the cylinder, $w_{c.v.}$, to the heat of combustion, q_c .

$$\eta = w_{c.v.} / q_c \quad (4.26)$$

Internal combustion engine efficiency can also be defined from the perspective of the second law of thermodynamics. While the first law takes the energy transfers to the surroundings by way of the coolant and the exhaust into account, it does not consider the maximum possible work. The second law definition of engine efficiency, η_{II} , is the ratio of the net work done by the engine to the maximum possible work:

$$\eta_{II} = W_{c.v.} / W_{\max} \quad (4.27)$$

Following Obert (1973), the maximum possible work, W_{\max} is found from application of the first and second law to the control volume shown in Figure 4.2. Note that the fuel and air reactants (r) flow into the engine at P_o, T_o , and the combustion products (p) are exhausted from the engine at P_o, T_o .

$$\dot{Q}_{c.v.} - \dot{W}_{c.v.} = \left(\frac{dE}{dt} \right)_{c.v.} + \sum_p \dot{m} h - \sum_r \dot{m} h \quad (4.28)$$

Let us integrate over one period of the engine's cycle

$$Q_{c.v.} - W_{c.v.} = \sum_p m h - \sum_r m h \quad (4.29)$$

The maximum work is obtained only if the process is reversible, in which case the second law applied to the control volume is an equality:

$$Q_{c.v.} = T_o \left(\sum_p m s - \sum_r m s \right) \quad (4.30)$$

The only way in which the reversible heat transfer of Equation 4.30 can occur between an engine and its surroundings is via an intervening Carnot engine. Upon substitution of Equation 4.30 into Equation 4.28, the maximum work is

$$\begin{aligned} W_{\max} &= \sum_r m h - \sum_p m h + T_o \left(\sum_p m s - \sum_r m s \right) \\ &= (H_r - H_p) - T_o (S_r - S_p) \\ &= B_r - B_p \end{aligned} \quad (4.31)$$

where the parameter B is the flow exergy

$$B = H - T_o S \quad (4.32)$$

Since the reactants and the products are both at reference conditions, the maximum work can also be expressed as the change in the Gibbs free energy, G :

$$W_{\max} = G_r - G_p \quad (4.33)$$

The available energy of combustion a_c is defined as the maximum work per unit mass (or mole) of fuel

$$\begin{aligned} a_c &= W_{\max}/m_f \\ &= \frac{1}{m_f} [(H_r - H_p) + T_o(S_p - S_r)] \\ &= (B_r - B_p)/m_f \end{aligned} \quad (4.34)$$

so the second law efficiency can be expressed as

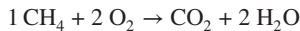
$$\eta_{II} = \frac{W_{c.v.}}{m_f a_c} \quad (4.35)$$

The difference between the available energy of combustion, $\Delta(H - T_o S)$, and the heat of combustion, ΔH , is that the available energy of combustion takes into account the change in entropy due to changes in composition of reactants.

EXAMPLE 4.5 Heat of Combustion and Available Energy of Combustion

Compare the available energy of combustion, a_c with the lower heat of combustion, q_{lhc} , for the stoichiometric combustion of methane at standard reference conditions.

SOLUTION Assume standard reference conditions $P = P_o = 1$ bar and $T_o = 298.15$ K, the air and fuel enter unmixed, and that the products leave in a gaseous state with a quality $\chi = 1$. Since the nitrogen enthalpy is zero for both the reactants and products it is not included in the computation. The chemical combustion equation per mole of methane is



and the molecular mass M of methane is 16.04.

Equations 4.3 and 4.34, per unit mass of fuel, are

$$q_c = H_r - H_p$$

$$a_c = B_r - B_p = (H_r - H_p) - T_o(S_r - S_p)$$

From the tabular data for \bar{h}_f^o and \bar{s}_i^o given in Table 4.1,

$$\begin{aligned} H_r &= \sum_{r_i} n_i \bar{h}_i \\ &= (1)(-74.87) + 0.21(0) = -74.87 \text{ MJ} \end{aligned}$$

$$H_p = \sum_{p_i} n_i \bar{h}_i$$

$$= (1)(-393.5) + (2)(-241.8) = -877.17 \text{ MJ}$$

$$S_r = \sum_{r_i} n_i [\bar{s}_i^o - R_u \ln y_i]$$

$$= (1)[186.2 - 8.314 \ln(1/1)] + (2)[205.15 - 8.314 \ln(0.21/1)] = 0.622 \text{ MJ/K}$$

$$S_p = \sum_{p_i} n_i [\bar{s}_i^o - R_u \ln y_i]$$

$$= (1)[213.79 - 8.314 \ln(0.0004/1)] + (2)[188.83 - 8.314 \ln(0.02/1)] = 0.721 \text{ MJ/K}$$

Therefore,

$$\begin{aligned} q_c &= H_r - H_p \\ &= -74.87 - (-877.17) \\ &= 802.3 \text{ MJ/kmol} = 50.01 \text{ MJ/kg} \end{aligned}$$

$$\begin{aligned} a_c &= (H_r - H_p) - T_o(S_r - S_p) \\ &= 802.3 - (298)(0.622 - 0.721) \\ &= 831.8 \text{ MJ/kmol} = 51.86 \text{ MJ/kg} \end{aligned}$$

Comment: At 298 K, N₂ and O₂ are assigned zero enthalpy, so the inclusion of N₂ will not change the results.

Figure 4.3 plots the available energy of combustion and the heat of combustion as a function of equivalence ratio at T_o = 298 K, P_o = 1 atm. The maximum work is attained only if the exhaust is in equilibrium at the state T_o, P_o. This also implies that each exhaust species such as CO₂ and H₂O is at the partial pressure that it is found in the environment. The exhaust water quality is evaluated by setting the partial pressure of the vapor equal to the saturation vapor pressure at T = T_o.

It is evident from Figure 4.3 that more energy is available per unit mass of fuel if an engine is fueled lean than if it is fueled rich. In the rich case, there is significant carbon monoxide and hydrogen in the exhaust. Thus, not all of the fuel's chemical energy is released and the exhaust gases could, in principle, be used as a fuel for some other engine. In practice, however, those gases are usually exhausted to the atmosphere and the energy is wasted. For this reason, in this chapter, we will base our fuel-air cycle thermal efficiency on the maximum available energy of combustion that occurs for very lean equivalence ratios. The value of $\phi = 0.01$ was chosen as being close enough to zero for practical purposes. Thus, letting

$$a_o = a_{c,\phi=0.01} \quad (4.36)$$

We define the second law thermal efficiency for a fuel-air cycle to be

$$\eta_{II} = \frac{W_{c.v.}}{m_f a_o} = \frac{w_{c.v.}(1 + \phi F A_s)}{(1 - f)\phi F A_s a_o} \quad (4.37)$$

where $w_{c.v.}$ is the work per unit mass done by the system.

To a certain extent, the definition of thermal efficiency is equivocal. It seems impractical to take into account the small amount of work that can in principle be realized because the exhaust composition is different than that of the atmosphere. One could make a case for defining efficiency in terms of the heat of combustion on the premise that never will a heat

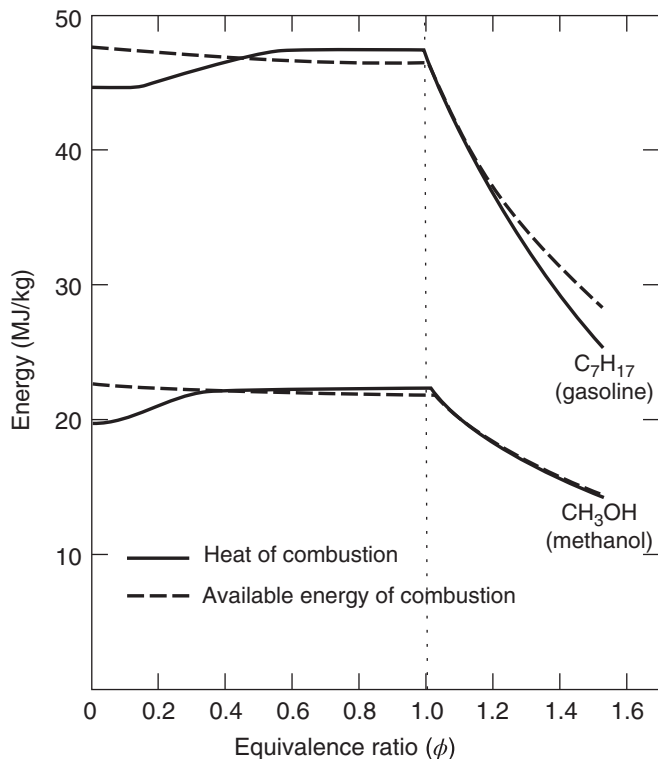


Figure 4.3 Available energy and heat of combustion for liquid gasoline and methanol. Fuel and air are unmixed. Products are mixed with equilibrium water quality. $P_o = 1.013$ bar, $T_o = 298$ K.

engine of any sort, including the Carnot engine, be used to reduce the irreversibilities associated with the heat transfer. By inspection of Figure 4.3, one would use the stoichiometric heat of combustion, for here the heat of combustion is maximum. Arguments can also be made for use of either the lower or the higher heat of combustion. Additionally, from Table 4.1, notice that for the most part there is little difference between the lower heat of combustion q_{lhc} and the maximum available energy a_o . Therefore, many engineers prefer to measure engine efficiency using the specific fuel consumption because its definition is unequivocal.

4.4 FUEL–AIR OTTO CYCLE

We now combine the thermodynamic processes discussed in previous sections with the fuel–air equations of state to form a fuel–air cycle analysis to compute the thermal efficiency, work, and imep produced by an internal combustion engine. A fuel–air cycle model includes the effect of the change in composition of the fuel–air mixture as a result of combustion. During compression, the gases in the cylinder are a mixture of air, fuel, and residual exhaust gas, and during expansion, the gases in the cylinder are equilibrium combustion products. Using these fuel–air combustion models, it is possible to compute the properties at states corresponding to the beginning and end of compression, combustion, and expansion for given fuel–air mixtures.

We start with a simple fuel–air Otto cycle in which the combustion process is assumed to be constant volume at top dead center. In a subsequent section, we develop a fuel–air finite energy release model in which the combustion occurs over a given change

in crank angle. The groundwork for introducing fuel-air cycles was laid in Chapter 2, where fundamental thermodynamic processes were presented; and in Chapter 3, where the thermodynamic properties and equations of state for equilibrium fuel-air-exhaust gas mixtures were developed.

Since the combustion process is assumed to be adiabatic and constant volume in an Otto cycle, the internal energy is constant, so $u_3 = u_2$, and the increase in temperature T and pressure P is due to the change in chemical composition from an unburned fuel air mixture to an equilibrium combustion product mixture. The basic processes of a fuel-air Otto cycle necessary to compute the efficiency and the indicated mean effective pressure are

- 1 to 2 Isentropic compression from v_1 to v_2 , with $s_2 = s_1$
- 2 to 3 Adiabatic, constant volume combustion, $v = \text{constant}$, with $u_3 = u_2$
- 3 to 4 Isentropic expansion from v_3 to v_4 , with $s_4 = s_3$

The work of the fuel-air Otto cycle is

$$w_{\text{net}} = (u_3 - u_4) - (u_2 - u_1) = u_1 - u_4 \quad (4.38)$$

and the imep is

$$\text{imep} = \frac{w_{\text{net}}}{v_1 - v_2} \quad (4.39)$$

The above equations are solved numerically in the fuel-air Otto cycle program *OttoFuel.m* listed in Appendix F.13. The engine parameters that are input to the Otto fuel-air cycle program are the compression ratio r , the fuel-air equivalence ratio ϕ , the residual mass fraction f , the fuel type, and the initial mixture temperature T_1 and pressure P_1 . Using the FARG and ECP routines to determine residual fraction and equilibrium properties, the program computes the mixture temperature, pressure, enthalpy, specific volume, and specific heat at each of the four states.

EXAMPLE 4.6 Fuel-Air Otto Cycle

Compute the state properties, work, imep, and thermal efficiency of a fuel-air Otto cycle with the following initial conditions: gasoline fuel with $P_1 = 101.3 \text{ kPa}$, $T_1 = 350 \text{ K}$, $\phi = 1.1$, residual fraction $f = 0.1$, and a compression ratio $r = 10$.

SOLUTION As described in detail in Appendix F.13, the fuel-air Otto cycle program *OttoFuel.m* computes the mixture properties at the four states, as well as the work, imep, and thermal efficiency.

The program input is

```
% program OttoFuel - computes const vol fuel air cycle
% first, isentropic compression from v1 to known v2
% establish initial conditions at state 1
clear;
T1 = 350;          %Kelvin
P1 = 101.3;        %kPa
phi = 1.1;         %equivalence ratio
f= 0.1;           %residual fraction
```

```
rc=10.; %compression ratio
...
```

The program output is

Ottofuel input conditions: phi= 1.10 fuel= 2					
State	1	2	3	4	
Pressure (kPa)	101.3	2113.1	8708.0	500.2	
Temperature (K)	350.0	730.1	2779.7	1604.9	
Enthalpy (kJ/kgK)	-390.8	47.3	677.8	-1167.3	
Volume (m ³ /kg)	0.956	0.096	0.096	0.956	
C _p (kJ/kg K)	1.078	1.23	2.052	1.424	
Work (kJ/kg)	1157.8				
Efficiency =	0.430				
Imep (kPa) =	1345.7				

The maximum temperature and pressure are $T_3 = 2780$ K and $P_3 = 8708$ kPa. The work produced is 1158 kJ/kg, the imep is 1346 kPa, and the thermal efficiency is 0.43.

Additional results obtained for the Fuel-Air Otto cycle model as a function of equivalence ratio, compression ratio, and residual fraction are plotted in Figures 4.4–4.6. The following are some of the important conclusions:

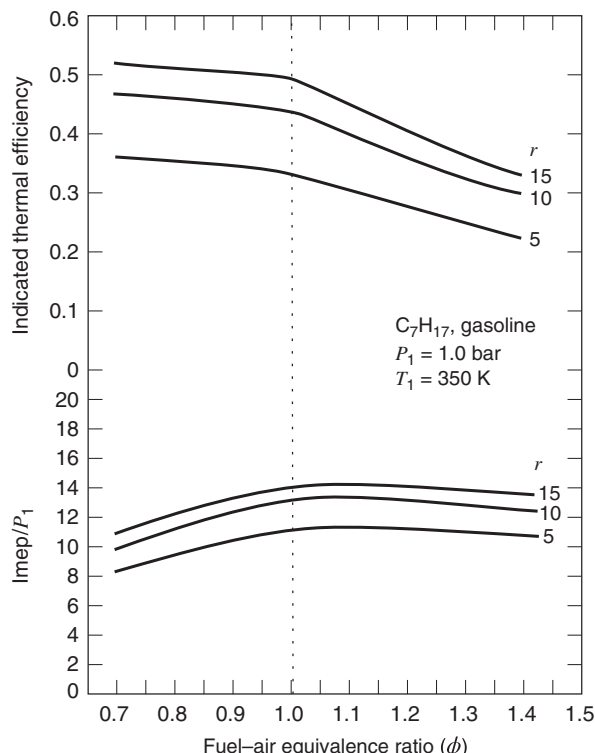


Figure 4.4 Effect of equivalence ratio on Otto fuel-air cycle.

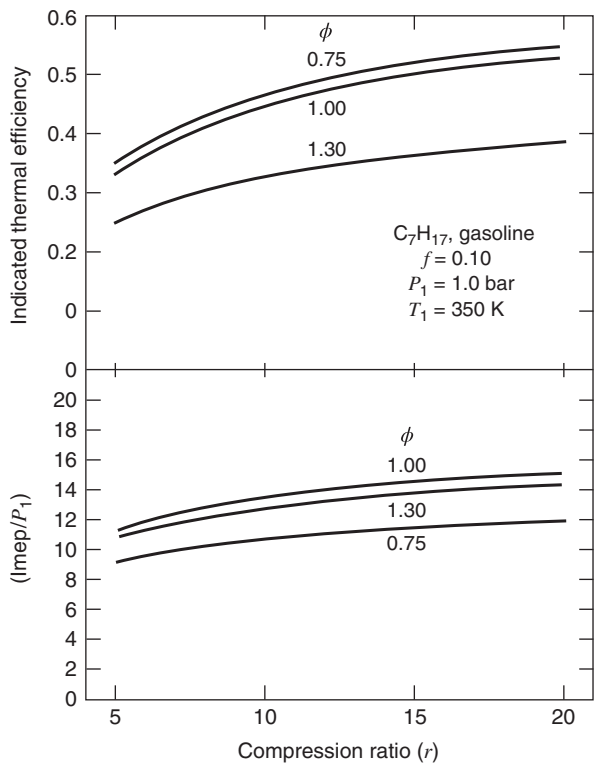


Figure 4.5 Effect of compression ratio on Otto fuel-air cycle.

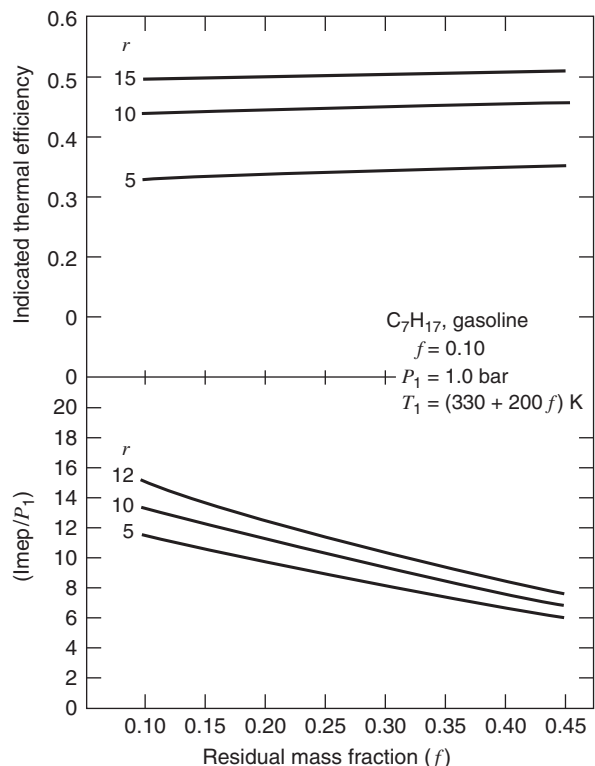


Figure 4.6 Effect of residual fraction on Otto fuel-air cycle.

1. The indicated efficiency increases with increasing compression ratio, is maximized by lean combustion, and is practically independent of the initial temperature and initial pressure. In actual engines, maximum efficiency occurs at stoichiometric or slightly lean; excessive dilution of the charge with air degrades the combustion.
2. The indicated mean effective pressure increases with increasing compression ratio, is maximized slightly rich of stoichiometric, and increases linearly with the initial density (i.e., $\text{imep} \sim P_1$ and $\text{imep} \sim 1/T_1$). The maximum imep at slightly rich equivalence ratio is due to the dissociation of the exhaust products.
3. For a given compression ratio, the peak pressure is proportional to the indicated mean effective pressure.
4. Peak temperatures in the cycles are largest for equivalence ratios slightly rich of stoichiometric.

The results shown are characteristic of most hydrocarbon fuels. It is of interest to explore the influence of fuel properties for some alternative fuels as we look to the future. Table 4.3 presents results obtained for two different compression ratios and five different fuels. Notice that there is very little difference among hydrocarbons. According to this analysis, diesel fuel would be just as good as gasoline in a homogeneous charge spark ignition engine; in reality, of course, knock would be a problem. Note that nitromethane is an excellent choice for a racing fuel, as it has the largest imep of the fuels in Table 4.3.

It is also of interest to examine the influence of the residual fraction, since a widely used technique for emission control is exhaust gas recirculation (EGR). By pumping exhaust gas into the intake manifold and mixing it with the fuel and air, one has, in essence, increased the residual gas fraction. Although the exhaust gas so recirculated is cooled before introduction into the induction system, it is still considerably warmer than the inlet air. Therefore, we will increase the inlet temperature in our computations simultaneously to examine the overall effect.

To illustrate, assume the initial temperature at the start of compression is $T_1 = 1330 + 200f$ (K). The results obtained for gasoline are given in Figure 4.6. Notice that the efficiency increases slightly with increasing dilution of the charge by residual gas. Notice too that imep falls with increasing residual fraction f ; it falls because the residual gas displaces the fuel–air mixture volume, and it also warms the fuel–air mixture, thereby reducing the

Table 4.3 Effect of Fuel Type on Otto Fuel–Air Cycle

Fuel	Formula	r	η_{Otto}	imep (bar)
Gasoline	C_7H_{17}	10	0.44	13.3
		15	0.49	14.4
Diesel	$\text{C}_{14.4}\text{H}_{24.9}$	10	0.44	13.7
		15	0.49	14.9
Methane	CH_4	10	0.44	12.2
		15	0.49	13.1
Methanol	CH_3OH	10	0.43	13.1
		15	0.48	14.2
Nitromethane	CH_3NO_2	10	0.39	21.0
		15	0.43	23.1

$$\phi = 1.0, f = 0.10, P_1 = 1.0 \text{ bar}, T_1 = 350 \text{ K}$$

charge density. As will be discussed later in this chapter, all of the conclusions drawn from Figures 4.4 to 4.6 apply to actual engines, provided that they are operated at optimum spark timing.

4.5 FOUR-STROKE FUEL–AIR OTTO CYCLE

In this section, we develop a four-stroke Otto fuel–air cycle with idealized inlet and exhaust processes. In this case, the input engine parameters T_1 , P_1 , and f are no longer the independent variables. Instead, the intake pressure P_i , the exhaust pressure P_e , and the intake temperature T_i are the independent variables and used as the input engine parameters.

The additional processes, introduced in Chapter 2, are reiterated here

- 4 to 5 Constant cylinder volume blowdown
- 5 to 6 Constant pressure exhaust
- 6 to 7 Constant cylinder volume reversion
- 7 to 1 Constant pressure induction

The exhaust blowdown is considered to be isentropic as far as the control mass is concerned. One solves for the temperature T_5 by requiring that $S_5 = S_4$ and $P_5 = P_e$. Application of the first law to the control mass during exhaust leads to the conclusion that

$$h_6 = h_5 \quad P_6 = P_5$$

$$T_6 = T_5 \quad V_6 = V_5$$

These are still valid conclusions even though now we are treating the exhaust gas as equilibrium combustion products.

The residual fraction, given by Equation 2.67, is

$$f = \frac{1}{r} \frac{v_4}{v_6} \quad (4.40)$$

The energy equation applied to the cylinder control volume during intake is given by Equation 2.71. Note that Equation 2.79 is no longer valid, since it assumes constant specific heats. In this case, Equation 2.79 is replaced by

$$h_1 = f[h_6 + (P_i - P_e)v_6] + (1 - f)h_i \quad (4.41)$$

and, of course, it is still true that if the pressure drop across the intake valves is neglected

$$P_1 = P_i \quad (4.42)$$

The volumetric efficiency and pumping work are

$$\epsilon_v = \frac{m_i}{\rho_i V_d} = \frac{r(1 - f)v_i}{(r - 1)v_1} \quad (4.43)$$

$$\text{pme} = P_e - P_i \quad (4.44)$$

Finally, the net imep and thermal efficiency are

$$\text{imep}_{\text{net}} = \text{imep} - \text{pme} \quad (4.45)$$

$$\eta_{\text{net}} = \eta (1 - \text{pme}/\text{imep}) \quad (4.46)$$

The above equations are solved numerically in the four-stroke fuel–air Otto cycle program `FourStrokeFuelAir.m` listed in Appendix F.14. The inputs to the four-stroke

Otto fuel-air cycle program are the compression ratio r , the fuel-air equivalence ratio ϕ , the intake pressure P_i , the exhaust pressure P_e , the intake temperature T_i , and the fuel type. Using the residual fraction (`farg.m`) and equilibrium combustion models (`ecp.m`) developed in Chapter 3, it is possible to compute the properties at states 1, 2, 3, and 4. As in the four-stroke gas cycle, analysis of the four-stroke fuel-air cycle requires an additional iteration loop to determine the residual fraction and exhaust conditions.

EXAMPLE 4.7 Four-Stroke Fuel-Air Otto Cycle

Compute the cycle properties, volumetric efficiency, residual fraction, net imep, and net thermal efficiency of a throttled four-stroke fuel-air Otto cycle with the following intake conditions: gasoline fuel with $P_i = 50$ kPa, $P_e = 105$ kPa, $T_i = 300$ K, $\phi = 0.8$, and a compression ratio of 10.

SOLUTION The four-stroke fuel-air Otto cycle program `FourStrokeFuelAir.m` is used to compute the desired cycle parameters. The code computes the mixture properties at the four cycle states, as well as the volumetric efficiency, residual fraction, net imep, and net thermal efficiency. The input parameters are entered into the program as shown below:

```
Program for four-stroke fuel air cycle
establish initial conditions for intake stroke
clear;
Ti = 300;      % intake temperature (K)
Pi = 52.5;     % intake pressure (kPa)
Pe = 105;      % exhaust pressure (kPa)
phi = .8;       % equivalence ratio
rc = 10.;       % compression ratio
...
...
```

The program output is

```
FourStrokeFuelAir Results
Inlet: Temp (K)= 300.0 Pressure (kPa)= 52.5
phi= 0.80 fuel= 2
```

State	----	1	----	2	----	3	----	4
Pressure (kPa) =	52.5	1128.2		4138.1		237.3		
Temperature (K) =	348.5	748.9		2615.3		1507.3		
Enthalpy (kJ/kgK) =	-196.5	254.5		810.8		-885.7		
Int. Energy (kJ/kg =	-293.6	45.8		45.4		-1324.6		
Volume (m ³ /kg) =	1.850	0.185		0.185		1.849		
Entropy (kJ/kgK) =	7.163	7.163		8.702		8.702		
Cp (kJ/kg K) =	1.059	1.199		1.903		1.366		

```
Work (kJ/kg) = 1031.0
Volumetric Efficiency = 0.9037
```

Ideal Thermal Efficiency = 0.491
 Net Thermal Efficiency = 0.4497
 Imep (kPa) = 619.4
 Pmep (kPa) = 52.5
 Exhaust Temperature (K) = 1262.6
 Residual Fraction f = 0.0528

Note that the entropy is constant during compression and expansion, and the internal energy and specific volume are constant during combustion. The temperature rise of the inlet fuel–air mixture is about 48 K when mixed with the $f = 0.053$ residual fraction. The maximum temperature and pressure are $T_3 = 2615$ K and $P_3 = 4138$ kPa. The exhaust temperature T_e is 1507 K. The volumetric efficiency is 0.904, net imep is 619 kPa, and the net thermal efficiency η_{net} is 0.45.

Results obtained from the program by varying the intake to exhaust pressure ratio and the compression ratio are given in Figures 4.7 and 4.8. The net efficiency and the net indicated mean effective pressure are each seen to be a strong function of the intake/exhaust pressure ratio. The advantage of turbocharging and the disadvantage of throttling are clear. For pressure ratios corresponding to supercharging, the curves are not representative, for one would have to also account for the work to drive the compressor.

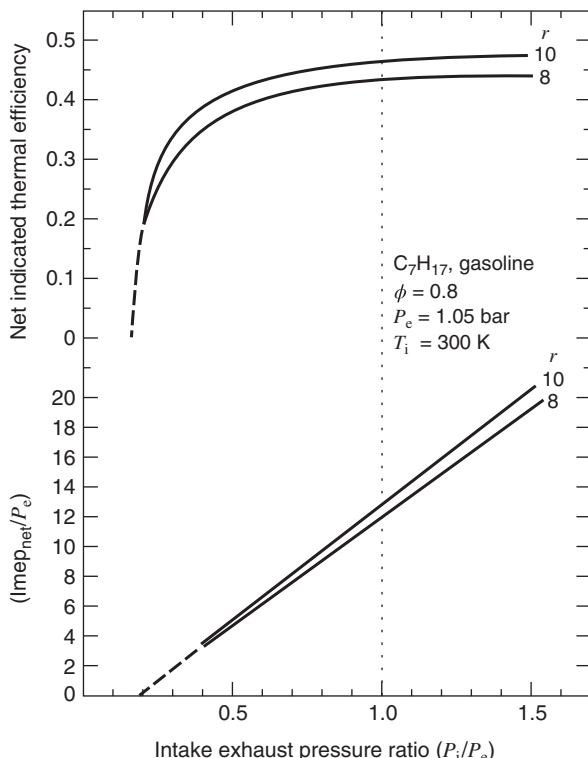


Figure 4.7 Effect of intake/exhaust pressure ratio on four-stroke Otto fuel–air cycle imep and thermal efficiency.

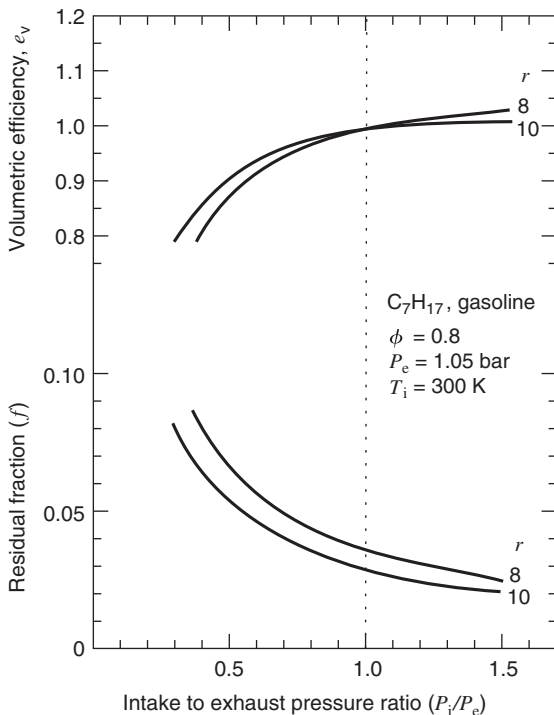


Figure 4.8 Effect of intake/exhaust pressure ratio on four-stroke Otto fuel–air cycle residual fraction and volumetric efficiency.

Notice that throttling also hurts the volumetric efficiency, mainly because of an increase in the residual fraction. The residual fraction decreases with increasing compression ratio, as one would expect.

The modeling of the intake and exhaust portion of the Otto cycle is not nearly as realistic as the compression, combustion, and expansion portion of the cycle. This is because of the assumptions of isobaric intake and exhaust processes and the neglect of heat transfer. Neglect of the heat transfer causes the residual fraction to be underpredicted by a factor on the order of 2. In Chapter 5, it will be shown that the processes are isobaric only at very low piston speeds; consequently, at high piston speeds, the pumping mean effective pressure can be in considerable error and can even have the wrong sign for super- or turbocharged engines.

4.6 HOMOGENEOUS TWO-ZONE FINITE HEAT RELEASE CYCLE

In this section, we analyze a homogeneous fuel–air cycle in which the fuel and air are fully mixed prior to the onset of combustion. We divide the combustion chamber into two zones, burned (b) and unburned (u), and develop differential equations for the change in pressure and change in temperature in each zone. The modeling is based on equations for energy and mass conservation, equation of state, and mass fraction burned. The assumption is made that both zones are at the same pressure P , and the ignition temperature is the adiabatic flame temperature based on the mixture enthalpy at the onset of combustion. The analysis includes heat loss to the combustion chamber surfaces, and the blowby mass loss past the rings.

In Chapter 2, we used a finite heat release function to express the fraction of heat added over a given crank angle change. In this section, we use a similar function to represent

the mass fraction x of the cylinder contents that have burned. The solution procedure is a simultaneous integration of a set of ordinary differential equations for P, T_u, T_b , and subsequent calculation of net work W , heat loss Q_1 , thermal efficiency η , and the indicated mean effective pressure. This two-zone model has been extended to multi-zone models by Raine et al. (1995).

The open system energy equation applied to the cylinder contents, is

$$\begin{aligned} \frac{dQ}{d\theta} - P \frac{dV}{d\theta} &= \frac{dU}{d\theta} + \frac{\dot{m}_1 h_1}{\omega} \\ &= m \frac{du}{d\theta} + u \frac{dm}{d\theta} + \frac{\dot{m}_1 h_1}{\omega} \end{aligned} \quad (4.47)$$

The specific volume v of the system is given by

$$v = \frac{V}{m} = xv_b + (1-x)v_u \quad (4.48)$$

Since $v = v(T, P)$, we can apply the chain rule to both zones:

$$\frac{\partial v_b}{\partial \theta} = \frac{\partial v_b}{\partial T_b} \frac{dT_b}{d\theta} + \frac{\partial v_b}{\partial P} \frac{dP}{d\theta} \quad (4.49)$$

$$\frac{\partial v_u}{\partial \theta} = \frac{\partial v_u}{\partial T_u} \frac{dT_u}{d\theta} + \frac{\partial v_u}{\partial P} \frac{dP}{d\theta} \quad (4.50)$$

Differentiating the equation for the specific volume, Equation 4.48, and incorporating Equations 4.49 and 4.50 yield

$$\frac{1}{m} \frac{dV}{d\theta} - \frac{V}{m^2} \frac{dm}{d\theta} = x \frac{dv_b}{d\theta} + (1-x) \frac{dv_u}{d\theta} + (v_b - v_u) \frac{dx}{d\theta} \quad (4.51)$$

$$\begin{aligned} \frac{1}{m} \frac{dV}{d\theta} + \frac{VC}{m\omega} &= x \frac{\partial v_b}{\partial T_b} \frac{dT_b}{d\theta} + (1-x) \frac{\partial v_u}{\partial T_u} \frac{dT_u}{d\theta} \\ &\quad + \left[x \frac{\partial v_b}{\partial P} + (1-x) \frac{\partial v_u}{\partial P} \right] \frac{dP}{d\theta} + (v_b - v_u) \frac{dx}{d\theta} \end{aligned} \quad (4.52)$$

The total internal energy u of the system is the sum of the internal energy of burned and unburned zones:

$$u = \frac{U}{m} = xu_b + (1-x)u_u \quad (4.53)$$

where u_b is the internal energy of the burned gas at temperature T_b , and u_u is the energy of the unburned gas at temperature T_u . Since $u = u(T, P)$, we can again apply the chain rule to both zones:

$$\begin{aligned} \frac{\partial u_b}{\partial \theta} &= \frac{\partial u_b}{\partial T_b} \frac{dT_b}{d\theta} + \frac{\partial u_b}{\partial P} \frac{dP}{d\theta} \\ &= \left(c_{pb} - P \frac{\partial v_b}{\partial T_b} \right) \frac{dT_b}{d\theta} - \left(T_b \frac{\partial v_b}{\partial T_b} + P \frac{\partial v_b}{\partial P} \right) \frac{dP}{d\theta} \end{aligned} \quad (4.54)$$

similarly,

$$\frac{\partial u_u}{\partial \theta} = \left(c_{pu} - P \frac{\partial v_u}{\partial T_u} \right) \frac{dT_u}{d\theta} - \left(T_u \frac{\partial v_u}{\partial T_u} + P \frac{\partial v_u}{\partial P} \right) \frac{dP}{d\theta} \quad (4.55)$$

Recall that the partial derivative terms $\frac{\partial v}{\partial T}$ and $\frac{\partial v}{\partial P}$ are computed by the programs ECP and FARG for given mixture states.

The $mdu/d\theta$ term in the energy equation is therefore

$$\begin{aligned} m \frac{du}{d\theta} &= m \left[x \frac{du_b}{d\theta} + (1-x) \frac{du_u}{d\theta} + (u_b - u_u) \frac{dx}{d\theta} \right] \\ &= mx(c_{pb} - P \frac{\partial v_b}{\partial T_b}) \frac{dT_b}{d\theta} + m(1-x)(c_{pu} - P \frac{\partial v_u}{\partial T_u}) \frac{dT_u}{d\theta} \\ &\quad - \left[mx \left(T_b \frac{\partial v_b}{\partial T_b} + P \frac{\partial v_b}{\partial P} \right) + m(1-x) \left(T_u \frac{\partial v_u}{\partial T_u} + P \frac{\partial v_u}{\partial P} \right) \right] \frac{dP}{d\theta} \\ &\quad + m(u_b - u_u) \frac{dx}{d\theta} \end{aligned} \quad (4.56)$$

The term $udm/d\theta$ is the blowby term. As we modeled blowby in Chapter 2, we write

$$\frac{dm}{d\theta} = -\frac{\dot{m}_1}{\omega} = \frac{-Cm}{\omega} \quad (4.57)$$

where C is the blowby coefficient depending on the ring design. This implies that the mass in the cylinder at a given crank angle θ , decreases as

$$m(\theta) = m_1 \exp[-C(\theta - \theta_1)/\omega] \quad (4.58)$$

where m_1 is the initial mass at state 1, the start of compression. The term $dQ/d\theta$ is the heat loss term, and as modeled in Chapter 2,

$$\frac{dQ}{d\theta} = -\frac{\dot{Q}_1}{\omega} = \frac{-\dot{Q}_b - \dot{Q}_u}{\omega} \quad (4.59)$$

from the burned and unburned gases. The heat loss terms are expressed with a convection equation,

$$\begin{aligned} \dot{Q}_b &= \mathbf{h} A_b (T_b - T_w) \\ \dot{Q}_u &= \mathbf{h} A_u (T_u - T_w) \end{aligned} \quad (4.60)$$

where \mathbf{h} is the convection heat transfer coefficient, and A_b and A_u are the areas of the burned and unburned gases in contact with the cylinder walls at temperature T_w . We have assumed, for convenience, that $\mathbf{h}_u = \mathbf{h}_b = \mathbf{h} = \text{constant}$. For the areas A_b and A_u , let us suppose that the cylinder area A_c can be divided as follows:

$$\begin{aligned} A_c &= \frac{\pi b^2}{2} + \frac{4V}{b} \\ A_b &= A_c x^{1/2} \\ A_u &= A_c (1 - x^{1/2}) \end{aligned} \quad (4.61)$$

The fraction of cylinder area contacted by the burned gas is assumed to be proportional to the square root of the mass fraction burned to reflect the fact, because of the density difference between burned and unburned gas, the burned gas occupies a larger volume fraction of the cylinder than the unburned gas. In practice, the exponent on x may be left as a free parameter to be determined from experiments or a more complicated scheme may be used based on an assumption about the flame shape.

We need to specify h_1 , the enthalpy of the mass loss due to blowby. Early in the combustion process, unburned gas leaks past the rings. Late in the combustion process,

burned gas leaks past the rings. Since a larger portion of unburned gas will be leaking than the unburned mass fraction, let us assume that

$$h_l = (1 - x^2)h_u + x^2h_b \quad (4.62)$$

As discussed in Chapter 3, the enthalpies $h_u = h(T_u, P)$ and $h_b = h(T_b, P)$ are computed by the program `ecp.m`.

The mass fraction burned, $x(\theta)$, is represented by the following finite heat release equation:

$$\begin{aligned} x &= 0 \quad \theta < \theta_s \\ x &= \frac{1}{2} \left(1 - \cos \left(\frac{\pi(\theta - \theta_s)}{\theta_b} \right) \right) \\ x &= 1 \quad \theta > \theta_s + \theta_b \end{aligned} \quad (4.63)$$

The remaining equation comes from introduction of the unburned gas entropy into the analysis. Treating the unburned gas as an open system losing mass via leakage and combustion, it can be shown that

$$-\dot{Q}_u = \omega m(1 - x)T_u \frac{ds_u}{d\theta} \quad (4.64)$$

Since $s_u = s_u(T_u, P)$ it follows that

$$\begin{aligned} \frac{\partial s_u}{\partial \theta} &= \frac{\partial s_u}{\partial T_u} \frac{dT_u}{d\theta} + \frac{\partial s_u}{\partial P} \frac{dP}{d\theta} \\ &= \frac{c_{pu}}{T_u} \frac{dT_u}{d\theta} + \frac{\partial v_u}{\partial T_u} \frac{dP}{d\theta} \end{aligned} \quad (4.65)$$

Elimination of $ds_u/d\theta$ between Equations 4.64 and 4.65 gives

$$c_{pu} \frac{dT_u}{d\theta} - T_u \frac{\partial v_u}{\partial T_u} \frac{dP}{d\theta} = \frac{-\mathbf{h}A_u}{\omega m(1 - x)} (T_u - T_w) \quad (4.66)$$

For convenience, let us define the following variables:

$$\begin{aligned} A &= \frac{1}{m} \left(\frac{dV}{d\theta} + \frac{VC}{\omega} \right) \\ B &= \frac{\mathbf{h}A_c}{\omega m} \left[\frac{1}{c_{pb}} \frac{\partial v_b}{\partial T_b} x^{1/2} (T_b - T_w) + \frac{1}{c_{pu}} \frac{\partial v_u}{\partial T_u} (1 - x^{1/2}) (T_u - T_w) \right] \\ C &= -(v_b - v_u) \frac{dx}{d\theta} - \frac{\partial v_b}{\partial T_b} \frac{h_u - h_b}{c_{pb}} \left[\frac{dx}{d\theta} - \frac{(x - x^2)C}{\omega} \right] \\ D &= x \left[\frac{T_b}{c_{pb}} \left(\frac{\partial v_b}{\partial T_b} \right)^2 + \frac{\partial v_b}{\partial P} \right] \\ E &= (1 - x) \left[\frac{T_u}{c_{pu}} \left(\frac{\partial v_u}{\partial T_u} \right)^2 + \frac{\partial v_u}{\partial P} \right] \end{aligned} \quad (4.67)$$

The six equations to be integrated are

$$\frac{dP}{d\theta} = \frac{A + B + C}{D + E}$$

$$\begin{aligned}
 \frac{dT_b}{d\theta} &= \frac{-\mathbf{h}A_c(T_b - T_w)}{\omega m c_{pb} x^{1/2}} + \frac{T_b}{c_{pb}} \frac{\partial v_b}{\partial T_b} \frac{A+B+C}{D+E} + \frac{h_u - h_b}{x c_{pb}} \left[\frac{dx}{d\theta} - (x - x^2) \frac{C}{\omega} \right] \\
 \frac{dT_u}{d\theta} &= \frac{-\mathbf{h}A_c(1 - x^{1/2})(T_u - T_w)}{\omega m c_{pu}(1-x)} + \frac{T_u}{c_{pu}} \frac{\partial v_u}{\partial T_u} \frac{A+B+C}{D+E} \\
 \frac{dW}{d\theta} &= P \frac{dV}{d\theta} \\
 \frac{dQ_1}{d\theta} &= \frac{\mathbf{h}A_c}{\omega} [x^{1/2}(T_b - T_u) + (1 - x^{1/2})(T_u - T_w)] \\
 \frac{dH_1}{d\theta} &= \frac{Cm}{\omega} [(1 - x^2)h_u + x^2h_b]
 \end{aligned} \tag{4.68}$$

The above equations are solved numerically in the homogenous two-zone finite heat release program `Homogeneous.m` listed in Appendix F.15. The inputs to the program are the compression ratio r , engine bore and stroke, engine speed, heat transfer and blowby coefficients, the fuel-air equivalence ratio ϕ , residual fraction, the initial pressure P_1 , and temperature T_1 . The initial burned gas temperature is assumed to be the adiabatic flame temperature based on the enthalpy at the time of spark. If $x < 0.001$, the system is treated as consisting of only unburned gas, and if $x > 0.999$, it is treated as being entirely composed of burned gas.

Using the residual fraction (`farg.m`) and equilibrium combustion models (`ecp.m`) developed in Chapter 3 to compute mixture mole fractions and properties, the `Homogeneous.m` program computes pressure, burned and unburned zone temperatures, work, and cumulative heat and mass loss as a function of crank angle. Finally, the program computes the net thermal efficiency of this cycle using Equation 4.69.

$$\eta = \frac{w_{c.v.}(1 + \phi F A_s)}{(1 - f)\phi F A_s a_o} \tag{4.69}$$

EXAMPLE 4.8 Homogeneous Two Zone Finite Heat Release

Compute the pressure and burned and unburned zone temperatures, net imep, and net thermal efficiency of a homogeneous finite heat release cycle with the following initial conditions: gasoline fuel with $P_1 = 100$ kPa, $T_1 = 350$ K, and $\phi = 0.8$.

The engine has a bore of 0.10 m and stroke of 0.10 m, with a half stroke to rod ratio $\epsilon = 0.25$, a compression ratio $r = 10$, residual fraction $f = 0.1$, and operates at $N = 2000$ rpm. The start of heat release is at -35° , and the combustion duration is 60° . Assume the cylinder wall temperature is 420 K, with a heat transfer coefficient of 500 W/(m²K), and blowby coefficient of 0.8 s^{-1} .

SOLUTION The input parameters are entered into the `Homogeneous.m` program as shown below:

```

Homogeneous Two Zone Combustion Cycle
This program computes the pressure and temperature
vs crank angle, the work, indicated thermal efficiency,
and the Indicated mean effective pressure (kPa)

```

R = 10; Compression ratio

```

B = .10;      Bore - B (m)
S = .08;      Stroke - S (m)
EPS = 0.25;   Half stroke to rod ratio
RPM = 2000;   Engine speed (RPM)
HEAT = 500;   Heat transfer coefficient (W/m2-K)
BLOWBY = 0.8; Blowby coefficient
THETAB = 60;   Burn angle (Deg)
THETAS = -35; Start of heat release (deg ATDC)
PHI = 0.8;    Equivalence ratio
F = 0.1;     Residual fraction
TW = 420;    Wall temperature (K)
fuel_id = 2;  gasoline
FS = 0.06548; gasoline stoichiometric fuel{---}air ratio
A0 = 47870;  maximum available energy (kJ/kg)
T1 = 350;    Initial temperature (K)
P1 = 100;    Initial Pressure (kPa)
...

```

The program output is shown in Figures 4.9–4.12, which are respectively plots of heat release fraction, pressure, unburned and burned temperatures, and cumulative work and heat loss as a function of crank angle. The burn fraction x begins at -35° , and ends at $+25^\circ$. The maximum pressure is about 6000 kPa at a crank angle of $+15^\circ$ atdc. The unburned gas temperature T_u profile rises due to the compression process and heat transfer from the cylinder walls, and ends at $+25^\circ$, as combustion is completed. The burned gas temperature T_b begins at -35° at the adiabatic flame temperature = 2140 K, as heat release is initiated, increases to about 2500 K, then decreases to about 1100 K as the cylinder volume increases.

The cumulative work is initially negative during compression, then becomes positive during expansion. The heat loss is very small during compression, then increases as the cylinder temperature increases during combustion. The mass loss is linear, due to the simple blowby model used.

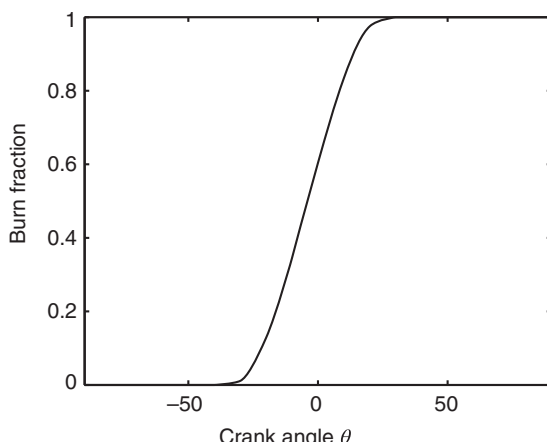


Figure 4.9 Heat release fraction versus crank angle.

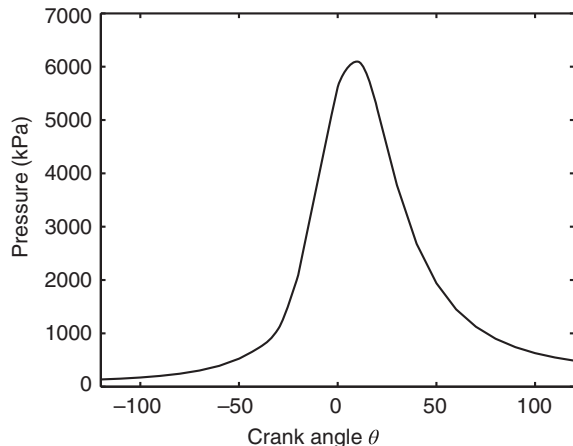


Figure 4.10 Pressure versus crank angle.

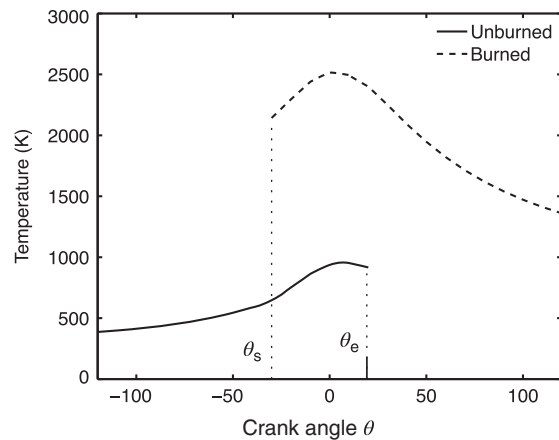


Figure 4.11 Unburned and burned zone temperature versus crank angle.

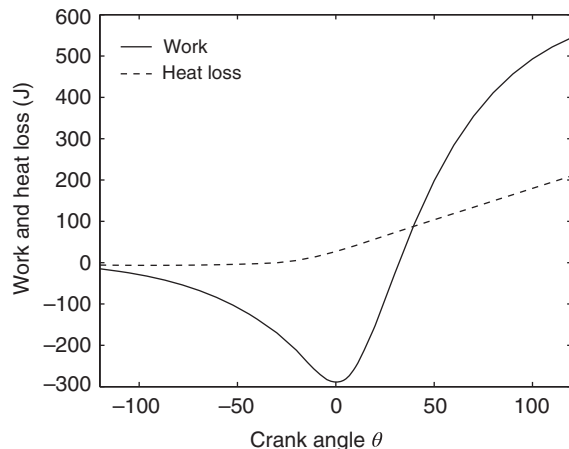


Figure 4.12 Work and heat loss (J) versus crank angle.

The net thermal efficiency, from Equation 4.69, is 0.388, and the net imep is 950 kPa. The equivalent fuel–air Otto cycle predicts $\eta = 0.460$, hence $\eta/\eta_{\text{Otto}} = 0.845$.

4.7 COMPARISON OF FUEL-AIR CYCLES WITH ACTUAL SPARK IGNITION CYCLES

Since the efficiency of an actual engine must be less than the efficiency of its equivalent Otto fuel-air cycle, the fuel-air cycle is a convenient reference for comparison. The indicated efficiency and mean effective pressure of actual engines are determined in practice by measuring the cylinder pressure as a function of cylinder volume and integrating $\int PdV$ to find the work. It is also possible to measure the residual fraction and charge density trapped within the cylinder.

With reference to Figure 4.13 an equivalent fuel-air cycle is constructed by matching the temperature, pressure, and composition (and thereby entropy) at some reference point after closing of the intake valve and prior to firing of the spark plug.

Since the actual process is nearly isentropic, the compression curves of the two cycles nearly coincide. Soon after the onset of combustion, the actual cycle pressure starts rising above that of the fuel-air cycle. Because the combustion actually is not at constant volume, the peak pressure is considerably less than that predicted by the fuel-air cycle. The expansion curve 3–4 is polytropic in character; measurements show that the entropy decreases during expansion, primarily due to heat transfer to the coolant. At point 4 the exhaust valve opens, and soon after, the pressure falls rapidly to the exhaust pressure. The cross-hatched area represents “lost work” that can mainly be attributed to the following:

- Heat loss
- Mass loss
- Finite burn rate
- Finite blowdown rate

By inspection of Tables 4.4–4.7, a series of CFR engine data sets from Taylor (1985), compared with equivalent fuel-air Otto cycle predictions, the following conclusions can be drawn:

1. The indicated mean effective pressure is maximized slightly rich of stoichiometric, and increases with increasing compression ratio and inlet pressure.

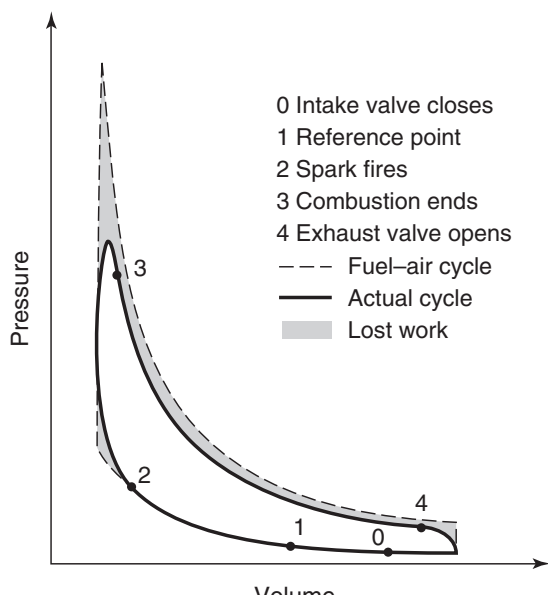


Figure 4.13 Comparison of an actual spark ignition cycle with its equivalent fuel-air cycle. Adapted from Taylor (1985).

Table 4.4 Effect of Equivalence Ratio ϕ on CFR Engine Performance

ϕ	θ_s (atdc) (deg)	θ_d (deg)	imep (bar)	η/η_{Otto}
0.74	-33	58	6.3	0.85
0.80	-23	39	6.4	0.83
1.17	-15	33	7.7	0.85
1.80	-20	39	7.0	0.83

 $N = 1200 \text{ rpm}$, $r = 7$,

Source: Taylor (1985).

Table 4.5 Effect of Spark Advance θ_s on CFR Engine Performance

θ_s (atdc) (deg)	θ_d (deg)	bmep (bar)	imep (bar)	η/η_{Otto}
0	40	5.0	6.0	0.73
-13	40	5.7	7.5	0.82
-26	38	5.8	7.5	0.82
-39	39	5.0	6.9	0.74

 $N = 1200 \text{ rpm}$, $r = 6$, $\phi = 1.13$,

Source: Taylor (1985).

Table 4.6 Effect of Engine Speed N on CFR Engine Performance

N (rpm)	θ_s (atdc) (deg)	θ_d (deg)	bmep (bar)	imep (bar)	η/η_{Otto}
900	-18	36	3.90	5.89	0.842
1200	-19	39	3.77	5.94	0.848
1500	-22	40	3.80	6.07	0.865
1800	-18	38	3.59	6.14	0.877

 $r = 6$, $\phi = 1.13$,

Source: Taylor (1985).

Table 4.7 Effect of Compression Ratio r on CFR Engine Performance

r	θ_s (atdc) (deg)	θ_d (deg)	bmep (bar)	imep (bar)	η/η_{Otto}
8	-13	29	5.5	7.9	0.79
7	-14	31	5.3	7.9	0.86
6	-15	33	5.3	7.2	0.84
5	-16	37	4.8	6.8	0.87
4	-17	39	4.1	6.1	0.86

 $N = 1200 \text{ rpm}$, $\phi = 1.13$,

Source: Taylor (1985).

2. The ratio of the actual efficiency to the equivalent fuel-air Otto cycle η/η_{Otto} is on the order of 0.85, and varies insignificantly with engine operating variables, at most decreasing slightly with increasing compression ratio.
3. The combustion duration, θ_d , is on the order of 35° , decreases with increasing compression ratio or inlet pressure, and is minimum at a slightly rich equivalence ratio.
4. The optimum spark advance, θ_s , increases with combustion duration and with increased engine speed. The optimum spark advance is defined as the crank angle θ that produces maximum brake torque (MBT).
5. The imep increases with engine speed, while bmep decreases, which, as we will see in Chapter 10, is caused by increased friction.

Based on the analysis done in Chapter 2, these results are to be expected. The differences between the fuel-air model and the actual engine is primarily due to heat loss, but also to mass loss and the finite burning rate. A small part of the discrepancy can be also attributed to opening the exhaust valve prior to bottom dead center to provide for the finite flowrate of the blowdown process.

For a given engine operated at optimum spark timing, the ratio η/η_{Otto} is nearly independent of the fuel-air equivalence ratio, the inlet temperature, the inlet pressure, the exhaust gas recirculation, and the engine speed. All the trends predicted by the Otto fuel-air cycle are, in fact, observed in practice.

This implies that there is slightly greater potential for improving the efficiency of spark ignition engines by increasing their theoretical efficiency through an increase in compression ratio rather than by reducing their losses. To illustrate, suppose that by reducing the heat loss or increasing the burn rate one could increase η/η_{Otto} from 0.80 to 0.90. The efficiency might be 0.32 instead of 0.29. On the other hand, suppose that research results showed that the compression ratio could be increased to 20. The fuel-air cycle efficiency would increase to about 0.46, and if η/η_{Otto} were still 0.8, the actual efficiency would now be 0.37. There is greater potential with this approach because the second law of thermodynamics does not limit the choice of variables that fix the theoretical efficiency but it does limit the gains that can be realized once the parameters that specify the fuel-air cycle are fixed.

4.8 LIMITED PRESSURE FUEL-AIR CYCLE

This cycle developed in this section models diesel engines and fuel-injected stratified charge engines in which the fuel is injected at the time it is intended to burn. The processes are

- | | |
|----------|--|
| 1 to 2 | Isentropic compression of air and residual gas |
| 2 to 2.5 | Constant volume, adiabatic fuel injection, and combustion |
| 2.5 to 3 | Constant pressure, adiabatic fuel injection, and/or combustion |
| 3 to 4 | Isentropic expansion |

These engines, in general, are fueled overall lean. In this case, the air-residual gas mixture is equivalent to equilibrium combustion products at an equivalence ratio given by Equation 4.70:

$$\phi_{12} = \frac{f\phi}{1 + (1 - f)\phi F_s} \quad (4.70)$$

where the residual fraction, f , is the ratio of the residual mass to the cylinder gas mass prior to fuel injection. The thermodynamic state during compression can then be determined with the equivalence ratio ϕ used as an argument.

The details of the fuel injection and combustion are of no concern at this level of modeling. We need only assume that at state 3 the gases in the cylinder are equilibrium combustion products at the overall fuel-air equivalence ratio. To specify the state, we know that

$$P_3 \leq P_{\text{limit}} \quad (4.71)$$

and we apply the energy equation to the process 2 to 3:

$$\Delta U = m_3 u_3 - m_2 u_2 = m_f h_f - P_3(m_3 v_3 - m_3 v_2) \quad (4.72)$$

It follows that

$$\frac{m_2}{m_3} = \frac{m_a + m_r}{m_a + m_r + m_f} = \frac{1}{1 + (1-f)\phi FA_s} \quad (4.73)$$

$$\frac{m_f}{m_3} = \frac{m_3 - m_2}{m_3} = \frac{(1-f)\phi FA_s}{1 + (1-f)\phi FA_s} \quad (4.74)$$

and the enthalpy at state 3 is

$$h_3 = u_3 + P_3 v_3 = \frac{u_2 + P_3 v_2 + (1-f)\phi FA_s h_f}{1 + (1-f)\phi FA_s} \quad (4.75)$$

The pressures during fuel injection P_f are high enough that Equation 3.42 should be used in lieu of Equation 3.47 to evaluate the fuel enthalpy. Hence,

$$h_{\text{fuel}} = h_{\text{o}} + v_o(P_{\text{fuel}} - P_o) \quad (4.76)$$

where the subscript zero denotes conditions at atmospheric pressure ($P_o = 1.01325$ bar).

In doing a computation, one should first assume that the combustion and fuel injection are entirely at constant volume. If the resultant P_3 satisfies Equation 4.71, then indeed the process is at constant volume. However, if Equation 4.71 is not satisfied, then $P_3 = P_{\text{limit}}$, and one solves Equation 4.75 to find the state 3.

The expansion occurs to a specific volume at state 4 different from that at state 1 because of the fuel injected. It can be shown that expansion must satisfy the following constraints:

$$s_4 = s_3 \quad (4.77)$$

$$v_4 = rv_3 = rv_2 \frac{m_2}{m_3} = \frac{rv_2}{1 + (1-f)\phi FA_s} \quad (4.78)$$

To evaluate the work $w_{c.v.}$, it is convenient to split it into three parts, w_{12} , w_{23} , and w_{34} , due to the change in mass and energy by fuel injection. The work components expressed per unit mass after fuel injection are

$$w_{c.v.} = w_{12} + w_{23} + w_{34} \quad (4.79)$$

$$w_{12} = \frac{W_{12} m_2}{m_2 m_3} = \frac{u_1 - u_2}{1 + (1-f)\phi FA_s} \quad (4.80)$$

$$w_{23} = P_3 \left[v_3 - \frac{v_2}{1 + (1-f)\phi FA_s} \right] \quad (4.81)$$

$$w_{34} = u_3 - u_4 \quad (4.82)$$

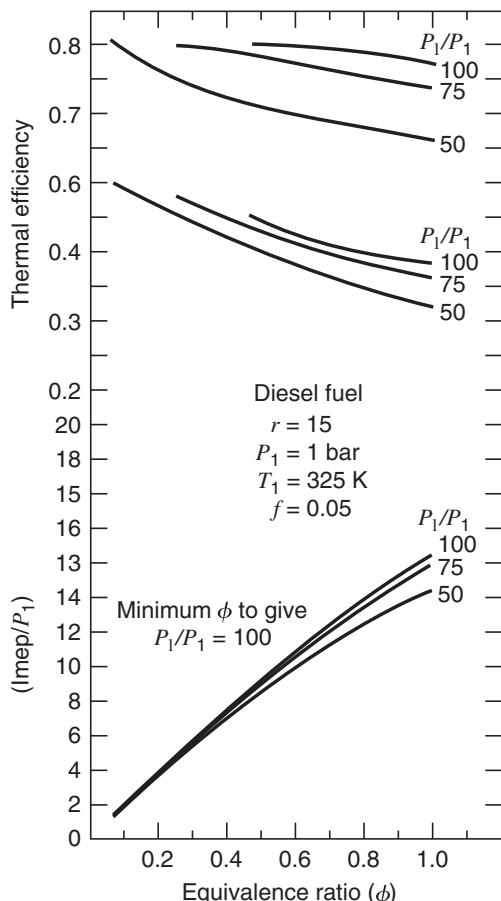


Figure 4.14 Effect of equivalence ratio on limited pressure fuel-air cycle.

The efficiency and imep are given by

$$\eta = \frac{w_{c.v.} m_3}{m_f a_o} = \frac{w_{c.v.}[1 + (1 - f)\phi F A_s]}{(1 - f)\phi F A_s a_o} \quad (4.83)$$

$$\text{imep} = \frac{w_{c.v.}[1 + (1 - f)\phi F A_s]}{v_1 - v_2} \quad (4.84)$$

Results obtained using the above modeling for different compression and equivalence ratios are given in Figures 4.14 and 4.15. Important conclusions are

1. The efficiency decreases with increased equivalence ratio. This is consistent with the Otto cycle fuel-air model, where the efficiency is maximum for lean mixtures.
2. The imep increases with equivalence ratio. This is also consistent with the Otto cycle fuel-air model, where the imep is maximum for slightly rich mixtures. Since the combustion is heterogeneous, the engine can be controlled without throttling the air.
3. The efficiency and imep are a weaker function of compression ratio relative to an Otto cycle. This is due to the constraint on peak pressure.
4. Both efficiency and imep increase with increasing limit pressure.
5. Even in the absence of heat and mass loss, the ratio η/η_{Otto} may be as low as 0.85.

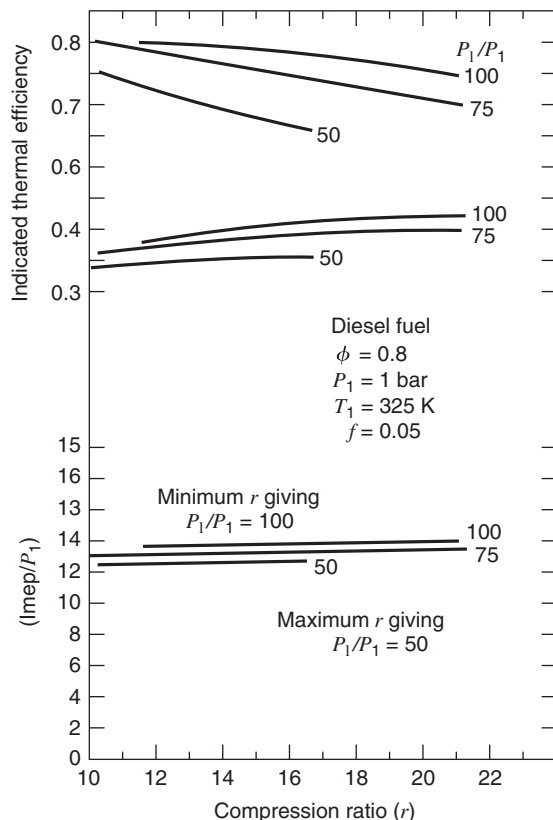


Figure 4.15 Effect of compression ratio on limited pressure fuel-air cycle.

The constraint on peak pressure results in the efficiency and imep being insensitive to compression ratio. In practice, the ratio η/η_{Otto} for diesel and fuel injected stratified engines is more sensitive to the particular design and the operating conditions than it is for homogeneous charge spark ignition engines. Thus, a greater range of indicated efficiencies exists among engines made by different manufacturers and among engines of different sizes. Divided chamber engines usually have a smaller η/η_{Otto} ratio than open chamber engines partly because of throttling losses through the throat between chambers, but mainly because of a greater heat loss.

4.9 COMPARISON OF LIMITED PRESSURE FUEL-AIR CYCLES WITH ACTUAL COMPRESSION IGNITION CYCLES

Diesel engines are designed to limit both the rates of pressure rise and the maximum pressures to satisfy durability, noise, and emissions considerations. Therefore, a convenient standard appears to be the equivalent limited pressure fuel-air cycle, and indeed this was the choice of Taylor (1985). As in the spark ignition engine, the losses are attributed to heat and mass loss, the finite blowdown rate, and combustion occurring at less than the maximum pressure.

The fuel-air cycle adequately models conventional spark ignition engines, but is not as useful for an engine as heterogeneous as a typical diesel engine. Diesel engine fuel flow rates are limited by the appearance of solid carbon in exhaust that did not burn to carbon

monoxide or carbon dioxide. This occurs even though the engine is running lean and is not predicted by fuel-air cycles. A more sophisticated model is required. These exist but are beyond the scope of this text.

There are two problems with using the limited pressure fuel-air cycle as a standard. The first is that an engine that can operate at a higher peak pressure and still satisfy the constraints imposed by durability, noise, and emissions considerations is a better engine and ought to be recognized as such. The second issue is that for some engines, it is not possible to construct an equivalent limited-pressure fuel-air cycle because the losses are so great that the peak pressure is less than would be achieved via isentropic compression alone.

We conclude this chapter by noting that if the ratio of η/η_{Otto} is a measure of how well an engine of a given compression ratio is developed, it appears that gasoline engines are more highly developed than diesel engines. This suggests that there is more potential for payoff from research and development on losses in diesel engines than there is on losses in spark ignition engines.

For further reading on the topic of how the second law of thermodynamics can be used to better understand internal combustion engine processes, especially combustion, the reader is referred to the text by Bejan (2006), and a series of papers by Caton (2000, 2010).

4.10 REFERENCES

- BEJAN, A. (2006), *Advanced Engineering Thermodynamics*, Wiley, New York.
- CATON, J. (2000), "On the Destruction of Availability (Exergy) Due to Combustion Processes: With Specific Application to Internal Combustion Engines," *Energy*, Vol. 25, pp. 1097–1117.
- CATON, J. (2010), "An Assessment of the Thermodynamics Associated the High-Efficiency Engines," ASME paper ICEF2010-35037.
- OBERT, E. (1973), *Internal Combustion Engines and Air Pollution*, Harper & Row, New York.
- RAINE, R., C. STONE, and J. GOULD (1995), "Modeling of Nitric Oxide Formation in Spark Ignition Engines with a Multizone Burned Gas," *Combust. Flame*, Vol. 102, p. 241–255.
- TAYLOR, C. (1985), *The Internal Combustion Engine in Theory and Practice*, Vol. 1, MIT Press, Cambridge, Massachusetts.

4.11 HOMEWORK

- 4.1** Compute the higher, lower, and equilibrium heats of combustion for methanol CH_3OH (*l*). The equilibrium computation determines the quality of the water in the products at standard atmospheric pressure and temperature.
- 4.2** The heat of combustion could have been defined without requiring complete conversion to carbon dioxide and water. What would the lower heat of combustion be for the case $\phi = 1.4$, fuel = C_8H_{18} (*l*) octane, $T_0 = 298 \text{ K}$, $P_0 = 1 \text{ atm}$? Assume the water quality $\chi = 1$ and that the equilibrium constant $K = 9.95 \times 10^{-6}$.
- 4.3** With reference to Figure 4.2, explain why the heats of combustion at $\phi = 0.2$ and $\phi = 1.2$ are less than those at $\phi = 1.0$.
- 4.4** What is the residual mass fraction required to reduce the adiabatic flame temperature of gasoline, diesel, methane, methanol, and nitromethane below 2000 K? Assume $\phi = 1.0$ at 101 kPa and 298 K.
- 4.5** Plot the adiabatic flame temperature of gasoline as a function of pressure ($50 < P < 5000$ kPa) for $T = 298 \text{ K}$, $\phi = 1.0$, and $f = 0.1$.

- 4.6** Equilibrium combustion products at $\phi = 0.9$ of methane CH_4 are expanded isentropically from $T_1 = 2000 \text{ K}$, $P_1 = 1000 \text{ kPa}$ to a pressure P_2 of 100 kPa. Find the final temperature T_2 and the work done.
- 4.7** Equilibrium combustion products of gasoline are expanded isentropically by a volume ratio of 10:1. (a) For $\phi = 1.1$ and an initial state of $T_1 = 3000 \text{ K}$, $P_1 = 5000 \text{ kPa}$, find the final state (T_2, P_2) and the work done. (b) Repeat the calculation for $\phi = 0.9$. What is the effect of equivalence ratio?
- 4.8** Show that Equation 4.35 for the second law efficiency reduces to Equation 4.26 for the first law efficiency when there is only heat transfer to the system instead of combustion.
- 4.9** Derive Equation 4.37 for the second law efficiency.
- 4.10** Derive Equation 4.43 for the volumetric efficiency.
- 4.11** What is the change in exergy $a_j - a_i$ (kJ/kg) for the compression (1–2), combustion (2–3), and expansion (3–4) strokes of the fuel–air cycle of Example 4.3?
- 4.12** Compute a_o , the maximum energy of combustion, for liquid gasoline C_7H_{17} based on equilibrium water quality, lean combustion at $\phi = 0.01$, and unmixed reactants.
- 4.13** Plot the second law thermal efficiency versus compression ratio (vary r from 5 to 20) for a methane fuel–air Otto cycle. Compare the results with the gas Otto cycle. Assume $T_i = 350 \text{ K}$, $\phi = 1.0$, $f = 0.05$, and $\gamma = 1.3$.
- 4.14** What compression ratio is required to have an imep of 1500 kPa with a methane fuel–air Otto cycle, assuming $T_1 = 325 \text{ K}$, $\phi = 0.95$, $f = 0.05$, and $P_1 = 101.3 \text{ kPa}$?
- 4.15** What value of the equivalence ratio will maximize the imep for a gasoline fuel–air Otto cycle with a compression ratio of 10? Assume $T_1 = 350 \text{ K}$, $f = 0.05$, and $P_1 = 101.3 \text{ kPa}$.
- 4.16** Exhaust gas recirculation (EGR) is used in spark ignition engines to reduce the peak combustion temperature and the concentration of NO_x . EGR can be modeled in a fuel–air cycle by varying the residual fraction. What residual fraction is needed to reduce T_3 to 2250 K in a gasoline engine with the following conditions: $T_1 = 350 \text{ K}$, $\phi = 0.95$, $r = 10$, and $P_1 = 101.3 \text{ kPa}$? If the original residual fraction was $f = 0.05$, what is the change in the imep, and why?
- 4.17** Plot and discuss the effect of supercharging on the volumetric and thermal efficiency of a four-stroke gasoline fuel–air Otto cycle model. Vary the intake pressure from 60 to 160 kPa, and assume $T_i = 300 \text{ K}$, $\phi = 1.0$, $r = 10$, and $P_e = 105 \text{ kPa}$.
- 4.18** As the intake pressure is throttled from 101.3 to 50 kPa, what is the change in the volumetric efficiency, imep, and residual fraction of a four-stroke gasoline fuel–air Otto cycle engine? Assume $T_i = 300 \text{ K}$, $\phi = 0.9$, $r = 11$, and $P_e = 105 \text{ kPa}$.
- 4.19** A CFR engine is operated at the following conditions: gasoline fuel with $P_1 = 100 \text{ kPa}$, $T_1 = 340 \text{ K}$, $r=10$, $\phi = 1.0$. The engine has a bore of 0.0825 m and stroke of 0.114 m. The other engine conditions are the same as in Example 4.8. Using the program Homogeneous .m, (a) compute the pressure and burned and unburned zone temperatures, imep, and thermal efficiency. (b) While keeping other parameters constant, compute and plot the effect of varying the spark advance (vary θ_s from 0 to -40°atdc), the equivalence ratio (vary ϕ from 0.7 to 1.3), and the compression ratio (vary r from 5 to 15). Compare and discuss the computational results with the experimental results given in Section 4.7.
- 4.20** Derive Equations 4.70–4.83 for the limited pressure fuel–air cycle.

Chapter 5

Intake and Exhaust Flow

5.1 INTRODUCTION

In this chapter, we examine the airflow into and out of the intake and exhaust systems in internal combustion engines. We will use compressible fluid mechanics to develop relationships between engine speed, mass flow rate, and valve geometry. A fundamental limiting factor affecting the performance of internal combustion engines is the onset of choked flow that occurs at high engine speeds. Since choked flow results from intake and exhaust valve flow area restrictions, most present-day engines have multiple intake and exhaust valves to minimize flow restrictions.

So far we have restricted our attention to constant pressure intake and exhaust flows. The constant pressure intake and exhaust model is qualitatively useful but quantitatively lacking, since no account is made of the unsteady and compressible flow phenomena affecting mass flow and pressure. Finally, we discuss the performance of superchargers and turbochargers, and how they can be incorporated into internal combustion engines to increase airflow and power.

5.2 VALVE FLOW

Valve Flow and Discharge Coefficients

The most significant airflow restriction in an internal combustion engine is the flow through the intake and exhaust valves. Typically the minimum cross-sectional area in the intake and exhaust system occurs at the valve, as shown in Figures 5.1 and 5.2. In accounting for the pressure drop across the intake and exhaust valves considerable success has been realized by modeling the gas flow through the valves as one-dimensional quasi-steady compressible flow. In this section, we obtain relationships for the mass flow rate through valves as a function of the intake and exhaust pressure ratio.

The velocity U in the intake and exhaust manifolds can be non dimensionalized by the speed of sound c to form the Mach number $M = U/c$, and conditions at various locations in the manifolds can be related to stagnation conditions where the Mach number $M = 0$. For steady adiabatic flow, the energy equation is

$$h_o = h + \frac{U^2}{2} = \text{const} \quad (5.1)$$

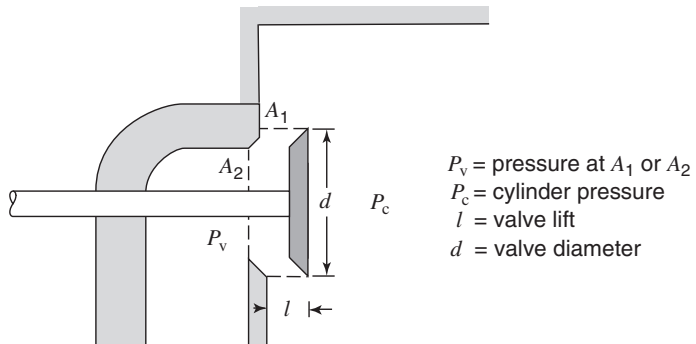


Figure 5.1 Schematic of valve flow areas.

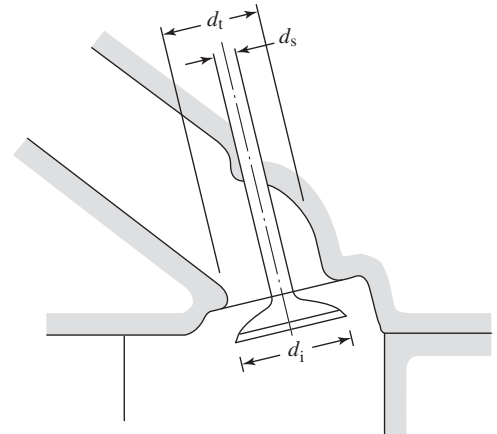


Figure 5.2 Schematic of valve flow blockage.

and for a gas with constant specific heats

$$\begin{aligned}
 \frac{T_o}{T} &= 1 + \frac{U^2}{2c_p T} \\
 &= 1 + \left(\frac{\gamma - 1}{2} \right) M^2
 \end{aligned} \tag{5.2}$$

For isentropic flow, the pressure and density are functions of the Mach number:

$$\begin{aligned}
 \frac{P_o}{P} &= \left[\frac{T_o}{T} \right]^{\gamma/(\gamma-1)} \\
 &= \left[1 + \left(\frac{\gamma - 1}{2} \right) M^2 \right]^{\gamma/(\gamma-1)}
 \end{aligned} \tag{5.3}$$

$$\begin{aligned}
 \frac{\rho_o}{\rho} &= \left[\frac{T_o}{T} \right]^{1/(\gamma-1)} \\
 &= \left[1 + \left(\frac{\gamma - 1}{2} \right) M^2 \right]^{1/(\gamma-1)}
 \end{aligned} \tag{5.4}$$

The pressure and density at the valve are related to the upstream stagnation pressure and density by the isentropic relation

$$\rho_v = \rho_o \left(\frac{P_v}{P_o} \right)^{1/\gamma} \quad (5.5)$$

and the ideal gas equation at stagnation conditions is

$$P_o = \rho_o R T_o \quad (5.6)$$

The stagnation sound speed c_o is

$$c_o = (\gamma R T_o)^{1/2} \quad (5.7)$$

The mass flow rate, \dot{m} , through a valve depends on the valve effective area A_f , fluid velocity and density:

$$\dot{m} = \rho_v A_f U_{is} \quad (5.8)$$

The velocity U_{is} is the reference isentropic velocity, and ρ_v is the fluid density at the valve. The isentropic velocity U_{is} depends on the pressure ratio and is calculated from the isentropic relation for flow in a converging nozzle:

$$U_{is} = \left[2 \frac{\gamma}{\gamma - 1} \frac{P_o}{\rho_o} \left(1 - \left(\frac{P_v}{P_o} \right)^{(\gamma-1)/\gamma} \right) \right]^{1/2} \quad (5.9)$$

where

P_o = upstream total or stagnation pressure

P_v = valve static pressure

ρ_o = upstream total or stagnation density

Upon substitution of Equations 5.5, 5.6, 5.7, and 5.9 into Equation 5.8, we obtain the desired relationship:

$$\dot{m} = \rho_o A_f c_o \left[\frac{2}{\gamma - 1} \left(\left(\frac{P_v}{P_o} \right)^{2/\gamma} - \left(\frac{P_v}{P_o} \right)^{(\gamma+1)/\gamma} \right) \right]^{1/2} \quad (5.10)$$

For intake flow into the cylinder, the stagnation conditions refer to conditions upstream of the valve in the intake port. For exhaust flow out of the cylinder, the stagnation conditions refer to conditions in the cylinder.

Choked flow occurs at a valve throat if the ratio of the upstream pressure to downstream pressure exceeds a critical value. When the flow is choked the Mach number at the valve throat is $M = 1$, and the critical pressure ratio is found from Equation 5.3 above to be

$$\begin{aligned} \frac{P_o}{P} &= \left[1 + \left(\frac{\gamma - 1}{2} \right) \right]^{\gamma/(\gamma-1)} \\ &= \left(\frac{\gamma + 1}{2} \right)^{\gamma/(\gamma-1)} \end{aligned} \quad (5.11)$$

For $\gamma = 1.35$, the critical pressure ratio is 1.86. Note that for choked flow, the valve static pressure P_v depends only on the upstream stagnation pressure P_o and is independent of the downstream pressure. For nonchoked flow into the cylinder, it may generally be assumed that the throat pressure is equal to the cylinder pressure. If the kinetic energy in

the cylinder is relatively negligible, one need not distinguish between static and stagnation cylinder pressure. However, for exhaust flow from the cylinder in nonchoked situations, one equates the throat pressure to the exhaust port static pressure and this may differ significantly from the exhaust port stagnation pressure.

Upon substitution of Equation 5.11 into Equation 5.10, we find the choked mass flow rate \dot{m}_{cr} to be

$$\begin{aligned}\dot{m}_{\text{cr}} &= \rho_0 A_f c_0 \left(\frac{2}{\gamma + 1} \right)^{(\gamma+1)/2(\gamma-1)} \\ &= K(\gamma) A_f \frac{P_0}{\sqrt{RT_0}}\end{aligned}\quad (5.12)$$

where $K(\gamma)$ is a parameter dependent only on the specific heat ratio γ . For $\gamma = 1.35$, $K = 6.76$.

$$K(\gamma) = \gamma^{1/2} \left(\frac{2}{\gamma + 1} \right)^{(\gamma+1)/2(\gamma-1)} \quad (5.13)$$

Alternatively, the effective area required for a given mass flow rate and stagnation pressure and temperature is

$$A_f = \frac{\dot{m}_{\text{cr}} \sqrt{RT_0}}{K P_0} \quad (5.14)$$

Equation 5.10 for the mass flow rate assumes flow from an upstream reservoir through an effective minimum valve area, A_f . The effective valve area depends on the valve diameter and lift, and two associated minimum areas are used, each with a corresponding flow coefficient. As shown in Figure 5.1, a geometric minimum area A_v can be defined using either the valve curtain area $A_1 = \pi d l$ or the valve seat area $A_2 = \pi d^2 / 4$. If the valve seat area is chosen, the flow coefficient is labeled C_f , as defined in Equation 5.15. If the valve curtain area is used, the flow coefficient is labeled C_d , a discharge coefficient, as shown in Equation 5.16.

$$A_f = C_f A_v = C_f \frac{\pi}{4} d^2 \quad (\text{Seat}) \quad (5.15)$$

$$A_f = C_d A_v = C_d \pi d l \quad (\text{Curtain}) \quad (5.16)$$

In the idealized model of a poppet valve shown in Figure 5.1, the two minimum geometric area A_v possibilities are evident, depending on the valve lift. For low lift the minimum area is the valve curtain area, and for larger lifts the minimum area is the valve seat area. In this idealized model, the geometric effects of the valve stem and valve seat angle are neglected. These considerations are addressed in Homework Problem 7.7. As shown in Figure 5.3, there is little reason to open a valve much beyond $l/d \approx 1/4$, since the flow area at such lifts would be limited by the port size. For intake ports, the maximum l/d is about 0.4, accounting for the flow coefficient of the port.

Flow or discharge coefficients are measured using steady flow benches like that illustrated in Figure 5.4. The mass flow rate and pressure drop across the valve are measured for a number of different valve lifts and pressure ratios. Equation 5.10 is then solved for the flow coefficient for a particular choice of representative valve area. It should be noted that flow bench pressure drops are of the order of 5 kPa, whereas actual pressure drops across exhaust valves are about two orders of magnitude larger, since the cylinder pressure at the exhaust valve opening is of the order of 500 kPa.

A typical plot of C_f versus lift is given in Figure 5.5. The flow coefficient C_f increases monotonically from zero with lift, since the effective flow area through the valve increases

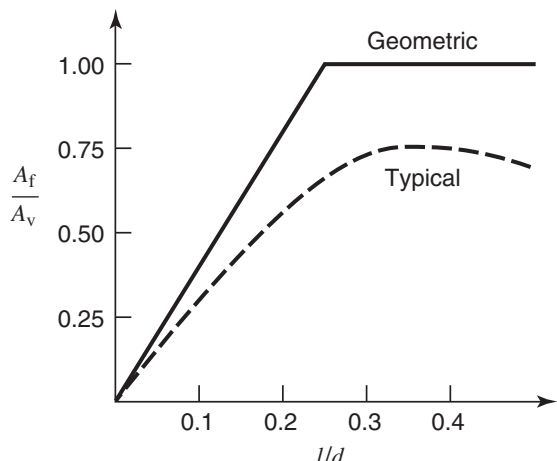


Figure 5.3 Valve flow coefficients versus lift.

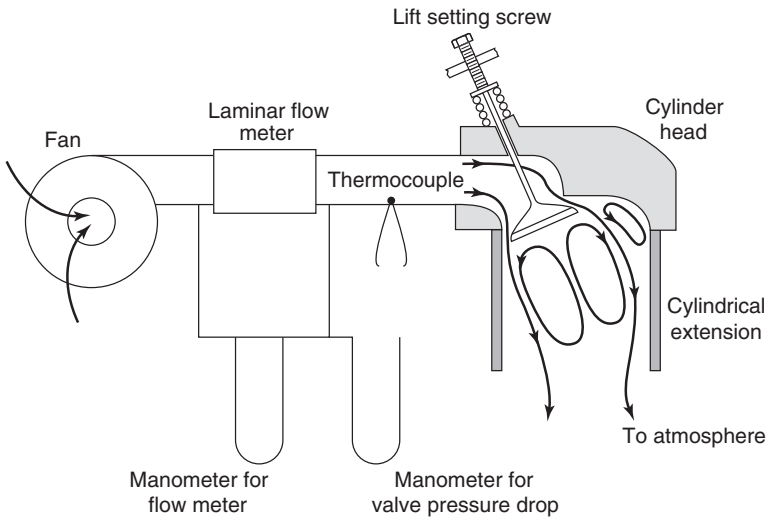


Figure 5.4 Schematic of a steady flow bench.

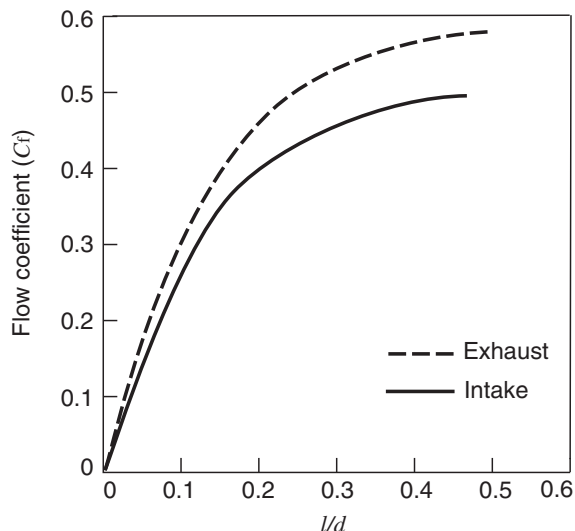


Figure 5.5 Intake and exhaust port flow coefficients. Adapted from Boretti et al. (1994).

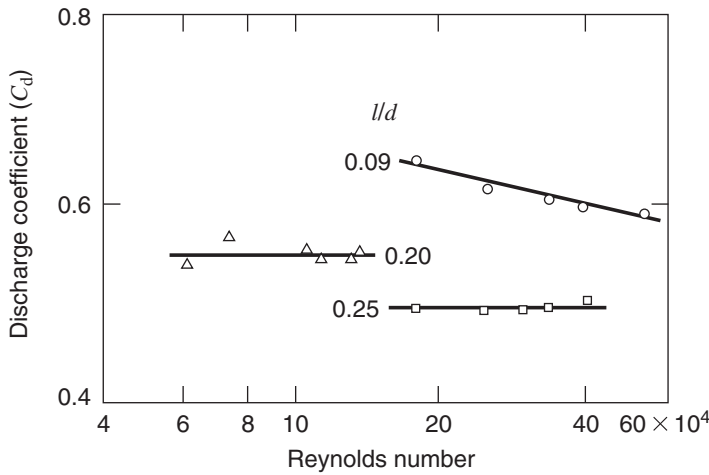


Figure 5.6 Effect of Reynolds number and nondimensional valve lift l/d on inlet valve discharge coefficient (Annand and Roe, 1974).

with lift, and the representative valve area $\pi d^2/4$ remains constant. The maximum value of C_f is seen to be about 0.6.

The discharge coefficient C_d is plotted versus Reynolds number in Figure 5.6. The discharge coefficient C_d is not a strong function of lift, since the curtain area is used to non-dimensionalize the valve area in forming C_d . The dependence of the discharge coefficient C_d on Reynolds number in Figure 5.6 can be understood in terms of the flow patterns shown in Figure 5.7.

At low lifts, $l/d = 0.0$, the inlet jet is attached to both the valve and the seat, and thus affected by viscous shear. The discharge coefficient, C_d , decreases slightly with lift, since the jet fills less of the reference curtain area as it transforms from an attached jet to a separated free jet. At high lifts, $l/d \geq 0.20$, the fluid inertia prevents the flow from turning along the valve seat, so the flow breaks away, forming a free jet. The flow area of a free jet is more or less independent of viscosity, thus the flow coefficient at high lifts is independent of Reynolds number.

Discharge coefficient results for exhaust valves are shown in Figure 5.8. Exhaust flow patterns are presented in Figure 5.9, and are basically unchanged as the exhaust valve opens, so the discharge coefficient is a weak function of the exhaust valve lift. Separation

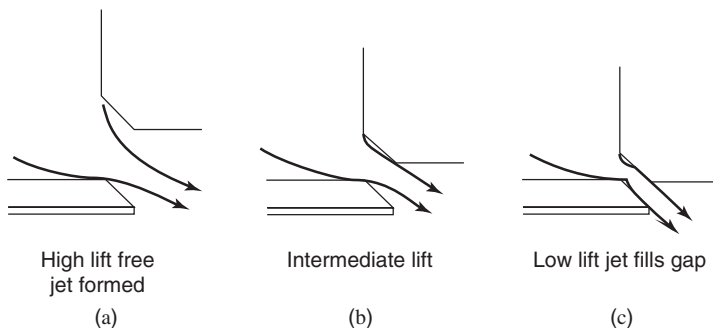


Figure 5.7 Flow patterns through an inlet valve (Annand and Roe, 1974).

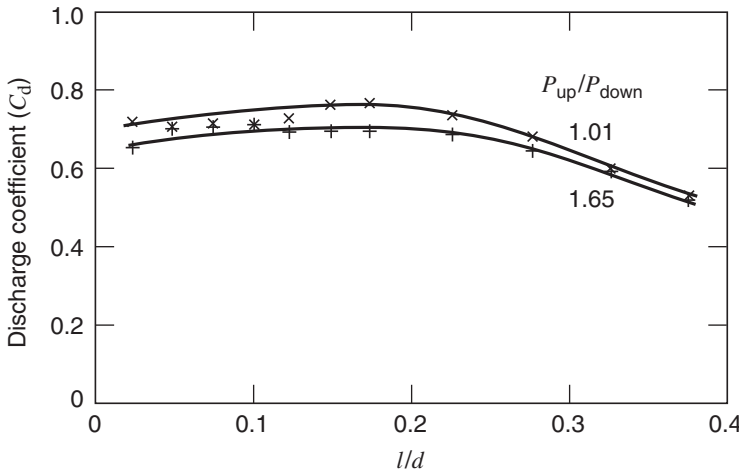


Figure 5.8 Effect of valve lift on exhaust valve discharge coefficient (Annand and Roe, 1974).

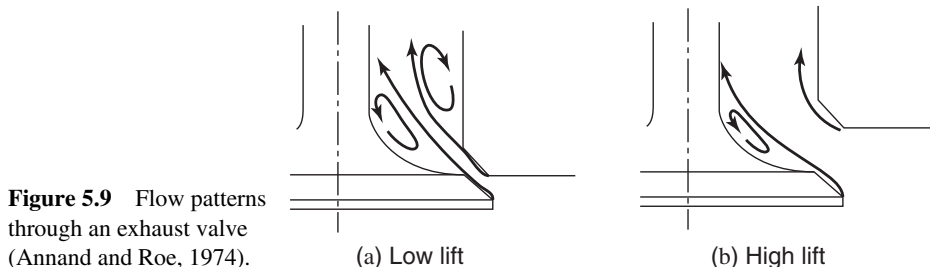


Figure 5.9 Flow patterns through an exhaust valve (Annand and Roe, 1974).

of the exhaust jet from the valve seat at high lift will cause the discharge coefficient to decrease slightly at high lifts.

EXAMPLE 5.1 Exhaust Mass Flow Rate

What is the initial mass flow rate through an exhaust valve, if the valve curtain area A_v is $2.7 \times 10^{-3} \text{ m}^2$, the valve discharge coefficient C_d is 0.6, and the cylinder pressure and temperature are initially at 500 kPa and 1000 K? Assume the exhaust system pressure is 105 kPa, $\gamma = 1.35$, and $R = 287 \text{ J/(kg K)}$.

SOLUTION First compute the pressure ratio and compare it to the critical pressure ratio to determine if the flow is choked:

$$\frac{P_o}{P_{exh}} = \frac{500}{105} = 4.76$$

$$\left(\frac{P_o}{P_{exh}} \right)_{cr} = \left(\frac{2}{\gamma + 1} \right)^{-\gamma/(\gamma-1)} = 1.86$$

Therefore, the flow is choked.

Second, use the choked flow equation, Equation 5.12, to compute the initial mass flow rate:

$$\dot{m} = \dot{m}_{\text{cr}} = \rho_0 C_d A_v c_0 \left(\frac{2}{\gamma + 1} \right)^{(\gamma+1)/2(\gamma-1)} \quad (5.17)$$

$$\rho_0 = P_0 / RT_0 = \frac{500 \times 10^3}{287 \times 1000} = 1.74 \text{ kg/m}^3 \quad (5.18)$$

$$\dot{m} = (1.74)(0.6)(2.7 \times 10^{-3})(1.35 \times 287 \times 1000)^{1/2}(2/2.35)^{3.36} = 1.02 \text{ kg/s} \quad (5.19)$$

Exhaust Gas Blowdown

In Chapter 2, we approximated the exhaust gas blowdown through a valve or port as a constant volume isentropic process. Using the unsteady mass and energy conservation equations, we can estimate a blowdown time, and compare to typical engine timescales.

If we define the control volume as the cylinder volume with instantaneous mass $m(t)$, pressure $P(t)$, temperature $T(t)$, and exiting (e) mass flow through an effective area A_f then

$$\frac{dm}{dt}|_{cv} = -\dot{m}_e \quad (5.20)$$

and if we assume no work or heat transfer during this process, the energy equation is

$$\frac{dE}{dt}|_{cv} = -\dot{m}_e h_e \quad (5.21)$$

Assuming an ideal gas with constant specific heats, at any time the energy in the control volume is

$$E|_{cv} = mc_v T \quad (5.22)$$

and the enthalpy of the exiting flow is

$$h_e = c_p T \quad (5.23)$$

The energy equation is then

$$\frac{d}{dt}(mc_v T) = c_v T \frac{dm}{dt} + c_v m \frac{dT}{dt} = -\dot{m}_e c_p T \quad (5.24)$$

or

$$mc_v \frac{dT}{dt} = -\dot{m}_e (c_p - c_v) T = -\dot{m}_e R T \quad (5.25)$$

If we assume the pressure differences are great enough across the valve to produce choked flow, then the exiting flow rate \dot{m}_e is

$$\dot{m}_{cr} = K A_f \frac{P}{\sqrt{RT}} \quad (5.26)$$

Upon substitution into the energy equation,

$$mc_v \frac{dT}{dt} = -K A_f P \sqrt{RT} \quad (5.27)$$

Since $P = \rho RT$, $R/c_v = \gamma - 1$, and $m = \rho V$, Equation 5.27 becomes

$$\frac{dT}{dt} = - \left[\frac{K(\gamma - 1)R^{1/2}A_f}{V} \right] T^{3/2} \quad (5.28)$$

If we let the initial temperature in the cylinder be $T = T_i$ at $t = 0$, and integrate to time t , with $V = \text{constant}$, then

$$\frac{T(t)}{T_i} = (1 + C T_i t)^{-2} \quad (5.29)$$

where

$$C = \frac{K(\gamma - 1)R^{1/2}A_f}{2V} \quad (5.30)$$

Assuming an isentropic blowdown process,

$$\begin{aligned} \frac{P}{P_i} &= \left(\frac{T}{T_i} \right)^{\gamma/(\gamma-1)} \\ &= \left(1 + C \sqrt{T_i} t \right)^{-2\gamma/(\gamma-1)} \end{aligned} \quad (5.31)$$

solving for time t ,

$$t = \frac{(P/P_i)^{(1-\gamma)/2\gamma} - 1}{C \sqrt{T_i}} \quad (5.32)$$

EXAMPLE 5.2 Characteristic Exhaust Blowdown Time

An engine operates at 2000 rpm. The cylinder volume V is $7.85 \times 10^{-4} \text{ m}^3$ when the exhaust valve opens to ambient conditions. The average valve effective area A_f is $2.50 \times 10^{-3} \text{ m}^2$. The cylinder pressure P and temperature T when the exhaust valve opens are at 500 kPa and 1500 K. Estimate the time t required for the cylinder pressure to be reduced to 200 kPa, and compare it to the time required for one stroke. Assume $\gamma = 1.35$, and $R = 287 \text{ J/(kg K)}$.

SOLUTION Assuming a constant cylinder volume and choked flow conditions, so Equation 5.32 is applicable. We first compute the constants K and C in Equation 5.32.

$$K = \gamma^{1/2} \left(\frac{2}{\gamma + 1} \right)^{(\gamma+1)/2(\gamma-1)} = 0.676 \quad (5.33)$$

$$\begin{aligned} C &= \frac{K(\gamma - 1)R^{1/2}A_f}{2V} \\ &= \frac{(0.676)(1.35 - 1)(\sqrt{287})(2.5 \times 10^{-3})}{2(7.85 \times 10^{-4})} \\ &= 6.38 \end{aligned} \quad (5.34)$$

$$\begin{aligned} t &= \frac{(P/P_i)^{(1-\gamma)/2\gamma} - 1}{C \sqrt{T_i}} \\ &= \frac{(200/500)^{-0.13} - 1}{6.38 \sqrt{1500}} \\ &= 0.51 \times 10^{-3} \\ &\approx 1/2 \text{ ms} \end{aligned} \quad (5.35)$$

A piston stroke is 180° , and an engine speed of 2000 rpm is equivalent to $12,000^\circ/\text{s}$, so the time required for one stroke is $180/12,000$ or 15 ms. For this engine, the blowdown from 500 to 200 kPa is thus about 1/30 of the piston stroke time, justifying the constant volume assumption.

Valve Mach Index

In this section, we examine the effect of valves on the engine volumetric efficiency. If we assume that the pressure in the intake and exhaust ports is equal to the pressure in the intake and exhaust plenums, respectively, then the mass inducted during the valve open period is

$$m_i = \frac{1}{\omega} \int_{\theta_{io}}^{\theta_{ic}} \dot{m} d\theta = \frac{1}{\omega} \int_{\theta_{io}}^{\theta_{ic}} \rho A_f c \left[\frac{2}{\gamma - 1} \left(\left(\frac{P_v}{P_o} \right)^{2/\gamma} - \left(\frac{P_v}{P_o} \right)^{(\gamma+1)/\gamma} \right) \right]^{1/2} d\theta \quad (5.36)$$

where θ_{io} is the crank angle at which the intake valve opens and θ_{ic} is the angle at which it closes. The terms A_f , ρ , c , P_v/P_o , and γ depend on the direction of flow, whether into or out of the cylinder. Let us normalize Equation 5.36 by the average effective intake flow area, \bar{A}_f ,

$$\bar{A}_f = \frac{1}{\theta_{ic} - \theta_{io}} \int_{\theta_{io}}^{\theta_{ic}} A_f d\theta = \bar{C}_f A_v \quad (5.37)$$

the intake plenum density, ρ_i , and sound speed, c_i :

The term \bar{C}_f is the average flow coefficient. We then have for the volumetric efficiency

$$e_v = \frac{m_i}{\rho_i V_d} = \frac{\bar{A}_f c_i}{\omega V_d} \int_{\theta_{io}}^{\theta_{ic}} \frac{\rho}{\rho_i} \frac{A_f}{\bar{A}_f} \frac{c}{c_i} \left[\frac{2}{\gamma - 1} \left(\left(\frac{P_v}{P_o} \right)^{2/\gamma} - \left(\frac{P_v}{P_o} \right)^{(\gamma+1)/\gamma} \right) \right]^{1/2} d\theta \quad (5.38)$$

Note that in the absence of reverse flow during induction $\rho/\rho_i = c/c_i = 1$; the terms are included as shown to cover the more general case in which reverse flow occurs. A more rigorous analysis would include the effect of engine speed.

Let us consider the limiting case in which the flow is always choked and into the cylinder. The pressure ratio given by Equation 5.11 is independent of crank angle, so

$$e_v = \left(\frac{2}{\gamma + 1} \right)^{(1+\gamma)/2(\gamma-1)} \frac{\bar{A}_f c_i}{\omega V_d} (\theta_{ic} - \theta_{io}) \quad (5.39)$$

We define a cycle averaged Mach number as the Mach index Z (Taylor, 1985) as

$$Z = \frac{\frac{\pi}{4} b^2}{\bar{A}_f} \frac{\bar{U}_p}{c_i} \quad (5.40)$$

so the volumetric efficiency becomes, assuming $\gamma = 1.4$,

$$e_v = 0.58 \left(\frac{\theta_{ic} - \theta_{io}}{\pi} \right) \frac{1}{Z} \quad (5.41)$$

Experimental results are available for an engine in which $(\theta_{ic} - \theta_{io})/\pi = 1.3$ and thus $e_v = 0.75/Z$. They are given in Figure 5.10. Equation 5.39 is an upper bound for the volumetric efficiency valid for large Z . It should be noted that the Mach index is not a parameter that characterizes an actual gas speed; rather, it characterizes what the average gas speed through the inlet valve would have to be to realize complete filling of the cylinder

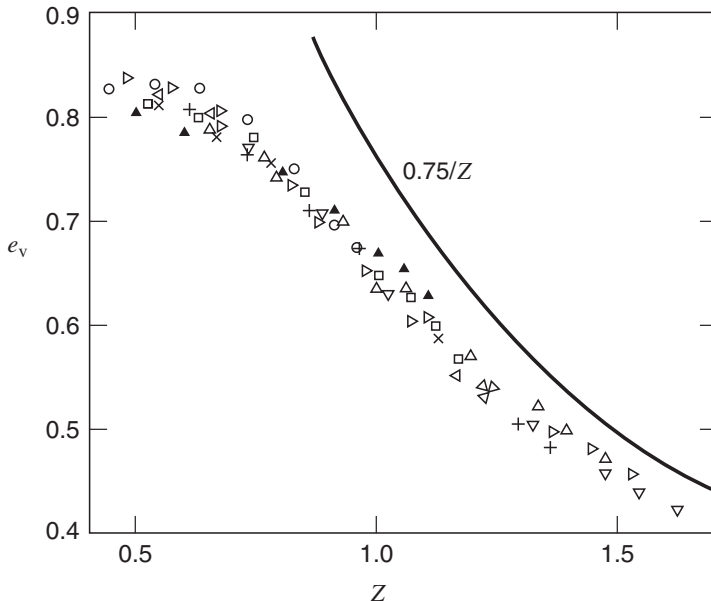


Figure 5.10 Volumetric efficiency versus inlet valve Mach index in the regime where choking occurs at the inlet valve (Livengood and Stanitz, 1943).

at that particular piston speed. The Mach number for that average inlet gas speed would be $Z/0.58$ for $\gamma = 1.4$.

The results in Figure 5.10 show that for good volumetric efficiency one should keep the Mach index down to less than about $Z = 0.6$. Based on the analyses that led to Equation 5.41, we can interpret this to mean that the average gas speed through the inlet valve should be less than the sonic velocity, so that the intake flow is not choked. Hence, inlet valves can be sized on the basis of the maximum piston speed for which the engine is designed. If we choose $Z = 0.6$ at this speed, it follows that the average effective area \bar{A}_i of the intake ($\bar{A}_f \rightarrow \bar{A}_i$) valves is

$$\bar{A}_i \geq 1.3 b^2 \frac{\bar{U}_p}{c_i} \quad \text{intake} \quad (5.42)$$

Likewise, for efficient expulsion of the exhaust gas, the average effective area \bar{A}_e , of the exhaust ($\bar{A}_f \rightarrow \bar{A}_e$) valves should be such that their Mach index is less than about 0.6, in which case, relative to intake conditions is

$$\frac{\bar{A}_e}{\bar{A}_i} \approx \frac{c_i}{c_e} = \left(\frac{T_i}{T_e} \right)^{1/2} \quad (5.43)$$

As suggested by the c_i/c_e ratio in Equation 5.43, a smaller exhaust valve diameter and lift ($l \sim d/4$) can be used because the speed of sound is higher in the exhaust gases than in the inlet gas flow. Current practice dictates that the exhaust to intake valve area ratio is on the order of 70–80%.

In many situations, it turns out that the intake valves are sized as large as possible while being consistent with Equation 5.43. This is because there is only so much room available for valves and it may not be possible to satisfy Equation 5.42, thereby compromising the maximum speed of the engine.

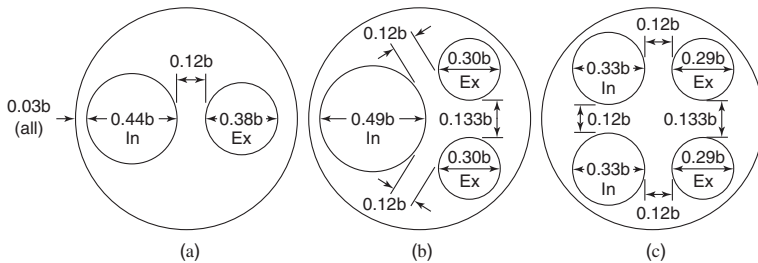


Figure 5.11 Valve diameter ratios for a flat cylinder head (b:bore, In: intake, Ex: exhaust). Adapted from Taylor (1985).

The use of multiple valves increases the valve area per unit piston area, and hence the speed at which the engine power becomes flow limited. Heads are often wedge-shaped or domed to increase the valve area to piston area ratio, so that intake valve area to piston area ratios of up to 0.5 can be obtained. Typical valve diameter ratios for two, three, and four valves per cylinder are given for a flat cylinder head in Figure 5.11.

EXAMPLE 5.3 Intake Valve Area

What is the intake valve area A_v and the ratio of the intake valve area to piston area required to have a Mach Index $Z = 0.6$ for an engine with a maximum speed of 8000 rpm, bore and stroke of 0.1 m, and inlet air temperature of 330 K? Assume $\gamma = 1.4$, $R = 287 \text{ J/kgK}$, and an average flow coefficient $\bar{C}_f = 0.35$.

SOLUTION

$$c_i = \sqrt{\gamma RT_o} = \sqrt{(1.4)(287)(330)} = 364 \text{ m/s}$$

$$\bar{U}_p = 2Ns = 2(0.1)(8000/60) = 26 \text{ m/s}$$

$$\bar{A}_i = 1.3 b^2 \frac{\bar{U}_p}{c_i} = (1.3)(0.1)^2 \frac{26}{364} = 9.3 \times 10^{-4} \text{ m}^2$$

Therefore,

$$A_v = \bar{A}_i / \bar{C}_f = 2.65 \times 10^{-3} \text{ m}^2$$

$$\frac{A_v}{A_p} = \frac{2.65 \times 10^{-3}}{\frac{\pi}{4}(0.1)^2} = 0.34$$

In a four-stroke engine, the pumping work is defined as the work required to push out the exhaust gas and to pull in the fresh charge. It is evaluated from a pressure–volume diagram from bottom center at the start of the exhaust stroke to bottom center at the end of the induction stroke. The ideal model, valid for engines operated at low Mach indices, predicts that the pme is the difference between the exhaust pressure and the inlet pressure. At higher speeds, the pressure difference across the valves at closing reduces or increases the pumping depending on whether or not the engine is supercharged. Data given by

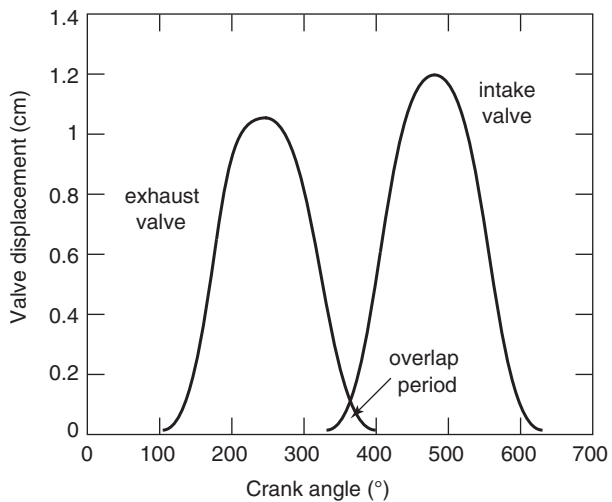


Figure 5.12 Representative exhaust and intake valve profiles.

Taylor (1985) for an engine with short intake and exhaust pipes are correlated by the following expression:

$$p_{mep} = (P_e - P_i) - (1.4 P_e - 2.6 P_i) Z^{1.5} \quad (5.44)$$

As $Z \rightarrow 0$, the p_{mep} goes to the ideal case of $P_e - P_i$.

Valve Timing

Intake and exhaust valve lifts are plotted as a function of crank angle in Figure 5.12. In order to ensure that a valve is fully open during a stroke for good volumetric efficiency, the valves are open for longer than 180° . The exhaust valve will open before bottom dead center and close after top dead center. Likewise, the intake valve will open before top dead center and close after bottom dead center. There is a valve overlap period at top dead center where the exhaust and intake valves are both open. This creates a number of flow effects. With a spark ignition engine at part throttle, there will be back flow of the exhaust into the inlet manifold since the exhaust pressure is greater than the throttled intake pressure. This will reduce the part load performance since the volume available to the intake charge is less, reducing the volumetric efficiency. Rough idle can also result due to unstable combustion. On the other hand, since this dilution will reduce the peak combustion temperatures, the NO_x pollution levels will also be reduced.

At wide open throttle, with both valves open, there will be some short-circuiting of the inlet charge directly to the exhaust, since in this case, the intake pressure is greater than the exhaust pressure. This will reduce the full load performance, since a fraction of the fuel is not burning in the cylinder.

Typical valve timing angles for a conventional and a high-performance automobile spark ignition engine are given in Table 5.1. The high-performance engine operates at much higher piston speeds at wide open throttle, with power and volumetric efficiency as the important factors, whereas the conventional engine operates at lower rpm, with idle and part load performance of importance. Therefore, the high-performance intake valve opens about 25° before the conventional intake valve, and closes about 30° after the conventional intake valve. As the engine design speed increases, to maintain a maximum valve opening during the intake and exhaust strokes, the intake and exhaust valves are open for a longer

Table 5.1 Representative Valve Timing Angles for Conventional and High-Performance Automobile Engines

		Open	Close	Duration
Intake	Conventional	5° before tdc	45° after bdc	230°
	High performance	30° before tdc	75° after bdc	285°
Exhaust	Conventional	45° before bdc	10° after tdc	235°
	High performance	70° before bdc	35° after tdc	285°

duration, from about 230° to about 285°. Early opening of the exhaust valve will reduce the expansion ratio, but will also reduce the exhaust stroke pumping work.

To minimize engine size and produce a given torque versus speed curve (with torque proportional to the volumetric efficiency at fixed thermal efficiency), it is clearly desirable to be able to vary valve timing with engine speed. Variable valve timing (VVT) is a technique that can address the problem of obtaining optimal engine performance over a range of throttle and engine speed. VVT allows the intake and exhaust valves to open and close at varying angles, depending on the speed and load conditions. At idle, with a nearly closed throttle, the intake and exhaust valve overlap is minimized to reduce exhaust back flow. At low speed, the intake valves are closed earlier to increase volumetric efficiency and torque. At high speed, with an open throttle, the intake valves are closed later to increase volumetric efficiency and power.

There have been a number of VVT mechanisms built and commercialized. As one might expect, the mechanical components of a VVT device are complex. Hydraulic mechanisms, dual lob camshafts with followers have been developed, and electromagnetic and electrohydraulic actuators that replace the camshaft have also been used, however, at greater expense.

Effect of Valve Timing on Volumetric Efficiency and Residual Fraction

The first law of thermodynamics applied to an open system doing boundary work is

$$\Delta E = - \int P dV + \int (\dot{m}_{in} h_{in} - \dot{m}_{out} h_{out}) dt + \int \dot{Q} dt \quad (5.45)$$

For an ideal gas with constant specific heat, it can be shown that

$$\Delta E = c_v \Delta(mT) = \frac{1}{\gamma - 1} \Delta(PV) \quad (5.46)$$

Let us assume that during overlap, residual exhaust gas flows up into the intake manifold and later an equal amount flows back into the cylinder. The flow into the cylinder is initially composed of residual exhaust gas until all of the residual gases in the intake manifold return back to the cylinder. It follows that for the intake process

$$\int_{io}^{ic} [(mc_p T)_{in} - (mc_p T)_{out}] dt = \int_{io}^{ec} [] + \int_{ec}^{is} [] + \int_{is}^{ic} [] \quad (5.47)$$

The integrand is the same in all integrals and is abbreviated on the right-hand side by brackets to save space. The event notation is

io = intake valve opens

ic = intake valve closes

ec = exhaust valve closes

is = intake of fresh mixture starts

The first integral on the right-hand side of Equation 5.47 has a positive component of enthalpy flow into the cylinder from the exhaust port and a negative component of enthalpy flow from the cylinder to the intake manifold. (We are neglecting the small decrease in temperature due to heat loss while the gas is in the intake port or pipe.) The second integral is equal to the amount of enthalpy that flows into the cylinder from the exhaust port during the overlap period, since we assume that this gas returns prior to the start of gas induction. Hence,

$$P_{ic}V_{ic} - P_{io}V_{io} = (\gamma - 1) \left[- \int_{io}^{ic} P dV + \int_{io}^{ec} (\dot{m}c_p T)_{ov} dt + c_p T_i \int_{is}^{ic} \dot{m}_{in} dt + \int_{io}^{ic} \dot{Q} dt \right] \quad (5.48)$$

Let us introduce the mass inducted, m_i

$$m_i = \int_{is}^{ic} \dot{m}_{in} dt \quad (5.49)$$

and the mass of exhaust, m_{ov} that flows into the cylinder from the exhaust system during overlap

$$m_{ov} = \int_{io}^{ec} \dot{m}_{ov} dt \quad (5.50)$$

We then have for the volumetric efficiency

$$e_v = \frac{m_i}{\rho_i V_d} = \frac{1}{\gamma} \frac{P_{ic}V_{ic} - P_{io}V_{io}}{P_i V_d} + \frac{\gamma - 1}{\gamma} \int_{io}^{ic} \frac{P dV}{P_i V_d} - \frac{\gamma - 1}{\gamma} \frac{Q}{P_i V_d} - \frac{T_{ov}}{T_i} \frac{m_{ov}}{\rho_i V_d} \quad (5.51)$$

Both heat transfer to the gas and gas exchange during the overlap period decrease the volumetric efficiency. Now let us consider the limiting case in which the piston speed is small, $U_p \rightarrow 0$. In this case there should be no pressure drop across the valves at closure, therefore

$$U_p \rightarrow 0 \Rightarrow P_{io} = P_e \text{ and } P_{ic} = P_i \quad (5.52)$$

Equation 5.51 then becomes

$$e_v = \frac{V_{ic} - V_{io}}{V_d} - \frac{1}{\gamma} \left(\frac{P_e}{P_i} - 1 \right) \frac{V_{io}}{V_d} - \frac{\gamma - 1}{\gamma} \frac{Q}{P_i V_d} - \frac{T_{ov}}{T_i} \frac{m_{ov}}{\rho_i V_d} \quad (5.53)$$

For engines with a short stroke to rod ratio, the cylinder volume can be approximated by

$$\frac{V}{V_o} \approx 1 + \frac{r - 1}{2}(1 - \cos \theta) \quad (5.54)$$

where θ is the crank angle measured from top dead center. Finally, we can write

$$e_v = \frac{\cos \theta_{io} - \cos \theta_{ic}}{2} - \frac{P_e/P_i - 1}{\gamma(r - 1)} \left[1 + \frac{r - 1}{2}(1 - \cos \theta_{io}) \right] - \frac{\gamma - 1}{\gamma} \frac{Q}{P_i V_d} - \frac{T_{ov}}{T_i} \frac{m_{ov}}{\rho_i V_d} \quad (5.55)$$

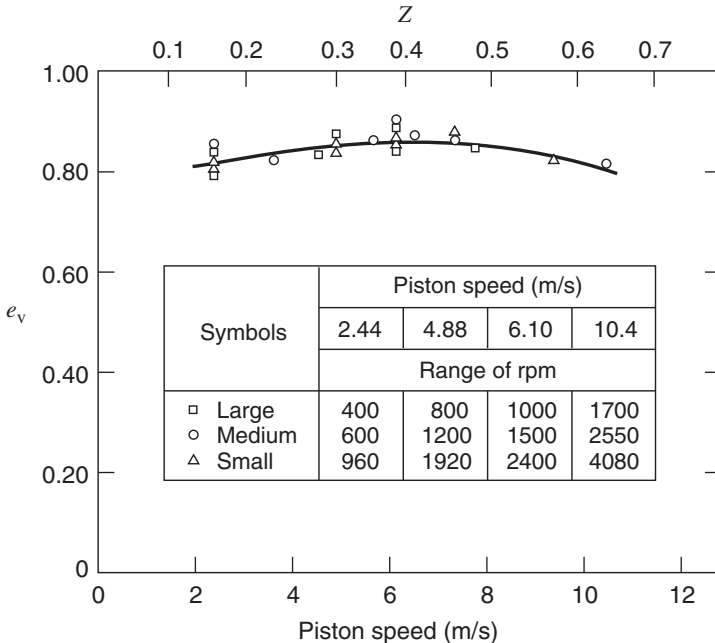


Figure 5.13 Volumetric efficiency versus mean piston speed of the MIT geometrically similar engines under similar operating conditions (Taylor, 1985).

Data are available for three geometrically similar engines in which the valve overlap is small and the cylinders are not much warmer than the inlet air; the overlap and heat loss terms are negligible in this case. Figure 5.13 presents the volumetric efficiency of those engines as a function of piston speed. The engines had similar operating conditions: $r = 5.74$, $\phi = 1.1$, $P_i = 0.95$ bar, $P_e = 1.08$ bar, $T_i = 339$ K, $T_c = 356$ K. Using the specified valve timings, compression ratio, exhaust to intake pressure ratio, and a specific heat ratio of $\gamma = 1.4$, Equation 5.55 predicts that $e_v \rightarrow 0.78$ as $U_p \rightarrow 0$. The prediction is seen to be quite good and similar agreement would be realized for different values of pressure ratio.

Our analysis shows that opening and closing valves at angles other than top and bottom center hurts the volumetric efficiency as the piston speed $U_p \rightarrow 0$. Why then are valves opened earlier and closed later than the ideal case? In addition to the finite valve opening and closing times discussed above, one needs to also consider that this analysis is only valid in the limit of zero piston speed.

For a finite piston speed there will be a pressure drop across the valves, the most important of which is at the intake valve at closing. In the limiting case, air is pushed out of the cylinder as the piston moves up during the time from bottom dead center to inlet valve closure. However, at a finite engine speed, the cylinder pressure at bottom center will be less than the inlet pressure because of the pressure drop across the valve as the charge was entering. Hence, as the piston begins the compression stroke, mixture can continue to flow into the cylinder until the pressure rises because of the filling and the upward moving piston. The flow will reverse itself when the two pressures are equal, and then flow back into the intake system until valve closure.

The volumetric efficiency increases with piston speed until a point is reached where the flow reversal starts at intake valve closure. For speeds beyond that point, volumetric

efficiency will drop because the valve will close during a time in which mixture is still flowing in the engine. The trend of volumetric efficiency with speed discussed here is shown very clearly in Figure 5.13.

Now consider the exhaust process. At any instant, the energy equation can be written as

$$-\dot{Q}_l - P \frac{dV}{dt} = c_v \left(m \frac{dT}{dt} + \frac{dm}{dt} T \right) + \frac{dm}{dt} c_p T \quad (5.56)$$

Combined with the equation of state and integrated, we have

$$f = \frac{m_{\text{io}}}{m_{\text{eo}}} = \left(\frac{P_i}{P_{\text{eo}}} \right)^{1/\gamma} \frac{V_{\text{io}}}{V_{\text{eo}}} \exp \left(\int_{\text{eo}}^{\text{io}} \frac{\dot{Q}_l}{PV} dt \right) \quad (5.57)$$

Integration is carried only to the time when the intake valve opens because during overlap it is assumed that the gases are pushed into the intake manifold only to return later. Notice that heat loss increases the residual fraction and is important here because the exhaust gases are considerably hotter than the cylinder walls.

5.3 INTAKE AND EXHAUST FLOW

In engines, the configuration of the inlet and exhaust flow networks employed plays an important role in determining the volumetric efficiency and residual fraction. Intake manifolds (see Figure 5.14) consisting of plenums and pipes are usually required to deliver the inlet air charge from some preparation device such as an air cleaner or compressor, and exhaust manifolds are used to duct the exhaust gases to a point of expulsion, often far removed from the engine. In multicylinder engines, manifolds are used so that cylinders can share the same compressor, muffler, and catalytic converter. The flow in the inlet and exhaust manifolds is unsteady due to the periodic piston and valve motion. The opening and closing of the intake and exhaust valves or ports create finite amplitude compression and rarefaction pressure waves that propagate at sonic velocity through the intake and exhaust airflow. Computed pressure and frequency profiles in an intake manifold are shown in Figure 5.15 in an engine operating at a low speed (≈ 3000 rpm), and in Figure 5.16 at a higher speed (≈ 6000 rpm). As the engine speed increases, the frequency and amplitude of the pressure waves increase proportionally.

Inlet and exhaust manifolds are sized or tuned to use the pressure waves to optimize the volumetric efficiency at a chosen engine speed. A tuned intake manifold will have a locally higher pressure when the intake valve is open, increasing the charge density. Likewise, a



Figure 5.14 Automotive engine intake manifold. (Courtesy Brodix, Inc.)

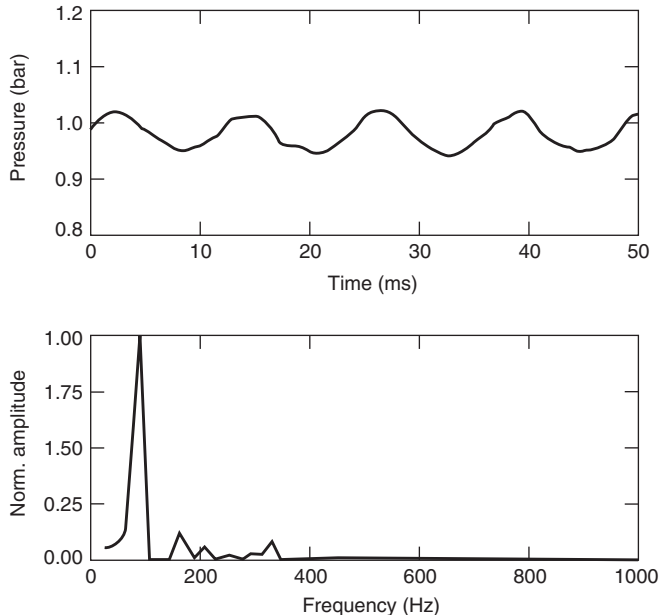


Figure 5.15 Intake manifold pressure and frequency at low speed (≈ 3000 rpm). Adapted from Silvestri et al. (1994).

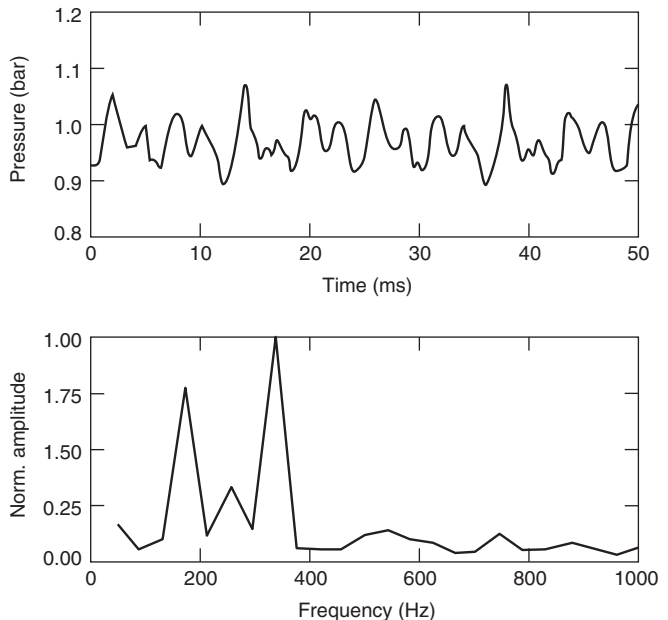


Figure 5.16 Intake manifold pressure and frequency at high speed (≈ 6000 rpm). Adapted from Silvestri et al. (1994).

tuned exhaust manifold will have a locally lower pressure when the exhaust valve is open, increasing the exhaust outflow.

Acoustic analytical models of inlet and exhaust flow have been developed. The acoustic analyses assume that valve opening and closing produces infinitesimal pressure waves traveling at the speed of sound c_o . A representative acoustic equation relating engine rpm, N_t , to a tuned intake runner length, L_t , is given by Equation 5.58:

$$N_t = a c_o / L_t \quad (5.58)$$

where L_t is the tuned intake runner length, and $a \approx 7.5$.

The inlet airflow in a single-cylinder four-stroke engine can also be modeled as a Helmholtz resonator with an effective volume of

$$V_{\text{eff}} = \frac{V_d}{2} \frac{r+1}{r-1} \quad (5.59)$$

The resonant tuning rpm N_t of the inlet pipe of length L_i and diameter D_i of a Helmholtz resonator is given by Equation 5.60:

$$N_t = \frac{15}{\pi} c_o \left(\frac{\frac{1}{4} \pi D_i^2}{L_i V_{\text{eff}}} \right)^{1/2} \quad (5.60)$$

where L_i is an effective length from the inlet valve to the atmosphere and D_i is an effective diameter that with L_i matches the inlet system volume.

The sensitivity of the volumetric efficiency to runner length and engine speed has been a challenge to engine design engineers. By choosing an intake runner of a given length, the volumetric efficiency can be increased for a particular engine speed, but it drops off more sharply at other speeds. A fixed length intake runner is desirable in engines with throttle body injectors or carburetors to minimize wall wetting and maldistribution of the fuel air mixture. With port fuel injection it is possible to use a variable runner length, and production engines with variable intake runner length are now becoming common in vehicles.

A representative plot of the effect of inlet runner length on the volumetric efficiency of an automobile engine is plotted as a function of engine speed in Figure 5.17. As the engine speed decreases, the volumetric efficiency approaches 0.8, and with no intake pipe or runner, the volumetric efficiency follows a shallow curve with a maximum at about 0.9, consistent with the analyses presented earlier in this chapter, in which the runner length for maximum volumetric efficiency is predicted to be inversely proportional to the engine speed.

Gas dynamics codes are used for the design of intake and exhaust plenums, runners, and ports, and to assess the effect of design changes on the flow patterns and the volumetric efficiency. There are a number of 1-D gas dynamics programs, such as WAVE (WAVE USER'S MANUAL, 2014) and GT-POWER (GT-POWER USER'S MANUAL, 2014), that numerically solve the compressible governing equations to predict intake and exhaust system pressure and flow profiles over an engine cycle. The governing equations for

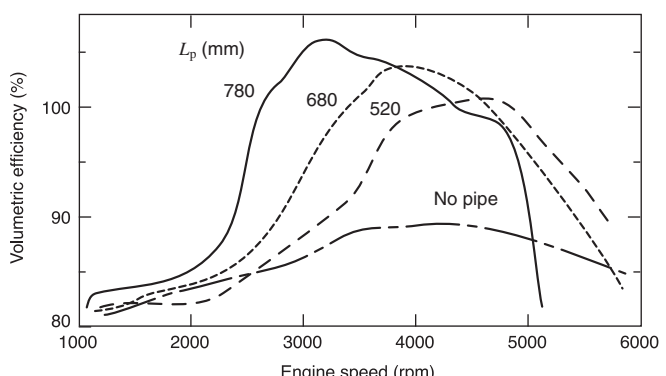


Figure 5.17 Volumetric efficiency versus engine speed and intake runner length. Adapted from Tabaczynski (1982).



Figure 5.18 CFD grid for intake manifold flow. (Courtesy Adapco.)

the intake and exhaust flow are the unsteady mass, momentum, and energy conservation equations, which for one dimension in vector form are

$$\frac{\partial \vec{f}}{\partial t} + \frac{\partial \vec{F}}{\partial t} = \vec{T} \quad (5.61)$$

$$\vec{f} = \begin{bmatrix} \rho A \\ \rho AU \\ \rho AE \end{bmatrix} \quad (5.62)$$

$$\vec{F} = \begin{bmatrix} \rho AU \\ \rho A(\rho U^2 + P) \\ \rho AUH \end{bmatrix} \quad (5.63)$$

$$\vec{T} = \begin{bmatrix} 0 \\ \tau_w \sqrt{4\pi A} + P \frac{\delta A}{\delta x} \\ q_w \sqrt{4\pi A} \end{bmatrix} \quad (5.64)$$

where ρ is the fluid density, A is the cross-sectional area of the duct, U is the fluid velocity, P is the pressure, E is the total specific energy, H is the total specific enthalpy, τ_w is the wall shear stress, and q_w is the wall heat flux. Physical effects such as wall friction, heat transfer, area changes, branches, and bends that occur in actual manifolds can be accounted for in the above equations.

The specific boundary condition geometry of the intake and exhaust ports is required for solution of Equations 5.61–5.64. A representative three-dimensional intake manifold geometry divided into computational mesh elements is shown in Figure 5.18. The modeling includes the intake manifold, the intake ports, valves, and cylinder volumes. The computed velocities with the middle cylinder open are shown in Figure 5.19. The CFD grid for the exhaust manifold shown in Figure 5.20 is for a three-cylinder engine with a closely coupled catalytic converter. The computed velocities with the middle cylinder exhaust valve open are shown in Figure 5.21.

5.4 SUPERCHARGERS AND TURBOCHARGERS

The power and efficiency of an internal combustion engine can be increased with the use of an air compression device such as a supercharger or turbocharger. Increasing the pressure and density of the inlet air will allow additional fuel to be injected into the cylinder, increasing the power produced by the engine. Spark ignition engines are knock limited,

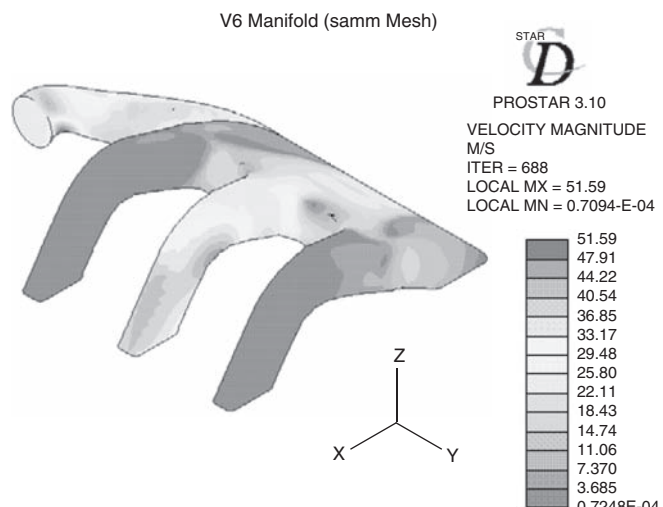


Figure 5.19 CFD velocity results for intake manifold flow. (Courtesy Adapco.)

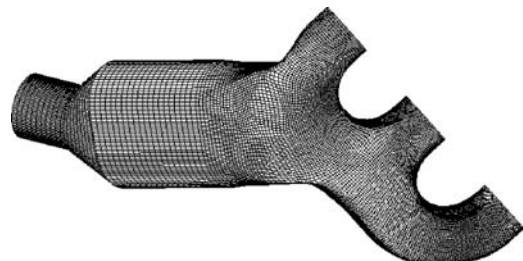


Figure 5.20 CFD grid for exhaust manifold flow. (Courtesy Adapco.)

restricting the allowable compressor pressure increase. An intercooler heat exchanger is used with turbochargers and superchargers to cool the intake air and increase its density after the compression process has raised its temperature, and reduce the tendency to knock. Superchargers and turbochargers are used extensively on a wide range of diesel engines, since they are not knock limited.

As shown in Figure 5.22, superchargers are classified as compressors that are mechanically driven off of the engine crankshaft. Superchargers are used in applications in which the increased density and pressure is desirable at all engine speeds. P. H. Roots, an American engineer, invented the supercharger in 1859, for use in the then-emerging steel industry. Superchargers have also been used in piston-driven airplane engines since about 1910 to compensate for the decrease in air pressure and density with altitude, and to increase the flight ceiling. Since it is mechanically driven, the rotational speed of a supercharger is limited to about speeds of the order of 10,000 rpm.

Turbomachinery considerations relative to engines include

- coupling compressors and turbines and matching them to the mass flow rate of the internal combustion engine;
- aftercooling of the compressed charge;
- relating steady-flow bench tests to actual periodic flow conditions; and
- transient response of the entire engine system.

RIGHT-HAND EXHAUST MANIFOLD AND CATALYST
Case 2: Runner 2 open, Velocity = 4 m/s, other runners closed.

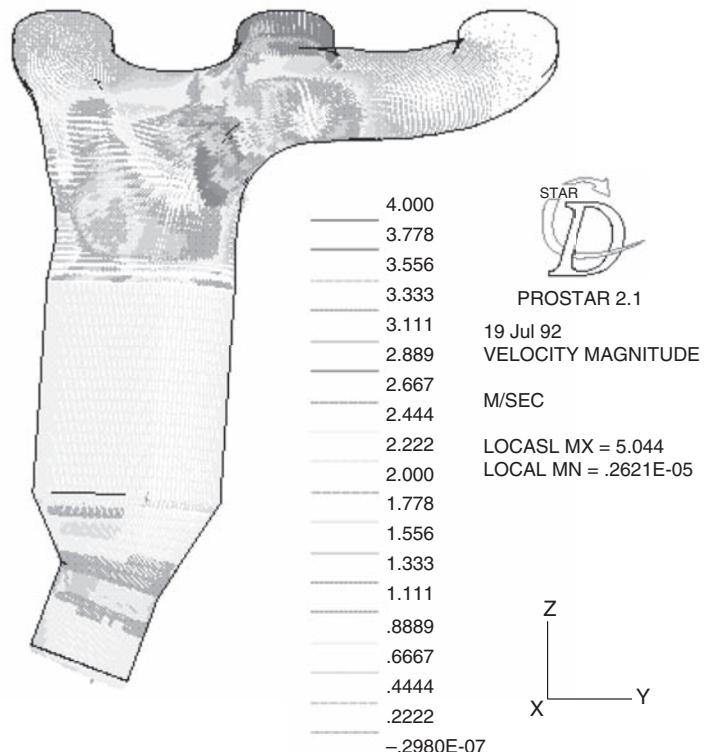


Figure 5.21 CFD results for exhaust manifold flow.
(Courtesy Adapco.)

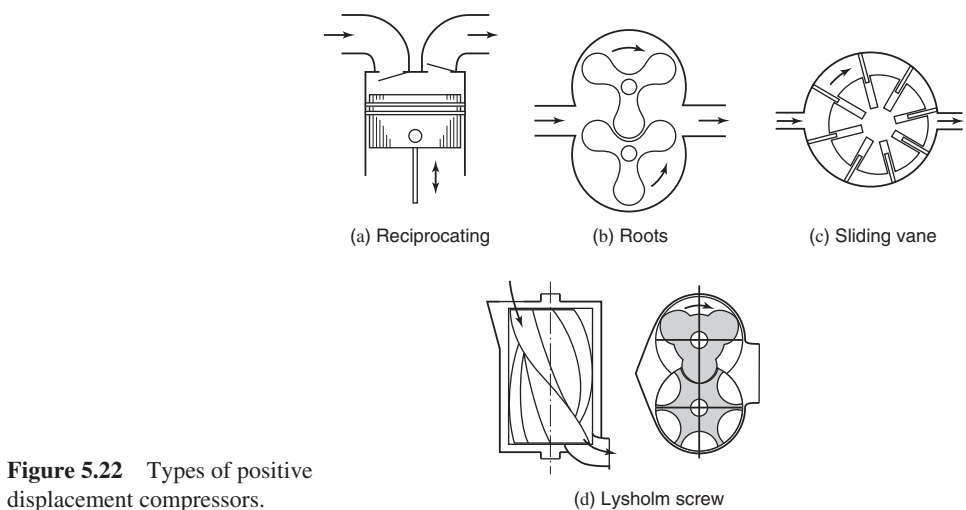


Figure 5.22 Types of positive displacement compressors.

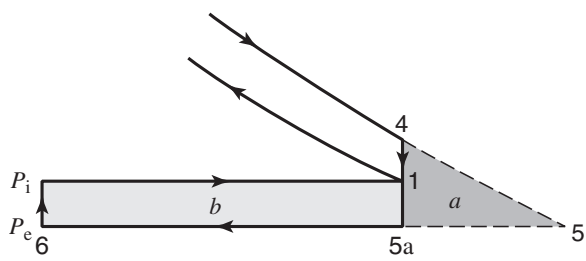


Figure 5.23 Comparison of turbine and compressor work.

a: blowdown work to turbine
b: compression work

The types of compressors used on internal combustion engines are primarily of two types: positive displacement and dynamic. With a positive displacement compressor, a volume of gas is trapped, and compressed by movement of a compressor boundary element. Three types of positive displacement compressors are the Roots, vane, and screw compressor, as shown in Figure 5.22. The efficiency of positive displacement compressors varies from about 50% for the Roots compressor to over 90% for the screw compressor. A dynamic compressor has a rotating element that adds tangential velocity to the flow which is converted to pressure in a diffuser. Two types of dynamic compressors and turbines are radial (centrifugal) and axial.

Turbochargers are defined as devices that couple a compressor with a turbine driven by the exhaust gases, so that the pressure increase is proportional to the engine speed. The turbocharger was first invented in 1906, and the applications have expanded from marine diesel engines, to vehicle diesel engines, and then to spark ignition engines. The potential increase in overall system efficiency with a turbocharger can be seen by inspection of Figure 5.23, in which a portion of the available work obtained from the blowdown of the exhaust gas can be used to compress the intake gas.

A turbocharger is a coupled dynamic compressor and dynamic turbine, due to the high rotational speeds, of the order of 100,000 rpm, required for efficient operation at typical internal combustion engine flow rates and pressure ratios. For automotive applications an outward radial flow geometry is used for the compressor, and an inward radial flow is used for the turbine. A cross section of a turbocharger with a radial compressor and turbine is shown in Figures 5.24 and 5.25. Turbochargers are controlled by varying the pressure ratio.

A waste gate is used to control the exhaust gas flow rate to the turbine. The waste gate is a butterfly or poppet valve controlled by the intake manifold pressure to prevent the turbocharger from compressing the intake air above a set knock or engine stress pressure limit. More recently, variable nozzles have been used to adjust the nozzle area to provide acceptable vehicular acceleration performance as well as efficient operation at high loads.

A turbine can also be mechanically connected to the engine drive shaft, a configuration called compounding. Turbochargers used in diesel locomotives use a clutch geared to the drive shaft to drive the compressor during low engine speed when there is insufficient power from the turbine. At higher engine speeds, the clutch disengages, and the compressor is driven by the exhaust gases flowing through the turbine. Axial flow compressors and turbines are typically used in marine turbocharger applications.



Figure 5.24 Turbocharger cutaway.
(Courtesy PriceWeber.)

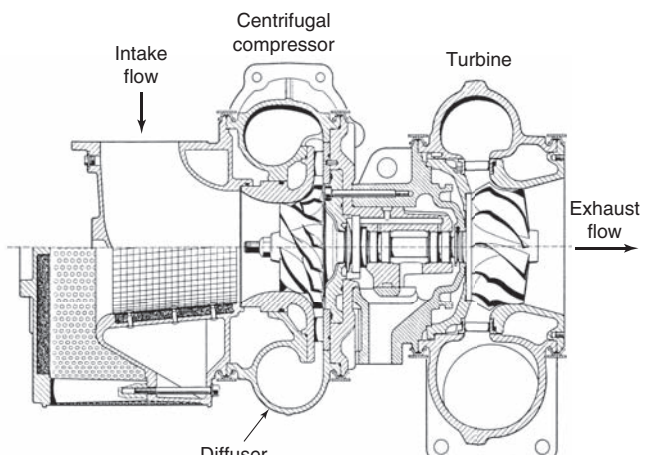


Figure 5.25 Turbocharger cross section (Laustela et al., 1995).

The adiabatic efficiency η_c of a compressor is defined as the isentropic work required to compress the gas over the specified pressure ratio divided by the actual work required to compress the gas over the same pressure ratio. The pressure ratio P_2/P_1 of compressors used for internal combustion engines is generally small enough that the gas may be assumed to have constant specific heat. It follows then that the isentropic work required per unit mass of gas to compress the gas from P_1 to P_2 is given by

$$w_{1-2s} = c_p(T_1 - T_{2s}) = -c_p T_1 \left[(P_2/P_1)^{(\gamma-1)/\gamma} - 1 \right] \quad (5.65)$$

In deriving Equation 5.65, it was tacitly assumed that the change in kinetic energy across the compressor was negligible compared to the change in enthalpy, an assumption usually valid in practice.

Experiments with compressors show that the adiabatic efficiency is dependent primarily upon the pressure ratio, the tip Mach number, and the mass flow rate ratio,

given below:

P_2/P_1	Outlet-inlet pressure ratio
s/c_o	Mach number based on rotor tip speed, $s = \omega D/2$
\dot{m}/\dot{m}_{cr}	Ratio of the mass flow rate to the critical mass flow rate

As shown previously in this chapter, the critical mass flow rate for choking flow with $\gamma = 1.4$ is

$$\dot{m}_{cr} = 0.578 \left(\frac{\pi D^2}{4} \right) \rho_o c_o \quad (5.66)$$

Compressor performance characteristics are plotted on a compressor map, with mass flow rate on the x axis and pressure rise on the y axis. Lines of constant adiabatic efficiency and constant rotational speed are plotted as a function of mass flow rate and pressure ratio. Note that the constant speed lines have a negative slope on the mass flow rate–pressure plane. Performance data for various piston, Roots, Lysholm, screw, centrifugal, and axial compressors are given in Figures 5.26–5.29. It can be seen that the various compressor configurations occupy different regions of the compressor map, allowing different compressors to be matched to a given conditions.

Dynamic compressors have surge and choking performance limits. The surge limit on the left side of the dynamic compressor map represents a boundary between stable and unstable operating points. For stable operation dynamic compressors operate to the right of the surge line, with a negative slope to the constant speed lines. Surge is a self-sustaining flow oscillation. When the mass flow rate is reduced at constant pressure ratio, a point arises where somewhere within the internal boundary layers on the compressor blades a flow reversal occurs. If the flow rate is further reduced, then a complete reversal occurs that relieves the adverse pressure gradient. That relief means a flow reversal is no longer needed and the flow then begins to return to its initial condition. When the initial condition is reached, the process will repeat itself, creating surge.

On the right side of the dynamic compressor map is a zone where efficiencies fall rapidly with increasing mass flow rate. The gas speeds are quite high in this zone and the attendant fluid friction losses are increasing with the square of the gas speed. In this region, there is also the choke limit, which occurs at a slightly different value of \dot{m}/\dot{m}_{cr} for each tip speed. Choking occurs when at some point within the compressor the flow reaches the speed of sound. It occurs at values of \dot{m}/\dot{m}_{cr} less than 1 because \dot{m}_{cr} is based on the compressor wheel diameter D rather than on the cross-sectional area where choking is occurring. The value of \dot{m}/\dot{m}_{cr} at choking varies with tip speed because the location within the compressor at which choking occurs depends on the structure of the internal boundary layers.

A procedure for matching a compressor with an internal combustion engine is listed below. Using the performance map, the compressor mass flow rate is matched to the engine mass flow rate, given the engine volumetric efficiency as a function of engine speed. The procedure is as follows:

- Assume a pressure ratio.
- Read the compressor efficiency and mass flow rate.
- Solve for the adiabatic temperature and density after compression.
- Calculate the engine mass flow rate with the density found in part (c) and the known volumetric efficiency.

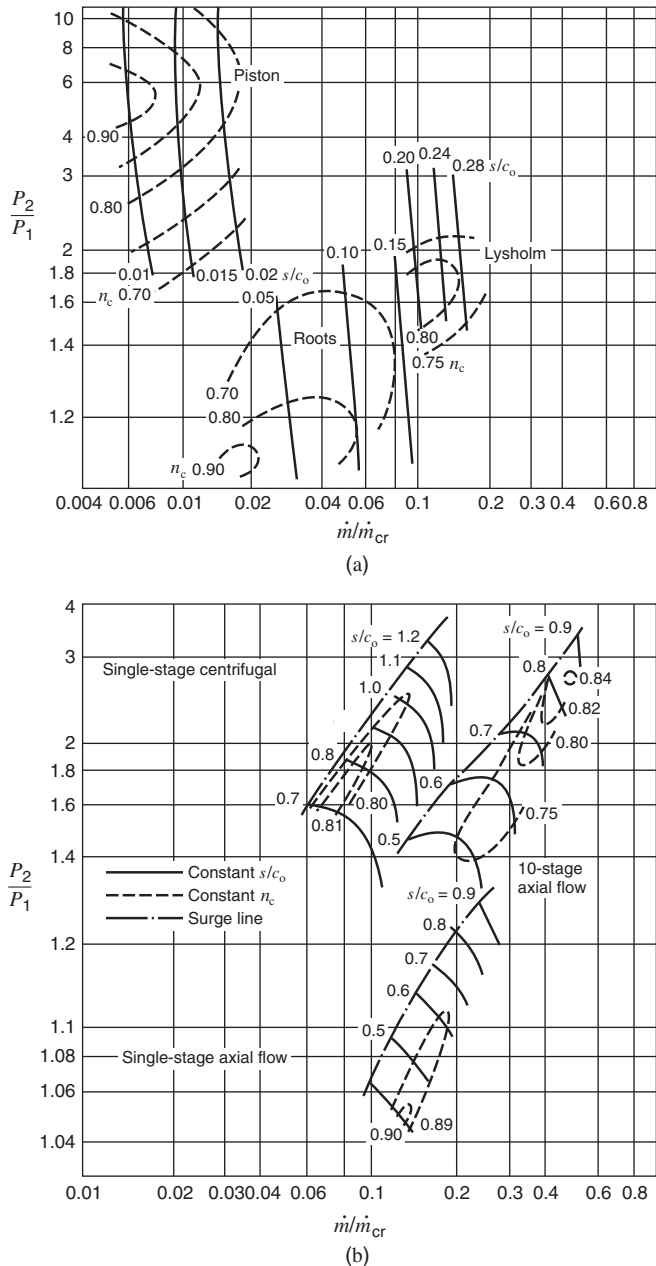


Figure 5.26 Comparative performance of various positive displacement and dynamic compressors (Taylor, 1985).

- (e) Iterate until the engine mass flow rate and compressor flow rate are equal.
- (f) Calculate the compressor power.

There are alternative devices that compete with positive displacement and dynamic turbomachines. Such alternatives include shock wave compressors (Weber, 1995), an example of which is a device called the Comprex in which air is compressed by means of exhaust pressure waves and momentary direct contact between the exhaust stream and the fresh air (Gaschler, Eib, and Rhode, 1983).

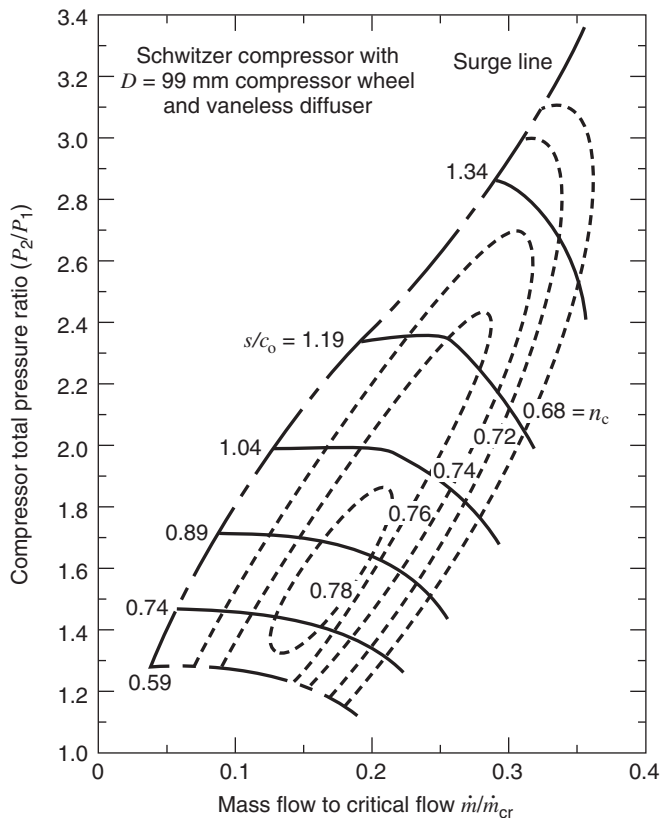


Figure 5.27 Centrifugal compressor map.
(Courtesy R. Hehman of Schwitzer.)

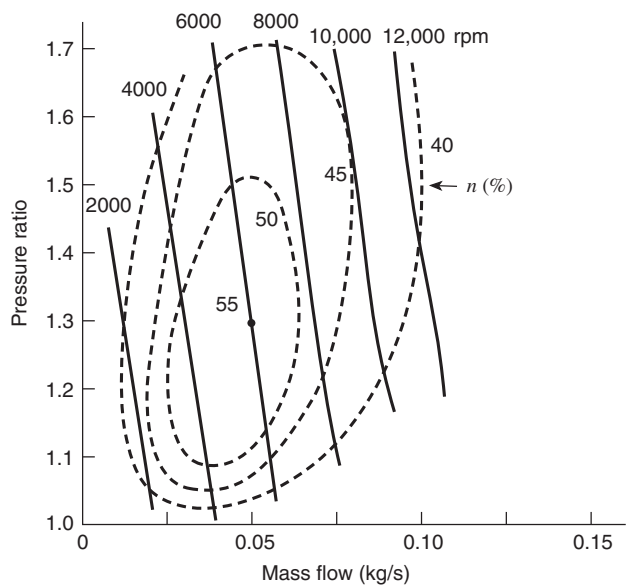


Figure 5.28 Representative Roots supercharger performance. (Adapted from Sorenson, 1984.)

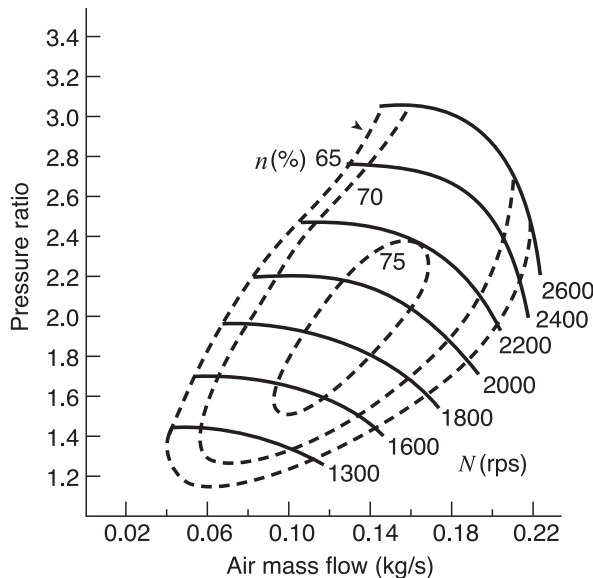


Figure 5.29 Representative centrifugal compressor map.
(Adapted from Andersson et al., 1984.)

5.5 EFFECT OF AMBIENT CONDITIONS ON ENGINE AND COMPRESSOR MASS FLOW

Engines are designed to operate over large ranges of ambient temperature, pressure, and humidity. The ambient pressure is to first order determined by the altitude above sea level. Engine tests are corrected for the effects of ambient pressure and temperature using the ideal gas compressible flow equation, Equation 5.10, restated below as Equation 5.67:

$$\dot{m}_a = A_{\text{eff}} \frac{P_o}{(RT_o)^{1/2}} \left[\frac{2\gamma}{\gamma - 1} \left(\left(\frac{P}{P_o} \right)^{2/\gamma} - \left(\frac{P}{P_o} \right)^{(\gamma+1)/\gamma} \right) \right]^{1/2} \quad (5.67)$$

If P/P_o is assumed to remain constant, then the mass flow rate through the engine varies as

$$\dot{m}_a \sim \frac{P_o}{(T_o)^{1/2}} \quad (5.68)$$

This parameter is also used as a correction factor on compressor maps to account for varying ambient conditions. For a constant fuel-air ratio, the above equation implies, as expressed below in Equation 5.69, that

$$\frac{\text{bmep}_m}{\text{bmep}_o} = \frac{P_m}{P_o} \left(\frac{T_o}{T_m} \right)^{1/2} \quad (5.69)$$

where the subscript m denotes the measured conditions and the subscript o denotes standard atmosphere conditions at sea level.

Two examples clearly illustrate the altitude effect on engine performance. Naturally aspirated diesel locomotive engines are usually derated by 2.5% per 300 m of elevation change, so at 10,000 ft (3.05 km) above sea level, the elevation of most mountain passes in the Western United States, they will produce 25% less power. Most locomotive diesels are now turbocharged to increase power and reduce the altitude effect.

Also, as an aircraft flies from sea level to an elevation of 20,000 ft (6.1 km), the density of the standard atmosphere decreases by 50% from 1.22 to 0.66 kg/m³. The bmep

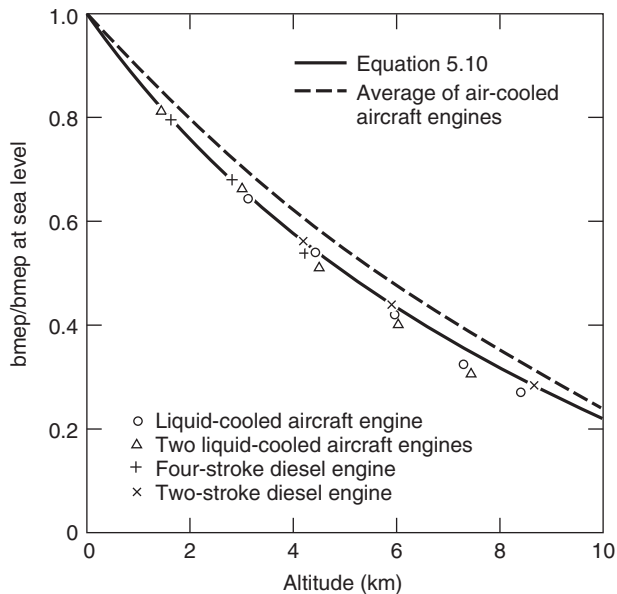


Figure 5.30 Effect of altitude on unthrottled engine performance at constant fuel-air ratio and coolant temperature.

performance of a number of naturally aspirated aircraft engines with altitude is shown in Figure 5.30. As a result of the density decrease, there is a 60% decrease in bmep at 6000 m relative to sea level. Equation 5.69 correlates the experimental data very well, as shown in Figure 5.28. Many piston-driven aircraft engines are supercharged to allow suitable operation at elevations above sea level.

For further information regarding intake and exhaust flow in engines and compressors, the reader is referred to the texts by Blair (1998), Watson and Janota (1982), Wilson and Korakianitis (2014), and Winterbone and Pearson (1999).

5.6 REFERENCES

- ANDERSSON, J., A. BENGTSSON, and S. ERIKSSON (1984), "The Turbocharged and Intercooled 2.3 L Engine for the Volvo 760," SAE paper 840253.
- ANNAND, W. and G. ROE (1974), *Gas Flow in the Internal Combustion Engine*, G. T. Foulis, Somerset, England.
- BLAIR, G. (1998), *Design and Simulation of Four Stroke Engines*, SAE International, Warrendale, Pennsylvania.
- BORETTI, A., M. BORGHI, and G. CANTORE (1994), "Numerical Study of Volumetric Efficiencies in a High Speed, Four Valve, Four Cylinder Spark Ignition Engine," SAE paper 942533.
- GASCHLER, E., W. EIB, and W. RHODE (1983), "Comparison of the 3-Cylinder DI-Diesel with Turbocharger or Comprex-Supercharger," SAE paper 830143.
- GT-POWER USER'S MANUAL (2014), Gamma Technologies, Westmont, Illinois.
- LAUSTELA, E., U. GRIBI, and K. MOOSER (1995), "Turbocharging the Future Gas and Diesel Engines of the Medium Range," ASME ICE Conf.; Vol 25-1, p. 1521.
- LIVENGOOD, J. and J. STANITZ (1943), "The Effect of Inlet Valve Design, Size and Lift on the Air Capacity and Output of a Four-Stroke Engine," NACA Technical Note TN-915.
- SILVESTRI, J., T. MOREL, and M. COSTELLO (1994), "Study of Intake System Wave Dynamics and Acoustics by Simulation and Experiment," SAE paper 940206.
- SORENSEN, S. (1984), "Simulation of a Positive Displacement Supercharger," SAE paper 820244.
- TABACZYNSKI, R. (1982), "Effects of Inlet and Exhaust System Design on Engine Performance," SAE paper 821577.
- TAYLOR, C. (1985), *The Internal Combustion Engine in Theory and Practice*. MIT Press, Cambridge, Massachusetts.

- WATSON, N. and M. JANOTA (1982), *Turbocharging the Internal Combustion Engine*, Wiley, New York.
- WAVE USER'S MANUAL (2014), Ricardo Software, Inc., Burr Ridge, Illinois.
- WEBER, H. (1995), *Shock Wave Engine Design*, Wiley, New York.
- WILSON, D. and T. KORAKIANITIS (2014), *The Design of High Efficiency Turbomachinery and Gas Turbines*, Second Edition, MIT Press, Cambridge, Massachusetts.
- WINTERBONE, D. and R. PEARSON (1999), *Design Techniques for Engine Manifolds*, Society of Automotive Engineers, Warrendale, Pennsylvania.

5.7 HOMEWORK

- 5.1 If an engine has a bore of 0.1 m, stroke of 0.08 m, inlet flow effective area of $4.0 \times 10^{-4} \text{ m}^2$, and inlet temperature of 320 K, what is the maximum speed it is intended to be operated while maintaining good volumetric efficiency?
- 5.2 Explain how unburned fuel can appear in the exhaust during the intake and exhaust strokes.
- 5.3 Combustion gases ($\gamma = 1.3$, $R = 280 \text{ J/(kg K)}$) exit through the exhaust port of a two-stroke engine during blowdown. The exhaust port geometry can be modeled as a converging nozzle with a port diameter of 2 cm. The cylinder gases are initially at 200 kPa and 393 K, and $P_{\text{atm}} = 101 \text{ kPa}$. What is the initial velocity and mass flow rate of the exhaust flow?
- 5.4 It was explained in the chapter that because of the pressure drop across a valve, it is advantageous to close the intake valve after bottom dead center. Use the same logic to explain why exhaust valves are closed after top dead center and what the effect of engine speed is on the residual fraction.
- 5.5 Suppose an engine were constructed with variable valve timing, thus ensuring optimum timing at all speeds. Explain how the volumetric efficiency would depend on speed for wide open throttle operation with short pipes and $Z < 0.6$.
- 5.6 Figure 5.2 shows an inlet valve opened to $l/d_i = 0.25$. If the stem is chosen to be $d_s = 0.15d_i$ and the throat of the port is $d_t = 0.85d_i$, what would be the flow coefficient based purely on the geometrical blockage?
- 5.7 Calculate the ratios of the inlet valve area to piston area for the three configurations a, b, and c in Figure 5.11.
- 5.8 Compare the performance of a single-inlet valve and a double-inlet valve configuration. The diameter of the inlet valve is 22 mm for the single-valve configuration, and 16 mm for the double-valve configuration. If the maximum valve lift $l/d = 0.25$, what is the difference in the valve curtain and the valve seat areas for both cases? What are some advantages to using four valves per cylinder?
- 5.9 If the inlet Mach index in each case in Figure 5.11 is held to $Z_i = 0.6$ and $c_i = 400 \text{ m/s}$, $\bar{A}_i = 0.35 n_i (\pi/4) d_i^2$ where n_i = number of intake valves, then what would be the mean piston speed in each case?
- 5.10 A four-stroke four-cylinder square (bore = stroke) engine has a displacement volume of 5 L and operates at 3000 rpm. The intake air temperature is 350 K, the intake manifold length is 1.25 m long, and $\bar{C}_f = 0.38$. (a) For a Mach index $Z = 0.6$, what is the mean piston speed and average effective intake valve flow area? (b) At what engine speed would the intake manifold be “tuned” for increased intake mass flow?

- 5.11** Compare the predicted resonant tuning rpm N_t (Equation 5.60) of a Helmholtz resonator model with the simple acoustic tuning rpm of Equation 5.58 and also the experimental results for maximum volumetric efficiency e_v plotted in Figure 5.17. Assume D_i is equal to the inlet pipe diameter. Make a table of the tuning rpm versus tuning inlet pipe length for the five cases shown in Figure 5.17. Assume $b = 83$ mm, $s = 106$ mm, $D_i = 0.05$ m, $r = 9$, $T_o = 300$ K.
- 5.12** Three camshafts are available for an engine. The valve maximum lift and intake and exhaust opening and closing angles in degrees relative to top dead center (tdc) and bottom dead center (bdc) are tabulated below.

CAM	IO (btdc)	IC (abdc)	EO (bbdc)	EC (atdc)	LIFT (mm)
Factory	30	60	60	30	9.5
A	26	66	66	26	11.4
B	22	62	62	22	10.3

Draw a sketch of the three cam timing diagrams. Discuss the effects these different cams might have, including duration and overlap effects.

- 5.13** Derive an expression for the volumetric efficiency of a supercharged engine, using an analysis similar to the derivation of Equation 5.51.
- 5.14** A supercharger has an isentropic efficiency of 0.75 and consumes 20 kW. If the volumetric flow rate of standard air into the supercharger is 250 L/s, what is the air temperature, pressure, and density exiting the supercharger? Assume standard inlet conditions.
- 5.15** Develop Equation 5.65 for the work done in an isentropic compression.
- 5.16** The airflow into a four-stroke 3.5 L engine operating at 3000 rpm with a volumetric efficiency of 0.75 is to be supercharged to 145 kPa from ambient P_o, T_o conditions. An intercooler cools the compressed air to 325 K. If the supercharger isentropic efficiency is 0.60, what is the power consumption of the supercharger?
- 5.17** A Roots supercharger map is given in Figure 5.28. Match (i.e., find the resultant pressure ratio) this supercharger to a 2.0 L, four-stroke engine with the following volumetric efficiencies.

N (rpm)	e_v (%)
1000	68
2000	68
3000	75
4000	76
5000	73
6000	70

Find the power required to drive the supercharger at each condition as well as the outlet temperature. Choose a compressor speed N_c equal to twice the engine speed N .

- 5.18** A naturally aspirated four-cylinder, four-stroke gasoline engine has the following specifications.

V_d	2316 cm ³
b	96 mm
s	80 mm
r	9.5
\dot{W}_b	83 kW at $N = 5400$ rpm
τ_b	184 N-m at $N = 2760$ rpm

A turbocharged version of the engine utilizes the compressor mapped in Figure 5.29. Estimate the brake power of the turbocharged engine at $N = 5400$ rpm if the compressor ratio is $P_2/P_1 = 1.5$. What is the cmeep and bmeep at this speed. What is the compressor efficiency and rotational speed? What is the heat transfer to the inter-cooler? Make the following assumptions.

- For the naturally aspirated (NA) engine
Inlet manifold conditions: $T_i = 310$ K, $P_i = 1.0$ bar, $\phi = 1.0$.
Volumetric efficiency: $e_v = 0.84$.
Mechanical efficiency: $\eta_m = \text{bmeep}/(\text{imep})_{\text{net}} = 0.90$.
- For the turbocharged (TC) engine
Aftercooled gas temperature: $T_i = 340$ K. Volumetric efficiency: $e_v = 0.91$.
Mechanical efficiency: $\eta_m = \text{bmeep}/(\text{imep})_{\text{net}} = 0.88$.
- For a given engine speed and displacement, the indicated power is proportional to airflow rate:

$$\dot{W}_i \propto \text{imep}_{\text{net}} \propto e_v P_i / T_i$$

In practice, the compression ratio was lowered to 8.7 to avoid knock and the engine produced 117 kW at 5280 rpm.

Chapter 6

Fuel and Airflow in the Cylinder

6.1 INTRODUCTION

In this chapter, we examine the delivery and in-cylinder flow of the fuel and air in both spark ignition and compression ignition engines. The basic principles of carburetors and fuel injection systems are laid out, providing an introduction to the various means employed to deliver fuel to the combustion chamber. In-cylinder flow is a large-scale turbulent mixing process initially governed by the momentum of the incoming air and fuel during the intake stroke, and then modified by the piston motion during the compression stroke.

Adequate mixing of the fuel and air is essential for a satisfactory combustion process that will produce the engine power required with minimum emissions. The timescales are very short, for example, in an automotive engine, the time available for mixing during the compression stroke is on the order of tens of milliseconds. During this time between injection and start of combustion, a liquid fuel needs to be broken up into droplets, vaporized, and mixed with the surrounding air.

Design of an engine's air-fuel mixing process is an engineering challenge as it is a compromise of many conflicting demands. For direct-injection (DI) engines, large-scale mixing and turbulence generation can be achieved by high-pressure fuel injection. In these cases, the mixing patterns are governed by the momentum flux of the injected fuel. Some engines rely on the angular momentum or swirl of the intake air for adequate mixing. However, increased swirl reduces volumetric efficiency and increases convective heat loss. Engines designed without swirl are termed quiescent and high-pressure fuel injection, which entrains cylinder air, is instead relied upon to fully mix the fuel and air. However, a higher required injection pressure will result in a more costly fuel injection system.

The chapter finishes with coverage of two-stroke engine configurations and airflow scavenging models.

6.2 CARBURETION

Carburetors are used on spark ignition engines to control the fuel flow delivered to an engine so that it is proportional to the airflow. As shown in Figures 6.1 and 6.2, carburetors are used for both liquid and gaseous fuels. With liquid fuels, they also serve to mix the fuel with the air by atomizing the liquid into droplets so that it will evaporate quickly. The liquid fuel carburetor was invented and patented in 1893 by W. Maybach (1846–

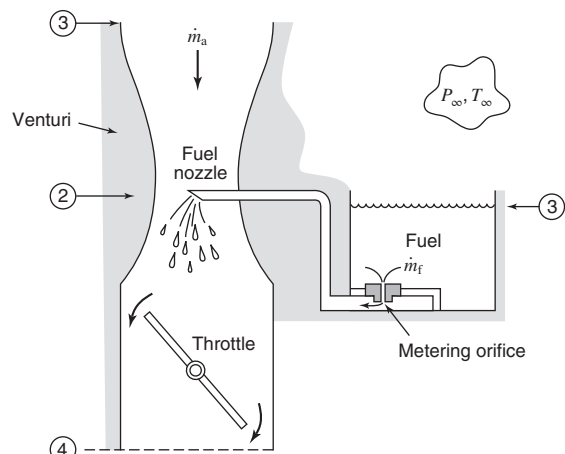


Figure 6.1 Carburetor for mixing liquid fuels with air.

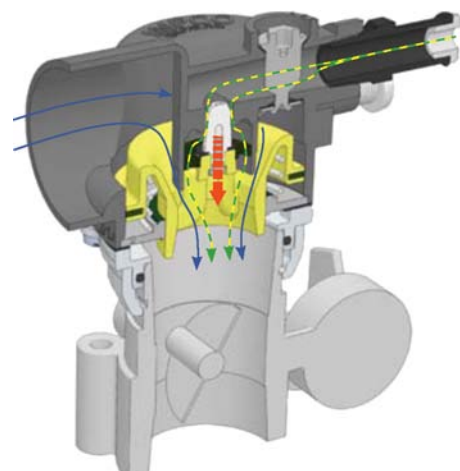


Figure 6.2 Carburetor for mixing gaseous fuels with air. (Courtesy Impco, Inc.)

1929), a German engineer, and used for mixture preparation in vehicular engines until the mid-1980s. Currently, due to emissions regulations, they are primarily used with small (<25 kW) engines.

The basic principle behind a liquid fuel carburetor is shown in Figure 6.1, indicating the inlet airflow through a venturi with a fuel nozzle at the throat and then past a throttle valve. In contrast to fuel injectors, liquid fuel carburetors atomize the fuel by processes relying on the air speed being greater than the fuel speed at the fuel nozzle. The pressure difference between the carburetor inlet and the nozzle throat is used to meter the fuel to achieve a desired air-fuel ratio. Therefore, the fuel is metered using the airflow as an independent variable. The mass flow between locations (1) and (4) is determined by the engine speed and throttle position. The pressure at location (2) and the fuel-air ratio, m_f/m_a , are dependent variables that adjust themselves to match the mass flow $\dot{m}_4 = \dot{m}_f + \dot{m}_a$ that the engine is demanding. For starting purposes, a choke is added upstream of the venturi to enrich the mixture. It is basically another throttle that acts to lower the air pressure and thus the airflow rate in the carburetor, while keeping the fuel flow rate relatively constant.

Assuming steady ideal gas flow through the carburetor, the airflow is given by Equation 6.1:

$$\dot{m}_a = \rho_\infty A_a c_\infty \left[\frac{2}{\gamma - 1} \left(\left(\frac{P_2}{P_\infty} \right)^{2/\gamma} - \left(\frac{P_2}{P_\infty} \right)^{(\gamma+1)/\gamma} \right) \right]^{1/2} \quad (6.1)$$

In Equation 6.1, c_∞ is the speed of sound in the atmospheric air, and $A_a = C_{d,a} A_v$ is the effective flow area at the venturi throat. That flow area is less than the venturi throat cross-sectional area because of blockage by the fuel nozzle and boundary layers along the venturi walls.

The fuel flow is computed assuming the fuel is incompressible, in which case

$$\dot{m}_f = A_f \sqrt{2\rho_f(P_\infty - P_2)} \quad (6.2)$$

where the area $A_f = C_{d,f} A_{\text{orifice}}$ is the effective flow area of the metering orifice. According to Obert (1973), the discharge coefficient of metering orifices used in carburetors is typically 0.75; it accounts for boundary layers in the orifice and for the small pressure drop from the orifice to the nozzle.

The maximum flow rate of air through a carburetor occurs when the flow chokes at the venturi nozzle. In this case,

$$\left(\frac{P_2}{P_\infty} \right)_{\text{cr}} = \left(\frac{2}{\gamma + 1} \right)^{\gamma/(\gamma-1)} \quad (6.3)$$

$$\dot{m}_{a,\text{cr}} = \rho_\infty A_a c_\infty \left(\frac{2}{\gamma + 1} \right)^{(\gamma+1)/2(\gamma-1)} \quad (6.4)$$

Equation 6.4 is useful in sizing a carburetor venturi; the effective area A_a is a function of the maximum airflow rate.

Let us call the ratio of the airflow to the critical or choked airflow, the carburetor demand D_c . It should be clear that $0 \leq D_c \leq 1$. Assuming $\gamma = 1.4$, which when substituted into Equations 6.1 and 6.4 and solved with Equation 6.2 for the fuel-air ratio FA yields

$$FA = \frac{\dot{m}_f}{\dot{m}_a} = \frac{1.73}{D_c} \frac{\rho_f}{\rho_\infty} \frac{A_f}{A_a} \left[\frac{2(P_\infty - P_2)}{\rho_f c_\infty^2} \right] \quad (6.5)$$

By definition, the carburetor demand D_c is then

$$D_c \equiv \frac{\dot{m}_a}{\dot{m}_{a,\text{cr}}} = 3.86 \left[\left(\frac{P_2}{P_\infty} \right)^{1.43} - \left(\frac{P_2}{P_\infty} \right)^{1.71} \right]^{1/2} \quad (6.6)$$

A graph of the fuel-air ratio as a function of carburetor demand is shown in Figure 6.3, assuming typical values for gasoline properties and different values of the effective area ratio A_f/A_a . The curves are based on Equation 6.5 for $P_\infty = 0.987$ bar, $\rho_f = 749$ kg/m³, $c_\infty = 346$ m/s, and $\rho_\infty = 1.17$ kg/m³. Note that for demands between 20 and 80%, the fuel-air ratio is a weak function of demand and its value is dependent primarily upon the geometric properties of the carburetor through the ratio A_f/A_a . At demand less than about 20%, the fuel-air ratio would in reality be much less than predicted by Equation 6.5 because of surface tension effects at the nozzle exit. The simple carburetor just described can then be expected to operate only over the demand range $0.20 < D_c < 0.80$.

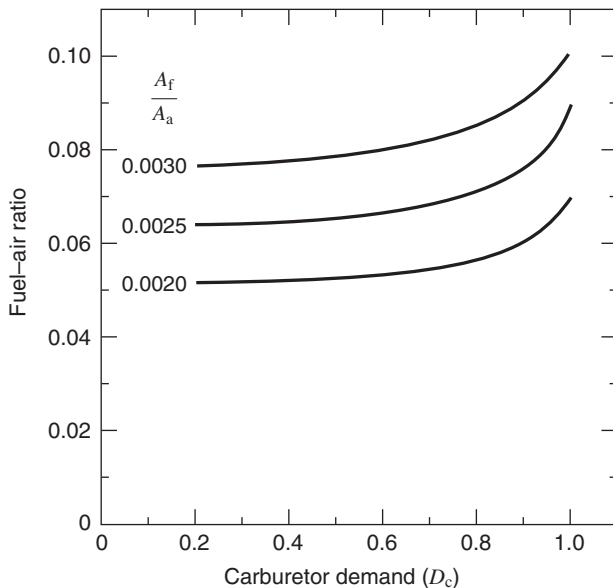


Figure 6.3 The fuel-air ratio as a function of carburetor demand.

6.3 FUEL INJECTION-SPARK IGNITION

Fuel Injection Systems

Spark ignition engines use fuel injectors to spray fuel into the air stream at the intake manifold (throttle body injection), at the inlet port (port fuel injection), or directly into the cylinder (direct-injection). Figure 6.4 shows an example of a system using port fuel injection and Figure 6.5 shows the fuel injector in a direct-injection engine. With port fuel injection, the fuel is sprayed into the port and onto the inlet valve to cool the valve and begin vaporization of the fuel. The amount of fuel required can be large enough so that the fuel injector will continue spraying into the port even when the valve is closed, so that the fuel can not enter the cylinder until the next intake stroke. For increased power, some spark ignition engines are configured with dual fuel injection, in which both port and direct fuel injectors are used to deliver fuel to the cylinder.

Digitally controlled fuel injectors were first patented in 1970 and were used on production vehicles in the United States beginning in 1982. Most automotive engines use port fuel injection, with direct fuel injection increasing in use. The required fuel pressure depends on the location of the fuel injector. A port fuel injector will have a fuel pres-

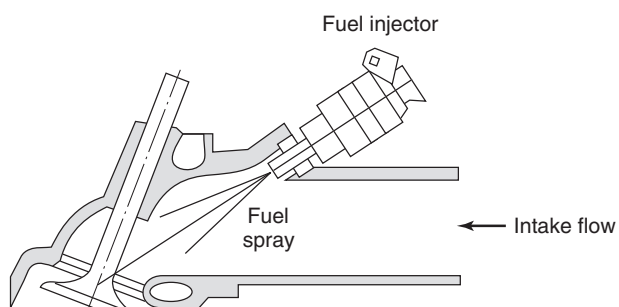


Figure 6.4 Schematic of port fuel injection.

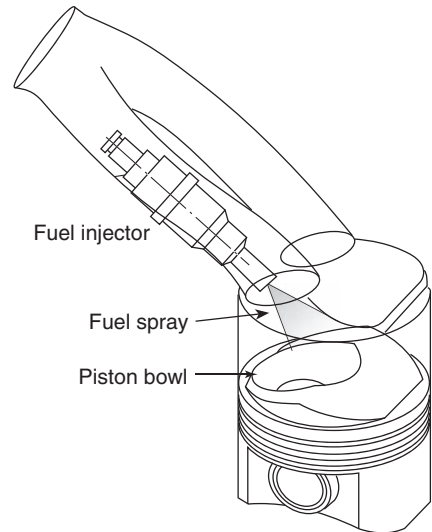


Figure 6.5 Schematic of gasoline direct fuel injection. (Adapted from Takagi et al., 1998.)

sure of about 2–5 bar, and a direct fuel injector will have a fuel pressure on the order of 30–130 bar.

Spark ignition engines primarily use a pintle nozzle fuel injector, where the upward motion of a pintle nozzle opens the valve. At an appropriate time in the engine cycle, the engine control computer issues a square wave pulse to open and close the pintle nozzle. The pintle is rapidly lifted off its seat by a solenoid and the quantity of fuel injected increases more or less linearly with the duration of the open period, since the opening and closing times are much less than the open duration time. Direct fuel injectors employ swirl ports to induce a tangential motion to the spray, resulting in a hollow cone spray for enhanced atomization and vaporization.

Bernoulli's equation can be used to estimate the mass of fuel injected as a function of the pressure and open period. Assuming quasi-steady flow through the fuel nozzle, the mass of fuel injected in one period Δt is the integral of the fuel flow rate:

$$m_f = \int_0^{\Delta t} \dot{m}_f dt = (2\rho_f \Delta P)^{1/2} \int_0^{\Delta t} A_f dt \quad (6.7)$$

where ΔP is the difference between the fuel delivery pressure and the air pressure upstream of the throttle, and A_f is the time-dependent nozzle effective area. The average effective flow area \bar{A}_f of the injector nozzle is given in Equation 6.8:

$$\bar{A}_f = \frac{1}{\Delta t} \int_0^{\Delta t} A_f dt \quad (6.8)$$

Defining the average injector discharge coefficient \bar{C}_d as

$$\bar{C}_d = \frac{\bar{A}_f}{A_o} \quad (6.9)$$

where A_o is the total geometric orifice area, the mass of fuel injected during the open duration period Δt can be expressed as

$$m_f = (2\rho_f \Delta P)^{1/2} \bar{C}_d A_o \Delta t \quad (6.10)$$

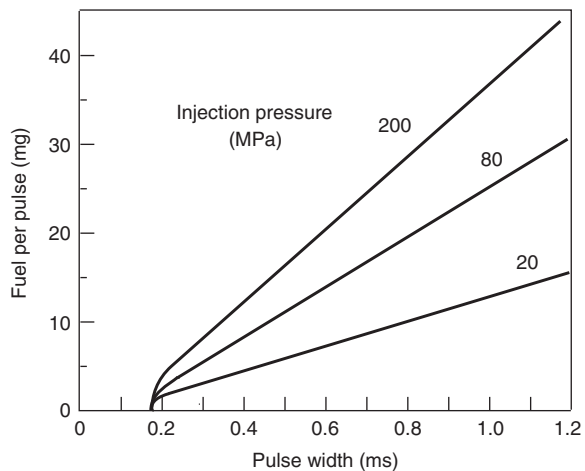


Figure 6.6 Mass of fuel injected as a function of injector pulse width and pressure.

The open duration period Δt of the fuel injection is typically 1–10 ms. The fuel per pulse is plotted in Figure 6.6 as a function of the pulse width and pressure for a representative automotive fuel injector. The prediction that the mass of fuel injected is linearly proportional to the open duration is borne out by experiment as evidenced by the results shown in Figure 6.6.

It is important that the fuel mostly evaporate before delivery to the cylinder. If the fuel in the air were to exist as large droplets, then these would collide with the intake manifold walls, and form a liquid fuel film on the walls. Accumulation of liquid fuel on the walls alters in an uncontrolled manner the fuel–air ratio of the fuel delivered to the cylinders. It causes lags and overshoots in the fuel flow with respect to the airflow delivered, and it causes variations in the fuel–air ratio from cylinder to cylinder.

Fuel injection in natural gas engines is discussed in Kim et al. (2004). Due to the relatively high-pressure involved, consideration needs to be given to the compressible flow features such as Mach disks that occur with natural gas fuel injection. For further information, the reader is referred to Li et al. (2004).

6.4 FUEL INJECTION–COMPRESSION IGNITION

Diesel Injection Systems

With compression ignition engines, fuel injection is classified as either direct-injection in which fuel is sprayed directly into the cylinders or indirect-injection (IDI), in which fuel is sprayed into a prechamber connected to the main chamber. One of the limiting features of compression ignition engines is the finite mixing rate of the fuel and air, especially for higher speed diesel engines, so a variety of DI and IDI systems have been developed to rapidly form a combustible fuel–air mixture. Fuel injection systems in the early parts of the twentieth century used air injection, a technique using the Venturi effect where compressed air entrained diesel fuel in the injector and carried it into the cylinder.

In direct-injection, the fuel is injected into the cylinder after the intake air has been compressed to about 50 bar and a temperature high enough (>850 K) for autoignition of the fuel–air mixture. The fuel flows through very small orifices in the injector tip, forming a liquid jet that subsequently breaks up into droplets that evaporate and mix with the surrounding air. Direct-injection systems operate at high-pressure, on the order of

1000 bar, so the fuel velocity will be high enough to penetrate deeply into the cylinder, and the atomized droplets will be small enough for rapid evaporation and subsequent ignition during the time available before the piston reaches top dead center. Distribution of the fuel in the cylinder is accomplished by both penetration along the streamwise flow direction, and dispersion perpendicular to the flow. The relative amounts of penetration and dispersion needed depend on the cylinder and piston geometry and the location of fuel injection.

We can again use Bernoulli's equation to examine an engine speed–injection pressure issue that arises with fuel injection systems. Assuming quasi-steady flow of an incompressible fluid, the total mass of fuel injected into a cylinder is

$$m_f = (2\rho_f \Delta P)^{1/2} \bar{A}_f \frac{\Delta\theta}{2\pi} \frac{1}{N} \quad (6.11)$$

Note that this expression is identical to Equation 6.10 except that Δt is expressed in terms of the crank angle change during the injection duration.

It is clear, in this form, that in order to hold $\Delta\theta$ constant as engine speed varies, one must accordingly increase or decrease the fuel pressure to hold m_f constant. In fact, since typically the fuel injection pressure is large compared with the cylinder pressure, one must vary the fuel injection pressure P_f with the square of engine speed:

$$P_f \approx \Delta P \propto N^2 \quad \text{if } m_f, \Delta\theta \text{ are constant} \quad (6.12)$$

Herein lies one basic problem with trying to build a diesel engine that will operate over a large speed range: if $N_{\max}/N_{\min} = 5$, then $P_{f,\max}/P_{f,\min} = 25$; furthermore, if at low speeds $P_{f,\min} = 50$ bar is needed to ensure good atomization and penetration into the combustion chamber, then $P_{f,\max} = 1250$ bar. This issue can be addressed with high-pressure fuel pumps.

Fuel injection systems are generally classified into two categories: systems that separate the fuel pressurization and injection, and those that combine fuel pressurization and injection.

The common rail injection system is an example of a system that separates fuel pressurization and injection. The high-pressure required for injection is generated mechanically using one common high-pressure pump. The high-pressure fuel is contained inside a thick-walled tube called a common rail. A control valve allows the fuel pressure to be maintained at a level set by the engine control unit. The fuel rail is large enough so that the internal pressure is not affected by operation of the fuel injectors. Since the fuel pressure is maintained at a constant value, this injection system is capable of multiple (pre-, main, and post-) injections for reduction of emissions and noise.

A schematic of a mechanically controlled common rail fuel injector is shown in Figure 6.7, and an electrically activated common rail fuel injector is shown schematically in Figure 6.8. In Figure 6.8, the electrically activated solenoid controls the motion of a control ball valve that regulates the flow of fuel from a valve control chamber. A needle valve is lifted, opening a flow path through the nozzle, and the fuel, which is already at a high-pressure, is injected into the engine cylinder. Excess fuel flows by the ball valve and back to the lower pressure fuel tank.

Examples of systems that combine the fuel pressurization and injection process are unit pumps and unit injectors. In these systems, there is simultaneous pressure generation and injection. The pressure generation is initiated by a camshaft or electric solenoid. These systems can have greater peak injection pressures than common rail systems, as the shape of the cam controls the pressure profile. Since the camshaft is coupled to the engine, the maximum injection pressure increases with engine speed.

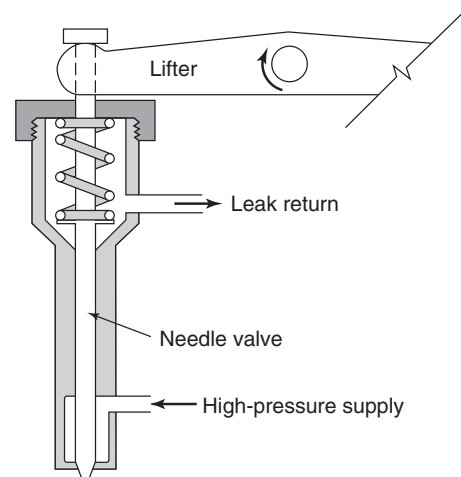


Figure 6.7 Common rail fuel injector-mechanical control.

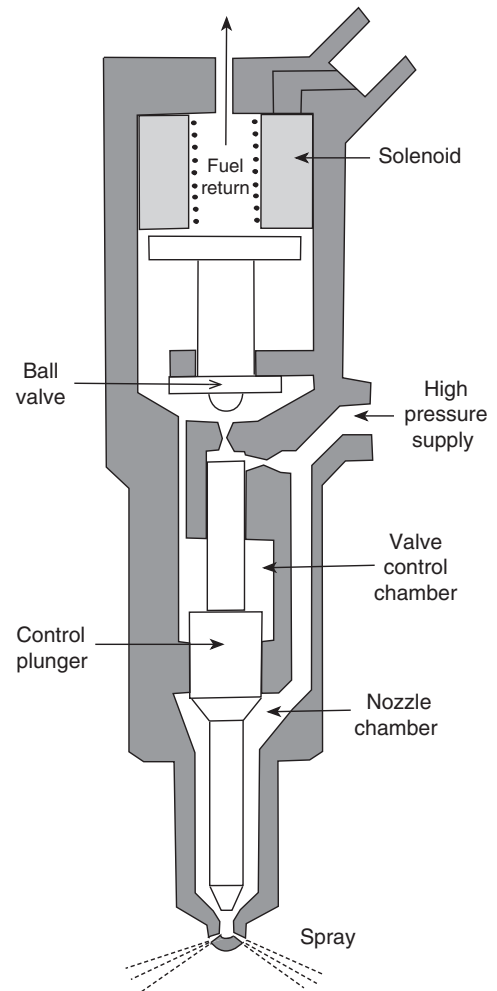


Figure 6.8 Common rail fuel injector-electrical control.

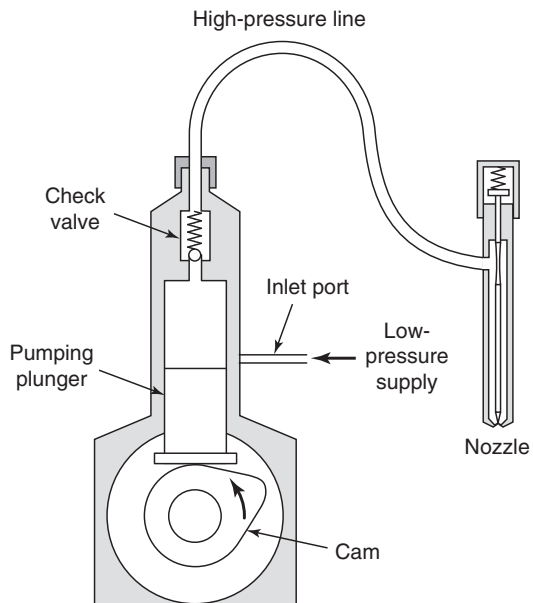


Figure 6.9 Unit pump fuel injection system.

The unit pump systems utilize the principle depicted in Figure 6.9. A low-pressure transfer pump fills the cavity ahead of a pumping plunger. A cam is configured to displace the plunger at the time when injection is to occur. The plunger moves up, shuts off the inlet port, and, because the fuel is nearly incompressible, it rapidly increases the fuel pressure. The rise in fuel pressure creates a pressure imbalance on the needle in the injector nozzle, causing it to open and allowing fuel to discharge into the engine cylinder through the nozzle. Once the fuel pressure falls to some predetermined value, a spring forces the needle down shutting off the injector. Typically, the injector pressure is about 500 bar when the needle opens, and it increases to a maximum of about 850 bar just before the needle closes.

With a unit pump injection system, the mass of fuel injected is controlled by varying the displacement of the pumping plunger. One way in which this is done is shown in Figure 6.10. A helix is cut into the pumping plunger that reopens the inlet port at some intermediate position in the plunger's stroke. A rack and pinion arrangement varies the effective stroke by rotating the plunger and therefore the position at which the port will reopen and thus dropping the fuel pressure. Some older diesel injection systems use a positive displacement pump so that the mass injected is the independent variable and the fuel pressure adjusts itself accordingly.

A unit injector is a combined unit consisting of both the pump and injector. Unit injectors were invented in 1934, and for many years were mechanically controlled. In

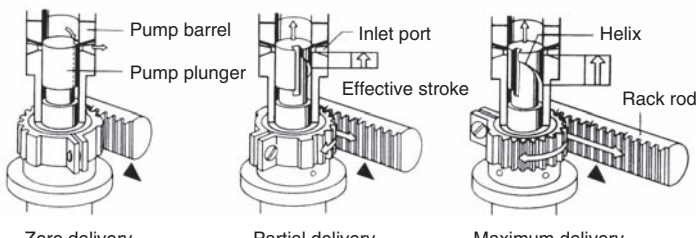


Figure 6.10 Unit pump operation.

1995, electronic unit injectors were developed. Metering is accomplished by actuation of a solenoid-operated valve, and closure of the solenoid valve initiates pressurization and subsequent fuel injection. The duration of valve actuation determines the amount of fuel injected. Unit injectors are commonly used on locomotive diesel engines.

Various nozzle configurations are used for diesel spray injection, including pintle, single, and multiorifice. Needle valves are used in diesel injection systems to control the amount of fuel injected. The sac volume, the volume of fuel in the space between the needle and the orifice is designed to be as small as possible to reduce unwanted fuel injection. Typical nozzle diameters d_n are on the order of $200 \mu\text{m}$, and length L_n about 1 mm.

EXAMPLE 6.1 Diesel Fuel Injection

The specifications for a 12-cylinder four-stroke diesel engine being designed are that it operate at a speed of $N = 1200$ rpm and produce $\dot{W}_b = 500$ kW of power, with a brake specific fuel consumption (bsfc) of 0.25 kg/kWh. The cylinder pressure at the start of injection is 30 bar, and the maximum cylinder pressure during combustion is 60 bar. The injection duration is nominally 10° of the crank angle. The unit pump injector nozzle is set to open at 200 bar, with a maximum injector pressure of 600 bar. The injector has a coefficient of discharge $\bar{C}_d = 0.60$.

- What is the mass of fuel injected per cylinder per cycle?
- What total orifice area A_o for each injector should be selected?

SOLUTION (a) The cycle average fuel consumption rate per cylinder is

$$\bar{m}_f = \text{bsfc} \cdot \dot{W}_b / n_c = 0.25 \cdot 500 / (12 \cdot 60) = 0.174 \text{ kg/min}$$

so the mass of fuel injected per cylinder per cycle is

$$m_f = \bar{m}_f / (N/2) = 0.174 / (1200/2) = 2.89 \times 10^{-4} \text{ kg}$$

(b) The pressure difference at the beginning of injection is $200 - 30 = 170$ bar, and at the end of injection is $600 - 60 = 540$ bar. For this preliminary design, let us estimate an average pressure difference of $(540 + 170) / 2 = 355$ bar between the fuel injector and the cylinder. Using Equation 6.11, and assuming the diesel fuel is incompressible with a density $\rho_f = 840 \text{ kg/m}^3$,

$$\begin{aligned} A_o &= \frac{m_f (2\rho_f \Delta P)^{-1/2}}{\bar{C}_d \left(\frac{\Delta\theta}{360} \cdot \frac{1}{N} \right)} \\ &= \frac{2.89 \times 10^{-4} (2 \cdot 840 \cdot 355 \times 10^5)^{-1/2}}{0.60 \left(\frac{10}{360} \cdot \frac{60}{1200} \right)} \\ &= 1.42 \times 10^{-6} \text{ m}^2 = 1.42 \text{ mm}^2 \end{aligned}$$

Diesel Sprays

The formation of a combustible mixture of diesel fuel and air in an engine cylinder is a very complex two-phase fluid mechanics process. Diesel fuel injection has a number of major

features, including an initial spreading angle, entrainment of surrounding gas, a liquid core surrounded by a vapor sheath, jet atomization into droplets, droplet evaporation, and gas jet wall impingement.

The spray is initially conical in shape, with the virtual origin of the jet inside the nozzle. The spreading angle of the spray, θ , depends on the ratio of the cylinder gas and diesel fuel densities. Experimental data in the atomization regime has been correlated by Reitz and Bracco (1979) with the following expression:

$$\tan \frac{\theta}{2} = \frac{4\pi}{A} \left(\frac{\rho_g}{\rho_l} \right)^{1/2} \frac{\sqrt{3}}{6} \quad (6.13)$$

where ρ_g is the gas density and the parameter A is a function of the nozzle diameter d_n and length L_n :

$$A = 3.0 + 0.28(L_n/d_n) \quad (6.14)$$

For example, for values of $\rho_g/\rho_l = 25 \times 10^{-3}$, and $A = 5$, the spread angle $\theta = 13^\circ$. As the gas density increases, the spreading angle of the spray increases.

There are different jet breakup mechanisms, depending on the outlet jet velocity and physical properties. The major governing parameters are the Weber number, the ratio of the shear and the surface tension forces; and the Reynolds number, the ratio of the inertial and the viscous forces:

$$We = \rho_l u^2 d_n / \sigma \quad (6.15)$$

$$Re = \rho_l u d_n / \mu_l \quad (6.16)$$

where ρ_l is the liquid jet density, u is the relative velocity of the jet, d_n is a nozzle or droplet diameter, σ is the surface tension, and μ_l is the dynamic viscosity of the jet.

Due to the high injection pressures, the outlet jet relative velocity is on the order of 100–200 m/s, which is in an atomization breakup regime. The shear forces on the liquid jet from the surrounding gas result in unstable surface waves that pinch off the liquid jet, producing droplets. In the atomization regime, the liquid fuel jet breaks up into liquid drops and ligaments, with dimensions much less than the injection nozzle diameter. With high injection pressures or short nozzles, the breakup length decreases, and breakup can occur at the nozzle exit. With the decrease in static pressure in the nozzle accompanying the fluid acceleration, it is also possible for cavitation to occur inside the nozzle, producing a bubbly two-phase injection flow from the nozzle. Collisions between droplets can also result in droplet coalescence.

The spray penetration distance has been the subject of extensive experimental and computational research due to its importance in the behavior of subsequent combustion processes. If the penetration is too short, air at the edges of the cylinder will not be involved in the combustion process, and if the penetration is too long, the jet spray will impinge on the cylinder walls, which will reduce the jet velocity and entrainment. Depending on the drop Weber number, the impact of a drop on the cylinder wall can result in the formation of a liquid film on the surface, breakup and vaporization, or rebound back into the cylinder.

A widely used correlation by Dent (1971) for the spray penetration distance is

$$S = 3.07 \left(\frac{\Delta P}{\rho_g} \right)^{1/4} (t d_n)^{1/2} \left(\frac{294}{T_g} \right)^{1/4} \quad (6.17)$$

where ΔP is the injector nozzle pressure drop, t is the time after start of injection. All the parameters in the above equation are in SI units. As the injection pressure or the nozzle diameter is increased, the penetration distance is increased. Once the startup phase of the

injection is complete, the length of the liquid core remains fairly constant until the end of injection.

The droplet sizes are characterized by a Sauter mean diameter, D_{SM} , named after a German scientist, J. Sauter, who in 1928 developed a measure of average particle size for a distribution of particles. The Sauter mean diameter, D_{SM} , is defined as the diameter of a model drop whose volume to surface ratio is equal to that of the total spray. A representative value of D_{SM} for diesel spray is 50 microns. As the gas density and nozzle diameter decrease, D_{SM} decreases, increasing the surface–volume ratio. Collisions between droplets also change the droplet size distribution.

$$D_{SM} = \frac{\sum_{i=1}^n d_i^3}{\sum_{i=1}^n d_i^2} \quad (6.18)$$

The next step in the diesel fuel injection process is the evaporation of the droplets. The evaporation time, on the order of 1 ms, depends on the droplet size, velocity, temperature, and droplet interaction. The energy for evaporation is heat transfer from the surrounding hot gases, an adiabatic saturation process that raises the droplet surface temperature to the saturation temperature, and lowers the surrounding gas temperature.

As mentioned earlier, the diesel combustion process is mixing limited. At the start of combustion, about 80% of the injected fuel has evaporated and is in the vapor phase. However, only about 20% of the fuel vapor has mixed with the surrounding air sufficiently to be flammable, so additional mixing is required for complete burning during the combustion process. For further information about the modeling and computation of fuel–air mixing processes in engines, the reader is referred to the book by Baumgarten (2006).

6.5 LARGE-SCALE IN-CYLINDER FLOW

Introduction

There are large-scale flow structures that are present in the cylinder during the intake and compression stroke, and are accompanied by the generation of small-scale turbulence. In this section, we discuss the physical and computational methods for quantification and characterization of these large-scale flow structures. Three parameters that are used to characterize the large-scale fluid motion and mixing in the cylinder are swirl, squish, and tumble. With large-scale mixing, the characteristic length of the fluid motion is on the order of the combustion chamber diameter, whereas with small-scale mixing, the turbulent fluid vortex size is many orders of magnitude smaller.

Cylinder Flow Measurement Techniques

Using lasers, it has become possible to measure local instantaneous velocities, temperatures, and some species concentrations within the cylinder without insertion of intrusive probes. Research engines and test rigs are built with optical access for the laser as one of the primary design features.

Figure 6.11 shows an arrangement for measuring velocity using a laser Doppler velocimetry (LDV) measurement technique. The arrangement shown is a steady-flow test rig. The beam from an argon-ion laser is split into two beams that are then focused to a small volume within the flow. Small particles, about $0.5 \mu\text{m}$ in diameter, are deliberately added to the flow to track the gas speed. As these particles pass through the probe volume made by the intersecting laser beams, they scatter radiation in all directions. The Doppler effect

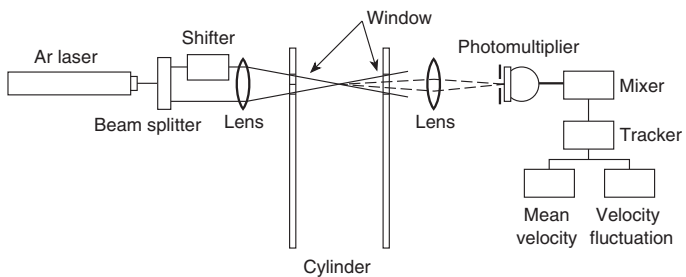


Figure 6.11 Laser Doppler velocimetry (LDV) steady-flow test rig.

shifts the frequency of the scattered light. The frequency shift is proportional to the particle velocity. The electronics of the LDV system filter and process the signal to detect the frequency shifts. Both the mean and turbulent velocity components are measured. By moving the laser beams and thus the probe volume, the velocity can be measured at different points within the cylinder.

Particle image velocimetry (PIV) systems measure velocity by determining particle displacement over time using a double-pulsed laser technique. A pulsed laser light sheet illuminates a plane in the flow, and the positions of particles in that plane are recorded by a video camera. A fraction of a second later, another laser pulse illuminates the same plane creating a second image. Images on the two planes are analyzed using cross-correlation techniques to compute the turbulent velocity field. Additional information about PIV and other laser-based measurement techniques is given in Adrian (1991).

Computational Simulation of In-Cylinder Flow Fields

The in-cylinder flow field can realistically be simulated using computational fluid dynamics (CFD) analysis. There are a number of CFD programs such as VECTIS (VECTIS USERS MANUAL, 2014), STAR-CD (STAR-CD USERS MANUAL, 2014), FLUENT (FLUENT USERS MANUAL, 2014), and CONVERGE (CONVERGE 2.1 MANUAL, 2013) that are available for computation of in-cylinder flow fields. These programs solve the discretized Navier–Stokes equations, with user chosen turbulence models, on a three-dimensional mesh or grid. The features and models included in current CFD codes include moving meshes, injection, spray and droplet evaporation, and turbulent combustion. Postprocessing is used for the analysis and visualization of the resulting solution.

A representative CFD grid for a four valve SI engine is given in Figure 6.12, and a close up cutaway of the port and valve region is shown in Figure 6.13. The computed flow field at 120° after tdc during the intake stroke is shown in Figure 6.14. Note that the computed flow field downstream of the intake valve is characterized by large-scale vortex motion.

With continued advances in high-speed digital computation, CFD calculations are now systematically included in internal combustion engine engineering design and optimization processes. For further information about the use of CFD analysis in the engine design process, the reader is referred to the book by Shi et al. (2011).

Swirl and Tumble

Swirl refers to a large-scale vortex motion within the cylinder about its long axis, and tumble is a large-scale vortex motion perpendicular to the cylinder axis. Swirl is generated during the intake stroke either by tangentially directing the flow into the cylinder using

Transient in-cylinder analysis of a four-valve SI engine
120° ATDC during the intake stroke

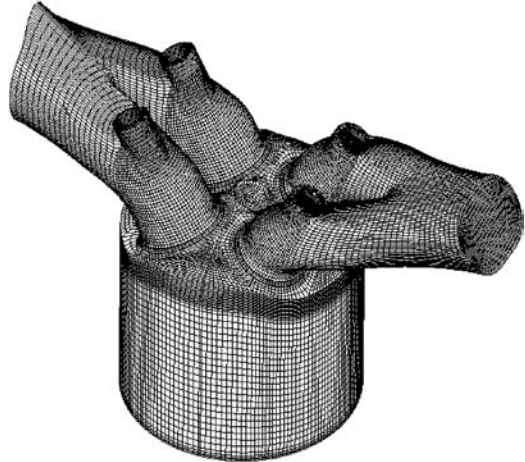


Figure 6.12 CFD grid for in-cylinder flow of a four-valve cylinder.
(Courtesy Adapco.)

Transient in-cylinder analysis of a four-valve SI engine
120° ATDC during the intake stroke

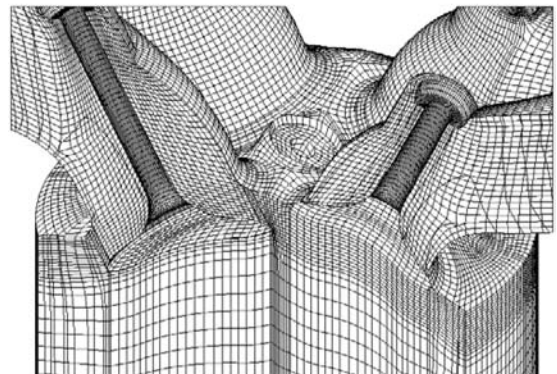


Figure 6.13 Close-up of CFD grid.
(Courtesy Adapco.)

Transient in-cylinder analysis of a four-valve SI engine
120° ATDC during the intake stroke

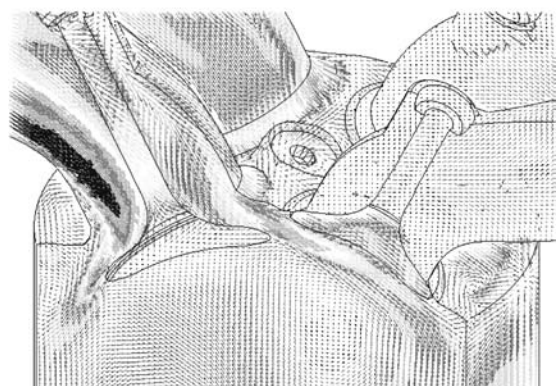


Figure 6.14 CFD flow field.
(Courtesy Adapco.)

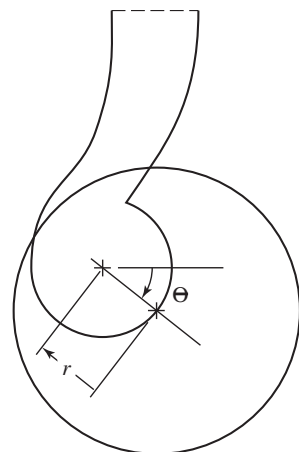


Figure 6.15 Schematic of intake port showing swirl parameters R_v and α . Adapted from Uzkan et al. (1983).

directed ports or by preswirling the incoming flow by use of a helical port. Helical ports are generally more compact than directed ports. They are capable of producing more swirl than directed ports at low lifts, but are inferior at higher lifts. Either design creates swirl at the expense of volumetric efficiency. Tumble is induced by the inlet poppet valve.

Swirl and tumble are one of the principal means to ensure rapid mixing between fuel and air in direct-injected engines. In diesel engines, as fuel is injected, the swirl bends the fuel jet and convects it away from the fuel injector, making fresh air available for the following fuel upstream. Swirl and tumble are also used in gasoline engines to promote rapid combustion, as they will result in higher turbulence levels at the start of ignition.

The swirl and tumble generated during the intake stroke will decay due to wall friction and turbulent dissipation. The swirl level at the end of the compression process is dependent upon the initial swirl generated during the intake process and how much it is amplified during the compression process.

Some parameters to consider in the design of a port for swirl are shown in Figure 6.15. These are the radius of the valve offset R_v and the orientation angle α . Research and development work, like that for maximizing the discharge coefficient, is typically done on a steady-flow bench. One way in which the swirl produced can be measured is shown in Figure 6.16. A honeycomb structure of low mass, supported by a low-friction air bearing straightens the flow. The change in angular momentum of the flow applies a torque to the honeycomb, which is measured by recording the force required to restrain it. The swirl is proportional to that torque.

The efficiency of the port as a swirl producer is characterized by a swirl coefficient C_s defined in Equation 6.19 as

$$C_s = \tau / (\dot{m}U b/2) \quad (6.19)$$

where

τ = torque applied to honeycomb

\dot{m} = mass flow rate

U = discharge velocity of gas

b = cylinder bore

The swirl coefficient C_s is equal to 1 for the limiting case where the inlet flow enters tangentially at the cylinder wall. C_s increases with the valve lift or offset, and the port

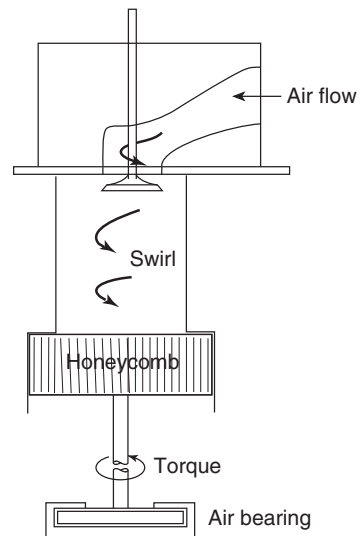


Figure 6.16 Steady-state flow and swirl system.
Adapted from Uzkan et al.(1983).

orientation is important only at the larger lifts. At zero offset, the port is producing swirl because of the helical path upstream of the valve. Since the swirl coefficient C_s characterizes the overall angular momentum of the flow, it does not capture all the complexity of the inlet flow, as it is possible for many different velocity distributions within the cylinder to yield the same angular momentum.

A bowl within the piston crown or cylinder head can be used to amplify swirl during the compression stroke, as shown in Figure 6.17. The swirl ratio in Figure 6.18 varies from zero to six times the engine speed. The swirl is proportional to the angular momentum, but it is also inversely proportional to the moment of inertia. At top center, the moment of inertia goes through a minimum in a manner dependent upon the design of the piston bowl. As seen in Figure 6.18, near top dead center of compression the swirl increases and decreases in a rather short period. The deeper the bowl, at constant compression ratio, the greater is the change in the moment of inertia and the greater is the swirl amplification.

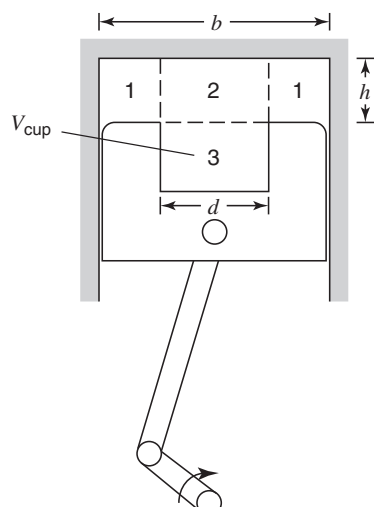


Figure 6.17 Schematic of bowl in piston crown for production of swirl and squish.

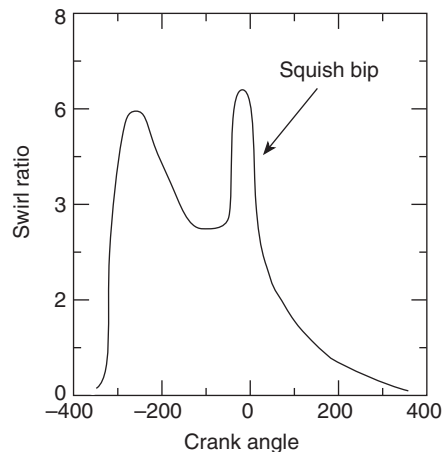


Figure 6.18 Example plot of swirl ratio versus crank angle. Adapted from Belaire et al. (1983).

In operating engines, a swirl ratio R_s is used to characterize the swirl:

$$R_s = \omega_s / 2\pi N \quad (6.20)$$

and similarly, a tumble ratio R_t is used to characterize the tumble:

$$R_t = \omega_t / 2\pi N \quad (6.21)$$

The swirl and tumble ratios are defined as the ratio of the solid body parallel and perpendicular rotational speeds of the intake flow ω_s and ω_t to the engine speed $2\pi N$. The solid body rotational speed is defined to have the same angular momentum as the actual flow. Additional discussion about the role of swirl and tumble in engines is contained in Kajiyama et al. (1984), Kawashima et al. (1998), and Lumley (1999).

There are limits to the amount of swirl that can be used effectively to minimize demands on the fuel injection system. Herein lies one of the primary reasons for building divided chamber, or, as they are often called, indirect-injection engines; less reliance on air motion induced by the fuel injection is required to effect large-scale mixing. A prechamber (Olsen and Kirkpatrick, 2008) used in large-bore natural gas fueled engines to increase in-cylinder fluid motion is shown in Figure 6.19.

With a prechamber or swirl chamber, air is forced to flow into the chamber during the compression stroke establishing three-dimensional air motion and generating turbulence.

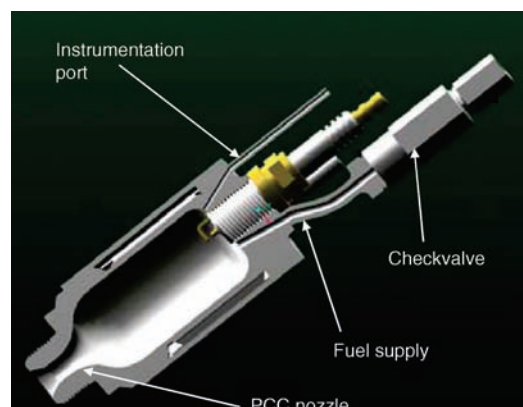


Figure 6.19 Prechamber for use in large-bore natural gas engine.

The pressure rise during combustion in the prechamber creates a flow out of the prechamber and back into the cylinder. The velocities of that backflow can be rather high, creating turbulence at the expense of an additional pressure loss. Flow passages are often contained within the piston top to organize the back flow into the cylinder to create large-scale mixing of the combustion products and the cylinder air.

Squish

Squish is a radial flow occurring at the end of the compression stroke in which the compressed gases flow into a cup located within the piston or a wedge in the cylinder head. The squish flow results from the cup-shaped geometry. The amount of squish is defined by the relative squish velocity. Incorporation of a bowl into the piston not only amplifies swirl, but also induces squish.

This can be appreciated in terms of a rather simple argument based on the continuity equation, and shown in Figure 6.17. The density within the cylinder at any time is more or less uniform (though time-dependent) during the compression stroke. Thus, at any instant, the mass within any of the zones labeled (1), (2), and (3) is proportional to the volume in these zones at any time. During compression, zones (1) and (2) get smaller, whereas zone (3) remains fixed. Thus, during compression, mass must flow out of zones (1) and (2), into zone (3). The velocity of the gas crossing the control surface between zones (1) and (2) is called the squish velocity and zone (1) is called the squish zone.

Use of squish was pioneered by H. Ricardo, in order to increase the turbulence level in side-valve engines, which were prevalent in the first half of the twentieth century (Lumley, 2001). In modern open chamber four-valve pent roof engines, the squish area is relatively low.

6.6 IN-CYLINDER TURBULENCE

Turbulence Parameters

The Reynolds numbers of flows in engine cylinders are on the order of 10,000–50,000, well into the turbulent flow regime. The turbulence results from the high-velocity inlet flow from the intake valve or port into the cylinder during the intake stroke. The inlet fluid jet flows across the cylinder, impinges on the piston top and cylinder walls, creating both large- and small-scale fluid flow features. The impinging flow is composed of turbulent eddies that have lifetimes comparable to the intake stroke timescale.

Turbulent flow in an engine can be envisioned as a mean fluid flow upon which are superimposed vortices of different sizes randomly dispersed in the flow. Turbulence is inherently three dimensional and time-dependent. A turbulent flow is composed of numerous vortices or eddies that have finite lifetimes and appear to be born at random times. The axes of the vortices also assume random orientations. There are even vortices within vortices. The turbulence in an engine is of importance as it controls the rate of combustion, since the combustion flame front is convected across the cylinder by turbulent vortices.

The turbulence in the flow field begins to appear above critical values, about 2300, of the mean flow Reynolds number, a ratio of the inertial to the viscous stresses. The Reynolds number is named after Osborne Reynolds (1842–1912), an English engineering professor who proposed it in 1883. The mean flow Reynolds number is defined in Equation 6.22, with the cylinder bore b as a length scale, and the mean piston speed \bar{U}_p as a velocity scale:

$$Re = \bar{U}_p b / \nu \quad (6.22)$$

It is not until the flow is analyzed statistically that any regularity in the flow field begins to appear. Flows that are statistically periodic, as in the case with reciprocating internal combustion engines, are treated using a statistical procedure called ensemble averaging. The ensemble average velocity $\bar{U}(x, \theta)$ is defined as

$$\bar{U}(x, \theta) = \frac{1}{n} \sum_{j=1}^n U(x, \theta, j) \quad (6.23)$$

where n is the number of cycles averaged and θ varies from 0 to 4π for a four-stroke engine and from 0 to 2π for a two-stroke engine. The left-hand side of Equation 6.23 is read as the ensemble average of the velocity at position x within the flow and at a time corresponding to the crank angle θ . The velocity summed on the right-hand side is the velocity at position x and angle θ for the j th cycle. As a consequence of the cycle-by-cycle variation in average velocity, there is a difference $\hat{U}(x, \theta, j)$ between the average velocity at a given location for a given cycle j and the ensemble average velocity:

$$\hat{U}(x, \theta, j) = \bar{U}(x, \theta, j) - \bar{U}(x, \theta) \quad (6.24)$$

To define the instantaneous turbulence within a given cycle j , one writes 6.25

$$U(x, \theta, j) = \bar{U}(x, \theta) + u'(x, \theta, j) \quad (6.25)$$

where u' is the turbulent fluctuation relative to the ensemble average, that is, the difference between the ensemble average and the instantaneous velocity, not the difference between a given cycle average and the instantaneous velocity. To quantify the magnitude of the turbulent fluctuations, a root-mean-square turbulence intensity $u_t(x, \theta)$ is defined in Equation 6.26, using ensemble averaging:

$$u_t(x, \theta) = \left[\frac{1}{n} \sum_{j=1}^n u'^2(x, \theta, j) \right]^{1/2} \quad (6.26)$$

The kinetic energy per unit mass of the turbulent fluctuations is

$$k = \frac{1}{2} u_t^2 \approx \frac{3}{2} u_t^2 \quad (6.27)$$

Determination of the turbulence intensity $u_t(x, \theta)$ requires measurements of $U(x, \theta, j)$ and u' as a function of position and crank angle. Turbulence characteristics of flows in engine cylinders have been measured using both hot-wire anemometry and laser Doppler velocimetry. Since the inlet jet velocity is proportional to piston speed, one would expect the in-cylinder mean and fluctuating velocities to also be proportional to piston speed, which then can be used as a normalizing parameter.

The results from experiments indicate that the turbulence intensity varies a great deal over a cycle. The maximum value of the turbulence intensity normalized by the piston speed, u_t/\bar{U}_p , is about ten, and occurs at 90° after top dead center, that is, halfway down the intake stroke, which is near the location of the maximum piston speed. The normalized turbulence intensity decreases to about one at bottom dead center, and remains at a value of order one during the compression stroke, and is almost homogeneous.

One of the most important conclusions reached to date is that the turbulence intensity increases linearly with piston speed. Liou, Hall, Santavicca, and Bracco (1984) conclude from a review of experimental results that the normalized top dead center turbulent intensity is

$$u_t/\bar{U}_p \approx 0.5 \quad (6.28)$$

Of course, there are differences from engine to engine at the same piston speed. The differences are caused partly by differences in the engine design and partly because flow cannot be quantitatively characterized by a measurement of only one velocity component at just one point. The turbulence measurements cover a range of engine configurations including engines with and without swirl. In the same engine with and without swirl, it has been found that the turbulent intensity is increased by swirling the flow.

The turbulence in an engine cylinder is characterized by four length scales: the characteristic length L , the integral length scale l , the Taylor microscale λ , and the Kolmogorov microscale η .

The characteristic length L of the enclosure represents the largest possible eddy size that the confining geometry of the walls will allow, such as the cylinder bore or clearance height. For a cylindrical combustion chamber, one should expect near top center, that the characteristic length should be roughly equal to the clearance height h ; whereas near bottom center, the characteristic length should be roughly equal to the bore b . With a cylindrical cup in the piston, near top center the characteristic length would be roughly the cup diameter.

The integral length scale l , represents the size of the largest and thus most energetic eddies in the turbulent flow field. For an inlet flow past a poppet valve, the integral scale is roughly equal to the inlet jet thickness. The integral scale is defined as the distance between two points where the autocorrelation coefficient of the fluctuating velocity at the points goes to zero. A number of significant turbulence parameters are based on the integral scale: The turbulence Reynolds number Re_t is based on the integral scale and the turbulent velocity, as given by Equation 6.29:

$$Re_t = \frac{u_t l}{\nu} \quad (6.29)$$

The integral scale is related to the rate of dissipation ϵ :

$$\epsilon = \frac{du_t^2}{dt} \sim \frac{u_t^2}{\tau_l} = \frac{u_t^3}{l} \quad (6.30)$$

and to the energy spectra $E(\kappa)$

$$l = \frac{\pi}{2u^2} \int_0^\infty \frac{E(\kappa)}{\kappa} d\kappa \quad (6.31)$$

The turbulent eddy viscosity v_t is the product of the integral scale and turbulent velocity:

$$v_t = u_t l \quad (6.32)$$

The integral timescale, $\tau_l = l/u_t$, represents the lifetime of a turbulent eddy. The Taylor microscale λ is useful in estimating the mean strain rate of the turbulence. It is defined as

$$\left(\frac{\partial u}{\partial x} \right)^2 = \frac{u_t^2}{\lambda^2} \quad (6.33)$$

The Kolmogorov microscale η is the smallest size viscous damping will allow. The Kolmogorov microscale is named after A. Kolmogorov (1903–1987), a Russian mathematician, who proposed that the smallest scales of turbulence are universal and depend only on the dissipation rate ϵ and viscosity ν . For turbulent flow in internal combustion engines, this scale is on the order of a few microns. From dimensional analysis, the Kolmogorov microscale is

$$\eta = \left(\frac{\nu^3}{\epsilon} \right)^{1/4} \quad (6.34)$$

Dimensional analysis of simple turbulent flows leads to the following relationships between the four length scales:

$$l = C_1 L \quad (6.35)$$

$$\frac{\lambda}{l} = \left(\frac{15}{C_\lambda} \right)^{1/2} Re_t^{-1/2} \quad (6.36)$$

$$\frac{\eta}{l} = \left(\frac{15}{C_\eta} \right)^{-1/4} Re_t^{-3/4} \quad (6.37)$$

The constants C_1 , C_λ , and C_η are numbers unique to the flow of interest and whose order of magnitude is unity.

Thus, we see that if the integral scale can be determined, so can the other scales. Note that the ratio of the largest to the smallest length scale is proportional to the Reynolds number raised to the 3/4 power. For example, if the Reynolds number of a flow is 10^4 , then L/l scales as 10^3 , and since turbulence is three dimensional, one would need about 10^9 grid points to resolve the entire range of length scales for each dependent variable. This has implications for the numerical solution of turbulent flows in engines and will be discussed in more detail in the next section.

As the turbulent Reynolds number increases, the smaller microscales decrease in size according to Equations 6.36 and 6.37. Since the turbulence in an engine increases with piston speed and the integral scale is independent of engine speed, we should expect that as engine speed goes up, the microscales of the turbulence will go down. Experiments clearly show that the flame wrinkling due to turbulence increases as the engine speed increases.

To fully characterize a turbulent flow, one needs to also specify the size distribution of the vortices and eddies that make up the turbulence. The largest eddies are generated by shear in the mean flow, and account for most of the transport of momentum and energy. Inertial effects spread the turbulent energy from the large eddies to smaller and smaller eddies until the viscous stresses are comparable to the inertial forces, a process called an energy cascade. The timescales of the eddies scale with the size of the eddies, so the rate at which energy is dissipated in the small eddies is controlled by the rate at which energy is transferred from the large eddies to the small eddies. Measurements of the eddy energy distribution indicate that the most energetic eddies initially have a size of about 1/6 of the largest eddy (Townsend, 1976).

EXAMPLE 6.2 *Turbulence Length Scales*

An engine has a mean piston speed \bar{U}_p of 5.0 m/s and a clearance volume height h of 10 mm. What is the characteristic length L , integral scale l , Taylor microscale λ , and Kolmogorov microscale η at the end of compression? Assume the fluid kinematic viscosity at the end of compression is 100×10^{-7} m²/s and $C_\eta = C_\lambda = 1$, $C_1 = 0.2$

SOLUTION $L = h$ since the flow is constrained by the clearance volume geometry

$$L = 10 \text{ mm}$$

$$l = C_1 L = (0.2)(10) = 2 \text{ mm}$$

$$\frac{\lambda}{l} = \left(\frac{15}{C_\lambda} \right)^{1/2} Re_t^{-1/2}$$

$$u_t = \bar{U}_p/2 = 2.5 \text{ m/s}$$

$$Re_t = \frac{u_t l}{\nu} = \frac{(2.5)(2 \times 10^{-3})}{(100 \times 10^{-7})} = 500$$

$$\lambda = \left(\frac{15}{1}\right)^{1/2} (500)^{-1/2}(2) = 0.30 \text{ mm}$$

$$\begin{aligned}\eta &= (C_\eta)^{-1/4} Re_t^{-3/4} l \\ &= (1)^{-1/4}(500)^{-3/4}(2) = 0.018 \text{ mm} = 18 \text{ microns}\end{aligned}$$

Turbulence Models

Turbulence models have been developed so that statistical approximations of the exact governing equations can be used. Due to the complexity of turbulent flow, turbulence modeling has been and will remain an active research area. The validation process of turbulence models is ongoing, and there are significant issues that need to be dealt with, for example, specifying the initial conditions throughout the flow and boundary conditions at the valves. In addition, the turbulence defined by Equation 6.26 does not recognize that a part of the fluctuation may be due to cycle-to-cycle variation in an organized flow that in any one cycle is different from the ensemble mean flow.

Turbulent flow fields in engines have been modeled for many years with a Reynolds-averaged Navier–Stokes (RANS) turbulent models. There are a number of turbulent eddy viscosity models currently being used by engine modelers. The most widely used is the $k - \epsilon$ model. The $k - \epsilon$ model is a two-equation model based on both a transport equation for turbulent kinetic energy k , and a transport equation for the dissipation of turbulent kinetic energy ϵ . The various forms of the $k - \epsilon$ model assume that the turbulent eddy viscosity depends on k and ϵ , as shown by the formulation given by Equations 6.38–6.40:

$$\nu_t = C_\mu k^2 / \epsilon \quad (6.38)$$

$$\frac{Dk}{Dt} = \frac{\partial}{\partial x_j} \left(\frac{\nu_t}{\sigma_k} \frac{\partial k}{\partial x_j} \right) + \nu_t \frac{\partial \bar{U}_i}{\partial x_j} \left(\frac{\partial \bar{U}_i}{\partial x_j} + \frac{\partial \bar{U}_j}{\partial x_i} \right) - \epsilon \quad (6.39)$$

$$\frac{D\epsilon}{Dt} = \frac{\partial}{\partial x_j} \left(\frac{\nu_t}{\sigma_\epsilon} \frac{\partial \epsilon}{\partial x_j} \right) + C_1 \frac{\epsilon}{k} \nu_t \frac{\partial \bar{U}_i}{\partial x_j} \left(\frac{\partial \bar{U}_i}{\partial x_j} + \frac{\partial \bar{U}_j}{\partial x_i} \right) - C_2 \frac{\epsilon^2}{k} \quad (6.40)$$

The constants σ_k , σ_ϵ , C_μ , C_1 , and C_2 are empirical constants that are flow field dependent. The $k - \epsilon$ model is based on a scalar eddy viscosity, so it does not take into account nonisotropic effects on the turbulence field such as streamline curvature resulting from cylinder swirl and tumble. It also assumes a fully developed turbulent flow field. Increased accuracy of in-cylinder mixing computations, prediction of the turbulence level, and the corresponding reaction rate can be accomplished by use of a compressible renormalized group (RNG) $k - \epsilon$ model, as discussed by Han and Reitz (1995).

Equations 6.38–6.40 are combined with the continuity, momentum, and energy equations to form a complete system for numerical analysis.

Large eddy simulation (LES) is a turbulence modeling procedure in which the large eddies are computed, and the smallest eddies are modeled. LES turbulence models are more computationally intensive than RANS models. The smallest eddies are more amenable to modeling as they have greater isotropic turbulence characteristics than the larger eddies. Eddies of size less than the grid size are removed from the dynamics. The grid cells can

be much larger than the Kolmogorov length scale. With LES modeling the time-dependent Navier–Stokes equations are spatially filtered over the computational grid.

The LES decomposition is written as

$$u(x, t) = u(x, t) + u''(x, t) \quad (6.41)$$

In this decomposition u is usually termed the large- or resolved-scale part of the solution, and u'' is called the small-scale or modeled part. It is important to note that both the large and small-scales depend on both space and time, as opposed to Reynolds averaging where only the fluctuating velocity component is time-dependent.

Both RANS and LES models are similar in that they both average over the small-scales, with the LES grid scales much smaller than the RANS grid scales. LES models are available in the CFD computer programs mentioned previously.

Direct numerical simulation (DNS) resolves the entire range of turbulent length scales. It is a complete time-dependent solution of the Navier–Stokes and continuity equations. Since no turbulence model is used at any length scale, the grid must be small enough to resolve the smallest turbulent eddy whose size is on the order of the Kolmogorov length scale. The main advantage of LES over DNS is the much smaller computational expense, as flow fields can be computed using LES at Reynolds numbers much higher than currently practical with DNS.

For further information, the reader is referred to the turbulence modeling text by Wilcox (2006). Garnier et al. (2009) also give further details about various aspects of LES modeling, especially for compressible flows.

6.7 AIRFLOW IN TWO-STROKE ENGINES

Two-Stroke Scavenging Configurations

The two-stroke engine combines the intake and compression stroke and the expansion and exhaust stroke in order to produce power every downward stroke. Two-stroke engines can be either spark or compression ignition. A large number of different two-stroke engine configurations have been designed, each with different scavenging or air-charging characteristics, airflow paths, and valve arrangements. In addition, there are many different valve arrangements used to open and close ports, including piston control, poppet valves, rotary valves, or sleeve valves. Considering the large number of possible permutations, based on classification of the pumping method, the air path, and the valving arrangement, it is clear why so many different types of two-stroke engines exist.

A crankcase-scavenged engine was discussed in Chapter 1. Air is inducted into the crankcase, subsequently compressed, and pumped into the cylinder. Lubricating oil is added to the intake airflow to lubricate the interior surfaces. Another class of two-stroke engines is the separately scavenged engine in which a separate compressor, driven by the crank or perhaps an exhaust turbine, delivers the air. Since there is no separate exhaust stroke, the scavenging process relies on air being forced at elevated pressures into the cylinder to expel the burnt exhaust gas from the previous cycle.

Two-stroke engines are classified on the basis of the air path during the course of scavenging. The three scavenging configurations are cross-, loop-, and uniflow-scavenging. Figure 6.20 illustrates various ways in which these three types of scavenging geometries can be realized.

The first two-stroke engines designed by Dugald Clerk in the late 1800's used cross scavenging and a piston with a deflector top. With cross scavenging, the intake and exhaust ports are located on opposite sides of the cylinder, 180° apart, and a deflector on the top of

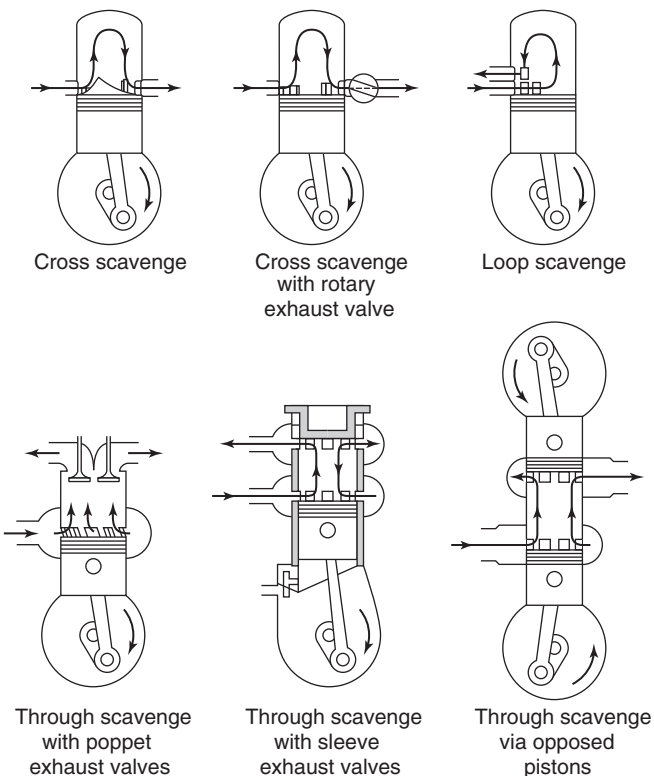


Figure 6.20 Two-stroke scavenging configurations (Taylor, 1985).

the piston ideally directs the incoming scavenging flow upward toward the upper portion of the cylinder. Since the ports are controlled by the piston, their opening and closing is symmetric about bottom dead center. This type of scavenging has good performance at low throttle and low engine speeds. The disadvantages are that the combustion chamber becomes irregularly shaped with a high surface to volume ratio, increasing the susceptibility for engine knock and possible overheating of the piston top.

With a cross-scavenging configuration, care must be taken to avoid short-circuiting. At wide open throttle with increased intake pressure, the scavenging airflow has a tendency to flow directly to the exhaust port. Notice in Figure 6.20 that without the deflector on the piston top, the incoming air would have a tendency to simply go in and out of the cylinder without displacing exhaust gas, that is, short circuit the intake and exhaust process. Insertion of the deflector is intended to force the gas to turn and mix with the exhaust gas, thus expelling a mixture of air and exhaust.

Experimental data suggest that the best scavenging that can be achieved via the cross scavenging method occurs when there is perfect mixing in which the fresh air introduced successively dilutes the residual exhaust gas. If sufficient air is used, at the end of scavenging an acceptable scavenging efficiency is then achieved.

Loop scavenging was developed by Adolf Schnurle, a German engineer, in 1926. With loop or Schnurle scavenging, the intake ports are angled and located 90–180° apart from the exhaust ports. The top of the piston is relatively flat, reducing the piston overheating issues. The angled intake ports produce a swirling scavenging flow that loops upward and around the combustion chamber and then downward to the exhaust port. Again, the ports are piston controlled. Numerical modeling of the fuel-air mixing in loop-scavenged engines is discussed further in Kim et al. (2007).

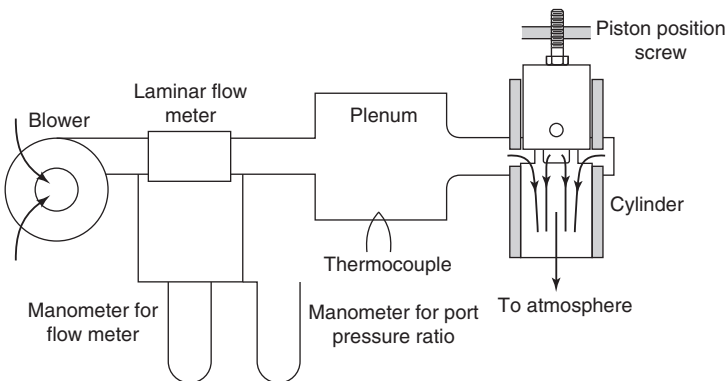


Figure 6.21 Flow bench measurement of effective flow areas and discharge coefficients of piston-controlled ports.

Uniflow scavenging is a scavenging method that uses ports for the intake and valves for the exhaust. The fresh air charge is admitted through piston-controlled ports near bottom dead center and the exhaust gas exits through exhaust valves located in the cylinder head, so the flow is ideally unidirectional. In theory, this method could result in perfect scavenging in which the incoming air displaces the exhaust gas without any mixing occurring between the incoming gas and the exhaust gas. The inlet ports are angled and located around the entire periphery of the cylinder, producing a swirling flow in the cylinder. Also, since the exhaust valves can be operated independently of the piston, it is possible to have greater control of the compression ratio and compression pressure. Due to its greater mechanical complexity compared with loop scavenging, uniflow scavenging is primarily used on large marine diesel two-stroke engines. For current applications of uniflow scavenging, the reader is referred to the numerical and experimental investigations of marine diesel engines in Anderson et. al. (2013), and of vehicular diesel engines in Laget et al. (2013).

As inspection of Figure 6.20 reveals, more often than not, two-stroke engines use piston-controlled ports rather than cam-actuated valves to admit the fresh charge and expel the exhaust. Therefore, for two-stroke flow analysis and modeling, one must specify the effective flow areas of the ports as functions of crank angle. A steady-flow apparatus for determining the effective flow area of piston-controlled ports is shown in Figure 6.21. Note the similarity with a valve flow bench apparatus. Solution of Equation 6.42 yields the effective port area A_f from measurements of the mass flow rate and the pressure ratio:

$$\dot{m} = \rho_o A_f c_o \left[\frac{2}{\gamma - 1} \left(\left(\frac{P_v}{P_o} \right)^{2/\gamma} - \left(\frac{P_v}{P_o} \right)^{(\gamma+1)/\gamma} \right) \right]^{1/2} \quad (6.42)$$

Some measured discharge coefficients, using the exposed geometric port area as the reference area, for a piston-controlled inlet port are shown in Figure 6.22. Part (b) of Figure 6.22 shows an important difference between results obtained for poppet valves and those obtained for simple ports. The discharge coefficient increases with Mach number, whereas, with poppet valves, it is nearly independent of Mach number. As the Reynolds number is not constant in Figure 6.22, the attribution of the observed effects to Mach number tacitly assumes that there is no dependence upon Reynolds number.

Crankcase, inlet, and exhaust pressures are plotted in Figures 6.23 and 6.24 for a loop-scavenged two-stroke motorcycle engine with piston-controlled induction operating at $N = 4000$ rpm. Finite-amplitude pressure waves occur in the intake and exhaust pipes. The

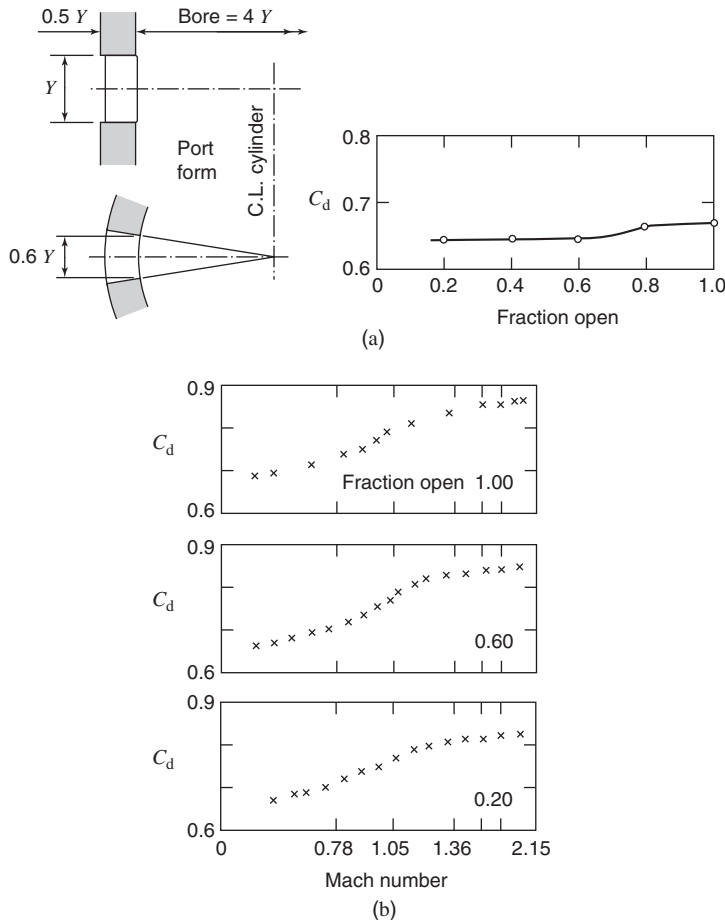


Figure 6.22 Port discharge coefficient. (a) Variation with port opening at low Mach number. (b) Variation with Mach number based on velocity and sound speed at the throat. (Annand and Roe, 1974.)

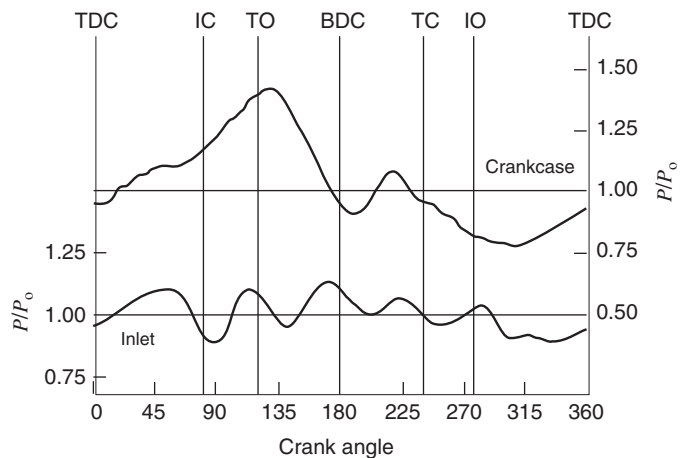


Figure 6.23 Crankcase and inlet pressure profiles for a two-stroke motorcycle engine. Adapted from Blair and Ashe (1976).

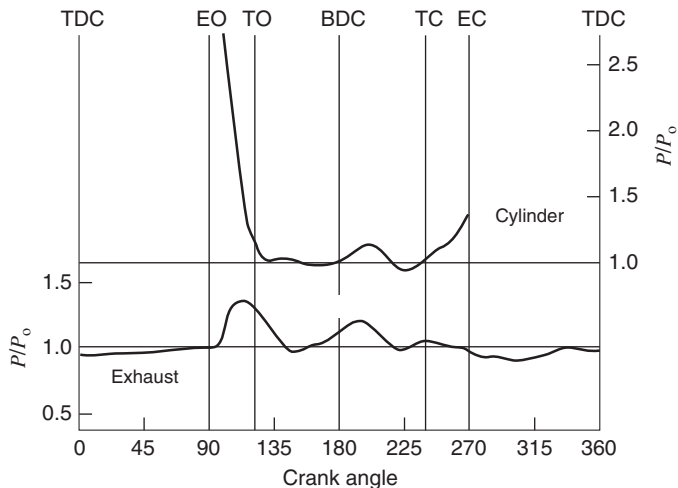


Figure 6.24 Cylinder and exhaust pressure profiles for a two-stroke motorcycle engine.
Adapted from Blair and Ashe (1976).

pressure waves are a significant influence in the performance of two-stroke engines, and thus need to be considered in the design of the intake and exhaust manifolds. Figure 6.23 indicates that the crankcase pressure increases fairly linearly as the piston moves downward until the transfer port is uncovered (TO), increases with an inlet pressure pulse, then continues to decrease. Figure 6.24 shows a positive fluctuation in the cylinder pressure as a plugging pulse returns in the exhaust. Additional information about two-stroke exhaust tuning is given in Adair et al. (2006).

Performance Parameters

The following discussion provides performance terminology according to SAE recommended practice. There are two reference masses used in two-stroke scavenging analyses. These are m_o , the mass of delivered charge in an ideal scavenging process using the displacement volume V_d and ambient air (or mixture) density, ρ_i . This reference mass is useful in experimental work.

$$m_o = \rho_i V_d \quad (6.43)$$

and m_{tr} , the trapped, that is, actual mass of gas in the cylinder at a given instant, including the delivered and the residual gas mass, useful in computational analysis. The relative charge, R_c , is defined as the ratio of these two masses:

$$R_c = \frac{m_{tr}}{m_o} \quad (6.44)$$

The trapped air–fuel ratio is a measure used to characterize the state of the mixture at the beginning of combustion:

$$\text{AF}|_{tr} = \frac{\text{mass of air retained}}{\text{mass of fuel retained}} \quad (6.45)$$

The delivery ratio, D_r , is the ratio of the actual mass of delivered charge to the ideal mass of delivered charge. It has values ranging from zero at intake port opening to values greater than one at exhaust port close depending on the amount of intake flow pressurization.

$$D_r = \frac{\text{mass of delivered charge}}{\rho_i V_d} \quad (6.46)$$

The scavenging ratio, S_r , is the ratio of the actual mass of delivered charge to the ideal mass of delivered charge, using the entire cylinder volume and ambient air (or mixture) density.

$$S_r = \frac{\text{mass of delivered charge}}{\rho_i V_{\text{cyl}}} \quad (6.47)$$

The trapping efficiency, η_{tr} , is the fraction of the delivered air (or mixture) retained in the cylinder at exhaust port close:

$$\eta_{\text{tr}} = \frac{\text{mass of delivered charge retained}}{\text{mass of delivered charge}} \quad (6.48)$$

The scavenging efficiency, η_{sc} , the ratio of the delivered charge retained to the mass of gas in the cylinder, is a measure of the replacement of the burnt exhaust gas with fresh charge at a given instant. It is used to compare the performance of various port and piston geometries as a function of the delivery or scavenging ratio.

$$\eta_{\text{sc}} = \frac{\text{mass of delivered charge retained}}{m_{\text{tr}}} \quad (6.49)$$

The charging efficiency, η_{ch} , the ratio of the delivered charge retained to the ideal mass of delivered charge, is a measure of the efficiency of the filling process:

$$\eta_{\text{ch}} = \frac{\text{mass of delivered charge retained}}{m_0} \quad (6.50)$$

The purity is defined as the fraction of air in the trapped cylinder charge:

$$\mathcal{P} = \frac{\text{mass of air in trapped cylinder charge}}{m_{\text{tr}}} \quad (6.51)$$

The parameters are defined for fuel-injected engines. For fuel-induced engines, as with a throttle-body injector, note that the air–fuel mixture is to be substituted for the air, and the mixture density at ambient pressure and temperature is to be substituted for the ambient air density.

The above parameters are not independent of each other. The scavenging efficiency η_{sc} , charging efficiency η_{ch} , and trapping efficiency η_{tr} are all measures of the success in clearing the cylinder of residual gases from the preceding cycle and as such can be mathematically related. By definition it follows that the trapping efficiency η_{tr} is

$$\eta_{\text{tr}} = \frac{\eta_{\text{ch}}}{D_r} = \frac{\eta_{\text{sc}} R_c}{D_r} \quad (6.52)$$

With excess air, the purity \mathcal{P} and scavenging efficiency η_{sc} differ because of the excess air λ in the residual gas. It can be shown that (Schweitzer, 1949)

$$\begin{aligned} \eta_{\text{sc}} &= \mathcal{P} \quad \text{if } \lambda \leq 1 \\ \eta_{\text{sc}} &= \frac{1}{1 + \lambda(1/\mathcal{P} - 1)} \quad \text{if } \lambda > 1 \end{aligned} \quad (6.53)$$

The scavenging efficiency is less than or equal to the purity. However, as the difference is usually small, the two quantities are often confused.

Finally, the residual mass fraction f required for thermodynamic analysis is

$$f = 1 - \eta_{\text{sc}} \quad (6.54)$$

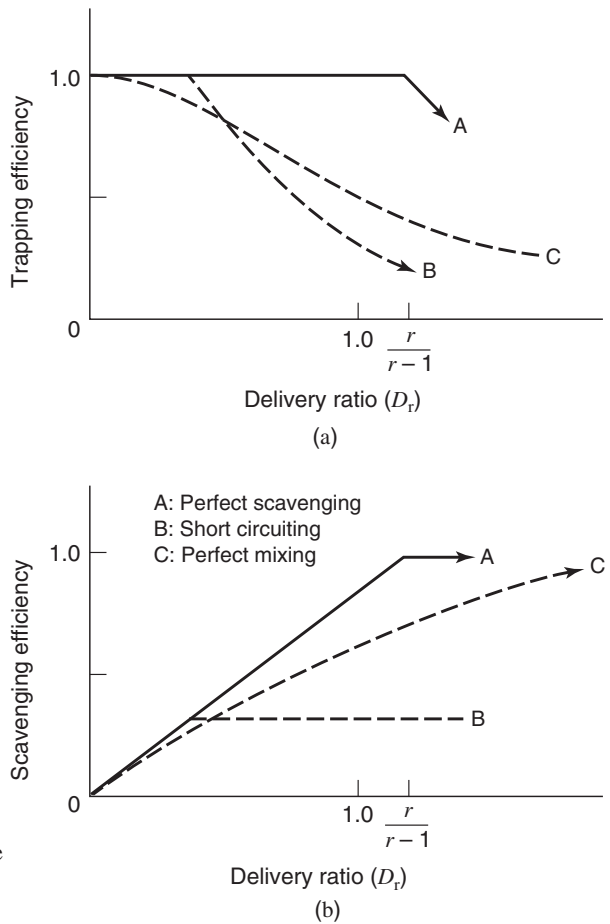


Figure 6.25 Two-stroke scavenging and trapping efficiencies.

Two-Stroke Scavenging Models

In this section, we will use three simple algebraic mixing models corresponding to perfect displacement, short-circuiting, and perfect mixing to find the relationships between the scavenging efficiency and the delivery ratio. These models are approximations of the actual scavenging process as they assume the process occurs at constant volume, temperature, and pressure in the cylinder. Experimental measurements of scavenging efficiency as a function of delivery ratio usually lie somewhere between the perfect displacement and perfect mixing limiting cases.

Let us consider first the case of perfect scavenging. In this ideal case no mixing occurs, and the inlet air simply displaces the exiting exhaust gas. The trapping and scavenging efficiencies as functions of the delivery ratio are given in Figure 6.25.

At a delivery ratio D_r given by

$$D_r = \frac{V_{bdc}}{V_d} = \frac{r}{r-1} \quad (6.55)$$

the cylinder volume at bottom center is filled with pure air ($P = \eta_{sc} = 1.0$), and if any more air is delivered, it is not retained. This occurs at a delivery ratio greater than one (see curve A in Figure 6.25) and dependent upon the compression ratio because the delivery ratio is defined in terms of the displacement volume V_d rather than the maximum cylinder

volume V_{cyl} corresponding to bottom dead center. Therefore,

$$\begin{aligned} \text{For } D_r &\leq r/(r-1), & \eta_{\text{sc}} &= D_r/R_c \\ && \eta_{\text{tr}} &= 1 \\ \text{For } D_r &> r/(r-1), & \eta_{\text{sc}} &= 1 \\ && \eta_{\text{tr}} &= R_c/D_r \end{aligned} \quad (6.56)$$

In the case of short-circuiting, the air initially displaces all the gas within the path of the short circuit and then simply flows into and out of the cylinder along that path. Thus, initially, the scavenging efficiency η_{sc} increases with delivery ratio as if scavenging were perfect. The scavenging efficiency then remains constant once the path has been displaced, see curve B in Figure 6.25.

For the case of perfect mixing, the first air to come in is assumed to be mixed with the exhaust gasses to form a homogeneous mixture. The composition of the mixture leaving the cylinder through the exhaust ports is the same as the instantaneous composition of the in-cylinder mixture. Thus, the first gas expelled is nearly all residual gas. As the scavenging process proceeds, the gas being expelled has an increasing concentration of fresh charge, decreasing the trapping efficiency.

The scavenging and trapping efficiencies as a function of the delivery ratio can be expressed via a mixing analysis based on the conservation of delivered air. Let m_a denotes delivered air, m'_a denotes delivered air retained, and m denotes the mass of the in-cylinder mixture. The instantaneous mass fraction of delivered air retained is

$$x = \frac{m'_a}{m} \quad (6.57)$$

and the airflow rate out of the cylinder is

$$\dot{m}'_{a,\text{out}} = x \dot{m}_{\text{out}} \quad (6.58)$$

The air mass continuity equation, Equation 6.59, is

$$\begin{aligned} \frac{dm'_a}{dt} &= \dot{m}'_{a,\text{in}} - \dot{m}'_{a,\text{out}} \\ &= \dot{m}_{\text{in}} - x \dot{m}_{\text{out}} \\ &= \dot{m}_{\text{in}}(1-x) \end{aligned} \quad (6.59)$$

The time derivative of Equation 6.57 is

$$\frac{dm'}{dt} = x \frac{dm}{dt} + m \frac{dx}{dt} = m \frac{dx}{dt} \quad (6.60)$$

assuming steady flow with equal mass flow rates into and out of the cylinder. Therefore,

$$m \frac{dx}{dt} = \dot{m}_{\text{in}}(1-x) \quad (6.61)$$

separating variables,

$$\frac{dx}{1-x} = \frac{\dot{m}_{\text{in}}}{m} dt \quad (6.62)$$

Integrating over the scavenging event, where at exhaust port close (ec), $x = \eta_{\text{sc}}$

$$\ln(1 - \eta_{\text{sc}}) = - \int_{\text{eo}}^{\text{ec}} \frac{\dot{m}_{\text{in}}}{m} dt \quad (6.63)$$

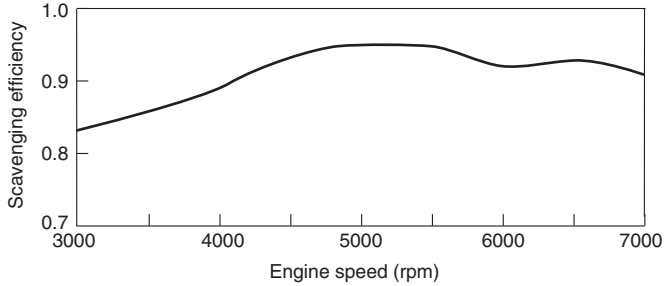


Figure 6.26 Two-stroke scavenging efficiency versus engine speed.
Adapted from Blair and Ashe (1976).

Since

$$\int_{eo}^{ec} \frac{\dot{m}_{in}}{m} dt = \frac{m_{in}}{m_{tr}} = \frac{D_r}{R_c}, \quad (6.64)$$

the scavenging and trapping efficiencies thus are

$$\begin{aligned} \eta_{sc} &= 1 - \exp\left(\frac{-D_r}{R_c}\right) \\ \eta_{tr} &= \frac{R_c}{D_r} \left[1 - \exp\left(\frac{-D_r}{R_c}\right) \right] \end{aligned} \quad (6.65)$$

The perfect mixing curves (C) are drawn in Figure 6.25 accordingly. The measured and predicted scavenging efficiencies using the perfect mixing model are compared in Figure 6.26 for a two-stroke motorcycle engine. The test engine is loop scavenged with piston-controlled induction. The scavenging efficiencies are about 90%. A more detailed review of scavenging modeling is given in Sher (1990).

State-of-the-art models use the differential mass and momentum conservation equations to predict the fluid flow and mixing conditions in a two-stroke engine as a function of the engine speed, and port and cylinder geometry. For further information regarding airflow in two-stroke engines, including the unsteady compressible flow characteristics of two-stroke engines, the reader is referred to the books by Heywood and Sher (1999), and Blair (1996).

6.8 REFERENCES

- ADAIR, J., D. OLSEN, and A. KIRKPATRICK (2006), “Exhaust Tuning for Large Bore 2-Stroke Cycle Natural Gas Engines,” *Int. J. Engine Res.*, Vol. 7, Issue 2, pp. 131–141.
- ADRIAN, R. (1991), “Particle-Imaging Techniques for Experimental Fluid Mechanics,” *Ann. Rev. Fluid Mech.*, Vol. 23, pp. 261–304.
- ANDERSON, F., J. HULT, K. NOGENMYR, and S. MAYER (2013), “Numerical Investigation of the Scavenging Process in Marine Two-Stroke Diesel Engines,” SAE paper 2013-01-2647.
- ANNAND, W. and G. ROE (1974), *Gas Flow in the Internal Combustion Engine*, G. T. Foulis, Somerset, England.
- BAUMGARTEN, C. (2006), *Mixture Formation in Internal Combustion Engines*, Springer-Verlag Publishing, Berlin.
- BELAIRE, R., R. DAVIS, J. KENT, and R. TABACZYNSKI (1983), “Combustion Chamber Effects on Burn Rates in a High Swirl Spark Ignition Engine,” SAE paper 830335.

- BLAIR, G. and M. ASHE (1976), "The Unsteady Gas Exchange Characteristics of a Two-Cycle Engine," SAE paper 760644.
- BLAIR, G. P. (1996), *Design and Simulation of Two Stroke Engines*, SAE International, Warrendale, Pennsylvania.
- CONVERGE 2.1 MANUAL (2013), Convergent Science, Inc., Madison, Wisconsin.
- DENT, J. C. (1971), "Basis for the Comparison of Various Experimental Methods for Studying Spray Penetration," SAE paper 710571.
- FLUENT USERS MANUAL (2014), Fluent Incorporated, Hanover, New Hampshire.
- GARNIER, E., N. ADAMS, and P. SAGAUT (2009), *Large Eddy Simulation for Compressible Flows*, Springer-Verlag Publishing, Berlin.
- HAN, Z. and R. REITZ (1995), "Turbulence Modeling of Internal Combustion Engines using RNG $k - \epsilon$ Models," *Comb. Sci. Tech.*, Vol. 106, pp. 207–295.
- HEYWOOD, J. and E. SHER (1999), *The Two-Stroke Cycle Engine*, SAE International, Warrendale, Pennsylvania.
- KAJIYAMA, K., K. NISHIDA, A. MURAKAMI, M. ARAI, and H. HIROYASU (1984), "An Analysis of Swirling Flow in Cylinder for Predicting D. I. Diesel Engine Performance," SAE paper 840518.
- KAWASHIMA, J., H. OGAWA, and Y. TSURU (1998), "Research on a Variable Swirl Intake Port for 4-Valve High Speed DI Diesel Engines," SAE paper 982680.
- KIM, G., A. KIRKPATRICK, and C. MITCHELL, 2004, "Computational Modeling of Natural Gas Injection in a Large-bore Engine," *ASME J. Eng. Gas Turbines Power*, Vol. 126, No. 3, pp. 656–654.
- KIM, G., A. KIRKPATRICK, and C. MITCHELL, 2007, "Supersonic Injection Virtual Valve Design for Three Dimensional Numerical Simulation of a Large-bore Natural Gas Engine," *ASME J. Eng. Gas Turbines Power*, Vol. 129, No. 4, pp. 1065–1071.
- LAGET, O., C. TERNEL, J. THIROT, and S. CHARMASSON (2013), "Preliminary Design of a Two-Stroke Uniflow Diesel Engine for Passenger Car," *SAE Int. J. Engines*, Vol. 6, No. 1, p. 596.
- LIOU, T. M., M. HALL, D. A. SANTAVICCA, and F. N. BRACCO (1984), "Laser Doppler Velocimetry Measurements in Valved and Ported Engines," SAE paper 840375.
- LI, Y., A. KIRKPATRICK, C. MITCHELL, and B. WILLSON (2004), "Characteristic and Computational Fluid Dynamics Modeling of High Pressure Gas Jet Injection," *ASME J. Eng. Gas Turbines Power*, Vol. 126, No. 1, pp. 1–6.
- LUMLEY, J. (1999), *Engines: An Introduction*, Cambridge University Press, Cambridge, England.
- LUMLEY, J. (2001), "Early Work on Fluid Mechanics in the IC Engine," *Annual Rev. Fluid Mech.*, Vol. 33, pp. 319–338.
- OBERT, E. F. (1973), *Internal Combustion Engines and Air Pollution*, Harper & Row, New York, pp. 388–389.
- OLSEN D. and A. KIRKPATRICK (2008), "Experimental Examination of Prechamber Heat Release in a Large Bore Natural Gas Engine," *ASME J. Eng. Gas Turbines Power*, Vol. 130, No. 5, pp. 052802: 1–7.
- REITZ, R. and F. BRACCO (1979), "On the Dependence of Spray Angle and Other Spray Parameters on Nozzle Design and Operating Conditions," SAE Paper 790494.
- SCHWEITZER, P. H. (1949), *Scavenging of Two-Stroke Diesel Engines*, Macmillan, New York.
- SHER, E. (1990), "Scavenging the Two-Stroke Engine," *Prog. Energy Combust. Sci.*, Vol. 16, pp. 95–124.
- SHI, Y., H. GE, and R. REITZ (2011), *Computational Optimization of Internal Combustion Engines*, Springer-Verlag, London, England.
- STAR-CD USERS MANUAL (2014), Computational Dynamics, Inc., London, England.
- TAKAGI, Y., T. ITOH, S. MURANAKA, A. IIYAMA et al., (1998), "Simultaneous Attainment of Low Fuel Consumption, High Output Power, and Low Exhaust Emissions in Direct Injection SI Engines," SAE Paper 980149.
- TAYLOR, C. (1985), *The Internal Combustion Engine in Theory and Practice*, Vols. 1 and 2, MIT Press, Cambridge, Massachusetts.
- TOWNSEND, A. (1976), *The Structure of Turbulent Shear Flow*, Cambridge University Press, Cambridge, England.

- UZKAN, T., C. BORGNAKKE, and T. MOREL (1983), "Characterization of Flow Produced by a High-Swirl Inlet Port," SAE paper 830266.
- VECTIS USERS MANUAL (2014), Ricardo Software, Inc., Burr Ridge, Illinois.
- WILCOX, D. (2006), *Turbulence Modeling for CFD*, Third Edition, DCW Industries, La Canada, California.

6.9 HOMEWORK

- 6.1** A four-cylinder, four-stroke, 3.0 L port-injected spark ignition engine is running at 2200 rpm on a stoichiometric mix of octane and standard air at 100 kPa and 298 K. If the average octane flowrate is 3.0 g/s, (a) what is the mass of fuel entering each cylinder per cycle?, (b) what is the volumetric efficiency, and (c) assuming complete combustion, what is the rate of heat release?
- 6.2** A carburetor has a pressure drop of 0.025 bar and a fuel-air ratio $FA = 0.06$ at a demand $D_c = 0.4$. (a) What is the fuel-air effective area ratio A_f/A_a ? (b) If the demand changes to $D_c = 0.6$, what is the change in the fuel-air ratio FA?
- 6.3** Carburetor venturis are sized assuming the maximum quasi-steady flow during the intake stroke is twice the average. Estimate the venturi throat diameter required for a four-cylinder 5.0 L engine with a volumetric efficiency of 0.9, and maximum speed of 6000 rpm. State clearly the assumptions you need to make.
- 6.4** What is the injection duration (deg) needed for fuel injection in a single cylinder diesel engine operating at 1500 rpm so that the engine produces 50 kW? The engine bsfc is 0.22 kg/kWh. Assume incompressible fuel flow, an average cylinder pressure of 50 bar during the fuel injection, an injector effective area $A_f = 1.0 \text{ mm}^2$, and an injection pressure equal to 550 bar.
- 6.5** If the diesel injector in problem 6.4 has a nozzle diameter d_n of 0.30 mm and length L_n of 1.0 mm, what is the spray angle? Assume the cylinder temperature is 800 K.
- 6.6** For problem 6.5, plot the spray tip penetration versus time, and determine the time and crank angle interval for the fuel to reach the cylinder wall for an engine with a bore of 150 mm operating at 1500 rpm.
- 6.7** A diesel fuel injector has a total orifice area of 0.15 mm^2 with an average $C_d = 0.60$. a.) If the average pressure difference between the fuel injector and cylinder is 400 bar, what is the amount of diesel fuel injected over a 8 ms period? b.) If the engine has a 50% thermal efficiency and operates at 1500 rpm, estimate the power produced by the engine.
- 6.8** To illustrate the effect of combustion chamber geometry on swirl amplification consider an axisymmetric engine where at bottom center the velocity field of the air inside the cylinder is approximately $v_r = v_z = 0$ and $v_\theta = V_0(2r/b)$. The cylinder has a bore b , and the piston has a disk-shaped bowl of diameter d and depth h . The motion is said to be solid body since the gas is swirling as though it were a solid. If at top dead center the motion is also solid body and angular momentum is conserved during compression, what is the ratio of the initial to final swirl speed, $\omega_{bdc}/\omega_{tdc}$, as a function of the compression ratio and the cylinder geometry? The moment of inertia of solid body rotation of a disk of diameter, d , and depth, h , is $I = \pi\rho hd^4/32$.

- 6.9** An engine has a mean piston speed \bar{U}_p of 10.0 m/s and a clearance volume height h of 5 mm. What is the characteristic length L , integral scale l , Taylor microscale λ , and Kolmogorov microscale η at the end of compression? Compare your calculations with Example 6.2 and explain the differences. Assume the fluid kinematic viscosity at the end of compression is 100×10^{-7} m²/s and $C_\eta = C_\lambda = 1$, $C_l = 0.2$.
- 6.10** A single-cylinder, two-stroke carbureted engine of 85 mm bore and 110 cm stroke is operating at 2500 rpm. It has a compression ratio $r = 8$, is fueled with gasoline, and is running rich with an equivalence ratio $\phi = 1.2$. If its indicated power is 20 kW with inlet air temperature of 345 K, inlet pressure of 101 kPa and exhaust pressure of 105 kPa, compute its scavenging ratio S_r and scavenging efficiency η_{sc} . Use Figure (4.4) to estimate the indicated thermal efficiency η_{Otto} of an equivalent fuel-air cycle, and assume $\eta/\eta_{Otto} = 0.80$.

Chapter 7

Combustion Processes in Engines

7.1 INTRODUCTION

In this chapter, we examine combustion processes in spark ignition and compression ignition engines. The combustion processes that occur in each of these types of engines are very different. A spark ignition engine has a relatively homogeneous turbulent mixture of fuel and air, which once ignited by a spark, sustains a reaction process that propagates a flame in the form of a thin wrinkled sheet through the mixture. During the combustion process, the energy release rate starts relatively slowly, increases to a maximum value, and then decreases near the end of the combustion process. Accordingly, the cylinder pressure increases to a maximum value after top dead center as the flame propagates across the cylinder, and then decreases during the expansion stroke. The performance of spark ignition engines is limited by the occurrence of an autoignition process called knock, which constrains the maximum compression ratio and thus the overall engine efficiency.

On the other hand, a compression ignition engine has separate fuel and air streams that combust as they are mixed together at a temperature greater than the autoignition temperature. The combustion reaction, which produces a diffusion flame, takes place at the interface between the fuel and the air. The energy release begins at a relatively high value, and then decreases as the available oxygen is depleted. The performance of compression ignition engines is limited by emissions of unburned hydrocarbons, including soot.

The combustion processes in both spark and compression ignition engines are very complex and depend on the type of fuel and the amount of air used in the combustion process. For example, the reaction pathways for the oxidation of a hydrocarbon fuel such as paraffin, C_nH_{2n+2} , a major component of gasoline, can include at least 10,000 different reactions. To keep such reactions computationally tractable, the large detailed reaction mechanisms are reduced to mechanisms with less species and reaction numbers, as discussed by Law et al. (2000).

Hydrocarbon reactions are generally grouped into three distinct steps. For example, the first step in the combustion of a fuel molecule is breaking up carbon–carbon bonds in the fuel molecule, forming alkenes (hydrocarbons with double carbon bonds) and hydrogen. The second step is further oxidation to form CO and hydrogen. The third and last step is the oxidation of CO to form CO_2 . Most of the energy release occurs during the last step, a

step independent of the molecular mass of the fuel. Consequently, hydrocarbon paraffins of different molecular mass have very similar heats of combustion.

Recently, with advances in injection and engine control technology, a variety of techniques, categorized as “low-temperature combustion” (LTC), have been developed to combine the best aspects of spark and diesel combustion, that is, combining the nearly homogeneous fuel–air mixture of a spark ignition engine with the higher compression of a diesel engine to achieve higher engine efficiencies with lower emissions. For the most part, these techniques are still in the research stage, but are very promising approaches.

7.2 COMBUSTION IN SPARK IGNITION ENGINES

Ignition

An energy source is needed to ignite the fuel–air mixture in a spark ignition engine. Early low compression engines used flames and spark ignition for this purpose, and as the compression ratio was increased, techniques such as high-voltage spark ignition, plasma jets, and laser ignition have been adopted. Spark ignition is by far the dominant ignition technology used currently in internal combustion engines. J. Lenoir used spark plug ignition to initiate combustion in his internal combustion engine in 1860, and R. Bosch and N. Tesla independently developed high-voltage spark plug technology in 1898. In 1911, C. F. Kettering, an American engineer, developed the electrical starter motor and high-voltage ignition for automobile engines, replacing the cumbersome hand cranked magneto.

With spark ignition, combustion is initiated by an electrical discharge across an electrode gap. The spark discharge requires about 20,000–30,000 V, and uses a spark plug configuration consisting of two electrodes, one grounded to the engine, and a center electrode insulated with porcelain. The spark discharge process has four main phases: predischarge, breakdown, arc, and glow. In the predischarge phase, energy is added to the gas molecules to ionize them. The voltage increases to the point that current can flow across the gap. The point at which current begins to flow through the ionized gas signals the onset of the breakdown phase. In the breakdown phase, the current increases to about 10^2 A in a few nanoseconds, establishing a low-impedance pathway between the electrodes. The sustainability of the plasma kernel is very dependent on the characteristics of the breakdown phase, since this phase has the highest voltage and current. In the low-impedance arc phase, the voltage is reduced to about 100 V, and the current decreases to about 1 A. The final phase of the spark discharge process is the glow discharge, which lasts much longer than the previous phases, with a voltage of about 500 V and current of about 0.1 A.

During the discharge process, electrical energy is transferred to the fuel–air mixture, raising its temperature high enough to initiate local chemical reactions. After approximately 20–100 ms after onset of ionization, if the chemical energy release exceeds the conduction heat transfer to the surrounding unburned mixture, the chemical reactions become self-sustaining, a glowing spherical flame kernel is formed, and a flame propagates radially away from the spark plug. The amount of ignition energy required decreases with increasing mixture temperature and pressure and is minimum at stoichiometric conditions. As the mixture becomes more lean, the laminar flame speed decreases, increasing the conduction heat transfer from the flame to the surrounding gas, and consequently increasing the ignition energy required. Variations in the mixture composition between the electrodes will contribute to variations in the flame propagation process, known as cyclic variation. Once established, the flame can also be transported by bulk flow motion.

Combustion Visualization

A wide variety of imaging techniques have been used to visualize the combustion processes in a spark ignition engine. In the late 1930s, Rassweiler and Withrow (1938) modified an L-head cylinder of a spark ignition engine so that a quartz window could be installed allowing an unobstructed view of the entire combustion space. Using high-speed motion photography, they were able to record the combustion process in a homogeneous charge, spark ignition engine. For the combustion process they photographed, ignition occurred at $\theta_s = -25^\circ$, and no flame was visible until $\theta_s = -16^\circ$, 9° later. That 9° period was called the ignition delay, $\Delta\theta_{id}$. Once formed, the flame spread like a spherical wave into the unburned gas with a ragged surface because of turbulence. The end of combustion at $\theta_s = +25^\circ$ was determined from simultaneous measurement of cylinder pressure.

More recently, Witze and Vilchis (1981) used a laser shadowgraph technique for combustion visualization. Shadowgraph photography is a method of flow visualization that shows contrasts due to differences in density of the flow. It does not record light emitted by the flame, rather it records light transmitted through and refracted by the gases. Figure 7.1 shows laser shadowgraph sequences for lean ($\phi = 0.55$) and slightly rich ($\phi = 1.1$) combustion and Figure 7.2 presents the corresponding pressure profiles. A ragged edge wave is seen propagating into the unburned mixture. Ignition delay (in degrees of crank angle) is on the order of 10° for the rich case and 20° for the lean case. At 20° and 25° after ignition in the rich case, the width of the flame front is clearly discernible. The width is more difficult to discern in the lean case because it is two or three times thicker. Thus, a completely burned region does not appear until approximately 40° after ignition. At this time, the whitest region is burned gas, the grayish region in front of the flame is unburned gas, and the highly convoluted dark and white region is a mixture of burned, burning, and unburned gas. There are also cycle-to-cycle variations in the flame propagation caused by the random features of the flow field. For further reading, a recent review of various optical diagnostic techniques is given in Soid and Zainal (2011).

Combustion Process Analysis

In a spark ignition engine, a flame propagates across a homogeneous fuel-air mixture. As shown in Figure 7.3, the concentration of reactants decreases, and the temperature of the mixture increases across the flame front. The flame front has two zones: a preheat zone in front of the flame in which the temperature of the reactants is raised to the ignition temperature by conduction heat transfer from the flame front into the unburned region, and a narrow reaction zone that contains the flame front where the combustion takes place. The energy release is negligible in the preheat zone. As the reactant's temperature rises in the reaction zone, the chemical reactions, which depend exponentially on temperature, increase until the reactants are consumed and their concentration then decreases to zero, forming the downstream side of the flame front.

There are a number of models of the homogeneous mixture combustion process in spark ignition engines. The models include zero-dimensional models, for example, two zone thermodynamic models that divide the combustion chamber into burned and unburned zones; quasi-dimensional models, for example, models that incorporate a turbulent flame speed to determine rate of mass burned; and multidimensional models, for example, flamelet, eddy break up, probability density function, and coherent flame models, which include combustion chamber geometry and associated boundary conditions. There are similar models for compression ignition engines.

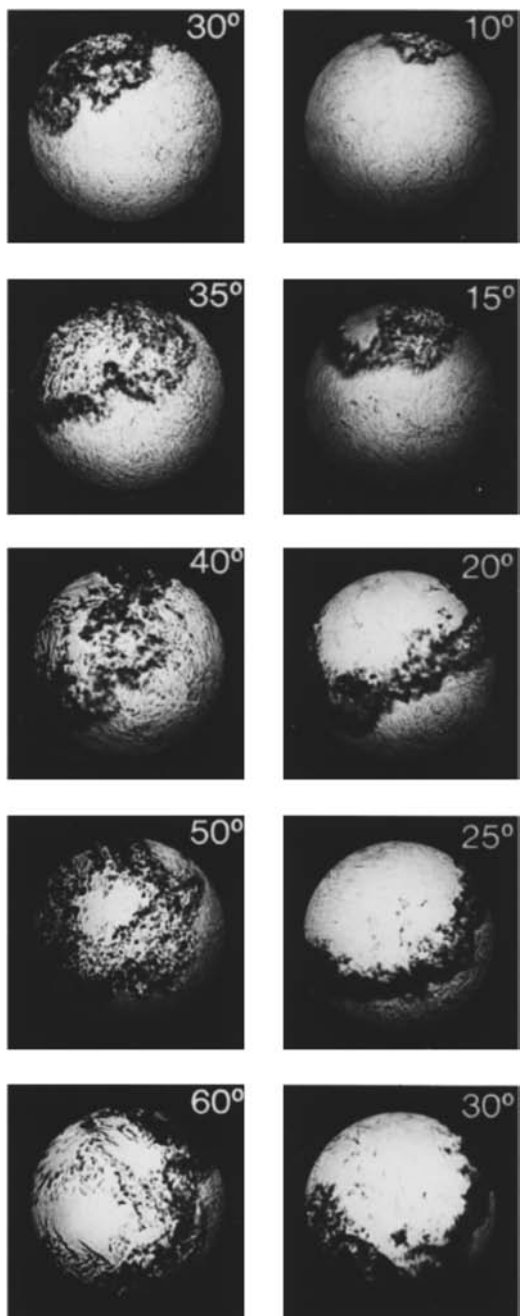


Figure 7.1 Laser shadowgraph of lean (left) and rich (right) combustion (Witze and Vilchis, 1981). Reprinted with permission, SAE.

Combustion modeling and incorporation into CFD models is a very active area of research. The CFD codes such as FLUENT, STAR-CD, and VECTIS that are referenced in the previous chapter also contain combustion models. The computer program CHEMKIN (Kee et al., 2006) is widely used in conjunction with CFD codes for combustion analysis in internal combustion engines, as it is able to model a variety and number of reactions.

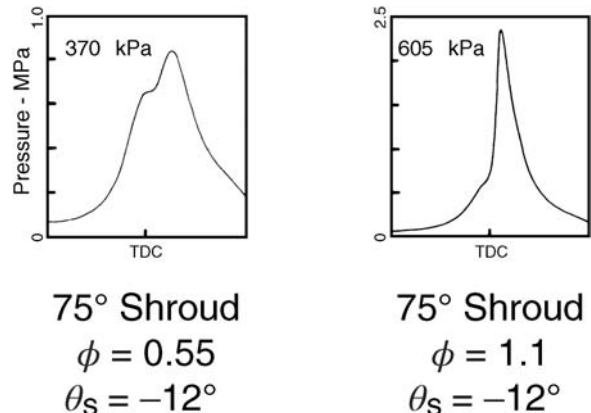


Figure 7.2 Pressure profiles for Figure 7.1 (Witze and Vilchis, 1981). Reprinted with permission, SAE.

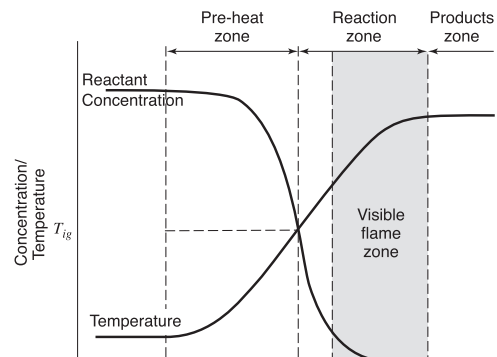


Figure 7.3 Temperature and species concentration profiles in laminar flames. Adapted from Borman and Ragland (1999).

The combustion parameters incorporated into these models include the laminar flame speed s_l , flame thickness δ_l , the turbulent flame speed s_t , and the turbulence intensity u_t . The laminar flame speed s_l , or burning speed, is a well-defined characteristic of a fuel-air mixture, and represents the speed at which a one-dimensional laminar flame propagates into the unburned gas under nonturbulent and adiabatic conditions.

The laminar flame speed depends on the pressure, temperature, equivalence ratio, and composition of the unburned gas. From measurements, Metghalchi and Keck (1982) developed the following correlation, Equation 7.1, for the laminar flame speed, based on the unburned (u) fuel-air properties, and valid for $T_u > 350$ K. The fuel-air mixtures measured were methanol, propane, isoctane, and indolene.

$$s_l = s_{l,o} \left(\frac{T_u}{T_{u,o}} \right)^a \left(\frac{P}{P_o} \right)^b (1 - 2.1 f) \quad (7.1)$$

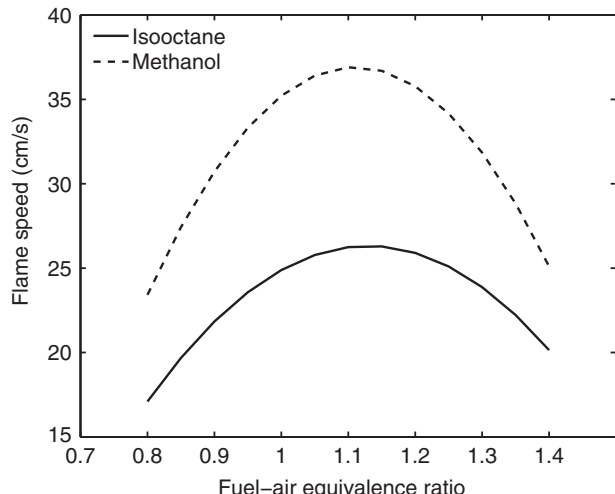
where $T_{u,o} = 298$ K and $P_o = 1$ atm, and f is the residual fraction, accounting for residual or recycled exhaust gases. The laminar flame speed was found to decrease linearly with residual fraction. The reference flame speed $s_{l,o}$ (cm/s) is given by Equation 7.2:

$$s_{l,o} = c_1 + c_2(\phi - \phi_o)^2 \quad (7.2)$$

where c_1 , c_2 , and ϕ_o are given in Table 7.1.

Table 7.1 Curve-Fit Parameters for Laminar Flame Speed Correlation, Equation 7.2

Fuel	c_1	c_2	ϕ_o
Methanol	36.92	-140.51	1.11
Propane	34.22	-138.65	1.08
Isooctane	26.32	-84.72	1.13

**Figure 7.4** Laminar flame speed versus equivalence ratio (Equation 7.1).

The parameters a and b depend on the equivalence ratio, and for the fuels tested by Metghalchi and Keck are given by

$$a = 2.18 - 0.8(\phi - 1) \quad (7.3)$$

$$b = -0.16 + 0.22(\phi - 1) \quad (7.4)$$

Some of these dependencies are illustrated in Figures 7.4 and 7.5, which plots the above correlation. The laminar flame speed that shows a maximum for slightly rich mixtures is a strong function of unburned gas temperature T_u and is a weak function of pressure P . The strong dependence of the laminar flame speed on unburned gas temperature is due to the exponential relation between the reaction kinetics and temperature.

There are three regimes for turbulent flames. The regimes are wrinkled laminar flame, flamelets in eddies, and distributed reaction. The characteristics of the regimes are outlined in Table 7.2. Internal combustion engines operate in the wrinkled laminar flame and the flamelets in eddies regimes, depending on the engine speed (Abraham et al., 1985).

In the wrinkled laminar flame regime, the flame thickness δ_l is thinner than the smallest Kolmogorov microscale η , and the turbulent intensity u_t is of the same order as the laminar

Table 7.2 Turbulent Flame Regimes

Wrinkled laminar flame	$\delta_l < \eta$	$u_t \sim s_l$
Flamelets in eddies	$\eta < \delta_l < l$	$u_t >> s_l$
Distributed reactions	$\delta_l > l$	

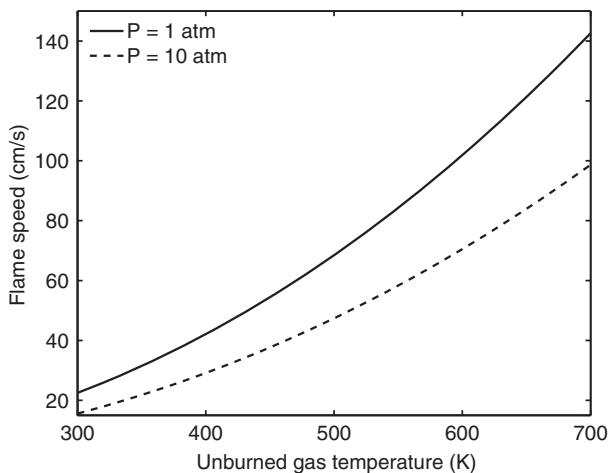


Figure 7.5 Laminar flame speed versus gas temperature (Equation 7.1).

flame speed s_l . The effect of turbulence in the cylinder therefore is to wrinkle and distort the laminar flame front. In the flow field, the turbulent vortices spread ignition sites via a ragged edge wave emerging from the spark plug. The position of the flame front moves irregularly, making the time average flame profile appear relatively thick, forming a “turbulent flame brush.” For the turbulent flow conditions of Example 7.3, the scale of the wrinkles is about 1 mm, and the flame is less than 0.01 mm thick.

The turbulent flame speed can be from 3 to 30 times greater than the laminar flame speed. In the wrinkled laminar flame regime, if one assumes that the area of the wrinkles is proportional to the turbulence intensity, then the turbulent flame speed s_t is simply the sum of the laminar flame speed and the turbulence intensity, represented by Equation 7.5 (Damkohler, 1947).

$$s_t = s_l + u_t \quad (7.5)$$

A convenient way to conceptualize the flame propagation in the wrinkled laminar flame regime is in terms of ink rollers. The ink roller model is shown in Figure 7.6. Imagine a bunch of cylindrical rolls as depicted to represent eddies of a similar diameter in the turbulent flow field. Now, consider ignition as being analogous to continuously depositing a stream of ink at the periphery of one roll. The rollers are rotating, and as a result, the ink spreads. A ragged edge wave emerges from the initial deposition site. The speed of the propagation is proportional to the velocity at the edge of the vortices. The front will take on a thickness determined by the speed of the rollers, their size, and the rate at which ink seeps into the rolls. In the flow field, the flame thickness will depend on the vorticity, the eddy sizes, and the laminar flame-spreading rate. As turbulence is a three-dimensional fluid phenomena, the eddies in the flow field are more likely to resemble a mesh of spaghetti than perfectly aligned ink rollers.

As discussed earlier, the turbulence intensity is proportional to the engine speed, so at higher engine speeds, the turbulent flame region can transition from a wrinkled sheet to the flamelets-in-eddies regime. In the flamelets-in-eddies regime, the flame thickness is greater than the small eddy thickness η , but less than the integral thickness l . The turbulent intensity is much greater than the laminar flame speed. The increased wrinkling can result in the creation of pockets of unburned gas mixture. Accordingly, in this regime, the burning rate is controlled by the turbulent mixing rate, that is, the integral length scale, not the chemical reaction rate.

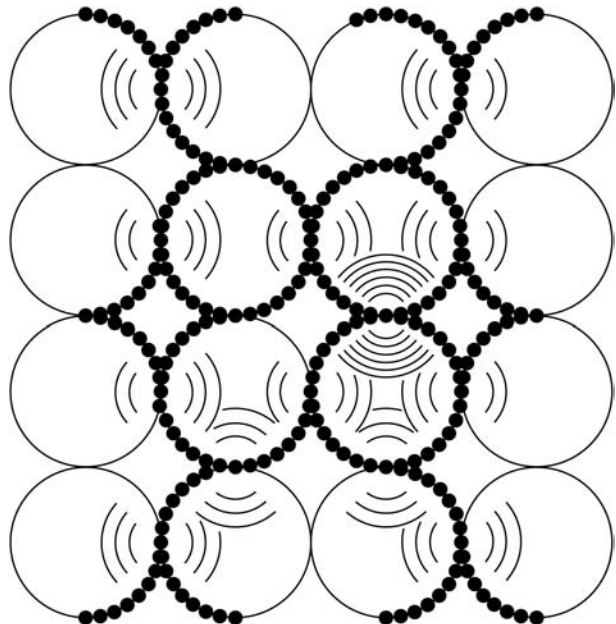


Figure 7.6 Ink roller model of turbulent combustion.

The combustion also depends on the combustion chamber geometry. To illustrate the effect of combustion chamber geometry, consider two limiting cases of combustion: (1) in a sphere centrally ignited and (2) in a tube ignited at one end. Assume that the sphere and the tube have the same volume. In each case, the flame will propagate as a ragged spherical front of radius r_f from the spark plug. In the sphere, the area of the front grows as r_f^2 . Thus, the entrainment rate gets faster and faster as the flame grows. On the other hand, in the tube, the flame front will initially grow as r_f^2 , but it will soon hit the walls and be constrained to be more or less constant from then on. Thus, combustion in a sphere can be expected to burn faster, that is, it will take less time to burn the charge. The maximum cylinder pressure occurs at about the time that the flame reaches the cylinder wall. This is also the point of largest flame surface area, with the maximum flow of unburned gases into the flame.

Energy Release Analysis

The differential energy equation analysis introduced in Chapter 2 can be used to compute the mass fraction burned x_b , and the combustion duration θ_d if the cylinder pressure versus crank angle is known. If one assumes thermal equilibrium at each crank angle, a uniform mixture, ideal gas behavior, and cylinder wall heat transfer loss Q_w , the first law for a single zone is

$$\frac{dQ}{d\theta} = \frac{\gamma}{\gamma - 1} \frac{PdV}{d\theta} + \frac{1}{\gamma - 1} \frac{VdP}{d\theta} + \frac{dQ_w}{d\theta} \quad (7.6)$$

Equation 7.6 can be solved numerically to obtain the net energy release per unit crank angle $dQ/d\theta$. The mass fraction burned $x_b(\theta)$ at any crank angle θ is then found from calculating

the integral of the energy release normalized by the total energy release integral:

$$x_b = \frac{\int_{\theta_s}^{\theta} \frac{dQ}{d\theta} d\theta}{\int_{\theta_s}^{\theta_e} \frac{dQ}{d\theta} d\theta} \quad (7.7)$$

Engine simulation programs typically use a energy release profile that has been curve-fitted with a Wiebe function, Equation 7.8:

$$x_b(\theta) = 1 - \exp \left[-a \left(\frac{\theta - \theta_s}{\theta_d} \right)^n \right] \quad (7.8)$$

This single zone analysis can be extended to two zones by assuming that the combusting mixture can be split into a burned and an unburned zone. The unburned zone includes the gas mixture ahead of the flame and unburned gas within the flame. The burned zone includes gas behind the flame and burned gas within the flame. Thus, the highly convoluted flame structure observed via flow visualization is accounted for, and the analysis is limited in principle only by the assumption that the mass of gas actually reacting is small.

In practice, the analysis is limited further by imprecise estimates of the heat transfer and mass loss as well as experimental error in the pressure measurement. For example, a model (Tabaczynski et al., 1980) has been developed to predict mass-fraction burned curves from fundamental quantities such as the laminar flame speed of the fuel and the turbulence intensity of the flow. Key to the analysis are the “ink roller” assumptions that ignition sites are spread by turbulence and the laminar burnup of material between shear layers occurs. Representative results are given in Figure 7.7, which show the ignition delay and combustion duration portions of the mass-fraction burned curve increasing as the equivalence ratio is decreased or the EGR increased.

Two aspects of the mass-fraction burned curve that are used to characterize the combustion are the ignition delay and the combustion duration. Figure 7.8 is a representative plot of the ignition delay angle versus equivalence ratio. The ignition delay is defined in this case as the crank angle change from spark firing to 1% mass fraction burned. The ignition delay depends on spark timing, residual fraction, and equivalence ratio.

Consistent with observations made via flame photography, ignition delay increases as the mixture is leaned out from stoichiometric. The ignition delay increases with spark advance because the laminar flame speed decreases as a result of lower temperatures at the time of spark, but it is not the sole effect, for the turbulent field is also different. Likewise, the ignition delay increases as the mixture is diluted either by leaning the charge or recirculating the exhaust. The change is proportionately less than the change in laminar flame speed. This is due to the influence of combustion on the turbulence field as the flame grows.

Figure 7.9 is a representative plot of combustion duration versus equivalence ratio. The combustion duration in this case is defined as the crank angle change from 1 to 90% burned fraction. Like ignition delay, the combustion duration depends on the equivalence ratio, the residual fraction, and the spark timing.

The combustion duration also depends on the laminar flame speed, the turbulence intensity of the flow, and the combustion chamber geometry. Minimizing the combustion duration in an engine requires a high turbulence intensity (which is often achieved at the expense of volumetric efficiency), a flame area that increases with distance from the spark plug, and a centrally located spark plug to minimize flame travel. As one expects, minimizing the combustion duration maximizes the work done, since the combustion approaches constant volume, and it also lowers the octane level required. Figure 7.10

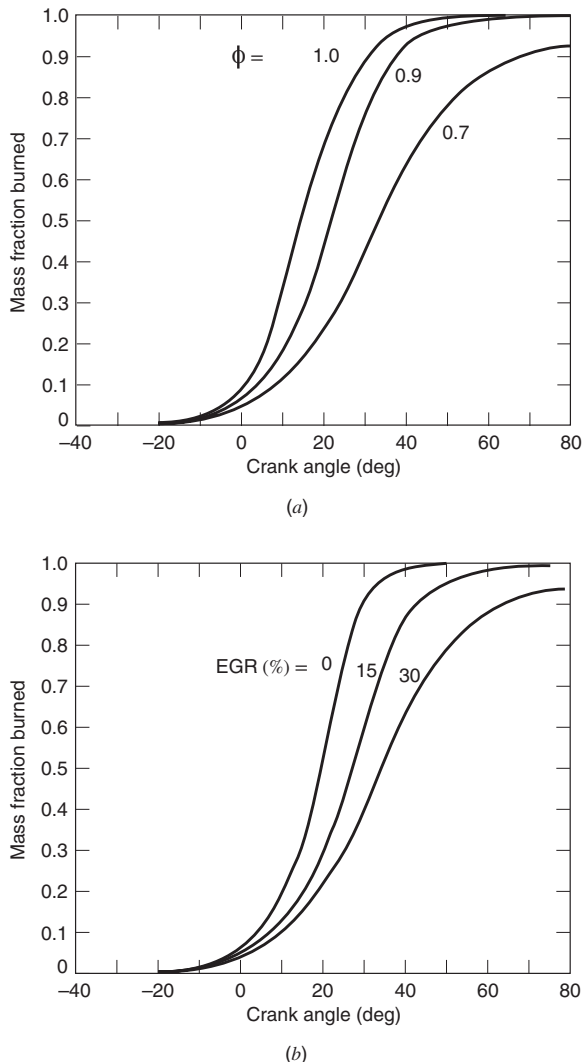


Figure 7.7 Representative mass-fraction burned curves: (a) for varying equivalence ratio and (b) for varying EGR.

shows experimental results for three different combustion chamber shapes, each with a compression ratio $r = 9$, engine speed $N = 1000$ rpm, and ignition at maximum torque. Note that the bowl shaped combustion chamber had the shortest combustion duration and the lowest required octane level.

7.3 ABNORMAL COMBUSTION (KNOCK) IN SPARK IGNITION ENGINES

Knock is the term used to describe an abnormal internal combustion engine phenomenon that produces an audible high frequency pinging or “knocking” noise. The performance of spark ignition engines is limited by the onset of knock. During knock, the unburned or end gas auto ignites and combusts before the arrival of the flame front. This combustion results from compression of the end gas by the expansion of the burned part of the charge, raising the end gas temperature to the autoignition point.

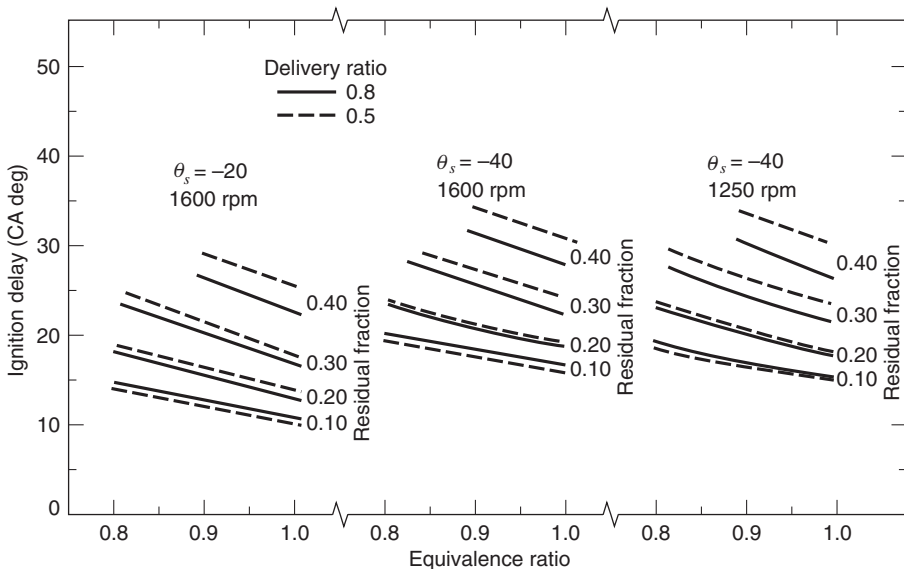


Figure 7.8 Ignition delay versus equivalence ratio and residual fraction. Adapted from Young (1980).

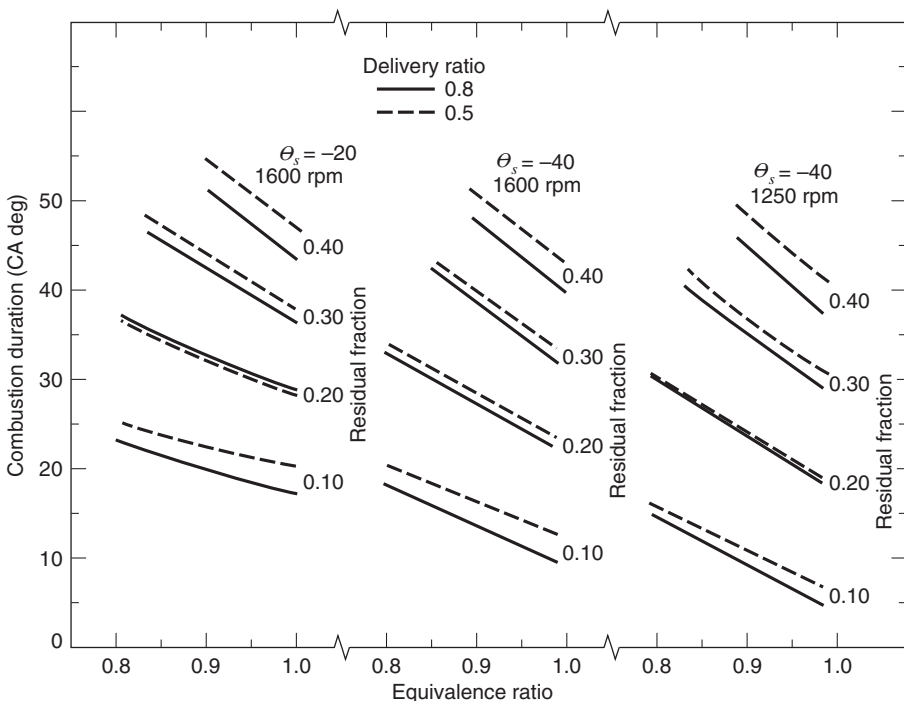


Figure 7.9 Combustion duration versus equivalence ratio and residual fraction. Adapted from Young (1980).

The autoignition in the end gas creates pressure waves that travel through the combustion gases, producing a rapid pressure rise and extremely high localized temperatures. The pressure waves can be of several different types. For example, they can take the form of finite amplitude supersonic pressure waves that decay rapidly to smaller amplitude

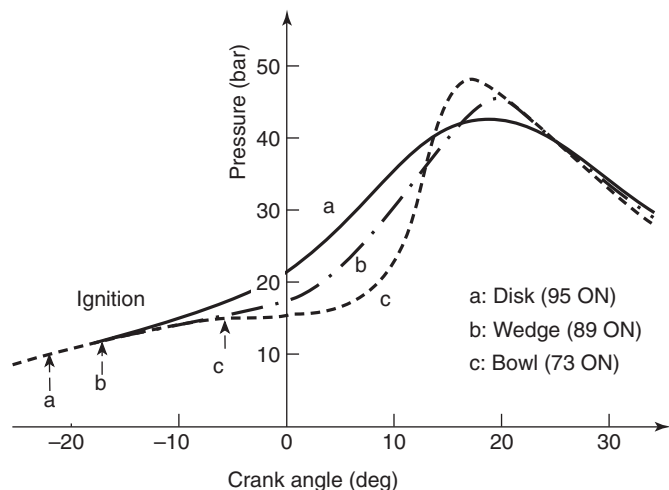


Figure 7.10 Effect of combustion chamber geometry on combustion duration and octane requirement. Adapted from Caris et al. (1956).

resonant sound waves. The attendant rapid fluctuations in pressure can be a serious problem, as they can disrupt the cylinder thermal boundary layers causing higher piston surface temperatures, resulting in surface erosion and failure. The onset of knock puts a constraint on spark ignition engine performance, since it limits the maximum compression ratio and thus the engine power.

Knock occurrence has been found to be dependent on many variables, including engine speed, fuel properties, combustion chamber design, equivalence ratio, and intake air temperature and pressure. The most important parameter is the end gas temperature, as the tendency to knock is directly proportional to the end gas temperature.

Characteristic cylinder pressure profiles for normal and knocking combustion are shown in Figure 7.11. The knock spectra of the pressure profiles depend on the cylinder chamber geometry and the speed of sound in the cylinder gases. Classic measurements by Draper (1938) indicate that the dominant acoustic frequency is the first tangential mode (1T) of vibration, followed by higher order harmonics. The 1T acoustic mode is one in which there are pressure fluctuations both in the tangential and radial directions. For a cylindrical combustion chamber, the dominant acoustic frequency f (Hz) is given by the following equation:

$$f = \frac{cn}{\pi b} \quad (7.9)$$

where c is the speed of sound (m/s), n is the wave mode eigenvalue, equal to 1.841 for the 1T mode, and b is the cylinder diameter. Typical knock frequency spectra are in the 2–10 kHz range for automobile size engines.

Using a single-cylinder research engine, the unburned end gas in a high swirl, homogeneous charge engine has been isolated in the center of the combustion chamber by simultaneous ignition at four equally spaced spark plugs mounted in the cylinder wall. High-speed schlieren photographs reveal that under knocking conditions, the flame spread occurs much faster than normal. Figure 7.12 shows the dramatic change in the schlieren pattern just before and just after ignition. The top line in the figure is the pressure versus crank angle, starting at TDC. It took about 2 ms for the flames to spread from the spark plugs to the position shown in the leftmost photograph just before knock, whereas it took only 0.1 ms to propagate through the end gas once autoignition occurred, as shown in the rightmost photograph. In this case, neither shock nor detonation waves were observed.

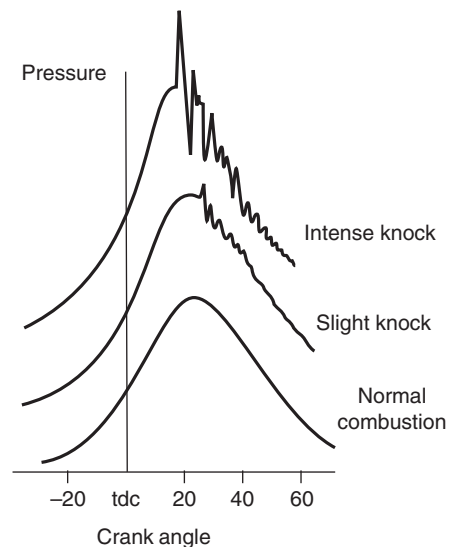


Figure 7.11 Pressure profiles for knocking conditions. Adapted from Douaud and Eyzat (1977).

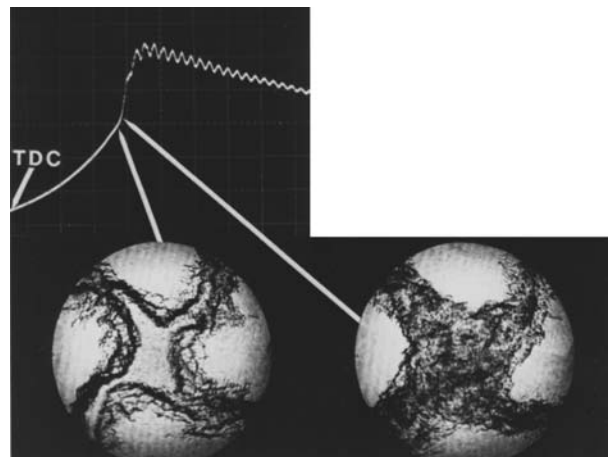


Figure 7.12 Schlieren photographs of knock process (Smith et al., 1984).

This is because the unburned gas involved is at an elevated temperature, so the laminar flame speed is substantially increased. More importantly, however, several autoignition sites appear almost simultaneously.

In these experiments, temperature measurements have been made of the end gas using a laser-based technique. For temperatures less than 1100 K, coherent antistokes Raman spectroscopy (CARS) is used, and at the higher temperatures, spontaneous Raman scattering is used. The results, shown in Figure 7.13, show that the end gas temperature, like the pressure, undergoes an abrupt change in the rate of change at the knock point. They also show that the temperature continues to rise even after the 0.1 ms required for the homogeneous ignition sites and the flame propagation to have consumed the end gas. Clearly, oxidation is not complete in the after-knock photograph of Figure 7.12.

Rapid compression machines (RCM) have been used to study combustion processes. The RCM has been used for many years to study autoignition phenomena and simulate the compression stroke of an internal combustion engine. With an RCM, a reactive mixture is introduced into a chamber, rapidly compressed by a moving piston, and the resulting

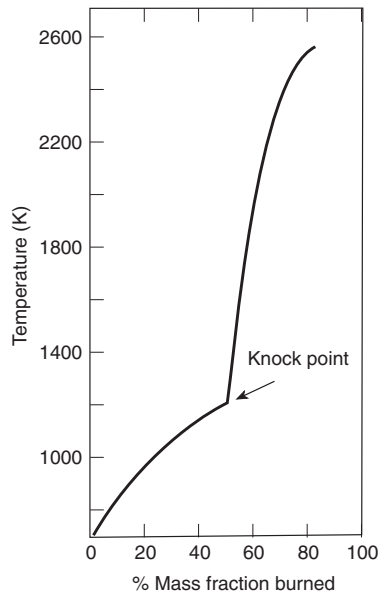


Figure 7.13 Temperature history of the end gas in Figure 7.12 as determined by CARS and Raman scattering (Smith et al., 1984).

temperature and pressure profiles measured. As discussed in Lee and Hochgreb (1998), the experimental results are used to verify proposed chemical kinetic mechanisms for autoignition.

Knock Modeling

One way to model engine knock is to suppose that there exists a critical mass fraction of combustion precursors that if attained anywhere within the end gas, that is, the unburned portion of the fuel–air mixture, will cause autoignition (Downs, 1951). Knock will then occur prior to the end of normal combustion if the integrated rate of formation equals this critical mass fraction.

The normalized rate of formation of precursors is represented by an equation, Equation 7.10 of the following form, where x_p is the mass fraction of precursors, x_c is the critical mass fraction, and T_u is the temperature of the unburned fuel–air mixture:

$$\frac{1}{x_c} \frac{dx_p}{dt} = A P^n \exp\left(\frac{-B}{T_u}\right) \quad (7.10)$$

The empirical constants A , B , and n are determined from a set of experimental results. Values of $A = 50.5$, $B = 3800$, and $n = 1.7$ were obtained by Douaud and Eyzat (1978). Like constants in algebraic burning laws, these constants will vary from engine to engine and from fuel to fuel.

We can define the extent of precursor reaction ζ as the ratio of the precursor mass fraction to the critical mass fraction:

$$\zeta = x_p/x_c \quad (7.11)$$

so upon differentiation with respect to time t ,

$$\frac{d\zeta}{dt} = \frac{1}{x_c} \frac{dx_p}{dt} \quad (7.12)$$

and

$$\zeta = \int_0^t \frac{d\zeta}{dt} dt = \frac{1}{x_c} \int_0^t \frac{dx_p}{dt} dt \quad (7.13)$$

The extent of precursor reaction ζ can be expressed in terms of crank angle θ and engine speed $\dot{\theta}$. Since $\dot{\theta} = d\theta/dt$,

$$\zeta = \frac{1}{\dot{\theta}} \int_{\theta_s}^{\theta} \frac{d\zeta}{dt} d\theta \quad (7.14)$$

If at any time prior to the end of combustion ζ reaches 1, knock is said to occur and the remaining unburned end gas burns instantaneously. The minimum engine speed $\dot{\theta}_{\min}$, above which there is not sufficient precursor formation time for knock to occur, is thus

$$\dot{\theta}_{\min} = \int_{\theta_s}^{\theta} \frac{d\zeta}{dt} d\theta \quad (7.15)$$

The reaction rate is an extremely strong function of the temperature (See homework problem 7.5). Indeed, at temperatures characteristic of the intake manifold, the rate of formation of precursors is negligible. Since the combustion in automotive class engines occurs over times of order 10^{-2} s, not until the rates approach 100 s^{-1} will knock occur with isoctane.

EXAMPLE 7.1 Spark Ignition Engine Knock

For a constant pressure combustion at 10 bar and unburned gas temperature of 1100 K, what is the precursor formation rate $d\zeta/dt$ and the minimum engine speed $\dot{\theta}_{\min}$ if the combustion duration is 40° ? Assume $A = 50.5$, $B = 3800$, and $n = 1.7$.

SOLUTION

$$\begin{aligned} \frac{d\zeta}{dt} &= A P^n \exp\left(\frac{-B}{T_u}\right) \\ &= (50.5)(10)^{1.7} \exp\left(-\frac{3800}{1100}\right) \\ &= 80.0 \text{ s}^{-1} \end{aligned}$$

$$\begin{aligned} \dot{\theta}_{\min} &= \int_{\theta_s}^{\theta} \frac{d\zeta}{dt} d\theta \\ &= \frac{d\zeta}{dt} (\theta - \theta_s) \\ &= (80.0)(40) \\ &= 3200 \text{ deg/s} = 533 \text{ rpm} \end{aligned}$$

A reduced kinetic model of autoignition chemistry and knock, known as the Shell model, frequently used in CFD simulations, is given by Halstead et al. (1977), and compared with a detailed kinetic knock model by Cowart et al. (1990).

Octane Number

To provide a standard measure of a fuel's knock characteristics, a scale has been devised in which fuels are assigned an octane number, ON. The first knock scale was developed by Ricardo (Ricardo, 1921), and fuels were rated by the highest useful compression ratio (HUCR) that could be used in an engine under a given set of conditions. Since the HUCR depended on the given engine, it was supplemented by a knock scale developed in the 1920s by the American Society for Testing Materials (ASTM) Cooperative Fuel Research Committee (CFR).

The Cooperative Fuel Research Committee also worked with the Waukesha Motor Company to develop a standardized CFR fuel research engine and specific operating conditions to measure the octane number of a fuel. The first CFR engine was designed and built in 1929, and it is still the standard by which liquid fuel octane measurements are made today. It is a single-cylinder (3.25 in. bore and 4.50 in. stroke) four-stroke valve in-head engine. The cylinder head and sleeve are one piece, so the compression ratio can be varied from 3:1 to 15:1 by lowering the entire cylinder with respect to the piston. It usually has a shrouded intake valve to induce swirl and turbulence, and to promote mixing. The CFR engine has no valve overlap, so the intake valve does not open substantially until the piston is about 1/3 to 1/2 of the way down the cylinder. The engine is coupled to a synchronous electric generator that is used to control the engine speed to a submultiple of the line frequency.

To measure knock, an ASTM pressure pickup that responds to the rate of pressure rise is used. The pickup consists of a core rod of magnetostrictive alloy. As the pressure rises in the combustion chamber, the diaphragm transmits this force to the core rod that in turn generates a magnetic field. The copper wire coil around the core converts the magnetic field to a voltage that is proportional to the rate of change of the combustion pressure. An evaporative cooling system is used to maintain constant cylinder jacket temperature. The coolant vaporizes in the cylinder jacket, with the vapor flowing to a condenser, and recirculates back to the cylinder.

Two sets of CFR engine operating conditions for engines are employed: the research (ASTM D908) and the motor (ASTM D357) methods, as detailed in Table 7.3. The table also includes specifications (ASTM D614) for testing aviation engines. Originally, the octane number measurement was performed using the research method; however, this method did not correlate well with the knocking found from actual road conditions at wide open throttle. The motor method, with increased engine speed and spark advance, was

Table 7.3 Octane Number Measurement Conditions

	Research	Motor	Aviation
ASTM method	D908	D357	D614
Air inlet temperature (K)	288	310	325
Jacket temperature (K)	373	373	463
Speed (rpm)	600	900	1200
Spark advance (degrees btdc)	13	19–26	35

developed to give an improved correlation between road and laboratory knocking results. The octane number label on gasoline pumps is the average of the research (R) and the motor (M) method octane numbers, $(R + M)/2$, and is also called the antiknock index (AKI).

The procedure to measure the octane number of a test fuel is as follows:

1. Run the CFR engine on the test fuel at either the motor or the research operating conditions.
2. Slowly increase the compression ratio until the standard amount of knock occurs.
3. At that compression ratio, run the engine on blends of the reference fuels isoctane and *n*-heptane.
4. The octane number is the percentage of isoctane in the blend that produces the standardized knock at that compression ratio.

One measure of an engine's octane requirement is its knock-limited indicated mean effective pressure (klimep). The greater the knock-limited imep, the smaller the octane requirement. Knock-limited imep is measured by increasing the inlet pressure P_i (which will increase the cylinder charge density and temperature) until knock occurs; the imep at that condition is the knock-limited imep. Experimental results (Hesselberg and Lovell, 1951) indicate that klimep decreases with increasing coolant temperature. Similar results are obtained with increasing inlet air temperature. Both results are to be expected, since chemical reaction rates are accelerated strongly by increase in temperature.

There are two problems with the octane number scale:

1. At low coolant temperatures, *di*-isobutylene performs better than isoctane (implying the octane number is greater than 100).
2. The relative ranking of isoctane and *di*-isobutylene depends on coolant temperatures. If the octane scale were decoupled from engine design, making the assigned number a fuel property, the fuel with the greater octane number would always yield the largest klimep.
3. Alcohol fuels have an octane number greater than 100.

The former problem is dealt with by extrapolation. A performance number defined as the ratio of the knock-limited imep for the fuel in question to the knock-limited imep of isoctane is used for this purpose. The latter problem is dealt with by using two standard operating conditions (research and motor) and reporting an average number. These shortcomings should be kept in mind; they are easy to forget because of the great utility of the octane number scale.

Typical results obtained for the effect of fuel-air ratio on the knock-limited imep are shown in Figure 7.14. Notice that near-stoichiometric mixtures have the lowest klimep (therefore the highest octane requirement). Also, notice that maximum klimep is attained with very rich ($\phi \sim 1.6$) mixtures. Therefore, to obtain maximum power from an engine, one should run very rich, near $\phi \sim 1.6$, with a compression ratio and inlet pressure such that imep is equal to knock-limited imep.

Since knock occurs if there is enough time for sufficient autoignition precursors to form, at high engine speeds one might not expect knock to be a problem since there is less time available for the precursors to form. On the other hand, as engine speed increases, there is less heat transfer from the gases to the cylinder walls so that gas temperatures will be higher. This accelerates the precursor formation rate so that less time is required to form a concentration high enough for autoignition to occur. As a result of these and other

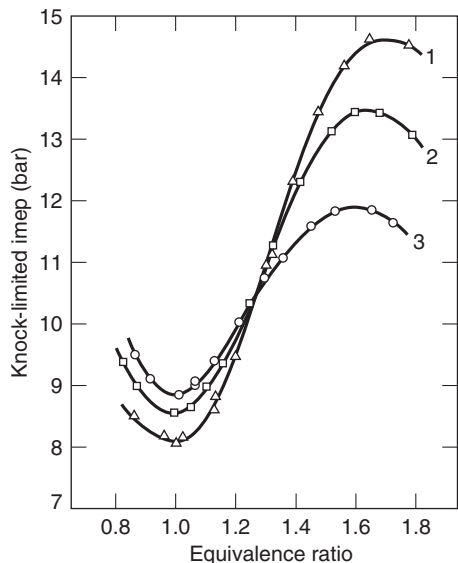


Figure 7.14 Effect of fuel–air ratio on knock-limited imep for three aircraft fuels (Cook et al., 1944).

competing effects, some engines show a klimep increasing with speed, and others show a decrease.

Knock in gaseous-fueled spark ignition engines is characterized with a methane number (MN), (Leiker et al., 1972), which is the percentage by volume of methane blended with hydrogen that exactly matches the knock intensity of the test gas mixture under specified operating conditions in a CFR engine. For example, a blend of 20% hydrogen and 80% methane has a methane number (MN) of 80. For the range beyond 100 MN, methane–carbon dioxide mixtures are used as reference mixtures. In this case, the MN is 100 plus the percent CO₂ by volume in the reference methane–carbon dioxide mixture. In order to replicate the ASTM D357 motor method, testing is conducted at the air–fuel ratio AF that produces maximum audible knock.

7.4 COMBUSTION IN COMPRESSION IGNITION ENGINES

Combustion Diagnostics

To better understand compression ignition combustion processes, we first discuss flow visualization and diagnostic techniques used in compression ignition engines. The application of optical diagnostics to diesel combustion is constrained by the need to maintain realistic combustion chamber geometry while maintaining satisfactory optical access.

High-speed cinematography is a qualitative measurement technique, since the image is integrated along the line of sight of an optically thick medium, and it is also not species specific, so additional diagnostic techniques have been developed. Various laser-based combustion diagnostic techniques developed by combustion researchers have been applied to diesel engines in order to obtain more detailed and species specific information about the combustion processes taking place in a diesel engine. The techniques include laser light scattering, and laser-induced incandescence and fluorescence.

With a light scattering technique, laser light is elastically scattered by fuel droplets and/or soot particles. The scattering distribution and intensity depends on the particle size. Mie scattering, named after Gustav Mie (1869–1957), is defined as elastic scattering

from particles whose diameter is of the same order of magnitude or smaller as the light wavelength. Liquid droplet spray patterns have been determined via measurements of the Mie scattering. Elastic scattering of light from molecules or small particles with diameters much smaller than the wavelength of the laser light is termed Rayleigh scattering, named after Lord Rayleigh (1842–1919). Vaporized fuel-air mixture patterns and temperature fields are determined through Rayleigh scattering measurements.

Laser light is also used to induce incandescence and fluorescence of given species. Both relative and absolute soot concentrations have been determined using laser-induced incandescence (LII). Planar laser-induced fluorescence (PLIF) has been used to determine polyaromatic hydrocarbon (PAH) concentrations, which are precursors to soot, OH distributions, and NO distributions. The OH radical distribution provides information about the location and intensity of diffusion and premixed flames. The NO radicals indicate the location of NO_x production in the cylinder.

An optical engine with an extended piston and a piston-crown window optical access was originally introduced by Bowditch (1961). A more recent example is a single-cylinder diesel engine modified for optical access by researchers at Sandia National Laboratory (Dec and Espey, 1995). This direct injection research engine is based on a typical commercial, heavy-duty diesel engine, with a stroke of 140 mm and a bore of 152 mm. It has an extended piston with a piston crown and a window at the top of the cylinder to provide for laser access along the axis of the fuel spray. The combustion bowl has a flat “pancake” bottom allowing the laser sheet to be viewed from above and below throughout the bowl and the squish region. The in-cylinder flow is quiescent with no swirl from the incoming airflow, and the test diesel fuel used in the engine had a cetane number of 42.5.

Figure 7.15 shows a high-speed cinematography sequence of the luminous combustion process in the above test engine. The high-speed photo sequence shows the fuel jet penetration and spread of the luminous combustion zones. The start of injection (SOI) is at 8.8° btdc, and each image is about 2.4° apart. The first luminosity is seen about 5° after the start of injection. The rapid appearance of widespread combustion indicates that the ignition occurs at multiple points throughout the jet. The luminosity is yellow, indicating the presence of hot soot particles and suggesting fuel-rich combustion. Between 2.9° and 1.8° btdc, the burning fuel jets contact the edge of the combustion bowl, and then spread along the circumference into the space between the jets and downward into the bottom of the bowl. The combustion heat release ends at about 17° atdc. For this case, about half of the fuel is injected after the burning fuel jet reaches the edge of the bowl. Since this is a quiescent engine, a significant portion of the in-cylinder air is not utilized for sometime after SOI, and as the injection proceeds, the fuel spray must travel ever farther through burned gases where combustion has already occurred.

Diesel Combustion Process

In a diesel engine, a low volatility fuel must be converted from a liquid state into a finely atomized state, vaporized, mixed with air, and its temperature raised to a point to support autoignition. The diesel combustion process is heterogeneous and controlled by the rate of fuel-air mixing. It has been classified into three phases: ignition delay, premixed combustion, and mixing-controlled combustion.

The time interval between the start of injection and the start of combustion is termed the ignition delay. Once regions of vapor-air mixture formed around the fluid jet as it is first injected into the cylinder are at or above the autoignition temperature, they will spontaneously ignite. The combustion of this initial vapor-air mixture is termed the

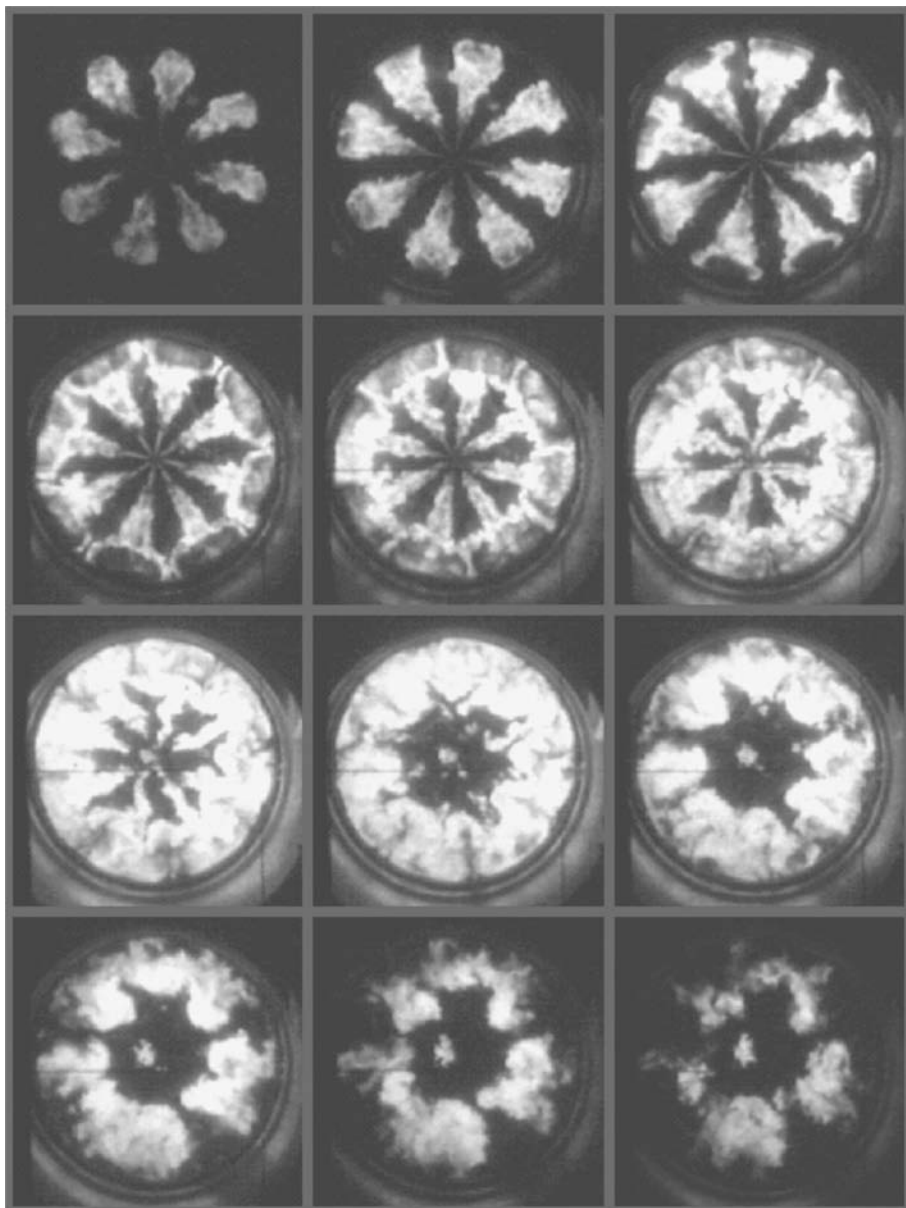


Figure 7.15 High-speed photographic sequence of the luminosity of a diesel flame (Espey and Dec, 1993).

premixed combustion phase. In the premixed combustion phase, ignition and combustion occurs around the fuel jet in regions that are fully mixed.

Next, in the mixing-controlled combustion phase, the fuel entering the cylinder does not mix fully with the air before combusting but burns in what is termed a diffusion flame. In a diffusion flame, the fuel in the main body of the fuel jet mixes with the surrounding air and ignites over a narrow range of equivalence ratios. Combustion in this phase occurs at a rate limited by the rate at which the fuel can be mixed with the entrained air.

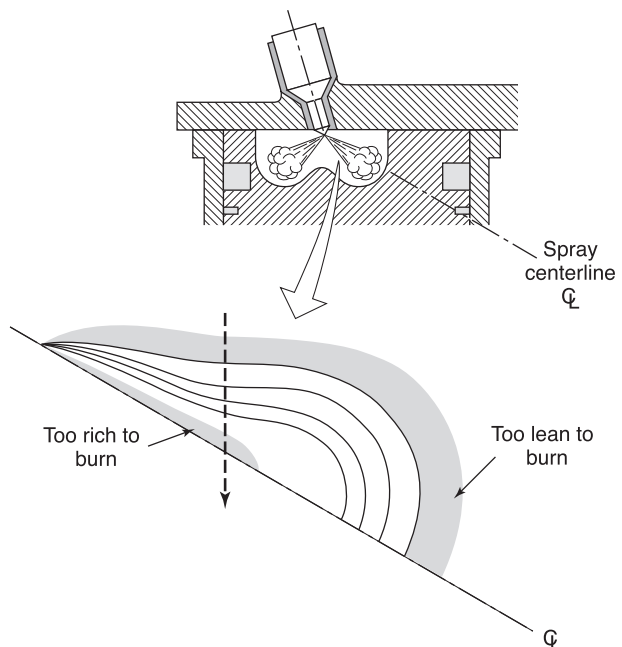


Figure 7.16 Simple model of diesel combustion.

The quantity of fuel burned in each of the premixed and mixing-controlled phases is not only influenced by the engine and injector design, but also by the fuel type and the load. At idle, most of the fuel injected in small bore diesel engines is burned in the premixed phase. As the load increases, the injection duration increases, and the relative size of the mixing-controlled phase increases relative to the premixed phase.

Early analyses of diesel combustion assumed that a burning diesel jet was composed of a dense fuel-rich core surrounded by a uniformly leaner fuel–air mixture, as shown in Figure 7.16. With reference to the models used for steady spray combustion in furnaces and gas turbines, the diesel fuel autoignition and premixed combustion phases were also assumed to occur in a diffusion flame in the near stoichiometric ($\phi \sim 1$) regions between the rich ($\phi > 1$) and the lean ($\phi < 1$) limits, at the outer edge of the jet. Soot was assumed to form in a narrow region on the fuel-rich side of the diffusion flame.

Recent laser sheet diagnostic experiments in diesel engines have indicated that the combustion process in diesel engines is different than that in furnaces and gas turbines. Dec (1997) has proposed an alternative conceptual model based on laser sheet experimental results. The Dec model features two stages of fuel oxidation for both of the premixed and mixing-controlled combustion phases. The first stage is partial oxidation of the fuel in a rich premixed reaction, and the second stage is combustion of the fuel-rich, partially oxidized products of the first stage in a near stoichiometric diffusion flame.

This conceptual model is shown schematically in Figure 7.17, a temporal sequence showing the progressive changes during the injection process. Significant events in the evolution of the jet state are drawn at successive degrees after the start of injection (ASI). Six parameters are shown in Figure 7.17: the liquid fuel, the vapor–air mixture, the PAHs, the diffusion flame, the chemiluminescence emission region, and the soot concentration. At 1.0° in Figure 7.17, near the beginning of the ignition delay phase, as the liquid fuel is injected into the cylinder, it entrains hot cylinder air along the sides of the jet, leading to fuel evaporation. Note that throughout the injection process, the liquid length portion of the jet remains relatively constant. There is limited penetration of the fuel droplets into

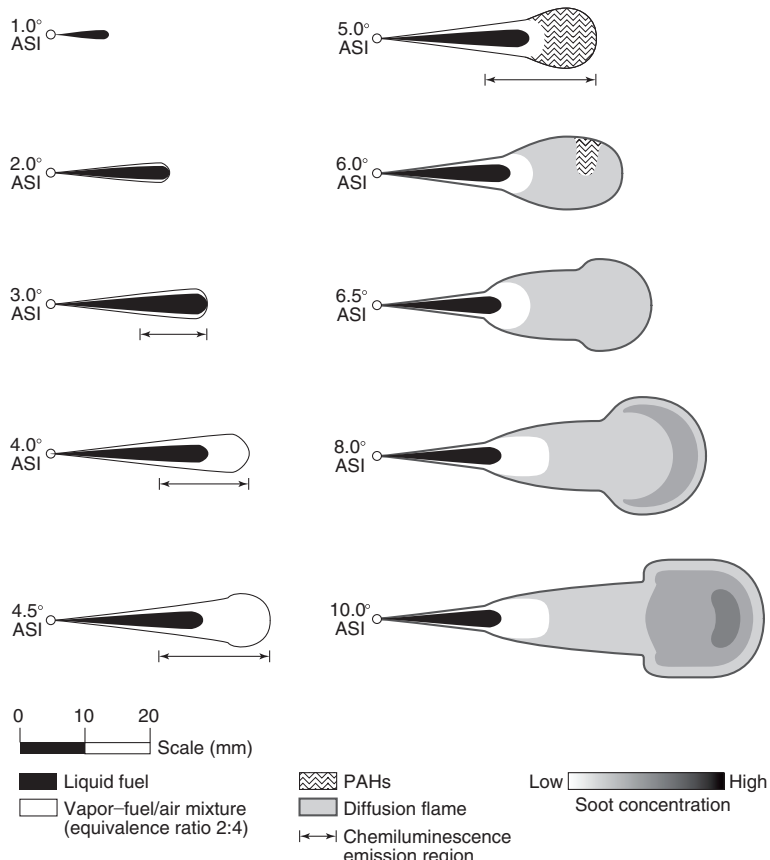


Figure 7.17 Detailed model of diesel combustion (Dec, 1997).

the combustion chamber. The penetration depth of the liquid jet has been found to be dependent on the volatility of the fuel, injector hole size, fuel and cylinder air temperature, and relatively insensitive to the injection pressure (Siebers, 1998).

At about 4.0° ASI, a vapor head vortex is beginning to form in the leading portion of the jet downstream of the liquid jet. The bulk of the vaporized fuel is in the head of the jet. The fuel vapor-air mixture region in the head vortex is relatively uniform, has a well-defined boundary separating it from the surrounding air, and has an equivalence ratio between 2 and 4 throughout its cross section. At about 5.0° ASI, premixed combustion begins in the head vortex. As a consequence of the high equivalence ratio, the initial premixed combustion is fuel-rich with a temperature of about 1600 K and produces PAHs and soot. The soot concentration is fairly uniform throughout the jet cross section.

At about 6.5° ASI, a turbulent diffusion flame forms at the edge of the jet around the products of the initial premixed stage. This turbulent diffusion flame begins the transition to the mixing-controlled phase and is near stoichiometric. The diffusion flame causes the formation of larger soot particles at the jet periphery. The soot concentration continues to increase throughout the head vortex region at the head of the jet. Since the head vortex of the jet is composed of recirculating gases, the soot particles also recirculate and grow in size.

At about 8° ASI, the jet reaches a quasi-steady condition in which the general features of the jet do not change significantly as it expands across the combustion chamber. The combustion is in the mixing-controlled phase. The fuel first passes through a very fuel rich ($\phi > 4$) premixed reaction stage and then burns out in the turbulent diffusion flame at the edge of the jet. Most of the soot is burned with the fuel in the diffusion flame. The fraction of soot that is not oxidized becomes an exhaust emission. NO_x is formed in the high-temperature regions in the diffusion flame where both oxygen and nitrogen are available, and in the post combustion hot gas regions.

Diesel Cetane Number

Diesel fuels are compared using an ignition delay metric and classified by cetane number (CN). The cetane number characterizes the ability of the fuel to autoignite, the opposite of octane number. The higher the cetane number, the shorter the ignition delay, as the ignition delay decreases approximately linearly with cetane number. If the cetane number is too low, the fuel will not ignite until late in the injection process. In this situation, the fuel is well mixed so that once combustion is initiated, the burning rate is very high, causing diesel knock to occur. At higher cetane numbers, combustion is initiated while the fuel is being injected, so the burning rate is controlled by the rate of fuel-air mixing. Cetane numbers for vehicular diesel fuels range from about 40 to 55. Additives such as nitrate esters can be used to increase the cetane number.

The cetane number scale varies from 0 to 100 and is measured for a given test fuel using a standard CFR engine with a prechamber and a variable compression ratio, and operated according to a standard set of operating conditions (ASTM D613) shown in Table 7.4. The compression ratio is adjusted until the ignition delay is 13° with the test fuel. At that compression ratio, reference fuels are blended to again produce an ignition delay of 13°. The cetane number is then computed from the relation below:

$$\text{CN} = \% \text{ hexadecane} + 0.15 \times (\% \text{ heptamethyl nonane})$$

The name cetane is derived from the fact that hexadecane is referred to as *n*-cetane ($\text{C}_{16}\text{H}_{34}$). The cetane number of *n*-cetane is assigned a value of 100. Originally, the cetane scale assigned a value of zero to a-methylnaphthalene as a reference fuel. Later, the low-cetane reference fuel was changed to heptamethylnonane (HMN), as it is less expensive and has better storage characteristics, and assigned a cetane number of 15 so that results obtained in the past were still valid. The cetane number and the octane number are inversely correlated, as shown in Figure 7.18. Gasoline is a poor diesel fuel and vice versa.

A low cetane number will mix more completely with the cylinder air before burning so that the local equivalence ratio of the initial premixed burn will be less ($\phi \sim 3$) than the local equivalence ratio ($\phi \sim 4$) for a greater cetane number.

Table 7.4 Cetane Number Measurement Conditions (ASTM D613)

Inlet temperature (°C)	66
Coolant temperature (°C)	100
Speed (rpm)	900
Injection timing (btdc)	13°
Injection pressure (MPa)	10.3

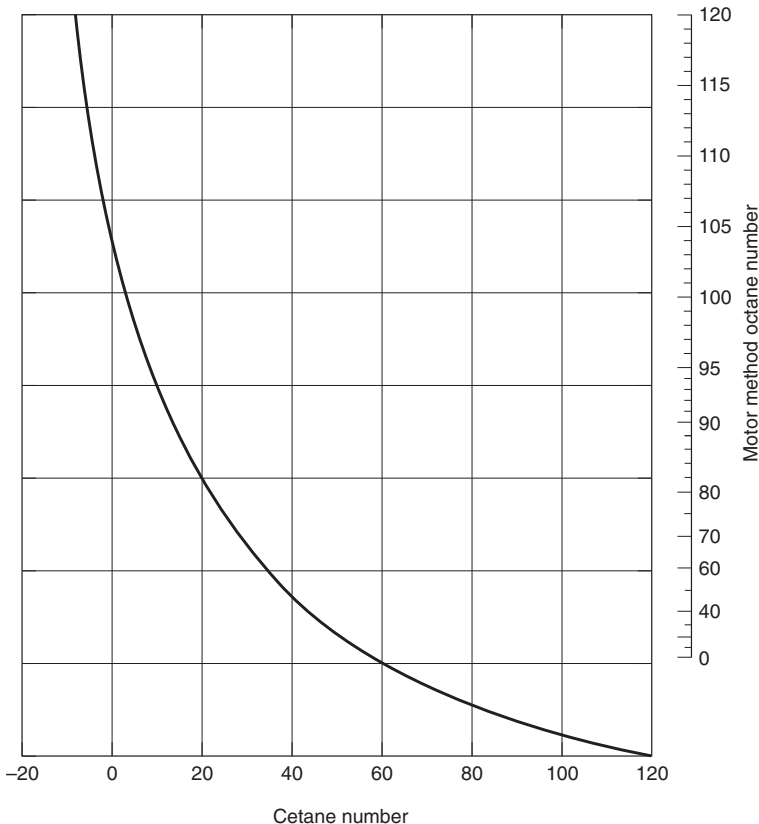


Figure 7.18 Cetane and octane number correlation for hydrocarbon fuels. (Adapted from Taylor, 1985.)

Diesel Ignition Delay

Diesel ignition delay is a physical process involving both fluid mechanics and combustion. During this process, the injected fuel is atomizing into droplets, vaporizing, mixing with the entrained air, and initiating preflame reactions. Accordingly, the diesel ignition delay period is defined as the time or crank angle between the start of injection (SOI) and the start of combustion (SOC). The start of injection begins when the injector needle lifts off its seat and fuel begins to flow into the combustion chamber. The start of combustion is determined indirectly using combustion analysis. One SOC metric is the crank angle location where 10% of the total energy release is reached. A similar SOC metric is the crank angle location where the rate of change of the slope of the cylinder pressure profile is a maximum.

The ignition delay period τ_{id} depends not only on the chemical characteristics of the fuel, but also on the fluid mechanics of atomization, vaporization, and mixing. Aromatic hydrocarbons and alcohols have chemical bonds that are difficult to break and result in a long ignition delay. If these fuels are injected rapidly enough to mix completely with air before autoignition occurs, they will all burn rapidly when ignition occurs in the premixed phase, producing a large rate of change of pressure and a high peak pressure.

On the other hand, the chemical bonds of some fuels, such as alkanes (straight chain paraffins), are easily broken. Ignition delay is then short, and with a long injection, most of the fuel to be burned is injected after autoignition occurs. Relatively little fuel burns in

the premixed phase and most of the fuel burns at a rate limited by the rate of mixing with the cylinder air.

As the engine speed increases, the ignition delay period will need to decrease to maintain a relatively constant combustion duration in crank angle degrees. In direct injection engines, the fuel–air mixing rate is increased using increased turbulence, swirl generated by the intake port geometry, and deeper piston bowls.

There have been a number of empirical correlations that have been developed for ignition delay that include the cetane number CN, the cylinder pressure P , temperature T , and mean piston speed \bar{U}_p . A correlation, Equation 7.16, by Hardenberg and Hase (1979) for direct injection engines is widely referenced, where the ignition delay is in crank angle degrees, piston speed in m/s, pressure in bars, and temperature in degrees Kelvin:

$$\tau_{id} = (0.36 + 0.22\bar{U}_p) \exp \left[E_a \left(\frac{1}{R_u T} - \frac{1}{17,190} \right) \left(\frac{21.2}{P - 12.4} \right)^{0.63} \right] \quad (7.16)$$

The term E_a is the apparent activation energy in J/mole,

$$E_a = \frac{618,840}{CN + 25} \quad (7.17)$$

and the temperature and pressure are computed at top dead center assuming a polytropic process with exponent n and compression ratio r :

$$\begin{aligned} T &= T_{tdc} = T_i r^{n-1} \\ P &= P_{tdc} = P_i r^n \end{aligned} \quad (7.18)$$

EXAMPLE 7.2 Diesel Engine Ignition Delay

A diesel engine with a stroke of 165 mm and compression ratio of 18 operates at 1500 rpm using a diesel fuel with a cetane number of 40. Given that the inlet manifold temperature and pressure $T_i = 283$ K, $P_i = 1.0$ bar, and $n = 1.35$, what is the estimated ignition delay (ms)?

SOLUTION

$$\bar{U}_p = 2Ns = (2)(1500/60)(0.165) = 8.25 \text{ m/s}$$

$$T = T_i r^{n-1} = (283)18^{1.35-1} = 780 \text{ K}$$

$$P = P_i r^n = (1)18^{1.35} = 49.5 \text{ bar}$$

$$E_a = \frac{618,840}{CN + 25} = 9521 \text{ J}$$

so the ignition delay is

$$\begin{aligned} \tau_{id} &= (0.36 + 0.22\bar{U}_p) \exp \left[E_A \left(\frac{1}{R_u T} - \frac{1}{17,190} \right) \left(\frac{21.2}{P - 12.4} \right)^{0.63} \right] \\ &= (0.36 + 0.22(8.25)) \exp \left[(9521) \left(\frac{1}{(8.314)(780)} - \frac{1}{17,190} \right) \left(\frac{21.2}{49.5 - 12.4} \right)^{0.63} \right] \\ &= 4.1 \text{ deg} \end{aligned}$$

and in terms of time,

$$\tau_{id} = 4.1 \text{ deg} (60 \text{ s/min}) (\text{rev}/360 \text{ deg}) (1000 \text{ ms/s})/(1500 \text{ rev/min}) = 0.45 \text{ ms}$$

Note that Equation 7.16 predicts that the ignition delay in crank angle degrees increases linearly with engine speed at a constant load, and that the ignition delay in terms of time is relatively constant.

For additional considerations regarding diesel ignition delay, the reader is referred to the paper by Assanis et al. (2003).

Diesel Energy Release Analysis

Diesel engine combustion analysis is performed using a differential energy equation analysis to determine either the effective energy release or the effective fuel injection rate for a given cylinder pressure profile. Typical calculations for a direct injection (DI) engine use Equation 7.20, which assumes homogeneous conditions throughout the combustion chamber during the injection and combustion process, and ideal gas behavior. The energy release in indirect injection engines (IDI) is modeled with an energy equation applied to both the main chamber and the prechamber so that pressure data are required for both chambers. Diesel energy release profiles will typically have two maxima, resulting from the premixed and the mixing-controlled combustion phases.

The double peak shape of the energy release profile in Figures 7.19 is characteristic of diesel combustion. The first peak occurs during the premixed combustion phase and results from the rapid combustion of the portion of the injected fuel that has vaporized and mixed with the air during this period. The energy release curve in the premixed combustion phase is relatively independent of the load, since the initial mixing is independent of the injection duration. The second peak occurs during the mixing-controlled combustion. The energy release during this phase depends on the injection duration. As the injection duration is increased to meet an increased engine load, the amount of fuel injected increases, thus increasing the magnitude and duration of the mixing-controlled energy release.

A dual Wiebe function (see Figure 7.20), which has two peaks, has been used to fit diesel combustion energy release data (Miyamoto et al., 1985). The dual equation,

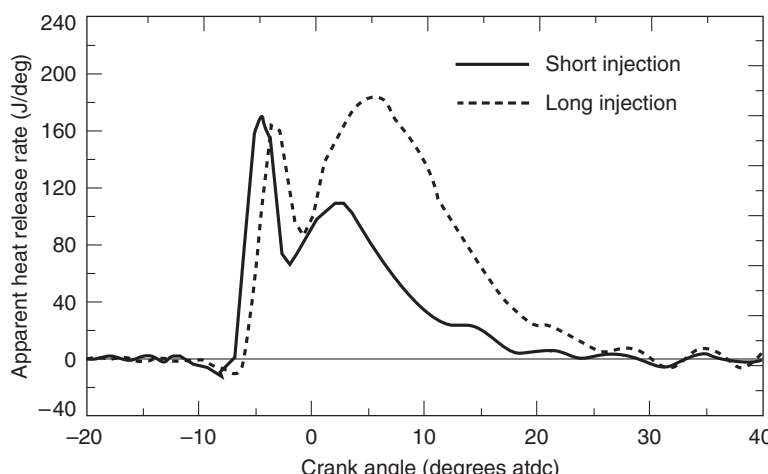


Figure 7.19 Example energy release profile for short- and long-fuel injection. Adapted from Dec (1997).

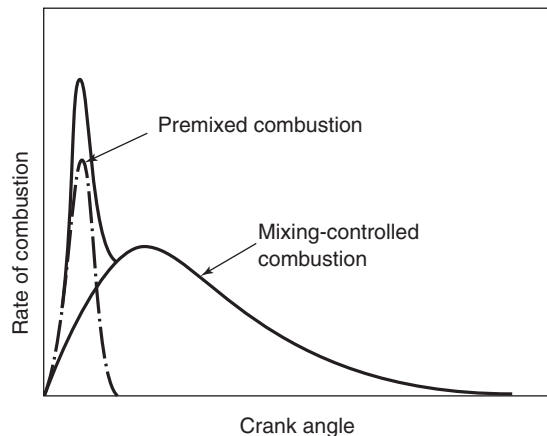


Figure 7.20 Dual Wiebe function for diesel energy release. Adapted from Miyamoto (1985).

Equation 7.19 with seven parameters is

$$\frac{dQ}{d\theta} = a m_p \frac{Q_p}{\theta_p} \left(\frac{\theta}{\theta_p} \right)^{m_p-1} \exp \left[-a \left(\frac{\theta}{\theta_p} \right)^{m_p} \right] + a m_d \frac{Q_d}{\theta_d} \left(\frac{\theta}{\theta_d} \right)^{m_d-1} \exp \left[-a \left(\frac{\theta}{\theta_d} \right)^{m_d} \right] \quad (7.19)$$

The subscripts p and d refer to the premixed and mixing-controlled combustion portions, respectively. The parameter a is a nondimensional constant, θ_p and θ_d are the burning duration for each phase, Q_p and Q_d are the integrated energy release for each phase, and m_p and m_d are nondimensional shape factors for each phase. The adjustable parameters are selected using a least squares fit. Miyamoto et al. (1985), for the specific direct (DI) and indirect injection (IDI) diesel engines tested in their experiments, reported that the m_p , m_d , and θ_p parameters were essentially independent of engine speed, load, and injection timing. The fitted values of these parameters is $a = 6.9$, $m_p = 4$, $m_d = 0.5$ (DI) or 0.9 (IDI), and $\theta_p = +7^\circ$.

The effective diesel fuel injection rate can also be obtained using the energy equation. The effective fuel injection rate \dot{m}_f is based on the assumptions that the chamber mixture is homogeneous and in thermodynamic equilibrium. The different liquid and vapor fuel fractions are not included at this level of modeling. The open system first law for the combustion chamber, Equation 7.20 with the injected fuel now explicitly included is

$$-\dot{Q}_l - P \dot{V} = \frac{d}{dt}(mu) - \dot{m}_f h_f \quad (7.20)$$

and the mass conservation equation, Equation 7.21 is

$$\frac{dm}{dt} = \dot{m}_f \quad (7.21)$$

In Equations 7.20 and 7.21, m is the fuel-air mass in the cylinder, \dot{m}_f is the fuel injection rate, h_f is the enthalpy of the injected fuel, and \dot{Q}_l is the heat transfer loss rate. With the above assumptions, the ideal gas equation in differential form is

$$P \dot{V} + V \dot{P} = RT \dot{m} + Rm \dot{T} \quad (7.22)$$

If dissociation is neglected, the internal energy is a function of temperature, pressure, and equivalence ratio only, so

$$u = u(T, P, \phi) \quad (7.23)$$

Differentiation of Equation 7.23 with respect to time gives

$$\dot{u} = \frac{\partial u}{\partial T} \dot{T} + \frac{\partial u}{\partial P} \dot{P} + \frac{\partial u}{\partial \phi} \dot{\phi} \quad (7.24)$$

If the mass of air in the cylinder is constant, with no residual fuel in the chamber at the beginning of injection, the overall equivalence ratio increases solely due to the fuel injection, and in differential form is

$$\dot{\phi} = \phi \frac{\dot{m}_f}{m_f} \quad (7.25)$$

Finally, combining Equations 7.20 through 7.25 leads to

$$\dot{m}_f = \frac{-\dot{Q}_1 - \left(1 + \frac{c_v}{R}\right) P \dot{V} - \frac{c_v}{R} V \dot{P}}{u - h_f - c_v T + \frac{m}{m_f} \frac{\partial u}{\partial \phi} \phi} \quad (7.26)$$

Equations 7.22, 7.25, and 7.26 are a set of ordinary, differential equations that when numerically integrated using measured values for P , \dot{P} , V , and \dot{V} yield T , \dot{T} , ϕ , $\dot{\phi}$, m_f and \dot{m}_f as functions of time. At each time step, an equilibrium combustion product numerical routine gives the required partial derivatives of the internal energy. The heat transfer loss \dot{Q}_1 is computed at each time step from an appropriate model.

Results obtained by an energy release computation that includes the relatively small effects of dissociation are given in Figure 7.21. The cylinder pressure and effective fuel injection rate (mg/deg) are plotted as a function of crank angle. The effective fuel injection rate curve is double peaked, similar to the effective energy release rate. The area under the curve is approximately equal to the actual mass of fuel injected.

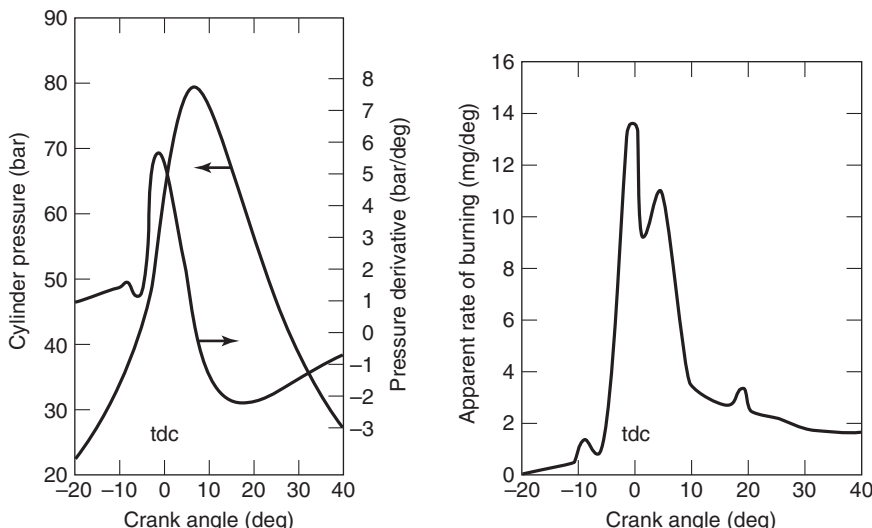


Figure 7.21 The effective fuel injection rate versus crank angle. Adapted from Krieger and Borman (1966).

Multidimensional Numerical Models of Diesel Combustion

Since diesel combustion is heterogeneous, numerical models need to be multidimensional to account for the spatial variations in temperature and species concentrations. There are a variety of turbulent combustion models, including probability density function (pdf) models, eddy break-up models, flamelet models, and coherent flame models that are used for both spark and diesel combustion modeling.

The research code KIVA (Amsden et al., 1985), developed at Los Alamos National Laboratory, is a public domain three-dimensional CFD program that has been used by a number of research groups to model compression ignition combustion. Reitz and coworkers at the University of Wisconsin (for example, see Kong et al., 1995) have added a number of improvements to the original KIVA model that incorporate more realistic analysis of the fuel spray breakup, vaporization, spray-wall impingement, wall heat transfer, ignition, combustion, and pollutant formation.

7.5 LOW-TEMPERATURE COMBUSTION

Introduction

Recently, there has been a great deal of interest and research activity worldwide in low-temperature combustion, in which combustion is initiated by the autoignition of a lean and nearly homogeneous fuel–air mixture. Over the last 20 years, a variety of techniques, categorized as ‘‘low-temperature combustion’’, have been developed to combine the best aspects of spark and diesel combustion, that is, combining the homogeneous fuel–air mixture of a spark ignition engine with the higher compression of a diesel engine to achieve lower emissions with much higher engine efficiencies.

The combustion process in a spark ignition engine produces less emissions than that of a diesel engine, but its compression ratio is knock-limited, and it has increased pumping losses at part load. The diesel engine is more fuel efficient, since it operates at a higher compression ratio and is unthrottled, but since it has higher NO_x and particulate (soot) emissions, it can require exhaust after treatment to meet emission standards.

In an LTC engine, the combustion begins whenever the autoignition temperature of a homogeneous or near homogeneous fuel–air mixture is reached. The low combustion temperatures greatly reduce the formation of nitric oxides and the heat transfer losses, and the lean air–fuel ratios reduce soot formation. Over the last decade, the hardware and software technology for control and operation of low-temperature combustion has advanced to a level that allows greater use of this combustion process. These techniques have taken advantage of the advances in injection technology, such as common rail injectors, allowing precise control of injection timing, multiple injection events, and use of multiple fuels.

An advantage of LTC is fuel flexibility, as both liquid fuels (gasoline, diesel, and biodiesel) and gaseous fuels (natural gas and hydrogen) can be used. The reactivity of the fuel is used as an ignition metric. Low reactivity fuels such as gasoline that have a high octane number are resistant to autoignition, and high reactivity fuels such as diesel fuel that have a high cetane number are more susceptible to autoignition. In addition to ignition delay, considerations such as fuel volatility, fuel composition, and initial cylinder temperature and pressure are important.

A volatile low reactivity fuel will vaporize and mix with the intake air more rapidly but will require higher cylinder temperatures for autoignition. A less volatile high reactivity fuel will require earlier injection for vaporization and mixing at a lower cylinder temperature. As the fuel molecular size increases, for example, from pentane to hexane and heptane, the

ignitability and rate of energy release increases, since the longer carbon chains break up more easily into radicals.

For the engine designer, with a low-temperature combustion approach, the energy release profile can be tailored to different modes of operation and fuel mixtures to meet emission requirements over the load and speed conditions of an engine. During low-temperature combustion, there is no distinct flame or wave front that propagates across the chamber but simultaneously ignites at a number of sites throughout the cylinder. With this propagation of ignition sites, the energy release is volumetric. The combustion duration is shorter, and the peak pressures and energy release rates are greater relative to conventional combustion. Soot production is greatly reduced, since the mixture is nearly homogeneous, with no locally rich combustion zones.

However, since the combusting mixture is nearly homogeneous, the start of ignition and the reaction rate is controlled by chemical kinetics, not turbulent diffusion as it is with non premixed combustion. Therefore, the cylinder temperature, pressure, equivalence ratio, and fuel composition govern the start of ignition. The low-temperature combustion duration can be very short, typically 5–10°, compared with 20–40° for a conventional spark or diesel engine, with an accompanying high rate of energy release.

The issues with low-temperature ignition that arise in engines are the high-energy release rates, adequate mixing of the fuel, air, and residual gases at high engine speeds, transient operation, cold starting, control of the start of ignition and the duration of ignition over a range of engine speeds and loads, and increased HC and CO emissions due to partial fuel oxidation. In response, researchers have developed a number of low-temperature combustion strategies to address these problems.

Three representative techniques that have been developed are homogeneous charge compression ignition (HCCI), premixed charge compression ignition (PCCI), and reactivity-controlled compression ignition (RCCI). In the latter two techniques, some degree of charge stratification is required to prevent excessive energy release rates and pressure rise. The charge stratification is accomplished using exhaust gas recirculation and multiple fuel injection.

Homogeneous Charge Compression Ignition (HCCI)

One of the first low-temperature combustion techniques developed was homogeneous charge compression ignition (HCCI). HCCI research began in the late 1970s, for example, see Onishi et al. (1979) for two-stroke engines and Najt and Foster (1983) for four-stroke engines. The two-stroke HCCI engines used very high EGR of up to 80% in which the goal was to improve combustion stability and reduce fuel consumption at part load. An HCCI engine operates without throttling, reducing the pumping losses, and the load is met by the control of the fuel-air ratio, so the mixture is very lean at low loads, and as the load increases, the mixture becomes more stoichiometric. The lean ($\phi < 0.3$) mixture in an HCCI combustion process results in lower peak combustion temperatures, about 1300 K, in comparison to spark ignition and diesel engines, depending on the fuel.

The lower peak temperatures significantly reduce NO_x . However, HCCI engines have an upper limit on the fuel-air ratio and peak torque. With an increase in load, there is an increase in the peak combustion temperature, and corresponding increase in the NO_x levels and susceptibility to knock. Also, as the load is increased, more fuel is added, increasing the fuel-air ratio, and thus advancing the start of combustion, increasing the net compression work. Experiments have shown there is a knock limit at higher loads, and partial combustion at high engine speeds. Since there are also lean flammability limits at

low load, the operating range of HCCI can be relatively narrow and limited to midload conditions.

The knock in an HCCI engine is a volumetric knock, in which autoignition is initiated simultaneously near TDC at multiple locations in the cylinder. Measurements by Vavra et al. (2012) indicate that the dominant frequency in HCCI knock is the first tangential (1T) mode with a uniform decrease in amplitude to other oscillation modes. This is in contrast to SI end gas knock which was found to begin after TDC near a wall with a greater energy density, more stochastic with less uniform distribution in frequencies, a larger difference in knock magnitude from the 1T to the 2T mode, and more cycle–cycle behavior.

In an HCCI engine, since the start and duration of combustion can not be directly controlled, it is controlled indirectly. Control techniques include varying inducted gas temperature, fuel–air ratio, high EGR rates, variable compression ratio, and variable valve timing. Using a variable compression ratio will control the temperature rise during compression. The residual fraction can be controlled using variable valve timing, for example, using early exhaust valve closing will increase the residual fraction.

The implementation of HCCI is different for gasoline and diesel fuels due to their different ignition characteristics. Dec and Yang (2010) used gasoline as a fuel for a medium duty diesel engine with a compression ratio of 14:1 operating in a HCCI mode, and reported that by boosting the intake pressure from 100 kPa to 325 kPa absolute while also increasing the EGR from 0 to 60%, they were able to increase the IMEP from 4 to 16 bar at the knock/stability limit. The gasoline entered the cylinder fully premixed in the intake plenum, eliminating fuel–air mixing issues.

Conversely, with diesel fuel, there is a need to cool the intake air to prevent knock and to start the fuel injection earlier in the compression stroke to give enough time for a homogeneous mixture to form. In this case, cooled EGR or reduced compression ratios are used to increase the ignition delay and decrease the rate of energy release. One method used to achieve adequate mixing in diesel-fueled LTC engines is early injection. However, the low volatility of diesel fuel can result in wall wetting, so low-penetration fuel injectors are used to increase entrainment and reduce wall impingement. The low penetration is achieved with higher pressure fuel injection together with an increased number of holes that have a smaller diameter. Multiple injection is also used to tailor the injection into several pulses with different durations. Also, with early injection, since the piston is lower in the cylinder, the fuel spray needs to have a larger downward direction.

Partially Premixed Compression Ignition (PPCI)

The partially premixed compression ignition (PPCI) technique is used to increase the combustion duration and reduce the rate of pressure rise through partial mixing of the fuel to create fuel stratification in the cylinder. With this technique, multiple injections of a single fuel are employed. The mixture is thus stratified, with a distribution of equivalence ratio. With a two injection strategy, as illustrated in Figure 7.22, a pilot injection is placed early in the compression stroke, typically about 150° btdc to create a homogeneous mixture, with the main injection near top dead center. Three injection event schemes have also been used. Combustion is initiated by the main injection near top dead center. High levels of EGR are also used to increase the ignition delay and prevent combustion during the first injection.

The relative amounts of fuel used in each injection depend on the engine load, fuel reactivity, and level of EGR. Both gasoline and diesel fuels have been used successfully in engines operating in a PPCI mode (Kalghatgi, 2007). A variation of PPCI (Dec et al., 2011)

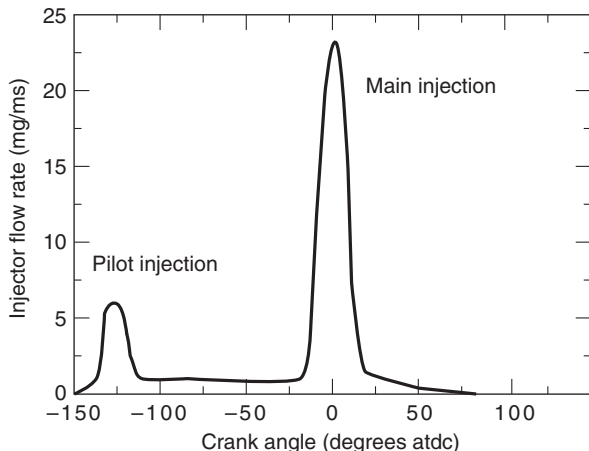


Figure 7.22 Example PCCI dual injection strategy.

is to premix the portion of the fuel with the intake air followed by directly injecting the remaining portion of the fuel into the cylinder during compression to initiate combustion. Ra et al. (2012), using a PCCI strategy with a triple injection of gasoline into a light duty 1.9 L single-cylinder diesel engine with a 16.5:1 compression ratio operating at about 16 bar and 2500 rpm, measured an indicated specific fuel consumption as low as 172 g/kWh. The EGR level was 48%.

Reactivity Controlled Compression Ignition (RCCI)

The reactivity-controlled compression ignition (RCCI) technique uses a dual fuel compression ignition strategy. As the schematic in Figure 7.23 illustrates, RCCI begins with port injection of a low reactivity (low cetane number) fuel such as gasoline followed by multiple direct injection of relatively small amounts ($\approx 15\%$) of a high reactivity (high cetane number) fuel such as diesel fuel. The mixture ignites when the diesel fuel is injected. As the directly injected diesel fuel is mixed with the low reactivity fuel, a gradient of fuel reactivity is established throughout the cylinder. The combustion is staged, reducing the rate of pressure rise, and progresses from regions of higher reactivity to regions of lower reactivity. There are three regions of energy release with the RCCI technique. The initial energy release is from the high reactivity diesel fuel, the second from a mixture of the two fuels, and the third from the low reactivity fuel.

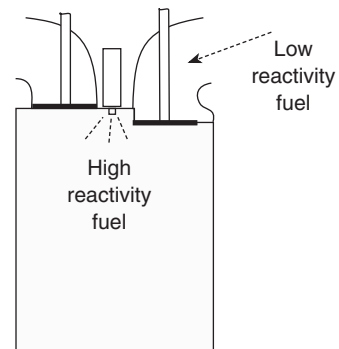


Figure 7.23 Example RCCI dual fuel operation.

Since two fuels are used, the RCCI technique has a greater operating range than HCCI and allows increased control of the start of combustion and the combustion duration. With this technique, it is possible to optimize the fuel reactivity for a range of engine operating conditions. For an engine with a 12:1 compression ratio, Bessonette et al. (2007) found that the optimum cetane number was about 45, that is, diesel fuel, at low loads, and at high loads, the optimum cetane number was about 27, that is, gasoline fuel. Therefore, as the load increases, one could specify a change in the fuel mixture from 20% gasoline/80% diesel at low load to 85% gasoline/15% diesel at high load.

Kokjohn et al. (2009) report net indicated thermal efficiencies of 50% ($\text{isfc} = 170 \text{ g/kWh}$) for dual fuel low-temperature combustion in a heavy duty 2.44 L single-cylinder diesel engine. They used port fuel injection of gasoline and direct injection of diesel fuel, with about 80% of the fuel energy from gasoline at high load (11 bar) conditions. The overall equivalence ratio was $\phi = 0.77$ and a high level of 45% EGR was used. The soot emissions were 0.004 g/kWh and NO_x emissions were 0.01 g/kWh, both well below emission standards, eliminating the need for exhaust after treatment. Similar results were reported by Hockett and Marchese (2015) in a CFD study of RCCI.

As of 2014, a number of manufacturers have vehicle prototypes in development, with planned commercial introduction in the coming decade. One approach that they have chosen to meet the high load/speed issues is to use the engine in a dual mode, that is, low-temperature combustion operation at lower loads, and spark or diesel operation at higher loads.

For further information about combustion processes in engines, books by Borman and Ragland (1998) and Turns (2012) cover combustion chemistry and kinetics in internal combustion engines from an engineering perspective. Detailed information about hydrocarbon chemical kinetics is given in Westbrook and Dryer (1984) and in the text by Law (2006).

7.6 REFERENCES

- ABRAHAM, J., F. WILLIAMS, and F. BRACCO (1985), "A Discussion of Turbulent Flame Structure in Premixed Charges," SAE paper 850345.
- AMSDEN, A., T. BUTLER, P. O'ROURKE, and J. RAMSHAW (1985), "KIVA-A Comprehensive Model for 2-D and 3-D Engine Simulations," SAE Paper 850554.
- ASSANIS, D., Z. FILIPPI, S. FIVELAND, and M. SYRIMIS (2003), "A Predictive Ignition Delay Correlation under Steady-State and Transient Operation of a Direct Injection Diesel Engine," *ASME J. Eng. Gas Turbines Power*, Vol. 125, No. 2, pp. 450–457.
- BESSONETTE, P., C. SCHLEYER, K. DUFFY, W. HARDY, and M. LIECHTY (2007), "Effects of Fuel Property Changes on Heavy-Duty HCCI Combustion," SAE paper 2007-01-0191.
- BORMAN, G. and K. RAGLAND (1998), *Combustion Engineering*, McGraw-Hill, New York.
- BOWDITCH, F. W. (1961), "A New Tool for Combustion Research: A Quartz Piston Engine," *SAE Trans.*, Vol. 69, p. 17.
- CARIS, D., B. MITCHELL, A. McDUFFIE, and F. WYCZALEK (1956), "Mechanical Octanes for Higher Efficiency," *SAE Trans.*, Vol. 64, p. 76100.
- COOK, H., J. VANDEMAN, and J. LIVENGOOD (1944), "Effect of Several Methods of Increasing Knock-Limited Power on Cylinder Temperatures," NACA ARR E4115 E-36.
- COWART, J., J. KECK, J. HEYWOOD, C. WESTBROOK, and W. PITZ (1990), "Engine Knock Predictions Using a Fully Detailed and a Reduced Chemical Kinetic Mechanism," Twenty Third Symposium (International) on Combustion, Combustion Institute, Pittsburgh, Pennsylvania.
- DAMKOHLER, G. (1947), "The Effect of Turbulence on Flame Velocity in Gas Mixtures," NACA Technical Memo TM-1112.
- DEC, J. (1997), "A Conceptual Model of DI Diesel Combustion Based on Laser-Sheet Imaging," SAE paper 970873.

- DEC, J. and C. ESPEY (1995), "Ignition and Early Soot Formation in a DI Diesel Engine Using Multiple 2-D Imaging Diagnostics," SAE paper 950456.
- DEC, J. and Y. YANG (2010), "Boosted HCCI for High Power without Engine Knock and with Ultra-Low NO_x Emissions - using Conventional Gasoline," SAE paper 2001-01-1086.
- DOUAUD, A. and P. EYZAT (1977), "DIGITAP An On-Line Acquisition and Processing System for Instantaneous Engine Data Applications," SAE paper 770218.
- DOUAUD, A. and P. EYZAT (1978), "Four-Octane-Number Method for Predicting the Anti-Knock Behavior of Fuels," SAE paper 780080.
- DOWNS, D., A. WALSH, and R. WHEELER (1951), "A Study of the Reactions that Lead to Knock in the Spark-Ignition Engine," *Phil. Trans. R. Soc. Lond. A*, Vol. 243, pp. 463–524.
- DRAPER, C. S. (1938), "Pressure Waves Accompanying Detonation in an Internal Combustion Engine," *J. Aero. Sci.*, Vol. 5, No. 6, pp. 219–226.
- ESPEY, C. and J. DEC (1993), "Diesel Engine Combustion Studies in a Newly Designed Optical-Access Engine Using High-Speed Visualization and 2-D Laser Imaging," SAE paper 930971.
- HALSTEAD, M., L. KIRSCH, and C. QUINN (1977), "The Autoignition of Hydrocarbon Fuels at High Temperatures and Pressures—Fitting of a Mathematical Model," *Combust. Flame*, Vol. 30, pp. 45–60.
- HARDENBERG, H. and F. HASE (1979), "An Empirical Formula for Computing the Pressure Rise Delay of a Fuel from Its Cetane Number and from the Relevant Parameters of Direct-Injection Diesel Engines," SAE paper 790493.
- HESELBERG, H. and W. LOVELL (1951), "What Fuel Antiknock Quality Means in Engine Performance," *J. SAE*, p. 32.
- HOCKETT, A. and A. MARCHESE (2015), "Modeling of a Natural Gas/Diesel Fuel RCCI Engine," *J. Eng. Res.*, In review.
- KALGHATGI, G., P. RISBERG, and H. ANGSTROM (2007), "Partially Pre-Mixed Auto-Ignition of Gasoline to Attain Low Smoke and Low NO_x at High Load in a Compression Ignition Engine and Comparison with a Diesel Fuel," SAE paper 2007-01-0006.
- KEE, R. (2006), CHEMKIN Computer Software, Reaction Design Inc., San Diego, California.
- KOKJOHN, S., R. HANSON, D. SPLITTER, and R. REITZ (2009), "Experiments and Modeling of Dual-Fuel HCCI and PCCI Combustion Using In-Cylinder Fuel Blending," SAE paper 2009-01-2647.
- KONG, S., Z. HAN, and R. REITZ (1995), "The Development and Application of a Diesel Ignition and Combustion Model for Multidimensional Engine Simulation," SAE paper 950278.
- KRIEGER, R. and G. BORMAN (1966), "The Computation of Apparent Heat Release for Internal Combustion Engines," ASME paper 66-WA-DGP-4.
- LAW, C. K. (2006), *Combustion Physics*, Cambridge University Press, New York.
- LAW, C. K., C. SUNG, and H. WANG (2000), "On the Development of Detailed and Reduced Reaction Mechanisms for Combustion Modeling," AIAA paper 2000-0860.
- LEE, D. and S. HOCHGREB (1998), "Rapid Compression Machines: Heat Transfer and Suppression of Corner Vortex," *Combust. Flame*, Vol. 114, pp. 531–545.
- LEIKER M., K. CHRISTOPH, M. RANKL, W. CANTELLIERI, and U. PFEIFER (1972), "Evaluation of Anti-knocking Property of Gaseous Fuels by Means of Methane Number and Its Practical Application to Gas Engines," ASME-72-DGP-4.
- METGHALCHI, M. and J. KECK (1982), "Burning Velocities of Mixtures of Air with Methanol, Isooctane and Indolene at High Pressure and Temperature," *Combust. Flame*, Vol. 48, No. 2, p. 191120.
- MIYAMOTO, N., T. CHIKAHISA, T. MURAYAMA, and R. SAWYER (1985), "Description and Analysis of Diesel Engine Rate of Combustion and Performance Using Wiebe's Functions," SAE paper 850107.
- NAJT, P. and D. FOSTER (1983), "Compression-Ignited Homogeneous Charge Compression," SAE Paper 830264.
- RASSWEILER, G. and L. WITHROW (1938), "Motion Pictures of Engine Flames Correlated with Pressure Cards," A landmark reprint paper commemorating SAE's 75th Anniversary, SAE paper 800131.
- RICARDO, H. (1921), "The Influence of Various Fuels on the Performance of Internal Combustion Engines," *Automot. Eng.*, Vol. 11, p. 92.
- SIEBERS, D. (1998), "Liquid-Phase Fuel Penetration in Diesel Sprays," SAE paper 980809.

- SMITH, J., R. GREEN, C. WESTBROOK, and W. PITZ (1984), "An Experimental and Modeling Study of Engine Knock," Twentieth Symposium (International) on Combustion, Combustion Institute, Pittsburgh, Pennsylvania.
- SOID, S. and Z. ZAINAL (2011), "Spray and Combustion Characterization for Internal Combustion Engines Using Optical Measuring Techniques—A Review," *Energy*, Vol. 36, No. 2, pp. 724–741.
- TABACZYNSKI, R., F. TRINKER, and B. SHANNON (1980), "Further Refinement and Validation of a Turbulent Flame Propagation Model for Spark Ignition Engines," *Combust. Flame*, Vol. 39, No. 2, p. 111–122.
- TURNS, S. (2012), *An Introduction to Combustion*, 3rd Edition, McGraw-Hill, New York.
- VAVRA, J., S. BOHAC, L. MANOFSKY, G. LAVOIE, and D. ASSANIS (2012), "Knock in Various Combustion Modes in a Gasoline Fueled Automotive Engine," *J. Eng. for Gas Turbines and Power*, Vol. 134, p. 082807-1 - 082807-8.
- WESTBROOK, C. and F. DRYER (1984), "Chemical Kinetic Modeling of Hydrocarbon Combustion," *Prog. Energy Combust. Sci.*, Vol. 10, p. 157.
- WITZE, P. and F. VILCHIS (1981), "Stroboscopic Laser Shadowgraph Study of the Effect of Swirl on Homogeneous Combustion in a Spark Ignition Engine," SAE paper 810226.
- YOUNG, M. (1980), "Cyclic Dispersion-Some Quantitative Cause and Effect Relationships," SAE paper 800459.

7.7 HOMEWORK

- 7.1** Compare the laminar flame speed s_l of isoctane, propane, and methanol for $P = 20$ atm, $T_u = 600$ K, $f = 0.05$, and $\phi = 0.9, 1.0, 1.1$, and 1.2 . At what equivalence ratios are the laminar flame speeds maximum for these fuels?
- 7.2** (a) Compute the laminar flame speed s_l at ignition for an isoctane-fueled engine with a compression ratio $r = 8$ and spark timing $\theta_s = -25^\circ$ atdc. The pressure and temperature at the time of ignition are given by

$$T_{u,s} = 350(V_{bdc}/V_s)^{(\gamma-1)/\gamma}$$

$$P_s = 0.5(V_{bdc}/V_s)^\gamma$$

The residual fraction is given by $f = 0.10(8/r)$, the combustion is stoichiometric with $\phi = 1$, and $\gamma = 1.3$.

(b) If the ignition delay $\Delta\theta_{id}$ is inversely proportional to the laminar flame speed at the time of ignition, and $\Delta\theta_{id} = 25^\circ$ for the conditions of part (a), plot the ignition delay $\Delta\theta_{id}$ versus θ_s for $-50^\circ < \theta_s < 0^\circ$ and show lines of constant compression ratio for $r = 8$ and $r = 10$. Discuss the results.

- 7.3** A turbocharged diesel engine has a compression ratio of 16:1 and stroke of 150 mm, with an inlet manifold conditions of 2 bar and 380 K. The cetane number of the diesel fuel is 40. What is the ignition delay τ_{id} in crank angle degrees if $N = 2500$ rpm? Assume a polytropic coefficient $n = 1.35$.
- 7.4** A maximum ignition delay τ_{id} of 20° is required for acceptable cold start ignition of an automobile diesel engine. The engine stroke is 80 mm, the cranking speed N is 200 rpm, and the polytropic coefficient n for compression to top dead center is 1.20. The fuel cetane number is 45, and the inlet air temperature and pressure are 250 K and 1 bar. What is the minimum compression ratio needed to have an ignition delay no longer than 20° ?

- 7.5** Consider the dependence of the precursor formation rate with temperature. For isoctane at $P = 10$ bar, plot the nondimensional precursor formation rate $d\zeta/dt$ versus temperature. Use the constants $A = 50.5$, $B = 3800$, and $n = 1.7$, and vary the unburned gas temperature T_u from 300 to 1100 K.
- 7.6** For an unburned gas temperature of 1200 K and pressure of 20 bar, with a combustion duration of 60°, what is the critical engine speed N above which knock will not have enough time to occur? Use the constants $A = 50.5$, $B = 3800$, and $n = 1.7$.
- 7.7** A combustion model produced the following data for an engine operated at wide open throttle on isoctane, where T_u is the temperature of the unburned gas mixture and P is the gas pressure. The start of combustion ($x_b = 0$) is -40° atdc, and the end of combustion ($x_b = 1.0$) is $+20^\circ$ atdc:

θ ($^\circ$ atdc)	P (bar)	T_u (K)
-40	5.6	600
-35	6.5	620
-30	7.5	650
-25	9.8	690
-20	14.6	745
-15	25.0	820
-10	35.0	880
0	52.8	965
10	58.6	996
15	54.0	990
20	45.2	975

If the precursor formation rate is given by Equation 7.10

$$\frac{d\zeta}{dt} = 50.5 P^{1.7} \exp(-3800/T_u)$$

- a.** Determine the minimum engine speed $\dot{\theta}_{\min}$ for which knock-free operation occurs, assuming the table is speed independent. Use the trapezoidal rule for integration of Equation 7.15.
- b.** Plot the extent of reaction ζ versus crank angle at that speed. Comment on assumptions implicit or explicit in the analysis.
- c.** Plot the extent of reaction ζ versus crank angle at engine speeds of 70 and 130% of the minimum engine speed $\dot{\theta}_{\min}$. For the slower engine speed, what is the crank angle θ at which knock is predicted to occur?
- 7.8** Estimate the dominant acoustic frequency (kHz) in a knocking CFR engine if the average end-gas temperature is assumed to be 1500 K.
- 7.9** The existence of a temperature gradient in the burned gas can be explained fairly simply using an ideal gas model in which the fluid is broken into an ensemble of elements. The average pressures and specific volumes of an Otto cycle are represented in Figure 7.24 by the diagram 1-2-3-4. All the gas is compressed isentropically from 1 to 2; hence at point 2, the gas is at a uniform temperature T_2 . The first element (infinitesimal) to burn will not

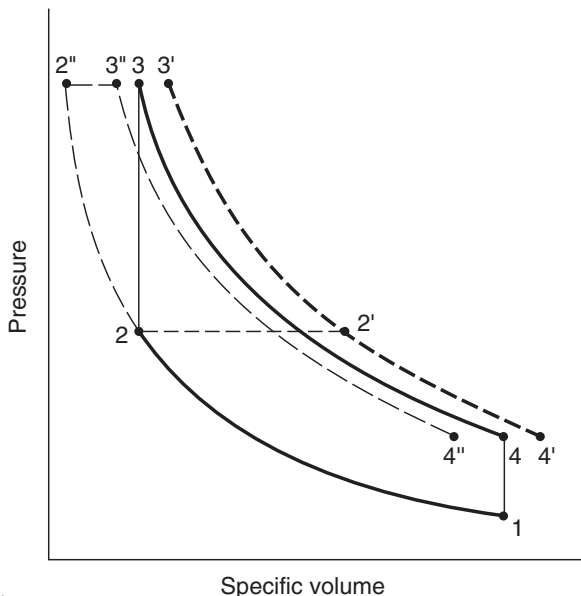


Figure 7.24 Ensemble of fluid elements in Otto cycle for Problem 7.9.

influence the cylinder pressure, and thus burns at constant pressure to $2'$. Thus

$$T_{2'} = T_2 + \frac{q}{c_p}$$

where q is the energy release per unit mass. That gas is then compressed isentropically to the peak pressure P_3 , hence

$$\frac{T'_3}{T'_2} = \left(\frac{P_3}{P_2} \right)^{(\gamma-1)/\gamma}$$

The last element to burn is compressed isentropically as unburned gas to the peak pressure at $2''$.

$$\frac{T''_2}{T'_2} = \left(\frac{P_3}{P_2} \right)^{(\gamma-1)/\gamma}$$

The last element then also burns at constant pressure so that

$$T_{3''} = T_{2''} + \frac{q}{c_p}$$

All the elements expand isentropically after the last element burns.

Taking as the average cycle the conditions used in Figure 2.1 of Chapter 2, find

(a) The ratio $T_{3'}/T_{3''}$

(b) The ratio $v_{3'}/v_{3''}$

- 7.10** Derive Equation 7.26 for the diesel fuel injection rate. Assume $u = u(T, \phi)$.

- 7.11** An HCCI engine needs to compress a fuel-air mixture to 1300 K at top dead center for proper autoignition. Assuming a residual gas fraction f of 0.35 at a temperature of 750 K, what should the inlet air temperature be if (a) the compression ratio is 11:1, and (b) the compression ratio is 18:1? Assume the specific heat ratio $\gamma = 1.35$.

Chapter 8

Emissions

8.1 INTRODUCTION

In this chapter, we discuss how pollutants are formed during the combustion process in an engine and examine measures that have been taken to reduce airborne emissions from engines. The major emissions from internal combustion engines include nitrogen oxides (NO_x), carbon monoxide (CO), hydrocarbons (HC), particulates (PM), and aldehydes. These combustion products are a significant source of air pollution, as internal combustion engines are the source of about half of the NO_x , CO, and HC pollutants in the atmosphere. The emissions from engines have a number of adverse health and environmental effects, as many research studies have shown a strong correlation between air pollution levels and human health effects. The health effects include reduced lung function, cardiovascular issues, coughs, asthma, and eye irritation.

Nitrogen oxides are formed during the combustion process, and in the atmosphere react with water vapor and solar radiation to form nitric acid, a component of acid rain, and ground level ozone, O_3 , a component of smog. In addition to creating significant respiratory system problems, both acid rain and smog damage forests, streams, and agricultural products. If transported over a wide area by prevailing winds, nitrogen oxides can create regional air quality issues.

Carbon monoxide is a product of rich combustion and reacts with oxygen and nitrogen oxides in the exhaust stream and atmosphere to form smog. When inhaled, carbon monoxide interferes with oxygen distribution throughout the circulatory system due to its high affinity for hemoglobin, about 200 times than that of oxygen. Carbon monoxide poisoning is the most common type of fatal air poisoning worldwide. The U.S. Environmental Protection Agency (EPA) first set air quality standards for CO in 1971, specifying an 8-h primary standard at 9 parts per million (ppm) and a 1-h primary standard at 35 ppm.

Hydrocarbon emissions result from release of unburned or partially combusted hydrocarbon fuels. Hydrocarbons also contribute to the chemical reactions that form ground level ozone. Various hydrocarbon compounds can cause increased incidence of respiratory problems and lung cancer. Finally, inhalation of particulates from engines causes increased respiratory problems.

Carbon dioxide (CO_2), a primary gaseous combustion product of internal combustion engines, is also a greenhouse gas and is in the process of being regulated as well, due to its increasing atmospheric concentration. The combustion of fossil fuels such as coal and petroleum is the leading cause of increasing CO_2 concentration in the atmosphere. About 60% of the CO_2 produced by combustion remains in the atmosphere; the remainder is removed from the atmosphere by plant photosynthesis and by diffusion into ocean water.

Before the advent of the industrial revolution, the average atmospheric concentration of CO₂ was about 280 ppm. Long-term precision monitoring began around 1960, when the average atmospheric concentration of CO₂ was measured at 316 ppm. By 1970, it was 325 ppm, in 1990, the concentration had risen to 354 ppm, and in 2010, it was 387 ppm, an increase of about 1–2 ppm per year.

8.2 NITROGEN OXIDES

Nitrogen oxides (NO_x) are formed throughout the combustion chamber during the combustion process due to the disassociation of N₂ and O₂ into their atomic states and subsequent reactions with molecular oxygen and nitrogen. The effect of engine operational parameters including equivalence ratio, spark timing, engine speed, and manifold pressure on nitrogen oxide concentration has been the goal of a great deal of research. The reactions forming NO_x are highly temperature dependent, so NO_x emissions are relatively low during engine start and warm-up, and then scale proportionally with the engine load. The total nitrogen oxide concentration is measured with a chemiluminescence analyzer, as discussed later in the text.

Nitrogen oxides (NO_x) are composed of NO and NO₂. Many complex reaction pathways for NO_x creation and decay have been formulated, and the corresponding rate parameters for the reactions have been established. In spark ignition engine exhaust, the dominant component of NO_x is nitric oxide, NO, with concentrations of the order of 1000 ppm, and the concentration of nitrogen dioxide, NO₂, is of the order of 10 ppm, that is, about 1%. In compression ignition engines, the concentration of NO₂ can be higher, approaching 10–30% of the total NO_x. In the atmosphere, nitric oxide will oxidize to nitrogen dioxide and react with unburned hydrocarbons in the presence of sunlight to form smog.

There are three major chemical mechanisms that produce NO. These are the thermal or Zeldovich mechanism, the prompt or Fenimore mechanism, and the combustion of fuel-bound nitrogen. For internal combustion engines, the most significant is the Zeldovich mechanism in which NO is formed in the high-temperature burned gases behind by the flame front. The prompt mechanism occurs within the relatively thin combustion flame front. Since the volume of the high-temperature burned gases is much larger than the instantaneous volume of the flame front, the amount of NO formed from the prompt mechanism is relatively small compared with that formed from the thermal or Zeldovich mechanism. Fuel-bound NO is formed from nitrogen in the fuel. Fossil fuels typically contain 0.5–2.0% nitrogen by weight, so during combustion of nitrogen-containing fuels, hydrogen cyanide and ammonia are formed, which react with O and OH to form NO.

The following three chemical equations form the extended Zeldovich reaction mechanism (Miller and Bowman, 1989):



The first two reactions, Zeldovich (1946), were proposed by Yakov Zeldovich (1914–1987), a Soviet physicist. They are chain-branching reactions, as two radical species are formed from a reaction that consumes only one radical. The first reaction,

Equation 8.1, is a nitrogen dissociation reaction triggered by an oxygen atom. This reaction is slow and therefore rate limiting, as it is endothermic with activation energy of 75.0 kcal. The second reaction, Equation 8.2, is very fast, as a nitrogen atom reacts exothermically (+31.8 kcal) with an oxygen molecule to form nitric oxide and an oxygen atom. The third reaction, Equation 8.3, is an exothermic (+49.4 kcal) reaction between a nitrogen atom and a hydroxide radical that forms nitric oxide and a hydrogen atom. This third reaction was proposed by Lavoie et al. (1970), and assumes partial equilibrium of the reaction:



The prompt mechanism, Fenimore (1971), occurs in rich combustion conditions at the flame zone. It is a reaction sequence initiated by reaction of hydrocarbon radicals with molecular nitrogen, leading to intermediate molecules, such as hydrogen cyanide, HCN, that then react to form NO, with concentrations of the order of 50 ppm.

The NO formed in the flame zone can be converted to NO_2 through the following reaction:



and converted back to NO through reactions with O and H, for example,



The rate constants for the extended Zeldovich reaction mechanism are given in Equation 8.7 (Hanson and Salimian, 1984). These rate constants are relatively slow compared with typical I. C. engine combustion timescales. The rate constants have units of $\text{cm}^3/(\text{mol s})$, the additional subscript r on the rate constants denotes the reverse reaction rate constant, and the temperature T is in Kelvin.

$$\begin{aligned} k_1 &= 1.8 \times 10^{14} \exp(-38,370/T) \\ k_{1r} &= 3.8 \times 10^{13} \exp(-425/T) \\ k_2 &= 1.8 \times 10^{10} T \exp(-4,680/T) \\ k_{2r} &= 3.8 \times 10^9 T \exp(-20,820/T) \\ k_3 &= 7.1 \times 10^{13} \exp(-450/T) \\ k_{3r} &= 1.7 \times 10^{14} \exp(-24,560/T) \end{aligned} \quad (8.7)$$

Following Heywood (1976), one can write the following expression for the rate of change of nitric oxide concentration, with the brackets denoting molar concentrations in units of mol/cm^3 .

$$\begin{aligned} \frac{d}{dt}[\text{NO}] &= +k_1[\text{O}][\text{N}_2] - k_{1r}[\text{NO}][\text{N}] + k_2[\text{N}][\text{O}_2] \\ &\quad - k_{2r}[\text{NO}][\text{O}] + k_3[\text{N}][\text{OH}] - k_{3r}[\text{NO}][\text{H}] \end{aligned} \quad (8.8)$$

To apply Equation 8.8, two approximations are introduced. First, that the C-O-H system is in equilibrium and is not perturbed by N_2 dissociation, and second, the N atoms change concentration by a quasi-steady process. The first approximation means simply that given the pressure, temperature, equivalence ratio, and residual fraction of a fluid element, one simply computes the equilibrium composition to determine the concentrations of N_2 , O_2 , O, OH, and H. The second approximation means that one can solve for the N atom concentration by setting the rate of change of N atoms to zero:

$$\begin{aligned} \frac{d}{dt}[\text{N}] &= +k_1[\text{O}][\text{N}_2] - k_{1r}[\text{N}][\text{NO}] - k_2[\text{N}][\text{O}_2] \\ &\quad + k_{2r}[\text{NO}][\text{O}] - k_3[\text{N}][\text{OH}] + k_{3r}[\text{NO}][\text{H}] \\ &= 0 \end{aligned} \quad (8.9)$$

With these two approximations, it can be shown that

$$\frac{d[\text{NO}]}{dt} = \frac{2R_1(1 - \alpha^2)}{1 + \alpha R_1/(R_2 + R_3)} \quad (8.10)$$

where α is the ratio of the nitric oxide concentration to its equilibrium value:

$$\alpha = \frac{[\text{NO}]}{[\text{NO}]_e} \quad (8.11)$$

and $R_i(i = 1, 2, 3)$ are various rates of reaction, with the equilibrium concentrations labeled with the subscript e :

$$R_1 = k_1[\text{O}]_e[\text{N}_2]_e$$

$$R_2 = k_{2r}[\text{NO}]_e[\text{O}]_e$$

$$R_3 = k_{3r}[\text{NO}]_e[\text{H}]_e$$

The total amount of nitric oxide that appears in the exhaust is computed by summing the mass fractions for all the fluid elements:

$$\bar{x}_{\text{NO}} = \int_0^1 x_{\text{NO}} dx \quad (8.12)$$

The above NO reaction mechanism has been incorporated into the two-zone finite heat release program *Homogeneous.m* introduced in Chapter 4. The program computes and plots both the equilibrium and the rate-limited NO concentrations as a function of crank angle, and also calculates NO concentration in the exhaust. Use of the program to compute NO formation is detailed in the following example:

EXAMPLE 8.1 NO Formation with a Homogeneous Two-Zone Finite Energy Release Model

A CFR engine is operated with gasoline using the following baseline conditions given in the table below. The start of heat release is -15° atdc and the burn duration is 45° . The inlet conditions are $P_1 = 100$ kPa and $T_1 = 350$ K. Using the *Homogeneous.m* program, plot the burn fraction, pressure, burned and unburned temperatures, equilibrium, and rate-limited NO values as a function of crank angle. This engine is similar to the CFR engine used in the NO study by Komiyama and Heywood (1973).

Parameter	Value
Bore (m)	0.0825
Stroke (m)	0.1143
Half stroke/rod ratio	0.25
Compression ratio	7
Engine speed (rpm)	1200
Equivalence ratio	0.88
Residual fraction	0.05
Cylinder heat transfer coefficient ($\text{W}/(\text{m}^2\text{K})$)	500
Mass blowby coefficient (s^{-1})	0.8
Cylinder wall temperature (K)	400

SOLUTION The input parameters are entered into the Homogeneous.m program as shown below:

```
% Homogeneous Two Zone Combustion Cycle
% This program computes the pressure and temperature
% vs crank angle, the work, indicated thermal efficiency
% and the Indicated mean effective pressure (kPa)

R = 10;           % Compression ratio
B = .10;          % Bore - B (m)
S = .08;          % Stroke - S (m)
EPS = 0.25;       % Half stroke to rod ratio
RPM = 2000;       % Engine speed (RPM)
HEAT = 500;        % Heat transfer coefficient (W/m2-K)
BLOWBY = 0.8;      % Blowby coefficient
THETAB = 60;       % Burn angle (Deg)
THETAS = -35;      % Start of heat release (deg ATDC)
PHI = 0.8;         % Equivalence ratio
F = 0.1;          % Residual fraction
TW = 420;          % Wall temperature (K)
fuel_id = 2;        % gasoline
FS = 0.06548;      % gasoline stoichiometric fuel-air ratio
A0 = 47870;        % maximum available energy (kJ/kg)
T1 = 350;          % Initial temperature (K)
P1 = 100;          % Initial Pressure (kPa)
...
...
```

The results of the computations are presented in the following four figures. The burn fraction profile is plotted in Figure 8.1, the calculated pressure profile in Figure 8.2, and the calculated unburned and burned temperature profiles in Figure 8.3. Each mass burns at its adiabatic flame temperature based on the unburned gas temperature at the time it burned. Once burned, the temperature of a mass tracks the pressure, as it is more or less isentropically compressed or expanded. Notice that the first mass to burn is compressed significantly. Each subsequent element to burn is compressed less, and the last element to burn undergoes no compression. As a result, the first mass to burn is hotter than all the rest, and the last mass to burn is the coolest.

The resulting NO profiles are plotted in Figure 8.4. Figure 8.4 illustrates how the nitric oxides vary with time in different fluid masses as the burned volume increases. The equilibrium concentration is computed based on the local temperature, pressure, equivalence ratio, and residual mass fraction.

The plot illustrates some important points about NO combustion. First, there is a significant difference between the equilibrium and the rate-limited concentrations of NO during the combustion process, as the rate-limited NO concentrations lag behind the equilibrium NO concentrations. Secondly, since the chemical reaction rates increase strongly

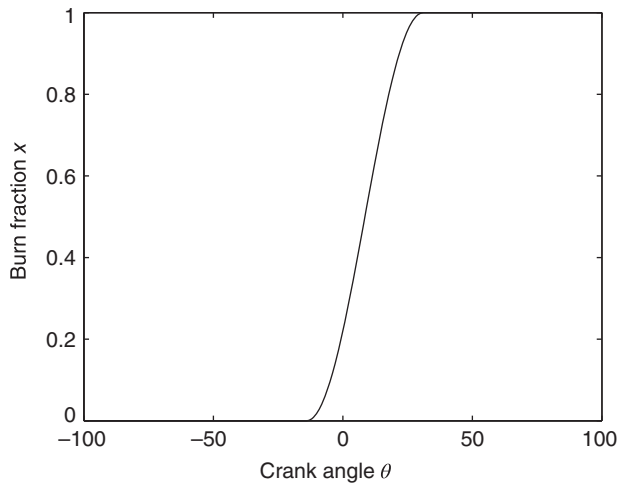


Figure 8.1 Mass fraction burned versus crank angle (Example 8.1).

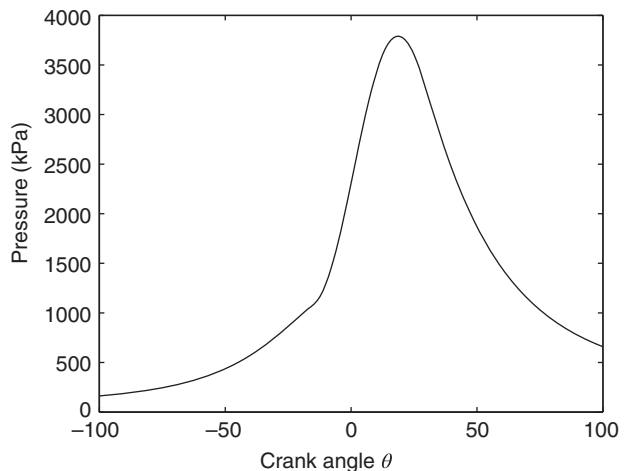


Figure 8.2 Pressure versus crank angle (Example 8.1).

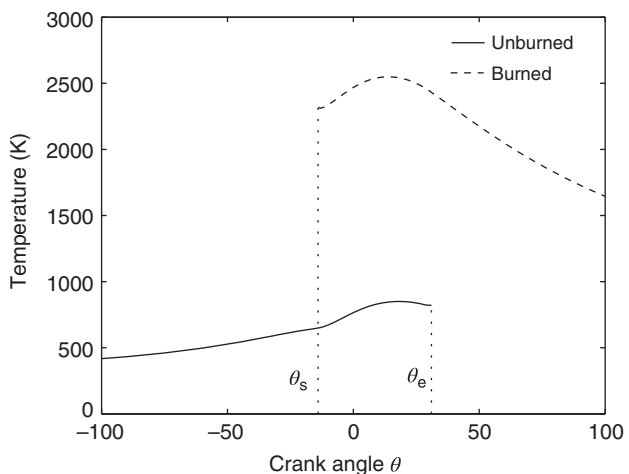


Figure 8.3 Calculated temperature of burned gas T_b and unburned gas T_u (Example 8.1).

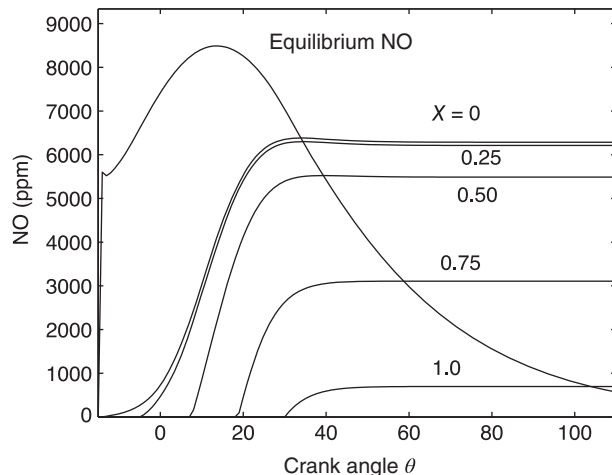


Figure 8.4 Predicted equilibrium and rate-limited NO concentrations (Example 8.1).

with temperature, there are large differences between the nitric oxide concentrations in the first mass to burn ($x = 0$) and last mass to burn ($x = 1$).

Furthermore, it can be seen that when the temperatures drop to about 2000 K, the decomposition rate becomes very slow, and for practical purposes, it may be said that the nitric oxides freeze at a concentration greater than the equilibrium values. The relatively high values of the “frozen” concentrations of nitric oxides in the exhaust are thus a function of the gas temperatures during combustion, not temperatures in the exhaust.

Some additional computational results using the engine of Example 8.1 are now presented to illustrate how nitric oxides in the exhaust depend on various engine parameters such as equivalence ratio, residual fraction, spark timing, engine speed, and cylinder wall temperature. The engine was operated at the baseline conditions given, and the various engine operational parameters were individually varied.

Figure 8.5 shows a result typical of all engines that nitric oxides are maximized with mixtures slightly lean of stoichiometric. Recall that increased temperatures favor nitric oxide formation and that burned gas temperatures are maximized with mixtures that are slightly rich. On the other hand, there is little excess oxygen in rich mixtures to dissociate and attach to nitrogen atoms to form nitric oxide. The interplay between these two effects results in maximum nitric oxides occurring in slightly lean mixtures, where there is a slight excess of oxygen atoms to react with the nitrogen atoms.

As the residual fraction is increased, the NO levels decrease, since the effective specific heat of the combusting mixture is increased. Note that since the program uses FARG to compute the residual gas mixture concentrations, the NO concentration in the residual fraction is not included in the exhaust NO concentrations.

Figures 8.6–8.10 lead to four additional observations, as follows:

- Increased cylinder wall temperature increases the nitric oxides, as the cylinder heat loss is decreased.
- The dependence on spark timing is strong for lean mixtures. As the timing is advanced, the NO levels increase, since the combustion temperatures increase.
- The dependence on engine speed has two competing factors to consider. These are the time available for heat loss and the time available for combustion. As the engine speed

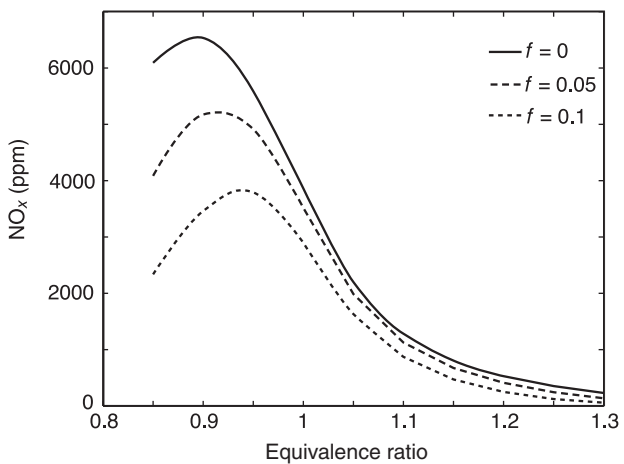


Figure 8.5 Calculated exhaust NO concentration versus equivalence ratio and residual fraction (Example 8.1).

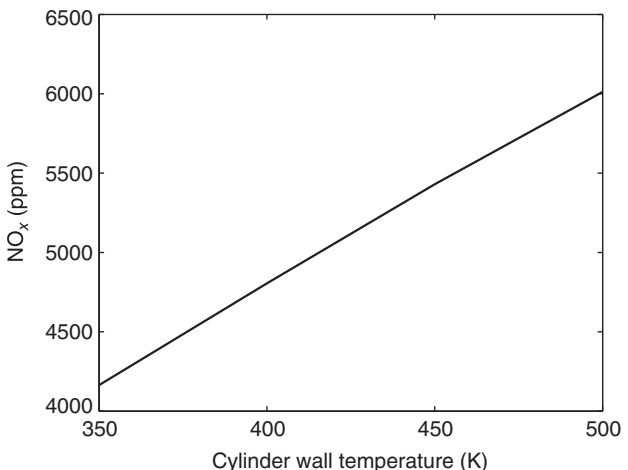


Figure 8.6 NO concentration versus cylinder wall temperature (Example 8.1).

increases, the heat loss decreases, causing an increase in combustion temperature, and the time available for combustion decreases, causing a decrease in combustion temperature. The overall result can be a maximum NO level at an intermediate engine speed.

- Increasing the inlet manifold pressure, and thus the imep, will increase the NO concentration.

At this point, it is useful to discuss the mixing of the burned gases. Fluid elements are mixed with one another via turbulence. If the rate of mixing is faster than the rate at which burned gas is produced, then the burned gas can be assumed to be homogeneous and characterized by a single temperature. If the mixing is slow, then the burned gas must be treated as an ensemble of fluid elements at different temperatures. Experimentally, it is observed that there are different temperature fluid elements in the burned gases but the differences are smaller than predicted. Thus, it can be inferred that mixing occurs, but it is not complete during combustion.

It can be shown using the analyses in Chapter 4 that the energy of the burned gas is a nearly linear function of temperature (i.e., the specific heat variation is relatively small over the range of temperatures encountered in the burned gas) so that for computing cylinder pressure, the overall average gas temperature can be used. The same cannot be said of

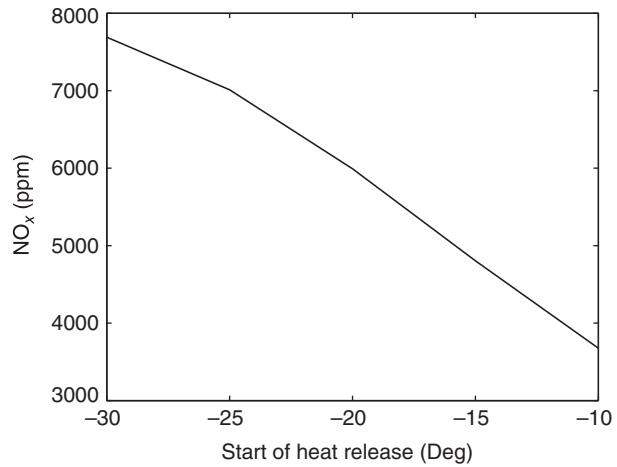


Figure 8.7 NO concentration versus start of heat release (Example 8.1).

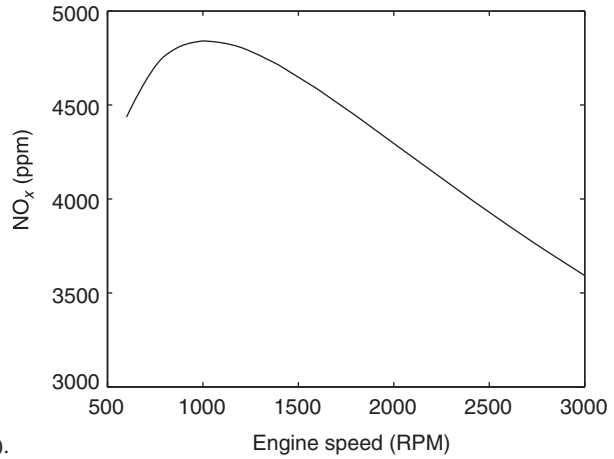


Figure 8.8 NO concentration versus engine speed (Example 8.1).

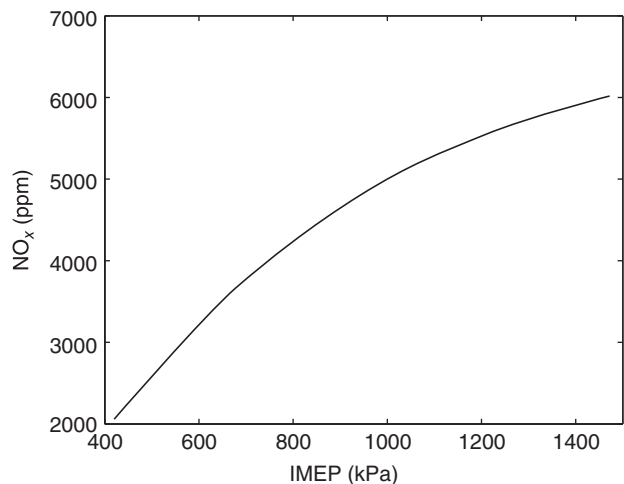


Figure 8.9 NO concentration versus IMEP (Example 8.1).

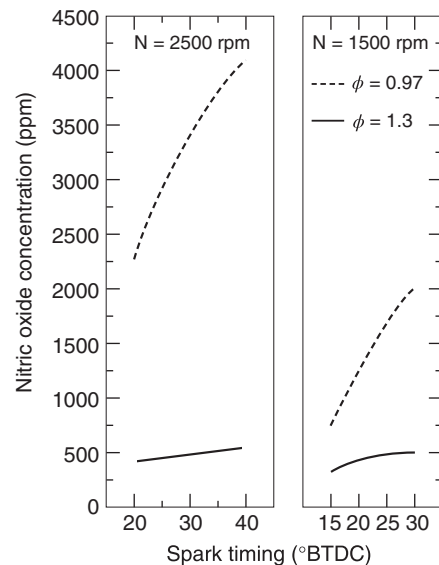


Figure 8.10 Advanced timing increases NO.
Adapted from Huls and Nickol (1967).

nitric oxides since the chemical rates are nonlinear functions of temperature. Using the Farg/Ecp formulation detailed in Chapter 4, Raine et al. (1995) have computed the nitric oxide formation in a multizone model. The NO model above does not include mixing and the temperature gradients due to wall boundary layers. The state of the art requires one to account for these effects to realize good agreement with experiment under all circumstances.

The trends shown above, although typical for homogeneous spark ignition engines, are by no means universal, especially for compression ignition engines. With compression ignition engines, one has to further account for variations in equivalence ratio from fluid element to fluid element. More complex combustion models also use detailed NO_x mechanisms that include more than 50 reactions.

8.3 CARBON MONOXIDE

Carbon monoxide (CO) appears in the exhaust of rich-running engines, since there is insufficient oxygen to convert all the carbon in the fuel to carbon dioxide. Another CO source is the dissociation of CO_2 at high combustion temperatures. The formation and destruction of CO is a principal reaction pathway in hydrocarbon combustion, which essentially consists of breakdown of the hydrocarbon fuel to carbon monoxide, and then the oxidation of carbon monoxide to carbon dioxide. The majority of the heat release for the combustion process occurs during the CO oxidation, given by the following reaction:



The most important engine parameter influencing carbon monoxide levels is the fuel-air equivalence ratio. Thus, results obtained when varying the fuel-air ratio are more or less universal. Typical results are shown in a classic plot of concentration versus fuel-air ratio, Figure 8.11, for a supercharged engine fueled with C_8H_{18} . Notice that at near stoichiometric conditions, carbon monoxide emission is a highly nonlinear function of equivalence ratio. Under these circumstances, in multicylinder engines, it becomes important to ensure that the same fuel-air ratio is delivered to each cylinder. If half the cylinders run lean and the

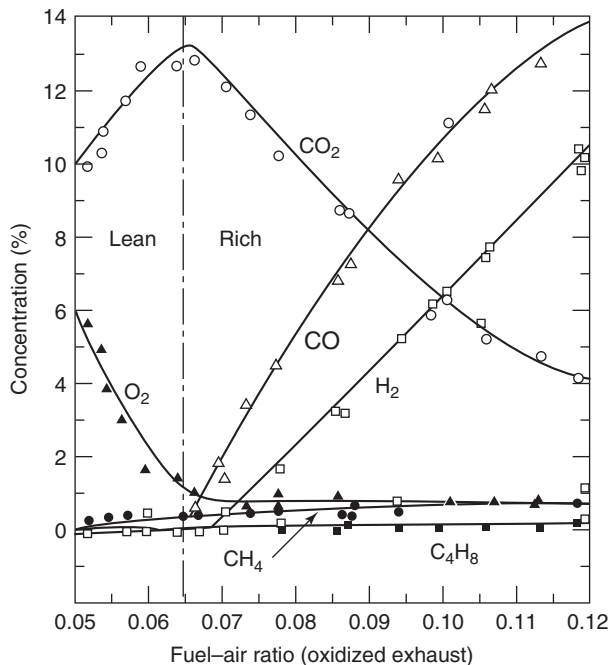


Figure 8.11 Exhaust gas composition versus fuel-air ratio for supercharged engine with valve overlap; fuel C_8H_{18} (Gerrish and Meem, 1943).

other half run rich, then the lean cylinder produces much less CO than the rich cylinders. The average CO emission of such an engine would correspond not to the average equivalence ratio but to an equivalence ratio richer than average, producing more CO than is necessary.

The C-O-H system is more or less in equilibrium during combustion and expansion up to the point where the nitric oxide chemistry freezes. Thus, whether it is a lean- or rich-running engine, one can determine the carbon monoxide concentration during these times using equilibrium chemistry assumptions. Late in the expansion stroke, with the gas temperatures down to about 1800 K, the chemistry in C-O-H systems starts to become controlled by chemical kinetics and is generally frozen by the time blowdown finishes, and the exhaust valve opens. Therefore, the measured values of CO in exhaust gases are lower than the peak values in the combustion chamber, but greater than equilibrium conditions for the exhaust gases.

The rate controlling reactions in the C-O-H systems are three-body recombination reactions such as



Results obtained by using an unmixed model for the burned gas and accounting for these rate-limiting reactions are illustrated in Figure 8.12. In these plots, x is the fraction of the total charge burned when an element is burned and z is the mass fraction that has left the cylinder at the time an element leaves the cylinder. Because that time is unknown, results are given for several values of z for each element. Gas that leaves early ($z \ll 1$) cools more rapidly than gas that leaves last ($z \approx 1$). The results show that gases that burn early carry more CO into the exhaust than gases that burn later. They also show the fortuitous fact that the frozen concentrations are close to the equilibrium concentrations that exist in the

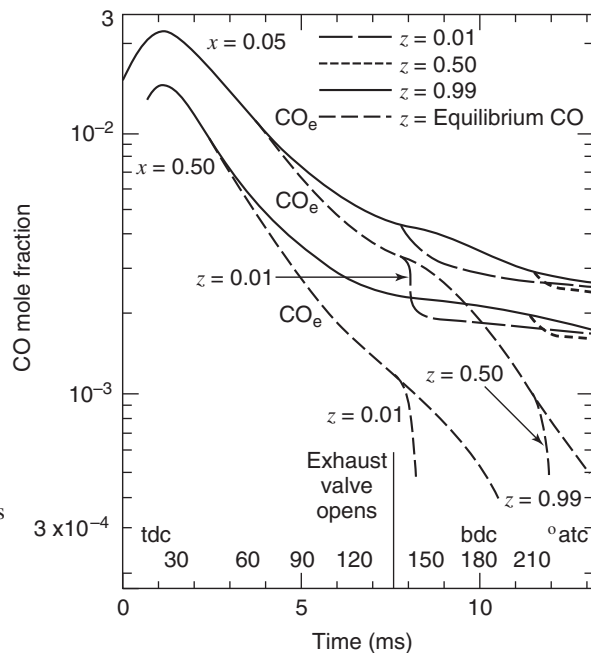


Figure 8.12 CO concentration in two elements of the charge that burned at different times during the combustion process; x is the mass fraction burned when the element burned and z is the fraction of gas that has left the cylinder during the exhaust process (Heywood, 1976).

cylinder at the time the exhaust valve opens. This suggests an approximation that is often used in practice, to assume that the C-O-H system is in equilibrium until the exhaust valve opens, at which time it then freezes instantaneously. In lean-running engines, there appears to be an additional source of CO caused by the flame-fuel interaction with the walls, the oil films, and the deposits. Under these circumstances, the exhaust concentrations are so low that they are not a practical problem, and thus details of these interactions remain largely unexplored.

Thus, the key to minimizing CO emissions is to minimize the times the engine must run rich (such as during start-up). Since diesel engines run lean overall, their emissions of carbon monoxide are low and generally not considered a problem. However, it does appear that direct injection diesel engines emit relatively more CO than indirect injection diesel engines.

8.4 HYDROCARBONS

Hydrocarbon emissions result from the presence of unburned fuel in the exhaust of an engine. Hydrocarbon emissions are greatest during engine start and warm-up, due to decreased fuel vaporization and oxidation. Hydrocarbon emissions from spark ignition engines and diesel engines are discussed separately in this section, as their combustion processes and resulting hydrocarbon emission sources are different.

Hydrocarbon emissions from engines have been grouped into a number of classifications for regulatory purposes. Two general classifications that are widely used are total hydrocarbons (THC) and nonmethane organic gases (NMOG). Methane is a greenhouse gas, but less photochemically reactive than the other hydrocarbons, so it is given a separate classification. The level of hydrocarbon emissions is usually expressed in terms of the total hydrocarbon concentration in parts per million carbon atoms.

Table 8.1 Hydrocarbon Emission Sources

Source	% HC Emissions
Crevices	38
Oil layers	16
Deposits	16
Liquid fuel	20
Flame quench	5
Exhaust valve leakage	5
Total	100

Source: Cheng et al., 1993.

Hydrocarbon fuels are composed of 10–20 major species and some 100–200 minor species. Most of these same species are found in the exhaust. However, some of the exhaust hydrocarbons are not found in the parent fuel but are hydrocarbons derived from the fuel whose structure was altered within the cylinder by chemical reactions that did not go to completion. These hydrocarbons represent about 50% of the total hydrocarbons emitted. The partial reaction hydrocarbon products, including acetaldehyde, formaldehyde, 1,3-butadiene, and benzene, are classified by the U.S. Environmental Protection Agency as toxic emissions.

Spark Ignition Engines

About 9% of the fuel supplied to a spark ignition engine is not burned during the normal combustion phase of the expansion stroke. There are additional pathways that consume 7% of the hydrocarbons during the other three strokes of the four-stroke spark ignition engine so that about 2% of the remaining unburned fuel will go out with the exhaust (Cheng et al., 1993). As a consequence, hydrocarbon emissions cause a decrease in engine thermal efficiency, as well as being an air pollutant. As listed in Table 8.1, six principal mechanisms are believed to be responsible for the alternative oxidation pathways and the exhaust hydrocarbons appearing: (1) crevices, (2) oil layers, (3) carbon deposits, (4) liquid fuel, (5) cylinder wall flame quenching, and (6) exhaust valve leakage.

The crevice mechanism is the most significant, responsible for about 38% of the hydrocarbon emissions. Crevices are narrow regions in the combustion chamber into which a flame cannot propagate. When a flame tries to propagate into a narrow channel, it may or may not be extinguished depending upon the ratio of the channel size and a characteristic of fuel-air mixtures called the quenching distance. By definition, crevices in engines have a characteristic size less than the quenching distance, so the cylinder gases in the crevices will not be consumed during the cylinder combustion process. Crevices occur around the piston, head gasket, spark plug, and valve seats, representing about 1–2% of the clearance volume. The largest crevice is the piston ring–liner crevice region. During compression and the early stages of combustion, the cylinder pressure rises, forcing a small fraction of the fuel–air mixture into the crevices. The crevice temperatures are approximately equal to the cooled wall temperatures, so the density of the fuel–air mixture in the crevices is greater than in the cylinder. When the cylinder pressure decreases during the latter portion of the expansion stroke, the unburned crevice gases will flow back into the cylinder, and contribute to the hydrocarbon emissions.

Wentworth (1971) was one of the first to recognize the importance of the crevice volume around the piston. He designed a special ring package to eliminate it. So far

it has found application only in research engines, where it allows one to make crevice hydrocarbons a negligible source. This allows study of the effects of engine variables on the remaining sources.

Oil layers within an engine can also trap some of the fuel and later release it during expansion. Kaiser et al. (1982) added oil to the engine cylinder and found that the exhaust hydrocarbons increased in proportion to the amount of oil added when the engine was fueled on isoctane. They verified that the increased emissions were unburned fuel and fuel oxidation species and not unburned oil and oil oxidation species. They also did experiments in which the engine was fueled with propane and found no increase in the exhaust hydrocarbons when oil was added. Since propane is not soluble in the oil, they concluded that the increase observed is caused by fuel having been absorbed into the oil layer during compression later being released into the cooling burned gas during the expansion stroke. Thus, one can conclude that hydrocarbon emissions from engines will also depend on the amount of oil in the cylinder and the solubility of the fuel in the oil.

With continued use, carbon deposits build up on the valves, cylinder, and piston heads of internal combustion engines. The deposits are porous, and the sizes of the pores in the deposits are smaller than the quenching distance, and as a result the flame cannot burn the fuel–air–residual gas mixture compressed into the pores. This mixture comes out of the pores during expansion and blowdown. Although some of it will burn up when mixed with the hotter gases within the cylinder, eventually cylinder gas temperatures will have dropped to the point where those reactions fail to complete, resulting in hydrocarbons being emitted from the engine.

Fuel injection past an open valve into the cylinder, as can be the case with port fuel injection, allows the fuel to enter the cylinder in the form of liquid droplets. The less volatile fuel constituents may not vaporize, especially during engine start and warm-up, and be adsorbed in the crevices, oil layers, and carbon deposits.

Flame quenching along the surfaces is a relatively minor mechanism. Daniel (1957) showed that as the flame propagates toward the walls in an engine, it is extinguished at a small but finite distance away from the wall. Flame photographs revealed a dark region near the wall of thickness about one-half the quench distance. Measurements have shown that these hydrocarbons are subsequently oxidized with a high efficiency as they diffuse into the burned gases during expansion, and thus do not contribute significantly to the engine out hydrocarbon emissions.

Hydrocarbons are exhausted from the engine in a complex process. At the end of combustion, there are hydrocarbons all along the walls trapped in deposits, oil layers, or the crevice volume. During expansion, hydrocarbons leave the crevice volume and are distributed along the cylinder wall. When the exhaust valve opens, the large rush of gas escaping drags with it some of the hydrocarbons released from oil layers and deposits. During the exhaust stroke, the piston rolls the crevice volume hydrocarbons that were distributed along the walls into a vortex that ultimately becomes large enough that a portion of it is exhausted.

As shown schematically in Figure 8.13, Tabaczynski et al. (1972) have verified in a water analog experiment that the piston rolls the wall layer into a vortex. They have also measured the hydrocarbon emission mass flow rate as a function of time during the exhaust stroke, plotted in Figure 8.14. Their results show that roughly one-half the hydrocarbons in their engine are exhausted during blowdown and one-half are exhausted during the latter portion of the exhaust stroke. The concentration profile has a peak during blowdown and a sudden increase at about 290°, when the vortex starts to exit the combustion chamber. Two-stroke spark ignition engines can produce a significant amount of hydrocarbon emissions. Short-circuiting of the fuel–air mixture during the scavenging process is the major source

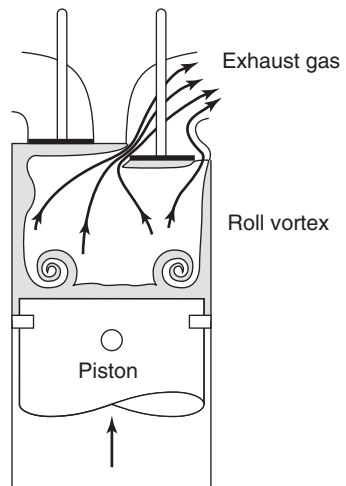


Figure 8.13 Wall vortex formed by exhaust stroke. Adapted from Tabaczynski et al. (1972).

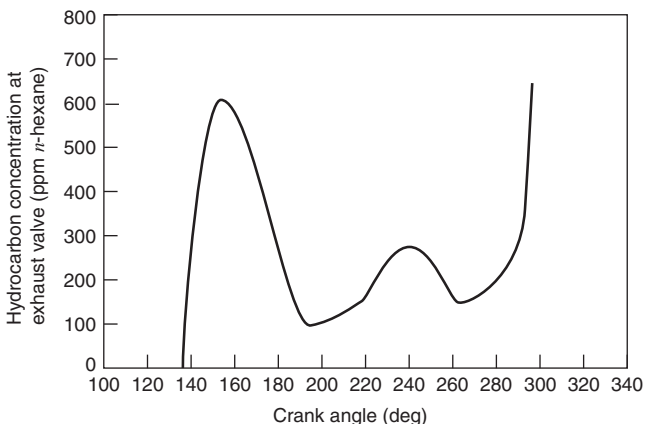


Figure 8.14 Variation of HC concentration at the exhaust valve during the exhaust process. Adapted from Tabaczynski et al. (1972).

of the hydrocarbon emissions. Direct fuel injection is increasingly being used in two-stroke engines to eliminate the short-circuiting of the fuel during scavenging. If crankcase compression is used, the unburnt lubrication oil is also a source of hydrocarbon emissions.

The hydrocarbon story does not end once the hydrocarbons leave the cylinder. There is considerable burn up in the exhaust port. Some emission control techniques use an air pump to inject ambient air into the exhaust manifold to further oxidize the hydrocarbons.

Compression Ignition Engines

Hydrocarbons from diesel engines come primarily from (1) fuel trapped in the injector at the end of injection that later diffuses out, (2) fuel mixed into air surrounding the burning spray so lean that it cannot burn, and (3) fuel trapped along the walls by crevices, deposits, or oil due to impingement by the spray (Greeves et al., 1977 and Yu et al., 1980).

The diesel combustion process relies on mixing fuel and air at the time they are intended to burn. As already mentioned, a combustion delay time is required for enough precursors to form in order for autoignition of the fuel to occur. The delay time is a strong function of equivalence ratio and is a minimum near stoichiometric proportions of fuel and air. However, since the delay time is finite, a fuel-air pocket can be mixed to stoichiometric

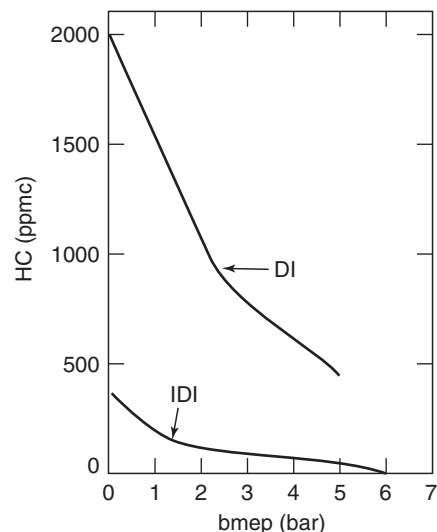


Figure 8.15 HC concentrations as a function of load for direct injection and prechamber engines.
Adapted from Pischinger and Cartellieri (1972).

proportions and then diluted by more air before autoignition occurs in that element. As a result, there are contours for lean equivalence ratios, and when autoignition occurs, there are fuel and air mixed locally to proportions less than the lean flammability limit. Thus, this local fuel mixture does not burn and will increase the hydrocarbon emission levels.

There is also fuel mixed too rich to burn at the time of autoignition. However, it will burn later with additional mixing, provided the gases are hot enough. Some hydrocarbons are also produced because some of this fuel does not have a stoichiometric air–fuel ratio to burn until late in the expansion stroke.

Pischinger and Cartellieri (1972) measured hydrocarbon emissions from both a naturally aspirated direct injection engine and a naturally aspirated indirect injection engine, see Figure 8.15. The results, although unique to the engines in question, indicated that in general, direct injection engines emit more hydrocarbons than indirect injection engines. For the direct injection engine, the hydrocarbons are greatest at light load. Thus, hydrocarbon emissions at idle have been a focus of attention. Pischinger and Cartellieri (1972) found that they can be influenced considerably by rather small changes in engine or injector geometry. Nozzles manufactured by different companies from the same specifications produced very different HC emissions. This illustrates the need for precise control in manufacturing to achieve low emissions. The other variable examined was the piston bowl diameter, which had a negligible influence on the bsfc, caused a slight change in NO_x, and a dramatic change in the hydrocarbons.

8.5 PARTICULATES

A high concentration of particulate matter (PM) is manifested as visible smoke or soot in the exhaust gases. Particulate emissions from engines are regulated, since inhalation of small particulate matter can create respiratory problems. Particulates are a major emissions problem for diesel engines, as their performance is smoke limited. With the mandated use of unleaded fuel for spark ignition engines, particulates are currently not as serious a problem for spark ignition engines as they are for diesel engines.

The U.S. Environmental Protection Agency defines a particulate as any substance other than water that can be collected by filtering diluted exhaust at or below 325 K. The

particulate material collected on a filter is generally classified into two components. One component is a solid carbon material or soot, and the other component is an organic fraction consisting of hydrocarbons and their partial oxidation products that have been condensed onto the filter or adsorbed to the soot. The organic fraction is influenced by the processes that dilute the exhaust with air upon expulsion from the engine. The methods used to measure particulate emissions are dilution tunnels, light absorption, filter discoloration, and filter paper trapped mass, and are discussed in more detail in Chapter 12.

Inspection of the soot fraction under an electron microscope reveals it to be agglomerates of spherical soot particles approximately 200 Å in diameter. The agglomerates can resemble a bunch of grapes in a more or less spherical configuration or be branched and chainlike in character. The agglomerates pose a health hazard because they are too small to be trapped by the nose and large enough that some particle deposition in the lungs occurs. Because of their small size, particles on the order of ~10 microns or less (PM_{10}) can penetrate the deepest part of the lungs such as the bronchioles or alveoli. Particles less than 2.5 microns in diameter ($PM_{2.5}$) are referred to as “fine” particles and are believed to pose the largest health risks. Particles with diameters between 2.5 and 10 microns are referred to as “coarse.”

The organic fraction results from all the processes that generate hydrocarbons and their partial oxidation products. During the dilution process, some of them cool enough to condense or adsorb the soot. In addition, some species originating from the lubricating oil are found in the particulate and may be anywhere from 25 to 75% of the organic fraction (Mayer et al., 1980).

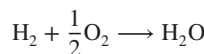
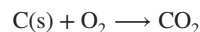
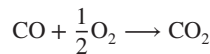
Smoke forms in diesel engines because diesel combustion is heterogeneous. Even though the diesel engine combustion process is lean overall, there are regions of fuel-rich combustion, in the premixed and in the mixing-controlled combustion phases of combustion, as shown by the combustion diagnostics presented in Chapter 7.

Consider a simple soot formation model with a two-stage reaction path for the fuel-rich combustion of a hydrocarbon fuel:

First stage: formation of CO



Second stage: oxidation of CO



According to this model, combustion takes place in two stages. If in the first stage, $c < a/2$, there is not enough oxygen present to convert all the carbon in the fuel to carbon monoxide, the carbon–oxygen ratio > 1 , resulting in the production of soot or solid carbon C(s). This is likely to occur locally within the fuel spray injected into the engine, since it takes time for air and its attendant oxygen to be mixed in with the fuel. The sooting starts with the formation of soot precursor species such as polycyclic aromatic hydrocarbon (PAH) molecules, then the growth and agglomeration of these molecules into particles.

The second stage burns the CO, soot, and other first stage products to completion in a diffusion flame. If there is enough oxygen present, that is, $c \geq a/2$, then the flame is

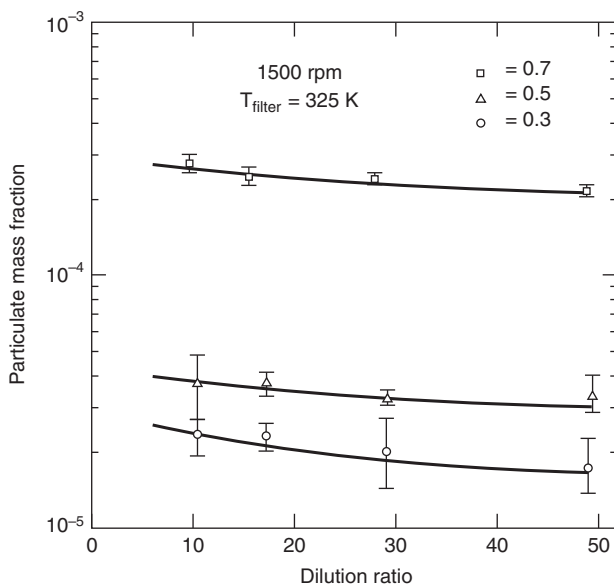


Figure 8.16 Particulate emission versus dilution ratio and equivalence ratio (Gillette and Ferguson, 1983).

clean since no solid carbon is formed. Incomplete oxidation will result in a sooting flame. A measure of the soot tendency of a fuel is termed the smoke point.

The detailed chemical processes leading to the formation of soot remain an active area of research. Measurements indicate that diesel soot particles contain hydrogen as well as carbon, with a C/H ratio of about 8. Particulate measurements by Gillette and Ferguson (1983) obtained using a direct injection diesel with a dilution tunnel are shown in Figure 8.16.

The amount of particulates is extremely dependent on the equivalence ratio. As the equivalence ratio is doubled, the particulates increase by an order of magnitude. Wood et al. (1982) measured the mass spectra of the organic fraction for particulates at three different engine speeds, $\phi = 0.5$, and a dilution ratio of 30. They reported that the spectrum changed with engine speed, particularly for molecular weights greater than 300. The mean molecular weight of the organic fraction was on the order of 200.

It is challenging to diesel engine designers that, generally, when a reduction in nitric oxides has been achieved, it is at the expense of an increase in soot. Using the diesel combustion model of Chapter 7, this is due to the fact that a decrease in the temperature of the diffusion flame will not only decrease the NO_x formation, but also decrease the oxidation of soot.

Figure 8.17 is a representative plot indicating that as the timing is retarded, the NO_x decreases, but the particulates increase, creating a trade-off between NO_x and smoke. Techniques used to decrease soot are to advance the injection timing and decrease the amount of EGR (see Figure 8.18). Another technique used to decrease soot is to increase the in-cylinder turbulence during the late stages of combustion. This increase in turbulence can be accomplished through the use of auxiliary gas injection (Kurtz et al., 2000).

8.6 EMISSIONS REGULATION AND CONTROL

Prior to the mid-1960s, exhaust emissions from vehicles were uncontrolled. Since then exhaust emissions from engines have been regulated worldwide by governmental agencies.

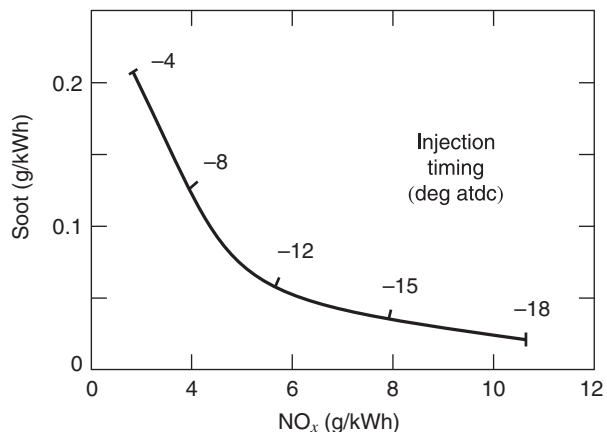


Figure 8.17 Example plot of soot and NO_x trade-off versus injection timing.

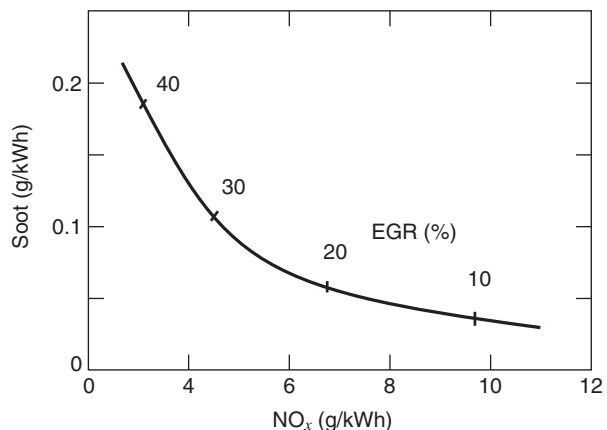


Figure 8.18 Example plot of soot and NO_x trade-off versus EGR.

In the United States, exhaust regulations are set by the U.S. Environmental Protection Agency. In 1966, in response to statewide air quality problems, The state of California introduced hydrocarbon and CO emission limits for vehicles. In 1968, the United States adopted the Clean Air Act that regulated vehicular and stationary emissions on a nationwide basis. The 1968 Clean Air Act requires the EPA to set national ambient air quality standards for “criteria pollutants.” Currently, there are six “criteria pollutants”:

- carbon monoxide,
- nitrogen oxides,
- sulfur oxides,
- ozone,
- lead, and
- particulate matter.

During the intervening years, emission requirements have become increasingly rigorous, and internal combustion engines today are allowed to generate significantly less pollution than their 1968 counterparts. Meeting these emission requirements has been a major challenge and also an opportunity for automotive engineers. As shown in Figure 8.19,

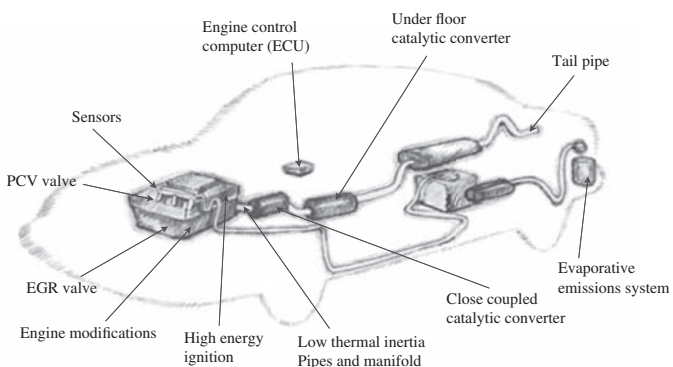


Figure 8.19 Engine emission control methods (Courtesy Englehard Corporation).

there are two basic methods used to control engine emissions: control of the combustion process, and the use of after-treatment devices in the exhaust system.

The current and past emission regulations for vehicles are tabulated in Table 8.2, and the emission standards for certification as a low emission vehicle (LEV) or ultralow emission vehicle (ULEV) are given in Table 8.3. Note that the emission requirements for nonstationary sources (vehicles) have units of grams per mile. The current hydrocarbon emission limits have been reduced to 0.9%, nitrogen oxides to 1.7%, and carbon monoxides to 4%, respectively, of the uncontrolled pre-1968 values.

Internal combustion engines used in applications other than vehicles, for example, large engines used in locomotive and marine applications, stationary power plants, and small engines used in nonroad applications, for example, lawn mowers, snow blowers, chainsaws, pumps, and generators, are also now regulated, since they also have been found

Table 8.2 U.S. Passenger Car and Light-Duty Truck Emission Standards (g/mile)

Year	HC	NO _x	CO
Precontrol	10.60	4.1	84.0
1968	4.10		34.0
1972	3.00	3.1	28.0
1975	1.50	3.1	15.0
1977	1.50	2.0	15.0
1980	0.41	2.0	7.0
1981	0.41	1.0	3.4
1993	0.25	1.0	3.4
1994	0.25	0.4	3.4
2009	0.10	0.07	3.4

Table 8.3 Low Emission Vehicle (LEV) and Ultralow Emission Vehicle (ULEV) Standards (g/mile)

	NMOG ^a	NO _x	CO
LEV	0.075	0.2	3.4
ULEV	0.040	0.2	1.7

^aNonmethane organic gas.

to be significant sources of hydrocarbon and carbon monoxide pollution. Stationary sources are regulated in terms of emissions normalized by the energy output, that is, g/kWh.

Combustion Process Control

Application of technological advances in fuel injectors, oxygen sensors, and onboard computers to engines has increased the control and subsequent optimization of the engine combustion process. Combustion process improvements include increased fluid turbulence and fuel mixing in the cylinder. As discussed earlier in the text, these improvements include modification of the intake valve size and position, and use of direct fuel injection into the cylinder. The use of alternative and oxygenated fuels to reduce emissions is the subject of Chapter 9.

Ignition Timing and Exhaust Gas Recirculation

Two NO_x control measures that have been used in automobile engines since the 1970s are retard of the ignition spark and exhaust gas recirculation (EGR). The aim of these measures is to reduce the peak combustion temperature and thus the formation of NO_x . As shown in Figure 8.7, retarding the spark timing lowers the NO_x , since a greater fraction of the combustion occurs in an expanding volume, lowering the peak cylinder pressure and temperature. However, this also decreases the engine thermal efficiency.

With the use of exhaust gas recirculation, some fraction of the exhaust gas is routed back into the intake manifold. The nonreactive exhaust gas acts as a diluent in the fuel–air mixture, lowering the combustion temperature, and the NO_x formation. This is suggested by the dependence on residual fraction plotted in Figure 8.5. The dilution by EGR of the mixture also reduces the combustion rate, so the spark timing is usually advanced to maintain optimal thermal efficiency. The EGR fraction increases with engine load up to the lean limit, which is about 15–20% of the fuel–air flow rate.

Catalytic Converters

A variety of exhaust after-treatment devices have been added to vehicles to meet emission requirements. These include catalytic converters, NO_x traps, and particulate filters. Currently, the most important after-treatment device is the three-way heterogenous catalyst (Kummer, 1981), invented in 1950 by Eugene Houdry, and first installed on the exhaust systems in passenger cars in 1975. It derives its name from the fact that it works on all three of the gaseous pollutants of concern: carbon monoxide, hydrocarbons, and nitric oxides. Heterogeneous catalysts provide a solid surface for gaseous reactions and reduce the activation energy required for the reaction. When the reactants are adsorbed on the catalyst surface, their internal molecular bonds are weakened, new bonds are more easily formed between fragments of different molecular species, forming reaction products, which then desorb from the catalyst surface back into the exhaust stream.

The surface area for reaction is important as it determines the number of catalytic sites. All catalytic converters are built in a porous honeycomb or pellet geometry (see Figure 8.20) to expose the exhaust gases to a larger surface made of small particles (<50 nm) of one or more of the noble metals, platinum (Pt), palladium (Pd), and rhodium (Rh). Platinum is the principal metal used to remove HC and CO, and rhodium is the principal metal used to remove NO. Figure 8.21 is a schematic of a three-way honeycomb catalyst. In the converter shown, a thin layer of the noble metals covers a washcoat of inert



Figure 8.20 Catalytic converter (Courtesy Englehard Corporation).

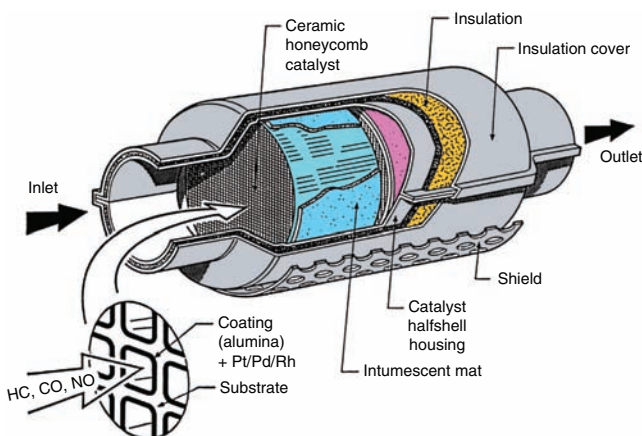
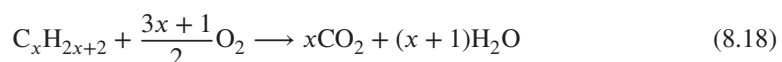


Figure 8.21 Catalytic converter components (Courtesy Englehard Corporation).

alumina Al_2O_3 on a cordierite honeycomb foundation. The operation of the catalytic converter is severely inhibited by lead and sulfur compounds in the exhaust so that vehicular fuels have been reformulated to reduce their lead and sulfur content.

The reactions removing CO and HC are oxidation reactions, as shown in Equations 8.17 and 8.18, thus work best in a lean environment with $\phi < 1$, as the excess oxygen will help drive the reactions to completion.



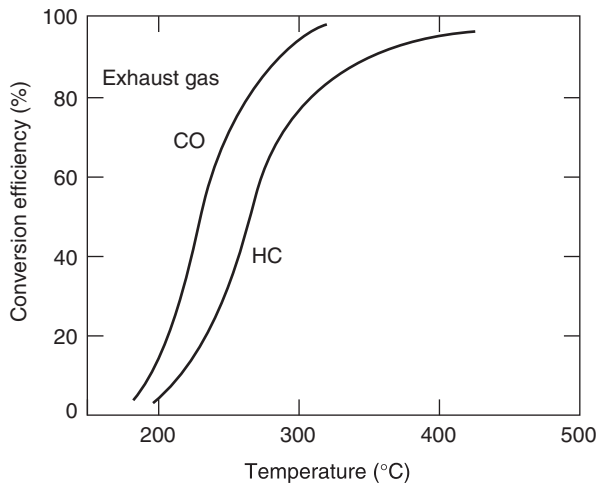


Figure 8.22 Conversion efficiencies for oxidizing catalysts. Adapted from Mondt (2000).

The reactions removing the NO are reduction reactions involving CO, H₂, and HC. Since these are reduction reactions, they work best in a rich environment with $\phi > 1$. Two representative reactions are given in Equations 8.19 and 8.20,



As the exhaust gases flow through the catalyst, the CO and hydrocarbons are removed through the above oxidation reactions forming CO₂ and H₂O products. The oxidation rate of hydrocarbons increases with molecular weight so that the oxidation of low molecular weight fuels such as methane is very slow in the converter. The NO reacts with the CO, hydrocarbons, and H₂ via reduction reactions on the surface of the catalyst.

The catalytic conversion efficiency is plotted versus temperature in Figure 8.22. The temperature at which a catalytic converter becomes 50% efficient is defined as the light-off temperature. The light-off temperature is about 220°C for the oxidation of CO and 270°C for the oxidation of HC. The conversion efficiency at fully warm conditions is about 98–99% for CO and 95% for HC, depending on the HC components. Various measures have been tried to decrease the converter warm-up time, including use of an afterburner, locating the converter or an additional start-up converter closer to the exhaust manifold, and electric heating.

A three-way catalyst will function correctly only if the exhaust gas composition corresponds to nearly 1% stoichiometric combustion. If the exhaust is too lean, nitric oxides are not destroyed and if it is too rich, carbon monoxide and hydrocarbons are not destroyed (see Figure 8.23). Herein lies one constraint that emission control imposes upon engine operation; to use a three-way catalyst, the engine must operate in a narrow window about stoichiometric fuel-air ratios. As discussed in Chapter 12, a closed-loop control system with an oxygen sensor is used to determine the actual fuel-air ratio, and adjust the fuel injector so that the engine operates in a narrow range about the stoichiometric set point. Ordinary carburetors run rich and are not able to maintain the fuel-air ratio in such a narrow set point range.

Analysis of fuel-air cycles in Chapter 4 showed that lean operation was beneficial to the thermal efficiency of the engine, and at first, it appears that operation at only stoichiometric conditions is a rather severe constraint. However, if one realizes that the excess air in

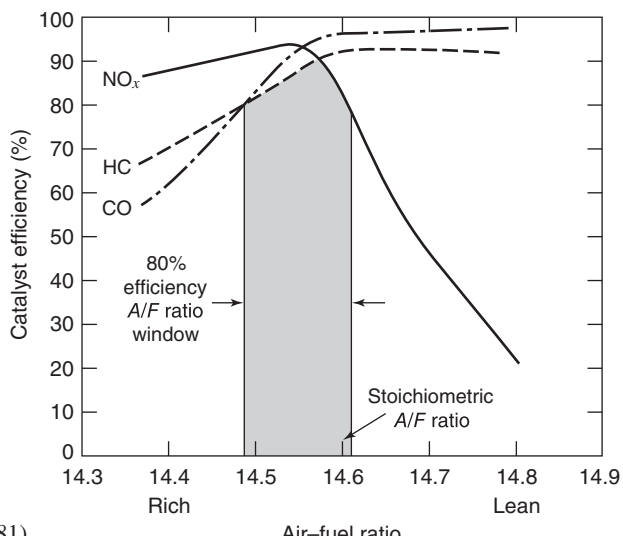


Figure 8.23 Conversion efficiencies for three-way catalyst versus air-fuel ratio (Kummer, 1981).

lean combustion is acting only as a dilutant, then one can appreciate that exhaust gas recirculation can be used to achieve the same effect. The difference is that the excess air is reactive, and the exhaust is nonreactive. Indeed, the fuel-air cycle computations (see Figure 4.6) showed that efficiency increases with increasing residual fraction.

Emission Control Techniques for Lean Combustion Engines

With lean combustion engines, such as diesel and natural gas engines, catalytic converters can be used to oxidize the HC and CO, but reduction of the exhaust nitric oxides is poor because of the high oxygen content of the exhaust gases. Two nitric oxide control techniques that have been developed for lean combustion conditions are selective catalytic reduction (SCR) and the lean NO_x trap.

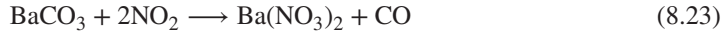
Selective catalytic reaction uses liquid ammonia (NH_3) or urea ($\text{CO}(\text{NH}_2)_2$) sprayed into the exhaust stream. As this mixture flows over a Pt/Rh catalyst, the NO and NO_2 are reduced as indicated by reactions, as shown in Equations 8.21 and 8.22:



This technique was developed by the Englehard Corporation in 1957. For vehicular applications, a mixture of about 32% urea and 68% water, called DEF (diesel exhaust fluid) is typically used, with an injection rate of about 2% of the diesel fuel flow rate. Use of ammonia injection systems is limited to large marine engines and large-bore stationary engines due to the toxicity of ammonia.

The lean NO_x trap technique operates in a cyclic fashion, in which the trap adsorbs and stores NO_x as a nitrate during lean burn operation, and releases it as molecular nitrogen during a short fuel-rich reducing desorption process. The NO_x trap is composed of alkali or alkaline earth materials, such as barium carbonate, that absorb and form nitrate species on the surface of the catalyst during the adsorption process. Once these nitrate species saturate the catalyst, the catalyst is regenerated by operating the engine in a rich condition to reduce the NO_2 to N_2 . After regeneration, the alkali or alkaline earth materials are again available for NO_2 trapping.

During the lean burn adsorption process, barium nitrate is formed from barium carbonate, as indicated by reaction, as shown in the Equation 8.23 below:



During the short fuel-rich desorption step, excess fuel is used to produce molecular nitrogen as indicated by reactions shown in the Equations 8.24 and 8.25:



The engine control system controls the cycling rate between lean and periodic-rich burn conditions to achieve a desired NO_x conversion efficiency. Lean NO_x traps have been used on diesel, gasoline, and natural-gas-fueled engines, in which the engine fuel was used as a fuel source for the rich reducing step, so this technique has a fuel penalty. Additional information about the lean NO_x trap technique is given by West et al. (2004), and diesel emission reduction is given in the review by Johnson (2011).

8.7 REFERENCES

- CHENG, W.K., D. HAMRIN, J. HEYWOOD, S. HOCHGREB, K. MIN, and M. NORRIS (1993), "An Overview of Hydrocarbon Emissions Mechanisms in Spark Ignition Engines," SAE paper 932708.
- DANIEL, W. (1957), "Flame Quenching at the Walls of an Internal Combustion Engine," Sixth Symposium (International) on Combustion, p. 886, Reinhold, New York.
- FENIMORE, C. (1971), "Formation of Nitric Oxide in Premixed Hydrocarbon Flames," Thirteen Symposium (International) on Combustion, the Combustion Institute (Pittsburgh), pp. 373–379.
- GERRISH, H. and J. MEEM (1943), "The Measurement of Fuel Air Ratio by Analysis of the Oxidized Exhaust Gas," NACA report 757.
- GILLETTE, A. and C. FERGUSON (1983), "Measurement and Analysis of the Particulate Emission from a Direct Injection Diesel," *Particulate Sci. and Tech.*, Vol. 1, No. 1, pp. 77–90.
- GREEVES, G., I. KHAN, C. WANG, and I. FENNE (1977), "Origins of Hydrocarbon Emissions from Diesel Engines," SAE paper 770259.
- HANSON, R. and S. SALIMIAN (1984), "Survey of Rate Constants in the N/H/O System," Chapter 6 in Combustion Chemistry (W. Gardiner, Jr., ed.), Springer-Verlag, New York, pp. 361–421.
- HEYWOOD, J. (1976), "Pollutant Formation and Control in Spark Ignition Engines," *Prog. Energy Combust. Sci.*, Vol. 1, pp. 135–164.
- HULS, T. and H. NICKOL (1967), "Influence of Engine Variables on Exhaust Oxides of Nitrogen Concentrations from a Multicylinder Engine," SAE paper 670482.
- JOHNSON, T. (2011), "Diesel Emissions in Review," SAE Paper 2011-01-0304.
- KAISER, E., J. LORUSSO, G. LAVOIE, and A. ADAMCZYK (1982), "The Effect of Oil Layers on the Hydrocarbon Emissons from Spark Ignited Engines," *Combustion Sci. Tech.*, Vol. 28, pp. 69–73.
- KOMIYAMA, K. and J. HEYWOOD (1973), "Predicting NOx Emissions and Effects of Exhaust Gas Recirculation in Spark-Ignition Engines," SAE paper 730475.
- KUMMER, J. (1981), "Catalysts for Automobile Emission Control," *Prog. Energy Combust. Sci.*, Vol. 6, pp. 177–199.
- KURTZ, E., D. FOSTER, and D. MATHER (2000), "Parameters that Affect the Impact of Auxiliary Gas Injection in a DI Diesel Engine," SAE Paper 2000-01-0233.
- LAVOIE G., J. HEYWOOD, and J. KECK (1970), "Experimental and Theoretical Study of Nitric Oxide Formation in Internal Combustion Engines," *Combust. Sci. Technol.*, Vol. 1, pp. 313–326.

- MAYER, W., D. LECHMAN, and D. HILDENS (1980), "The Contribution of Engine Oil to Diesel Exhaust Particulate Emissions," SAE paper 800256.
- MILLER, J., and BOWMAN, C. (1989), "Mechanism and Modeling of Nitrogen Chemistry in Combustion," *Prog. Energy Combust. Sci.*, Vol. 15, pp. 287–338.
- MONDT, J. (2000), *Cleaner Cars: The History and Technology of Emission Control Since the 1960's*, SAE International, Warrendale, Pennsylvania.
- PISCHINGER, R. and W. CARTELLIERI (1972), "Combustion System Parameters and Their Effect Upon Diesel Engine Exhaust Emissions," SAE paper 720756.
- RAINE, R., C. STONE, and J. GOULD (1995), "Modeling of Nitric Oxide Formation in Spark Ignition Engines with a Multizone Burned Gas," *Combust. Flame*, Vol. 102, pp. 241–255.
- TABACZYNSKI, R., J. HEYWOOD, and J. KECK (1972), "Time Resolved Measurements of Hydrocarbon Mass Flowrate in the Exhaust of a Spark Ignition Engine," SAE paper 72112.
- WENTWORTH, J. (1971), "Effect of Combustion Chamber Surface Temperature on Exhaust Hydrocarbon Concentration," SAE paper 710587.
- WEST, B., S. HUFF, J. PARKS, S. LEWIS, J. CHOI, W. PARTRIDGE, and J. STOREY (2004), "Assessing Reductant Chemistry During In-Cylinder Regeneration of Diesel Lean NO_x Traps," SAE Paper 2004-01-3023.
- WOOD, K., J. CIUPEK, R. COOKS, and C. R. FERGUSON (1982), "Characterization of Diesel Particulates by Mass Spectrometry Including MS-MS," SAE paper 821217.
- YU, R., V. WONG, and S. SHAHED (1980), "Sources of Hydrocarbon Emissions from Direct Injection Diesel Engines," SAE paper 800049.
- ZELDOVICH, Y. (1946), "The Oxidation of Nitrogen in Combustion and Explosions," *Acta Physiochim. U.R.S.S.*, Vol. 21, pp. 577–628.

8.8 HOMEWORK

- 8.1** Consider an equilibrium mixture of exhaust gases composed of O₂, N₂, and NO. Using the equilibrium constant K_p equation for the reaction $\frac{1}{2} \text{O}_2 + \frac{1}{2} \text{N}_2 \rightleftharpoons \text{NO}$ (see Chapter 3), plot the equilibrium mole fraction of NO as a function of temperature from 1000 to 4000 K for (a) $P = 1 \text{ atm}$, and (b) $P = 40 \text{ atm}$.
- 8.2** The rate of change of nitric oxide mass fraction for a fluid element because of chemical reaction is given by Equation 8.10. The mass fraction can also change because of NO convected in and out of the fluid element. Consider the control volume shown in Figure 8.24. Write an expression for the rate of change of nitric oxide mass fraction for this element assuming the fluid entering is devoid of nitric oxides, the fluid leaving has the same properties as fluid in the element, and the generation of NO within the control volume is given by Equation 8.10.

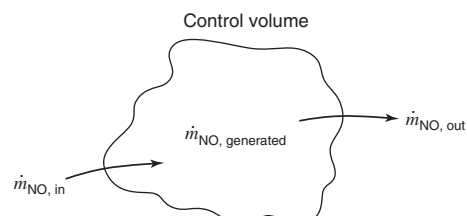


Figure 8.24 Illustration for Homework Problem 8.2.

- 8.3** The initial NO formation rate ($\text{mol}/(\text{cm}^3\text{s})$) can be estimated (Heywood, 1976) given the equilibrium (e) concentrations (mol/cm^3) of oxygen and nitrogen, from the relation

$$\frac{d[\text{NO}]}{dt} = \frac{6 \times 10^{16}}{T^{1/2}} \exp\left(\frac{-69,090}{T}\right) [\text{O}_2]_e^{1/2} [\text{N}_2]_e \quad (8.26)$$

Plot the exponential dependence of NO formation on temperature by computing the formation rate over a range of temperatures from 1000 to 3000 K at $P = 10$ bar and equilibrium mole fractions of $y_{\text{N}_2} = 0.79$ and $y_{\text{O}_2} = 0.20$.

- 8.4** A CFR engine is operated with methane using the conditions given in Example 8.1. The start of heat release is -15° atdc and the burn duration is 40° . The inlet conditions are $P_1 = 100$ kPa and $T_1 = 350$ K. Using the Homogeneous.m program, plot the burn fraction, pressure, burned and unburned temperatures, equilibrium and rate-limited NO values as a function of crank angle.
- 8.5** A CFR engine is operated with gasoline using the conditions given in Example 8.1. The start of heat release is -25° atdc and the burn duration is 60° . The inlet conditions are $P_1 = 100$ kPa and $T_1 = 350$ K. Using the Homogeneous.m program, plot the maximum burned temperature T_b and the exhaust NO concentration as a function of compression ratio. Vary the compression ratio from 7 to 12. Is engine knock a concern under these conditions?
- 8.6** What are the equilibrium constants K_p at 650 K for the two ammonia reactions given by Equations 8.21 and 8.22?
- 8.7** A large-bore two-stroke stationary engine uses an ammonia injection system to remove NO from the exhaust. The engine has a displacement of 300 L and speed of 400 rpm. It is fueled with methane, operates lean at an equivalence ratio of 0.80, and has a delivery ratio of 0.92. If 0.1% of the nitrogen entering the exhaust has been converted to NO during the combustion process, what is the mass flow (kg/h) of ammonia needed to reduce the NO to N_2 ?
- 8.8** Use the equilibrium combustion solver program ecp.m to compute the exhaust CO concentration for an engine fueled with C_7H_{17} . Plot the CO concentration versus ϕ for two different gas temperatures at the time of exhaust valve opening, $T = 1800$ K and $T = 1500$ K. Assume an exhaust pressure of 200 kPa.

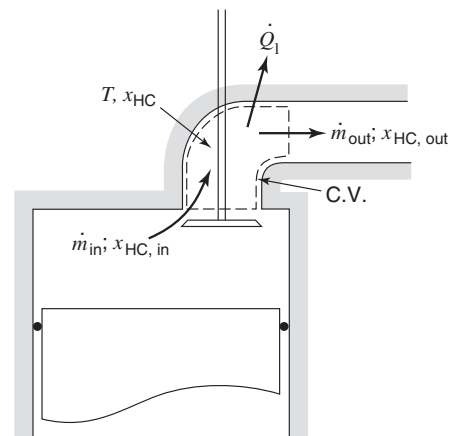


Figure 8.25 Illustration for Homework Problem 8.9.

- 8.9** Reaction of hydrocarbons in the exhaust port of an engine is an important process since it alters the HC emission levels from gasoline and diesel engines. The rate of change of the HC mass fraction due to chemical reaction is given by

$$-\frac{dx_{\text{HC}}}{dt} = A x_{\text{HC}} x_{\text{O}_2} \exp\left(\frac{-E}{RT}\right)$$

Assuming that gases in the port shown in Figure 8.25 are well mixed, show that

$$\left(\frac{dx_{\text{HC}}}{dt}\right)_{\text{c.v.}} = \frac{\dot{m}_{\text{in}}}{m} (x_{\text{HC,in}} - x_{\text{HC}}) - A x_{\text{HC}} x_{\text{O}_2} \exp\left(\frac{-E}{RT}\right)$$

- 8.10** As an engine warms up, clearance between various parts change because of differing amounts of thermal expansion. Explain how this can affect hydrocarbon emissions from a spark ignition, homogeneous charge engine.
- 8.11** Explain how blowby can affect hydrocarbon exhaust emissions (not crankcase emissions that are no longer a problem). Specifically discuss the influence of engine speed.

Chapter 9

Fuels

9.1 INTRODUCTION

So far our attention has been on fuels composed of only one chemical species. However, a typical gasoline or diesel fuel may consist of 100 different hydrocarbons and another 100–200 trace species. In this chapter, we discuss why fuels are so complex, how they are manufactured, their thermodynamic properties, and how they perform in engine applications.

Gasoline and diesel fuels for internal combustion engines are primarily obtained by distillation from petroleum oil. Petroleum oil has a relatively low cost and a high-energy density. It is a fossil fuel composed from ancient organic materials. Formation of petroleum and natural gas reservoirs occurs underground during the pyrolysis of hydrocarbons in a variety of endothermic reactions at high-temperature and/or pressure. Wells are drilled into oil reservoirs to extract the crude oil. In 1858, Edwin Drake drilled the first U.S. oil well, a 21-m deep well in Titusville, Pennsylvania. He is credited with inventing the technique of drilling inside a pipe casing to prevent water seepage. Innovations in the technology for oil recovery have allowed deeper and deeper wells to be drilled. For example, oil is currently pumped from reservoirs about 3000 m below the North Sea seabed in Europe.

The petroleum industry classifies crude oil by its geographical origin, its API (American Petroleum Institute) gravity (light or heavy), and its sulfur content (low sulfur is labeled as sweet, and high sulfur is labeled as sour). Light crude oil produces a higher gasoline fraction. Sweet crude oil is more valuable than sour crude oil because it requires less refining to meet sulfur standards.

The identified worldwide crude oil reserves are estimated by the American Petroleum Institute to be about 1 trillion barrels, with 0.6 trillion barrels remaining to be identified. At present consumption rates, at about 30 billion barrels per year, it is estimated that petroleum reserves will last for 60–95 years. Technological advances in extraction have created continual increases in the size of the worldwide petroleum reserves. For example, in 1950 the identified worldwide petroleum reserves were estimated to be about 0.09 trillion barrels, so in the last 60 years the identified petroleum reserves have increased tenfold. To put the consumption of petroleum into perspective, about 0.7 trillion barrels of petroleum have been consumed since the advent of the industrial revolution. The current U.S. production of crude oil is about 10 million barrels per day. The recent invention and commercialization of hydraulic fracturing, commonly known as “fracking”, has enabled greater production of petroleum and natural gas from underground shale formations.

Since petroleum contains carbon, its combustion produces carbon dioxide, a greenhouse gas linked to global warming. There are a number of private and governmental

initiatives underway to reduce the amount of greenhouse gas emissions from internal combustion engines. These initiatives include increased combustion and process efficiency, and increased use of biofuels. The price of crude oil is dependent on geopolitical factors, and has risen over the last 50 years to a maximum of about \$100 U.S. per barrel. At that price level, alternative fuels such as biodiesel are becoming economically competitive.

The earliest internal combustion engines in the late 1800s were fueled with coal gas. Coal gas is obtained by the coking, that is, partial pyrolysis of coal, similar to the process of producing charcoal from wood. The pyrolysis process drives off the volatile constituents in the coal. Coal gas is typically 50% hydrogen, 35% methane, 10% carbon monoxide, and other trace gases such as ethylene. Coal gas was the primary source of gaseous fuel in the United States until replaced by natural gas in the 1940s. Use of gaseous fuels such as methane for internal combustion engines is increasing, due to increased availability and relatively lower emissions relative to liquid fuels.

9.2 HYDROCARBON CHEMISTRY

Gasoline and diesel fuels are composed of blends of hydrocarbons, grouped into families of hydrocarbon molecules termed paraffins, olefins, naphthenes, and aromatics. The hydrocarbon families each have characteristic carbon–hydrogen bond structures and chemical formulae.

Paraffins (alkanes) are molecules in which carbon atoms are chained together by single bonds. The remaining bonds are with hydrogen. They are called saturated hydrocarbons because there are no double or triple bonds. The general formula for the paraffin family is $C_nH_{(2n+2)}$. The number of carbon atoms is specified by a prefix:

1-meth	2-eth	3-prop	4-but
5-pent	6-hex	7-hept	8-oct
9-non	10-dec	11-undec	12-dodec

Paraffin is designated as an alkane by the suffix *-ane*. Examples of paraffins are methane, CH_4 , and octane, C_8H_{18} , as shown schematically in Figure 9.1. Compounds with straight chains are also labeled as normal or *n*-. For example, octane is sometimes called normal octane or *n*-octane. Isooctane, shown in Figure 9.1, is an example of a branched chain isomer of octane. That is, it has the same number of carbon atoms as octane but not in a straight chain. The group CH_3 attached to the second and fourth carbons from the right is called a methyl radical, *meth* because it has one carbon atom and *yl* because it is of the alkyl radical family C_nH_{2n+1} . Isooctane is more properly called 2,2,4-trimethylpentane, 2,2,4 because methyl groups are attached to the second and fourth carbon atoms, *trimethyl* because three methyl radicals are attached, and *pentane* because the straight chain has five carbon atoms.

Olefins (alkenes) are molecules with one or more carbon–carbon double bonds. Monoolefins have one double bond, the general formula is C_nH_{2n} , and their names end with *-ene*. For example, 1-octene, C_8H_{16} is shown in Figure 9.1. Isomers are possible not only by branching the chain with the addition of a methyl radical but also by shifting the position of the double bond without changing the carbon skeleton. Olefins with more than one carbon–carbon double bond are undesirable components of fuel that lead to storage problems. Consequently, they are refined out and the only olefins of significance in diesel fuel or gasoline fuel are monoolefins.

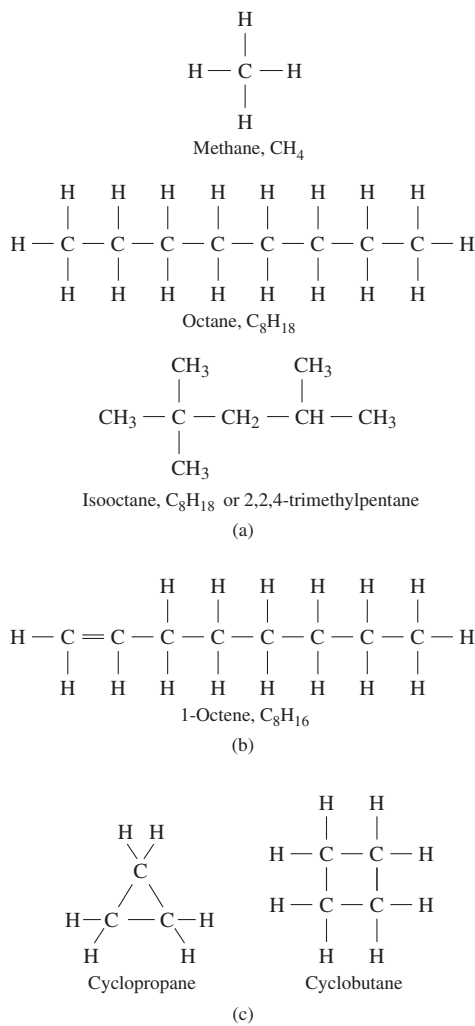
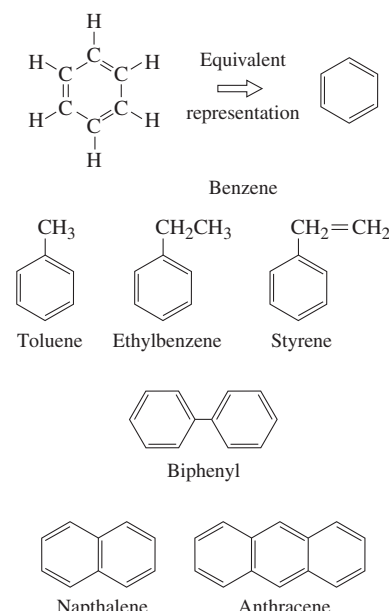


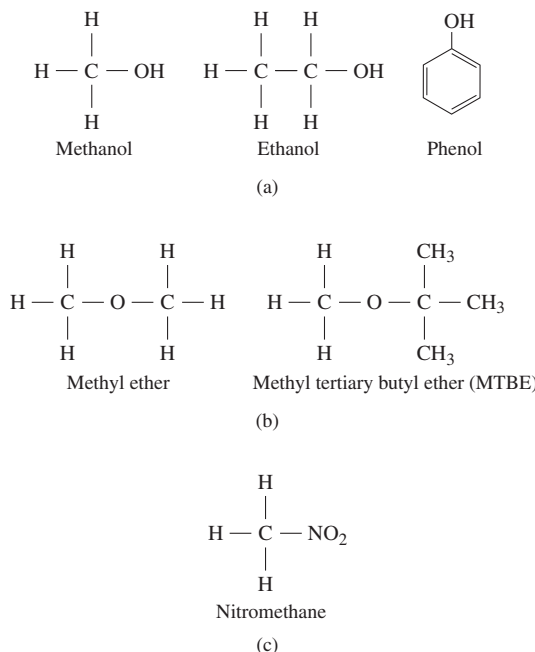
Figure 9.1 (a) Paraffins, (b) olefins, and (c) naphthenes.

Naphthenes (cycloalkanes) have the same general formula as olefins, C_nH_{2n} , but there are no double bonds. They are called *cyclo* because the carbon atoms are in a ring structure. Two examples are cyclopropane and cyclobutane, shown in Figure 9.1. Cycloalkane rings having more than six carbon atoms are not as common.

Aromatics are hydrocarbons with carbon–carbon double bonds internal to a ring structure. The most common aromatic is benzene, shown schematically in Figure 9.2. Benzene is a regulated toxic compound, as it is a known carcinogen. Notice that the double bonds alternate in position between the carbon atoms. This makes the molecule's bonds difficult to break so that a greater temperature is required to initiate combustion. As a result, aromatics are desirable in gasoline since they increase the octane number. Aromatics are undesirable components of diesel fuels. Some common aromatics (toluene, ethylbenzene, and styrene) have groups such as methyl radicals substituted for hydrogen atoms, and others (biphenyl) have more than one ring. Finally, there are polycyclic aromatic hydrocarbons (PAH) that are aromatics with two carbon atoms shared between more than one ring (naphthalene and anthracene).

**Figure 9.2** Aromatics.

An alcohol is a partially oxidized hydrocarbon, formed by replacing a hydrogen atom with the hydroxyl radical OH. If the hydrogen atom attached to an aromatic ring is replaced by the hydroxyl radical, the molecule is called a phenol. Ethers are isomers of alcohol with the same number of carbon atoms. Some examples, shown in Figure 9.3, are methanol, ethanol, phenol, and methyl ether.

**Figure 9.3** (a) Alcohols, (b) ethers, and (c) nitroparaffins.

Nitromethane, CH_3NO_2 , is formed from a paraffinic hydrocarbon by replacing a hydrogen atom with a NO_2 group, as shown in Figure 9.3. It has twice the bound oxygen as monohydric alcohols, and can combust without air. At ambient temperature, it is a liquid, and it is widely used as a drag racing fuel.

9.3 REFINING

Crude oil contains a large number of various hydrocarbon fractions. For example, 25,000 different compounds have been found in a sample of petroleum-derived crude oil. The compounds range from gases to viscous liquids and waxes. The purpose of a refinery is to physically separate crude oil into various fractions, and then chemically process the fractions into fuels and other products. A full-scale crude oil refinery produces fuels for engines (gasoline, diesel, and jet), fuels for heating (burner, coke, kerosene, and residual), chemical feedstock (aromatics and propylene), and asphalt. On an average, a refinery will refine about 40% of the input crude oil into gasoline, 20% into diesel and heating fuel, 15% into residual fuel oil, 5% into jet fuel, and the remainder into the other listed hydrocarbons. The fraction separation process is called distillation and the device employed is a fractionating column.

The generic features of a small-scale fractionating column or still are illustrated in Figure 9.4. The fractions at the top of the column have lower boiling points than the fractions at the bottom. The column is heated preferentially, boiling off the lighter components. The classification of the various fractions is arbitrary. In the order in which they leave the still, the various fractions are commonly referred to as naphtha, distillate, gas oil, and residual oil. Further subdivision uses the adjectives *light*, *middle*, or *heavy*. The adjectives *virgin* or *straight run* are often used to signify that no chemical processing has been done to the fraction. For example, since light, virgin naphtha can be used as gasoline, it is often called straight run gasoline. The physical properties of any fraction depend on the distillation temperatures of the products collected.

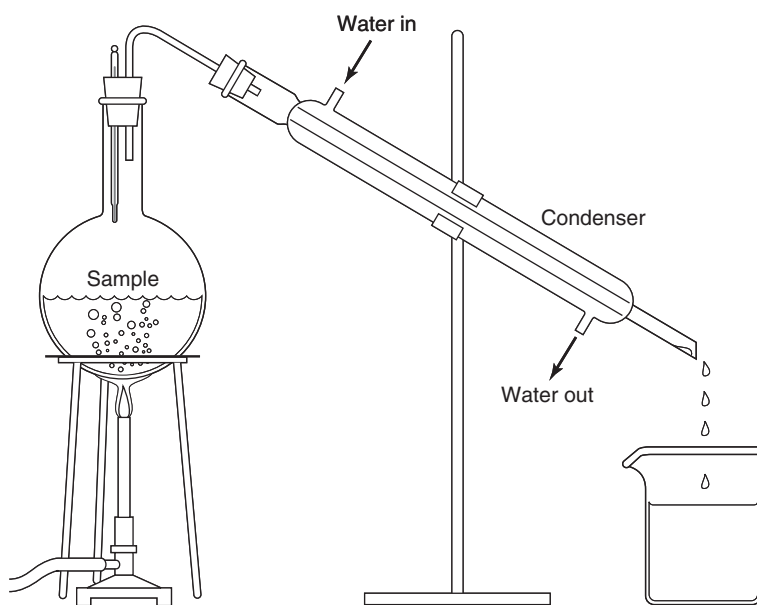


Figure 9.4 Distillation process.

A broad cut fraction is collected over a large range of distillation temperatures, a narrow cut over a small range, a light fraction over a low-temperature range, and a heavy fraction over a high-temperature range. Gasoline fuel is a blend of hydrocarbon distillates with a range of boiling points from about 25°–225°C, and diesel fuel is a blend of hydrocarbon distillates with a range of boiling points from about 180°–360°C.

Chemical processing is required to convert one fraction into another. For example, a crude might yield, on an energy basis, 25% straight run gasoline but the product demand could be 50%. In this situation, the other 25% would be produced by chemical processing of some other fraction into gasoline. Chemical processing is also used to upgrade a given fraction. For example, straight run gasoline might have an octane number of 70, whereas the product demand could be for an octane number of 90. In this case, chemical processing would be needed to increase the octane number from 70 to 90.

Alkylation is used to increase the molecular weight and octane number of gasoline by adding alkyl radicals to a gaseous hydrocarbon molecule. Light olefin gases are reacted with isobutane using a catalyst. Isooctane results from reacting butene with isobutane. This process requires relatively low-temperature (275 K) and pressure (300 kPa) and therefore consumes relatively less energy than other refining processes.

Catalytic cracking uses activated catalysts to break the molecular chains of a distillate to produce naphthas. Naphtha is a liquid mixture consisting of straight-chained and cyclic aliphatic hydrocarbons having from five to nine carbon atoms per molecule. The naphtha products of catalytic cracking are blended with other hydrocarbons to produce high octane number gasolines. The reactions occur at high-temperature (700–800 K) and at low to moderate pressure (200–800 kPa). Considerable energy is consumed in the process.

Reforming refers to reactions designed to alter molecular structure to yield higher octane gasoline (e.g., conversion of paraffins into aromatic hydrocarbons). This is often done using catalysts in a hydrogen atmosphere at high-temperature (800 K) and high pressure (3000 kPa). Considerable hydrogen is produced as a result of the reaction:



Coking is the process used to convert heavy reduced crude fraction to the more usable naphtha and distillate fractions. The reduced crude is heated in an oven. Upon heating, the molecules undergo pyrolytic decomposition and recombination. The average molecular weight of the fraction remains the same, but a greater spectrum of components is produced. The heaviest component, called coke, is a solid carbon material similar to charcoal.

9.4 FUEL PROPERTIES

The thermophysical properties, that is, enthalpy, specific heat, and entropy, of some single hydrocarbons were given in Chapter 3. In general, the equivalent chemical formula C_aH_b of a hydrocarbon–fuel mixture can be determined given the molecular weight M and the hydrogen to carbon ratio HC of the fuel:

$$a = M / (12.01 + 1.008 \text{ HC}) \quad \text{and} \quad b = \text{HC} \cdot a$$

Using the first law, the enthalpy of formation, h_f^o , at 298 K for a hydrocarbon fuel of formula C_aH_b can be determined from the heat of combustion q_c and the product enthalpies, Equation 9.1:

$$h_f^o = q_c + ah_{f,\text{CO}_2} + \frac{b}{2} \left[h_{f,\text{H}_2\text{O}} - (1 - \chi)h_{fg,\text{H}_2\text{O}} \right] \quad (9.1)$$

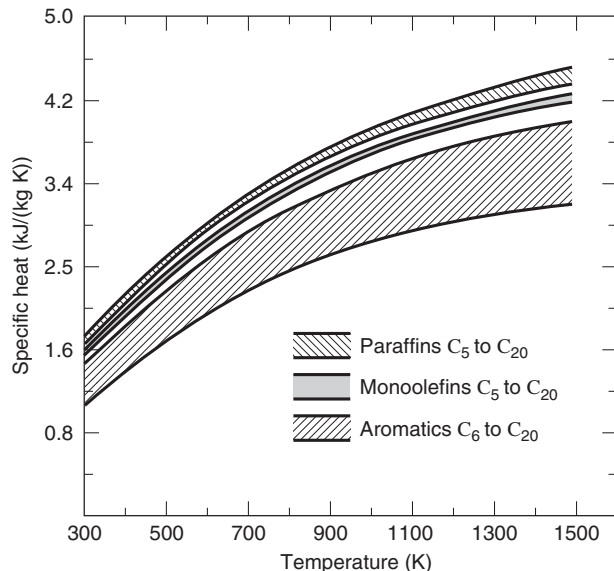


Figure 9.5 Specific heat of various hydrocarbons.

where χ is the quality of water in the products. The lower heat of combustion assumes $\chi = 1.0$, whereas the higher heat of combustion assumes $\chi = 0$.

Figures 9.5 and 9.6 show the ideal gas constant pressure specific heat, $c_{p,i}$ of the hydrocarbon constituents (paraffins, monoolefins, aromatics, naphthenes, and alcohols) found in fuels as a function of temperature. The figures show that on a per unit mass basis the specific heat depends on temperature and carbon type and is a weak function of carbon number. This is not unexpected since the specific heat of a molecule depends on the number and type of bonds. Assuming the specific heat per bond is constant, one expects the specific heat to increase with the number of bonds, and on a per mole basis this is true. However, since both the number of bonds and the mass of the molecule scale with the number of carbon atoms, the specific heat is nearly constant on a per unit mass basis.

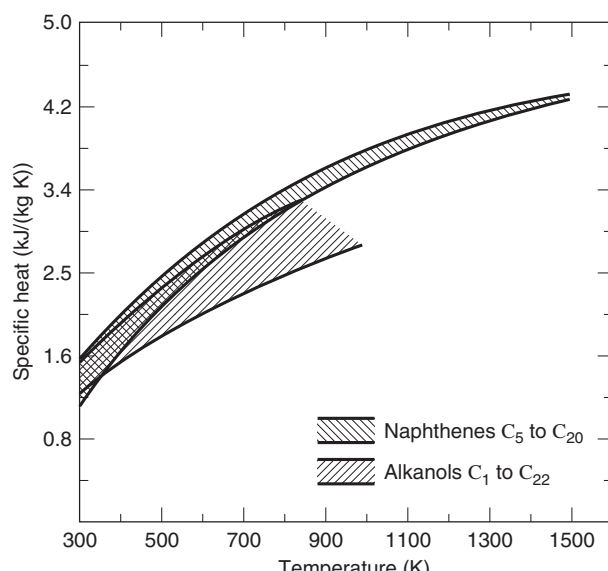


Figure 9.6 Specific heat of various hydrocarbons.

Table 9.1 Specific Heat Curve-Fit Coefficients for Fuel Components

Type	<i>i</i>	<i>a_i</i>	<i>b_i</i>	<i>c_i</i>
Paraffins	1	0.33	5.0	-1.5
Monoolefins	2	0.33	4.6	-1.3
Aromatics	3	0.21	4.2	-1.3
Naphthenes	4	0.04	5.0	-1.4
Alkanols	5	0.50	3.3	-0.71

The results shown are correlated by Equation 9.2:

$$c_{p,i} = a_i + b_i t + c_i t^2 \quad (9.2)$$

where $t = T(\text{K}) / 1000$, and $300 < T < 1500 \text{ K}$. The a_i, b_i, c_i coefficients of Equation 9.2 are listed in Table 9.1 for various hydrocarbon constituents. The specific heat, c_p of a motor fuel is

$$c_p = \sum_i x_i c_{p,i} \quad (9.3)$$

where x_i is the mass fraction of component i .

The absolute entropy (kJ/(kmol K)) of a liquid hydrocarbon fuel with formula $C_a H_b O_c N_d$ has been correlated by Ikumi and Wen (1981):

$$s = 4.69a + 18.41b + 44.55c + 85.97d \quad (9.4)$$

The octane numbers of various single hydrocarbon fuels are tabulated in Table 9.2. In general, it has been found that the octane number is increased by reducing the straight chain length. This can be accomplished by reducing the total number of carbon atoms or by rearranging them into a branched chain structure. These generalizations are illustrated in Figure 9.7. The critical compression ratio is determined by increasing the compression ratio of a CFR engine ($N = 600 \text{ rpm}$ and inlet temperature $T_i = 311 \text{ K}$) until incipient knock occurs. The correlation with octane number is evident. For further information about the properties of internal combustion engine fuels, the reader is referred to Owen and Coley (1995).

9.5 GASOLINE FUELS

Gasoline has been the dominant vehicular fuel since the early 1900s. It has a very high volumetric energy density and a relatively low cost. It is composed of a blend of light distillate hydrocarbons, including paraffins, olefins, naphthenes, and aromatics. It has a hydrogen to carbon ratio varying from 1.6 to 2.4. A typical formula used to characterize gasoline is C_8H_{16} , with a molecular weight of 111. A high hydrogen content gasoline is C_7H_{17} .

Gasoline properties of interest for internal combustion engines are given in Table 9.3. The properties include the octane number, volatility, gum content, viscosity, specific gravity, and sulfur content. The American Society for Testing and Materials (ASTM) has established a set of gasoline specifications for each property, also listed in Table 9.3. The antiknock index (AKI) is the average of the research (D2699) and motored (D2700) octane numbers, and it is displayed on gasoline pumps at service stations (e.g., 85, 87, and 91).

Table 9.2 Knock Characteristics of Single-Component Fuels

Formula	Name	Compression ratio	Octane number Research	Octane number Motor
CH_4	Methane	12.6	120	120
C_2H_6	Ethane	12.4	115	99
C_3H_8	Propane	12.2	112	97
C_4H_{10}	Butane	5.5	94	90
C_4H_{10}	Isobutane	8.0	102	98
C_5H_{12}	Pentane	4.0	62	63
C_5H_{12}	Isopentane	5.7	93	90
C_6H_{14}	Hexane	3.3	25	26
C_6H_{14}	Isohexane	9.0	104	94
C_7H_{16}	Heptane	3.0	0	0
C_7H_{16}	Triptane	14.4	112	101
C_8H_{18}	Octane	2.9	-20	-17
C_8H_{18}	Isooctane	7.3	100	100
$\text{C}_{10}\text{H}_{12}$	Isodecane		113	92
C_4H_8	Methylcyclopropane		102	81
C_5H_{10}	Cyclopentane	12.4	101	95
C_6H_{12}	Cyclohexane	4.9	84	78
C_6H_{12}	1,1,2-trimethylcyclopropane	12.2	111	88
C_7H_{14}	Cycloheptane	3.4	39	41
C_8H_{16}	Cyclooctane		71	58
C_6H_6	Benzene			115
C_7H_8	Toluene	15	120	109
C_8H_{10}	Ethyl benzene	13.5	111	98
C_8H_{10}	<i>m</i> -Xylene	15.5	118	115
C_3H_6	Propylene	10.6	102	85
C_4H_8	Butene-1	7.1	99	80
C_5H_{10}	Pentene-1	5.6	91	77
C_6H_{12}	Hexene-1	4.4	76	63
C_5H_8	Isoprene	7.6	99	81
C_6H_{10}	1,5-Hexadiene	4.6	71	38
C_5H_8	Cyclopentene	7.2	93	70
CH_4O	Methanol		106	92
$\text{C}_2\text{H}_6\text{O}$	Ethanol		107	89

Source: Obert, (1973).

For many years, the octane number of gasoline was above 90, and reached a maximum in the 1960s, with leaded premium gasoline available with AKI ratings of 103+. As of 2014, regular gasoline has a 87 AKI octane.

The octane number for aviation fuels is based on the motored (D2700) and supercharged (D909) test methods.

Knowledge of gasoline volatility is important not only in designing fuel delivery and metering systems, but also in controlling evaporative emissions. The volatility is quantified by three related specifications: (1) the distillation curve (D86), (2) the Reid vapor pressure (D323), and (3) the vapor–liquid ratio (D439). With the D86 distillation

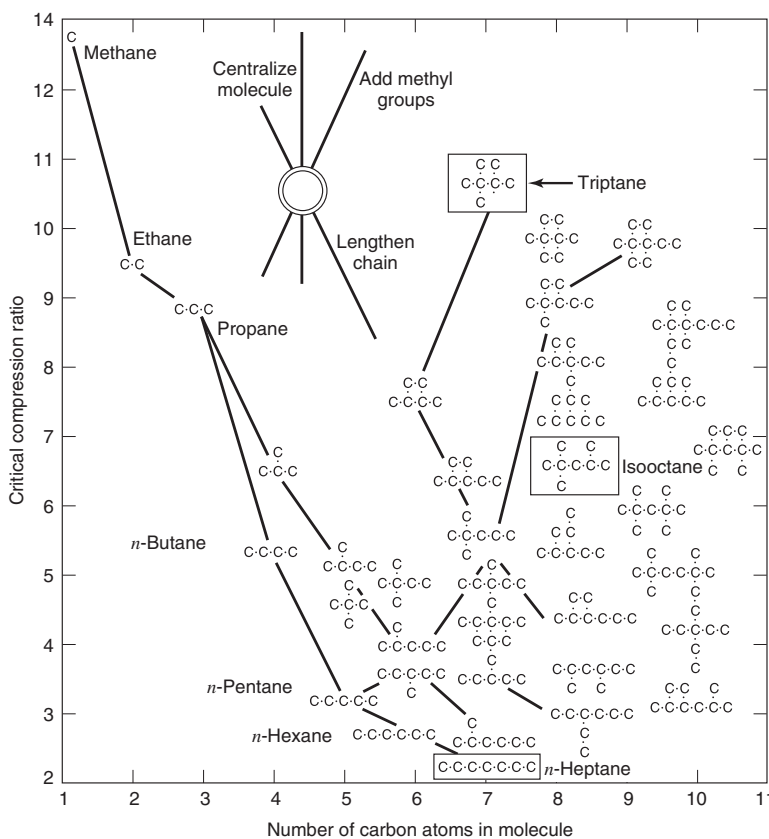


Figure 9.7 Effect of fuel structure on detonation tendency on paraffinic hydrocarbons (Lovell, 1948).

method, a still is used to evaporate the fuel. The fuel vapor is condensed at atmospheric pressure. The heating rate is adjusted continuously such that the condensation rate is 4–5 mL/min. The heating process is stopped when the fuel starts to smoke and decompose, typically around 370°C. The vapor temperature at the top of the distillation flask is measured

Table 9.3 Gasoline Property Specifications

Property	ASTM method
Benzene, vol%	D3606
Distillation, K	D86
Gum, mg/mL	D381
Heating value	D240
Hydrocarbons, %	D1319
Octane, motored	D2700
Octane, research	D2699
Octane, supercharged	D909
Reid vapor pressure, kPa	D323
Specific gravity	D287
Sulfur, wt%	D1266

throughout the test. The volume fraction of condensate is plotted versus temperature to form a distillation curve. The 10% and 90% evaporation temperatures, T_{10} and T_{90} , are used in the volatility specifications. The T_{10} temperature, indicating the start of vaporization, is used to characterize the cold starting behavior, and the T_{90} temperature, indicating the finish of vaporization, is used to characterize the possibility of unburned hydrocarbons. The ASTM drivability index (DI) is also a measure of fuel volatility and is defined in Equation 9.5 as

$$\text{DI} = 1.5T_{10} + 3T_{50} + T_{90} \quad (9.5)$$

Gum is a product of oxidation reactions with certain molecules often found in fuels. Use of gasoline with a high gum component can lead to sticking of valves and piston rings, carbon deposits, and clogging of fuel metering orifices. Inhibitors are often added to gasoline to reduce the gum formed in such a test under an assumption that they will also reduce gum formation in service. The ASTM D381 test method involves evaporating 50 mL of gasoline in a glass dish at approximately 430 K by passing heated air over the sample for a period of about 10 min. The difference in weight of the dish before and after the test is called the existent gum content.

Reformulated Gasoline (RFG) and Renewable Fuel Standard (RFS)

The U.S. Clean Air Act of 1990 set up two programs, an oxygenated fuels program and a reformulated gasoline (RFG) program, which resulted in mandated changes in the composition of gasoline. The oxygenated fuels program is a winter program used to reduce carbon monoxide and hydrocarbon levels in major cities that have carbon monoxide levels that exceed federal standards. The oxygenated fuels program requires that gasoline contain at least 2.7% by weight of oxygen. The first cities to use oxygenated gasoline were Denver, CO, and Phoenix, AZ, and it is now required in about 40 cities in the United States.

The reformulated gasoline program is a year-round program used to reduce ozone levels. It was mandated for metropolitan areas that have ozone levels that exceed federal standards. The program requires that gasoline sold year-round in these areas have minimum oxygen content of 2% by weight and maximum benzene content of 1%. It is now required in 10 cities in the United States, and an additional 21 areas have voluntarily entered the program. The primary oxygenate used is ethanol (EtOH). In 1996, California required use of Tier 2 RFG, that has stricter standards than Tier 1 RFG.

The requirements for increased production volume of renewable fuels have greatly expanded the market for biofuels. The U.S. Energy Policy Act of 2005 amended the Clean Air Act and established a national renewable fuel standard (RFS) requiring that gasoline contain 10% renewable fuels such as ethanol (E10). Studies are underway to allow use of midrange blends such as E15 (15% ethanol) and E20 (20% ethanol) in standard gasoline-fueled vehicles; however, there are fuel compatibility issues with the existing vehicle fleet.

The properties of various gasolines are compared in Table 9.4. The gasolines listed are

- Industry average gasoline
- Gasoline oxygenated with ethanol (gasohol)
- Phase 1 reformulated gasoline
- California Phase 2 reformulated gasoline

The volume percentage of olefins and benzene in reformulated gasoline is lower than industry average gasoline. The Reid vapor pressure is reduced in the summer in reformulated gasoline to reduce the emissions due to fuel evaporation. The 90% distillation temperature

Table 9.4 Properties of Gasoline Fuels

	Average gasoline	Gasohol	Phase 1 RFG	Phase 2 RFG
Aromatics, vol%	28.6	23.9	23.4	25.4
Olefins, vol%	10.8	8.7	8.2	4.1
Benzene, vol%	1.60	1.6	1.3	0.93
Reid vapor pressure, kPa (S: summer and W: winter)	60-S 79-W	67-S 79-W	50-S 79-W	46
T_{50} , K	370	367	367	367
T_{90} , K	440	431	431	418
Sulfur, mass ppm	338	305	302	31
Ethanol, vol%	0	10	4	0

Source: Adapted from EPA 420-F-95-007.

Table 9.5 FTP Regulated Emissions (g/mile) from Industry Average and Reformulated Gasoline

	Industry average gasoline	Phase 2 reformulated gasoline
HC	0.226	0.167
NMHC	0.203	0.148
CO	3.22	2.25
NO_x	0.394	0.321

Source: Cadle et al., 1997.

T90 is decreased to increase the vaporization and oxidation of the gasoline, which reduces the hydrocarbon emissions.

Since sulfur has an adverse impact on the performance of catalytic converters, the EPA Tier 2 gasoline sulfur regulations, phased in from 2004 to 2007, reduced the sulfur level in reformulated gasoline by 90% from about 300 to 30 ppm.

Table 9.5 compares the FTP regulated emissions from industry average gasoline and Tier 2 reformulated gasoline for a group of fleet vehicles. The use of the reformulated gasoline decreased the HC emissions by 26%, NMHC emissions by 27%, CO emissions by 30%, and NO_x emissions by 18%.

Gasoline Additives

Gasoline additives include octane improvers, anti-icers to prevent fuel line freeze-up, detergents to control deposits on fuel injectors and valves, corrosion inhibitors, and antioxidants to minimize gum formation in stored gasoline. Alcohols, ethers, and methyl cyclopentadienyl manganese tricarbonyl (MMT) are now used as octane improvers.

Many compounds have been tested for use as octane improvers in gasoline. Tetraethyl lead was the primary octane improver in general use from 1923 to 1975. Its use in motor vehicles was prohibited in 1995 due to its toxicity and adverse effect on catalytic converters.

and oxygen sensors. Currently, lead is only used in aviation and off-road racing gasolines. Thomas Midgley (1889–1944), a mechanical engineer from the General Motors Research Laboratory, discovered lead additives in 1921, as outlined in Midgley and Boyd (1922). Midgley also was the inventor of Freon (F-12), a refrigerant initially developed for automotive air conditioning systems. Freon was the most widely used refrigerant in the world until the mid-1990s when it was determined that the ultraviolet decomposition of Freon in the stratosphere releases chlorine, causing depletion of the stratospheric ozone layer. The manufacturing of Freon in the United States was prohibited in 1998.

9.6 ALTERNATIVE FUELS FOR SPARK IGNITION ENGINES

Important alternative fuels for spark ignition engines are compressed natural gas (CNG), propane or liquid petroleum gas (LPG), alcohols, and hydrogen. Alternative fuels are of interest, since they can be refined from renewable feedstocks, and their emission levels can be much lower than those of gasoline and diesel-fueled engines (Dhaliwal et al., 2000). If there are availability problems with crude oil, due to worldwide geopolitical problems, alternative fuels can also be used as replacements. As of the year 2015, the most commonly used alternative fuel for vehicles is propane, followed by natural gas, and methanol.

The cost of alternative fuels per unit of energy delivered can be greater than gasoline or diesel fuel, and the energy density of alternative fuels by volume is less than gasoline or diesel fuel. The smaller volumetric energy density requires larger fuel storage volumes to have the same driving range as gasoline-fueled vehicles. This can be a drawback, particularly with dual fuel vehicles, where a significant portion of the trunk space is used by the alternative fuel storage tank. Alternative fuels also lack a wide-scale distribution and fueling infrastructure comparable to that of conventional fuels. In recent years, fleet vehicles, such as buses, trucks, and vans have been a growing market for alternative fuels, as they can operate satisfactorily with localized fueling. In 1990, there were about 4 million propane-fueled vehicles, 3 million ethanol-fueled vehicles, and about 1 million natural gas-fueled vehicles worldwide, compared with about 150 million gasoline-fueled vehicles in the United States alone (Webb and Delmas, 1991).

Existing gasoline or diesel engines can be retrofitted fairly easily for operation with alternative fuels. However, various operational considerations need to be taken into account. The different combustion characteristics of alternative fuels require a change in the injection and ignition timing. Also, many alternative fuels, especially those in gaseous form, have very low lubricity, causing increased wear of fuel components such as fuel injectors and valves.

The properties of various alternative fuels are tabulated in Table 9.6, and are compared with the properties of *n*-octane. The first three columns contain gaseous fuels (methane, propane, and hydrogen) and the next three columns are liquid fuels (methanol, ethanol, and *n*-octane). While there is a range of energy densities on a fuel mass ($\text{MJ}/\text{kg}_{\text{fuel}}$) basis, the energy densities are comparable on a stoichiometric air mass ($\text{MJ}/\text{kg}_{\text{air}}$) basis. Octane has the greatest energy density by volume (MJ/L). Alternate fuels have higher octane levels than gasoline, so engines fueled with alternative fuels can operate at higher compression levels, and thus at higher efficiency. Further information about alternative fuels and their use is given in Owen and Coley (1995).

The methane number is a measure of the tendency for a gaseous fuel to knock. As indicated in Table 9.7, Malenshek and Olsen (2009) found a linear relationship between the maximum compression ratio and the methane number, for a variety of gaseous fuels, including coal gas, wood gas, digester gas, and landfill gas. A fuel's methane number limits

Table 9.6 Thermodynamic Properties of Spark Ignition Fuels

	Propane	Natural gas	Hydrogen	Methanol	Ethanol	Gasoline
Molecular weight	44.10	18.7	2.015	32.04	46.07	~110
Boiling point (°C), at 1 bar	-42	-160	-253	65	78	30–225
Mass A/F ratio, stoichiometric	15.58	17.12	34.13	6.43	8.94	15.04
Vapor pressure (kPa), at 32°C				32	17	62–90
Enthalpy of vaporization, h_{fg} (kJ/kg), at 298 K				1215	850	310
Adiabatic flame temperature (K)	2268	2227	2383	2151	2197	2266
Vapor flammability limits (% volume)	2.1–9.5	5.3–15	5–75	5.5–26	3.5–26	0.6–8
Lower heating value, mass, (MJ/kg _{fuel})	46.4	50.0	120	19.9	26.8	44.5
Lower heating value, volume, (MJ/kg _{fuel})	25.5	8.1		15.7	21.1	32.9
Lower heating value, stoichiometric (MJ/kg _{air})	2.98	2.92	3.52	3.09	3.00	2.96
Octane number, research	100	120	106	112	111	90–98
Octane number, motor	95.4	120		91	92	80–90
Stoichiometric CO ₂ emissions, (g CO ₂ /MJ _{fuel})	64.5	54.9	0	69	71.2	71.9

Source: Adapted from Black, 1991 and Unich et al., 1993.

Table 9.7 Critical Compression Ratio Versus Methane Number

Gas	Compression ratio	Methane number
Coal gas	8.0	23.9
Steam-reformed natural gas	10.5	62.4
Wood gas	10.3	70.2
Natural gas		78–98
Methane	14.4	100
Digester gas	17.6	139.1
Landfill gas	17.6	139.6

Source: Malenshek and Olsen, 2009.

the maximum compression ratio and thus the theoretical engine efficiency. For example, an engine optimized to operate on natural gas with a methane number of about 90 is susceptible to knock when operated on gases that have a lower methane number, such as coal gas which has a methane number of 24. The octane number of methane is 120 (RON), one of the highest values for hydrocarbon fuels.

Propane

Propane (C_3H_8), is a saturated paraffinic hydrocarbon. When blended with butane (C_4H_{10}) or ethane (C_2H_6), it is also designated as liquefied petroleum gas. A common LPG blend is P92, which is 92% propane and 8% butane. In the United States, about one-half of the LPG supply is obtained from the lighter hydrocarbon fractions produced during crude oil refining, and the other half from heavier components of wellhead natural gas.

Propane has been used as a vehicular fuel since the 1930s. In 1993, there were about 4 million LPG vehicles operating worldwide, with the majority in the Netherlands, followed by Italy, the United States, and Canada. There is a relatively extensive refueling network for propane, with over 15,000 refueling stations available in North America. There are a number of original equipment manufacturers that currently sell propane-fueled vehicles, primarily light- and medium-duty fleet vehicles, such as pick-up trucks and vans. Conversion kits are also available to convert gasoline or diesel-fueled engines to dedicated propane or dual fuel use.

In vehicles, propane is stored as a compressed liquid, typically from 0.9 to 1.4 MPa. Its evaporative emissions are essentially zero, since it is used in a sealed system. A pressure regulator controls the supply of propane to the engine and converts the liquid propane to a gas through a throttling process. Propane gas can be injected into the intake manifold, into the ports, or directly into the cylinder. Propane has an octane number of 112 (RON), so vehicular applications of propane can operate at a raised compression ratio.

As shown in Table 9.6, the CO_2 emissions on an equivalent energy basis are about 90% that of gasoline. Liquid propane has three-fourths of the energy density by volume of gasoline so that the fuel economy is correspondingly reduced. The volumetric efficiency and the power are also reduced due to the displacement of about 5–10% of the intake air by propane and the loss of evaporative charge cooling. Propane requires about a 5°spark advance at lower engine speeds due to its relatively low flame speed.

Representative FTP emissions from an LPG-fueled engine are shown in Table 9.8. The engine used was a 3.1 L engine with an LPG conversion system using an intake manifold mixer. The LPG fuel used was HD5 propane (96% propane and 4% ethane). The results indicate that the HC and CO emissions were lower with LPG than gasoline, 43 and 53% respectively, but the NO_x levels were higher. The toxic emissions are also given in

Table 9.8 LPG-Fueled Vehicle (3.1 L Engine) Emissions

	Propane	Gasoline
Regulated emissions (g/mile)		
HC	0.21	0.37
CO	2.55	5.4
NO_x	0.67	0.42
Toxic emissions (mg/mile)		
Benzene	<0.1	16.7
1,3-Butadiene	<0.1	2.5
Formaldehyde	1.2	3.1
Acetaldehyde	0.3	1.5
Total	1.5	23.8

Source: Bass et al., 1993.

Table 9.8. The levels of toxic emissions are typically an order of magnitude less than the baseline gasoline toxic emissions.

Natural Gas

Natural gas is a naturally occurring fuel found in oil fields. It is primarily composed of about 90–95% methane (CH_4), with small amounts of additional compounds such as 0–4% nitrogen, 4% ethane, and 1–2% propane. Methane is a greenhouse gas, with a global warming potential approximately 10 times that of carbon dioxide. As shown in Table 9.6, since methane has a lower carbon to hydrogen ratio relative to gasoline, its CO_2 emissions are about 22–25% lower than gasoline.

Natural gas has been used for many years in stationary engines for gas compression and electric power generation. An extensive distribution network of natural gas pipelines exists to meet the need for natural gas for industrial processes and heating applications. Natural gas-fueled vehicles have been in use since the 1950s, and conversion kits are available for both spark and compression ignition natural gas and gasoline or diesel fuel. As of 2013, there are about 18 million natural gas-fueled road vehicles worldwide, and the number of natural gas-fueled vehicles is expected to double by 2020. One advantage of a bifuel operation is that the operating range of a vehicle is extended in comparison with a dedicated natural gas-vehicle. Currently, original equipment manufacturers are selling production natural gas-fueled vehicles, primarily to fleet owners. Natural gas vehicles were the first vehicles to meet the California ULEV emission standards.

Natural gas is stored in a compressed (CNG) state at room temperatures and also in a liquid (LNG) form at 160°C. Natural gas has an octane number (RON) of about 120 so that natural gas engines can operate at a compression ratio higher than that of gasoline-fueled engines. Natural gas is pressurized to 20 MPa in vehicular storage tanks so that it has about one-third of the volumetric energy density of gasoline. The storage pressure is about 20 times that of propane. Like propane, natural gas is delivered to the engine through a pressure regulator, either through a mixing valve located in the intake manifold, port fuel injection at about 750 kPa, or direct injection into the cylinder. With intake manifold mixing or port fuel injection, the engine's volumetric efficiency and power is reduced due to the displacement of about 10% of the intake air by the natural gas, and the loss of evaporative charge cooling. Natural gas does not require mixture enrichment for cold starting, reducing potential cold start HC and CO emissions.

The combustion of methane is different from that of liquid hydrocarbon combustion, since only carbon–hydrogen bonds are involved, and no carbon–carbon bonds, so the combustion process is more likely to be more complete, producing less nonmethane hydrocarbons. Optimal thermal efficiency occurs at rich conditions with equivalence ratios of 1.3–1.5. The total hydrocarbon emission levels can be higher than gasoline engines due to unburned methane. The combustion of methane can produce formaldehyde, a regulated toxic pollutant. The particulate emissions of natural gas are very low relative to diesel fuel. Natural gas has a lower adiabatic flame temperature (2240 K) than gasoline (2310 K), due to its higher product water content. Operation under lean conditions will also lower the peak combustion temperature. The lower combustion temperatures lower the NO formation rate, and produce less engine-out NO_x .

To meet vehicular emission standards, catalytic converters are used with natural gas-fueled engines. Since three way catalytic converters are most effective at stoichiometric conditions, natural gas combustion needs to be maintained at stoichiometric, and exhaust gas recirculation (EGR) is used to reduce the peak combustion temperatures and thus the

Table 9.9 CNG-Fueled Vehicles (2.2 L Engine) Regulated Emissions (g/mile)

Emission	Toyota engine	GMC engine	GMC engine
	CNG	CNG	Gasoline
NMOG	0.007	0.027	0.08
CO	0.69	1.01	1.54
NO _x	0.015	0.10	0.17

Source: Sun et al., 1998, Kato et al., 1999.

nitrogen oxide levels. Table 9.9 gives the exhaust emissions for a 2.2 L bifuel gasoline and CNG engine, and a 2.2 L dedicated CNG engine. When the bifuel engine is switched from gasoline to CNG, the nonmethane organic gases (NMOG), carbon monoxide (CO), and nitrogen oxide (NO_x) levels were reduced to 60%, 34%, and 41%, respectively. The dedicated CNG engine was modified to operate specifically with natural gas, with a higher compression ratio, intake valves with early closing timing, and intake and exhaust valves with increased lift.

The emissions of FTP toxics from a 0.75 ton light-duty truck operated with gasoline and with natural gas are given in Table 9.10. The engine emission control system included a heated oxygen sensor and a standard three-way catalyst. The same compression ratio of 8.3:1 was used for both fuels. Table 9.9–9.11 also indicate that the CNG toxic emissions are much less than the gasoline toxic emissions. The highest mass emissions with gasoline were benzene and formaldehyde, and the highest mass emissions with CNG was formaldehyde, at a level about half of that of gasoline.

Natural gas can replace diesel fuel in heavy-duty engines with the addition of a spark ignition system. A number of heavy-duty diesel engine manufacturers are also producing dedicated natural gas heavy-duty engines. The natural gas-fueled engines are operated lean with an equivalence ratio as low as $\phi = 0.7$. The resulting lower in-cylinder temperatures reduce the NO_x levels. Heavy-duty natural gas engines are designed to meet LEV emission standards without the use of an exhaust catalyst and will meet ULEV emission standards with the addition of a catalyst. The emission certification data for three heavy-duty natural gas engines are given in Table 9.11.

Natural gas can also be used in compression ignition engines if diesel fuel is used as a pilot fuel, since the autoignition temperature of methane is 540°C, compared with 260°C for diesel fuel. This fueling strategy is attractive for heavy-duty diesel applications, such as trucks, buses, locomotives, and ships, compressors, and generators. These engines are

Table 9.10 CNG-Fueled Vehicles Toxic Emissions (mg/mile)

Toxic	CNG	CNG start/ gasoline run	Gasoline
Benzene	0.2	14.8	31.2
1,3-Butadiene	6.0.1	0.1	1.5
Formaldehyde	3.4	4.1	5.9
Acetaldehyde	0.2	0.3	2.0
Total	3.8	19.3	40.6

Source: Springer et al., 1994.

Table 9.11 Heavy-Duty Natural Gas Engine Emission Certification Data (g/bhp-h)

	Hercules GTA 5.6	Cummins L10	Detroit Diesel 50G
Power (hp)	190	240	275
NMHC	0.9	0.2	0.9
CO	2.8	0.2	2.8
NO _x	2.0	1.4	2.6
PM	0.10	0.02	0.06

Source: Owen and Coley, 1995.

also operated with a lean combustion mixture so that the NO_x emissions are decreased. However, since diesel engines are unthrottled, at low loads the lean combustion conditions can degrade the combustion process, increasing the hydrocarbon and carbon monoxide emissions.

Ethanol

Ethanol (C₂H₅OH) is an alcohol fuel formed from the fermentation of sugar and grain stocks, primarily sugar cane and corn, which are renewable energy sources. Its properties and combustion characteristics are very similar to those of methanol. Ethanol is also called “grain” alcohol. It is a liquid at ambient conditions and nontoxic at low concentrations.

Gasohol (E10) is a gasoline–ethanol blend with about 10% ethanol by volume. E85 is a blend of 85% ethanol and 15% gasoline. In Brazil, about half of the vehicles use an ethanol-based fuel “alcool,” primarily E93, produced from sugar cane. In the United States, the primary source of ethanol is currently from starch feedstocks, such as corn, and there are efforts underway to produce ethanol from cellulosic feedstocks such as corn fiber, forestry waste, poplar, and switch grass. The energy density by volume of ethanol is relatively high for an alternative fuel, about two-thirds that of gasoline. The octane rating of ethanol of 111 RON allows use of an increased compression ratio. The cetane number of ethanol is low, at about 8, and it can be used in compression ignition engines with diesel fuel pilot ignition.

As shown in Table 9.6, the CO₂ emissions from ethanol on an equivalent energy basis are about 99% that of gasoline. With a switch from RFG to E85, for a fleet of flexible-fueled vehicles, Cadel et al. (1997) report that the NO_x emissions decreased by 29%, the nonmethane hydrocarbons (NMHC) decreased by 10%, and the CO emissions increased by 8%. The corresponding FTP toxic emissions are shown in Table 9.12. There was a 71% reduction in 1,3-butadiene, and a 64% reduction in benzene. However, for E85 the acetaldehyde emissions were almost two orders of magnitude higher than those of RFG, leading to almost a fourfold increase in the toxic emission levels.

Methanol

Methanol (CH₃OH) is an alcohol fuel formed from natural gas, coal, or biomass feedstock. Methanol has been used as a vehicular fuel since the early 1900s, and is also used as a fuel for diesel engines and fuel cells. It is also called wood alcohol. It is a liquid at ambient conditions. Its chemical structure is a hydrocarbon molecule with a single hydroxyl (OH)

Table 9.12 FTP Toxic Emissions (mg/mile) from Ethanol-Fueled Vehicles

Toxic	E85	Phase 2 RFG
Benzene	1.8	5.1
1,3-Butadiene	0.2	0.7
Formaldehyde	4.1	2.1
Acetaldehyde	24.8	0.5
Total	20.7	8.4

Source: Cadle et al., 1997.

radical. The hydroxyl radical increases the polarity of the hydrocarbon so that methanol is miscible in water, and has a relatively low vapor pressure. Since oxygen is part of the chemical structure, less air is required for complete combustion. Methanol is very toxic, and ingestion can cause blindness and death.

Pure methanol is labeled M100, and a mix of 85% methanol and 15% gasoline is labeled M85. M85 has an octane rating of 102. Adding gasoline to methanol provides more volatile components that can vaporize more easily at low-temperatures. Methanol has been adopted as a racing fuel, both for performance and safety reasons. Since methanol mixes with water, a methanol fire can be extinguished with water, which is not the case with gasoline. The octane rating of methanol M100 of 111 RON allows use of an increased compression ratio. The relatively high enthalpy of evaporation (1215 kJ/kg) of methanol relative to gasoline (310 kJ/kg) produces greater intake air-cooling and a corresponding increase in volumetric efficiency relative to gasoline. The energy density by volume of methanol is about half that of gasoline. However, because of its oxygen content, it has a higher stoichiometric energy density (3.09 MJ/kg air) relative to gasoline (2.96 MJ/kg air). For maximum power, a rich equivalence ratio of $\phi = 1.6$ is used.

Flexible-fuel vehicles (FFV) have been developed to use a range of methanol and gasoline blends ranging from 100% gasoline to M85. An optical fuel sensor is used to determine the alcohol content and adjust the fuel injection and spark timing. The engine compression ratio is not increased, to allow for the lower octane level of gasoline. The low vapor pressure of methanol causes cold starting problems. Satisfactory cold starting with M85 requires a rich mixture so that enough volatiles are present to form a combustible mixture. Methanol is corrosive, especially to rubber and plastic, so alcohol tolerant components, such as stainless steel, are required for its storage and transport.

The cetane number of methanol is low at about 5, and it can be used in compression ignition engines with diesel fuel pilot ignition. Methanol burns with a nearly invisible flame, and a relatively high flame speed. Formaldehyde is a significant decomposition product from methanol combustion and is expected to be higher from methanol than other fuels. The formaldehyde emissions are proportional to the equivalence ratio, so rich combustion will produce increased emissions of formaldehyde. Special lubricants also need to be used in methanol-fueled engines.

As shown in Table 9.6, the CO₂ emissions of methanol on an equivalent energy basis are about 96% that of gasoline. With a change in the fuel for a fleet of flexible-fueled vehicles from RFG to M85, the nonmethane hydrocarbons (NMHC) and CO emissions decreased by 30% and 17% respectively, and the NO_x emissions remained about the same (Cadle et al., 1997). The FTP toxic emissions for the methanol- and gasoline-fueled-flexible-fueled vehicles are given in Table 9.13. There was an 83% reduction in 1,3-butadiene, a 50% reduction in benzene, and a 25% increase in acetaldehyde. However, for M85 the

Table 9.13 Toxic Emissions (mg/mile) from Methanol-Fueled Vehicles

Toxic	M85	Phase 2 RFG
Benzene	3.0	6.0
1,3-Butadiene	0.10	0.6
Formaldehyde	17.1	1.6
Acetaldehyde	0.5	0.4
Total	20.7	8.6

Source: Cadle et al., 1997.

formaldehyde emissions were almost an order of magnitude higher than those of RFG, leading to more than a twofold increase in the toxic emission levels.

9.7 HYDROGEN

Hydrogen (H_2) can be produced from many different feedstocks, including natural gas, coal, biomass, and water. The production processes include steam reforming of natural gas, presently the most economical method, electrolysis of water, and gasification of coal, which also produces CO_2 . Hydrogen is colorless, odorless, and nontoxic, and hydrogen flames are invisible and smokeless. The global warming potential of hydrogen is insignificant in comparison to hydrocarbon-based fuels, since combustion of hydrogen produces no carbon-based compounds such as HC, CO, and CO_2 .

At present, the largest user of hydrogen fuel is the aerospace community for rocket fuel. Hydrogen can also be used as a fuel in fuel cells. There have been a number of vehicular demonstration projects, but the relatively high cost of hydrogen fuel has hindered adoption as an alternative fuel. Dual fuel engines have been used with hydrogen, in which hydrogen is used at start up and low load, and gasoline at full load (Fulton et al., 1993) to reduce the cold start emissions levels.

One of the major obstacles related to the use of hydrogen fuel is the lack of any manufacturing, distribution, and storage infrastructure. The most economical method would be to distribute hydrogen through pipelines, similar to natural gas distribution. The three methods used to store hydrogen are: (1) in a liquid form at $-253^{\circ}C$ in cryogenic containers, (2) as a metal hydride, such as iron–titanium hydride $FeTiH_2$, or (3) in a pressurized gaseous form at 20–70 MPa. The metal hydride releases hydrogen when heated by a heat source, such as a vehicle exhaust system. The most common storage methods are liquid and hydride storage, which have comparable volumetric storage capabilities, both requiring about 10 times the space required by an equivalent 5-gallon gasoline tank, as shown by Table 9.14. At least a 55-gallon tank of compressed hydrogen is needed to store the energy equivalent of 5 gallons of gasoline.

Compressed hydrogen at 70 MPa has one-third the energy density by volume of compressed natural gas, and liquid hydrogen has one-fourth the energy density by volume of gasoline. Use of liquid hydrogen has an additional energy cost, as liquefaction of hydrogen to -20 K requires an expenditure of energy approximately equal to the energy content of liquid hydrogen. If mixed with air in the intake manifold, the volume of hydrogen is about 30% of the intake mixture volume at stoichiometric, decreasing the volumetric efficiency. The octane rating of hydrogen of 106 (RON) allows use of an increased compression ratio.

Table 9.14 Comparison of Hydrogen Storage Methods

	Gasoline (5 gallons)	Liquid H ₂	Hydride Fe Ti (1.2%)	Compressed (70 MPa) H ₂
Energy (kJ)	6.64×10^5	6.64×10^5	6.64×10^5	6.64×10^5
Fuel mass (kg)	14	5	5	5
Tank mass (kg)	6.5	19	550	85
Total fuel system mass (kg)	20.5	24	555	90
Volume (gal)	5	47	50	60

Source: Kukkonen and Shelef, 1994.

The combustion characteristics of hydrogen are very different from gasoline combustion characteristics, as the laminar flame speed of a hydrogen–air mixture is about 3 m/s, about 10 times that of methane and gasoline, and the adiabatic flame temperature is about 100°C higher than gasoline and methane. Since it has a wide flammability limit (5–75%), preignition and backfiring can be a problem. The flammability limits correspond to equivalence ratios of from 0.07 to 9.0. Water injection into the intake manifold is used to mitigate preignition and provide cooling. Exhaust gas recirculation and lean operation are used to reduce NO_x levels.

9.8 DIESEL FUELS

Diesel fuel consists of a mixture of light distillate hydrocarbons that have molecular weights from about 170 to 200, with a corresponding range of 12–20 carbon atoms per molecule. Diesel fuels vaporize in the range between about 180 and 360°C, higher than gasoline. It is estimated that there are more than 10,000 isomers in diesel fuel. Like gasoline, diesel fuels are mixtures of paraffinic, olefinic, naphthenic, and aromatic hydrocarbons, but their relative proportions are different. Diesel fuels have about an 8% greater energy density by volume than gasoline, and are the primary fuel used by heavy-duty vehicles. Diesel fuel is also much less flammable than gasoline, as the flash point temperature of diesel 2-D is 52°C, much higher than that of gasoline, which is about –40°C. The flash point is defined as the lowest temperature at which a vapor–air mixture will ignite when an ignition source is applied.

Diesel fuels are classified both by a numerical scale and by use. The use designations are bus, truck, railroad, marine, and stationary. The American Society for Testing and Materials, ASTM D975, numerical classification scheme for diesel fuels ranges from one to six, with letter subcategories. Diesel fuel number 1-D is a light (approximated by C₁₂H₂₂) distillate cold weather fuel with a flash point of 38°C. Diesel fuel 2-D is a middle (approximated by C₁₅H₂₅) distillate diesel fuel of lower volatility and is the most common fuel for vehicular applications. Diesel fuel 4-D is a heavy distillate fuel used for stationary applications where the engine speed is low and more or less constant. It has a flash point of 55°C. As the number designation increases, the mean molecular weight and viscosity of the fuel increases.

The specification chart contained in ASTM D975 is shown here as Table 9.15. These specifications are used by refiners as a basis for the control of diesel fuel compositions. The corresponding European Standards Organization (CEN) standard for diesel fuel is EN 590, listed in Table 9.16. The thermodynamic properties of diesel fuel 2-D are listed in

Table 9.15 Diesel Fuel Specifications (ASTM D975)

	ASTM Method	No. 1-D	No. 2-D	No. 4-D
Minimum cetane number	D613	40	40	30
Minimum flash point, °C	D93	38	52	55
Cloud point, °C	D2500	Local	Local	Local
Maximum water and sediment, vol%		0.05	0.05	0.05
Maximum carbon residue	D524	0.15	0.35	
Maximum ash, wt%	D482	0.01	0.01	0.10
T_{90} , K	D86	561 max	555–611	
Kinematic viscosity at 40 °C (mm ² /s)	D445	1.3–2.4	1.9–4.1	5.5–24
Maximum copper strip corrosion		No. 3	No. 3	

Table 9.18. In CFD simulations, diesel fuel is often approximated by tetradecane ($n\text{-C}_{14}\text{H}_{30}$) for computation of evaporation, ignition, and combustion.

One component of diesel fuel that has attracted particular regulatory attention is sulfur, due to the adverse impact that sulfur-containing particulate emissions have on air quality. During combustion the sulfur in the diesel fuel forms sulphates (SO_4^-), and sulfur dioxide (SO_2), which reacts with water to form sulfuric acid, a component of acid rain. Ultralow sulfur diesel (ULSD) has a sulfur content of 15 ppm or less. As part of the Euro V emission standards, ULSD is required in Europe. After December 1, 2014, all highway, nonroad, locomotive, and marine diesel fuel produced and imported in the United States will be mandated to be ultralow sulfur diesel. Sulphur reacts with the nickel in metal alloys in fuel injectors to form a eutectic alloy with increased lubricity. Therefore, with decreased sulfur concentration, additional fuel additives will be needed to maintain the lubricity of diesel fuel.

At low-temperatures, the higher molecular weight components in diesel fuel have a tendency to jell or crystallize into solid wax particles giving it a cloudy appearance. The onset of this crystallization is called the cloud point. A standardized test is used to specify the cold filter plugging point (CFPP) temperature for various grades of diesel fuel. Additives are used to modify the crystal structure of the wax particles to reduce the plugging of the fuel filter at low-temperatures.

The cetane numbers of various hydrocarbons used in diesel fuel are listed in Table 9.17. The octane number and the cetane number of a fuel are inversely correlated. As shown in Figure 7.18, when the octane number is decreased from 85 to 0, the corresponding cetane number increases from 20 to 60. Therefore, diesel fuel is a poor spark ignition fuel and vice versa. Since a low cetane number fuel will mix more completely with the cylinder air before burning, the local equivalence ratio of the initial premixed burn will be less ($\phi \sim 3$) than the local equivalence ratio ($\phi \sim 4$) for a higher cetane number.

There are a number of correlations used to approximate the ignition quality of a diesel fuel. One widely used approximation is the calculated cetane index, CCI. The CCI is an approximation to the cetane number using the ASTM D976 empirical correlation for petroleum-based diesel fuels, and is based on the API gravity and the midpoint (50% evaporated) boiling temperature.

$$\text{CCI} = -420.34 + 0.016 G^2 + 0.192 G \log T_{50} + 65.01 (\log T_{50})^2 - 0.0001809 T_{50}^2$$

Table 9.16 European Diesel Fuel Specifications (EN 590)

	Temperate climate	ISO Test method
Minimum cetane number	51	51-65
Minimum cetane index	46	42-64
Density at 15°C, (kg/m ³)	820-845	3675
Polycyclic aromatic hydrocarbons, %	11	12916
Minimum flash point, (°C)	55	2719
Maximum water, (mg/kg)	200	12937
Total contamination, (mg/kg)	24	12662
Maximum ash, wt%	0.01	6245
Distillation recovered 95% (v/v), (°C)	360	3405
Kinematic viscosity at 40°C (mm ² /s)	2.00-4.50	3104
Maximum sulfur, ppm	10	20884
Maximum copper strip corrosion	Class 1	2160
Lubricity, wear scar diameter (wsd), (μm)	460	12156

Table 9.17 Centane Numbers of Hydrocarbon Fuels

Formula	Name	Cetane number
C ₁₆ H ₃₂	Heptamethylnonane	15
C ₇ H ₁₆	<i>n</i> -Heptane	56
C ₈ H ₁₈	<i>n</i> -Octane	64
C ₁₂ H ₂₆	<i>n</i> -Dodecane	88
C ₁₄ H ₃₀	<i>n</i> -Tetradecane	96
C ₁₆ H ₃₄	<i>n</i> -Hexadecane (cetane)	100

Source: Hurn and Smith (1951).

Table 9.18 Comparison of Thermodynamic Properties of Compression Ignition Fuels

	Diesel (2D)	Dimethyl ether (DME)	Rapeseed methyl ester (RME)
Formula	C ₁₅ H ₂₅	CH ₃ OCH ₃	
Molecular weight	170-200	46.07	
Liquid density (kg/m ³)	820-860	668	882
Kinematic viscosity (m ² /s) at 40°C	2.8 × 10 ⁻⁶	2.2 × 10 ⁻⁷	4.1 × 10 ⁻⁶
Lower heating value, mass (MJ/kg _{fuel})	42.5	28.4	37.7
Lower heating value, volume (MJ/L _{fuel})	34.8-36.5	19.0	
Boiling point at 1 bar (°C)	180-360	-25	
Vapor pressure at 38°C (bar)	0.0069	8	
Cetane number	40-55	55-60	48-58
Stoichiometric A/F ratio	14.7	9.0	11.2-12.5

where

$$G = \text{API gravity} = 141.5 / (\text{Specific gravity}) - 131.5$$

$$T_{50} = \text{Midpoint boiling temperature, } ^\circ\text{F}$$

The cetane index is useful because it is less expensive to obtain than a measurement of the actual cetane number. It is also used as a surrogate specification of aromatics content. In addition, it illustrates that not all diesel fuel properties can be specified independently of one another.

The regulated emissions from vehicular diesel combustion include CO, HC, NO_x, and particulate matter (PM). The emissions regulations have been imposed in response to concerns about the adverse effect that compression ignition engines have had on ambient air quality, specifically NO_x and PM. Nitrogen oxides are a precursor to ground-level ozone formation, and particulate emissions are a respiratory hazard. As discussed earlier, there is a trade-off between NO_x and particulate matter (PM) emissions from compression ignition engines, as techniques to lower NO_x will generally increase PM, and vice versa. With the increased availability of diesel after treatment devices, such as lean NO_x traps, U.S. manufacturers have increased their production and sales of diesel vehicles.

9.8.1 Alternative Fuels for Compression Ignition Engines

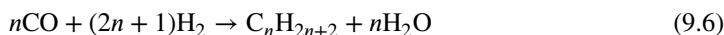
A number of fuels can be used as an alternative for petroleum-based diesel fuels. One alternative is biodiesel, that is, methyl ester vegetable oils, such as soybean, castor, canola, sunflower, cotton, palm, coconut, Jatropha, and algae oils. Other diesel alternative fuels are dimethyl ether (DME), and Fischer–Tropsch (F-T) fuel.

Biodiesel fuels are designated with the prefix B, so a mixture of 20% biodiesel is labeled B20. A number of U.S. states have mandated the use of biodiesel, and the levels vary by state, from B2 to B20. Diesel engines are rated for a maximum percentage of biodiesel, typically from B5 to B20. The most common blend in the United States is B20. In Europe, diesel fuel is blended with 7% biodiesel to produce B7. Biodiesel is also a ULSD (Ultralow sulfur diesel) because it contains very low levels of sulfur.

Biodiesel fuels are produced through the transesterification of triglycerides in vegetable oil using a low molecular weight alcohol, such as methanol. The methyl ester is obtained through a process in which methyl alcohol and a catalyst (such as sodium hydroxide or potassium hydroxide) chemically breaks down the triglyceride molecule into methyl esters of the oil and a glycerin byproduct. Biodiesel is not a single chemical compound, as the triglycerides in vegetable oils are a variable mixture of unsaturated and saturated fatty acids.

The thermodynamic properties of a widely used biodiesel fuel, rapeseed methyl ester (RME) are listed in Table 9.18. The interest in algae-based biodiesel has been increasing, due to the far greater sunlight–oil conversion efficiency of algae relative to land-based crops.

Fischer–Tropsch (F-T) fuel is produced from a mixture of CO and H₂ using a catalytic reforming process with iron or cobalt. The CO is generated by pyrolysis of woody materials, such as switchgrass. The Fischer–Tropsch reaction is a water–gas reaction:



Dimethyl ether (DME) is an oxygenated fuel produced by dehydration of methanol or from synthesis gas. The volumetric energy density (MJ/L) of DME is about half that of diesel fuel. It burns with a visible blue flame, similar to that of natural gas. It is noncorrosive to metals but does deteriorate some elastomers.

Alternative diesel fuels have a higher cost, and lower volumetric energy density than fossil-based diesel fuel, but do produce lower CO and particulate emissions. Numerous studies have shown slightly greater NO_x levels from diesel engines fueled with biodiesel relative to petroleum-based diesel. For example, Krahl et al. (1996) report that RME had about 40% lower HC emissions, 35% lower CO, 35% lower PM, but about 15% greater NO_x emissions. One explanation is that the oxygen atoms in the biodiesel molecule give rise to a leaner premixed ignition zone during combustion resulting in increased combustion temperatures.

Clark et al. (1999) measured the transient emissions of a number of blends of Fischer-Tropsch fuel. All of the regulated emissions were lower in comparison with low-sulfur diesel fuel, with 43% lower HC emissions, 39% lower CO, 14% lower PM, and 14% lower NO_x emissions.

9.9 REFERENCES

- BASS, E., B. BAILEY, and S. JAEGER (1993), "LPG Conversion and HC Emissions Speciation of a Light Duty Vehicle," SAE paper 932745.
- BLACK, F. (1991), "An Overview of the Technical Implications of Methanol and Ethanol as Highway Motor Vehicle Fuels," SAE paper 912413.
- CADLE, S., P. GROBLICKI, R. GORSE, J. HOOD, D. KARDUBA-SAWICKY, and M. SHERMAN (1997), "A Dynamometer Study of Off-Cycle Exhaust Emissions—The Auto/Oil Air Quality Improvement Research Program," SAE paper 971655.
- CLARK, N., C. ATKINSON, G. THOMPSON, and R. NINE (1999), "Transient Emissions Comparisons of Alternative Compression Ignition Fuels," SAE paper 1999-01-1117.
- DHALIWAL, B., N. YI, and D. CHECKEL (2000), "Emissions Effects of Alternative Fuels in Light-Duty and Heavy-Duty Vehicles," SAE paper 2000-01-0692.
- FULTON, J., F. LYNCH, R. MARMARO, and B. WILLSON (1993), "Hydrogen for Reducing Emissions from Alternative Fuel Vehicles," SAE paper 931813.
- HURN, R. W. and H. M. SMITH (1951), "Hydrocarbons in the Diesel Boiling Range," *J. Ind. Eng. Chem.*, Vol. 43, pp. 2788–2793.
- IKUMI, S. and C. WEN (1981), "Entropies of Coals and Reference States in Coal Gasification Availability Analysis," West Virginia University Internal Report.
- KATO, K., K. IGARASHI, M. MASUDA, K. OTSUBO, A. YASUDA, and K. TAKEDA (1999), "Development of Engine for Natural Gas Vehicle," SAE paper 1999-01-0574.
- KRAHL, J., A. MUNACK, M. BAHADIR, L. SCHUMACHER, and N. ELSER (1996), "Review: Utilization of Rapeseed Oil, Rapeseed Oil Methyl Ester or Diesel Fuel: Exhaust Gas Emissions and Estimation of Environmental Effects," SAE paper 962096.
- KUKKONEN, C. and M. SHELEF (1994), "Hydrogen as an Alternative Fuel," SAE paper 940766.
- LOVELL, W. (1948), "Knocking Characteristics of Hydrocarbons," *J. Ind. Eng. Chem.*, Vol. 40, pp. 2388–2438.
- MALENSHEK, M. and D. OLSEN, (2009), "Methane number testing of alternative gaseous fuels", *Fuel*, Vol. 88, p. 650–656.
- MIDGLEY, T. and T. BOYD (1922), "The Chemical Control of Gaseous Detonation with Particular Reference to the Internal-Combustion Engine," *J. Ind. Eng. Chem.*, Vol. 14, pp. 894–898.
- OWEN, K. and T. COLEY (1995), *Automotive Fuels Reference Book*, Society of Automotive Engineers, Warrendale, Pennsylvania.

- SPRINGER, K., L. SMITH, and A. DICKINSON (1994), "Effect of CNG Start-Gasoline Run on Emissions from a 34 Ton Pick Up Truck," SAE paper 941916.
- SUN, X., A. LUTZ, E. VERMIGLIO, M. AROLD, and T. WIEDMANN (1998), "The Development of the GM 2.2L CNG Bi-Fuel Passenger Cars," SAE paper 982445.
- WEBB, R. and P. DELMAS (1991), "New Perspectives on Auto Propane as a Mass-Scale Motor Vehicle Fuel," SAE paper 911667.

9.10 HOMEWORK

- 9.1** What is the chemical structure of (a) 3-methyl-3-ethylpentane, and (b) 2,4-diethylpentane?
- 9.2** If a hydrocarbon fuel is represented by the general formula C_xH_{2x} , what is its stoichiometric mass air-fuel ratio?
- 9.3** A fuel has the following composition by mass: 10% pentane, 35% heptane, 30% octane, and 25% dodecane. If its general formula is of the form C_xH_y , find x and y .
- 9.4** If the mass composition of a hydrocarbon fuel mixture is 55% paraffins, 30% aromatics, and 15% monoolefins, what is its specific heat? Compare with the value of specific heat for C_7H_{17} using Equation 3.37. Assume $T = 1000$ K.
- 9.5** Compute the enthalpy of formation of C_8H_{18} .
- 9.6** A four-stroke engine operates on methane with an equivalence ratio of 0.9. The air and fuel enter the engine at 298 K, and the exhaust is at 800 K. The heat rejected to the coolant is 350 MJ/kmol_{fuel}. (a) What is the enthalpy of the exhaust combustion products? (b) What is the specific work output of the engine? (c) What is the first law efficiency of the engine?
- 9.7** A fuel blend has a density of 700 kg/m³ and a midpoint boiling temperature of 90°C. What is its cetane index?
- 9.8** What is the decrease in volumetric efficiency of a 5 L gasoline-fueled engine when it is retrofitted to operate with propane? The decrease is due to the displacement of a portion of the inlet air by the propane fuel. Assume standard temperature and pressure inlet air conditions.
- 9.9** Repeat Problem 9.8 for hydrogen and methane.
- 9.10** A flexible fuel vehicle operates with a mixture of 35% iso-octane and 65% methanol, by volume. If the combustion is to be stoichiometric, what should the mass air-fuel ratio be?
- 9.11** If an dragster fuel tank contains a mixture of 70% octane and 30% nitromethane, by volume, what should the mass air-fuel ratio be to run rich at $\phi = 1.24$?
- 9.12** A vehicle is equipped with a flex-fuel eight-cylinder 6.0 L spark ignition engine running on a mixture of octane and ethanol at $\phi = 0.95$. At an operating condition of 2500 rpm, the thermal efficiency is 0.30 and the volumetric efficiency is 0.80. If the fuel mixture is changed from 10% ethanol (E10) to 85% ethanol (E85), (a) What is the change in the overall mass air-fuel ratio, and (b) What is the change in the engine power?
- 9.13** Verify the CO₂ concentration values resulting from the combustion of propane, methane, methanol, ethanol, and gasoline given in Table 9.6.

Chapter 10

Friction and Lubrication

10.1 INTRODUCTION

In this chapter, we will examine the frictional processes in internal combustion engines and learn about the properties of engine lubricating oils. Engines are lubricated not only to reduce friction but also to prevent engine failure. Since frictional losses are a significant fraction of the power produced in an internal combustion engine, minimization of friction has long been a major consideration in engine design and operation. The friction forces in engines are a consequence of both hydrodynamic stresses in oil films and also metal-to-metal contact. Minimum friction is obtained by use of low shear strength lubricating oil and hardened metallic surfaces.

Lubricants also reduce component wear during metal-to-metal contact, and reduce corrosion from the acidic products of combustion. Additives are added to lubricating oils that preferentially adsorb to bearing surfaces and lower the coefficient of friction. A pressurized system is used to circulate lubricants to the bearings, piston rings, and valve trains.

The frictional processes in an internal combustion engine can be categorized into three main components: (1) the mechanical friction, (2) the pumping work, and (3) the accessory work. The mechanical friction includes the friction of internal moving parts such as the crankshaft, piston, rings, and valve train. The pumping work is the net work done to draw in a fresh mixture during the intake stroke and push out the combustion gases during the exhaust stroke. The accessory work is the work required for operation of accessories such as the oil pump, fuel pump, alternator, and a fan.

The study of friction in engines is highly empirical and depends on experimental measurements, especially, as we will see, on motored engine tests. We will use scaling arguments to develop relations for the dependence of the various modes of friction work on overall engine parameters such as the bore, stroke, and engine speed, then construct an overall engine friction model. The coefficients for the scaling relations are obtained from experimental data and include lubrication oil properties such as viscosity.

10.2 FRICTION COEFFICIENT

The friction coefficient f defined in Equation 10.1 is the ratio of the shear force F_f to the normal force F_n acting on a surface. The friction coefficient depends on the type of lubrication and the fluid stress between two surfaces.

$$f = \frac{F_f}{F_n} = \frac{\tau}{\sigma_n} \quad (10.1)$$

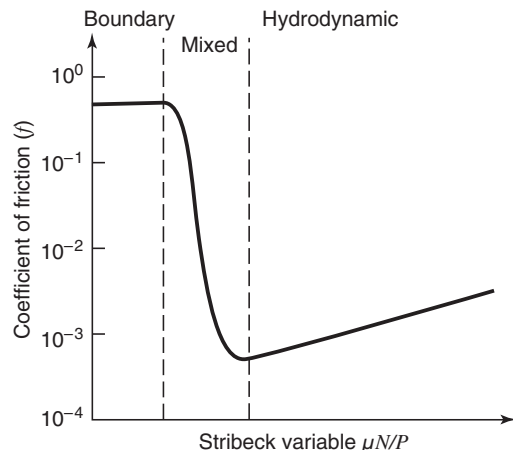


Figure 10.1 Stribeck diagram showing friction regimes.

Generally speaking, there are three friction regimes: hydrodynamic, mixed, and boundary friction. In an engine, the frictional losses have a variety of sources, for example, hydrodynamic friction in the crankshaft and camshaft journal bearings, mixed lubrication in the piston ring pack and skirt, and rolling contact friction in the valve train. The friction mean effective pressure (fmep) of an engine component depends on the friction regime and the lubricating surface geometry, such as whether the contacting surfaces are sliding (piston) or rotating (bearings) relative to each other.

The three friction regimes are shown on a Stribeck diagram in Figure 10.1. The diagram is named after Richard Stribeck (1861–1950), a German engineering professor who published pioneering studies of rotating bearing friction in 1901. The Stribeck diagram plots the friction coefficient as a function of a Stribeck variable or duty parameter. For rotating surfaces, the duty parameter is $\mu N / \sigma_n$, where μ is the lubricant dynamic viscosity, N is the relative rotational speed between surfaces, and σ_n is a normal stress, that is, the fluid pressure. For sliding surfaces, the duty parameter is $\mu U L / F_n$, where U is the relative velocity of the two surfaces, and L is the contact length in the direction of motion. In the hydrodynamic friction regime, the surfaces are completely separated by a liquid film of thickness h . This is a preferred mode of operation since mechanical wear is minimized. The shear stress is entirely due to the lubricant viscosity. Therefore in this regime, the friction coefficient f is given by Equation 10.2:

$$f = \frac{\mu}{\sigma_n} \frac{du}{dy} \quad (10.2)$$

and is a straight line on the Stribeck diagram. Crankshafts, connecting rods, and piston rings are designed to operate in the hydrodynamic regime as much as possible. An increase in lubricant temperature will decrease its viscosity, decreasing the duty parameter and the coefficient of friction. The relationship between the film thickness and the Stribeck duty parameter is shown schematically in Figure 10.2, indicating that the film thickness increases nonlinearly as the duty parameter increases.

As the pressure load on the lubricant is increased or the relative velocity decreased, the oil film thins out to the point where its thickness is comparable to the size of the surface irregularities. This is the mixed lubrication regime. The liquid film no longer completely separates the surfaces, and intermittent metal-to-metal contact occurs, causing an increase in the friction coefficient. The friction coefficient in the mixed regime is a combination of hydrodynamic and metal-to-metal contact friction.

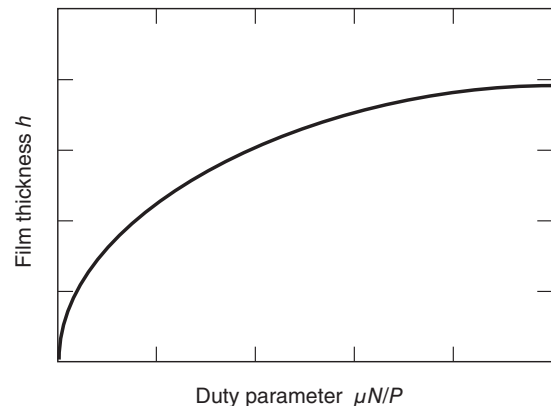


Figure 10.2 Schematic of lubricant film thickness versus Stribeck duty parameter.

With further increase in load or decrease in speed, the metal-to-metal boundary lubrication regime is reached. Boundary lubrication occurs at either end of the piston stroke when the piston velocity approaches zero, in relatively slow moving valve train components, and during engine start-up and shutdown. In boundary lubrication, oil film patches separate the sliding surfaces where the thickness is just a few molecular diameters of the lubricant, as shown in Figure 10.3. The force required to cause tangential motion in boundary lubrication is approximately the area of contact times the shear strength of the adsorbed oil layer, σ_o . It is important to know how the lubricant can be adsorbed by the surfaces, how rough the surfaces are, and whether or not the surface molecules themselves are prone to adhering to one another. The real area of contact depends primarily on the applied load, the yield strength, and the asperities of the softer material. The yield stress, σ_m , of the softer material balances the applied load, so that as the load increases, there is a proportional increase in the area of contact. The coefficient of friction in the metal-to-metal boundary lubrication regime is given by Equation 10.3:

$$f = \frac{\sigma_o}{\sigma_m} \quad (10.3)$$

and is independent of the engine design and operating parameters such as engine speed. The friction depends on the properties of the lubricant (excluding viscosity), and the properties of the sliding surfaces, such as the roughness, plasticity, elasticity, shear strength, and hardness.

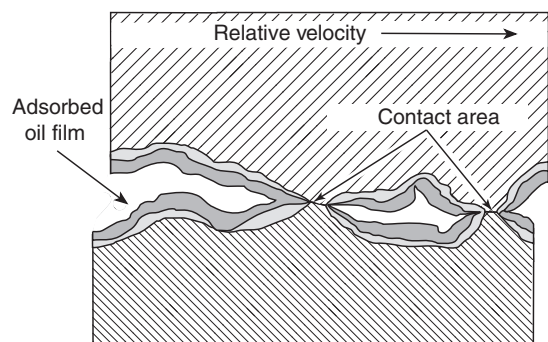


Figure 10.3 Metal-to-metal contact in boundary lubrication. Adapted from Rosenberg (1982).

10.3 FRICTION MEAN EFFECTIVE PRESSURE

The engine friction work, \dot{W}_f reduces the mechanical efficiency of an engine, and is the difference between the indicated work \dot{W}_i and the brake work \dot{W}_b . The friction work is eventually removed as waste heat by the engine cooling system. We can represent friction as a power loss:

$$\dot{W}_f = \dot{W}_i - \dot{W}_b \quad (10.4)$$

It is useful to normalize the engine friction power into a mean effective pressure (mep) form by dividing by displacement volume and engine speed so that the friction losses of engines of different sizes can be directly compared.

$$fmep = \frac{\dot{W}_f}{V_d N/2} \quad (10.5)$$

Therefore,

$$fmep = imep - bmep \quad (10.6)$$

The indicated mean effective pressure (imep) is the net work per unit displacement volume done by the gas during compression and expansion, and the brake mean effective pressure (bmep) is the external shaft work per unit displacement volume done by the engine. With this definition, the pumping losses during the intake and exhaust strokes are considered to be part of the overall engine friction. It is customary to also include the work to run auxiliary components with the mechanical friction when the friction mean effective pressure is defined as in Equation 10.6. Accordingly, the friction mean effective pressure is the sum of the mechanical friction (mfmeep), pumping (pmep), and accessory (amep) mean effective pressure.

$$fmep = mfmeep + pmep + amep \quad (10.7)$$

If a supercharger is connected to the engine crankshaft, then

$$fmep = imep - bmep - cmep \quad (10.8)$$

The term cmep is the work per unit volume required to power the supercharger compressor.

The friction power \dot{W}_f is the product of the friction force F_f and a characteristic velocity U :

$$\dot{W}_f = F_f U \quad (10.9)$$

Therefore, the mechanical friction mean effective pressure scales as

$$mfmeep \sim \frac{\dot{W}_f}{V_d N} \sim \frac{F_f U}{n_c b^2 s N} \quad (10.10)$$

where V_d is the displacement volume, n_c is the number of cylinders, b is the cylinder bore, s is the piston stroke, and N is the engine speed.

10.4 FRICTION MEASUREMENTS

There are a number of measurement methods used to determine the friction force and the friction mean effective pressure. The most direct method is to use Equation 10.6. The indicated mean effective pressure is computed from cylinder pressure measurements during compression and expansion, and the brake mean effective pressure is determined

from dynamometer measurements. Such measurements are discussed in Chapter 11. A more commonly used method that does not require the measurement of cylinder pressure is motoring the engine without combustion. This method measures the motoring mean effective pressure (mmeep), defined as the work per unit displacement volume required to rotate an engine operated without combustion. A direct current (dc) electric cradle-type dynamometer is an appropriate apparatus for such a measurement. The dynamometer is mounted on bearings and is restrained from rotation by only a strut connected to a load beam. When the dynamometer is absorbing or providing power, a torque is applied to the load cell of the dynamometer either by the engine or by the dc motor. The work done in rotating the crankshaft through one revolution is $2\pi\tau$. Hence, for two- and four-stroke engines, respectively

$$mep = \frac{4\pi\tau}{V_d} \quad (\text{four-stroke engine}) \quad (10.11)$$

$$mep = \frac{2\pi\tau}{V_d} \quad (\text{two-stroke engine}) \quad (10.12)$$

The above equations are valid whether or not the engine is firing. Although the sign of τ changes, we think of bmeep and mmeep as positive numbers. Practical application comes from the observation that under controlled conditions,

$$fmeep \approx mmeep \quad (10.13)$$

Therefore, motoring tests are useful because it is very much easier to measure mmeep than fmeep. However, it needs to be noted that the motored engine friction and the fired engine friction are not the same, since the thermodynamic state of the engine is different in each case. The motored friction can be more or less than the fired friction, depending on the relative magnitudes of the various friction components. The piston and cylinder bore temperatures are lower for the motored state, which will increase the viscosity and thus the hydrodynamic friction of the lubricating film, but also increase the clearances that lowers the friction. Since the combustion pressure on the piston rings is much greater for the fired case, the ring friction for the fired case will be greater than the motored case. Similarly, the bearing loads will be greater for the fired case. The cooler exhaust gas for the motoring case will have a greater density, producing a larger motored pmep. Finally, temperature gradients within the engine are much less in the motored engine than in the fired engine. To obtain approximately the same heat loss, oil and coolant temperatures should be matched between the motored and fired engines.

Comparisons between motoring and firing friction are given in Figure 10.4 for a diesel engine, and Figure 10.6 for a spark ignition engine. The total fmeep is on the order of 1 bar for both engines. The results illustrate the differences between a fired and a motored test. In both figures, the friction for motored and fired cases is determined by integrating

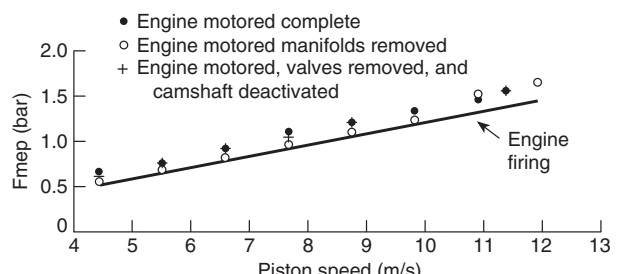


Figure 10.4 Diesel engine fmeep versus piston speed. (Brown, 1973.)

the pressure–volume diagram to obtain the imep and subtracting the measured bmep as per Equation 10.6. Therefore, the motored friction labeled in Figures 10.4 and 10.6 is the motored fmep, not the mmeep, which is obtained from dynamometer measurements alone.

The diesel engine tested by Brown (1973) in Figure 10.4 is a six-cylinder, in-line engine. As the piston speed is increased from 4 to 12 m/s, the fmep increases nearly linearly, with no significant variation with load. The motored fmep is slightly greater than the fired fmep, a consequence of cooler wall temperatures and higher oil viscosity during motoring. Since the airflow in a diesel engine is unthrottled, the pumping friction is not a function of the load.

The most important advantage of a motoring test is that the engine can be partially disassembled, which precludes firing, and motored to study the distribution of friction among the various parts. Figure 10.5 is typical of the results that can be obtained by this method. In this experiment by Brown (1973), the diesel engine was systematically disassembled, and the resulting fmep measured. To measure the pumping loss, the first items removed were the manifolds and turbocharger. Next the valves were removed and the camshafts disconnected. As disassembly proceeds, it became clear that pistons and rings are responsible for about one-half to three fourths of the friction. The last curve, H, shows the friction due to spinning only the crankshaft.

The spark ignition engine of Figure 10.6 is a four-cylinder, in-line engine with a 12 : 1 compression ratio. The mechanical friction (mfmep) and pumping (pmep) are plotted versus load for a constant mean piston speed of 6.1 m/s. As the throttle of the spark

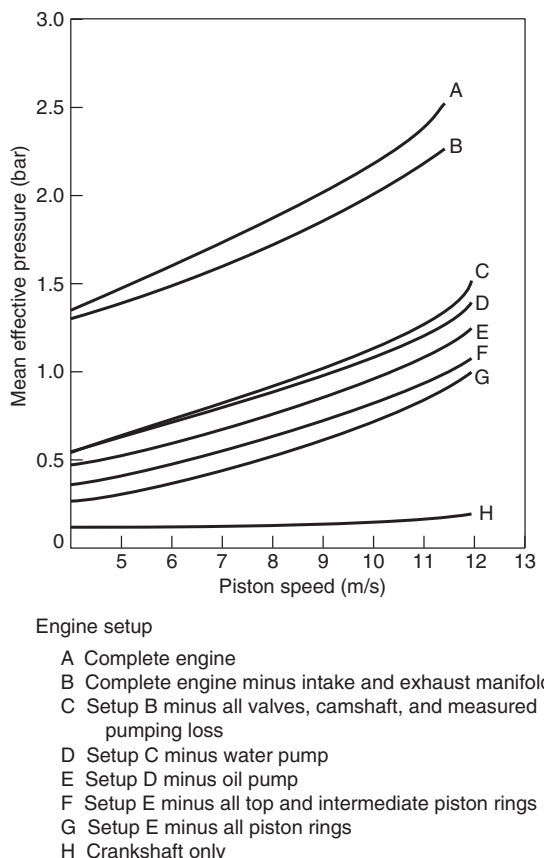


Figure 10.5 Motored friction mean effective pressure (fmep) during disassembly of a diesel engine.
Adapted from Brown (1973).

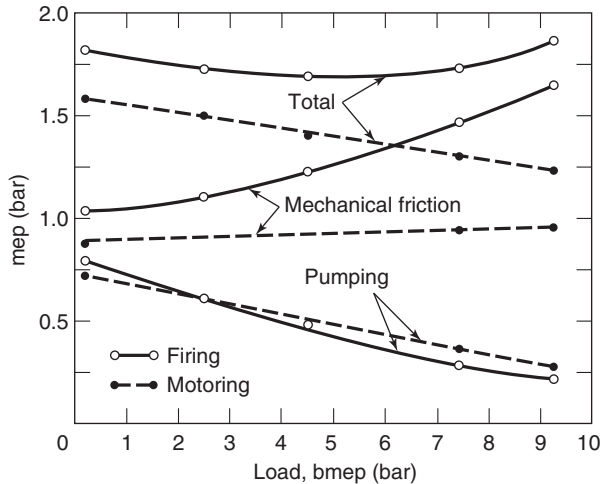


Figure 10.6 Gasoline engine friction versus load.
(Gish et al., 1957.)

ignition engine is opened to meet an increased load, the pmeep decreases for both the fired and motored cases. However, the fired mechanical friction increases with load due to the increased gas pressure, while the motored mechanical friction is unchanged. Consequently, for this engine, the total fired friction is greater than the motored total friction. Note that Equation 10.13 is a rather crude approximation at high loads for this spark ignition engine. For further reading in this area, an overview of techniques for measuring friction in fired engines is given in Noorman et al. (2000).

10.5 FRICTION MODELING

The above experimental results indicate that friction depends on the piston speed and the load. Other variables that immediately come to mind are the oil viscosity μ_o , oil density ρ_o , the compression ratio r , the bore b , and other geometrical parameters that specify the bearings, rings, pistons, cams, lifters, and so on. Mathematically,

$$f_{mep} = f \left[\bar{U}_p, \mu_o, \rho_o, r, imep, b, l_i (i = 1, 2, \dots), \sigma_j (j = 1, 2, \dots) \right] \quad (10.14)$$

where the $l_i (i = 1, 2, \dots)$ represent all the lengths and $\sigma_j (j = 1, 2, \dots)$ all the relevant material properties. The dimensionless groups are therefore

$$\frac{f_{mep}}{\rho_o \bar{U}_p^2} = f_1 \left[\frac{\rho_o \bar{U}_p b}{\mu_o}, r, \frac{imep b}{\mu_o \bar{U}_p}, \frac{l_i}{b}, \frac{\sigma_j}{b} \right] \quad (10.15)$$

The first dimensionless group in the argument list is a Reynolds number based on the piston speed, bore, and the oil dynamic viscosity μ_o .

$$Re = \frac{\rho_o \bar{U}_p b}{\mu_o} = \frac{\bar{U}_p b}{v_o} \quad (10.16)$$

since $v_o = \mu_o / \rho_o$. In the case of motoring mean effective pressure, the dependence on load is no longer necessary and we conclude that

$$\frac{mmeep}{\rho_o \bar{U}_p^2} = f_2 \left[Re, r, \frac{l_i}{b}, \frac{\sigma_j}{b} \right] \quad (10.17)$$

That the Reynolds number based on mean piston speed is the proper scaling parameter has been demonstrated by Taylor (1985), who did experiments with geometrically similar engines. Geometrically similar engines refer to any family of engines manufactured from the same materials with same l_i/b , σ_i/b , that is, same compression ratio and stroke to bore ratio. In Taylor's experiments, the motoring mean effective pressures for three different engines (with $b = 6.35$ cm, 10.2 cm, and 15.2 cm), fell on a common curve when plotted as a function of mean piston speed. The oil viscosities were chosen to be proportional to the bore, so the mmeep was a function of the Reynolds number. This implies that

$$\frac{\text{mmeep}}{\rho_0 \bar{U}_p^2} = f_3(Re) \quad (\text{Geometrically similar engines}) \quad (10.18)$$

When one recognizes that to a certain degree, all reciprocating piston engines are geometrically similar, then Equation 10.18 applies in an order of magnitude analysis for any engine. Since the viscosity of oil used in engines is more or less independent of size, the friction can be expected to be relatively less in larger engines than in smaller engines.

As an illustration of the application of Equation 10.18, the correlation of Bishop (1964) is

$$\frac{\text{mmeep}}{\rho_0 \bar{U}_p^2} = \frac{1.3 \times 10^5}{Re} + \frac{1.7 \times 10^8}{Re^2}(r + 15) \quad (10.19)$$

Equation 10.19 implies that the motoring mean effective pressure decreases as engine size increases, as shown by writing it in dimensional form:

$$\text{mmeep} = 1.3 \times 10^5 \frac{\bar{U}_p \mu}{b} + 1.7 \times 10^8(r + 15) \frac{\mu^2}{\rho b^2} \quad (10.20)$$

Engine friction models have been developed to account for different types of friction and are used in the engine design process to estimate the influence of parameters such as engine speed and geometry on engine friction. The process used in the modeling is to develop component fmep models, then sum the component fmep values to arrive at a prediction of overall engine fmep. Papers by Sandoval and Heywood (2003) and Shayler et al. (2005) develop engine friction models and explicitly include the dependence on oil viscosity. There has been a continued decrease in engine friction over the last 50 years due to advances in component design and manufacturing, so the coefficients used in friction models always need to be adjusted for a given engine.

10.6 JOURNAL BEARING FRICTION

The journal bearings used in an internal combustion engine include the main crankshaft bearings, connecting rod bearings, and accessory bearings and seals. A crankshaft with main and connecting rod journal bearing shafts is shown in Figure 10.7. Note the lubrication ports on the shafts and the different main and connecting rod bearing diameters. A journal bearing is shown schematically in Figure 10.8. The journal bearing is cylindrical, with as smooth a finish as possible. The journal bearing operates in the hydrodynamic friction regime during normal operation. During start-up and shutdown, the friction regimes are mixed and boundary friction due to the low bearing speed.

Journal bearings are relatively soft to allow foreign particles to be embedded without damaging the journal and have a low melting point to reduce the risk of seizure. Materials used in journal bearings in internal combustion engines are composed of babbitt, which is an alloy of lead (Pb), tin (Sn), antimony (Sb), and copper (Cu), specified by ASTM Standard

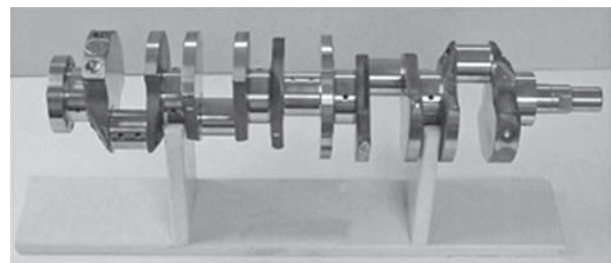


Figure 10.7 Engine crankshaft.
(Courtesy Norton Manufacturing.)

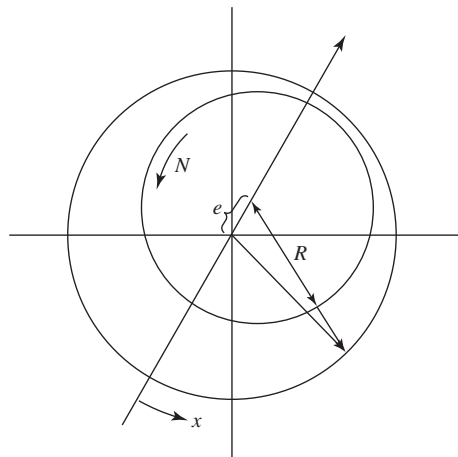


Figure 10.8 Journal bearing geometry.

B23-2010. The bearing material is named after Isaac Babbitt (1799–1862), an American engineer who invented a low-friction tin-based metal alloy for use in bearings. The babbitt alloy has a relatively low load-carrying capacity, so it is bonded to a stronger substrate such as steel or aluminum. Babbitt thicknesses in engine bearings currently range from 20 to 200 μm , a significant improvement from typical babbitt thicknesses of the order of 5 mm in 1900. A lead-based babbitt is composed of roughly 89% Pb, 9% Sn, and 2% Cu.

Loads on crankshaft bearings vary significantly with crank angle, the connecting rod geometry, and the combustion gas pressure. To meet the bearing loads, crankshaft main bearings for automotive spark ignition engines are typically sized to be about 65% of the cylinder bore, and connecting rod bearings are sized to be about 55% of the cylinder bore. Bearing lengths are sized at 35–40% of the cylinder bore. In addition to the crankshaft and connecting rod journal bearings, there are journal bearings on the camshaft rotating at one-half the engine speed. Also, the piston pin on the connecting rod oscillates back and forth without completing a revolution.

The difference in the diameters of the inner shaft and the outer bearing creates a thin annulus through which the lubricant flows. At rest the shaft sits in contact with the bottom of the bearing. As the shaft begins to rotate, its center line shifts eccentrically in the bearing maintaining metal-to-metal contact with the bearing. As the engine speed increases, the bearing will “aquaplane” and enter the hydrodynamic regime, in which the rotating shaft carries the oil all the way around the annulus between the two cylinders. If the bearing is not sealed, oil will leak out at the ends, so oil is pumped at relatively low pressures through internal passages to the bearing annulus.

A minimum oil film thickness is required to maintain hydrodynamic lubrication as operation in the mixed or boundary lubrication regime increases engine wear. For automotive class engines, the minimum thickness is on the order of $2\mu\text{m}$. The oil film thickness can be determined by resistance and capacitance measurements. Measurements by Tseregounis et al. (1998) in a multicylinder engine indicated that the minimum film thickness occurs during the power stroke of the cylinder nearest the bearing.

The oil film in a journal bearing is thin compared with the diameter of the bearing, so if one neglects the bearing curvature, the flow in a journal bearing can be modeled as Couette flow with constant dynamic viscosity μ . The velocity gradient in a bearing of diameter D_b , length L_b , and annular clearance c is therefore

$$\frac{du}{dr} = \pi D_b N / c \quad (10.21)$$

The friction force, F_f , in the bearing is

$$F_f = A\mu \frac{du}{dr} = (\pi D_b L_b) \mu \pi D_b N / c = \pi^2 \mu D_b^2 L_b N / c \quad (10.22)$$

Equation 10.22 is known as Petrov's equation, named after the Russian scientist Nikolai Petrov (1836–1920), who published his analyses of hydrodynamic flow in bearings in 1883. The friction coefficient in the Petrov model is

$$f = \frac{F_f}{P\pi D_b L_b} = \pi(\mu N / P) D_b / c \quad (10.23)$$

In the hydrodynamic regime, the Petrov flow model predicts that the friction coefficient increases linearly with the Stribeck variable, and the slope is dependent on the ratio of the bearing diameter to clearance. The friction of real bearings approaches the Petrov value at high values of the Stribeck variable, $\mu N / P$. More rigorous analyses include the bearing load and eccentricity, but the results still retain the scaling of the Petrov equation.

Using the Petrov equation, the nondimensional fmep of n_c journal bearings is inversely proportional to the oil Reynolds number:

$$\frac{\text{fmep}}{\rho_o \bar{U}_p^2} \sim \frac{1}{n_c} \left[\frac{\frac{D_b L_b}{b s}}{\frac{c}{D_b}} \right] \frac{1}{Re} \quad (10.24)$$

The friction mean effective pressure of a journal bearing array, such as the crankshaft main bearings or the connecting rod bearings, scales with engine speed to the 0.6 power (Shayler et al. 2005), assuming constant bearing clearance and oil viscosity, as shown in Equation 10.25:

$$\begin{aligned} \text{fmep}_{\text{bearings}} &\sim \frac{F_f U}{n_c N b^2 s} \\ &= c_b \left(\frac{n_b N^{0.6} D_b^3 L_b}{n_c b^2 s} \right) \left(\frac{\mu}{\mu_{\text{ref}}} \right)^{0.4} \end{aligned} \quad (10.25)$$

Shayler et al. (2005) suggest a proportionality constant $c_b = 0.0202$ ($\text{kPa}\cdot\text{min}^{0.6}/\text{rev}^{0.6}\cdot\text{mm}$) for automotive diesel engines.

The crankshaft bearing seals operate in a boundary lubrication regime, since the seals directly contact the crankshaft surface. As the normal force, which is the seal lip load, is constant, the friction force will be constant, and the friction mean effective pressure of the

crankshaft bearing seal will be independent of engine speed, and will scale as

$$\text{fmePseals} \sim \frac{ND_b}{n_c Nb^2 s} = c_s \frac{D_b}{n_c b^2 s} \quad (10.26)$$

Shayler et al. (2005) suggest a proportionality constant $c_s = 9.36 \times 10^4 \text{ kPa-mm}^2$.

10.7 PISTON AND RING FRICTION

Piston assembly friction is the major component of engine friction. The piston assembly is composed of compression rings, oil control rings, piston skirts, and piston pins. Advances in materials and increased understanding of friction have reduced the energy lost to friction; however, due to the reciprocating relative motion between the cylinder and the piston surfaces, piston and ring friction remain a major source of friction loss. Over the years, due to improvements in materials and manufacturing techniques, piston skirts have become smaller, the number of rings has decreased, and the piston has become lighter.

Illustrations of a piston and connecting rod, piston head and skirt, and a piston ring assembly are shown in Figures 10.9–10.11, respectively, showing the relative sizes and locations of the piston head, skirt, and rings.



Figure 10.9 Piston and connecting rod. (Courtesy Mahle, Inc.)

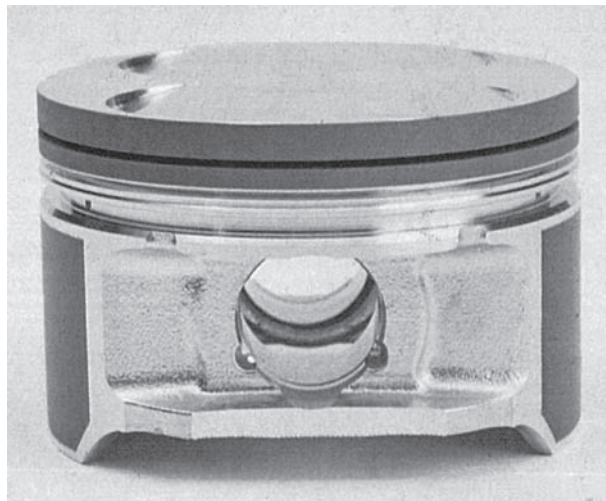


Figure 10.10 Piston head for a spark ignition engine. (Courtesy Mahle, Inc.)

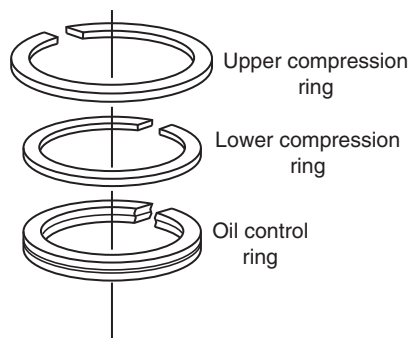


Figure 10.11 Piston ring assembly schematic.
Adapted from Merrion (1994).

The friction of the piston and rings results from the reciprocating contact between the piston skirt and the ring pack with the cylinder bore. The cylinder bore is rougher than a journal bearing bore, since the cylinder bore must retain some oil during operation. The clearance c between the piston and the cylinder wall is typically specified to be about 0.050 mm for street automobile engines and is increased to 0.100 mm or greater for race engines to reduce friction losses.

The piston ring pack has three main functions. The rings seal the combustion chamber, control the lubrication oil flow, and transfer heat from the piston to the cylinder. In order to preserve a seal against the cylinder bore, each ring has some amount of radial tension. Current ring pack designs generally use three piston rings, two compression rings, and an oil control ring. Common types of piston rings are shown in Figure 10.12. Various cross sections are available, such as rectangular, crown or barrel face, taper, and dykes. The top compression ring can have a bevel on the upper inside edge of the ring to produce a positive twist, and a seal on the bottom edge of the ring. The second ring can have a bevel on the bottom inside edge to produce a reverse twist that will help scrape oil off the cylinder wall. The oil control ring typically has two narrow rails and an expander that wipes off excess oil from the cylinder liner.

Ring materials include cast iron, ductile (nodular) iron, and stainless steel. A ring pack will often have a ductile iron top ring, a cast iron second ring, and a stainless steel oil ring. Coatings available for ring faces are molybdenum and chrome. The space between

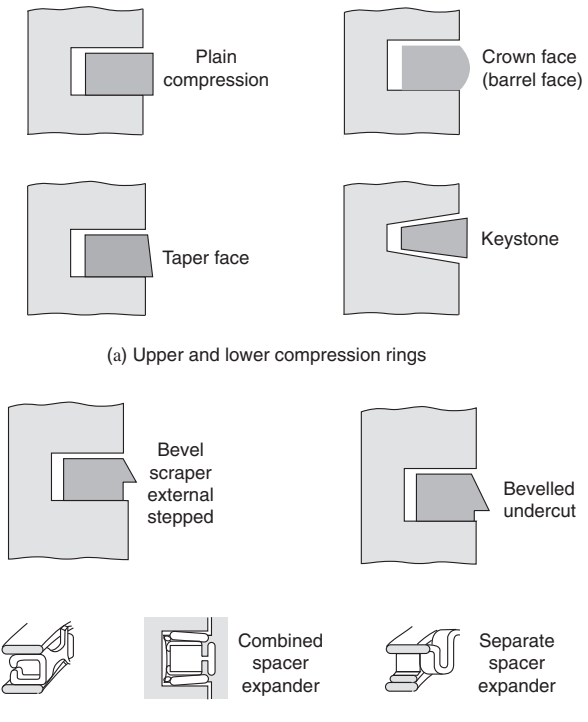


Figure 10.12 Common types of piston rings.

the side of the ring and the groove is called the side clearance, and the space between the back of the ring and the groove is called the back clearance. The back clearance is minimized in high-performance engines to increase the sealing effectiveness. The side and back clearances allow the pressure in the piston groove to follow the cylinder pressure, so as the cylinder pressure increases, the increasing groove pressure presses the compression rings more firmly against the cylinder wall, increasing the sealing. Piston rings are split, forming an end gap, so that they can be slipped onto the piston and also accommodate thermal expansion of the piston ring. Engine power is sensitive to the size of the end gap, so the end gap is minimized in high-performance engines.

The piston skirt is designed to meet the side thrust forces originating from the rotation of the connecting rod. The side thrust force on the piston skirt depends on the crank angle, cylinder pressure, piston speed, acceleration, and connecting rod geometry. In addition, the wrist pins are offset slightly by 1–2 mm to reduce the side thrust force. Offsetting the wrist pins will also reduce piston noise.

Figure 10.13 illustrates a force balance applied to the piston. The forces on the piston result from the gas pressure P , connecting rod applied force F_r , friction force F_f , the side thrust force F_t , and the piston inertia $m_p a_p$. These forces can be resolved into x - and y -direction force balances as given by Equations 10.27 and 10.28:

$$\sum F_x = m_p a_p = -F_r \cos \phi + P \frac{\pi}{4} b^2 \pm F_f \quad (10.27)$$

$$\sum F_y = F_t - F_r \sin \phi = 0 \quad (10.28)$$

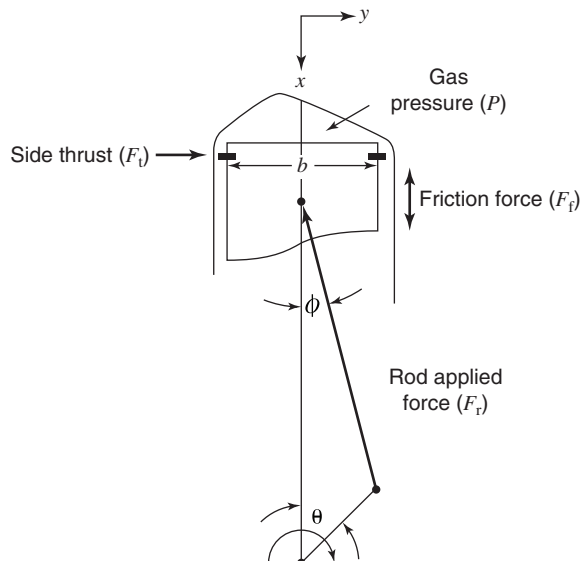


Figure 10.13 Piston force balance.

The sign on the friction force depends on the crank angle θ . It is negative when the piston is moving downward toward the crankshaft ($0^\circ < \theta < 180^\circ$) and positive when the piston is moving upward ($180^\circ < \theta < 360^\circ$). Solving for the side thrust force F_t :

$$F_t = \left(+P \frac{\pi}{4} b^2 \pm F_f - m_p a_p \right) \quad (10.29)$$

The piston acceleration a_p , Equation 1.33 from Chapter 1, for small $\epsilon = s/2l$ is

$$a_p = \frac{\omega^2 s}{2} [\cos \omega t + \epsilon \cos 2\omega t] \quad (10.30)$$

Results of piston force balance calculations for a particular engine are given in Figure 10.14. A detailed calculation of side thrust force versus crank angle requires data from the P-V diagram, the mass and moment of inertia of the piston and connecting rod, and the engine speed. The largest side thrust forces occur during the expansion stroke when

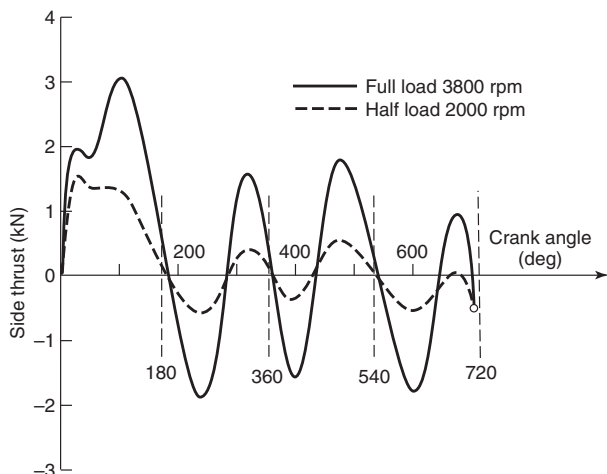


Figure 10.14 Piston side thrust load and the switch of contact sides. Adapted from Ting and Mayer (1974).

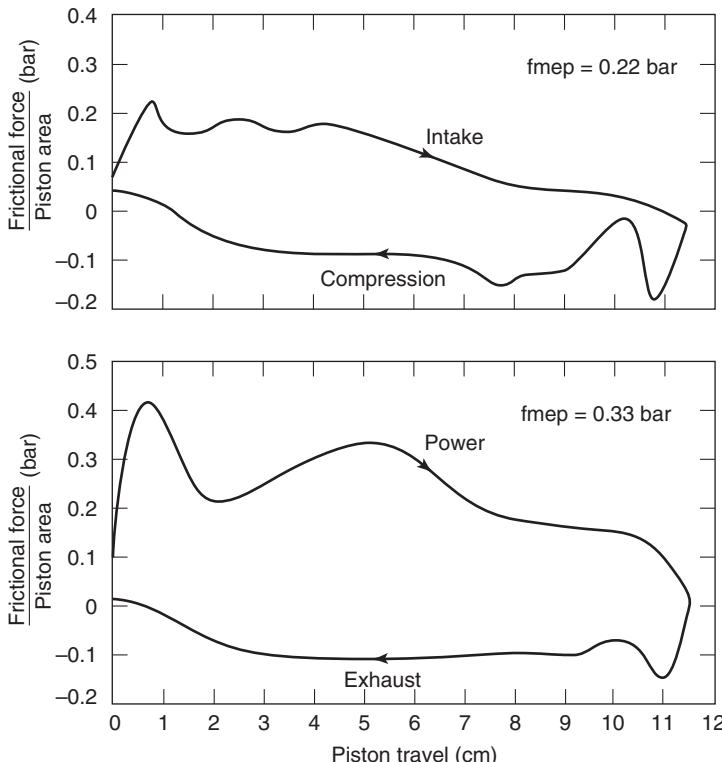


Figure 10.15 Piston and ring friction, $\bar{U}_p = 4.57 \text{ m/s}$, $\text{bmep} = 5.78 \text{ bar}$, $T_c = T_{\text{oil}} = 356 \text{ K}$ (Leary and Jovellanos, 1944).

the cylinder pressures are largest. The side thrust force changes sides as the piston passes through top and bottom center since the connecting rod changes sides.

As a consequence of the force balance, the “left” side of the clockwise rotating piston in Figure 10.13 is subjected to larger forces than the “right” side. In this case, the left side is referred to as the major thrust side, whereas the right side is called the minor thrust side. Since the friction work is the product of the friction force and piston velocity, the friction work will be the largest during the middle of the stroke where the piston velocity is greatest. Engines show more upper cylinder wear on the major thrust side than on the minor thrust side as a result.

The friction due to the piston–ring assembly has been directly measured in a friction research engine. Typical results are shown in Figure 10.15. The following features should be noted (Taylor, 1985):

- The fmep due to piston and ring friction is on the order of 20–30 kPa for this engine.
- Friction forces occurring during expansion are about twice as large as those occurring during any other stroke.
- Friction forces are comparable on the compression and exhaust strokes.
- Friction forces tend to be high just after top and bottom dead center, which Taylor hypothesized was due to metallic contact between the rings and the cylinder wall.
- The friction force is nonzero at the top and bottom dead centers, due to the type of friction research engine, which had a spring-loaded cylinder head for measurement of the axial friction force.

Support for Taylor's hypothesis that metallic contact occurs in the vicinity of top dead center comes from measurements of the oil film in running engines. Measurements of the oil film thickness have been performed (e.g., see McGeehan, 1978) using electrical resistance and capacitance techniques. The results show that resistance is low in the vicinity of top and bottom dead center, as one would expect, if there is metallic contact. The electrical resistance is higher at the middle of each stroke where piston speed is high and hydrodynamic lubrication is expected. Similar results have been reported by Arcoumanis et al. (1998) using a laser-induced fluorescence system. Therefore, it has generally been concluded that a boundary lubrication regime exists at the ends of the stroke where the piston speed is low, and hydrodynamic lubrication exists in the middle of each stroke where the piston speed is higher.

Friction correlations for piston and ring friction have been developed that take both the boundary lubrication and the hydrodynamic friction regimes into account. The hydrodynamic friction component depends on the contact area. Setting L_s as the average piston skirt and ring contact length, and c as an average skirt clearance, the friction force, F_f , of the piston skirt scales as

$$F_f = A\mu \frac{du}{dy} \sim bL_s\mu \frac{\bar{U}_p}{c} \quad (10.31)$$

and for n_c pistons, the piston skirt fmep scales as

$$\begin{aligned} \text{fmep}_{\text{skirt}} &\sim \frac{F_f U}{n_c N b^2 s} \sim \frac{(\mu n_c b L_s \bar{U}_p) \bar{U}_p}{c n_c N b^2 s} \\ &= \mu \frac{L_s \bar{U}_p}{bc} \end{aligned} \quad (10.32)$$

It is reasonable to assume that the piston skirt length and the clearance scale directly with the bore, that is, $L_s \sim b$, and $c \sim b$. The skirt length scaling is based on geometrical similarity, and the clearance scaling is based on thermal expansion considerations. Therefore, the piston skirt hydrodynamic fmep is inversely proportional to the bore and can be expressed as

$$\text{fmep}_{\text{skirt}} \sim \mu \frac{\bar{U}_p}{b} = c_{ps} \frac{\bar{U}_p}{b} \quad (10.33)$$

Patton et al. (1989) suggest a coefficient $c_{ps} = 294 \text{ kPa-mm-s/m}$ for the piston skirt friction, including the oil properties in the proportionality constant.

The friction force of the piston rings has two components, one resulting from the ring tension and the other component from the gas pressure loading. The component of piston friction due to ring tension in the mixed lubrication regime will have a friction coefficient inversely proportional to the engine speed. Patton et al. (1989) recommend a scaling for piston-ring friction that bridges the boundary and hydrodynamic lubrication regimes given by

$$F_f \sim f F_n \sim \left(1 + \frac{1000}{N}\right) \quad (10.34)$$

The piston ring scaling is

$$\text{fmep}_{\text{rings}} \sim \frac{n_c \left(1 + \frac{1000}{N}\right) \bar{U}_p}{n_c N b^2 s} = c_{pr} \left(1 + \frac{1000}{N}\right) \frac{1}{b^2} \quad (10.35)$$

The proportionality constant recommended by Patton et al. (1989) is $c_{pr} = 4.06 \times 10^4 \text{ kPa-mm}^2$.

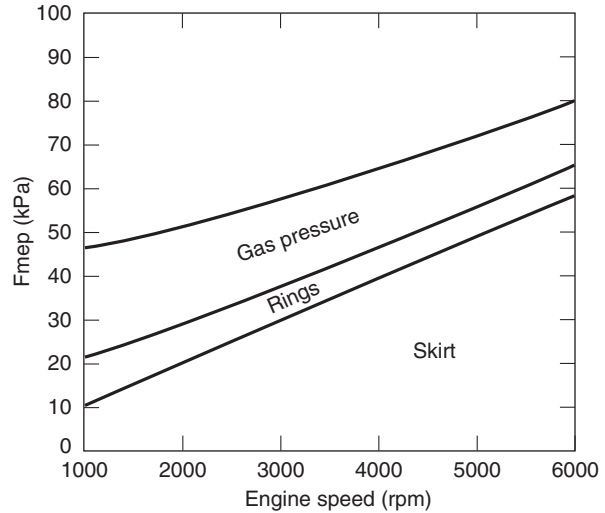


Figure 10.16 Components of piston friction.

A correlation for the component of piston friction due to the gas pressure loading recommended by Bishop (1964) is

$$fmep_{\text{gas}} = c_g \frac{P_i}{P_a} \left(0.088r + 0.182r^{(1.33-K\bar{U}_p)} \right) \quad (10.36)$$

where P_i is the intake manifold pressure, P_a is the atmospheric pressure, r is the compression ratio, $c_g = 6.89$, and $K = 2.38 \times 10^{-2}$ s/m. The correlation includes the effect of compression ratio and a decrease in the friction coefficient in the mixed lubrication regime.

Relative magnitudes of the three piston friction terms: skirt, ring pack, and bearings are shown in Figure 10.16 for the 82-mm bore diesel engine specified in Table 10.4. The skirt and rod bearing fmep increase linearly with engine speed, while the piston ring fmep decreases with engine speed. At low speeds, most of the friction is due to the piston rings, and at higher speeds, the majority of the friction is from the piston skirt.

Figure 10.17 illustrates some concepts used for a theoretical analysis of ring friction. There is an oil layer separating the ring from the cylinder wall whose thickness, δ , is both time and spatially dependent. The oil pressure P_{oil} is also time and spatially dependent. Since the bore is much larger than the oil film thickness, a one-dimensional approximation can be used. In the situation shown, the coordinate system is defined so that the ring is stationary and the cylinder wall is moving with the instantaneous piston speed, U_p . For the case in which the oil film is much thinner than the ring width, that is

$$\delta(x, t) \ll L \quad (10.37)$$

the Navier–Stokes equations for the oil motion reduce to a Reynolds equation, which is

$$\frac{d}{dx} \left[\delta^3 \frac{dP_{\text{oil}}}{dx} \right] = 6\mu U \frac{d\delta}{dx} + 12\mu \frac{d\delta}{dt} \quad (10.38)$$

The boundary conditions to be applied to the Reynolds equation in the case illustrated by Figure 10.17 are

$$P_{\text{oil}}(0, t) = P_{\text{top}}(t) \quad (10.39)$$

$$P_{\text{oil}}(L, t) = P_{\text{bot}}(t) \quad (10.40)$$

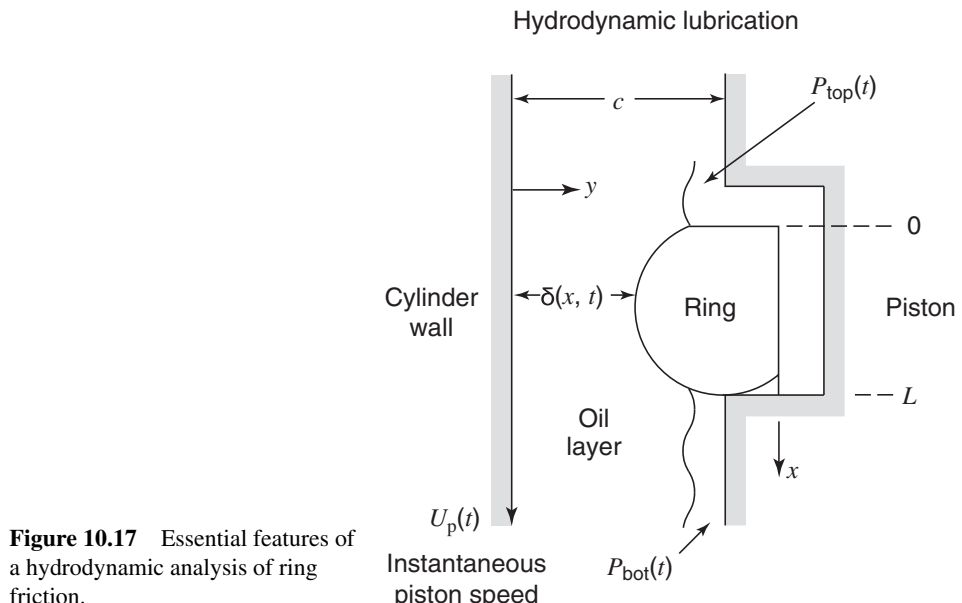


Figure 10.17 Essential features of a hydrodynamic analysis of ring friction.

where $P_{top}(t)$ and $P_{bot}(t)$ are periodic functions known either from direct measurements or from a combustion model complete with a blowby model. Numerical solution of the Reynolds equation yields the oil film thickness $\delta(x, t)$ and the oil pressure $P_{oil}(x, t)$ such that the boundary conditions are satisfied.

Models that include both boundary and hydrodynamic lubrication are available for analysis of the piston ring pack. The models also account for piston tilt, blowby and inter-ring pressures, ring and piston curvature, ring tension, and surface roughness. The results of the modeling predict the oil film thickness and pressure distribution for each ring. Some calculated oil film thicknesses for a particular engine are shown in Figure 10.18. In the

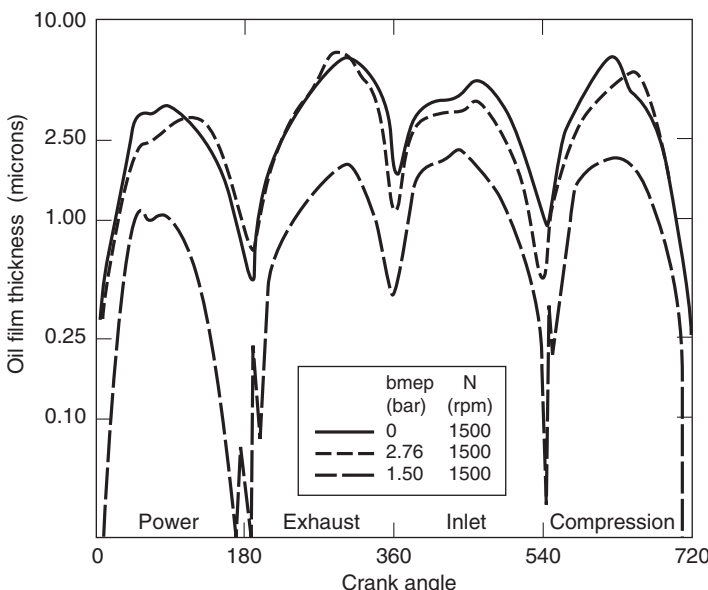


Figure 10.18 Effect of load and speed on minimum oil film thickness (Allen et al., 1976).

Table 10.1 Types of Valve Trains

Type I	OHC	Direct acting/flat or roller follower
Type II	OHC	End pivot rocker/flat or roller follower
Type III	OHC	Center pivot rocker/flat or roller follower
Type V	CIB	Rocker arm/flat or roller follower

graph, the minimum oil thickness is plotted for different speeds and loads. The results are similar in shape for all conditions and are fairly insensitive to speed and load. Surface roughness in engines is such that for film thicknesses less than about a micron, metal-to-metal contact can be expected to occur. The results in Figure 10.18 show that metal-to-metal contact can be expected to occur at top and bottom dead center for all speeds and loads. The results also show that at high load, metal-to-metal contact can occur for most, if not all, of the power stroke.

10.8 VALVE TRAIN FRICTION

The valve train friction results from the camshaft, cam follower, and valve components. Common valve train designs are listed in Table 10.1. The designs listed in Table 10.1 include overhead cam (OHC) and cam-in-block (CIB) with push rods. Either flat (ff) or roller (rf) cam followers are used. A schematic of these valve train designs is given in Figure 10.19. The shape and orientation of the camshaft lobes of a type V push rod V8 engine is shown in Figure 10.20. A type V rocker arm with a roller follower is shown in Figure 10.21 and rocker arms mounted on a cylinder head are shown in Figure 10.22. Example engine poppet valves are shown in Figure 10.23.

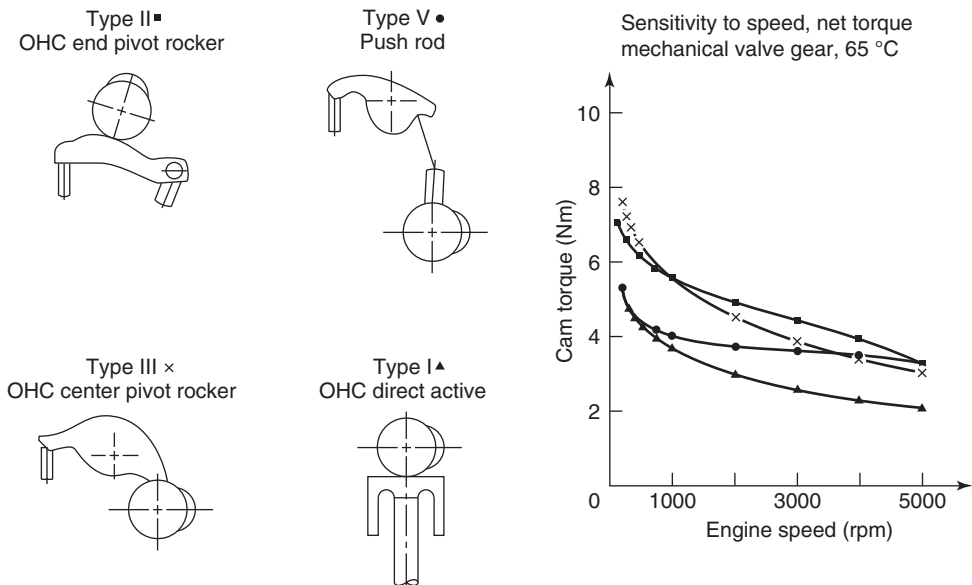


Figure 10.19 Various valve train designs (Rosenberg, 1982).

Figure 10.20 Example V8 engine camshaft. (Courtesy COMP Cams.)



Figure 10.21 Type V push rod rocker arm with roller follower. (Courtesy Jesel Valve train Components.)



Figure 10.22 Rocker arms on cylinder head. (Courtesy Jesel Valve train Components.)



Figure 10.23 Engine poppet valves. (Courtesy Wesco Valve.)



The valve train frictional losses are due to the following: hydrodynamic friction in the camshaft bearing, mixed lubrication in the flat followers, rolling contact friction in the roller followers, and both mixed and hydrodynamic friction due to the oscillating motion of the lifters and valves.

The hydrodynamic friction in the camshaft is similar to that in the main and connecting rod bearings. If the camshaft bearing diameter and length are assumed to be constant and not a function of engine size, the fmep scales as

$$\text{fmep}_{\text{cam}} \sim \frac{N n_{\text{cs}}}{n_c b^2 s} = c_c \frac{N n_{\text{cs}}}{n_c b^2 s} \quad (10.41)$$

where n_{cs} is the number of camshaft bearings, assumed equal to the product of the number of camshafts and the number of main bearings. Shayler et al. (2005) suggest a value of $c_c = 6720 \text{ kPa-mm}^3 \cdot \text{min}^{0.6}/\text{rev}^{0.6}$ as the proportionality constant, plus an additional value of 1.2 kPa to account for the camshaft oil seals.

For scaling purposes, the normal force in the valve mechanism components such as followers, rocker arms, valve lifters, and valves is assumed to be proportional to the product of the effective valve train mass and acceleration. The valve train effective mass is proportional to valve area, which is in turn proportional to the cylinder cross-sectional area. Therefore, the normal force in the valve train scales as the square of the cylinder bore.

A flat follower (ff) is assumed to operate in the mixed lubrication regime, and can be scaled with a friction coefficient inversely proportional to engine speed.

$$F_f = f F_n = \left(2 + \frac{10}{5 + \mu N} \right) b^2 \quad (10.42)$$

Therefore, the flat follower fmep can be expressed as

$$\text{fmep}_{\text{ff}} \sim \frac{F_f U}{n_c N b^2 s} = c_{\text{ff}} \left(2 + \frac{10}{5 + \mu N} \right) \frac{n_v}{n_c s} \quad (10.43)$$

where n_v is the total number of valves, and c_{ff} is the flat follower coefficient.

A roller follower (rf) operates in the rolling contact friction regime and therefore is scaled with a friction coefficient proportional to engine speed:

$$F_f = f F_n \sim N b^2 \quad (10.44)$$

$$\text{fmep}_{\text{rf}} = c_{\text{rf}} \frac{n_v N}{n_c s} \quad (10.45)$$

where c_{rf} is the roller follower coefficient.

The coefficients for the valve train friction terms are given in Table 10.2 for the four types of valve train mechanisms. In Table 10.2, the coefficients for the flat follower, the roller follower, oscillating hydrodynamic, and oscillating mixed fmep have the units of kPa-mm, kPa-mm-min/rev, kPa-(mm-min/rev)^{1/2}, and kPa, respectively.

10.9 ACCESSORY FRICTION

The accessory mean effective pressure (amep) is the sum of the remaining crankcase friction terms other than the journal bearing, piston and rings, and valve train losses. It includes the oil pump (Figure 10.24), water pump (Figure 10.25), and noncharging alternator friction. If these terms are assumed to be proportional to engine displacement, then by reference to Equation 10.10, the mean effective pressure of the accessories is a function of engine speed only and can be represented by a second-order polynomial.

Table 10.2 Coefficients for Valve Train Friction Terms

Configuration	Type	Flat follower c_{ff} (kPa-mm)	Roller follower c_{rf} (kPa-mm-min/rev)	Oscillating hydrodynamic c_{oh} (kPa-mm-min/rev) $^{1/2}$	Oscillating mixed c_{om} (kPa)
Single overhead cam (SOHC)	Type I	200	0.0076	0.5	10.7
Double overhead cam (DOHC)	Type I	133	0.0050	0.5	10.7
Single overhead cam (SOHC)	Type II	600	0.0227	0.2	42.8
Single overhead cam (SOHC)	Type III	400	0.0151	0.5	21.4
Cam in block (CIB)	Type IV	400	0.0151	0.5	32.1

Source: Patton et al., 1989.



Figure 10.24 Engine oil pump.
(Courtesy Melling Engine Parts.)



Figure 10.25 Engine water pump.
(Courtesy Airtex Products.)

Table 10.3 Coefficients for Auxiliary Friction Terms

	c_1 (kPa)	c_2 (kPa-min/rev)	c_3 (kPa-min ² /rev ²)	n
Oil pump	1.28	0.0079	-8.4×10^{-7}	0.3
Water pump	0.13	0.002	$+3.0 \times 10^{-7}$	0.7

Source: Shayler et al., 2005.

The accessory mean effective pressure with a viscosity correction suggested by Shayler (2005) is

$$\text{amep} = c_1 + (c_2 N + c_3 N^2)(\mu/\mu_{\text{ref}})^n \quad (10.46)$$

where the coefficients are given in Table 10.3.

10.10 PUMPING MEAN EFFECTIVE PRESSURE

The pumping mean effective pressure (pmeep) is the sum of the pressure drops across flow restrictions during the intake and exhaust strokes. It is a measure of the work required to move the fuel-air mixture into and out of an engine. The flow restrictions are categorized into four main areas: the intake system (is), the inlet valves (iv), the exhaust valves (ev), and the exhaust system (es). The major intake system flow restrictions are the throttle valve, air filter, intake manifold, and carburetor. The exhaust system flow restrictions include the exhaust manifold, catalytic converter, muffler, and tail pipe. Accordingly, the total pmeep is given by Equation 10.47:

$$\text{pmeep} = \Delta P_{\text{is}} + \Delta P_{\text{iv}} + \Delta P_{\text{ev}} + \Delta P_{\text{es}} \quad (10.47)$$

The pressure drop in the intake system ΔP_{is}

$$\Delta P_{\text{is}} = P_a - P_i \quad (10.48)$$

where P_i is the manifold pressure upstream of the inlet valves and P_a is the atmospheric pressure. The pressure drop across the inlet valves scales with the density, mass flow rate, and the open valve area

$$\Delta P_{\text{iv}} \sim \rho U^2 \sim \frac{1}{\rho} \left(\frac{\dot{m}}{n_{\text{iv}} A_{\text{iv}}} \right)^2 \quad (10.49)$$

where n_{iv} is the number of intake valves per cylinder. The mass flow rate scales with the volumetric efficiency that in turn is proportional to the intake/atmospheric pressure ratio:

$$\dot{m} \sim V_d N \sim e_v b^2 s N \sim \frac{P_i}{P_a} b^2 \bar{U}_p \quad (10.50)$$

Neglecting the density change across the valves, the inlet valve pressure drop therefore scales as the square of the mean piston speed

$$\Delta P_{\text{iv}} = c_v \left(\frac{P_i}{P_a} \frac{\bar{U}_p b^2}{n_{\text{iv}} D_{\text{iv}}^2} \right)^2 \quad (10.51)$$

where D_{iv} is the intake valve diameter. Similarly, the exhaust valve pressure drop ΔP_{ev} scaling is

$$\Delta P_{ev} = c_v \left(\frac{P_i}{P_a} \frac{\bar{U}_p b^2}{n_{ev} D_{ev}^2} \right)^2 \quad (10.52)$$

where D_{ev} is the exhaust valve diameter, and n_{ev} is the number of exhaust valves per cylinder. The constant of proportionality determined by Millington and Hartles (1968) for small high-speed diesel engines is $c_v = 4.12 \times 10^{-3}$ kPa·s²/m².

The exhaust system pressure drop ΔP_{es} also scales with the square of the mass flow rate:

$$\Delta P_{es} \sim \frac{\dot{m}^2}{\rho_{es}} = c_{es} \left(\frac{P_i}{P_a} \bar{U}_p \right)^2 \quad (10.53)$$

If the total exhaust system pressure drop is assumed to be 40 kPa at a piston speed of 15 m/s at wide open throttle conditions, then the proportionality constant c_{es} equals 0.178 kPa·s²/m² (Patton et al., 1989).

10.11 OVERALL ENGINE FRICTION MEAN EFFECTIVE PRESSURE

The preceding component analyses can be combined to form an overall engine friction mep model. The component equations have been used to develop a fmep program, *Friction.m* that is included in Appendix F.16. The effect of throttling on fmep is examined in a chapter homework problem.

EXAMPLE 10.1 *Friction Mean Effective Pressure*

What are the crankshaft, piston, valve train, pumping, and accessory fmep for the four-cylinder engine specified in Table 10.4, if it is operated at wide open throttle (WOT) at speeds varying from 1000 to 6000 rpm?

SOLUTION The input parameters for a SOHC four-cylinder in-line engine with two intake and two exhaust valves per cylinder are given in Table 10.2. Note that a wide open throttle condition is one in which the intake pressure is the same as the atmospheric pressure. Using the *Friction.m* program, the fmep components are plotted as a function of engine speed in Figure 10.26. The friction from the piston rings and skirt is the largest component. As the engine speed increases from 1000 to 6000 rpm, the total fmep increases nonlinearly from about 100 to 260 kPa, with a large increase in the pumping friction proportion.

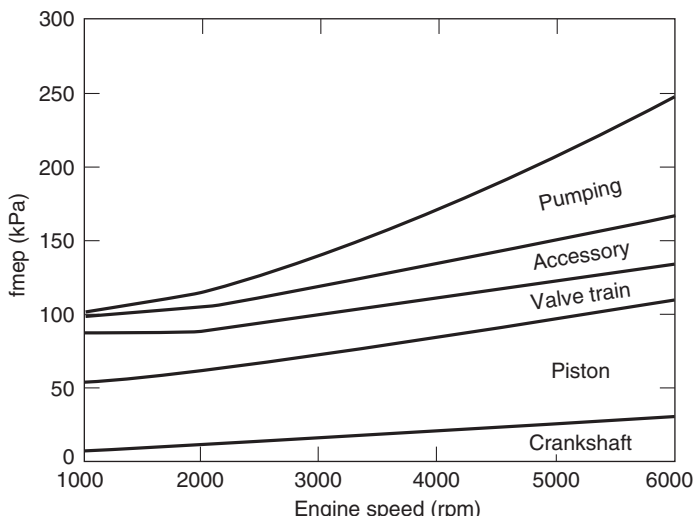
A quadratic correlation of the total fmep for this engine is given by Equation 10.54:

$$fmep = 94.8 + 2.3 \left(\frac{N}{1000} \right) + 4.0 \left(\frac{N}{1000} \right)^2 \quad (10.54)$$

The relative contributions of the crankshaft, piston, valve train, accessory, and pumping to the overall fmep are plotted in Figure 10.27. For wide open throttle conditions at low engine speeds, the overall fmep is primarily due to piston and valve train friction. As the engine speed increases, the pmep fraction increases to about 35%, and the valve train fmep fraction decreases from 35 to 10%.

Table 10.4 Representative Engine Parameters for Example 10.1

Bore (mm)	82.5
Stroke (mm)	82
Number of cylinders	4
Compression ratio	19.4
Atmospheric pressure (kPa)	101
Intake pressure (kPa)	101
Exhaust pressure (kPa)	103
Intake valves/cylinder	1
Exhaust valves/cylinder	1
Intake valve diameter (mm)	36.5
Exhaust valve diameter (mm)	31.5
Number of crankshaft bearings	5
Crankshaft bearing dia. (mm)	54
Crankshaft bearing length (mm)	21.6
Number of connecting rod bearings	4
Connecting rod bearing dia. (mm)	49
Connecting rod bearing length (mm)	21.4
Number of camshaft bearings	5

**Figure 10.26** Friction mean effective pressure versus engine speed.

10.12 LUBRICATION

Oil is used as a lubricant to reduce the friction between the principal moving parts of an engine. In addition to lubricating, engine oil is expected to meet a number of other service requirements: to act as a coolant for the pistons, rings, and bearings, to enhance the rings combustion seal, to control engine wear or corrosion, and to remove impurities from lubricated regions. To meet these requirements, additives are used with petroleum or synthetic base oil stocks. The additives include antifoam agents, antirust agents, antiwear agents, corrosion inhibitors, detergents, dispersants, extreme pressure agents, friction reducers,

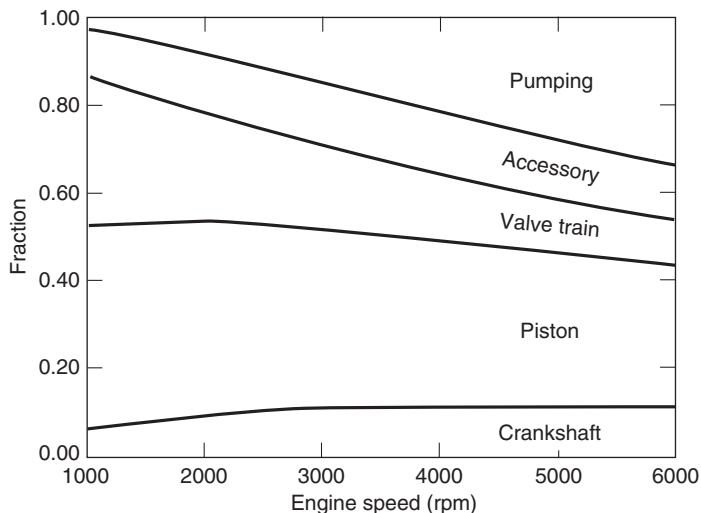


Figure 10.27 Relative contributions of fmeep components versus engine speed.

oxidation inhibitors, pour point depressants, and viscosity index improvers. Additives range in concentration from several parts per million up to 10%.

The portion of the crude oil refiners use to make lubricants is on the order of 1% and comes from the higher-boiling fraction and undistilled residues that possess the necessary viscosity. Refiners use chemical processing and additives to produce oils with desirable characteristics. Straight-run base stock from petroleum crude oil is referred to as a petroleum oil, whereas those base stocks produced by chemical processing are called synthetic oils. Some synthetic base stocks are compatible with petroleum base stocks and the two types may be blended, in which case the stock is referred to as a blend.

The viscosity of a lubricating oil decreases with increasing temperature and increases with pressure. A Newtonian oil is one in which the viscosity is independent of the shear rate. Shear rates in engines are sometimes high enough that the viscosity decreases, and some oils are deliberately made non-Newtonian via the introduction of polymeric materials into low-viscosity oils. At some times during hydrodynamic lubrication, the loads increase the oil pressure, which increases the viscosity, increasing the load capacity. It has been suggested that this stabilizing effect is a part of the reason for effects attributed to the “property” oiliness. These polymeric materials also thicken oil more at high temperatures than at low temperatures. The invention of viscosity modifiers eliminated the need to use different viscosity oils in summer and winter operation.

The SAE classifies oils by their viscosity. Two series of grades are defined in Table 10.5. Grades with the letter W(Winter) are based on a maximum low-temperature dynamic viscosity, a maximum borderline pumping temperature, and a minimum kinematic viscosity at 100°C. Grades without the letter W are based on a minimum and a maximum kinematic viscosity at 100°C. Increasing SAE grade numbers correspond to increasing viscosity. In terms of carbon content of the SAE grades, Gruse (1967) offers the guidelines listed in Table 10.6. Note that the SAE grade and thus the viscosity, increases with increasing molecular weight.

The borderline pumping temperature is measured via a standard test procedure, ASTM D3829, and is a measure of an oil's ability to flow to an engine oil pump inlet and provide adequate oil pressure during warm-up. This is to ensure that the oils meeting this standard will all flow readily on cold start-up and reach moving parts as quickly as possible. The dynamic viscosity is measured using the standard procedure SAE J300, and the kinematic

Table 10.5 SAE Specifications for Engine Oils

SAE viscosity grade	Dynamic viscosity μ (cP) at temperature (°C), maximum	Borderline pumping temperature (°C), maximum	Kinematic viscosity v (cSt) at 100 °C	
			Minimum	Maximum
0W	3250 at -30	-35	3.8	
5W	3500 at -25	-30	3.8	
10W	3500 at -20	-25	4.1	
15W	3500 at -15	-20	5.6	
20W	4500 at -10	-15	5.6	
25W	6000 at -5	-10	9.3	
20	-	-	5.6	<9.3
30	-	-	9.3	<12.5
40	-	-	12.5	<16.3
50	-	-	16.3	<21.9

Source: SAE Handbook, 2003.

Table 10.6 SAE Engine Oil Carbon Content

	Range	Average
SAE 10	C ₂₅ –C ₃₅	C ₂₈
SAE 30	C ₃₀ –C ₈₀	C ₃₈
SAE 50	C ₄₀ –C ₁₀₀	C ₄₁

Source: Gruse, 1967.

viscosity is determined following ASTM D445, a procedure that measures the time required for a given volume of oil to flow through a capillary tube. This is to ensure that oils meeting this standard will all exhibit proper lubricating properties under the high pressures and temperatures found at normal engine operating conditions.

As shown in Figure 10.28, a multiviscosity grade of oil is one that satisfies one of each of the two grades at different temperatures. When the engine is cold, a relatively low oil viscosity, such as 10W, is required, and when the engine is warmed up, there is a need for a higher viscosity, such as 30W, for adequate lubrication and sealing. Multigrade oils have been created to meet both cold start and normal operation requirements by adding polymeric high molecular weight compounds that reduce the viscosity change with temperature. As

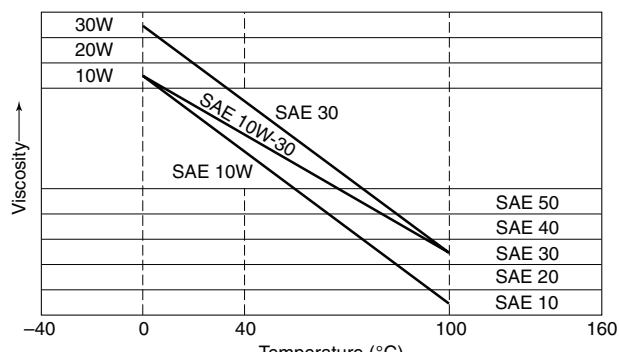
**Figure 10.28** Engine oil viscosity grades.

Table 10.7 Constants for Equation 10.55

SAE grade	C_1 (N s/m ²)	C_2 (°C)
10	1.09×10^{-4}	1157.5
20	9.38×10^{-5}	1271.6
30	9.73×10^{-5}	1360.0
40	8.35×10^{-5}	1474.4
50	1.17×10^{-4}	1509.6
60	1.29×10^{-4}	1564.0

Source: Hamrock et al. (1999).

Figure 10.28 indicates, at low-temperatures, the viscosity of an SAE 10W30 oil will be less than that of a SAE 30 oil to meet cold start requirements.

The dynamic viscosity μ (N s/m²) of SAE oils as a function of temperature is correlated by Equation 10.55:

$$\mu = C_1 \exp \left[\frac{C_2}{1.8 T(\text{°C}) + 127} \right] \quad (10.55)$$

Values of the constants C_1 and C_2 of Equation 10.55 for various SAE grades of engine oils are given in Table 10.7, as a function of temperature $T(\text{°C})$.

Finally, it should be mentioned that many two-stroke engines, especially small ones, achieve upper cylinder lubrication by mixing oil with the gasoline. The oil used is typically SAE 30 or 40, and formulated specifically to minimize combustion chamber deposits. In this situation, additional control of the oil (and the fuel) is required to prevent spark fouling, to assure miscibility with the fuel, and to provide for a hydrodynamic film of the proper viscosity. The fuel–oil mixture that contacts the cold walls separates during compression and combustion, leaving an oil film on the wall.

10.13 REFERENCES

- ALLEN, D. G., B. R. DUDLEY, J. MIDDLETOWN, and D. A. PANKA (1976), “Prediction of Piston Ring–Cylinder Bore Oil Film Thickness in Two Particular Engines and Correlation with Experimental Evidences,” *Conference on Piston Ring Scuffing*, Mechanical Engineering Pub. Ltd., London, p. 107.
- ARCOUMANIS, C., M. DUSZYNSKI, H. LINDENKAMP, and H. PRESTON (1998), “Measurements of Lubricant Film Thickness in the Cylinder of a Firing Diesel Engine Using LIF,” SAE paper 982435.
- BISHOP, I. N. (1964), “Effect of Design Variables on Friction and Economy,” SAE paper 640807.
- BROWN, W. L. (1973), “The Caterpiller Imep Meter and Engine Friction,” SAE paper 730150.
- GISH, R., S. McCULLOUGH, J. RETZLOFF, and H. MUELLER (1957), “Determination of True Engine Friction,” SAE paper 117.
- GRUSE, W. A. (1967), *Motor Oils: Performance and Evaluation*, Van Nostrand Reinhold, New York.
- HAMROCK, W., B. JACOBSON, and S. SCHMID (1999), *Fundamentals of Machine Elements*, McGraw-Hill Publishing, New York.
- LEARY, W. A. and J. U. JOVELLANOS (1944), “A Study of Piston and Piston–Ring Friction,” NACA ARR-4J06.
- MCGEEHAN, J. A. (1978), “A Literature Review of the Effects of Piston and Ring Friction and Lubricating Oil Viscosity on Fuel Economy,” SAE paper 780673.
- MERRION, D. (1994), “Diesel Engine Design for the 1990’s,” SAE SP-1011.
- MILLINGTON, B. and E. HARTLES (1968), “Frictional Losses in Diesel Engines,” SAE paper 680590.

- NOORMAN, M., D. ASSANIS, D. PATTERSON, S. TUNG, and S. TSEREGOUNIS (2000), "Overview of Techniques for Measuring Friction Using Bench Tests and Fired Engines," SAE paper 2000-01-1780.
- PATTON, K. J., R. G. NITSCHKE, and J. B. HEYWOOD (1989), "Development and Evaluation of a Friction Model for Spark Ignition Engines," SAE paper 890836.
- ROSENBERG, R. C. (1982), "General Friction Considerations for Engine Design," SAE paper 821576.
- SAE Handbook (2003), *Fuels and Lubricants*, Society of Automotive Engineers, Warrendale, Pennsylvania.
- SANDOVAL, D. and J. HEYWOOD (2003), "An Improved Friction Model for Spark Ignition Engines," SAE paper 2003-01-0725.
- SHAYLER, P., D. LEONG, and M. MURPHY (2005), "Contributions to Engine Friction During Cold, Low Speed Running and the Dependence on Oil Viscosity," SAE paper 2005-01-1654.
- TAYLOR C. (1985), *The Internal Combustion Engine in Theory and Practice*, Vol. 2, MIT Press, Cambridge, Massachusetts.
- TING, L. L. and J. E. MAYER, Jr. (1974), "Piston Ring Lubrication and Cylinder Bore Analysis, Part I Theory and Part II Theory Verification," *J. Lubr. Tech.*, Vol. 96, pp. 305–314.
- TSEREGOUNIS, S., M. VIOLA, and R. PARANJPE (1998), "Determination of Bearing Oil Film Thickness (BOFT) for Various Engine Oils in an Automotive Gasoline Engine Using Capacitance Measurements and Analytical Predictions," SAE paper 982661.

10.14 HOMEWORK

- 10.1** How is the fmep computed from the data in Figure 10.15?
- 10.2** It has been observed that the oil film thickness on the cylinder wall tends to be greater at lower loads. Relate this observation to the fmep versus load curves in Figure 10.6.
- 10.3** A four-cylinder engine has a 85 mm bore b and 90 mm stroke s , and operates at 5000 rpm. What is the power lost to piston skirt friction?
- 10.4** What is the power (W) lost to main crankshaft friction in a four-cylinder engine with a 100 mm bore and stroke if the engine is operating at 1500 rpm? Assume the main crankshaft has five bearings, each with a diameter of 50 mm and length of 25 mm.
- 10.5** Racing mechanics will often modify an engine by increasing the bearing clearances above the manufacturer specifications. This can increase the power of an engine. With reference to Equation 10.2, discuss why the power is increased, and the tradeoffs that should be considered in choosing a clearance.
- 10.6** Using Petrov's equation, Equation 10.22, show that the nondimensional fmep of journal bearings is inversely proportional to the oil Reynolds number, as indicated by Equation 10.24.
- 10.7** Using a piston force balance, discuss the zero crossings in Figure 10.14, and the absence of zero crossings between 0 and 180°.
- 10.8** With reference to a piston force balance, how is the piston and ring friction affected by the mass of the piston?
- 10.9** For the piston specifications given in Table 10.4, at what engine speed will the piston skirt friction be equal to the piston ring friction?
- 10.10** What are the pumping, accessory, valve train, piston, and crankshaft fmeps for a six-cylinder engine at 3000 rpm and WOT with 0.1-m bore and stroke, and compression ratio of 11? The number of crankshaft bearings is seven. Assume the other engine specifications are as given in Table 10.4.

- 10.11** Compute the fmep components (pumping, accessory, valve train, piston, and crankshaft) for the engine specified in Table 10.4 but throttled to 50 kPa inlet pressure. Plot the results versus engine speed from 1000 to 6000 rpm.
- 10.12** If one cylinder of a multicylinder spark ignition engine is motored by disconnecting the spark plug, it has been observed that the motored cylinder pressure increases with load. Discuss why this is to be expected.
- 10.13** Oil companies are advertising “slippery oils,” that is, non-Newtonian, that if used in your automobile will slightly reduce the fuel consumption. The implication is that when the slippery oil is compared with conventional oil of equal viscosity, the slippery oil will have a reduced friction coefficient. How is this possible?

Chapter 11

Heat and Mass Transfer

11.1 INTRODUCTION

Satisfactory engine heat transfer is required for a number of important reasons, including material temperature limits, lubricant performance limits, emissions, and knock. Since the combustion process in an internal combustion engine is not continuous, as is the case for an external combustion engine, the time average component temperatures are much less than the peak combustion temperatures. However, the temperatures of certain critical areas need to be kept below material design limits. Aluminum alloys begin to melt at temperatures greater than 775 K, and the melting point of iron is about 1800 K. Temperature gradients around the cylinder bore will cause bore distortion and subsequent increased blowby, oil consumption, and piston wear. Cooling of the engine cylinder is also required to prevent knock from occurring in spark ignition engines.

Exhaust system heat transfer is also an important factor in emissions and exhaust turbine performance. Satisfactory catalytic converter performance only occurs above a threshold or light-off temperature. The threshold temperature (catalyst oxidation efficiency greater than 50%) for the catalyzed oxidation of hydrocarbon and carbon monoxide emissions is about 500 K so that at exhaust temperatures less than 500 K, catalytic converter performance is adversely affected. In addition, the continued oxidation of hydrocarbons and other pollutants in the exhaust system is a function of the exhaust system temperature.

Heat transfer to the airflow in the intake manifold is also an important consideration. The heat transfer lowers the volumetric efficiency, since the density of the intake air is decreased. Plastic intake manifolds with reduced thermal conductivity (as well as reduced weight) are now being used to reduce intake air heating.

The heat transfer rate in an engine is dependent on the coolant temperature and the engine size, among other variables. There are complex interactions between the various engine parameters. For example, as the temperature of the engine coolant decreases, the heat transfer to the coolant will increase, and the combustion temperature will decrease. This will cause a decrease in the combustion efficiency and an increase in the volumetric efficiency. It will also cause an increase in the thermal stresses in the cylinder sleeve, and increase the size of the radiator needed, since the coolant ambient temperature difference will decrease. The formation of nitrogen oxides will decrease, and the oxidation of hydrocarbons will decrease. The exhaust temperature will also decrease, causing a decrease in the performance of the catalytic converter and a turbocharger.

11.2 ENGINE COOLING SYSTEMS

There are two types of engine cooling systems used for heat transfer from the engine block and head liquid cooling and air cooling. With a liquid coolant, thermal energy is removed through the use of internal cooling channels within the engine block, as shown schematically in Figure 11.1. With air as a coolant, thermal energy is removed through the use of fins attached to the cylinder wall, as shown schematically in Figure 11.2. Both types of cooling systems have various advantages and disadvantages. Liquid systems are much quieter than air systems, since the cooling channels absorb the noise from the combustion processes. However, liquid systems are subject to freezing, corrosion, and leakage problems that do not exist in air systems.

As indicated in Figure 11.1, the water cooling system is usually a single loop where a water pump sends coolant to the engine block and then to the head. The coolant will then flow to the top of a radiator or heat exchanger and exit at the bottom to flow back to the pump. Early engines, such as the Ford Model T engine, did not have a water pump, and used a thermosyphon natural convection loop to circulate the coolant from the engine to the radiator. The water pump is located at the bottom of the engine to minimize cavitation. The pump is usually powered by the engine; however, electric water pumps have also been used. During engine warm-up, a thermostatically controlled valve will recycle the coolant flow through the engine block, bypassing the heat exchanger. As the engine heats up, the valve will open up, and allow the coolant to flow to the radiator. The time required for engine warm-up to a steady-state operating temperature depends on the engine size, speed, and load and is typically of the order of 10 min for an automotive engine. Dual circuit cooling with separate circuits to the head and block has also been used.

The design of the liquid cooling passages in the engine block and head is done empirically. The primary design consideration is to provide for sufficient coolant flow at the high heat flux regions, such as the exhaust valves. Since the area between exhaust valves is difficult to cool, some automotive engine designs use only one exhaust valve to reduce the heating of the inlet air–fuel mixture, and thus increase the volumetric efficiency. A review of precision cooling considerations is given in Robinson et al. (1999).

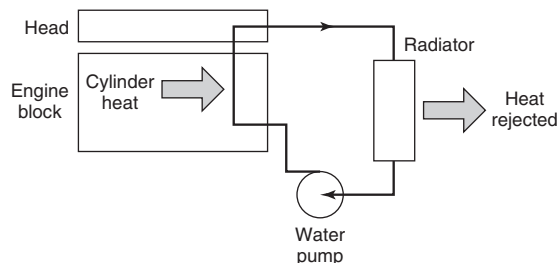


Figure 11.1 Liquid cooling system schematic.

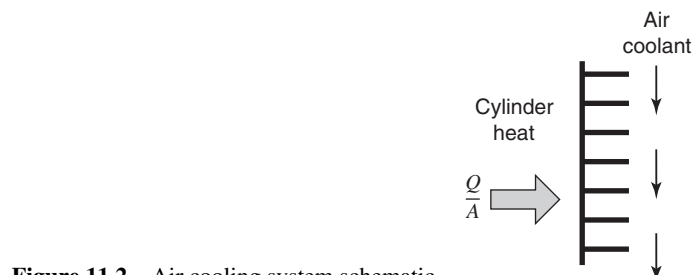


Figure 11.2 Air cooling system schematic.

The boiling point temperature of the liquid coolant can be raised by increasing the pressure or by adding an additive with a high boiling point, such as ethylene glycol. The heat fluxes and surface temperatures near the exhaust manifold and port are high enough so that nucleate boiling can occur in the coolant at those locations. The boiling heat transfer coefficients are much larger than single-phase forced convection, so that the surface temperatures will be correspondingly lower. For heat fluxes of the order of 1.5 MW/m^2 , the resulting surface temperature of the cooling jacket will be about $20\text{--}30^\circ\text{C}$ above the saturation temperature, which is typically 130°C (400 K). The nucleate boiling process is very complex, as bubbles formed on the cooling channel surface are swept downstream and then condensed in cooler fluid. Engines with relatively low-power output, less than 20 kW, primarily use air cooling, shown schematically in Figure 11.2. Because the thermal conductivity of air is much less than that of water, air systems use fins to lower the air-side surface temperature. For higher power output, an external cooling fan is used to increase the air-side heat transfer coefficient. Aircraft engines are, for the most part, air cooled; supplying the required airflow is not a problem, since the engine need not be enclosed and is usually located right behind a propeller. Engines that are operated for very short periods of time, such as engines used in 1/4-mile dragsters, do not use a cooling system but use the thermal capacitance of the engine block to keep the gas-side surface temperatures within limits.

Since about one-third of the fuel energy is lost as heat transfer to the coolant, it would seem reasonable to try to reduce this heat loss, thereby increasing the efficiency of the engine. One way to reduce the heat flow to the coolant is to increase the thermal resistance of the engine block through the use of lower thermal conductivity materials, such as ceramics, or adding thermal insulation to the engine. Ceramic wall materials that can operate at higher temperatures and have a lower thermal conductivity than cast iron are silicon nitride and zirconia.

Experimental results from such engines show that a reduction in the coolant heat loss does not result in a corresponding increase in the efficiency of the engine (Sun et al., 1993). There are a number of reasons for this. First, by insulating the engine, the average cylinder temperature increases, and the exhaust temperature and enthalpy increase. The thermal energy that had been conducted to the coolant is now added to the exhaust stream. Secondly, since the penetration depth of the combustion heat flux is only about a millimeter, the coolant heat transfer is a relatively steady-state process throughout the cycle, but the positive work is produced only during the expansion stroke. The coolant heat transfer that occurs during the other strokes is not available to be converted to work. Thirdly, the higher wall temperatures will heat the incoming gas during the intake stroke lowering its volumetric efficiency. For spark ignition engines, the higher wall temperatures during the compression stroke can give rise to knock problems. Therefore, the majority of the engines that have employed increased cylinder thermal resistance are compression ignition engines.

11.3 ENGINE ENERGY BALANCE

An engine energy balance is obtained through experiments performed on instrumented engines. Figure 11.3 depicts an engine instrumented to determine the quantities of heat rejected to oil, water, and to the ambient air. Flow meters are installed in the water, and oil circuits and thermocouples measure the inlet and outlet temperatures. An energy balance, Equations 11.1 and 11.2, applied to the water coolant and the oil flowing through the engine yields

$$\dot{Q}_{\text{water}} = (\dot{m}c_p)_{\text{water}}(T_3 - T_4) \quad (11.1)$$

$$\dot{Q}_{\text{oil}} = (\dot{m}c_p)_{\text{oil}}(T_1 - T_2) \quad (11.2)$$

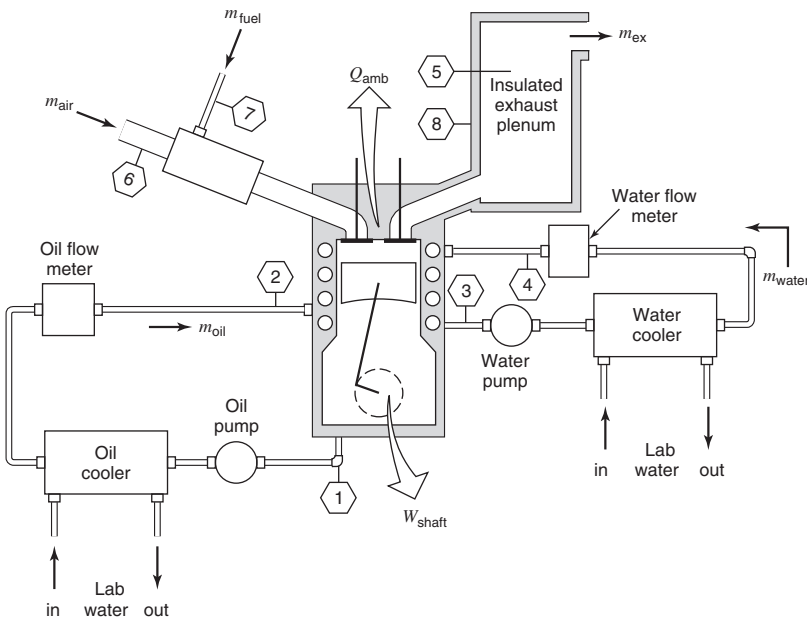


Figure 11.3 Engine instrumented for energy balance measurements.

Determining the heat loss to the ambient air is more involved. The first law, Equation 11.3, applied to the engine system is

$$\begin{aligned}\dot{Q}_{\text{amb}} &= (\dot{m}h)_{\text{air}} + (\dot{m}h)_{\text{fuel}} - (\dot{m}h)_{\text{exh}} \\ &\quad - \dot{Q}_{\text{water}} - \dot{Q}_{\text{oil}} - \dot{W}_{\text{shaft}}\end{aligned}\quad (11.3)$$

The mass flow rate of the exhaust is known in terms of the measured mass flow rates of air and fuel since

$$\dot{m}_{\text{exh}} = \dot{m}_{\text{air}} + \dot{m}_{\text{fuel}} \quad (11.4)$$

The enthalpies of the exhaust, the air, and the fuel are based on the measured temperatures T_5 , T_6 , and T_7 , respectively. The exhaust composition can be calculated theoretically from the known fuel-air equivalence ratio or it may be measured. In either case, it is important that the temperature T_5 corresponds to the mass-averaged temperature of the exhaust; for this reason, there is an insulated plenum that serves to mix the hot exhaust gas emitted early in the cycle with the cool exhaust gas emitted later in the cycle. A further complication is that the thermocouple measurement must be corrected for radiation heat transfer to obtain the true gas temperature. An energy balance on the thermocouple tip, Equation 11.5, yields

$$T_{\text{exh}} = T_5 + \frac{\epsilon\sigma}{h}(T_5^4 - T_8^4) \quad (11.5)$$

where ϵ is the emissivity of the thermocouple tip, σ is the Stefan–Boltzmann constant, \mathbf{h} is the heat transfer coefficient at the tip (printed in bold to distinguish it from the symbol h for enthalpy), T_5 is the tip temperature, and T_8 is the exhaust plenum inner wall temperature.

In doing these energy balances, it is common practice to evaluate the maximum heat that can be recovered from the exhaust gas. This is computed from an energy balance,

Table 11.1 Energy Balance on a Medium Speed, Four-Stroke, Turbocharged Diesel Engine (All energy rates are normalized by the fuel rate, \dot{Q}_{in})

N (rpm)	bmep (bar)	\dot{Q}_{exh}	\dot{Q}_{water}	\dot{Q}_{oil}	\dot{Q}_{amb}	\dot{W}_{shaft}	$\dot{W}_{friction}$	\dot{Q}_{loss}
500	9.90	0.459	0.118	0.037	0.069	0.317	0.100	0.124
500	3.52	0.437	0.108	0.065	0.092	0.298	0.178	0.087
400	3.50	0.432	0.151	0.074	0.026	0.315	0.092	0.159

Source: Whitehouse(1970).

Equation 11.6, on the exhaust where it is cooled to ambient temperature:

$$\dot{Q}_{exh} = \dot{m}_{exh} [h_{exh}(T_{exh}) - h_{exh}(T_{amb})] \quad (11.6)$$

In evaluating the exhaust enthalpy at ambient temperature, equilibrium water quality should be used, as discussed in Chapter 4. If Equation 11.6 is substituted into Equation 11.3, one obtains

$$\dot{Q}_{amb} = \dot{Q}_{in} - \dot{Q}_{exh} - \dot{Q}_{water} - \dot{Q}_{oil} - \dot{W}_{shaft} \quad (11.7)$$

where, by definition

$$\dot{Q}_{in} = (\dot{m}h)_{air} + (\dot{m}h)_{fuel} - (\dot{m}h)_{exh} \quad (11.8)$$

Finally, if the fuel and air are at an ambient temperature, the engine runs lean or stoichiometric, and the ambient temperature and pressure are coincident with the reference temperature and pressure, then the inlet enthalpy is the product of the fuel flow rate and the fuel's stoichiometric heat of combustion.

Some results obtained by Whitehouse (1970) for a medium-speed diesel engine are given in Table 11.1. The terms in the table are normalized by the input energy of the fuel \dot{Q}_{in} . The diesel engine used was a single-cylinder test engine with a bore of 304.8 mm, a stroke of 381 mm, and a compression ratio of 12.85. The table also gives the heat equivalence of the friction so that one can ascertain how much of the heat lost to the ambient air, to the oil, and to the water, is from the working fluid and how much is from friction. The overall heat loss is the sum of the heat transfer to the water, oil, and ambient air minus the friction work:

$$\dot{Q}_{loss} = \dot{Q}_{water} + \dot{Q}_{oil} + \dot{Q}_{amb} - \dot{W}_{friction} \quad (11.9)$$

Inspection of the shaft work term reveals that the engine has a brake thermal efficiency of about 30%. About 45% of the energy is rejected in the exhaust, 10–15% is dissipated by friction, and 10–15% is dissipated with heat loss.

We now examine representative energy balance results for spark ignition engines. Figure 11.4 shows the results of an energy balance on a small, spark ignition automobile engine. This engine has an internal oil pump, and the heat rejected to the oil is carried away partly by the coolant and partly by the heat lost to ambient air. As the load increases and the intake manifold pressure increases from $P_i = 0.4$ bar to $P_i = 0.8$ bar, the energy converted to shaft work increases from about 20 to 30%, the coolant load decreases from about 40 to 30%, the exhaust energy varies from about 30 to 35%, and the heat lost to ambient air decreases from about 10 to 5%. The energy dissipated by friction decreases from about 14 to 7% for the same loads. The total heat loss from the gas to the coolant and ambient air during the cycle is about 28–36%.

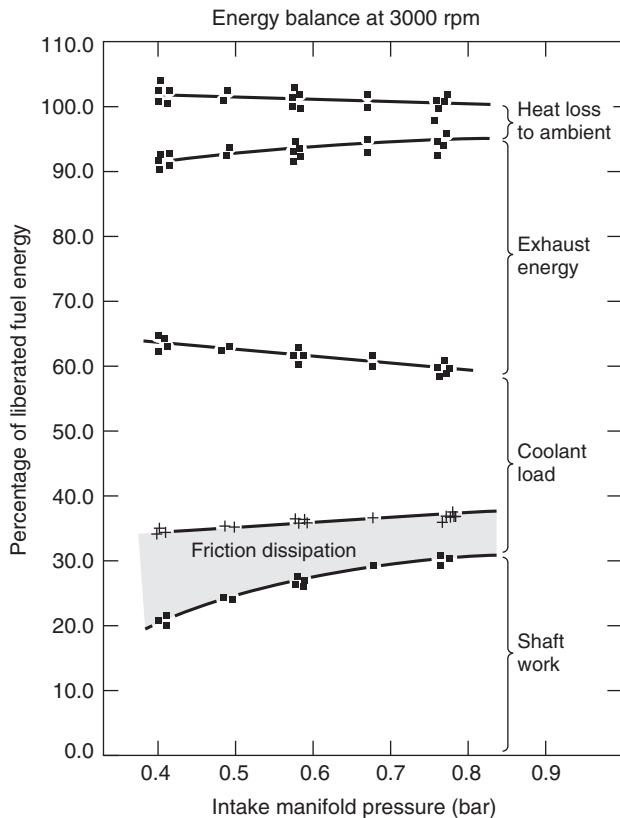


Figure 11.4 Energy balance on an automotive engine.

(Courtesy D. Brigham of Ford Motor Co.)

Ryder (1950) performed an energy balance on a Pratt and Whitney Mark R-2800 air-cooled aircraft engine, as shown in Table 11.2. Under cruise conditions, the engine runs at 1800 rpm, with the engine fueled slightly lean at $\phi = 0.90$, producing a bmepl = 8.75 bar, and brake thermal efficiency of $0.98 \times 29\% = 28\%$. During takeoff, the engine speed is increased to 2700 rpm, and the engine is fueled extremely rich with $\phi = 1.65$. Only about 46% of the fuel's heat of combustion is released, producing a bmepl = 13.72 bar. This is done to utilize the liquid fuel's latent heat for cooling and to avoid knock limiting the power. Because the fuel consumed during takeoff is small compared with that used in the entire trip, the fact that fuel is wasted is of secondary concern. Notice that during takeoff, 35% of the heat released is converted to shaft work, and the brake thermal efficiency of the engine is reduced to $0.46 \times 35\% = 16.1\%$.

Upon comparison, we see that the diesel engine loses only about one-half as much heat to the coolant and ambient air as the gasoline engine, yet their shaft efficiencies are

Table 11.2 Energy Balance on an Air-Cooled, Spark Ignition Aircraft Engine

ϕ	N (rpm)	bmepl (bar)	\dot{Q}_{exhaust}	\dot{Q}_{oil}	\dot{Q}_{ambient}	\dot{W}_{shaft}	$\dot{Q}_{\text{in}}/\dot{m}_f q_c$
0.90	1800	8.75	0.44	0.09	0.18	0.29	0.98
1.65	2700	13.72	0.44	0.08	0.12	0.35	0.46

Source: Ryder (1950).

All energy rates are normalized by the fuel rate, \dot{Q}_{in} .
Engine: $b = 146.1$ mm, $s = 152.4$ mm.

about equal since the diesel engine has more exhaust heat loss than the gasoline engine. As discussed above, experiments with insulated engines show that a reduction in the coolant heat loss has a small impact on the shaft efficiency and that the energy no longer lost to the coolant mostly appears in the exhaust flow. If a turbocharger is used, the available portion of the exhaust energy can be converted to useful work.

11.4 CYLINDER HEAT TRANSFER

There are a wide range of temperatures and heat fluxes throughout an internal combustion engine. The value of the local heat flux can vary by an order of magnitude depending on the spatial location in the combustion chamber and the relative crank angle. The sources of the heat flux are not only the hot combustion gases, but also the friction that occurs between moving surfaces, such as the piston rings and the cylinder wall. When an engine is running at a steady state, the heat transfer rates throughout most of the engine structure are relatively constant. As will be shown, unsteady periodic effects are limited to a penetration layer about 1–5 mm thick at the combustion gas cylinder wall interface.

Experiments indicate that the heat flux increases with increasing engine load and speed, with the maximum heat flux through the engine components occurring at fully open throttle and at maximum speed. Peak heat fluxes are on the order of 1–10 MW/m². The heat flux is largest in the center of the cylinder head, the exhaust valve seat, and the center of the piston. About 50% of the heat flow to the engine coolant is through the engine head and valve seats, 30% through the cylinder sleeve or walls, and the remaining 20% through the exhaust port area.

The piston and valves, since they are moving, are difficult to cool, and operate at the highest temperatures. Temperature measurements indicate that the greatest temperatures occur at the top, that is, the crown of the piston, since it is in direct contact with the combustion gases. The crown temperatures can be as high as 550 K. The temperatures of the piston and valves depend on their thermal conductivity. As the thermal conductivity increases, the conduction resistance decreases, resulting in lower surface temperatures. For the same speed and loading, aluminum pistons are about 40 K cooler than cast iron pistons.

The main cooling paths for the piston are conduction through the piston rings to the cylinder wall and conduction through the piston body to the air–oil mist on the underside of the piston, as shown in Figure 11.5. About half of the heat rejected to the cylinder wall from the piston is from cylinder friction. The main cooling path for the exhaust valves is through the valve seat, since the exhaust valve is closed for about three strokes of the four-stroke cycle. The cooling mechanism is thermal contact conduction. The conductance depends on the maximum cylinder pressure, which compresses the valve onto the valve seat. Values of the thermal contact conductance between 5000 and 35,000 W/mK have been measured (Wisniewski, 1998). Hollow valve stems partially filled with sodium have been used to increase the effective axial thermal conductivity of the exhaust valve. The sodium melts at 370 K, so at temperatures greater than 370 K, there is internal natural conduction heat transfer in the axial direction inside the valve stem.

In order to accurately calculate the total heat loss from the combustion chamber, one must evaluate the heat flux at every location in the combustion chamber and integrate over the active cylinder area, as indicated by Equation 11.10. For this reason, a number of surface thermocouples are installed into the engine at representative locations.

$$\dot{Q}(t) = \int_{A(t)} q''(t) dA \quad (11.10)$$

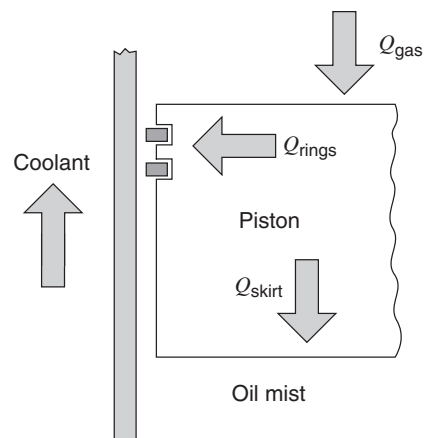


Figure 11.5 Piston cooling paths.

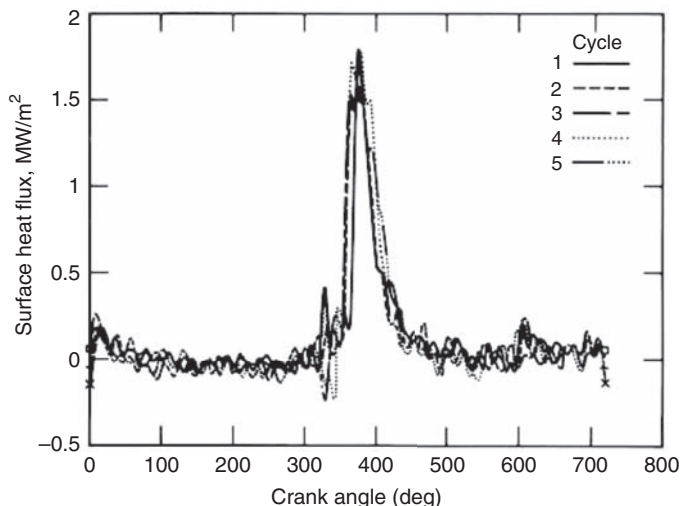


Figure 11.6 Cylinder head heat flux profiles of five consecutive combustion cycles in a spark ignition engine. Adapted from Alkidas and Myers (1982).

Resolution of the instantaneous heat transfer at the cylinder surface can be achieved by inserting a surface thermocouple into the engine structure. Figure 11.6 shows the heat flux measurements made by Alkidas and Myers (1982) using a surface thermocouple in a cylinder head of a propane-fueled engine. Five consecutive combustion cycles are shown, with a peak heat flux of about 1.8 MW/m^2 . Note that most of the heat transfer occurs early in the expansion stroke from 360° to 420° crank angle, when the combustion gas temperatures are greatest. Negative heat flux, that is, from cylinder surface to combustion gases, can occur late in the expansion stroke and during the intake stroke. The cycle-to-cycle variations noted in Figure 11.6 are caused by cycle-to-cycle variations in arrival times of the turbulent flame at the thermocouple.

The surface thermocouple used for instantaneous heat flux measurements was originally developed by Bendersky (1953). The essential features of a surface thermocouple are shown in Figure 11.7. Within the plug are two iron–constantan thermocouple junctions, one at the surface and one at a depth Δx from the surface. The basic idea is that according to Fourier's law, Equation 11.11, for small Δx ,

$$q'' = -k \frac{\Delta T}{\Delta x} \quad (11.11)$$

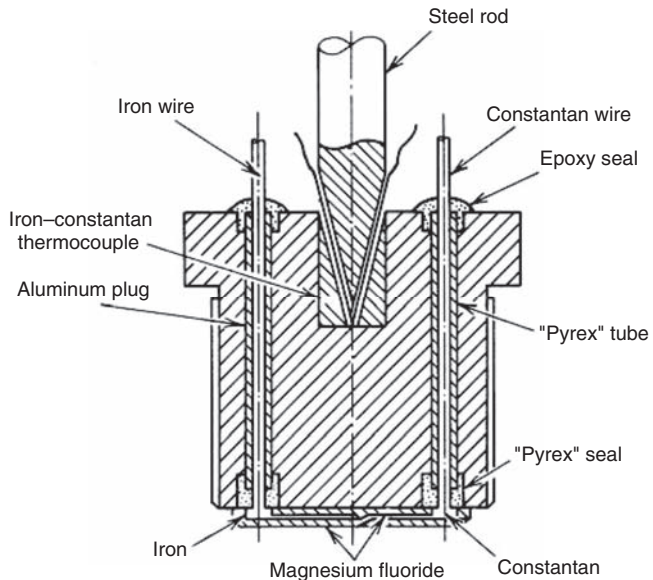


Figure 11.7 Surface thermocouple plug used to measure instantaneous heat flux.
Adapted from Dent and Suliaman (1977).

The criterion for small Δx is that it be small compared with the thermal penetration layer δ . Unfortunately, it is just not practical to build a plug with $\Delta x \ll \delta$. Therefore, instead, one solves the heat conduction equation between the two thermocouples, assuming that it is one-dimensional. The measured surface temperature variation in time for one cycle is curve-fitted by a Fourier series, shown in Equation 11.12, with Fourier coefficients A_i and B_i :

$$T(0, t) = \bar{T}(0) + \sum_{i=1}^N [A_i \cos(i\omega t) + B_i \sin(i\omega t)] \quad (11.12)$$

The heat flux is then given by Equation 11.13:

$$q'' = -k \left[\frac{\Delta \bar{T}}{\Delta x} + \sum_{i=1}^N \sqrt{\frac{i\omega}{2\alpha}} [(B_i - A_i) \sin(i\omega t) + (B_i + A_i) \cos(i\omega t)] \right] \quad (11.13)$$

The parameter ω is one-half the engine frequency for a four-stroke engine and equal to the engine frequency for a two-stroke engine.

11.5 HEAT TRANSFER MODELING

The heat transfer processes in an internal combustion engine can be modeled with a variety of methods. These methods range from simple thermal networks to multidimensional differential equation modeling. The choice of modeling method involves considerations such as the computational accuracy required and the data that are available to model the engine configuration and operation.

Thermal network models, using resistors and capacitors, are very useful for rapid and efficient estimation of the conduction, radiation, and convection heat transfer processes in engines. Using a thermal network, the significant resistances to heat flow, and the effects of changing material thermal conductivity, thickness, and coolant properties can be easily determined. Thermal networks can be used directly for convection and conduction heat

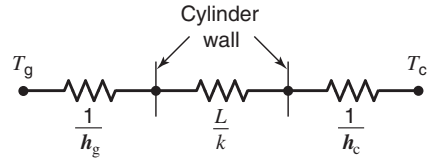


Figure 11.8 Three resistor thermal network.

transfer, and the radiation heat transfer equation needs to be linearized to conform to the resistance model.

A simple three resistor series network, which includes convection and conduction resistances shown in Figure 11.8, is an illustration of the steady-state heat transfer from the engine cylinder gas to the coolant. This series path is composed of convection through the cylinder gas boundary layer, conduction across the cylinder head wall, and convection through the coolant liquid boundary layer. The cylinder gas boundary layer insulates the cylinder wall from the high-temperature cylinder gases. From Fourier's equation, Equation 11.14, the conduction resistance is

$$R_{\text{cond}} = \frac{\Delta T}{Q/A} = \frac{L}{k} \quad (11.14)$$

and using Newton's equation, Equation 11.15 the convection resistance is

$$R_{\text{conv}} = \frac{\Delta T}{Q/A} = \frac{1}{h} \quad (11.15)$$

Examples of resistor–capacitor thermal networks applied to engine warm-up and steady-state operation are given in Shayler et al. (1993) and Bohac et al. (1996).

We now analyze the unsteady nature of the heat flux from the combustion gas to the cylinder wall. The cylinder wall has a periodic heat flux on the gas side and a constant surface temperature on the coolant side. The problem posed requires solution of the transient heat conduction equation, Equation 11.16

$$\frac{\partial T}{\partial t} = \alpha \frac{\partial^2 T}{\partial x^2} \quad (11.16)$$

subject to the following boundary conditions

$$\begin{aligned} -k \frac{\partial T}{\partial x} &= q_0'' + q_1'' \sin(\omega t) && \text{at } x = 0 \\ T &= T_L && \text{at } x = L \end{aligned} \quad (11.17)$$

as well as an initial condition

$$T = T_i(x) \quad \text{at } t = 0 \quad (11.18)$$

An exact solution can be written in closed form but it is quite cumbersome and as a result, not very illustrative. Fortunately, an approximate solution can be derived for the practical case where

$$\omega t \gg 1 \quad \text{and} \quad \frac{\omega L^2}{2\alpha} \gg 1 \quad (11.19)$$

In this case, the temperature field is given by Equation 11.20:

$$T = T_L + \frac{q_0''}{k}(L - x) + \frac{q_1''}{(\alpha/\omega)^{1/2}} \exp \left[\left(-\frac{\omega}{2\alpha} \right)^{1/2} x \right] \sin \left(\omega t - \left(\frac{\omega}{2\alpha} \right)^{1/2} x - \frac{\pi}{4} \right) \quad (11.20)$$

Inspection of this solution shows that

- the surface temperature at $x = 0$ oscillates with the same frequency as the imposed heat flux but with a phase difference of $\pi/4$;
- the amplitude of the oscillations decays exponentially with the distance x from the surface; the amplitude is reduced to 10% of that at the surface at a penetration distance δ given by Equation 11.21

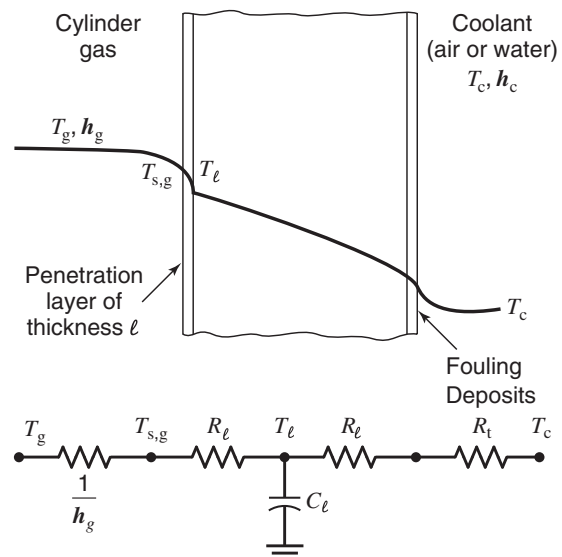
$$\delta = -\ln(0.10) (2\alpha/\omega)^{1/2} = 2.3 (2\alpha/\omega)^{1/2} \quad (11.21)$$

For a two-stroke engine operating at 2000 rpm ($\omega = 209 \text{ s}^{-1}$) and made of cast iron ($\alpha = 21 \times 10^{-6} \text{ m}^2/\text{s}$), the penetration distance $\delta = 0.7 \text{ mm}$, and for aluminum, $\delta = 2.2 \text{ mm}$.

The penetration distance δ is a measure of how far into the material fluctuations about the mean heat flux penetrates. For distances x greater than δ , the temperature profile is more or less steady and driven only by the time-average heat flux. Since the length δ is small compared with the dimensions (wall thickness, bore, etc.) over which conduction heat transfer occurs, two simplifications can be made:

- Conduction heat transfer in the various parts can be assumed steady and driven by the average flux.
- Heat transfer from the gas can be coupled to the conduction analysis accounting for capacitance only in a penetration layer of thickness δ in series with a resistance computed or measured for a steady state.

A five node thermal network for a cylinder wall is given in Figure 11.9. The modeling of the penetration layer can be complicated by the presence of an oil film or deposits. Fortunately, an accurate model is not required as the fluctuations about the mean \bar{T}_δ tend



$R_t = \text{conduction path resistance to coolant}$

$$R_\ell = \ell/2k$$

$$C_\ell = \rho c \ell$$

Figure 11.9 Thermal network with capacitance node for penetration layer.

to be small compared with the gas penetration depth temperature difference $T_g - \bar{T}_\delta$. For an engine operated at a steady state, the penetration layer is thin because the engine frequency, which dictates the frequency components of the heat flux imposed on the gas-solid interfaces, is rather high. On the other hand, in the case of an engine being accelerated or decelerated, the penetration layer is thicker because lower frequency components are added to the heat flux that are characteristic of the rates of change of engine speed. For example, one could define a characteristic time τ by

$$\tau^{-1} = \frac{1}{\omega} \frac{d\omega}{dt} \quad (11.22)$$

The penetration distance δ at time τ is

$$\delta = 2.3(2\alpha\tau)^{1/2} \quad (11.23)$$

For $\tau = 5$ s, the penetration distance $\delta = 33$ mm for cast iron and is no longer small compared with the typical dimensions over which the heat is transferred. Therefore, to accurately model heat transfer in engines operated on a transient mode, the three dimensional and unsteady features should be included.

Determination of the temperature profile of an engine component such as the piston requires solution of the three-dimensional heat conduction equation. As mentioned earlier, the piston can be treated as steady and driven by an average heat flux, since the penetration layers are small. The mean cylinder gas temperature is computed using a cycle simulation to predict instantaneous gas temperatures which are then integrated over crank angle according to Equation 11.24:

$$\bar{T}_g = \frac{1}{4\pi\bar{h}_g} \int_0^{4\pi} \mathbf{h}_g T_g d\theta \quad (11.24)$$

where \mathbf{h}_g is the instantaneous heat transfer coefficient (the determination of which is the subject of the next section). Likewise, an average heat transfer coefficient, Equation 11.25, is used in estimating the heat transfer coefficients on the crown of the piston in contact with the cylinder gas.

$$\bar{h}_g = \frac{1}{4\pi} \int_0^{4\pi} \mathbf{h}_g d\theta \quad (11.25)$$

Results obtained by Li (1982) for the combustion gas and piston temperatures of a 2.5 L, four-cylinder engine at WOT, are given in Table 11.3 and in Figure 11.10. Notice that both the mean combustion gas temperature and the mean heat transfer coefficient increase with engine speed. The mean gas temperature increases because there is less time for the

Table 11.3 Variation of the Mean Gas Temperature and Heat Transfer Coefficient at the Top of the Piston with Engine Speed

Engine speed (rpm)	\bar{T}_g (C)	\bar{h}_g (W/m ² K)
2400	990	1820
3600	1037	2430
4600	1062	2800

Source: Li (1982).

^aA dished piston running in a 2.5 L engine WOT.

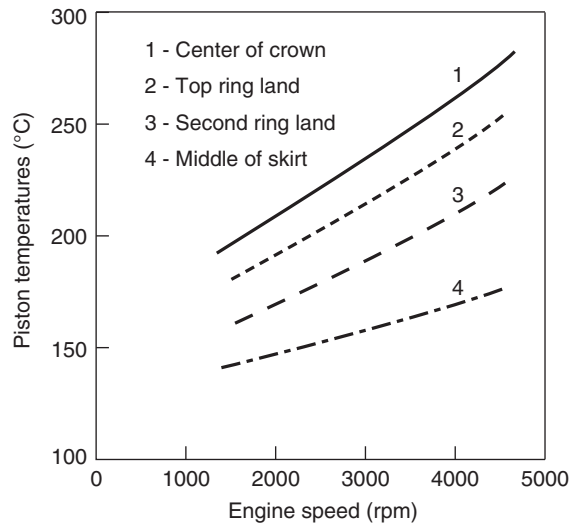


Figure 11.10 Piston temperature distribution versus engine speed at WOT. Adapted from Li (1982).

gases to lose heat as engine speed increases, whereas the mean heat transfer coefficient increases because of increased gas motion at higher speeds.

Temperatures in the piston are determined by the average heat flow into the piston and the effectiveness with which the heat can be dissipated to the oil and the coolant. As speed increases, the heat flow increases, whereas the overall heat transfer coefficients to the coolant and oil change little, thus piston temperature increases.

The calculated results show that three areas are particularly important in dissipating the piston heat input: (1) the ring groove surfaces, (2) the underside of the dome, and (3) the upper portion of the pin-bearing surface. From the ring grooves, heat flows into the rings, through the bore, and is eventually absorbed by the coolant. From the underside of the dome and the surface of the pin bearing, the heat is convected into an air-oil mist and is eventually absorbed by the oil in the sump.

In zonal modeling of the cylinder gas, the cylinder volume is divided into individual control volumes, each with its own thermodynamic properties and heat transfer coefficient. For example, a two-zone model separating the cylinder gases into unburned and burned gas fractions, with the moving flame separating the two zones is given in Krieger and Borman (1966). A four-zone model consisting of the central core zone, a squish zone, a head recess zone, and a piston recess zone was used by Tillock and Martin (1996). With zonal modeling, the characteristic length and velocity are zone dependent. The characteristic velocity is usually taken as an effective velocity with components from the mean and turbulent flow field.

As the number of zones increases to length scales that are much less than the cylinder bore, the modeling is termed multidimensional. With multidimensional models, the mass, momentum, and energy conservation equations take the form of partial differential equations, which are solved numerically. Detailed turbulence and reaction rate models are also required. For example, the use of turbulent heat transfer models in the multidimensional KIVA code is given in Reitz (1991).

11.6 HEAT TRANSFER CORRELATIONS

Engine heat transfer data can be correlated with the engine thermal conditions using two nondimensional parameters, the Nusselt and Reynolds numbers. The Nusselt number, Nu ,

is the ratio of the convection to the conduction heat transfer over the same temperature difference, expressed in Equation 9.29 as

$$Nu = \frac{\mathbf{h} b}{k} \quad (11.26)$$

where \mathbf{h} is the heat transfer coefficient, b is a length scale, usually the cylinder bore, and k is the working fluid thermal conductivity. The Nusselt number is named after Wilhelm Nusselt (1882–1957), a German engineering professor who made many contributions to heat transfer, primarily in dimensional analysis, condensation, and heat exchangers.

The Reynolds number, Re , a ratio of the inertial to viscous fluid forces, is defined in Equation 11.27:

$$Re = \frac{\rho U b}{\mu} \quad (11.27)$$

where ρ is the fluid density, U is a characteristic gas velocity, and μ is the dynamic viscosity.

The characteristic gas velocity in the cylinder depends on a number of parameters, such as the piston speed, the degree of combustion, the level of turbulence, and the amount of swirl and tumble present. Since the gas velocity in the cylinder scales with the piston speed, the mean piston speed is usually chosen as a first order estimate of the characteristic gas velocity in the cylinder for the Reynolds number. As discussed in Chapter One, the mean piston speed \bar{U}_p is

$$\bar{U}_p = 2 N s$$

Correlations have been developed for three types of engine heat transfer: (a) $Q(\bar{x}, \bar{\theta})$, the time and spatially averaged engine heat transfer, used in overall energy balance calculations, (b) $Q(\bar{x}, \theta)$, the instantaneous spatially averaged cylinder heat transfer, used in engine performance and heat release analysis, and (c) $Q(x, \theta)$, the instantaneous local heat transfer, typically used in CFD simulations of the detailed combustion and flow fields in the cylinder.

From dimensional analysis, the heat transfer correlations are of the form, Equation 11.28:

$$Nu = f(Re, Pr) = a Re^b Pr^c \quad (11.28)$$

where Pr is the Prandtl number, $Pr = \nu/\alpha$. The Prandtl number is named after Ludwig Prandtl (1875–1953), a German engineering professor who made many significant contributions to fluid mechanics and aerodynamics.

The convective heat flux q'' from the cylinder gases to the cylinder wall is

$$q'' = Q/A = \mathbf{h}(T_g - T_w) \quad (11.29)$$

Combustion gas properties are evaluated at the appropriate mean effective cylinder gas temperature T_g , which can be obtained using the ideal gas equation for known cylinder pressure and volume. Because of the approximate nature of the correlations, it has been recommended (Krieger and Borman, 1966) that using air properties for the thermal conductivity and viscosity of the combustion gases is adequate. Values of the thermal conductivity and dynamic viscosity of air are given in Appendix A. The radiation heat transfer is included implicitly in the convection correlations or as a stand-alone term, depending on the computational accuracy desired. For further reading about engine heat transfer, a comprehensive review is given in Borman and Nishiwaki (1987), and more recently by Finol and Robinson (2011).

Overall Average Heat Transfer Coefficient

A classic correlation for the overall average engine heat transfer coefficient, h_o , between the cylinder and the coolant is that of Taylor (1985). The correlation, Equation 11.30 was developed from engine energy balance data from a variety of engine types – two- and four-stroke engines, compression and spark ignition. Typical energy balance measurement data include engine air and fuel flow rates, coolant flow rate, and temperature rise. The Nusselt number in the Taylor correlation implicitly includes the conduction and radiation heat transfer components:

$$Nu = 10.4 Re^{0.75} \quad (11.30)$$

In terms of the mass flow rate into the engine per unit piston area, the Reynolds number is defined in Equation 11.31 as

$$Re = \frac{(\dot{m}_a + \dot{m}_f) b}{A_p \mu_g} \quad (11.31)$$

The overall heat flux q'' from an engine cylinder to the coolant is calculated using the piston area $A = A_p = 1/4 \pi b^2$ as a reference area:

$$q'' = \frac{\bar{Q}}{A_p} = h_o (\bar{T}_g - T_c)$$

EXAMPLE 11.1 Overall Average Heat Transfer Coefficient

Compute the overall average heat transfer coefficient h_o and heat flux q'' for a single-cylinder engine with a 0.1 m bore and stroke, average combustion gas temperature of 1000 K, coolant temperature of 350 K, and fuel-airflow rate of 2×10^{-3} kg/s. Assume $k = 0.06$ W/(m K) and $\mu = 20 \times 10^{-6}$ Ns/m².

SOLUTION The Reynolds number is

$$Re_b = \frac{(\dot{m}_a + \dot{m}_f) b}{A_p \mu_g} = 1274$$

The heat transfer coefficient is found using the Taylor correlation:

$$h_o = 10.4 Re_b^{0.75} \frac{k}{b} = 1330 \text{ W}/(\text{m}^2 \text{ K})$$

The heat flux from the cylinder to the coolant is therefore

$$q'' = \frac{\bar{Q}}{A_p} = h_o (\bar{T}_g - T_c) \approx 0.86 \text{ MW}/\text{m}^2$$

Instantaneous Cylinder Average Heat Transfer Coefficient

The instantaneous cylinder average heat transfer coefficient, $h_g(\theta)$, between the combustion gas and cylinder wall is a function of crank angle, and is an input to the finite heat

release model in this Section represented by Equation 11.39. Since $h_g(\theta)$ is a single-zone cylinder average, properties such as the thermal conductivity and viscosity to be used in the correlation are the instantaneous spatially averaged values. The instantaneous gas temperature and density can be determined from the known gas mass and cylinder volume. Two instantaneous cylinder average heat transfer correlations that have been widely used are the Annand and the Woschni correlations.

The Annand (1963) correlation was developed from cylinder head thermocouple measurements of instantaneous heat flux. It uses a constant characteristic velocity, the mean piston speed \bar{U}_p , and a constant characteristic length, the cylinder diameter b . The Annand correlation is

$$q'' = a_1 \frac{k}{b} Re^{0.7} (T - T_w) + a_2 \sigma (T^4 - T_w^4) \quad (\text{W/m}^2) \quad (11.32)$$

where $350 < a_1 < 800$ depending on the intensity of the charge motion, which was found to be larger in two-stroke engines than in four-stroke engines. The recommended radiation term a_2 is equal to 0.58 for diesel combustion and 0.075 for spark ignition engines, and is relatively small compared with the convection term. The Stefan–Boltzmann constant σ is $5.67 \times 10^{-8} \text{ W/(m}^2\text{ K}^4)$.

Another popular correlation for the instantaneous cylinder average heat transfer coefficient is due to Woschni (1967). The Woschni correlation was developed using a heat balance analysis for each stroke of a direct injection diesel engine and uses a variable characteristic gas velocity to account for the increased gas velocity induced by combustion. The Woschni correlation is

$$Nu = 0.035 Re^{0.8} \quad (11.33)$$

The characteristic gas velocity in the Woschni correlation is proportional to the mean piston speed during intake, compression, and exhaust. During combustion and expansion, with the valves closed, it is assumed that the gas velocities are increased by the combustion process, so the characteristic gas velocity has both piston speed and combustion pressure rise terms:

$$U = 2.28 \bar{U}_p + 0.00324 T_r \frac{V_d}{V_r} \frac{P - P_m}{P_r} \quad (11.34)$$

where

\bar{U}_p = mean piston speed (m/s)

T_r = temperature at intake valve closing (K)

V_r = cylinder volume at intake valve closing (m^3)

P_r = pressure at intake valve closing (kPa)

V_d = displacement volume(m^3)

P_m = motored pressure (kPa)

The pressure rise due to combustion is the cylinder pressure P in the firing engine minus the cylinder pressure P_m in the motored engine at the same crank angle. The latter can be estimated by use of the isentropic relation $P_m V_m^\gamma = P_r V_r^\gamma = \text{constant}$, where the subscript r indicates reference conditions, such as intake valve closing.

The previous equation for the characteristic gas velocity is applicable when the intake and exhaust valves are closed and combustion is taking place. When the valves are open, the cylinder gases have a different characteristic velocity resulting from the flow into or

out of the cylinder. In this case, the Woschni correlation uses

$$U = 6.18 \bar{U}_p \quad (11.35)$$

Since thermal conductivity $k \sim T^{0.75}$, and dynamic viscosity $\mu \sim T^{0.62}$, the Woschni heat transfer coefficient in dimensional form (W/(m² K)) is given by Equation 11.36:

$$h_g = 3.26 P^{0.8} U^{0.8} b^{-0.2} T^{-0.55} \quad (11.36)$$

where the units of P , U , b , and T are in kPa, m/s, m, and K, respectively.

The constants in the Woschni correlation were determined by matching experimental results from a given engine. When applied to any other engine, the constants for the heat transfer coefficient and characteristic velocity are estimates at best, and it is not uncommon to find engineers adjusting them to better match their own engine. Additional correlations are discussed in Hohenberg (1979).

An illustrative cylinder heat transfer coefficient match is given in Chang et al. (2004). They modified the Woschni correlation to obtain agreement with measured instantaneous surface heat flux data in an HCCI engine, especially the effect of engine load. They reduced the combustion pressure rise term by a factor of six, used the instantaneous chamber height y as the characteristic length scale, and changed the temperature exponent to 0.73. Their correlation is

$$h_g = 3.4 P^{0.80} U^{0.80} y^{-0.20} T^{-0.73} \quad (11.37)$$

where

$$U = 2.28 \bar{U}_p + \frac{0.00324}{6} T_r \frac{V_d}{V_r} \frac{P - P_m}{P_r} \quad (11.38)$$

The finite heat release model introduced in Chapter 2 can now be modified to include the heat transfer dQ_w to the cylinder walls, since we have an expression for the instantaneous average cylinder heat transfer coefficient $h_g(\theta)$. The finite heat release equation, Equation 11.39, with the addition of cylinder wall heat transfer is

$$\frac{dP}{d\theta} = \frac{\gamma - 1}{V} \left[Q_{in} \frac{dx_b}{d\theta} - \frac{dQ_w}{d\theta} \right] - \gamma \frac{P}{V} \frac{dV}{d\theta} \quad (11.39)$$

The heat transfer rate at any crank angle θ to the exposed cylinder surfaces at an engine speed N is determined with Equation 11.40:

$$\frac{dQ_w}{d\theta} = h_g(\theta) A(\theta) (T_g(\theta) - T_w) / (2\pi N) \quad (11.40)$$

The combustion chamber area A is a function of crank angle θ , and is the sum of the combustion chamber area at top dead center A_o and the instantaneous cylinder wall $A_w(\theta)$ area. The instantaneous combustion chamber area and volume are thus

$$A = A_o + \pi b y(\theta)$$

$$V = V_o + \frac{\pi b^2}{4} y(\theta)$$

or

$$A = (A_o - 4V_o/b) + 4V/b \quad (11.41)$$

where V_o is the cylinder volume at top dead center. By reference to Chapter 1, the dimensionless cylinder volume $\tilde{V}(\theta) = V(\theta)/V_{bdc} = V(\theta)/V_1$ for $l \gg s$ is

$$\tilde{V}(\theta) = \frac{1}{r} + \frac{r-1}{2r}(1 - \cos \theta) \quad (11.42)$$

When the parameters in the heat loss equation are normalized by the conditions at state 1, bottom dead center, they take the form

$$\tilde{Q} = \frac{Q_{\text{in}}}{P_1 V_1} \quad \tilde{T} = \frac{T}{T_1} \quad \tilde{Q}_1 = \frac{Q_1}{P_1 V_1} \quad (11.43)$$

and

$$\tilde{h} = \frac{4hT_1}{P_1 \omega \beta b} \quad \beta = \frac{4V_1}{b(A_o - 4V_o/b)} \quad (11.44)$$

The dimensionless heat loss is then

$$\frac{d\tilde{Q}_1}{d\theta} = \tilde{h}(1 + \beta\tilde{V})(\tilde{P}\tilde{V} - \tilde{T}_w) \quad (11.45)$$

The original Woschni heat transfer correlation equation, Equation 11.36, is incorporated in the Matlab® program `WoschniHeatTransfer.m` that is listed in Appendix F.17. The program is a finite heat release program that can be used to compute the performance of an engine and calculates the instantaneous heat and mass transfer. The engine performance is determined by numerically integrating the finite heat release equation for the pressure, work, heat loss, and cylinder gas mass as a function of crank angle. The integration starts at bottom dead center ($\theta = -180^\circ$), with initial inlet conditions given. The integration proceeds degree by degree to top dead center and back to bottom dead center. Once the pressure and other terms are computed as a function of crank angle, the overall cycle parameters of network, thermal efficiency, and imep are also computed. The use of the program is detailed in the following example:

EXAMPLE 11.2 Instantaneous Heat Transfer Coefficient

For the same engine conditions as in Example 2.3 with the start of combustion at $\theta_s = -20^\circ$, (a) Find the maximum imep and thermal efficiency when cylinder heat transfer is accounted for using the Woschni heat transfer correlation. (b) Plot the instantaneous heat transfer coefficient $h_g(\theta)$, the heat flux q'' to the cylinder wall, and the cylinder pressure P as a function of crank angle.

SOLUTION Assume that the specific heat ratio $\gamma = 1.3$, inlet mixture pressure $P_1 = 1$ bar, inlet temperature $T_1 = 300$ K, cylinder wall temperature $T_w = 360$ K, the top dead center area/volume ratio $A_o/V_o = 306.6 \text{ m}^{-1}$, the engine speed $\omega = 200 \text{ rad/s}$, and that mass loss can be neglected. The nondimensional volume parameter β and wall temperature \tilde{T}_w for this problem are

$$\beta = \frac{4r}{b(A_o/V_o) - 4} = \frac{(4)(10)}{(0.1)(306.6) - 4} = 1.50$$

$$\tilde{T}_w = T_w/T_1 = 360/300 = 1.2$$

The given engine parameters are entered into the `WoschniHeatTransfer.m` program as shown below:

```
function [ ] = WoschniHeatTransfer( )
% Gas cycle heat release code with Woschni heat transfer
```

```

thetas = -20; % start of heat release (deg)
thetad = 40; % duration of heat release (deg)
r = 10; % compression ratio
gamma = 1.3; % gas const
Q = 20; % dimensionless total heat release
beta = 1.5; % dimensionless volume
a = 5; % wiebe parameter a
n = 3; % wiebe exponent n
omega = 200.; % engine speed rad/s
c = 0; % mass loss coeff
s = 0.1; % stroke (m)
b = 0.1; % bore (m)
T_bdc = 300; % temp at bdc (K)
tw = 1.2; % dimensionless cylinder wall temp
P_bdc = 100; % pressure at bdc (kPa)
...

```

The predicted instantaneous heat transfer coefficient $h_g(\theta)$ is plotted in Figure 11.11. It rises sharply as heat release commences and has a maximum value of about $2200 \text{ W}/(\text{m}^2 \text{ K})$. The resulting wall heat flux q'' is presented in Figure 11.12, with a peak heat flux of about $3.6 \text{ W}/\text{m}^2$. The cylinder pressure profile and cumulative work and heat loss are plotted in Figures 11.13 and 11.14. As discussed earlier, the cumulative work is initially negative due to the piston compression and becomes positive on the expansion stroke. The heat loss is very small during compression, indicating a nearly isentropic compression process, and rises rapidly during the heat release process.

Representative thermodynamic parameters are compared with the simple heat release computation with no heat loss in Table 11.4. With the instantaneous heat transfer included, the maximum efficiency is reduced from 0.49 to 0.41, and the maximum nondimensional imep is reduced from 10.96 to 9.11.

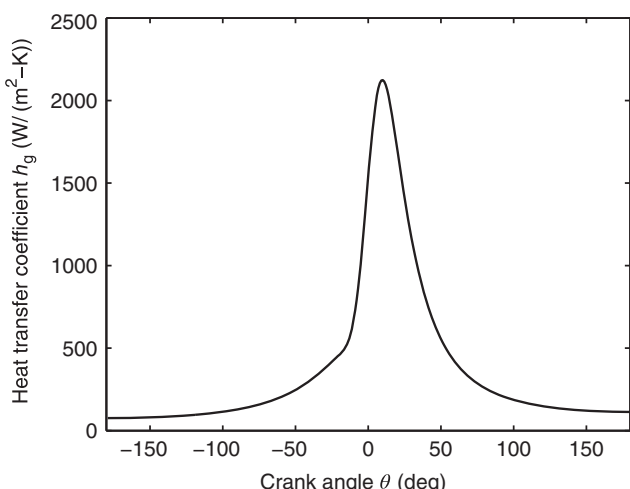


Figure 11.11 Instantaneous heat transfer coefficient $h_g(\theta)$ (Example 11.2).

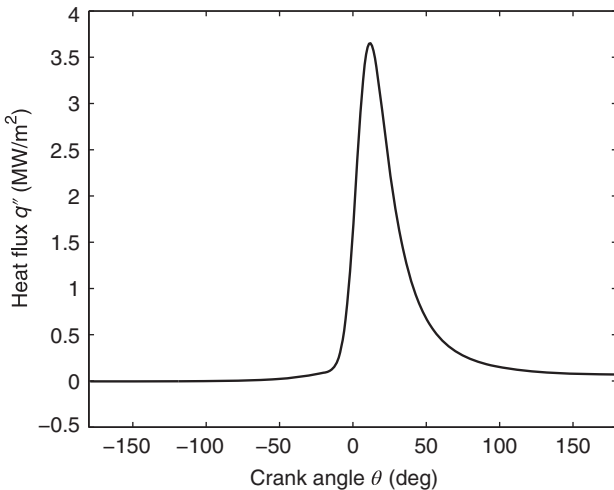


Figure 11.12 Heat flux q'' (Example 11.2).

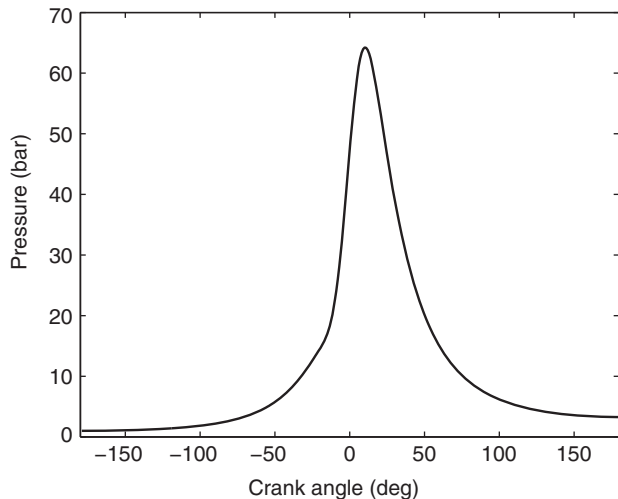


Figure 11.13 Cylinder pressure profile (Example 11.2).

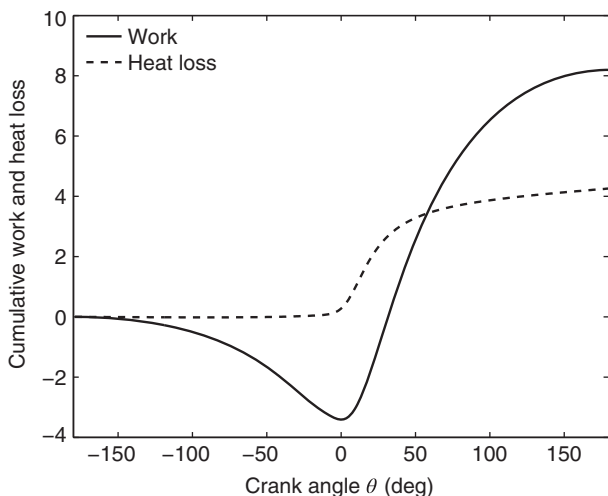


Figure 11.14 Cumulative work and heat loss for (Example 11.2).

Table 11.4 Comparison of Heat Release Models With and Without Heat/Mass Loss (Example 11.2)

	w/ heat loss	w/o heat loss
θ_s	-20.00	-20.00
θ_d	40.00	40.00
P_{\max}/P_1	64.22	67.23
θ_{\max}	11.0	11.0
Net work/ $P_1 V_1$	8.20	9.86
Heat loss/ $P_1 V_1$	4.26	0
Efficiency η	0.41	0.493
η/η_{Otto}	0.82	0.988
Imep/ P_1	9.11	10.96

11.7 HEAT TRANSFER IN THE EXHAUST SYSTEM

Convective heat loss is an important consideration in exhaust pipe and port design, especially for engines with exhaust turbines or catalytic converters. The ports are relatively short and curved with highly unsteady flow due to valve and piston motion, so the flow will not be fully developed. The resulting maximum heat flux is of short duration and relatively high due to the high exhaust gas velocities and temperatures.

Nusselt-Rayleigh number correlations have been developed for the time-averaged heat transfer in the exhaust system. Malchow et al. (1979) obtained the following correlation, Equation 11.46 for the average heat loss in a straight circular exhaust pipe with $D/L = 0.3$, where D is the exhaust pipe diameter and L is the pipe length:

$$Nu = 0.0483 Re^{0.783} \quad (11.46)$$

A steady-state correlation for developing flow in a smooth pipe (Incropera and DeWitt, 2007) is

$$Nu = 0.023 Re^{0.8} Pr^{0.33} (1 + D/L)^{0.7} \quad (11.47)$$

In Equation 11.47, Pr is the Prandtl number and L is the pipe length. Comparison of the correlations indicate that the heat transfer in the exhaust pipe is about 50% greater than would exist in a steady flow in the same pipe.

Hires and Pochmara (1976) correlated experimental results for the instantaneous heat loss from 10 different exhaust port designs. The suggested correlation equation, Equation 11.48, is

$$Nu = 0.158 Re^{0.8} \quad (11.48)$$

where their Reynolds number is defined as

$$Re = \frac{\dot{m}d}{\mu A} \quad (11.49)$$

and \dot{m} is the instantaneous flow rate, d is the throat diameter, A is the exit cross section, and μ is the exhaust gas viscosity. In an exhaust port, it appears that the heat transfer coefficient is about eight times what it would be in a steady flow in the same port. This is probably caused by increased turbulence generated by flow separation near the poppet valve.

In that neither Equation 11.46 nor 11.48 includes information about the exhaust valve, such as lift or valve seat angle, they are applicable to other engines only in so far as they

are geometrically similar. As discussed in Chapter 5, at low valve lifts, the port flow is in the form of a jet, and for larger lifts, the port flow is in the form of developing pipe flow. The valve geometry and lift have been incorporated into heat transfer correlations by Caton and Heywood (1981).

11.8 RADIATION HEAT TRANSFER

During the combustion process in an engine, high temperature gases and particulate matter radiate to the cylinder walls. In a spark ignition engine, the fraction of the gaseous and particulate matter radiation is very small in comparison to the convection heat transfer to the cylinder wall. The flame front propagates quickly across the combustion chamber through a nearly homogeneous fuel–air mixture. Most of the gaseous radiation is in narrow bands from the H₂, CO₂, and H₂O molecules.

In a compression ignition engine, fuel burns in a turbulent diffusion flame formed around the fuel spray in the region where the equivalence ratio is close to 1. Soot particles are formed as an intermediate step in the combustion process. The radiation from the soot particles during their existence is significant, comprising about 20–40% of the total heat transfer to the cylinder wall (Dent and Sulaiman, 1977). In contrast to the gaseous radiation, the soot particles radiate over the entire spectrum. The radiant heat transfer from the flame will reduce its temperature, which affects the local rate of NO formation. The Woschni correlation, since it is based on heat flux, includes the radiation heat transfer to the cylinder wall. The Annand correlation does not include the radiation heat flux.

Radiation heat transfer in participating media, such as the case in a combusting gas–particulate mixture, is modeled with the radiation transfer equation (RTE). The equation includes the radiant energy absorbed, emitted, and scattered along a given solid angle direction:

$$\frac{dI}{ds} = -(K + \sigma)I + KI_b + \frac{\sigma}{4\pi} \int P(\Omega, \Omega') I(\Omega') d\Omega' \quad (11.50)$$

where I is the radiant intensity in the direction of a solid angle Ω , s is the distance in that direction, I_b is the black body intensity, K is an extinction coefficient, σ is a scattering coefficient, P is the phase function or probability for scattering from solid angle Ω' into solid angle Ω . There are a variety of numerical methods for solution of the radiative transfer equation including flux methods, Monte Carlo techniques, the discrete ordinates method (DOM), and the discrete transfer method (DTM). The discrete ordinates method discretizes the radiative transfer equation for a set of finite solid angle directions. The resulting discrete ordinates equations are solved along the solid angle directions using a control volume technique.

The radiation transfer equation has been incorporated into multi-dimensional CFD codes, such as KIVA. Blunsdon et al. (1992) applied the discrete transfer method to the CFD code KIVA for the simulation of diesel combustion, and also modeled the radiation from combustion products in a spark ignition engine (Blunsdon et al., 1993). Using the discrete ordinates method, Abraham and Magi (1997) computed the radiant heat loss in a diesel engine. Inclusion of the radiant heat loss reduced the peak temperature by about 10% relative to a nonradiative computation, lowering the predicted frozen NO concentrations.

The exhaust system operates at a temperature high enough so that radiation heat transfer from the exhaust system to the environment is significant. At full load with a stationary engine on a test stand, it is possible to make the exhaust system glow red, which indicates that the radiation emission is in the visible wavelength range. In many engines, a radiation

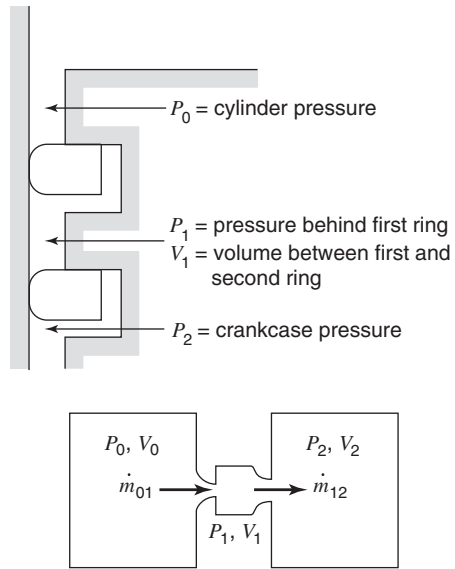


Figure 11.15 Ring pack and 1-D flow model of blowby.

shield is used to reduce the radiation heat transfer from the exhaust manifold to the engine block and head through the exhaust manifold gasket.

11.9 MASS LOSS OR BLOWBY

There are three primary reasons for an interest in blowby. It influences (1) the gas pressure acting on the rings that influences the friction and wear characteristics, (2) the indicated performance, and (3) the hydrocarbon emissions.

Typically, a ring pack consists of two compression rings and an oil ring. The pressure drop across the oil ring is generally negligible. Such a ring pack is represented in Figure 11.15. A one-dimensional representation of the ring pack is also shown; it consists of three plenums in series through passages whose sizes are dependent upon the ring gaps, the piston to cylinder wall clearance, and any ring tilt present. The volumes are all time dependent: V_0 changes because of piston motion; V_1 changes because of ring motion; and V_2 changes because of piston motion (including those of the other cylinders in a multicylinder engine).

Figure 11.16 shows the results of measurements made for ring gas pressures in a two-stroke diesel engine (Ruddy, 1979). Notice that about 70° after top dead center, the pressure between the rings P_1 is greater than the cylinder pressure P_0 which, if the flows are quasi-steady, means there is flow of compressed gas from the ring pack back to the cylinder.

The mass flow from one ring pack plenum to another is governed by the compressible flow equation, Equation 11.51:

$$\dot{m} = \rho_0 C_d A_t c_o \left[\frac{2}{\gamma - 1} \left(\left(\frac{P_1}{P_0} \right)^{2/\gamma} - \left(\frac{P_1}{P_0} \right)^{(\gamma+1)/\gamma} \right) \right]^{1/2} \quad (11.51)$$

The requisite stagnation properties and the specific heat ratio are based on current values in the upstream plenum. The throat area A_t is proportional to the ring gap and the bore to cylinder clearance. The orifice coefficient C_d , which depends at least on the

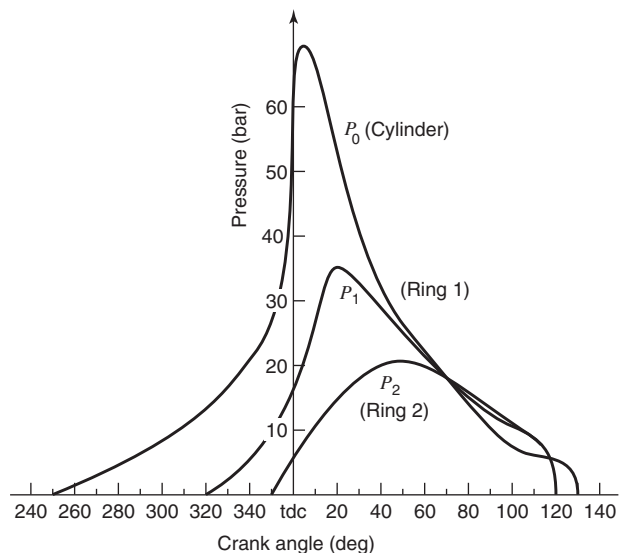


Figure 11.16 Measured interring pressure. Adapted from Ruddy (1979).

Reynolds number of the flow and also on whether or not the ring is tilted, is not known with certainty. It is of order unity and its magnitude is fixed by matching between measured and predicted data, typically the average blowby rate and the interring pressure distribution.

It is typical in such computations to assume that the gas between rings is at a temperature equal to the average of the piston temperature and the cylinder liner temperature. In so doing, there is no need to solve the energy equation for each plenum. The equation of continuity for mass conservation is applied to each plenum where the mass flows in and out are determined as just described. By simultaneously integrating the resultant ordinary differential equations, one obtains the mass within each plenum. These are coupled to equations of motion for each ring, thereby obtaining the plenum volumes. With the plenum volumes and the mass contained therein, one then uses an equation of state to compute the pressure in each plenum. A representative computer simulation program used for computation of ring pack gas flow is RINGPACK (Ricardo, 2014).

It was mentioned that blowby influences the hydrocarbon emissions. During compression and the early stages of combustion, unburned fuel and air is being compressed into the plenums between the rings. As mentioned, the gases rapidly equilibrate thermally to the environment and are thus at the average of the piston and liner temperature. In fact, the heat transfer is so effective that the flame propagating in the cylinder is extinguished when it tries to propagate into the spaces between the rings. The unburned fuel and air pushed into the ring pack remains unburned.

Soon after the blowby flow reverses itself due to the decreasing cylinder pressure, unburned fuel and air emerges from the ring pack back into the cylinder. Since this occurs late in the expansion stroke, the burned gases in the cylinder are relatively cold, and thus a large part of this reemerging fuel and air will not be oxidized as it mixed with the in-cylinder combustion products. Thus, unburned fuel or hydrocarbons will be expelled from the engine during the exhaust process. Namazian and Heywood (1982) estimated that anywhere from 2 to 7% of the fuel is wasted in this way. It is interesting to note that this is another advantage of diesel engines, since in diesel engines, the composition of the cylinder gas compressed into the ring pack will be primarily air.

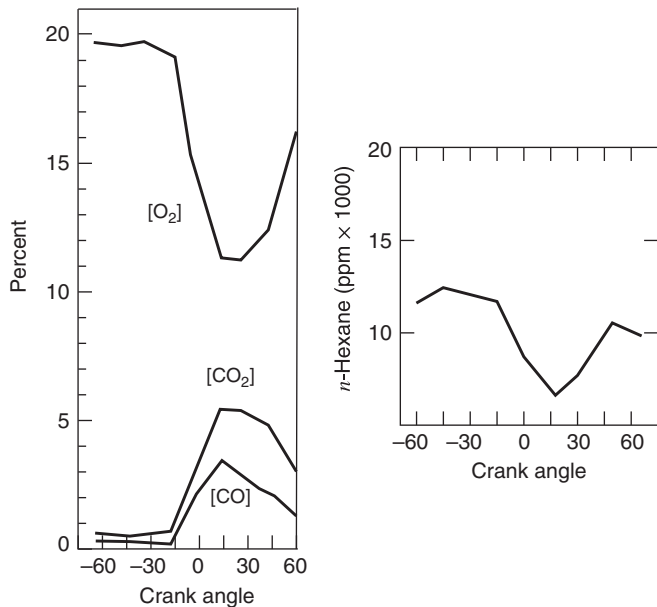


Figure 11.17 Measured gas composition at the top land of a gasoline engine at WOT. Adapted from Furuhama and Tateishi (1972).

Figure 11.17 shows gas concentrations at the top land of a 1.3 L four-cylinder gasoline engine at WOT at 2000 rpm measured by Furuhama and Tateishi (1972). They mounted a sampling valve in the piston and opened the valve for 1.25 ms at the same angle in consecutive cycles. Gases were withdrawn for analysis from the space between the top land and the cylinder for a variety of crank angles during the cycle.

Their measurements indicated that during the compression stroke, concentrations of oxygen and hydrocarbons (as *n*-hexane equivalent) are high because fuel and air is entering the ring pack. Likewise, carbon dioxide and carbon monoxide are low in concentration attributable to the residual gas content. About 15° before top dead center, there is a sudden drop in oxygen and hydrocarbon concentration as burned gases are beginning to enter the ring pack. About 30° after top dead center, it appears that the unburned gases that entered earlier reemerge, though diluted somewhat by the burned products that entered the ring pack.

In Chapters 2 and 4, we investigated the influence of blowby on indicated performance. It was assumed that the flow was always out of the cylinder and that the rate was proportional to the mass of the cylinder contents. The constant of proportionality C was selected so that about 2.5% of the charge leaked out, consistent with observation. The computations were deliberately simple for illustration purposes. They ignored the fact that a flow reversal occurs during the expansion stroke, and thus underestimate the mass of gas that is pushed into the ring pack during the subsequent compression stroke. As mentioned, when this gas re-emerges, much of it fails to oxidize and thus fuel is wasted.

11.10 REFERENCES

- ABRAHAM, J. and V. MAGI (1997), "Application of the Discrete Ordinates Method to Compute Radiant Heat Loss in a Diesel Engine," *Numer. Heat Transfer, Part A: Appl.*, Vol. 31, No. 6, pp. 597–610.
 ALKIDAS, A. C. and J. P. MYERS (1982), "Transient Heat-Flux Measurements in the Combustion Chamber of a Spark Ignition Engine," *ASME J. Heat Transfer*, Vol. 104, pp. 62–67.

- ANNAND, W. J. D. (1963), "Heat Transfer in the Cylinders of a Reciprocating Internal Combustion Engine," *Proc. Instn. Mech. Engrs.*, Vol. 177, p. 973.
- BENDERSKY, D. (1953), "A Special Thermocouple for Measuring Transient Temperature," *Mech. Eng.*, Vol. 75, p. 117.
- BLUNSDON, C., J. DENT, and W. MALALASEKERA (1993), "Modeling Infrared Radiation from the Combustion Products in a Spark Ignition Engine," SAE paper 932699.
- BLUNSDON, C., W. MALALASEKERA, and J. DENT (1992), "Application of the Discrete Transfer Model of Thermal Radiation in a CFD Simulation of Diesel Engine Combustion and Heat Transfer," SAE paper 922305.
- BOHAC, S., D. BAKER, and D. ASSANIS (1996), "A Global Model for Steady State and Transient S. I. Engine Heat Transfer Studies," SAE paper 960073.
- BORMAN, G. and K. NISHIWAKI (1987), "Internal Combustion Engine Heat Transfer," *Prog. Energy Combust. Sci.*, Vol. 13, pp. 1-46.
- CATON, J. A. and J. B. HEYWOOD (1981), "An Experimental and Analytical Study of Heat Transfer in an Engine Exhaust Port," *Int. J. Heat Mass Transfer*, Vol. 24 (4), pp. 581-595.
- CHANG, J. O. GURALP, Z. FILIP, D. ASSANIS, T. KUO, P. NAJT, and R. RASK (2004), "New Heat Transfer Correlation for an HCCI Engine Derived from Measurements of Instantaneous Surface Heat Flux," SAE paper 2004-01-2996.
- DENT, J. C. and S. J. SULAIMAN (1977), "Convective and Radiative Heat Transfer in a High Swirl Direct Injection Diesel Engine," SAE paper 770407.
- FINOL, C. and K. ROBINSON (2011), "Thermal Modeling of Modern Diesel Engines: Proposal of a New Heat Transfer Coefficient Correlation," *Proc. IMechE Part D: J. Automobile Eng.*, Vol. 225, No. 11, p. 1544-1560.
- FURUHAMA, S. and Y. TATEISHI (1972), "Gases in Piston Top-Land Space of Gasoline Engine," *Trans. Soc. Automotive Eng. of Japan*, Vol. 4, pp. 30-39.
- HIRES, S. D. and G. L. POCHMARA (1976), "An Analytical Study of Exhaust Gas Heat Loss in a Piston Engine Exhaust Port," SAE paper 760767.
- HOHENBERG, G. (1979), "Advanced Approaches for Heat Transfer Calculations," SAE paper 790825.
- INCROPERA, F. , D. DEWITT, T. BERMAN, and A. LAVINE (2007), *Fundamentals of Heat and Mass Transfer*, 6th edition, Wiley, New York.
- KRIEGER, R. and G. BORMAN (1966), "The Computation of Apparent Heat Release for Internal Combustion Engines," *ASME Proc. of Diesel Gas Power*, paper 66-WA/DPG-4.
- LI, C. (1982), "Piston Thermal Deformation and Friction Considerations," SAE paper 820086.
- MALCHOW, G., S. SORENSEN, and R. BUCKIUS (1979), "Heat Transfer in the Straight Section of an Exhaust Port of a Spark Ignition Engine," SAE paper 790309.
- NAMAZIAN, M. and J. B. HEYWOOD (1982), "Flow in the Piston-Cylinder-Ring Crevices of a Spark Ignition Engine: Effect on Hydrocarbon Emissions, Efficiency and Power," SAE paper 820088.
- REITZ, R. (1991), "Assessment of Wall Heat Transfer Models for Premixed Charge Engine Combustion Computations," SAE 910267.
- RINGPACK V.3 Users Manual (2014), Ricardo Software, Inc.
- ROBINSON, K., N. CAMPBELL, J. HAWLEY, and D. TILLEY (1999), "A Review of Precision Engine Cooling," SAE paper 1999-01-0578.
- RUDDY, B. (1979), "Calculated Inter-Ring Gas Pressures and Their Effect on Ring Pack Lubrication," DAROS Information, Vol. 6, pp. 2-6, Sweden.
- RYDER, E. A. (1950), "Recent Developments in the R-4360 Engine," *SAE Quart. Trans.*, Vol. 4(4), p. 559.
- SHAYLER, P., S. CHRISTIAN, and T. MA (1993), "A Model for the Investigation of Temperature, Heat Flow, and Friction Characteristics During Engine Warm-up," SAE paper 931153.
- SUN, X., W. WANG, D. LYONS, and X. GAO (1993), "Experimental Analysis and Performance Improvement of a Single Cylinder Direct Injection Turbocharged Low Heat Rejection Engine," SAE paper 930989.
- TAYLOR, C. F. (1985), *The Internal Combustion Engine in Theory and Practice*, MIT Press, Cambridge, Massachusetts.

- TILLOCK, B. and J. MARTIN (1996), "Measurement and Modeling of Thermal Flows in an Air-Cooled Engine," SAE paper 961731.
- WHITEHOUSE, N. (1970), "Heat Transfer in Compression-Ignition Engines: First Paper: Heat Transfer in a Quiescent Chamber Diesel Engine," *Proc. Inst. Mech. Engrs.*, Vol. 185, pp. 963–975.
- WISNIEWSKI, T. (1998), "Experimental Study of Heat Transfer in Exhaust Valves of 4C90 Diesel Engine," SAE paper 981040.
- WOSCHNI, G. (1967), "A Universally Applicable Equation for the Instantaneous Heat Transfer Coefficient in the Internal Combustion Engine," SAE paper 670931.

11.11 HOMEWORK

- 11.1** Practical applications of Equation 11.7 are limited because the heat loss to ambient air is determined by the small differences between much larger numbers. Suppose each term on the right-hand side can be determined to within $\pm 5\%$. What tolerances could then be attached to Q_{amb} ? For nominal values, use the results given in Table 11.1. The most probable error is computed from the square root of the sum of the squares of the errors of the RHS terms.
- 11.2** The average heat flux through a water cooled engine's cylinder head ($k = 65 \text{ W}/(\text{m K})$) 1.0 cm thick is $0.2 \text{ MW}/\text{m}^2$. If the coolant temperature is 85°C and the coolant side heat transfer coefficient is $750 \text{ W}/(\text{m}^2 \text{ K})$, what is the average surface temperature on the combustion chamber and the coolant sides of the cylinder head?
- 11.3** If an engine cylinder head is changed from iron ($k = 60 \text{ W}/(\text{m K})$) to aluminum ($k = 170 \text{ W}/(\text{m K})$), estimate the change in the heat flux from the head. What is the change in the gas-side cylinder head temperature?
- 11.4** At an engine speed of 1000 rpm, what is the approximate penetration depth of the temperature fluctuations in (a) a cast iron block and (b) an aluminum engine block?
- 11.5** Determine the effect of engine speed on the overall engine heat transfer coefficient of Example 11.1. Plot h_o versus N for $1000 < N < 6000$ rpm. Assume the volumetric efficiency $e_v = 0.9$.
- 11.6** Using the Taylor correlation, Equation 11.30, develop an equation for the overall heat transfer coefficient h_o as a function of the engine speed, bore, and volumetric efficiency.
- 11.7** With reference to the Taylor correlation, Equation 11.30, the heat transfer coefficient h_o increases with engine speed to the 0.75 power, whereas the time available for heat transfer decreases with engine speed. What is the net effect of increasing engine speed on engine thermal efficiency?
- 11.8** Calculate the time-averaged heat transfer (kW) to the coolant from a four-cylinder propane-fueled engine with a 120 mm bore and stroke operating at 1200 rpm. The propane fuel flow rate to the engine is 1.0 g/s with an equivalence ratio $\phi = 0.8$. The time-averaged combustion gas temperature is 1200 K, and the coolant temperature is 340 K.
- 11.9** If $k \sim T^{0.75}$ and $\mu \sim T^{0.62}$, how does the heat transfer coefficient of the Woschni correlation, Equation 11.33 vary with pressure and temperature?
- 11.10** How would you expect the leading coefficient of Equation 11.35 to change if Woschni had included the effect of the intake valve size?

- 11.11** A single-cylinder spark ignition cycle engine with a compression ratio $r = 10$ is operated at full throttle. The initial cylinder pressure and temperature at bottom dead center are $P_1 = 1$ bar and $T_1 = 300$ K. The bore and stroke of the engine are $b = 80$ mm and $s = 90$ mm, with the top dead center area/volume ratio $A_o/V_o = 320 \text{ m}^{-1}$. The average cylinder wall temperature $T_w = 400$ K. The total heat addition, $Q_{in} = 2000$ J, the start of combustion is at $\theta_s = -15^\circ$, and the combustion duration $\theta_d = 40^\circ$. Assume that the ideal gas specific heat ratio γ is 1.4, the Wiebe energy release parameters are $a = 5$ and $n = 3$, and the blowby mass loss coefficient $c = 0.70$.

Using the program `WoschniHeatTransfer.m`, (a) Find the imep and thermal efficiency. (b) Plot the instantaneous heat transfer coefficient $h_g(\theta)$, the heat flux q'' to the cylinder wall, and the cylinder pressure P as a function of crank angle.

- 11.12** For the engine in Homework 11.11, if the start of combustion is changed to $\theta_s = -25^\circ$, and the combustion duration $\theta_d = 50^\circ$, using the program `WoschniHeatTransfer.m` program, (a) Find the imep and thermal efficiency. (b) Plot the instantaneous heat transfer coefficient $h_g(\theta)$, the heat flux q'' to the cylinder wall, and the cylinder pressure P as a function of crank angle.
- 11.13** What is the average heat transfer coefficient for an exhaust pipe that has an average mass flow rate of 0.08 kg/s at a mean temperature of 700 K and a pipe diameter of 0.045 m?

Chapter 12

Engine Testing and Control

12.1 INTRODUCTION

The purpose of this chapter is to introduce engine testing, measurement, and control. One instruments the engine to determine the value of engine parameters such as the engine torque, engine speed, fuel flow rate, airflow rate, emissions, cylinder pressure, residual fraction, coolant temperature, oil temperature, and the spark or fuel injection timing. To measure the performance of an engine one needs to connect the engine to a dynamometer to control the speed and load.

The testing procedure generally consists of operating the engine at different speeds and loads and measuring the parameters of interest for a given test. An energy balance can also be performed as a check to determine the various energy flow paths in the engine, that is, to the dynamometer, coolant, ambient, and exhaust. Exhaust gas measurement and analysis are performed to determine the emissions produced by the engine.

Some measurements are rather straightforward and require little, if any, explanation. The coolant temperature is easily measured by insertion of a thermocouple or thermistor into the coolant. Some of the measurements require analysis to obtain the desired result. For example, the air-fuel equivalence ratio is determined from the combustion equations and measurements of the composition of the exhaust gases. The testing results are normalized into parameters such as the specific fuel consumption or the mean effective pressure.

The internal combustion engine is a complex electromechanical system with a number of embedded sensing and control systems. These systems include air-fuel ratio, spark timing, knock, idle speed, and exhaust gas recirculation (EGR) control. There is a need to provide real-time information about the engine state to an engine control system, and subsequently the control system needs to be able to change the operating state of the engine.

The two primary inputs to the control system for engine testing are the engine speed and engine torque. The control parameters for a spark ignition engine are the spark timing, valve timing, exhaust gas recirculation, and fuel injector flow. With a spark ignition automobile engine, the air-fuel ratio is tightly controlled to stoichiometric conditions to ensure proper performance of the exhaust three-way catalytic converter, and the ignition timing is controlled to prevent knock. For a compression ignition engine, major control parameters are the fuel injector flow rate and the injection timing.

Sensors for additional engine parameters are in development for use in production vehicles. These include an optical combustion sensor to detect the peak combustion pressure, that is, peak torque. Similarly, a crankshaft torque sensor is also under development. These two sensors can be used to maintain the engine at maximum brake torque conditions. In the emissions area, a vehicle NO_x sensor is being developed to allow an engine to be operated with closed-loop control of the NO_x levels.

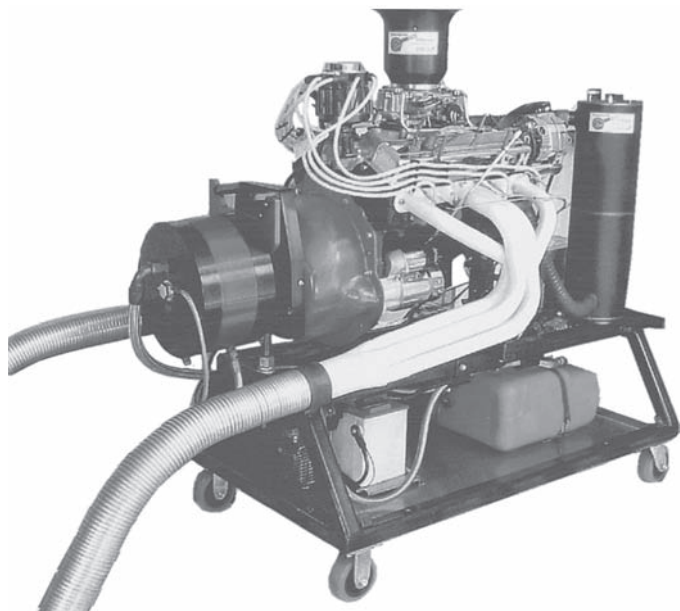


Figure 12.1 Engine on hydraulic dynamometer test stand. (Courtesy Land & Sea, Inc.)

12.2 INSTRUMENTATION

Dynamometers

The dynamometer is a device that provides an external load on the engine and absorbs the power produced by the engine, as shown in Figure 12.1. The earliest dynamometers were brakes that used mechanical friction to absorb the engine power, hence the power absorbed was called the “brake horsepower.” The types of dynamometers currently used are hydraulic or electric. A hydraulic dynamometer or water brake is constructed of a vaned rotor mounted in a casing mounted to the rotating engine shaft. A continuous flow of water is maintained through the casing. The power absorbed by the rotor is dissipated in fluid friction as the rotor shears through the water. Adjusting the level of water in the casing varies the torque absorbed.

There are a number of different kinds of electric dynamometers. These include direct current, regenerative alternating current, and eddy current. The power absorbed in an electric dynamometer is converted into electrical energy, either as power or eddy currents. The electricity can then be dissipated as heat by resistance heating and transferred to a cooling water or air stream. In direct current or regenerative alternating-current machines, the electricity generated can be used, and transformers are available that allow it to supplement a power system. Historically, direct-current machines have offered the greatest testing flexibility but at the greatest cost.

Engine dynamometers can further be classified depending upon whether or not they also have the capability to motor an engine, that is, spin an engine not producing power, similar to the operation of an electric the starter motor of an automobile engine. Hydraulic dynamometers cannot motor an engine. Strictly speaking, neither can eddy-current machines, but because they are often configured into a package with an electric motor to run an engine, for practical purposes the distinction is moot.

The method most commonly employed to measure torque is shown in Figure 12.2. The dynamometer is supported by trunnion bearings and restrained from rotation only a

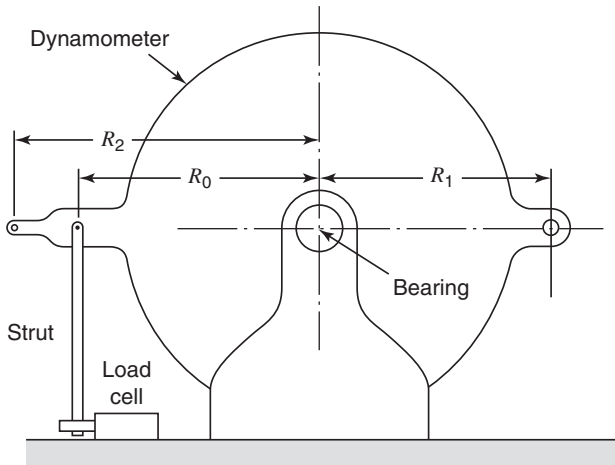


Figure 12.2 Torque measurement using a cradle-mounted dynamometer.

strut connected to a load cell. Whether the dynamometer is absorbing or providing power, a reaction torque is applied to the dynamometer. Hence, if the force applied by the strut is F , then the torque applied to the engine is given by Equation 12.1:

$$\tau = FR_o \quad (12.1)$$

where R_o is defined in Figure 12.2. The load cell measures the force F . For calibration, lever arms are located at R_1 and R_2 for hanging known weights.

Since the work done in rotating the engine's crankshaft through one revolution, or 2π radians, is $2\pi\tau$, it follows that the mean effective pressure for two-stroke engines is equal to $2\pi\tau/V_d$ and the mean effective pressure for four-stroke engines is equal to $4\pi\tau/V_d$, respectively.

If the engine is absorbing energy, then the brake mean effective pressure (bmep) is determined. If the engine is being motored, then the motoring mean effective pressure (mmep) is determined (which, as explained in Chapter 10, is an approximate measure of the friction losses in an engine).

With an appropriate control system, the dynamometer can be used to control either engine speed or torque. For control of engine speed, the dynamometer applies whatever load is required to maintain that speed. For example, if the engine being tested were a spark ignition engine, then the response of the dynamometer to the operator increasing the inlet manifold pressure by opening the throttle would be to increase the load (resistance to turning or applied torque) to maintain the speed.

With torque control selected, the dynamometer maintains a fixed load. For example, the dynamometers response to opening the throttle of a spark ignition engine would be to maintain a constant applied torque. In this case, the engine speed would increase to a point where the friction mean effective pressure in the engine would have increased by an amount equal to the increase in the net indicated mean effective pressure.

Since about one third of the input fuel energy to the engine ends up as heat transfer to the coolant, a cooling tower or radiator is required for the dynamometer stand. The cooling tower will control the coolant temperature. A complete test stand has, in addition, provisions to control the fuel and air temperature, the atmospheric pressure, and the air humidity.

Crank Angle

The crankshaft position is used by the engine control system for ignition timing control, that is, spark advance, which is defined as degrees before top dead center. The crankshaft position can be determined from measurements made in a number of locations on the mechanical drive train, for example, on the crankshaft, camshaft, or distributor shaft. Noncontacting methods are used, which are usually electrical, but optical methods have also been devised.

A Hall effect sensor is commonly used on the camshaft or distributor shaft. The Hall effect, discovered in 1879 by E. H. Hall (1855–1938), an American physicist, is due to electromagnetic forces acting on electrons in metals and semiconductors. If a current is passed through a semiconductor that is placed near a magnet, a voltage is developed across the semiconductor perpendicular to the direction of current flow \vec{V} and perpendicular to the direction of magnetic flux \vec{B} . The voltage results from the Lorentz force $(\vec{V} \times \vec{B})$ acting on the electrons in the semiconductor. The Lorentz force is named after H. Lorentz (1853–1928), a Dutch physicist. The voltage is proportional to the magnetic flux so that if the magnetic flux is changed, the voltage will change. There are a number of Hall effect sensor configurations. With a shielded field sensor, tabs are placed on a rotating disc, mounted on the distributor shaft, and the Hall sensor and magnet are placed on opposite sides of the tab. Each time the tab passes between the magnet and the Hall sensor, the magnetic reluctance of the tab will decrease the magnetic flux intensity at the sensor that causes a corresponding decrease in the sensor Hall voltage. The voltage is independent of engine speed, so the Hall effect sensor can be used even if the engine is not running.

Engine Speed

The engine speed is measured with optical or electrical techniques. One optical technique uses a disk with holes mounted on the revolving engine shaft. A light-emitting diode is mounted on one side of the disk and a phototransistor is mounted on the other side. Each time a hole on the disk passes by the optical sensor, a pulse of light impinges on the phototransistor that generates a periodic signal, the frequency of which is proportional to engine speed.

Many engines use a notch in the flywheel and a magnetic reluctance sensor. The engine speed is found by measuring the frequency at which the notch passes by the position sensor. The sensor is an electromagnet whose induced voltage varies with the change in the magnetic flux. As the notch in the flywheel passes by the sensor, the induced voltage will first decrease, then increase. If the engine is not running, there will be no change in the magnetic flux, and the magnetic reluctance sensor will not produce any voltage.

Fuel Flow Measurement

An old, but accurate and simple, way to measure the cumulative fuel flow to an engine is to locate the fuel supply on a weighing bridge and time the period required to consume a certain weight of fuel. The essence of such a system is shown in Figure 12.3. This method works equally well for both liquid and gaseous fuels. For liquid fuels, a pipette and stopwatch can be used, a method used to calibrate fuel flow meters. A small positive displacement turbine can be installed in the fuel line as an electronic fuel flow transducer. Basically, the rotational speed of the turbine is proportional to the fuel flow rate. These transducers are also convenient in terms of minimizing bulk in the test cell, maximizing safety, and maintaining a clean fuel system. Unfortunately, they measure a volumetric

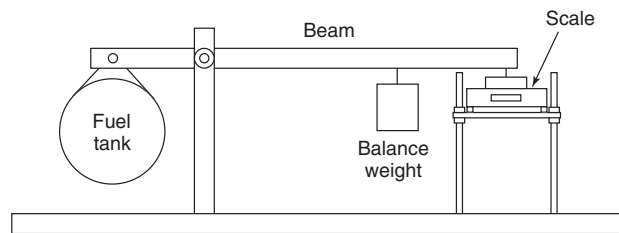


Figure 12.3 Fuel flow measurement using a weighing bridge. Adapted from Lynch and Smith (1997).

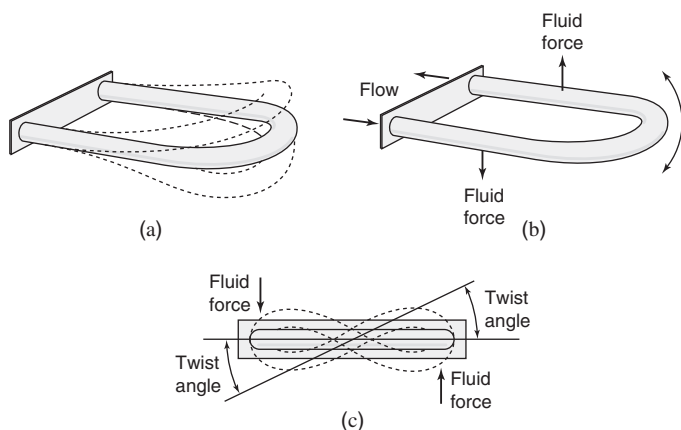


Figure 12.4 Coriolis effect flow meter.

- (a) Sensor tube vibration.
- (b) Forces acting on sensor tube in upward motion.
- (c) End view indicating the force couple and tube twist. (Courtesy Micro Motion, Inc.)

flow rate instead of a mass flow rate, and the calibration is weakly dependent upon the fuel viscosity. Thus, in practice, calibration curves have to be established as a function of the fuel temperature (and possibly pressure) and new ones generated if the fuel type is varied. The calibration curve needs to span the nominal range of fuel flow rates that can be as large as 50 : 1. At considerably greater cost than the turbine-type flow meters, there are other types, such as the ‘‘Flowtron’’ meter, and the Coriolis flow meter. The ‘‘Flowtron’’ meter is the hydraulic equivalent of the Wheatstone bridge circuit. The bridge comprises four matched orifices and a recirculating pump. The external fuel flow through the meter generates a pressure imbalance that is proportional to the mass flow rate. Coriolis flow meters pass the fuel flow through a vibrating U-tube, as shown in Figure 12.4. The Coriolis force ($2\bar{\omega} \times \vec{U}$) acting on the flow will generate a twisting moment in the tube since the flow reverses direction as it passes through the U-tube. A strain gage mounted on the tube measures the magnitude of the twist that is proportional to the flow rate. The accuracy and repeatability of the Flowtron and Coriolis meters is excellent, better than 0.5% or less.

The return flow from fuel injection systems needs to be taken into account in fuel flow measurements, since it is of the same order of magnitude as the fuel flow through the fuel injectors. One approach is to cool the return fuel to the temperature of the supply fuel and connect it to the supply fuel downstream of the fuel flow meter.

Airflow Measurement

The inlet air mass flow rate in vehicular engines is measured by a constant temperature hot film anemometer. The principle of operation is very elegant. A small resistive wire or film

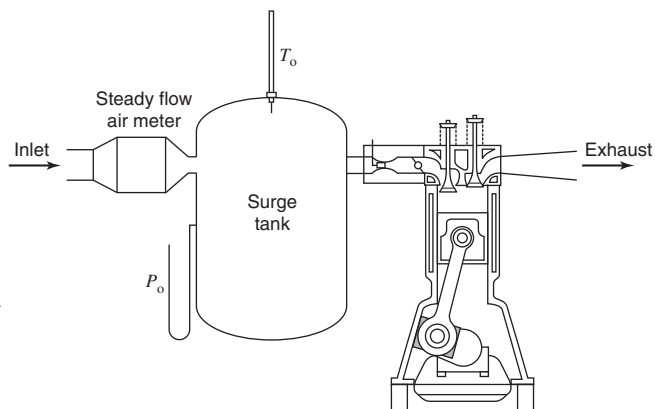


Figure 12.5 Single-cylinder engine equipped with inlet surge tank and steady flow air meter.

placed in the airflow is heated by an electric current. The current required to maintain the film at a constant temperature above the ambient is proportional to the mass flow rate of the air. The sensor is placed at one leg of a Wheatstone bridge circuit so that the proper current is sent through the sensor to maintain a constant sensor temperature.

Airflow to engines cannot be measured with the same precision as the fuel flow. There are two main reasons for this: (1) the instrumentation available is at best accurate to within about 1%, and (2) it is harder to ensure that all of the air delivered to the engine is metered or retained. Air can leak into and out of the cylinder of engines, for example, through the valve guides. As a result, as recommended by Stone (1989), it is wise to measure airflow not only directly but also indirectly using exhaust gas analysis. A discussion of airflow measurement via exhaust gas analysis is given later in this chapter.

A common problem in measuring airflow is that the flow is unsteady or periodic; however, the available meters are usable only in a steady flow. A similar problem can be encountered in measuring fuel flow. The severity of the problem decreases with an increasing number of cylinders sharing a common intake manifold and with an increase in the volume between the meter and the intake ports. The volume acts as a fluid capacitor to damp out fluctuations at the meter. The flow at the meter is smoother with multicylinder engines than with single-cylinder engines because the cylinders are out of phase with one another; thus, as the peaks and valleys in the flow rates to individual cylinders are superimposed, the flow at the meter becomes smooth.

A solution for the worst case, that is, for a single-cylinder engine, that can be applied to steady-state engine testing is illustrated in Figure 12.5. All of the air to be delivered to the engine is metered by a steady-state airflow meter located upstream of a surge tank. Kastner (1947) recommends that the volume of the surge tank be at least about 250 times the displacement volume of the engine. The various types of airflow meters that can be used include the following:

ASME Orifice Often employed as a secondary standard to calibrate other meters; flow rate depends on the square root of the pressure drop across the orifice, so a range of orifice sizes is used to cover the airflow rate range.

Laminar Flow Meter A bundle of tubes (not necessarily round in cross section) sized so that the Reynolds number in each is well within the laminar regime; flow rate depends linearly on the pressure drop across the meter.

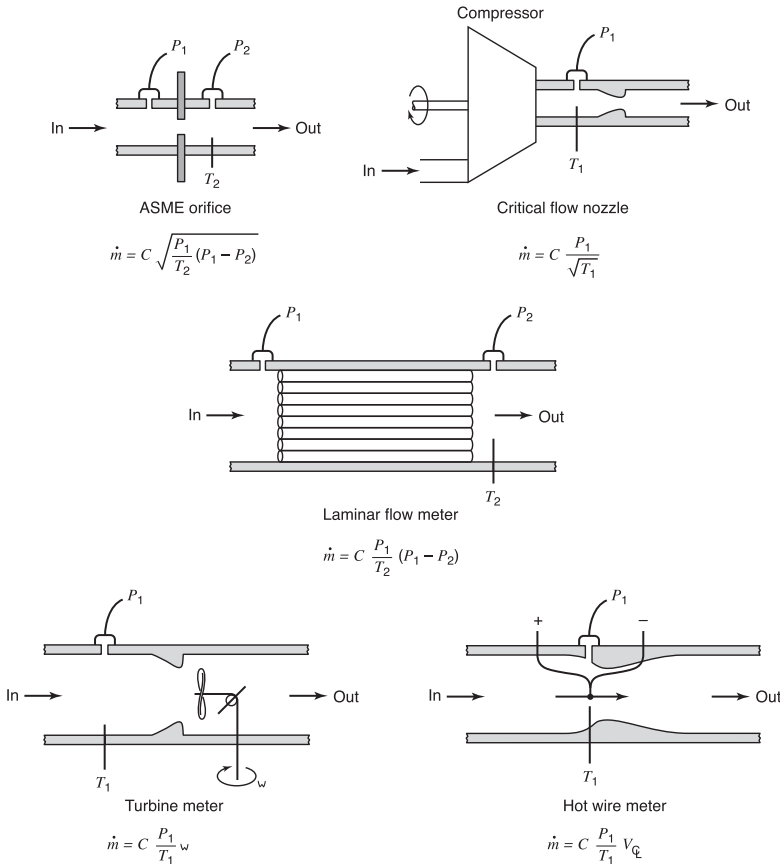


Figure 12.6 Various air flow meters and associated pressure/temperature measurements.

Critical Flow Nozzle A Venturi in which the flow is choked; the flow rate is then linearly dependent upon the delivery pressure (an external compressor is thus required) and independent of the pressure in the surge tank.

Turbine Meter The airflow rate is linearly dependent upon the rotational speed of the turbine.

Hot Wire Meter A hot wire anemometer is inserted into the flow to measure the center-line velocity; the airflow rate is proportional to center-line velocity.

No matter which of the various methods is used, measurements of temperature and pressure also have to be made. Key components of systems employed using these various meters are identified in Figure 12.6. The calibration coefficients of the meters are a function of the Reynolds number of the flow through the meters. For transient engine testing, only the hot wire meter can be used, as it can measure the instantaneous mass flow rate; it can also be used in steady-state testing where the required air box is viewed as a nuisance. It must, however, be used with care because it is possible that in some engines a flow reversal will occur and the meter does not know whether the flow is going forward or backward.

Correction factors are used to adjust measured data to standard atmospheric temperature and pressure conditions. The specific correction procedures are usually included in the laboratory practice manual.

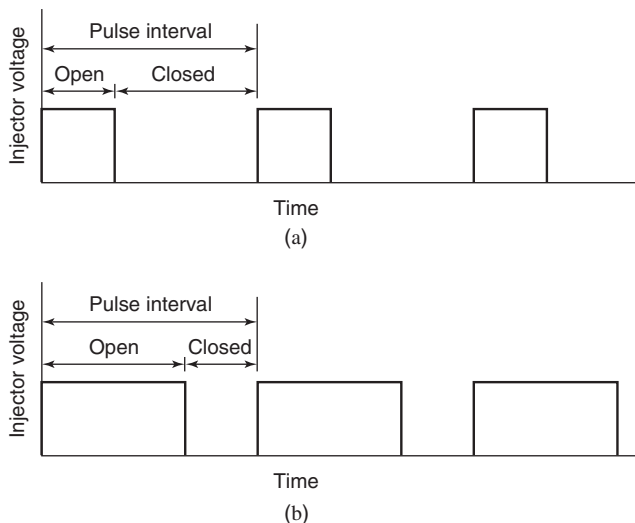


Figure 12.7 Fuel injector control voltage. (a) Part load.
(b) Full load.

Air–Fuel Ratio

The fuel flow rate is computed from the air mass flow rate and the requirement that a spark ignition engine maintains a stoichiometric air–fuel ratio, so the fuel flow rate is directly proportional to the airflow rate. The fuel metering of a fuel injector is performed by a solenoid-operated plunger attached to a needle valve. The plunger is normally closed, so that when the solenoid is not energized, no fuel can flow through the fuel injector. When the engine control unit energizes the solenoid, the valve is lifted and allows fuel to flow through the injector nozzle into the intake port.

The fuel pressure is regulated to a fixed value, so the amount of fuel injected is proportional to the time that the valve is open. The proportionality constant for fuel flow and injector pulse width is determined experimentally. The fuel injector control voltage is pulse-width modulated, as shown in Figure 12.7. The ECU uses a torque-based mean value model to control the pulse width. The width of the solenoid voltage pulse from the ECU depends on the engine load, and the frequency is proportional to engine speed.

Manifold and Ambient Air Pressure

The air pressure in the intake manifold is used by the engine control system as an indication of engine load. Higher manifold pressures correspond to higher loads, since as the throttle is opened to meet an increasing load, the pressure drop across the throttle decreases, and the manifold pressure increases. The manifold air pressure is measured by the displacement of a diaphragm that is deflected by manifold pressure. There are several types of diaphragm sensors. A common one is the silicon-diffused strain gauge sensor. This sensor is a thin square silicon diaphragm with sensing resistors at each edge. One side of the diaphragm is sealed under vacuum, and the other side is exposed to the manifold pressure. The resistors are piezoresistive so that their resistivity is proportional to the strain of the diaphragm. A Wheatstone bridge circuit is used to convert the resistance change to a voltage signal. The pressure fluctuations from the finite opening and closing of the intake valves are filtered out with a small diameter vacuum hose so that the time-average pressure is measured.

Throttle Position

The throttle position is a control system input as it is controlled by the engine operator. The throttle position is measured by a variable resistor or potentiometer attached to the axis of the sensor butterfly throttle valve. As the throttle rotates, the internal resistance of the sensor is changed proportional to the throttle angle change. For a spark ignition engine, the airflow rate into the intake manifold is governed by the throttle position, that is, the throttle functions as a mass airflow control valve. The airflow rate is a nonlinear function of throttle position, and for relatively small throttle angle changes, the airflow versus throttle angle relationship is linearized in control modeling.

Exhaust Gas Recirculation

Exhaust gas recirculation is used to reduce peak combustion temperatures and thus NO_x emission levels. The exhaust gas recirculation actuator is a vacuum-operated, spring-loaded diaphragm valve. The amount of EGR depends on the combustion stability limits, engine speed, and temperature. The EGR valve is normally closed. When EGR is needed, the engine control system energizes a solenoid valve to supply vacuum to the diaphragm valve. The diaphragm valve opens to allow exhaust gases to flow into the intake manifold and mix with the incoming fuel-air mixture.

Inlet Air and Coolant Temperature

The inlet air temperature and coolant temperature are measured with thermistors. The thermistors are mounted in a housing placed in the fluid stream. The coolant temperature is used to indicate engine warm-up and overheating states.

12.3 COMBUSTION ANALYSIS

A number of methods have been used to measure pressure as a function of cylinder volume for combustion analysis purposes. We will restrict our attention to piezoelectric transducers, since they are the method preferred by most engine laboratories.

The piezoelectric effect is the generation of an electric charge on a solid by a change in pressure. Consider that a crystalline solid is made up of positive and negative charges distributed over a space in a lattice structure. If the distribution of charges is nonsymmetrical, stressing the crystal will distort the lattice and displace positive charges relative to negative charges. A surface that was electrically neutral may become positive or negative. Substances such as salt (NaCl) have a symmetrical distribution of charges and therefore stresses do not lead to piezoelectricity. There are two primary piezoelectric effects: (1) the transversal effect in which charges on the x -planes of the crystal result from forces acting upon the y -plane, and (2) the longitudinal effect in which charges on the x -planes of the crystal result from forces acting upon the x -plane. In Figure 12.8(a), an example of the transversal effect, the quartz is cut as a cylinder with two 180° or three 120° sectors. The potential difference between the outer and inner curved surfaces of the cylinder is a measure of the gas pressure. In Figure 12.8(b), an example of the longitudinal effect, the quartz is cut into a number of wafers electrically connected in parallel. The potential difference is measured between the plane surfaces.

Piezoelectric transducers can be obtained with internal coolant passages and with a temperature compensator. Note that a rise in temperature will cause the housing to expand

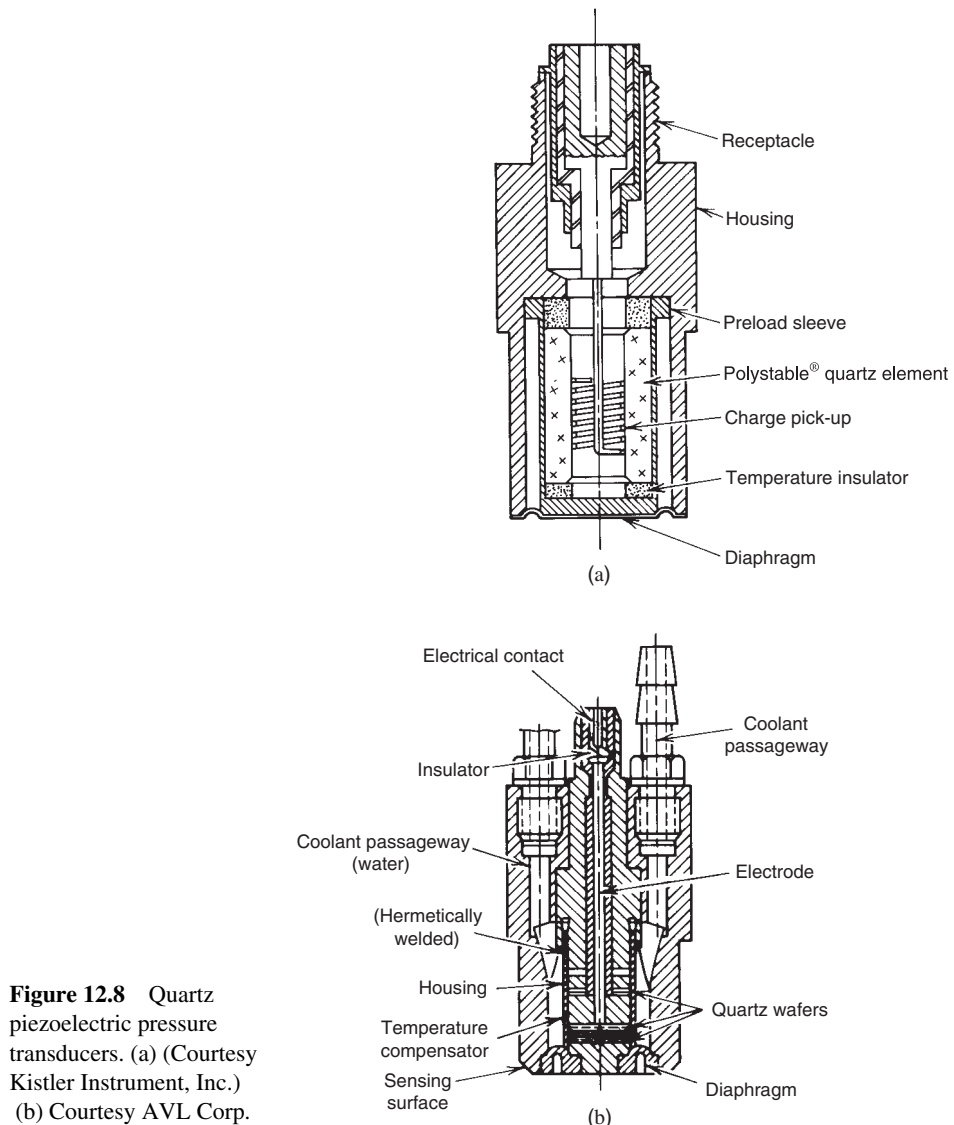


Figure 12.8 Quartz piezoelectric pressure transducers. (a) (Courtesy Kistler Instrument, Inc.) (b) Courtesy AVL Corp.

and thereby relieve the precompressed crystals from load. Piezoelectric transducers can also be obtained with flame shields to reduce flame impingement errors. Such errors are also reduced by coating the diaphragm with a silicone rubber to act as a heat shield.

Quantitative use of piezoelectric transducers is nontrivial. Care and methodical procedure is required. The reader who is using these transducers is advised to also consult classic SAE papers by Brown (1967), Lancaster et al. (1975), and Randolph (1990), as well as to follow the manufacturer's calibration procedures methodically. A typical system for measuring cylinder pressure as a function of cylinder volume is shown in Figure 12.9. A crank angle encoder is used to establish the top dead center position and the phasing of cylinder pressure to crank angle.

Computer-based combustion analysis hardware and software are used to acquire and analyze the pressure data. The hardware consists of high-speed A/D data acquisition systems

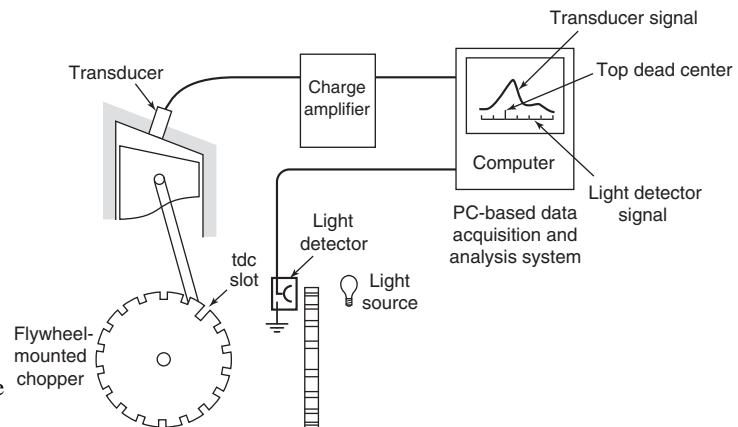


Figure 12.9
Schematic of pressure measurement system.

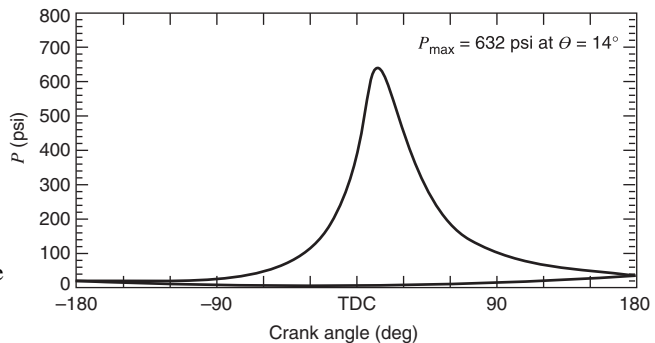


Figure 12.10 Representative cylinder pressure versus crank angle.

and dedicated digital signal processors. The software performs statistical and thermodynamic analysis of the pressure data in real time. To study the effect of cycle-to-cycle variation, the analysis can be performed on an individual cycle and also on an ensemble average of many cycles. Measurements of cylinder pressure can be used to determine not only the location of peak pressure but also the instantaneous heat release, burn fraction, and gas temperature. For additional information, the reader is referred to papers by Foster (1985) and Cheung and Haywood (1993). Representative pressure versus crank angle data are plotted in Figure 12.10. Using the known slider–crank geometry, the pressure data can be plotted as a function of cylinder volume, see Figure 12.11, and in the form $\log P$ versus $\log V$, see Figure 12.12. The nonreacting portions of the compression and expansion strokes are modeled as polytropic processes where $PV^n = \text{constant}$. The polytropic exponent n can be found from the slope of the curve on the $\log P$ versus $\log V$ plot. Note that the intake and exhaust pumping loop characteristics and the pressure sensor fluctuations are much more evident when the pressure data are plotted on logarithmic coordinates.

The instantaneous heat release, see Figure 12.13, is deduced from the cylinder pressure measurements through the use of the differential energy equation, Equation (2.34), rearranged in this chapter as Equation 12.2, where dQ_{wall} is the heat transfer to the wall.

$$\frac{dQ}{d\theta} = \frac{1}{\gamma - 1} V \frac{dP}{d\theta} + \frac{\gamma}{\gamma - 1} P \frac{dV}{d\theta} + \frac{dQ_{\text{wall}}}{d\theta} \quad (12.2)$$

The integral of the instantaneous heat release provides the burn fraction curve, shown in Figure 12.14. The average gas temperature can be computed from the measured pressure

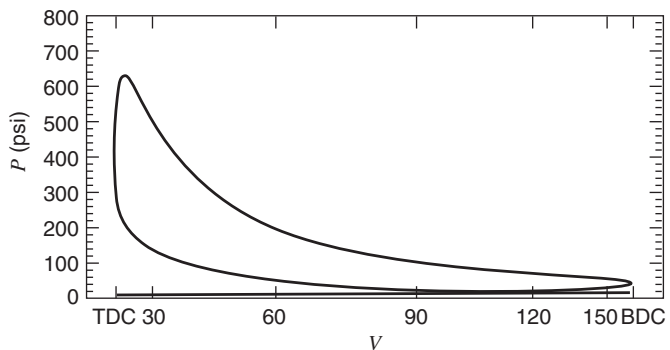


Figure 12.11 Cylinder pressure versus volume.

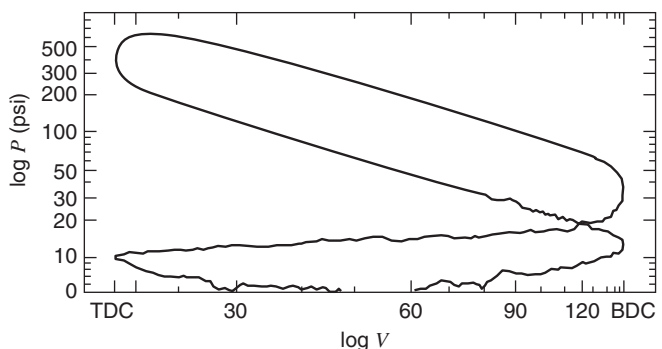


Figure 12.12 Log cylinder pressure versus log volume.

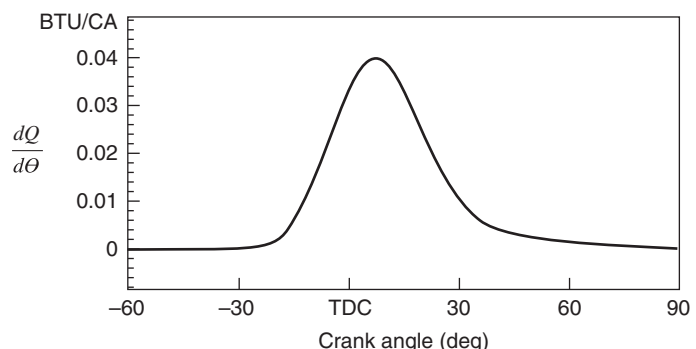


Figure 12.13 Instantaneous heat release versus log volume.

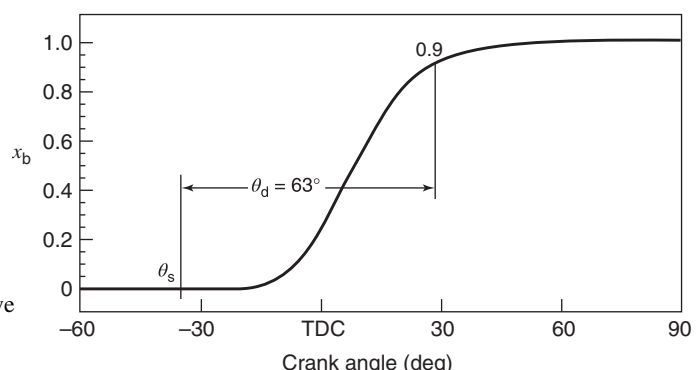


Figure 12.14 Cumulative heat release versus crank angle.

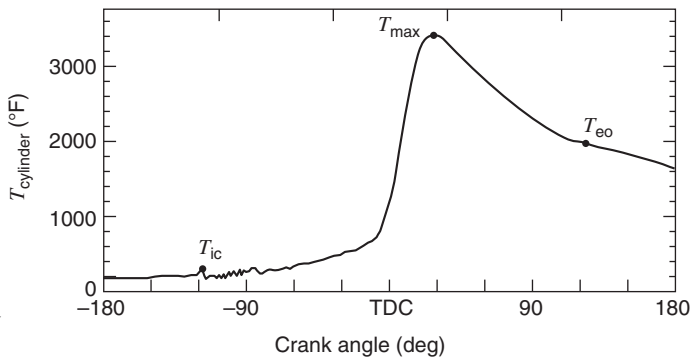


Figure 12.15 Cylinder average temperature versus crank angle.
(ic: intake valve close and eo: exhaust valve open.)

and the ideal gas equation, Equation 12.22. The temperature shown in Figure 12.15 is an average of the burned and unburned gas temperatures. The mixture mass m is evaluated from the conditions at a convenient reference, such as intake valve closing.

12.4 EXHAUST GAS ANALYSIS

Electronic instruments that are easy to use and reliable are available for several of the exhaust constituents of interest to us including carbon dioxide, carbon monoxide, hydrocarbons, oxygen, and nitrogen oxides. Many laboratories, especially those studying or testing emissions, have a set of these instruments mounted together with a suitable sample handling system. We will briefly explain how the instruments for the species mentioned operate, and then we will look at how experimental data can be used to compute a fuel-air ratio.

Carbon Dioxide and Carbon Monoxide

Nondispersive infrared analyzers (NDIR) are used for carbon dioxide and carbon monoxide. They can also be used for methane, hexane, nitric oxide, sulfur dioxide, ethylene, and water. The principle of operation of the infrared analyzer is based on the infrared absorption spectrum of gases. For the most part, gases are transparent to electromagnetic radiation. However, at certain frequencies in the infrared spectrum, the energy associated with a photon coincides with that required to change a molecule from one quantized energy level to another. At those frequencies, a gas will absorb radiation. The concentration of a given compound in a gas mixture can then be determined from the absorption characteristics. As shown in Figure 12.16, carbon dioxide absorbs at about 4.2 μm ; whereas carbon monoxide absorbs at about 4.6 μm . Thus, by using a radiation analyzer with a sensitivity as shown, one can detect carbon dioxide in a sample without interference from any carbon monoxide that may also be present.

The operation of an infrared analyzer is shown in Figure 12.17. The analyzer passes infrared radiation through two cells: one a reference cell containing a nonabsorbing background gas and the other a sample cell containing a continuous flowing sample. The detector is filled with the component gas of interest to absorb infrared radiation transmitted through the two cells. The detector will absorb less radiation on the right than on the left because of the attenuation in the sample cell causing a diaphragm to deflect in proportion to the difference in the rates of energy absorption. Since the deflection will depend on the component density in the sample stream, the amount of deflection can be sensed and displayed

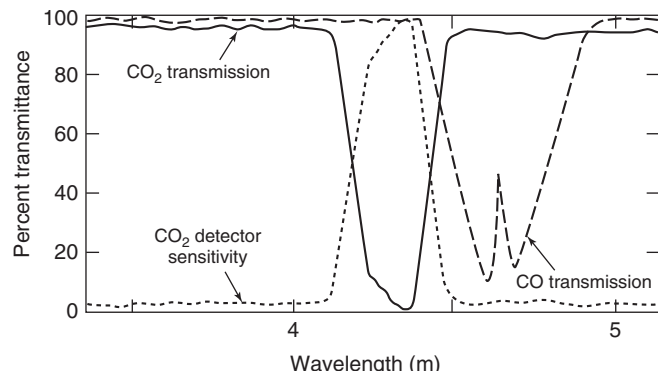


Figure 12.16 CO and CO₂ infrared transmittance spectra.

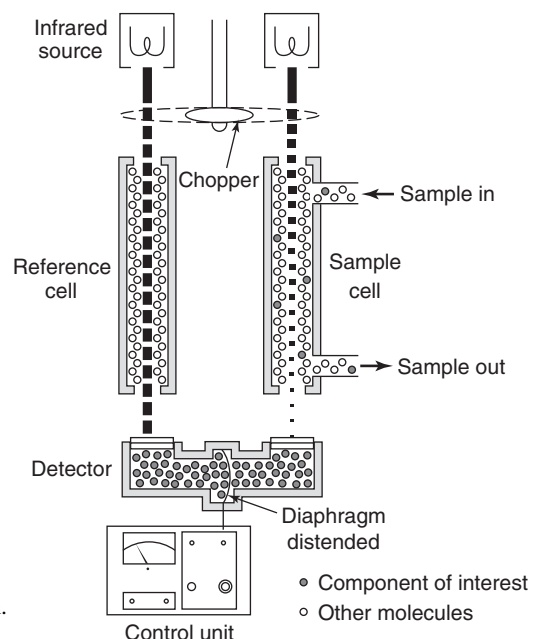


Figure 12.17 Infrared analyzer operation.
(Courtesy Beckman Instruments, Inc.)

on an electric meter calibrated to read in units of concentration. Notice that by filling the detector with the component of interest, one automatically obtains the desired sensitivity so as to eliminate interference from other components.

Hydrocarbons

Hydrocarbon detection is performed with a flame ionization detector (FID). Introduction of hydrocarbon molecules into a hydrogen–air flame produces, in a complex process, electrons and positive ions. By burning a sample of the exhaust gas in an electric field, positive ions are produced in an amount proportional to the number of carbon atoms introduced into the flame. A schematic of such a burner is shown in Figure 12.18. The sample is mixed with the hydrogen and diluent fuel and burned in a diffusion flame. The combustion products pass between electrodes producing an ion current. The hydrocarbon concentration is proportional to the ion current.

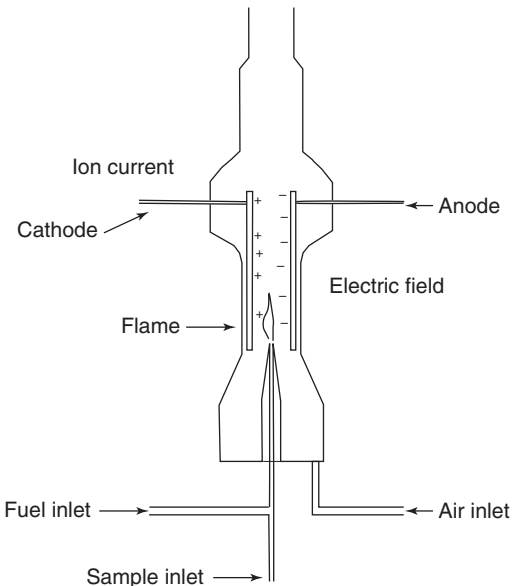


Figure 12.18 Schematic of a flame ionization detector (FID).

Table 12.1 FID Characteristic Response

Molecular structure	Approximate response
Methane	1.0
Alkanes	1.0
Aromatics	1.0
Alkenes	0.95
Alkynes	1.3
Carbonyl radical	0
Nitrile radical	0.3

The magnitude of the current depends somewhat on the molecular structure of the hydrocarbon being detected. The characteristic response of a given molecular structure normalized by the response to methane is given in Table 12.1.

According to Table 12.1, the following concentrations would all read approximately 1% on the meter:

1.00% of CH_4 , methane;
0.1% of $\text{C}_{10}\text{H}_{22}$, decane;
0.132% of C_8H_{16} , octene; and
0.385% of C_2H_2 , acetylene.

The flame ionization detector gives no information about the type of hydrocarbons in the exhaust or their average hydrogen to carbon ratio. In recognition of this latter point, it is preferred to report measurements as ppmC (particles per million carbon) rather than as ppm CH_4 or C_3H_8 or C_aH_β equivalent.

Hydrocarbon speciation is performed with a Fourier transform infrared analyzer (FTIR), a gas chromatograph, or a mass spectrometer. The FTIR operates on the same principle as the NDIR but also computes a Fourier transform of the infrared absorption

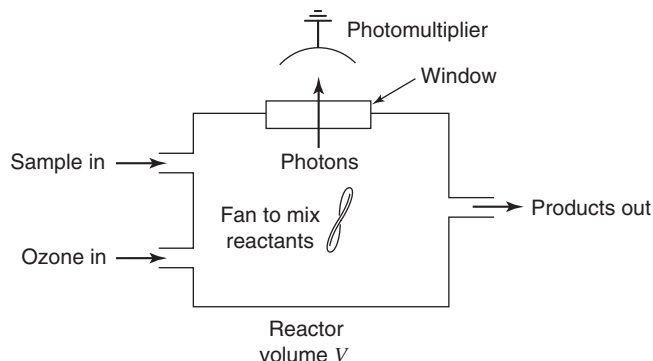


Figure 12.19 Model representation of the reactor in a chemiluminescence nitric oxide reactor.

spectrum of the gas mixture. It is useful for the detection of methanol and formaldehyde. A gas chromatograph uses a solid or solid–liquid column to separate the hydrocarbon species. The detection limits for gas chromatographs used in conjunction with a flame ionization detector are on the order of 10 parts per billion carbon (ppbC).

Nitrogen Oxides

Nitrogen oxides (NO_x) are measured with a chemiluminescence detector (CLD). Chemiluminescence is the process of photon emission during a chemical reaction. When nitric oxide (NO) reacts with ozone (O_3), chemiluminescence from an intermediate product nitric dioxide (NO_2) occurs during the reaction. The amount of nitric oxide present is proportional to the number of photons produced.

A chemiluminescence reactor model is shown in Figure 12.19. The exhaust gas sample is first passed through a catalyst to convert nitric dioxide (NO_2) to nitric oxide (NO) prior to delivery to the reactor. The reactor has an exhaust gas sample port, an ozone inlet port, and an outlet port. The photons produced are measured with a photomultiplier. An optical filter is used to filter out photons from non- NO_2 chemiluminescence reactions that produce photons outside the wavelength band between 0.60 and 0.66 μm .

To simplify the reaction analysis, the reactor is assumed to be perfectly stirred, so the concentration of reactants is uniform throughout the reactor. The chemical reactions involved in this process are



The asterisk in the above equations denotes NO_2 in an electronically excited state and M is a symbol chemists use to denote any molecule in the system. The nitric oxide (NO) reacts with ozone O_3 to produce electronically excited nitric dioxide NO_2^* . The excited nitric oxides can be deactivated by emission of a photon or by collision with any other molecule.

The conservation equation for excited nitric dioxide is

$$\frac{d}{dt}[\text{NO}_2^*] = k_1[\text{NO}][\text{O}_3] - k_2[\text{NO}_2^*] - k_3[\text{NO}_2^*][\text{M}] - \dot{V}_f[\text{NO}_2^*] = 0 \quad (12.6)$$

Equation 12.6 indicates that the rate at which excited nitric dioxide NO_2^* is produced by reaction with ozone in the reactor is balanced by the reduction rates due to photon emission, molecular collision, and the rate at which it flows out of the reactor. The braces in the conservation equation denote the concentrations in units of mol/m³ and \dot{V}_f is the volumetric flow rate of products leaving the reactor. The k 's are the rate coefficients for the three reactions, Equations 12.3–12.5. When the system is in steady state, the rate of change of concentration of any species in the reactor is zero. The steady-state concentration of NO_2^* is therefore

$$[\text{NO}_2^*] = \frac{k_1[\text{NO}][\text{O}_3]}{k_2 + k_3[\text{M}] + \dot{V}_f} \quad (12.7)$$

At steady state, the rate at which photons leave the system is equal to the rate at which they are produced in reaction 12.4. Therefore, the photon intensity, I , measured by the photomultiplier is

$$I = k_2[\text{NO}_2^*] = \frac{k_2 k_1[\text{NO}][\text{O}_3]}{k_2 + k_3[\text{M}] + \dot{V}_f} \quad (12.8)$$

The rate of change of concentration of nitric oxide is assumed to be zero, so

$$\frac{d}{dt}[\text{NO}] = k_1[\text{NO}][\text{O}_3] - \dot{V}_f[\text{NO}]_{\text{sample}} = 0 \quad (12.9)$$

Upon substitution of Equation 12.9 into Equation 12.8, the photon intensity is

$$I = \frac{k_2 \dot{V}_f [\text{NO}]_{\text{sample}}}{k_2 + k_3[\text{M}] + \dot{V}_f} \quad (12.10)$$

If the reactor is operated such that the ozone flow rate is large compared with the sample flow rate, then

$$\begin{aligned} \dot{V}_f &= \dot{V}_{f,\text{O}_3} \\ [\text{M}] &= [\text{O}_3] = P/RT \end{aligned} \quad (12.11)$$

Fixing the reactor temperature fixes the chemical rate constants k_1 , k_2 , and k_3 , and fixing the pressure fixes the ozone concentration. Therefore, as indicated by Equation 12.10, for a given volumetric flow rate of ozone and exhaust gas sample, the photon intensity is proportional to the concentration of nitric oxide in the entering sample stream.

Exhaust Gas Oxygen Concentration

The exhaust gas oxygen concentration is measured with an oxygen sensor. The oxygen sensor is used to control the air-fuel ratio, since the operation of a three-way catalyst requires that the air-fuel ratio be maintained within about 1% of stoichiometric. The sensor is constructed out of a thimble-shaped solid zirconium oxide (ZrO_3) electrolyte stabilized with yttrium oxide (Y_2O_3). The development of the zirconia sensor is detailed in Hamann et al. (1977). The interior and exterior surfaces of the electrolyte are coated with porous platinum to form interior and exterior electrodes. Electrochemical reactions on the electrodes produce negatively charged oxygen ions that then produce a voltage across the electrolyte. The voltage V produced depends on the oxygen ion flow rate that in turn is proportional to the oxygen partial pressure at the electrodes, as indicated by Equation 12.12. The symbol F is the Faraday constant equal to $9.649 \times 10^7 \text{ C/kmol}$. The

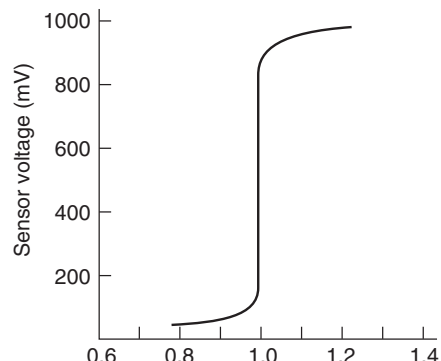


Figure 12.20 Oxygen sensor voltage versus equivalence ratio.

oxygen partial pressure for a lean $\phi = 0.82$ mixture is about 0.04 bar.

$$V = \frac{RT}{4F} \ln \left(\frac{P_{O_2\text{atm}}}{P_{O_2\text{exhaust}}} \right) \quad (12.12)$$

The voltage output is highly nonlinear at stoichiometric conditions, with a large change in the voltage between rich and lean conditions. If the exhaust mixture is rich, with a lack of O₂, oxygen ions will flow from the air-side electrode across the electrolyte to the exhaust side. If the mixture is lean, with excess oxygen, oxygen ions also form at the exhaust gas electrode, and the migration of oxygen ions across the electrode drops. For rich conditions, a voltage of about 800 mV is formed and for lean conditions about 50 mV is produced, as indicated in Figure 12.20. A control set point voltage of about 0.5 V is used to maintain stoichiometric conditions. If the sensor voltage is below the set point voltage, the exhaust is considered by the control system to be lean, and vice versa. The behavior of the oxygen sensor is temperature dependent, as the electrolyte needs to be above 280°C for proper operation. A heating electrode is sometimes embedded in the sensor to rapidly bring it up to operating temperature.

Particulates

There are a number of techniques used to characterize and measure particulate emissions. These include light absorption, filter discoloration, and measurement of the total mass of particulates trapped on a filter paper. The exhaust particle size distribution can be measured using aerosol instruments such as the scanning mobility particle sizer (Wang and Flagan, 1990).

The absorption-type smoke meter uses the principle of light absorption by particles. A pump is used to draw undiluted exhaust gas into a measuring chamber that has a light source at one end and a photodiode at the opposite end. The attenuation of the beam of light by the exhaust is proportional to the particle concentration. The filter-type smoke meter draws a metered amount of exhaust gases through a filter paper. The blackening of the filter paper is compared against a “Bacharach grey scale.”

Standards, such as SAE J 1280, that employ direct mass measurement also specify the use of a dilution tunnel in order to simulate the exhaust conditions near a vehicle. The particulates leaving the exhaust pipe are at a relatively high-temperature and concentration in the outlet exhaust flow. These gases cool during the mixing process with the atmosphere, and the associated condensation and agglomeration processes will change the structure and

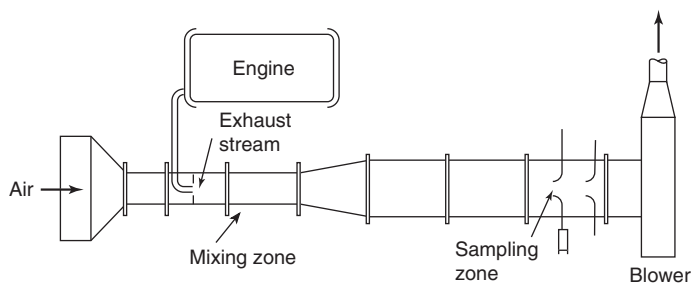


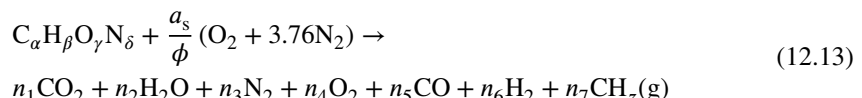
Figure 12.21 Exhaust gas dilution tunnel.

density of the particulates in the exhaust gases. Dilution tunnels are used to standardize this near-field ($< 3\text{ m}$) mixing process. A dilution tunnel is shown in Figure 12.21. The tunnel is about 0.3 m in diameter. By flowing dilution air at a constant speed, typically 10 m/s , through a converging–diverging nozzle, the Venturi effect can be used to remove exhaust gas from the exhaust pipe. Minidilution tunnels with a 25-mm diameter have also been developed. Downstream of the nozzle, the exhaust is well mixed with the dilution air. The diluted exhaust gas is sampled and drawn through Teflon-coated glass fiber paper filters.

The total particulate mass is trapped by the filter found by the increase in weight of the sample filter. In order to compute the dilution ratio, which is defined as the ratio of dilute mixture flow rate to exhaust gas flow rate, the carbon dioxide concentration is measured in both the engine exhaust and the diluted sample. The dilution ratio is typically about $10 : 1$.

Fuel–Air Equivalence Ratio

To solve for the fuel–air equivalence ratio from exhaust gas analysis, let us write the combustion reaction as



where the subscript z is defined as

$$z = \beta/\alpha \quad (12.14)$$

In Equation 12.13, $\text{CH}_z(\text{g})$ represents the gaseous hydrocarbons that a flame ionization detector records. The parameter z is the average hydrogen to carbon ratio of the hydrocarbons and is unknown. In engines that function properly, the exhaust gas contains negligible hydrocarbons, as far as atom balancing is concerned. They are included in the analysis because they are important in engines that misfire. A carbon and oxygen balance on this equation leads to Equation 12.15 for the equivalence ratio:

$$\phi = \frac{2(1 + (1/4)\beta/\alpha - (1/2)\gamma/\alpha)(y_1 + y_5 + y_7)}{2y_1 + y_2 + 2y_4 + y_5} \quad (12.15)$$

Notice that if we had an instrument to measure the mole fraction of water (y_2) in the exhaust gas (generally we do not), then the equivalence ratio could be determined with no further analysis or approximations. A complication arises in that most emission instruments do not function if water condenses in them. A common way to handle this is to condense the water from the sample prior to delivery to the instruments. With no water vapor in the sample, we then say the concentration is ‘‘dry,’’ as opposed to ‘‘wet.’’ The dry concentration depends

on the amount of water condensed out. Denoting a dry concentration with a superscript zero, we can relate the dry concentration of any species i to the wet concentration by

$$y_i^0 = \frac{y_i}{1 - y_2} \quad (12.16)$$

Of course there is no physical significance to “dry water” ($i = 2$). It is mathematically convenient, however, to speak of dry water defined by Equation 12.16. In terms of dry concentrations, the equivalence ratio is

$$\phi = \frac{2(1 + (1/4)(\beta/\alpha) - (1/2)(\gamma/\alpha))(y_1^0 + y_5^0 + y_7^0)}{2y_1^0 + y_2^0 + 2y_4^0 + y_5^0} \quad (12.17)$$

There is no change in the function since the wet water term $(1 - y_2)$ factors out. The water concentration is found from a hydrogen atom balance. However, that does not solve the problem completely because it introduces two new unknowns: y_6 , the hydrogen concentration; and z , the hydrogen to carbon ratio of the exhaust hydrocarbons, Equation 12.15.

Spindt (1965) has found by experiments that it is satisfactory to assume

$$\frac{y_2 y_5}{y_1 y_6} = 3.5 \quad (12.18)$$

Substitution of these relationships into the hydrogen balance gives, after much manipulation

$$y_2^0 = \frac{(1/2)(\beta/\alpha)(y_1^0 + y_5^0)}{1 + (y_5^0/3.5 y_1^0)} \quad (12.19)$$

In experiments, the measured fuel–air ratios and those determined from exhaust gas analysis agree to within $\pm 2\%$. For greater accuracy, Lynch et al. (1997) recommend that the NO concentration be measured and also included in the analysis.

Residual Fraction

The residual fraction can be determined directly by use of a sampling valve to withdraw gases from the compression stroke for analysis with the same instruments already described. The mole fraction of carbon dioxide in those gases is

$$y_{\text{CO}_2} = y_r y''_{\text{CO}_2} \quad (12.20)$$

where y_r is the residual mole fraction and y''_{CO_2} is the carbon dioxide mole fraction in the exhaust gases. The residual mass fraction is, by Equation 12.20,

$$f = \left[1 + \frac{m'}{m''} \left(\frac{y''_{\text{CO}_2}}{y_{\text{CO}_2}} - 1 \right) \right]^{-1} \quad (12.21)$$

The molecular weights of the residual gas M'' and fuel–air mixture M' are known if the mole fractions of their constituent gases are known.

A typical sampling valve is shown in Figure 12.22. The seat (2) has threads that are screwed into a receiving hole that provides access to the combustion chamber. In this application, the valve is mounted in the cylinder head, and when it is opened, gases in the cylinder are withdrawn. The poppet valve (1) is opened by a trigger signal corresponding to a given crank angle and is open for 1–2 ms. It is electromagnetically opened by passing 2–5 A of current through a coil (19). A spring (10) closes the valve when the current stops.

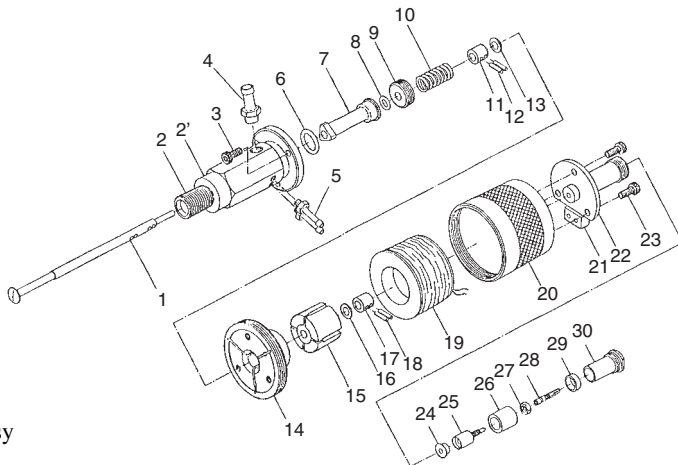


Figure 12.22 Typical sampling valve. (Courtesy Tsukasa Sokkler, Ltd.)

A capacitance type of valve motion detector (24 and 25) is incorporated into the valve, and the sampled gases flow out the port (4). By opening the valve at the same angle in successive cycles, it is possible to have a steady flow of gas for delivery to the exhaust gas analyzers.

It is also possible, though certainly more difficult, to determine the residual fraction by measuring the temperature at some angle during the compression stroke and applying the equation of state.

$$PV = mRT \quad (12.22)$$

For further information about engine testing and measurement, the reader is referred to Plint and Martyr (2012).

12.5 CONTROL SYSTEMS IN ENGINES

The control systems in internal combustion engines operate using sensors, microprocessors, and actuators. The sensors measure temperatures, pressures, flow rates, and concentrations at various locations throughout the engine. The sensor information is provided to the engine control microprocessors to characterize the instantaneous state of the engine. The control systems are quite complex, as they interact with each other, are nonlinear, and need to have robust operation over a wide range of transient speed and load conditions.

The parameters that characterize the engine state include, at a minimum, the engine speed, throttle position, crank angle, intake airflow rate, intake manifold and ambient pressure, inlet air and coolant temperature, exhaust gas oxygen concentration, and onset of knock. The engine components that need to be controlled include not only the fuel injectors or carburetor but also the spark plugs, the exhaust gas recirculation valve, the turbocharger waste gate or variable area nozzle, and for a vehicle, the transmission. An example engine control system diagram is presented in Figure 12.23.

There are two types of control systems used on engines: memory-based systems and adaptive systems. Memory systems store the optimum values of control variables such as spark timing and fuel injector pulse width for a range of engine operating conditions in a table or map. The optimum values include both efficiency and emissions considerations. For a given engine load (that is, manifold air pressure) and engine speed, the engine control

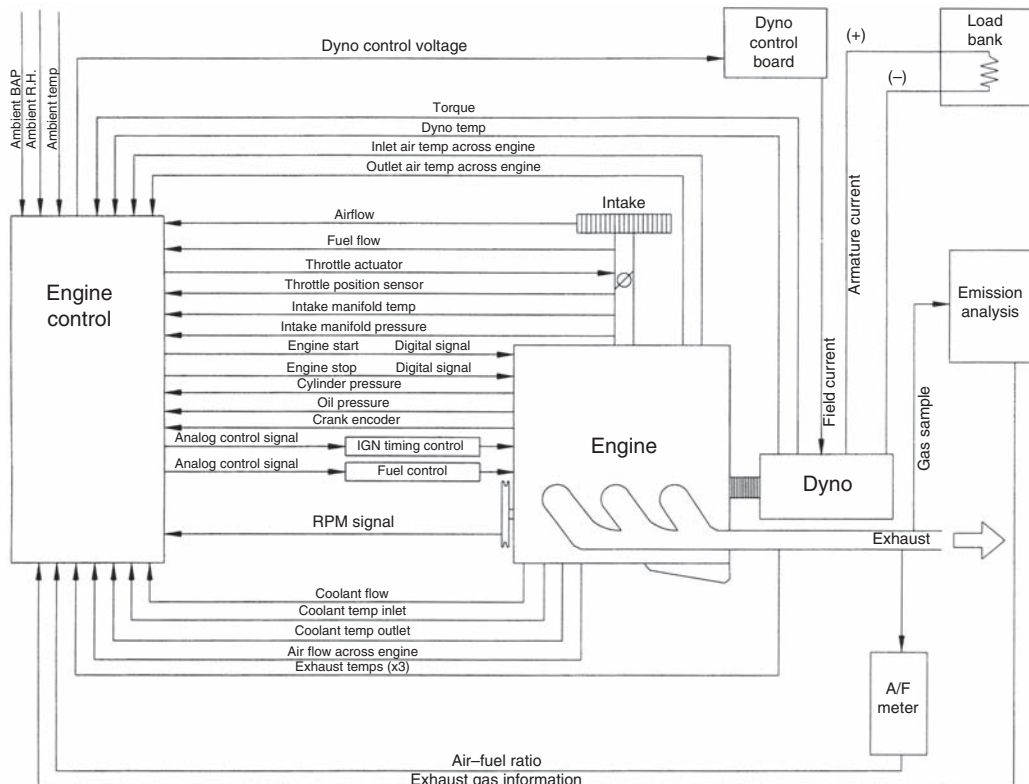


Figure 12.23 Example diagram of engine control system. Adapted from Kirkpatrick and Willson (1998).

computer will ‘‘look up’’ the optimum timing and then change the spark timing to that optimum value. In feed-forward operation, the spark advance is computed from a spark advance map as a function of engine speed and load. The spark advance map is determined from engine calibration testing. Memory-based control systems have the disadvantage of not accounting for part-to-part variation in engine components, the effect of deposits, and fuel property changes. Also, the optima determined from mapping measurements on a test engine are not exactly the same from engine to engine.

The engine control systems operate with both open- and closed-loop feedback control. Some of the critical sensors, such as the oxygen sensor, operate properly only when an engine has warmed up. When an engine is cold, it operates on an open-loop control without input from the oxygen sensor. When the engine has warmed up, it switches to closed-loop feedback control and uses the oxygen sensor data to compute the required fuel flow rate. If the oxygen sensor indicates a rich mixture ($\phi > 1$), the pulse width of the fuel injector actuator signal is reduced to decrease the equivalence ratio. After a time lag, primarily the time required for the leaner fuel–air mixture to flow from the injector to the oxygen sensor located in the exhaust system, the oxygen sensor will indicate a lean mixture ($\phi < 1$). In response, the controller will increase the injection pulse width to enrich the mixture. With this type of closed-loop control, known as a limit cycle, the air–fuel mixture continually oscillates about stoichiometric conditions, with a time average value of $\phi < 1$.

Adaptive systems determine an operating point from real-time measurement of engine variables and subsequent correction of the look-up tables. The subsystems that have used

adaptive control are the exhaust gas recirculation, evaporative emissions, idle air control, and air-fuel ratio control. Various calibrations need to be periodically reset due to wear, aging, and replacement of components, such as fuel injectors or sensors.

Subsystems that alternate between open- and closed-loop control, such as the air-fuel ratio, will perform periodic adaptive corrections. If a system is in closed-loop control, it can compare the closed-loop values with the open-loop values. If there is a significant change, the open-loop table values are corrected. The corrections to the look-up tables are also obtained by driving the vehicle through specified driving cycles, typically stop-and-go traffic with intermittent idle periods. During the driving cycle, the control system applies very small perturbations to the parameters, such as the ignition timing, and measures the response in other parameters, such as the fuel flow. Optimum values are then stored in the various tables such as the ignition-timing table.

The U.S. Environmental Protection Agency has mandated the use of on-board diagnostics (OBD) on passenger cars and light- and heavy-duty trucks built after 1994. These regulations are designed to detect emissions-related malfunctions. The diagnostic system uses various methods to communicate diagnostic information to operators. If a fault is detected, such as a faulty sensor, a fault code corresponding to the fault is stored. One type of diagnostic system flashes the “check engine” light using a variation of the Morse code signaling system. Alternatively, a computer or some similar type of digital analysis tool can be connected to the communications port of the diagnostic system.

If a sensor fails, the engine control system is able to maintain engine operation. It substitutes a fixed value for the sensor input, sends out a fault code, and continues to monitor the incorrect sensor input. If the sensor returns to normal limits, the engine control system will then return to processing the sensor data.

Some automotive engine control systems disable a number of fuel injectors if a cylinder head sensor indicates that the engine is overheating, perhaps from a loss of coolant. Varying and alternating the number of disabled fuel injectors controls the engine temperature. When a fuel injector is disabled, its cylinder works as a convective heat exchanger since airflow into and out of the cylinder continues to take place, and no combustion is occurring in the cylinder. One consequence of this strategy is that the engine will produce proportionally less power with disabled fuel injectors. Fuel injector disabling is also used if an engine or vehicle over-speed condition is detected. Once the speed is reduced, the engine returns to normal operating mode.

The onset of knock is detected by a knock detector. The methods used to detect knock include piezoelectric and magnetostrictive techniques. If a knock signal is sent to the engine control unit, the timing will be retarded, and then the throttle will be closed until the knock ceases. The delay in ignition will reduce the torque produced by the engine.

The sensor information stored by the engine control unit can also be sent via telemetry or wireless Internet to a host computer. Racing teams use this technique to debug and fine-tune high-performance race cars. Many rental car and trucking firms are tracking the operation of their vehicles in this manner. In the near future, wireless communication technologies will be used by engine and vehicle manufacturers not only for routine engine diagnostics but also to collect information about long-term engine performance and reliability.

Recent developments in control systems are the development of parametric engine performance models, two examples of which are mean value models and discrete-time models. The mean value engine model (MVE) is physics based, and is an intermediate level engine model that has been used in applications where overall engine parameters such as engine efficiency, emissions, airflow rate, air-fuel ratio, maximum cylinder pressure, and exhaust pressure are of primary interest, as opposed to crank angle resolved behavior. The MVE models are highly compatible with model-based engine control systems, as

they predict the cycle-averaged engine behavior. Calibration and validation of MVEMs is accomplished both by comparison to more complex engine models and engine test data.

A classic paper outlining engine control systems is by Cook and Powell (1988). For further information about recent developments in engine control systems, the reader is referred to books by Guzzella and Onder (2010), and by Ulsoy et al. (2012).

12.6 VEHICLE EMISSIONS TESTING

For emissions testing of engines in vehicles, a chassis dynamometer is used. The chassis dynamometer is used to put vehicles through a driving cycle, with the advantage of not having to instrument a moving vehicle. Chassis dynamometers were first developed for locomotives and more recently for road vehicles. The U.S. Environmental Protection Agency requires chassis dynamometer testing of many classes of vehicular engines for emissions purposes. The word ‘‘homologation’’ is used to describe this certification process.

The chassis dynamometer is composed of a series of rollers, flywheels, and dynamometers. The vehicle to be tested is driven onto the top of the chassis dynamometer and its drive tires rotate between two rollers that are mechanically connected to flywheels and electric dynamometers. The rolling inertia of the vehicle is simulated with rotating flywheels and electronic inertia. A cooling fan is used to produce adequate airflow to prevent the engine from overheating.

The United States, the European Community, and Japan have developed their own driving cycles that simulate a variety of driving conditions for various classes of vehicles. Two United States driving schedules are shown in Figure 12.24. The United States driving cycle for passenger cars and light-duty trucks is the Federal Test Procedure (FTP). The test

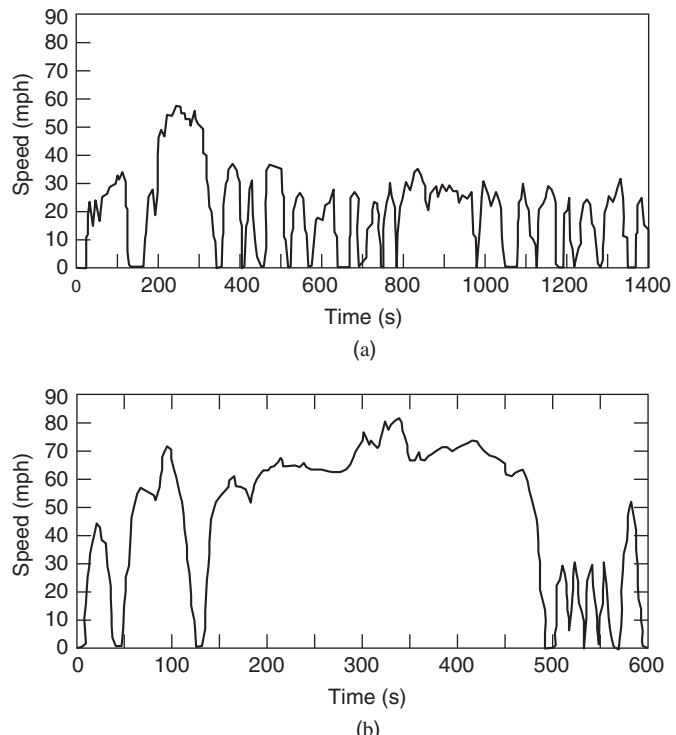


Figure 12.24 (a) Federal Test Procedure LA4 driving schedule. (b) US06 driving schedule.

procedure for heavy-duty (gross vehicle weight > 8500 lbs.) highway engines is the EPA transient test procedure and the EPA smoke test procedure.

12.7 REFERENCES

- BROWN, W. L. (1967), "Methods for Evaluating Requirements and Errors in Cylinder Pressure Measurement," SAE paper 670008.
- CHEUNG, H. and J. HEYWOOD (1993), "Evaluation of a One-Zone Burn Rate Analysis Procedure Using Production SI Engine Pressure Data," SAE paper 932749.
- COOK, J. and B. POWELL (1988), "Modeling of an Internal Combustion Engine for Control Analysis," *IEEE Control Syst. Mag.*, August, pp. 20–26.
- FOSTER, D. (1985), "An Overview of Zero-Dimensional Thermodynamic Models for IC Engine Data Analysis," SAE Technical Paper 852070.
- GUZZELLA, L. and C. ONDER (2010), *Introduction to Modeling and Control of Internal Combustion Engine Systems*, Springer-Verlag, Berlin.
- HAMANN, E., H. MANGER, and L. STEINKE (1977), "Lambda-sensor with Y_2O_3 -Stabilized ZrO_2 -Ceramic for Application in Automotive Emission Control Systems," SAE paper 770401.
- KASTNER, L. J. (1947), "An Investigation of the Airbox Method of Measuring the Air Consumption of Internal Combustion Engines," *Proc. Inst. Mech. Eng.*, Vol. 157, pp. 387–404.
- KIRKPATRICK, A. and B. WILLSON (1998), "Computation and Experimentation on the Web with Application to Internal Combustion Engines," *ASSE J. Eng. Educ.*, Vol. 87, No. 5, pp. 529–537.
- LANCASTER, D. R., R. B. KRIEGER, and J. H. LIENESCH (1975), "Measurement and Analysis of Engine Pressure Data," SAE paper 750026.
- LYNCH, D. and W. SMITH (1997), "Comparison of AFR Calculation Methods Using Gas Analysis and Mass Flow Measurement," SAE paper 971013.
- PLINT, M. and A. MARTYR (2012), *Engine Testing: Theory and Practice*, 4th Edition, Elsevier, Ltd., Oxford.
- RANDOLPH, A. (1990), "Methods of Processing Cylinder-Pressure Transducer Signals to Maximize Data Accuracy," SAE paper 900170.
- SPINDT, R. S. (1965), "Air–Fuel Ratios from Exhaust Gas Analysis," SAE paper 650507.
- STONE, C. R. (1989), "Airflow Measurement in Internal Combustion Engines," SAE paper 890242.
- WANG, S. and R. FLAGAN (1990), "Scanning Electrical Mobility Spectrometer," *Aerosol Sci. Tech.*, Vol. 13, pp. 257–261.
- ULSOY, A., H. PENG, and M. CAKMAKCI (2012), *Automotive Control Systems*, Cambridge University Press, New York.

12.8 HOMEWORK

- 12.1** Measurements of the exhaust gases of a hydrogen-fueled engine indicate a composition of 71.0% N_2 , 25.0% O_2 , and 3.9% H_2O . At what equivalence ratio was the engine operated?
- 12.2** The exhaust composition of a test engine is as follows:

$$\begin{array}{ll}
 \text{CO}_2 = 11.5\% & \text{NO} = 310 \text{ ppm} \\
 \text{H}_2\text{O} = 7.11\% & \text{NO}_2 = 20 \text{ ppm} \\
 \text{N}_2 = 77.99\% & \text{CH}_4 = 350 \text{ ppm} \\
 \text{O}_2 = 3.19\% & \text{C}_3\text{H}_8 = 225 \text{ ppm} \\
 \text{CO} = 0.06\% & \text{C}_7\text{H}_{17} = 475 \text{ ppm} \\
 \text{H}_2 = 0.01\% &
 \end{array}$$

Find the following:

- (a) Wet concentration in ppm of HC and NO_x as would be indicated by heated flame ionization and chemiluminescence detectors, respectively. (Assume the FID responds to all carbon atoms equally.)
 - (b) Dry concentrations of CO_2 , O_2 in percent, and CO in ppm.
 - (c) Fuel-air equivalence ratio if the hydrogen to carbon ratio of the fuel is 1.3.
- 12.3** Explain how Equation 12.22 could be used to measure the residual fraction.
- 12.4** A diesel engine operated on $\text{C}_{14}\text{H}_{27}$ produced exhaust gas of the following dry composition:

$$\begin{array}{ll} \text{CO}_2 = 6.22\% & \text{N}_2 = 81.51\% \\ \text{O}_2 = 12.20\% & \text{NO}_x = 400 \text{ ppm} \\ \text{CO} = 0.024\% & \text{HC} = 200 \text{ ppm C} \end{array}$$

- (a) Explain how the method of hydrocarbon measurement can yield a situation wherein the sum of the exhaust constituents adds up to slightly greater than 100%.
 - (b) At what equivalence ratio was the engine operated? How would the answer differ if one neglected the carbon monoxide and hydrocarbons?
- 12.5** An isoctane-fueled engine has a measured fuel mass flow rate of 0.5 g/s and air mass flow rate of 7.0 g/s. The exhaust gas composition (dry) is measured to be $\text{CO}_2 = 11\%$ and $\text{CO} = 3.0\%$. Compare the equivalence ratio computed from the exhaust gas composition with that from the fuel-airflow rate ratio. Assume an equilibrium exhaust composition to estimate the exhaust H_2 concentration.
- 12.6** A test engine operates on methane at a mass flow rate of 2.0 g/s with an equivalence ratio $\phi = 0.8$. (a) What is the inlet air mass flow rate? (b) If the exhaust is at standard conditions, what are the volumetric flow rates of the exhaust products N_2 , H_2O , CO_2 , and O_2 ?
- 12.7** Manufacturers of laminar airflow meters typically provide a calibration curve of the following form:
- $$\dot{V}_{\text{stp}} = c_1 \Delta P + c_2 \Delta P^2$$
- where \dot{V}_{stp} is the volumetric flow rate at standard temperature (298.15 K), and pressure (1 bar), and ΔP is the pressure drop across the meter.
- (a) Use dimensional analysis to show how the constants c_1 and c_2 would change for measurements made at conditions other than standard temperature and pressure.
 - (b) How can one determine the mass flow rate rather than the volumetric flow rate?
- 12.8** Assuming one-dimensional, isentropic steady flow of an ideal gas with constant specific heats, derive an expression for the constant C of the critical flow nozzle in Figure 12.6. The calibration constant depends on the nozzle throat area A , the gas constant R , and the ratio of specific heats γ . You may assume the upstream area is large enough that measured P_1 and T_1 are stagnation properties.
- 12.9** Figure 12.12 is a plot of $\log P$ versus $\log V$. Estimate the polytropic exponents in the expression $PV^n = \text{constant}$ in the middle of both the expansion and compression strokes. How do these exponents relate to the specific heat ratio?

Chapter 13

Overall Engine Performance

13.1 INTRODUCTION

In this chapter, we take an overall view of the performance of internal combustion engines. We use the information about friction, heat transfer, and combustion presented in the previous chapters to explain and discuss the influence of various factors, such as engine and piston speed, load, compression ratio, and ignition timing. Performance maps for various representative spark ignition and compression ignition engines are introduced. The frictional and aerodynamic drag components of road load are also discussed for application to vehicle performance simulation.

13.2 EFFECT OF ENGINE AND PISTON SPEED

The effects of engine speed on the power and coolant load of an automotive spark ignition engine at full load, that is, wide open throttle, are shown in Figure 13.1. The graphs in Figure 13.1 plot the performance of an unthrottled 4.7 L V-8 spark ignition engine with a bore $b = 95.2$ mm and stroke $s = 86$ mm at three different compression ratios, $r = 8, 10,$ and 12 . Note that the indicated specific fuel consumption decreases with increasing engine speed and then levels out. This is mainly because the percentage heat loss to the coolant is decreasing with increasing engine speed. On the other hand, the brake specific fuel consumption (bsfc) is fairly flat or decreasing at low speeds and is increasing at higher speeds. At higher speeds, the friction and pumping losses become more significant, as they increase quadratically with engine speed.

The power curves in Figure 13.1 are conveniently explained in terms of the expression relating the power \dot{W}_b of an engine to the volumetric efficiency e_v , the net indicated thermal efficiency η_i , and the mechanical efficiency η_{mech} . The relationship (four stroke) is given in Equation 13.1:

$$\begin{aligned}\dot{W}_b &= \eta_{\text{mech}} \dot{W}_i \\ &= \eta_{\text{mech}} \eta_i a_0 \frac{\text{FA}}{1 + \text{FA}} e_v \rho_i V_d N / 2\end{aligned}\tag{13.1}$$

where, as before, FA is the fuel–air ratio, a_0 is the maximum available energy of combustion, and ρ_i is the mixture density in the intake manifold.

Figure 13.1 also gives the indicated power as a function of engine speed. Since the engine is unthrottled, we can assume for qualitative purposes that the curve is the net indicated power versus engine speed. All the terms multiplying the mechanical efficiency

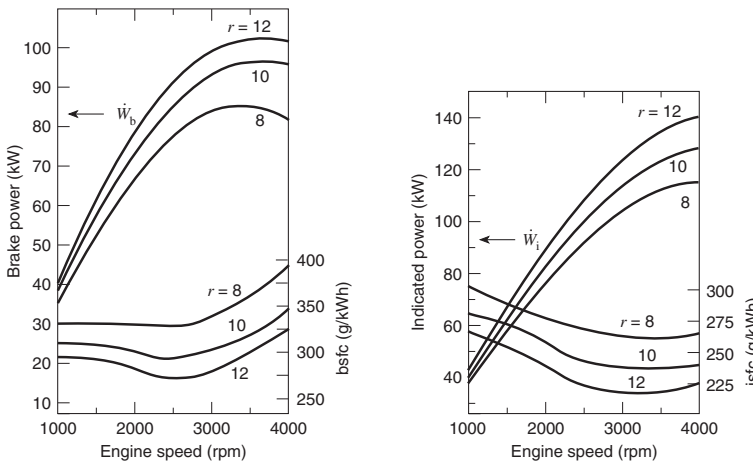


Figure 13.1 Performance of a V-8 spark ignition engine at three different compression ratios.
(Adapted from Roensch, 1949.)

in Equation 13.1 constitute the net indicated power. If the indicated torque were constant, then the indicated power would increase linearly with engine speed.

Torque as a function of engine speed usually reflects the variation in volumetric efficiency with engine speed. A falling off in volumetric efficiency at the higher speeds causes the falling off of the indicated power at high engine speeds. Recall that the speed at which the volumetric efficiency peaks is dependent upon the valve timing. The indicated power is not decreasing as fast as it would if the volumetric efficiency were the only parameter changing with speed. The indicated efficiency is increasing slightly with speed.

The brake power is the product of the net indicated power and the mechanical efficiency. Friction power increases with the square of engine speed, since the friction torque (proportional to brake mean effective pressure (bmep)) increases linearly with engine speed. The mechanical efficiency therefore decreases linearly with engine speed, causing the brake power to exhibit a maximum even though the indicated power is still increasing.

It was stated earlier that these generalizations are expected to apply to all engines. That statement needs qualification in the case of two-stroke engines, especially carbureted ones. Recall that in two-stroke engines, there is a significant difference between the delivered mass and the trapped mass, because of short-circuiting. Any fuel that is short-circuited is wasted and represents a loss not discussed in the context of Figure 13.1, since this effect is usually negligible in four-stroke engines. As the trapping efficiency generally increases with engine speed, the amount of fuel short-circuited will decrease with engine speed.

13.3 EFFECT OF AIR–FUEL RATIO AND LOAD

The effect of the air–fuel ratio on brake specific fuel consumption of a spark ignition engine at a constant load is shown in Figure 13.2 for three different compression ratios, ($r = 8, 9$, and 11). Figure 13.2 indicates that the spark ignition engine is most efficient when running stoichiometrically or slightly lean. At very lean fuel–air ratios, the engine wastes fuel because of misfire, and at rich fuel–air ratios it wastes fuel since there is not enough oxygen present to liberate all of the fuels energy.

The effect of fuel–air ratio on the brake specific fuel consumption and exhaust emissions of a number of indirect-injection (IDI) and direct-injection (DI) compression ignition

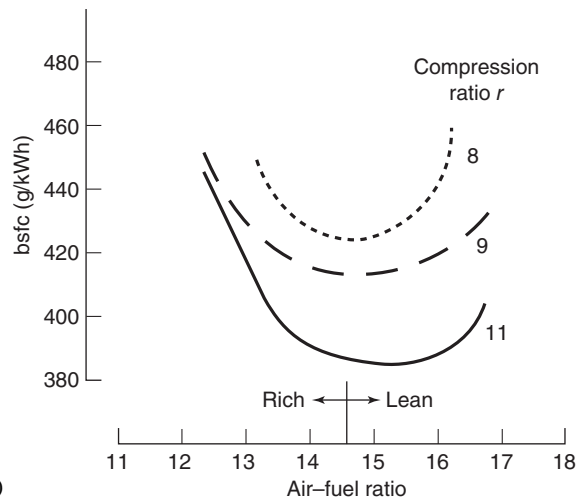


Figure 13.2 Brake specific fuel consumption of a single cylinder research engine versus air-fuel ratio. (Adapted from French, 1983.)

engines is plotted in Figure 13.3. Since the stoichiometric fuel-air ratio for diesel fuel is about 0.07, the equivalence ratio for the data plotted ranges from 0.14 to 0.85. As the mixture is leaned out, the NO_x decrease, due to the lower combustion temperatures. The smoke readings are in Bosch smoke number (BSN) units, a scale that measures the reflectivity of a piece of filter paper through which some of the exhaust gas is passed.

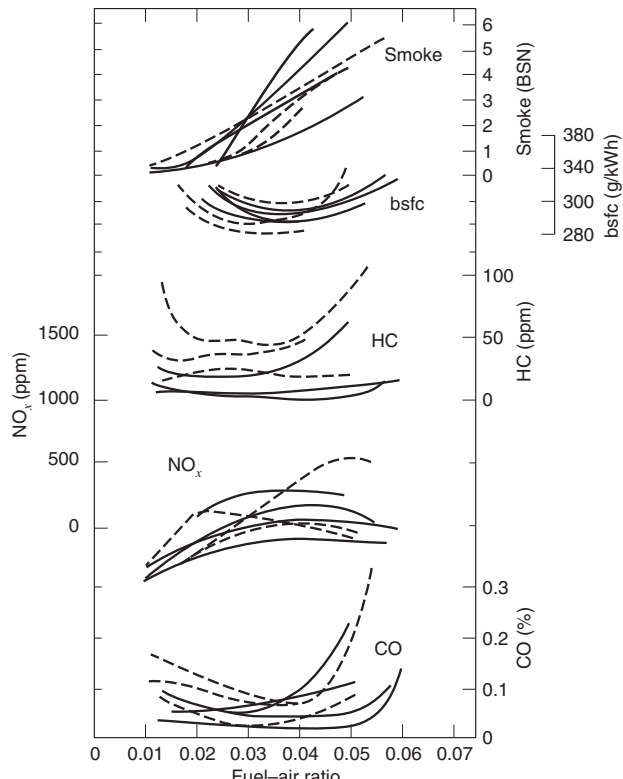


Figure 13.3 The effect of air-fuel ratio on the bsfc and exhaust emissions of a number of IDI and DI diesel engines. (Adapted from Motoyoshi et al., 1976.)

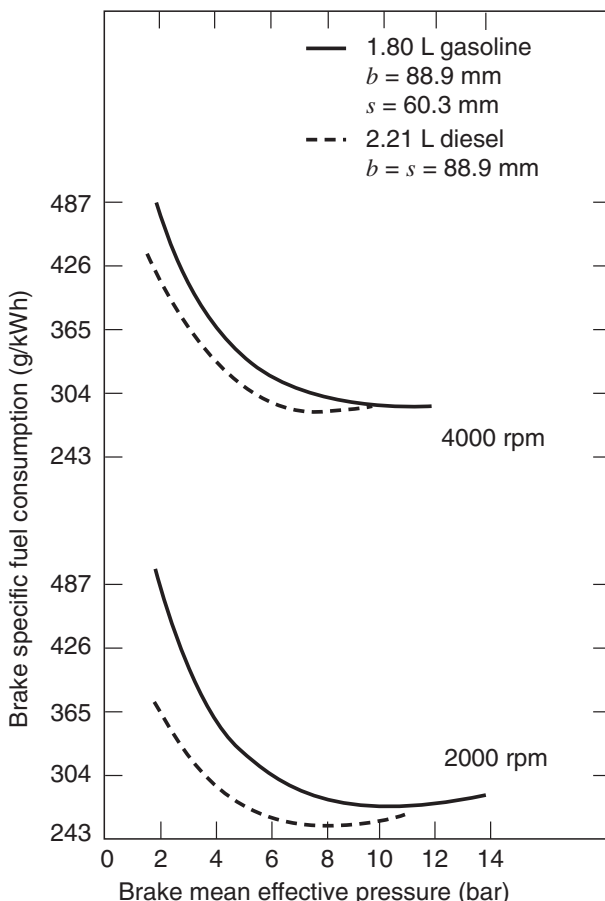


Figure 13.4 Comparison of an SI engine with an IDI–CI engine design to produce equal torque speed characteristics. (Adapted from Walder, 1965.)

The effect of load, that is, the brake mean effective pressure, on the brake specific fuel consumption is qualitatively the same for both compression ignition and spark ignition engines, as shown by representative examples in Figure 13.4, which compares a gasoline and a diesel engine, and Figure 13.5 for a marine diesel with two types of prechambers. In both cases, the bsfc will be infinite at idle, since the engine is producing no useful work but is consuming fuel. As the load increases, the brake specific fuel consumption drops, goes through a minimum, and may or may not increase depending on how the load is increased at this point.

In the case of spark ignition engines, opening the throttle and increasing the delivery ratio increases the load. This has little effect on the indicated efficiency, slightly increases the friction, and significantly reduces the pumping losses. Again, the dominant factor is the increase in mechanical efficiency. At constant fuel–air ratio, the brake specific fuel consumption drops with increasing load all the way to the point of maximum load so long as the imep increases faster than the fmep. In engines running at a fuel–air ratio less than that corresponding to maximum power (about $\phi = 1.1$, as we saw in our studies with fuel–air cycles), the load can be increased further by increasing the fuel–air ratio. This causes the brake specific fuel consumption to begin increasing with load once the engine is running rich.

In the case of compression ignition engines, increasing the fuel–air ratio increases the load; although this slightly drops the indicated efficiency and slightly increases the

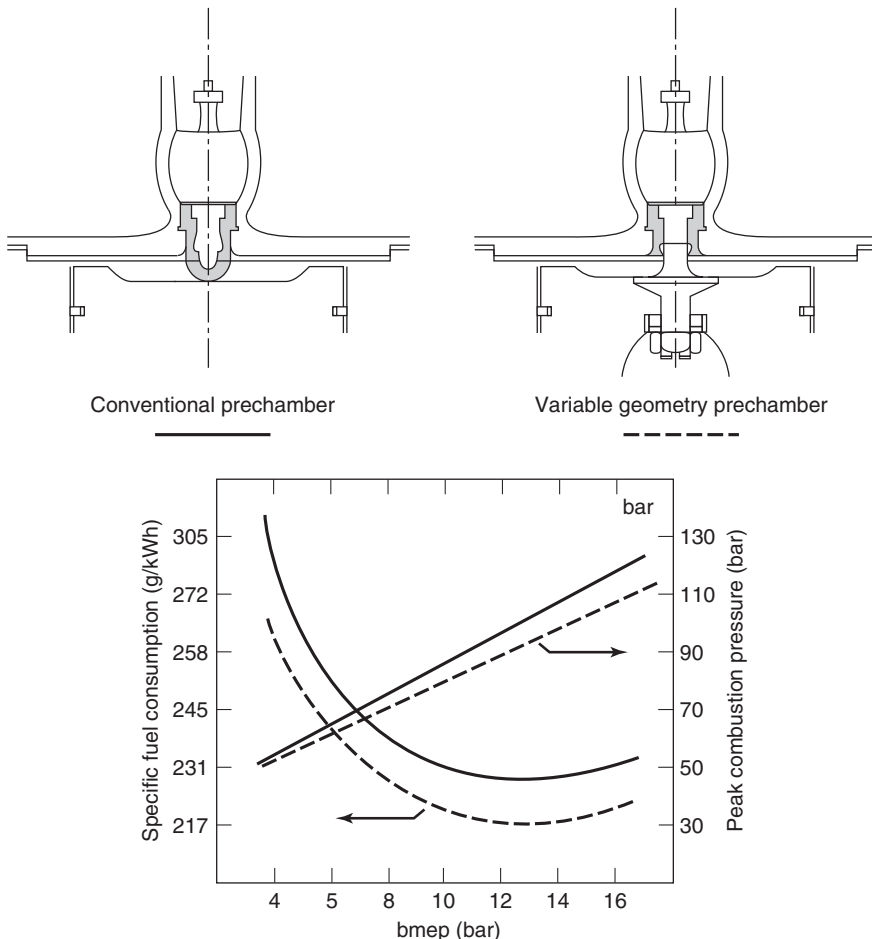


Figure 13.5 Brake specific fuel consumption of a marine diesel engine versus load (Hermann, 1980).

friction, the increase in mechanical efficiency is so great that it improves the specific fuel consumption. Just before the load is about to become smoke limited, the brake specific fuel consumption begins to increase because significant quantities of fuel begin to be only partially oxidized and thus are wasted.

The variable geometry prechamber of Figure 13.5 improved the fuel economy of the marine engine by about 10 g/kWh or about 5%. The 5% improvement is small and does not affect the trend shown for brake specific fuel consumption with load. Nevertheless, from an economic perspective that 5% improvement is very significant since the cost of fuel saved by a ship on a trip, although small compared with the total fuel cost, will be comparable to the trip's profit.

13.4 ENGINE PERFORMANCE MAPS

A common way of presenting the effects of both speed and load on engine performance is shown in Figure 13.6, an engine performance map. The engine speed N or the mean piston speed \bar{U}_p is plotted on the x -axis, and the brake mean effective pressure is plotted

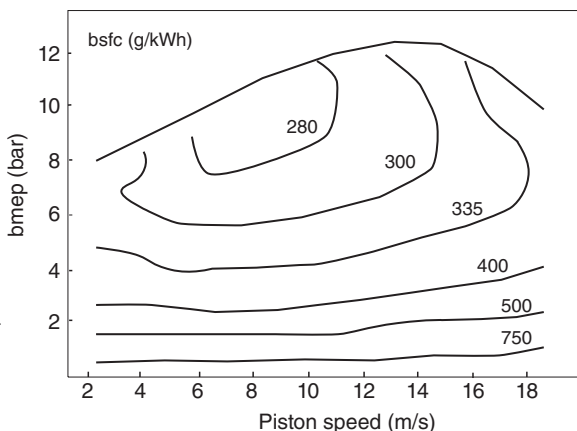


Figure 13.6 Performance map of bmep and bsfc versus mean piston speed for an automotive spark ignition engine.

on the *y*-axis. Contour lines of constant brake specific fuel consumption are plotted on this load–speed plane. The lines of constant bsfc are usually size independent for a given engine family, so performance maps can be used to match an engine with a given load profile. The upper envelope on a map is the wide open throttle performance curve. Its shape reflects variations in the volumetric efficiency with engine speed, although small changes in inlet air density are also involved. Performance maps can also be generated for emissions levels, with contour lines of constant emission level.

A representative spark ignition automotive engine performance map is given in Figure 13.6. The engine was a turbocharged four-cylinder engine with a 92-mm bore and 80-mm stroke, and compression ratio of $r = 8.7$. For general automotive applications, engines are designed to have the region of minimum bsfc located at relatively low engine speeds (40–60% of maximum engine speed) and at relatively high loads (60–80% of maximum bmep).

Representative diesel performance maps are given in Figure 13.7 as a function of engine speed, and in Figure 13.8 as a function of piston speed. With a diesel engine, the power is smoke limited, as the fuel–air ratio needs to be reduced relative to stoichiometric to reduce exhaust particulates. The relative position of the point of minimum fuel consumption can be moved up or down depending on the degree of mixture enrichment allowed.

At lower loads, the diesel bsfc is less than the SI engine bsfc due to its lower pumping work and leaner air–fuel ratio. Increasing the fuel–air ratio increases the load; although this slightly drops the indicated efficiency and slightly increases the friction, the increase in mechanical efficiency is so great that it improves the specific fuel consumption. Just before the load is about to become smoke limited, the brake specific fuel consumption begins to increase because significant quantities of fuel begin to be only partially oxidized and thus are wasted.

Engine performance maps generally have a single-valued minimum brake specific fuel consumption operating point. Starting at the location of minimum bsfc on the map, the fuel consumption increases in all directions. If one increases the engine speed, the fuel consumption increases because of an increase in the friction loss. If one decreases the engine speed, the fuel consumption increases because of an increase in the heat loss per cycle. At very lean fuel–air ratios, the engine wastes fuel because of misfire, and at rich fuel–air ratios it wastes fuel since there is not enough oxygen present to liberate all of the fuel’s energy. If one increases the load, the fuel consumption increases because the mixture must be enriched beyond stoichiometric. If one decreases the load, the fuel consumption

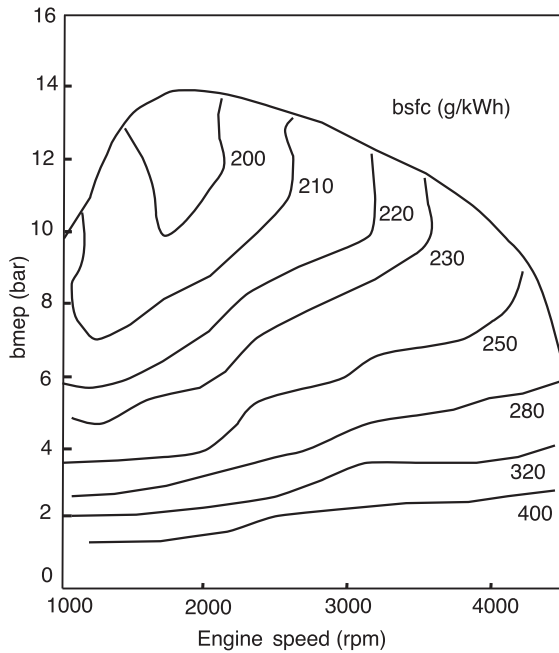


Figure 13.7 Performance map of bmepl and bsfc versus engine speed for a representative automobile diesel engine.

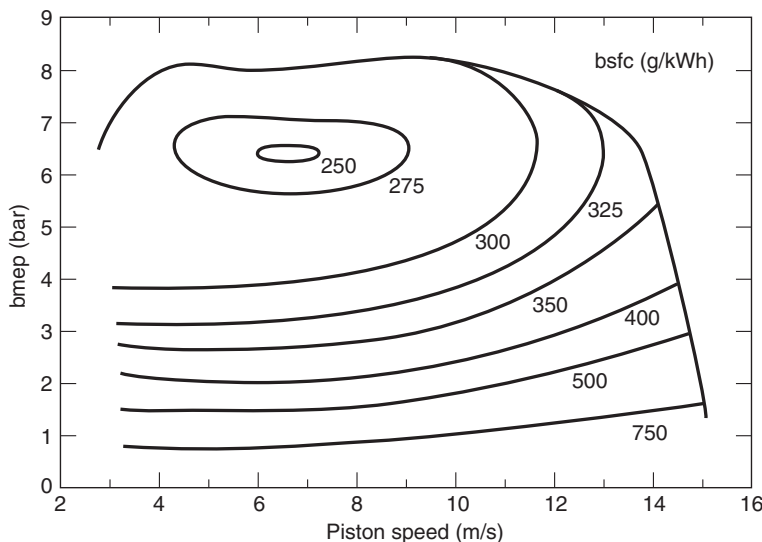


Figure 13.8 Performance map of a four-cylinder naturally aspirated indirect-injection (NA-IDI) diesel engine: $b = 76.5$ mm, $s = 80$ mm and $r = 23$. (Adapted from Hofbauer and Sator, 1977.)

increases because the friction is becoming a larger proportion of the indicated work. Finally, for a spark ignition engine with an intake throttle valve, as the load decreases, the throttle is closed, increasing the throttling losses, and increasing the bsfc.

Performance maps for large stationary and marine engines are not typically produced, since such engines usually operate at one speed. For more information about the use of automotive class spark ignition performance maps, the reader is referred to Shayler et al. (1999).

13.5 EFFECT OF ENGINE SIZE

We now look at the effect of engine size. The torque an engine will produce, by definition of the mean effective pressure, is

$$\tau_b = \frac{1}{4\pi} \text{bmep } V_d \quad (\text{four-stroke engine}) \quad (13.2)$$

$$\tau_b = \frac{1}{2\pi} \text{bmep } V_d \quad (\text{two-stroke engine}) \quad (13.3)$$

The power can also be expressed in terms of the mean effective pressure:

$$\dot{W}_b = \frac{1}{4} \text{bmep } A_p \bar{U}_p \quad (\text{four-stroke engine}) \quad (13.4)$$

$$\dot{W}_b = \frac{1}{2} \text{bmep } A_p \bar{U}_p \quad (\text{two-stroke engine}) \quad (13.5)$$

Therefore, for a given stress level (bmep, \bar{U}_p), the torque is proportional to the displacement volume V_d and the power is proportional to the piston area A_p

$$V_d = n_c \frac{\pi}{4} b^2 s \quad (13.6)$$

$$A_p = n_c \frac{\pi}{4} b^2 \quad (13.7)$$

Finally, we can also write for four- and two-stroke engines:

$$\dot{m}_f = \text{bsfc} \cdot \text{bmep} \cdot V_d \cdot N/2 \quad (\text{four-stroke engine}) \quad (13.8)$$

$$\dot{m}_f = \text{bsfc} \cdot \text{bmep} \cdot V_d \cdot N \quad (\text{two-stroke engine}) \quad (13.9)$$

$$\text{bsfc} = \frac{\text{FA}}{1 + \text{FA}} \frac{e_v \rho_i}{\text{bmep}} \quad (13.10)$$

where, as before, FA is the fuel-air ratio, e_v is the volumetric efficiency, and ρ_i is the mixture density in the intake manifold. Notice that Equation 13.10 does not explicitly include engine size, so the efficiency of engines is expected to be a weak function of size for a given stress.

The specific fuel consumption versus cylinder bore for representative diesel engines is shown in Figure 13.9. This figure is based on two- and four-stroke designs with bores from 62 to 900 mm. For bores greater than 500 mm, the thermal efficiency is about 50%. The ratio of the maximum bore to minimum bore is about 15, corresponding to a 3400 to 1 displacement volume ratio, whereas the brake specific fuel consumption varies by only a factor of 1.6. Although it is indeed a weak function with respect to the bore, the change in specific fuel consumption with the bore is significant with respect to fuel economy. An important factor underlying the trend shown in Figure 13.9 is that the surface to volume ratio of the cylinder is decreasing with increasing bore:

$$(A/V) \sim b^{-1}$$

This means that there will be proportionally less heat lost as the bore increases. Another factor working in the favor of large engines is that the rotational speed decreases with the bore size for a constant piston speed,

$$N \sim s^{-1} \sim b^{-1}$$

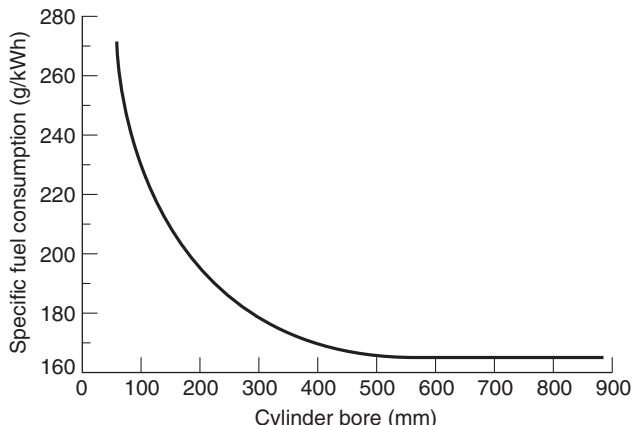


Figure 13.9 Brake specific fuel consumption of two- and four-stroke engines versus cylinder bore. (Thomas et al., 1984.)

so that there is more time near top center for fuel injection and combustion. This means that there will be less of a volume change during combustion and thus there will be a closer approach to constant volume combustion.

As discussed in Chapter 11, measurements indicate that the motoring mean effective pressure decreases as engine size increases, Equation 13.11:

$$\text{memp} = 1.3 \times 10^5 \frac{\bar{U}_p \mu}{b} + 1.7 \times 10^8 (r + 15) \frac{\mu^2}{\rho b^2} \quad (13.11)$$

Therefore, the friction can be expected to be relatively less in large engines than in small engines. The brake thermal efficiency of the state-of-the-art large ($b > 500$ mm) diesel engines is about 50%. Surely, they are among the most efficient engines in the world. Their low losses due to heat transfer, combustion, and friction have already been mentioned. They also use late-closing intake valves to realize a longer expansion stroke than compression stroke.

The generalizations just drawn ought to hold true for spark ignition engines too, although the point is academic, for they are not practical unless care is taken to stratify the charge. Large homogeneous charge spark ignition engines are not practical because their octane requirements are too high. In earlier chapters, it was pointed out that the flame speed is in part controlled by the magnitude of the turbulence, and that the turbulence is proportional to the piston speed. It follows that the combustion duration in crank angle is constant, but in the time domain is inversely proportional to the engine's rotational speed. There is consequently more time for knock precursors to form in relatively low speed, large engines. For similar reasons, the engineering of small high-speed diesel engines is a challenge, as there is little time for autoignition to occur and/or inject the fuel at reasonable pressures.

13.6 EFFECT OF IGNITION AND INJECTION TIMING

For spark ignition gasoline engines, the timing parameter is the spark timing, and for diesel engines the timing parameter is the fuel injection timing. A classic plot of the effect of spark timing on the brake mean effective pressure for a number of automotive engines at different chassis dynamometer speeds is given in Figure 13.10. Note that the variations in spark timing have the same percentage effect on the bmep at all the tested dynamometer

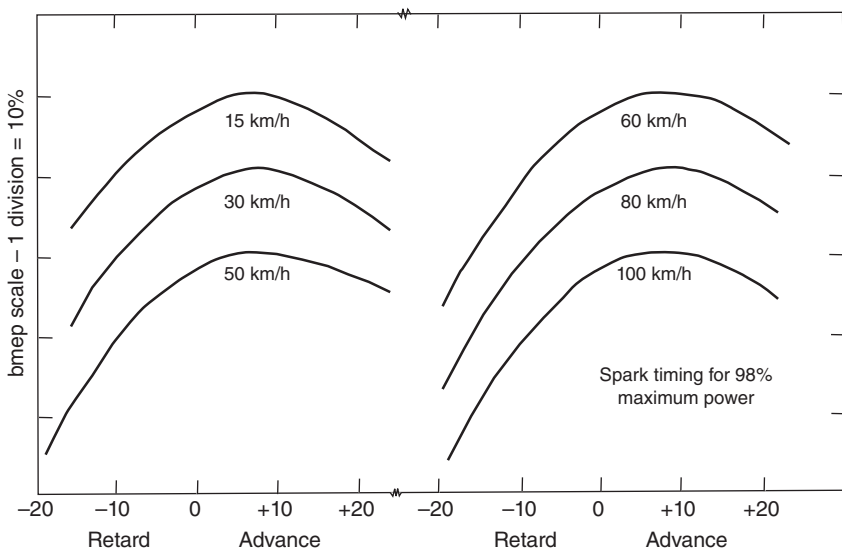


Figure 13.10 Effect of spark timing on bmeep for a number of different chassis dynamometer speeds. (Adapted from Barber, 1948.)

speeds. The data are well correlated by Equation 13.12:

$$\frac{\text{bmeep}}{(\text{bmeep})_{\max}} = 1 - (\Delta\theta/53)^2 \quad (13.12)$$

where $\Delta\theta$ is the change in degrees of crank angle from the angle of maximum bmeep. Although the data correlated are rather old, they are still representative of today's engines. Engines today are usually timed to a crank angle referred to as MBT (minimum advance for best torque). Examine Figure 13.10 and notice how relatively flat the bmeep curve is in the vicinity of the maximum. Now, reexamine Figure 7.30 and notice how sensitive the nitric oxide emissions are to variations in spark timing. Clearly, if the timing is slightly retarded, say 5° from that of maximum bmeep, then the engine power will decrease very little, and under some operating conditions the nitric oxides will be greatly reduced. Retarded timing also somewhat reduces the engine's octane requirement.

The term MBT spark timing is widely accepted, yet there is no quantitative definition in terms of how far the spark should be retarded from the point of maximum torque. Therefore, we will define MBT timing as a spark retard of 4° from the angle of maximum torque. This definition agrees with values reported in the literature to a tolerance of about $\pm 2^\circ$.

Figure 13.11 shows how the MBT timing can be expected to vary with engine speed, equivalence ratio, and residual mass fraction. Because the charge is diluted by either air (in which case it is lean) or exhaust gas, the combustion duration and ignition delay both increase, thereby requiring a greater spark advance to more or less center the combustion about top center. Likewise, as engine speed increases, ignition delay and the MBT spark advance increase.

One way to illustrate the trade-offs involved in controlling nitric oxides by retarding the fuel injection timing is to plot the brake specific nitric oxides versus the brake specific fuel consumption at full load as in Figure 13.12. The graph shows the response of two different

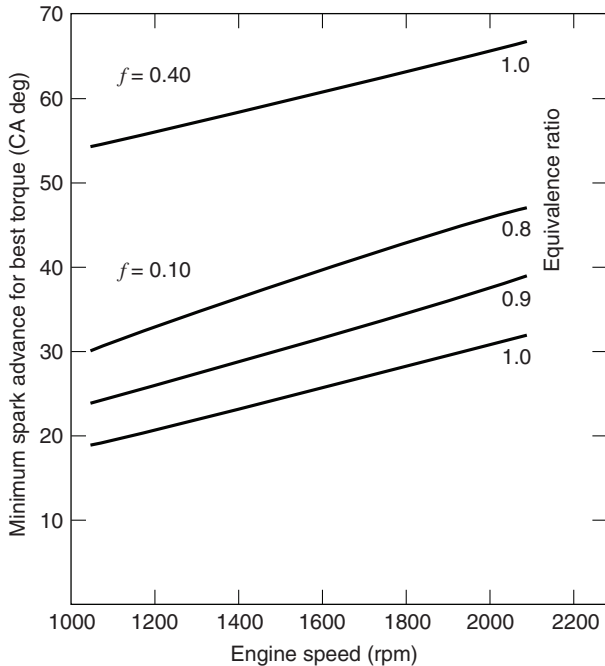


Figure 13.11 Minimum spark advance for best torque.
(Adapted from Young, 1980.)

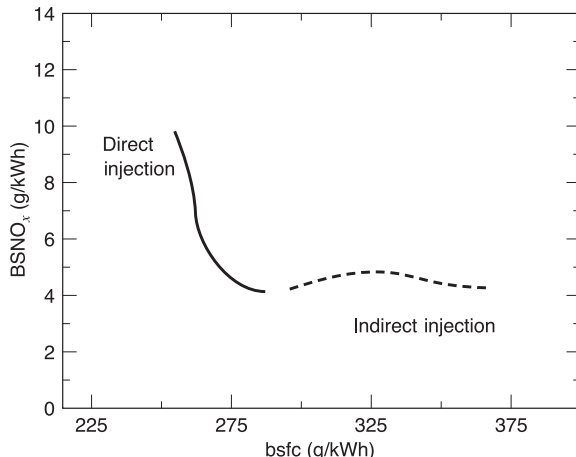


Figure 13.12 Brake specific nitric oxide emissions versus brake specific fuel consumption at full load as fuel injection timing is varied.
(Adapted from Pischinger and Cartelleri, 1972.)

diesel engines to changes in timing at full load and rated speed of $N = 2800$ rpm. The engines are production, in-line six-cylinder, naturally aspirated four-stroke diesel engines with $V_d = 5.9$ L and a compression ratio of $r = 17$. For the direct-injection engine, a significant reduction in the nitric oxide emissions can be realized at the expense of a slight increase in the brake specific fuel consumption. With indirect-injection engines, there is no appreciable change in the nitric oxides as injection timing is changed. However, at part loads the IDI engine shows response curves more like those shown for the direct injection engines. Retarding the injection timing is an effective means of controlling the nitric oxide emissions, but with diesel engines, it is usually at the expense of an increase in the particulate or smoke emissions. Furthermore, with indirect injection, retarding the timing does not always reduce the nitric oxides. The results discussed point out that it is more

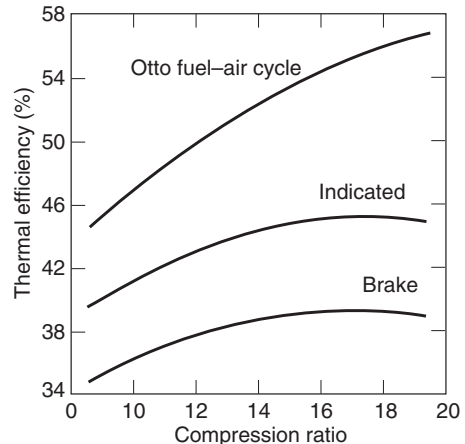


Figure 13.13 Thermal efficiency of a spark ignition engine as a function of the nominal compression ratio. (Adapted from Caris and Nelson, 1959.)

difficult to generalize about the performance of diesel engines than about gasoline engines. This is because there are many more degrees of freedom available in the design of a diesel engine.

13.7 EFFECT OF COMPRESSION RATIO

As shown previously in Figure 13.1, increasing the compression ratio decreases the brake specific fuel consumption. The particular results shown are, of course, unique to the specific engine design tested. The compression ratio trends depicted and their underlying causes, however, are typical to all engines, compression or spark-ignited engines, two or four-stroke engines.

Figure 13.13 indicates that the indicated specific fuel consumption improves at a faster rate with increasing compression ratio than the brake specific fuel consumption, because both friction and heat losses are increasing with compression ratio. In fact, there is an optimum compression ratio due to these effects. The spark advance is set for best efficiency, as is the fuel–air equivalence ratio at a lean setting of $\phi = 0.91$. The compression ratios of spark ignition engines are less than the optima shown in Figure 13.13 to avoid knock.

Computer simulations of diesel engines show similar trends (McAulay et al., 1965). An optimum compression ratio of 12–18 is typical, and is the underlying reason why direct-injection diesel engines have compression ratios in the same range. The compression ratios of indirect-injection diesel engines are greater than optimum to assist in cold starting, which is harder than with direct-injection engines because of the high heat loss in the prechamber.

13.8 VEHICLE PERFORMANCE SIMULATION

We finish this chapter with a vehicular application. For a vehicle, the power requirements that need to be met by an engine are specified by a road load power equation, Equation 13.13, which includes the effects of aerodynamic drag and rolling resistance:

$$\begin{aligned}\dot{W}_v &= \sum F \cdot U_v \\ &= (C_r m_v g + \frac{1}{2} C_d \rho_o A_v U_v^2) U_v\end{aligned}\quad (13.13)$$

where

C_r = coefficient of rolling resistance

m_v = mass of vehicle (kg)

g = gravitational constant, 9.81 m/s²

C_d = drag coefficient

A_v = vehicle front cross-sectional area, (m²)

U_v = vehicle speed (m/s)

Automotive engines are expected to operate well over a wide range of speeds and loads. Figure 12.24 in Chapter 12 presents two driving cycles used by the U.S. Environmental Protection Agency for regulatory purposes. In each case, vehicle speed as a function of time is specified. A vehicle simulation using Equation 13.13 can be used to assess the fuel economy performance of various candidate engines and vehicle combinations. From knowledge of the vehicle's characteristics, including frontal area, drag coefficient, weight, and gear ratios, the driving cycle can be transformed into a specification of the required engine torque and speed as a function of time.

The total fuel consumed by the engine during the driving cycle will be the integral of the fuel flow rate, Equation 13.14:

$$m_f = \int_0^t \dot{m}_f(t) dt = \frac{A_p}{4} \int_0^t \text{bsfc}(t) \text{bmep}(t) \bar{U}_p(t) dt \quad (13.14)$$

For a two-stroke engine, the factor of four would instead be a factor of two. In order to do the integration, one needs bsfc, bmep, and \bar{U}_p as functions of time. The latter two are known since the engine torque and speed is known from the driving cycle requirements and the vehicle characteristics.

The brake specific fuel consumption can be determined for each load and speed point of the driving cycle from the engine performance map. If an emissions map is available, a similar computation can be performed to compute the total emissions produced during the driving cycle. For further information about the trends in the performance characteristics of modern automobile engines, the reader is referred to Heywood and Welling (2009).

13.9 REFERENCES

- BARBER, E. M. (1948), "Knock Limited Performance of Several Automobile Engines," SAE Trans., Vol. 2, p. 401.
- CARIS, D. F. and E. E. NELSON (1959), "A New Look at High Compression Engines," SAE Trans., Vol. 67, p. 112.
- FRENCH, C. (1983), "A Universal Test Engine for Combustion Research," SAE paper 830453.
- HERMANN, R. (1980), "PA4-200 Engines with Variable Geometry Precombustion Chamber and Two Stage Turbocharging System," ASME paper 80-DGP-22.
- HEYWOOD, J. and O. WELLING (2009), "Trends in Performance Characteristics of Modern Automobile SI and Diesel Engines," SAE paper 2009-01-1892.
- HOFBAUER, P. and K. SATOR (1977), "Advanced Automotive Power Systems, Part 2: A Diesel for a Subcompact Car," SAE Trans., Vol. 86, paper 770113.
- MCAULAY, K., T. WU, S. CHEN, G. BORMAN, P. MYERS, and O. UYEHARA (1965), "Development and Evaluation of the Simulation of the CI Engine," SAE paper 650451.
- MOTOYOSHI, E., T. YAMADA, and M. MORI (1976), "The Combustion and Exhaust Emission Characteristics and Starting Ability of Y.P.C. Combustion System," SAE paper 760215.
- PISCHINGER, R. and W. CARTELLIERI (1972), "Combustion System Parameters and Their Effect upon Diesel Engine Exhaust Emissions," SAE paper 720756.
- ROENSCH, M. (1949), "Thermal Efficiency and Mechanical Losses of Automotive Engines," SAE J., Vol. 51, p. 1730.

- SHAYLER, P., J. CHICK, and D. EADE (1999), "A Method of Predicting Brake Specific Fuel Consumption Maps," SAE paper 1999-01-0556.
- THOMAS, F. J., J. S. AHLUWALIA, E. SHAMAH, and G. W. VAN DER HORST (1984), "Medium-Speed Diesel Engines Part 1: Design Trends and the Use of Residual/Blended Fuels," ASME paper 84-DGP-15.
- WALDER, C. J. (1965), "Problems in the Design and Development of High Speed Diesel Engines," SAE paper 978A.
- YOUNG, M. B. (1980), "Cyclic Dispersion-Some Quantitative Cause and Effect Relationships," SAE paper 800459.

13.10 HOMEWORK

- 13.1** Derive Equation 13.1, which relates the power of an engine to its volumetric efficiency, net indicated thermal efficiency, mechanical efficiency, and engine speed.
- 13.2** Derive Equation 13.1 as a function of mean piston speed \bar{U}_p , instead of engine speed.
- 13.3** What is the specific brake work ($\text{kJ/kg}_{\text{fuel}}$) of a 4 L single-cylinder propane engine operating stoichiometrically, if the heat transfer to the coolant is 17 kW, the air and fuel enter the engine at 298 K, the exhaust is 700 K, and the propane mass flow rate is 1.2 g/s?
- 13.4** A hydrogen engine operates with an air mass flowrate of 2.0 kg/s and produces 1 MW of power. The exhaust enthalpy is equal to $-40,000 \text{ kJ/kg}_{\text{fuel}}$, and the heat losses from the engine total $50,000 \text{ kJ/kmol}_{\text{fuel}}$. At what equivalence ratio ϕ is the engine being operated?
- 13.5** A four-stroke 6 L engine is fueled lean with methane at an equivalence ratio $\phi = 0.8$. It operates at 2000 rpm with a volumetric efficiency of 0.80. The exhaust temperature is 800 K, and the heat transfer to the coolant is $3.4 \times 10^5 \text{ kJ/kmol}_{\text{fuel}}$. What is the engine's thermal efficiency and power?
- 13.6** A car traveling steadily on a level road at 100 km/h requires about 15 kW of power from the engine. For the engine families represented by the performance maps of Figure 13.6 and Figure 13.7, estimate the fuel economy of the vehicle (km/g), the bore required of a four-cylinder engine, and the maximum power the engine will produce. Assume that the engine is operating at its best fuel economy point when the vehicle is cruising at 100 km/h, that engine controls limit the piston speed to 10 m/s, and that the performance map is size independent.
- 13.7** Using the performance map of Figure 13.6, calculate the required cylinder bore, for a six-cylinder engine with equal bore and stroke that is to produce 200 kW with a maximum piston speed of 12 m/s. Plot the bsfc, torque, and power versus engine speed.
- 13.8** A six-cylinder diesel engine with equal bore and stroke is being designed to provide a maximum brake torque of 200 Nm at 2000 rpm. Using the performance map of Figure 13.7, estimate the required engine displacement, and maximum brake power.
- 13.9** What is the engine power required for an automobile to travel up a hill with a 10° slope at 50 mph? Assume a vehicle frontal cross-sectional area A_v of 2.0 m^2 , $C_d = 0.3$, $C_r = 0.015$, $m_v = 1500 \text{ kg}$.
- 13.10** If the power required for a truck to travel up a 12° incline at 70 mph is 91 kW, what is the mass m of the truck? The frontal area is 2.5 m^2 , $C_d = 0.5$, and $C_r = 0.02$.

- 13.11** The price of large diesel engines is roughly proportional to their rated power. Let c_1 be the engine price per kilowatt per year and c_2 the fuel price per kilogram. At low values of c_1 , it pays to buy an engine bigger than required and operate it at its best fuel economy point. For low values of c_2 , it pays to buy a smaller engine and run it at its rated power. For the diesel engine family performance map of Figure 13.8, at what ratio c_1/c_2 will two different sized engines yield the same total annual cost? Assume the engines are run 20 h/day and their rated power is at a speed-load point of $U_p = 8$ m/s and bmep = 8 bar.
- 13.12** Write an expression resembling Equation 13.14 for the mass of pollutant species i (given its emission index at any load–speed point) emitted by an engine operated over a duty cycle from $0 < t < t_d$.

Appendix A

Physical Properties of Air

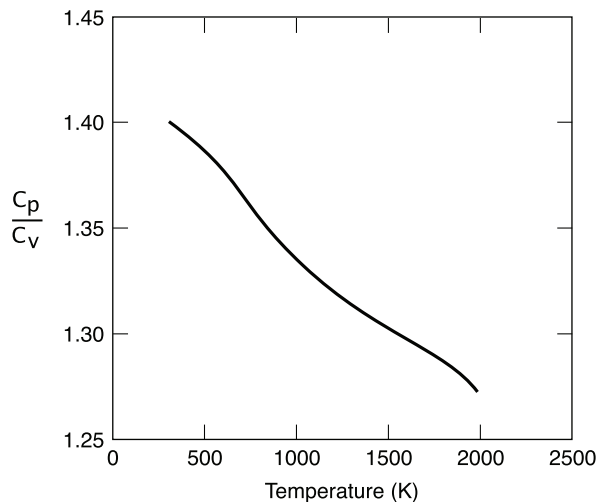


Figure A.1 Specific heat ratio for air

Table A.1 Properties of Air at Atmospheric Pressure

T (K)	ρ (kg/m ³)	c_p (kJ/(kg K))	$\mu \times 10^7$ (N s/m ²)	$\nu \times 10^6$ m ² /s ²	$k \times 10^3$ (W/(m K))	$\alpha \times 10^6$ (m ² /s ²)	Pr
100	3.5562	1.032	71.1	2.00	9.34	2.54	0.786
150	2.3364	1.012	103.4	4.426	13.8	5.84	0.758
200	1.7458	1.007	132.5	7.590	18.1	10.3	0.737
250	1.3947	1.006	159.6	11.44	22.3	15.9	0.720
300	1.1614	1.007	184.6	15.89	26.3	22.5	0.707
350	0.9950	1.009	208.2	20.92	30.0	29.9	0.700
400	0.8711	1.014	230.1	26.41	33.8	38.3	0.690
450	0.7740	1.021	250.7	32.39	37.3	47.2	0.686
500	0.6964	1.030	270.1	38.79	40.7	56.7	0.684
550	0.6329	1.040	288.4	45.57	43.9	66.7	0.683

(continued)

Table A.1 (Continued)

T (K)	ρ (kg/m ³)	c_p (kJ/(kg K))	$\mu \times 10^7$ (N s/m ²)	$\nu \times 10^6$ m ² /s ²	$k \times 10^3$ (W/(m K))	$\alpha \times 10^6$ (m ² /s ²)	Pr
600	0.5804	1.051	305.8	52.69	46.9	76.9	0.685
650	0.5356	1.063	322.5	60.21	49.7	87.3	0.690
700	0.4975	1.075	338.8	68.10	52.4	98.0	0.695
750	0.4643	1.087	354.6	76.37	54.9	109	0.702
800	0.4354	1.099	369.8	84.93	57.3	120	0.709
850	0.4097	1.110	384.3	93.80	59.6	131	0.716
900	0.3868	1.121	398.1	102.9	62.0	143	0.720
950	0.3666	1.131	411.3	112.2	64.3	155	0.723
1000	0.3482	1.141	424.4	121.9	66.7	168	0.726
1100	0.3166	1.159	449.0	141.8	71.5	195	0.728
1200	0.2902	1.175	473.0	162.9	76.3	224	0.728
1300	0.2679	1.189	496.0	185.1	82	238	0.719
1400	0.2488	1.207	530	213	91	303	0.703
1500	0.2322	1.230	557	240	100	350	0.685
1600	0.2177	1.248	584	268	106	390	0.688
1700	0.2049	1.267	611	298	113	435	0.685
1800	0.1935	1.286	637	329	120	482	0.683
1900	0.1833	1.307	663	362	128	534	0.677
2000	0.1741	1.337	689	396	137	589	0.672
2100	0.1658	1.372	715	431	147	646	0.667
2200	0.1582	1.417	740	468	160	714	0.655
2300	0.1513	1.478	766	506	175	783	0.647
2400	0.1448	1.558	792	547	196	869	0.630
2500	0.1389	1.665	818	589	222	960	0.613
3000	0.1135	2.726	955	841	486	1570	0.536

Source: F. Incropera, D. DeWitt, T. Bergman, and A. Lavine (2007), *Fundamentals of Heat and Mass Transfer*, Wiley, New York.

Table A.2 Physical Properties of Air at Atmospheric Conditions
($T = 298$ K, $P = 1$ atm = 1.0133 bar)

Molecular mass	$M = 28.966$ kg/kmol
Gas constant	$R = 0.28704$ kJ/(kg K)
Speed of sound	$c = 345.9$ m/s
Binary diffusion with octane	$D = 5.68 \times 10^{-6}$ m ² /s
Schmidt number	$Sc = \nu/D = 2.77$
Lewis number	$Le = \alpha/D = 3.91$

Appendix B

Thermodynamic Property Tables for Various Ideal Gases

Table B.1 Properties of Various Ideal Gases at 298 K (SI Units)

Gas	Chemical formula	M (kg/kmol)	R (kJ/(kg K))	c_{po} (kJ/(kg K))	c_{vo} (kJ/(kg K))	γ
Air		28.97	0.287	1.004	0.717	1.40
Ethane	C_2H_6	30.07	0.27650	1.7662	1.4897	1.186
Ethanol	C_2H_5OH	46.069	0.18048	1.427	1.246	1.145
Ethylene	C_2H_4	28.054	0.29637	1.5482	1.2518	1.237
Helium	He	4.003	2.07703	5.1926	3.1156	1.667
Hydrogen	H_2	2.016	4.12418	14.2091	10.0849	1.409
Methane	CH_4	16.04	0.51835	2.2537	1.7354	1.299
Methanol	CH_3OH	32.042	0.25948	1.4050	1.1455	1.227
Nitrogen	N_2	28.013	0.29680	1.0416	0.7448	1.400
Nitrous oxide	N_2O	44.013	0.18891	0.8793	0.6904	1.274
<i>n</i> -Octane	C_8H_{18}	114.23	0.07279	1.7113	1.6385	1.044
Oxygen	O_2	31.999	0.25983	0.9216	0.6618	1.393
Propane	C_3H_8	44.097	0.18855	1.6794	1.4909	1.126
Steam	H_2O	18.015	0.46152	1.8723	1.4108	1.327

Source: R. Sonntag, C. Borgnakke, and G. Van Wylen (2003), *Fundamentals of Thermodynamics*, Wiley, New York.

Table B.2 Binary Diffusion Coefficients at 1 atm ($D_{AB} \sim T^{3/2}/P$)

Substance A	Substance B	T (K)	$D_{AB} \times 10^5$ (m ² /s)
Benzene	Air	273	0.77
Carbon dioxide	Air	273	1.38
Cyclohexane	Air	318	0.86
<i>n</i> -Decane	Nitrogen	363	0.84
<i>n</i> -Dodecane	Nitrogen	399	0.81
Ethanol	Air	273	1.02
<i>n</i> -Hexane	Nitrogen	288	0.757
Hydrogen	Air	273	0.611
Methanol	Air	273	1.32
<i>n</i> -Octane	Air	273	0.505
Water	Air	273	2.2

Source: Perry, Green, and Maloney (1984), Perry's Chemical Engineers' Handbook, McGraw-Hill, New York.

Table B.3 Ideal Gas Properties of N₂ and N (SI Units), Entropies at 0.1-MPa (1-bar) Pressure

T (K)	Nitrogen, Diatomic (N ₂)		Nitrogen, Monatomic (N)	
	$\bar{h}_{f,298}^o = 0$ kJ/kmol	$M = 28.013$	$\bar{h}_{f,298}^o = 472,680$ kJ/kmol	$M = 14.007$
	($\bar{h} - \bar{h}_{298}^o$) (kJ/kmol)	\bar{s}^o (kJ/(kmol K))	($\bar{h} - \bar{h}_{298}^o$) (kJ/kmol)	\bar{s}^o (kJ/(kmol K))
0	-8670	0	-6197	0
100	-5768	159.812	-4119	130.593
200	-2857	179.985	-2040	145.001
298	0	191.609	0	153.300
300	54	191.789	38	153.429
400	2971	200.181	2117	159.409
500	5911	206.740	4196	164.047
600	8894	212.177	6274	167.837
700	11,937	216.865	8353	171.041
800	15,046	221.016	10,431	173.816
900	18,223	224.757	12,510	176.265
1000	21,463	228.171	14,589	178.455
1100	24,760	231.314	16,667	180.436
1200	28,109	234.227	18,746	182.244
1300	31,503	236.943	20,825	183.908
1400	34,936	239.487	22,903	185.448
1500	38,405	241.881	24,982	186.883
1600	41,904	244.139	27,060	188.224
1700	45,430	246.276	29,139	189.484
1800	48,979	248.304	31,218	190.672
1900	52,549	250.234	33,296	191.796
2000	56,137	252.075	35,375	192.863

(continued)

Table B.3 (Continued)

Nitrogen, Diatomic (N_2)			Nitrogen, Monatomic (N)	
$\bar{h}_{f,298}^o = 0 \text{ kJ/kmol}$			$\bar{h}_{f,298}^o = 472,680 \text{ kJ/kmol}$	
$M = 28.013$			$M = 14.007$	
$T \text{ (K)}$	$(\bar{h} - \bar{h}_{298}^o)$ (kJ/kmol)	\bar{s}^o (kJ/(kmol K))	$(\bar{h} - \bar{h}_{298}^o)$ (kJ/kmol)	\bar{s}^o (kJ/(kmol K))
2200	63,362	255.518	39,534	194.845
2400	70,640	258.684	43,695	196.655
2600	77,963	261.615	47,860	198.322
2800	85,323	264.342	52,033	199.868
3000	92,715	266.892	56,218	201.311
3200	100,134	269.286	60,420	202.667
3400	107,577	271.542	64,646	203.948
3600	115,042	273.675	68,902	205.164
3800	122,526	275.698	73,194	206.325
4000	130,027	277.622	77,532	207.437
4400	145,078	281.209	86,367	209.542
4800	160,188	284.495	95,457	211.519
5200	175,352	287.530	104,843	213.397
5600	190,572	290.349	114,550	215.195
6000	205,848	292.984	124,590	216.926

Source: R. Sonntag, C. Borgnakke, and G. Van Wylen (2003), *Fundamentals of Thermodynamics*, John Wiley, New York.

Table B.4 Ideal Gas Properties of O₂ and O (SI Units), Entropies at 0.1-MPa (1-bar) Pressure

Oxygen, Diatomic (O ₂)		Oxygen, Monatomic (O)	
	$\bar{h}_{f,298}^o = 0 \text{ kJ/kmol}$		$\bar{h}_{f,298}^o = 249,170 \text{ kJ/kmol}$
	$M = 31.999$		$M = 16.00$
$T \text{ (K)}$	$(\bar{h} - \bar{h}_{298}^o)$ (kJ/kmol)	\bar{s}^o (kJ/(kmol K))	$(\bar{h} - \bar{h}_{298}^o)$ (kJ/kmol)
0	-8683	0	-6725
100	-5777	173.308	-4518
200	-2868	193.483	-2186
298	0	205.148	0
300	54	205.329	41
400	3027	213.873	2207
500	6086	220.693	4343
600	9245	226.450	6462
700	12,499	231.465	8570
800	15,836	235.920	10,671
900	19,241	239.931	12,767
1000	22,703	243.579	14,860
1100	26,212	246.923	16,950
1200	29,761	250.011	19,039
1300	33,345	252.878	21,126
1400	36,958	255.556	23,212
1500	40,600	258.068	25,296
1600	44,267	260.434	27,381
1700	47,959	262.673	29,464
1800	51,674	264.797	31,547
1900	55,414	266.819	33,630
2000	59,176	268.748	35,713
2200	66,770	272.366	39,878
2400	74,453	275.708	44,045
2600	82,225	278.818	48,216
2800	90,080	281.729	52,391
3000	98,013	284.466	56,574
3200	106,022	287.050	60,767
3400	114,101	289.499	64,971
3600	122,245	291.826	69,190
3800	130,447	294.043	73,424
4000	138,705	296.161	77,675
4400	155,374	300.133	86,234
4800	172,240	303.801	94,873
5200	189,312	307.217	103,592
5600	206,618	310.423	112,391
6000	224,210	313.457	121,264

Source: R. Sonntag, C. Borgnakke, and G. Van Wylen (2003), *Fundamentals of Thermodynamics*, John Wiley, New York.

Table B.5 Ideal Gas Properties of CO₂ and CO (SI Units), Entropies at 0.1-MPa (1-bar) Pressure

Carbon Dioxide (CO ₂)			Carbon Monoxide (CO)	
	$\bar{h}_{f,298}^o = -393,522 \text{ kJ/kmol}$	$M = 44.01$	$\bar{h}_{f,298}^o = -110,527 \text{ kJ/kmol}$	$M = 28.01$
$T \text{ (K)}$	$(\bar{h} - \bar{h}_{298}^o)$ (kJ/kmol)	\bar{s}^o (kJ/(kmol K))	$(\bar{h} - \bar{h}_{298}^o)$ (kJ/kmol)	\bar{s}^o (kJ/(kmol K))
0	-9364	0	-8671	0
100	-6457	179.010	-5772	165.852
200	-3413	199.976	-2860	186.024
298	0	213.794	0	197.651
300	69	214.024	54	197.831
400	4003	225.314	2977	206.240
500	8305	234.902	5932	212.833
600	12,906	243.284	8942	218.321
700	17,754	250.752	12,021	223.067
800	22,806	257.496	15,174	227.277
900	28,030	263.646	18,397	231.074
1000	33,397	269.299	21,686	234.538
1100	38,885	274.528	25,031	237.726
1200	44,473	279.390	28,427	240.679
1300	50,148	283.931	31,867	243.431
1400	55,895	288.190	35,343	246.006
1500	61,705	292.199	38,852	248.426
1600	67,569	295.984	42,388	250.707
1700	73,480	299.567	45,948	252.866
1800	79,432	302.969	49,529	254.913
1900	85,420	306.207	53,128	256.860
2000	91,439	309.294	56,743	258.716
2200	103,562	315.070	64,012	262.182
2400	115,779	320.384	71,326	265.361
2600	128,074	325.307	78,679	268.302
2800	140,435	329.887	86,070	271.044
3000	152,853	334.170	93,504	273.607
3200	165,321	338.194	100,962	276.012
3400	177,836	341.988	108,440	278.279
3600	190,394	345.576	115,938	280.422
3800	202,990	348.981	123,454	282.454
4000	215,624	352.221	130,989	284.387
4400	240,992	358.266	146,108	287.989
4800	266,488	363.812	161,285	291.290
5200	292,112	368.939	176,510	294.337
5600	317,870	373.711	191,782	297.167
6000	343,782	378.180	207,105	299.809

Source: R. Sonntag, C. Borgnakke, and G. Van Wylen (2003), *Fundamentals of Thermodynamics*, John Wiley, New York.

Table B.6 Ideal Gas Properties of H₂O and OH (SI Units), Entropies at 0.1-MPa (1-bar) Pressure

Water (H ₂ O)		Hydroxyl (OH)	
	$\bar{h}_{f,298}^o = -241,826 \text{ kJ/kmol}$		$\bar{h}_{f,298}^o = 38,987 \text{ kJ/kmol}$
	$M = 18.015$		$M = 17.007$
$T \text{ (K)}$	$(\bar{h} - \bar{h}_{298}^o)$ (kJ/kmol)	\bar{s}^o (kJ/(kmol K))	$(\bar{h} - \bar{h}_{298}^o)$ (kJ/kmol)
0	-9904	0	-9172
100	-6617	152.386	-6140
200	-3282	175.488	-2975
298	0	188.835	0
300	62	189.043	55
400	3450	198.787	3034
500	6922	206.532	5991
600	10,499	213.051	8943
700	14,190	218.739	11,902
800	18,002	223.826	14,881
900	21,937	228.460	17,889
1000	26,000	232.739	20,935
1100	30,190	236.732	24,024
1200	34,506	240.485	27,159
1300	38,941	244.035	30,340
1400	43,491	247.406	33,567
1500	48,149	250.620	36,838
1600	52,907	253.690	40,151
1700	57,757	256.631	43,502
1800	62,693	259.452	46,890
1900	67,706	262.162	50,311
2000	72,788	264.769	53,763
2200	83,153	269.706	60,751
2400	93,741	274.312	67,840
2600	104,520	278.625	75,018
2800	115,463	282.680	82,268
3000	126,548	286.504	89,585
3200	137,756	290.120	96,960
3400	149,073	293.550	104,388
3600	160,484	296.812	111,864
3800	171,981	299.919	119,382
4000	183,552	302.887	126,940
4400	206,892	308.448	142,165
4800	230,456	313.573	157,522
5200	254,216	318.328	173,002
5600	278,161	322.764	188,598
6000	302,295	326.926	204,309

Source: R. Sonntag, C. Borgnakke, and G. Van Wylen (2003), *Fundamentals of Thermodynamics*, John Wiley, New York.

Table B.7 Ideal Gas Properties of H₂ and H (SI Units), Entropies at 0.1-MPa (1-bar) Pressure

T (K)	Hydrogen (H ₂)		Hydrogen, Monatomic (H)	
	$(\bar{h} - \bar{h}_{298}^o)$	\bar{s}^o	$(\bar{h} - \bar{h}_{298}^o)$	\bar{s}^o
	(kJ/kmol)	(kJ/(kmol K))	(kJ/kmol)	(kJ/(kmol K))
0	-8467	0	-6197	0
100	-5467	100.727	-4119	92.009
200	-2774	119.410	-2040	106.417
298	0	130.678	0	114.716
300	53	130.856	38	114.845
400	2961	139.219	2117	120.825
500	5883	145.738	4196	125.463
600	8799	151.078	6274	129.253
700	11,730	155.609	8353	132.457
800	14,681	159.554	10,431	135.233
900	17,657	163.060	12,510	137.681
1000	20,663	166.225	14,589	139.871
1100	23,704	169.121	16,667	141.852
1200	26,785	171.798	18,746	143.661
1300	29,907	174.294	20,825	145.324
1400	33,073	176.637	22,903	146.865
1500	36,281	178.849	24,982	148.299
1600	39,533	180.946	24,060	149.640
1700	42,826	182.941	29,139	150.900
1800	46,160	184.846	31,218	152.089
1900	49,532	186.670	33,296	153.212
2000	52,942	188.419	35,375	154.279
2200	59,865	191.719	39,532	156.260
2400	66,915	194.789	43,689	158.069
2600	74,082	197.659	47,847	159.732
2800	81,355	200.355	52,004	161.273
3000	88,725	202.898	56,161	162.707
3200	96,187	205.306	60,318	164.048
3400	103,736	207.593	64,475	165.308
3600	111,367	209.773	68,633	166.497
3800	119,077	211.856	72,790	167.620
4000	126,864	213.851	76,947	168.687
4400	142,658	217.612	85,261	170.668
4800	158,730	221.109	93,576	172.476
5200	175,057	224.379	101,890	174.140
5600	191,607	227.447	110,205	175.681
6000	208,332	230.322	118,519	177.114

Source: R. Sonntag, C. Borgnakke, and G. Van Wylen (2003), *Fundamentals of Thermodynamics*, John Wiley, New York.

Table B.8 Ideal Gas Properties of NO and NO₂ (SI Units), Entropies at 0.1-MPa (1-bar) Pressure

Nitric Oxide (NO)			Nitrogen Dioxide (NO ₂)	
	$\bar{h}_{f,298}^o = 90,291 \text{ kJ/kmol}$	$M = 30.006$	$\bar{h}_{f,298}^o = 33,100 \text{ kJ/kmol}$	$M = 46.005$
$T \text{ (K)}$	$(\bar{h} - \bar{h}_{298}^o)$ (kJ/kmol)	\bar{s}^o (kJ/(kmol K))	$(\bar{h} - \bar{h}_{298}^o)$ (kJ/kmol)	\bar{s}^o (kJ/(kmol K))
0	-9192	0	-10186	0
100	-6073	177.031	-6861	202.563
200	-2951	198.747	-3495	225.852
298	0	210.759	0	240.034
300	55	210.943	68	240.263
400	3040	219.529	3927	251.342
500	6059	226.263	8099	260.638
600	9144	231.886	12,555	268.755
700	12,308	236.762	17,250	275.988
800	15,548	241.088	22,138	282.513
900	18,858	244.985	27,180	288.450
1000	22,229	248.536	32,344	293.889
1100	25,653	251.799	37,606	298.904
1200	29,120	254.816	42,946	303.551
1300	32,626	257.621	48,351	307.876
1400	36,164	260.243	53,808	311.920
1500	39,729	262.703	59,309	315.715
1600	43,319	265.019	64,846	319.289
1700	46,929	267.208	70,414	322.664
1800	50,557	269.282	76,008	325.861
1900	54,201	271.252	81,624	328.898
2000	57,859	273.128	87,259	331.788
2200	65,212	276.632	98,578	337.182
2400	72,606	279.849	109,948	342.128
2600	80,034	282.822	121,358	346.695
2800	87,491	285.585	132,800	350.934
3000	94,973	288.165	144,267	354.890
3200	102,477	290.587	155,756	358.597
3400	110,000	292.867	167,262	362.085
3600	117,541	295.022	178,783	365.378
3800	125,099	297.065	190,316	368.495
4000	132,671	299.007	201,860	371.456
4400	147,857	302.626	224,973	376.963
4800	163,094	305.940	248,114	381.997
5200	178,377	308.998	271,276	386.632
5600	193,703	311.838	294,455	390.926
6000	209,070	314.488	317,648	394.926

Source: R. Sonntag, C. Borgnakke, and G. Van Wylen (2003), *Fundamentals of Thermodynamics*, John Wiley, New York.

Appendix C

Curve-Fit Coefficients for Thermodynamic Properties of Various Fuels and Ideal Gases

Specific heats of fuels and ideal gases are curve-fitted to polynomials of the form below. For any given species, the specific heat is approximated by

$$\frac{c_p}{R} = \frac{\bar{c}_p}{R_u} = a_1 + a_2 T + a_3 T^2 + a_4 T^3 + a_5 T^4$$

For an ideal gas, $dh = c_p dT$ and $ds = (c_p/T) dT$. It follows that the enthalpy and entropy at atmospheric pressure are

$$\frac{h}{RT} = \frac{\bar{h}}{R_u T} = a_1 + \frac{a_2}{2} T + \frac{a_3}{3} T^2 + \frac{a_4}{4} T^3 + \frac{a_5}{5} T^4 + \frac{a_6}{T}$$

$$\frac{s^0}{R} = \frac{\bar{s}^0}{R_u} = a_1 \ln T + a_2 T + \frac{a_3}{2} T^2 + \frac{a_4}{3} T^3 + \frac{a_5}{4} T^4 + a_7$$

The temperature range 300–1000 K is useful for unburned mixture property computation, and the temperature range 1000–3000 K is useful for burned mixture property computation.

Table C.1 Curve-Fit Coefficients for Ideal Gas Properties of Selected Fuels in Vapor Phase ($300 \leq T \leq 1000$ K)

Fuel	Formula	a_1	a_2	a_3	a_6	a_7
Methane	CH ₄	1.971324	7.871586E -03	-1.048592E -06	-9.930422E -03	8.873728
Gasoline	C ₇ H ₁₇	4.0652	6.0977E -02	-1.8801E -05	-3.5880E +04	1.545E +01
Diesel	C _{14.4} H _{24.9}	7.9710	1.1954E -01	-3.6858E -05	-1.9385E +04	-1.7879
Methanol	CH ₃ OH	1.779819	1.262503E -02	-3.624890E -06	-2.525420E +04	1.50884E +01
Nitromethane	CH ₃ NO ₂	1.412633	2.087101E -02	-8.142134E -06	-1.026351E +04	1.917126E +01

($a_4 = a_5 = 0$)

Table C.2 Curve-Fit Coefficients for Thermodynamic Properties of Combustion Products ($1000 \leq T \leq 3000$ K)

Species	a_1	a_2	a_3	a_4	a_5	a_6	a_7
CO_2	0.24007797E + 01	0.87350957E - 02	-0.66070878E - 05	0.20021861E - 08	0.63274039E - 15	-0.48377527E + 05	0.96951457E + 01
H_2O	0.40701275E + 01	-0.11084499E - 02	0.41521180E - 05	-0.29637404E - 08	0.80702103E - 12	-0.30279722E + 05	-0.32270046E + 00
N_2	0.36748261E + 01	-0.12081500E - 02	0.23240102E - 05	-0.63217559E - 09	-0.22577253E - 12	-0.10611588E + 04	0.23580424E + 01
O_2	0.36255985E + 01	-0.18782184E - 02	0.70554544E - 05	-0.67635137E - 08	0.21555993E - 11	-0.10475226E + 04	0.43052778E + 01
CO	0.37100928E + 01	-0.16190964E - 02	0.36923594E - 05	-0.20319674E - 08	0.23953344E - 12	-0.14356310E + 05	0.2955535E + 01
H_2	0.30574451E + 01	0.26765200E - 02	-0.58099162E - 05	0.55210391E - 08	-0.18122739E - 11	-0.98890474E + 03	-0.22997056E + 01
H	0.25000000E + 01	0	0	0	0	0.25471627E + 05	-0.46011762E + 00
O	0.29464287E + 01	-0.16381665E - 02	0.24210316E - 05	-0.16028432E - 08	0.38906964E - 12	0.29147644E + 05	0.29639949E + 01
OH	0.38375943E + 01	-0.10778858E - 02	0.96830378E - 06	0.18713972E - 09	-0.22571094E - 12	0.36412823E + 04	0.49370009E + 00
NO	0.40459521E + 01	-0.34181783E - 02	0.79819190E - 05	-0.61139316E - 08	0.15919076E - 11	0.97453934E + 04	0.29974988E + 01

Source: Gordon, S. and B. McBride (1971), "Computer Program for Calculation of Complex Chemical Equilibrium Compositions, Rocket Performance, Incident and Reflected Shocks, and Chapman-Jouquet Detonations," NASA SP-273.

Table C.3 Curve-Fit Coefficients for Thermodynamic Properties of Combustion Products ($1000 \leq T \leq 3000$ K)

Species	a_1	a_2	a_3	a_4	a_5	a_6	a_7
CO_2	0.446080E + 01	0.309817E - 02	- 0.123925E - 05	0.227413E - 09	- 0.155259E - 13	- 0.489614E + 05	- 0.986359
H_2O	0.271676E + 01	0.294513E - 02	- 0.802243E - 06	0.102266E - 09	- 0.484721E - 14	- 0.299058E + 05	0.663056e + 01
N_2	0.289631E + 01	0.151548E - 02	- 0.572352E - 06	0.998073E - 10	- 0.652235E - 14	- 0.905861E + 03	0.616151e + 01
O_2	0.362195E + 01	0.736182E - 03	- 0.196522E - 06	0.362015E - 10	- 0.289456E - 14	- 0.120198E + 04	0.361509e + 01
CO	0.298406E + 01	0.148913E - 02	- 0.578996E - 06	0.103645E - 09	- 0.693535E - 14	- 0.142452E + 05	0.634791e + 01
H_2	0.310019E + 01	0.511194E - 03	0.526442E - 07	- 0.349099E - 10	0.369453E - 14	- 0.877380E + 03	- 0.196294e + 01
H	0.25E + 01	0	0	0	0	0.254716E + 05	- 0.460117
O	0.254205e + 01	- 0.275506E - 04	- 0.310280E - 08	0.455106E - 11	- 0.436805E - 15	0.292308E + 05	0.492030E + 01
OH	0.291064E + 01	0.959316E - 03	- 0.194417E - 06	0.137566E - 10	0.142245E - 15	0.393538E + 04	0.544234E + 01
NO	0.3189E + 01	0.133822E - 02	- 0.528993E - 06	0.959193E - 10	- 0.648479E - 14	0.982832E + 04	0.674581E + 01

Source: Gordon and McBride, 1971.

Appendix D

Conversion Factors and Physical Constants

Table D.1 Unit Conversion Factors

Area	1 m ²	= 1550.0 in. ² = 10.764 ft ²
Energy	1 J	= 9.4787 × 10 ⁻⁴ Btu
Energy/mass	1 kJ/kg	= 0.4303 Btu/lb _m
Force	1 N	= 0.22481 lb _f
Heat transfer rate	1 W	= 3.4123 Btu/h
Heat flux	1 W/m ²	= 0.3171 Btu/(h·ft ²)
Heat transfer coefficient	1 W/(m ² ·K)	= 0.17612 Btu/(h·ft ² °F)
Thermal diffusivity	1 m ² /s	= 3.875 × 10 ⁴ ft ² /h
Length	1 m	= 39.370 in. = 3.2808 ft = 0.62137 mile
	1 km	
Mass	1 kg	= 2.2046 lb _m
Mass density	1 kg/m ³	= 0.062428 lb _m /ft ³
Mass flow rate	1 kg/s	= 7936.6 lb _m /h
Mass transfer coefficient	1 m/s	= 1.1811 × 10 ⁴ ft/h
Power	1 kW	= 1.341 hp
Pressure and stress	1 Pa (1 N/m ²)	= 0.020886 lb _f /ft ²
	1.0133 × 10 ⁵ N/m ²	= 1 standard atmosphere = 760 mmHg
	1 × 10 ⁵ N/m ²	= 1 bar = 750.06 mmHg
Rotational speed	1 rev/min	= 0.10472 rad/s
Specific heat	1 J/(kg·K)	= 2.3886 × 10 ⁻⁴ Btu/(lb _m °F)
Temperature	K	= (5/9)°R = (5/9) (°R + 459.67) °C + 273.15
Temperature difference	1 K	= 1°C = (9/5)°R = (9/5)°F

(continued)

Table D.1 (Continued)

Thermal conductivity	1 W/(m·K)	= 0.57782 Btu/(h ft·°F)
Thermal resistance	1 K/W	= 0.52750°F/(h-Btu)
Torque	1 Nm	= 0.73756 lb _f ft
Viscosity (dynamic)	1 kg/(m·s ²)	= 2419.1 lb _m /(ft·h)
Viscosity (kinematic)	1 m ² /s	= 3.875 × 10 ⁴ ft ² /h
Volume	1 m ³ (10 ³ L)	= 6.1023 × 10 ⁴ in. ³ = 35.314 ft ³ = 264.17 gal
Volume flow rate	1 m ³ /s	= 2.1189 × 10 ³ ft ³ /min = 1.5850 × 10 ⁴ gal/min

Source: F. Incropera, D. DeWitt, T. Bergman, and A. Lavine, (2007), *Fundamentals of Heat and Mass Transfer*, John Wiley, New York.

Table D.2 Physical Constants

Universal gas constant	R_u	= 8.315 kJ/(kmol·K) = 8.314 × 10 ⁻² m ³ bar/(kmol·K) = 8.205 × 10 ⁻² m ³ atm/(kmol·K) = 1545 ft lb _f /(lbmole·°R) = 1.986 Btu/(lbmole·°R)
Avogadro's number	N	= 6.024 × 10 ²³ molecules/mol
Planck's constant	h	= 6.625 × 10 ⁻³⁴ (J·s)/molecule
Boltzmann's constant	k	= 1.380 × 10 ⁻²³ J/(K-molecule)
Speed of light in vacuum	c_0	= 2.998 × 10 ⁸ m/s
Stefan–Boltzmann constant	σ	= 5.670 × 10 ⁻⁸ W/(m ² ·K ⁴) = 0.1714 × 10 ⁻⁸ Btu/(h ft ² ·°R ⁴)
Gravitational acceleration	g	= 9.807 m/s ²
Standard atmospheric pressure	P	= 101,325 N/m ² = 101.325 kPa

Appendix E

Thermodynamic Analysis of Mixtures

E.1 THERMODYNAMIC DERIVATIVES

As shown by Bridgman (1914), any thermodynamic derivative can be expressed in terms of three independent derivatives. These derivatives are

$$\begin{aligned} \left(\frac{\partial h}{\partial T}\right) &= c_p \\ \left(\frac{\partial v}{\partial P}\right)_T & \\ \left(\frac{\partial v}{\partial T}\right)_P & \end{aligned} \quad (\text{E.1})$$

For example, γ , the ratio of specific heats, is given by

$$\gamma = \frac{c_p}{c_v} = \frac{c_p}{c_p + T(\partial v/\partial T)_P^2 / (\partial v/\partial P)_T} \quad (\text{E.2})$$

These derivatives were chosen by Bridgman as they can be determined directly by experiment. The term $(\partial v/\partial P)_T$ is the isothermal compressibility, the term $(\partial v/\partial T)_P$ is the coefficient of volumetric expansion, and the term $(\partial h/\partial T)$ is the specific heat at constant pressure. These three variables are used in this text to compute fuel–air mixture properties and perform cycle analysis.

For a gas mixture, the derivatives can be expressed as functions of pressure P , specific volume v , temperature T , and molecular mass M . Using the ideal gas law, the specific volume v of a mixture is

$$v = \frac{R_u T}{M P} \quad (\text{E.3})$$

Upon differentiation of Equation E.3 with respect to pressure P ,

$$\begin{aligned} \left(\frac{\partial v}{\partial P}\right)_T &= \frac{R_u T}{M} \frac{\partial}{\partial P} \left(\frac{1}{P}\right) + \frac{R_u T}{P} \frac{\partial}{\partial P} \left(\frac{1}{M}\right) \\ &= -\frac{v}{P} - \frac{v}{M} \frac{\partial M}{\partial P} \\ &= -\frac{v}{P} - \frac{v}{M} \sum M_i \frac{\partial y_i}{\partial P} \end{aligned} \quad (\text{E.4})$$

where

$$\frac{\partial M}{\partial P} = \sum M_i \frac{\partial y_i}{\partial P} \quad (\text{E.5})$$

and upon differentiation of Equation E.3 with respect to temperature T ,

$$\begin{aligned} \left(\frac{\partial v}{\partial T} \right)_P &= \frac{R_u}{PM} + \frac{R_u T}{P} \frac{\partial}{\partial T} \left(\frac{1}{M} \right) \\ &= \frac{v}{T} - \frac{v}{M} \frac{\partial M}{\partial T} \\ &= -\frac{v}{T} - \frac{v}{M} \sum M_i \frac{\partial y_i}{\partial T} \end{aligned} \quad (\text{E.6})$$

where

$$\frac{\partial M}{\partial T} = \sum M_i \frac{\partial y_i}{\partial T} \quad (\text{E.7})$$

Note that the important role of the changes in mole fraction with respect to pressure and temperature, $\partial y_i / \partial P$ and $\partial y_i / \partial T$, have in determination of the mixture properties and thermodynamic derivatives.

Adopting the notation used by Bridgeman (1914),

$$\left(\frac{\partial y}{\partial x} \right)_z = \frac{(\partial y)_z}{(\partial x)_z}$$

the following list can be used to construct any other required thermodynamic first derivative in terms of $c_p = \partial h / \partial T$, $\partial v / \partial P$, and $\partial v / \partial T$:

$$(\partial T)_P = -(\partial P)_T = 1$$

$$(\partial v)_P = -(\partial P)_v = \left(\frac{\partial v}{\partial T} \right)_P$$

$$(\partial s)_P = -(\partial P)_s = \frac{c_p}{T}$$

$$(\partial u)_P = -(\partial P)_u = c_p - P \left(\frac{\partial v}{\partial T} \right)_P$$

$$(\partial h)_P = -(\partial P)_h = c_p$$

$$(\partial v)_T = -(\partial T)_v = - \left(\frac{\partial v}{\partial P} \right)_T$$

$$(\partial s)_T = -(\partial T)_s = \left(\frac{\partial v}{\partial T} \right)_P$$

$$(\partial u)_T = -(\partial T)_u = T \left(\frac{\partial v}{\partial T} \right)_P + P \left(\frac{\partial v}{\partial P} \right)_T$$

$$(\partial h)_T = -(\partial T)_h = -v + T \left(\frac{\partial v}{\partial T} \right)_P$$

$$(\partial s)_v = -(\partial v)_s = \frac{c_p}{T} \left(\frac{\partial v}{\partial P} \right)_T + \left(\frac{\partial v}{\partial T} \right)_P^2$$

$$(\partial u)_v = -(\partial v)_u = c_p \left(\frac{\partial v}{\partial P} \right)_T + T \left(\frac{\partial v}{\partial T} \right)_P^2$$

$$\begin{aligned}
(\partial h)_v &= -(\partial v)_h = c_p \left(\frac{\partial v}{\partial P} \right)_T + T \left(\frac{\partial v}{\partial T} \right)_P^2 - v \left(\frac{\partial v}{\partial T} \right)_P \\
(\partial u)_s &= -(\partial s)_u = \frac{P}{T} \left[c_p \left(\frac{\partial v}{\partial P} \right)_T + T \left(\frac{\partial v}{\partial T} \right)_P^2 \right] \\
(\partial h)_s &= -(\partial s)_h = -\frac{vc_p}{T} \\
(\partial h)_u &= -(\partial u)_h = -v \left[c_p - P \left(\frac{\partial v}{\partial T} \right)_P \right] - P \left[c_p \left(\frac{\partial v}{\partial P} \right)_T + T \left(\frac{\partial v}{\partial T} \right)_P^2 \right]
\end{aligned}$$

E.2 NUMERICAL SOLUTION OF EQUILIBRIUM COMBUSTION EQUATIONS

The 4×4 nonlinear system of equations developed in Chapter 3.7 with unknowns y_3, y_4, y_5, y_6 , that is, the mole fractions of N₂, O₂, CO, H₂, respectively, is solved using Newton–Raphson iteration and Gaussian elimination.

$$f_j(y_3, y_4, y_5, y_6) = 0 \quad j = 1, 2, 3, 4 \quad (\text{E.8})$$

A first-order Taylor series expansion of the solution mole fraction vector $[y_3^*, y_4^*, y_5^*, y_6^*]$ is $y_i^* = y_i^{(1)} + \Delta y_i$, where y_i^* is a set of mole fractions reasonably close to the solution vector. The steps Δy_i are computed from the matrix equation

$$\mathbf{A}\Delta y_i = \mathbf{F} \quad (\text{E.9})$$

where \mathbf{A} is the Jacobian matrix of the partial derivative of each equation with respect to each mole fraction, $A_{ij} = \partial f_j / \partial y_i$. At each iteration denoted by k , the new y_i solution vector is thus given by

$$y_i^{k+1} = y_i^k - \mathbf{A}^{-1} \mathbf{F} \quad (\text{E.10})$$

Iteration continues until the maximum step change Δy_i is below a specified tolerance. In certain cases, Newton–Raphson iteration may run into difficulties due to the numerical precision of the computer, and the solution of the matrix equation for Δy_i may yield singularities. This behavior is reduced by introducing an underrelaxation parameter, which was determined by trial and error to be 0.05.

The elements of the Jacobian matrix \mathbf{A} are determined by first defining the following partial derivatives:

$$\begin{aligned}
D_{ij} &= \frac{\partial y_k}{\partial y_l} \quad i = 1, 2, 7, 8, 9, 10 \\
&\quad j = 3, 4, 5, 6 \\
D_{jj} &= \frac{\partial y_j}{\partial y_j} = 1
\end{aligned}$$

Performing the mole fraction differentiations yields

$$\begin{aligned}
D_{76} &= \frac{1}{2} \frac{c_1}{y_6^{1/2}} & D_{103} &= \frac{1}{2} \frac{c_4 y_4^{1/2}}{y_3^{1/2}} \\
D_{84} &= \frac{1}{2} \frac{c_2}{y_4^{1/2}} & D_{26} &= c_5 y_4^{1/2}
\end{aligned}$$

$$\begin{aligned}
 D_{94} &= \frac{1}{2} \frac{c_3 y_6^{1/2}}{y_4^{1/2}} & D_{24} &= \frac{1}{2} \frac{c_5 y_6}{y_4^{1/2}} \\
 D_{06} &= \frac{1}{2} \frac{c_3 y_4^{1/2}}{y_6^{1/2}} & D_{14} &= \frac{1}{2} \frac{c_6 y_5}{y_4^{1/2}} \\
 D_{104} &= \frac{1}{2} \frac{c_4 y_3^{1/2}}{y_4^{1/2}} & D_{15} &= c_6 y_4^{1/2}
 \end{aligned}$$

The matrix elements A_{ij} are

$$\begin{aligned}
 A_{11} &= 1 + D_{103} & A_{12} &= 1 + D_{14} + D_{24} + D_{84} + D_{104} + D_{94} \\
 A_{13} &= 1 + D_{15} & A_{14} &= 1 + D_{26} + D_{76} + D_{96} \\
 A_{21} &= 0 & A_{22} &= 2D_{24} + D_{94} - d_1 D_{14} \\
 A_{23} &= -d_1(1 + D_{15}) & A_{24} &= 2D_{26} + 2 + D_{76} + D_{96} \\
 A_{31} &= D_{103} & A_{32} &= 2 + (2 - d_2)D_{14} + D_{24} + D_{84} + D_{104} + D_{94} \\
 A_{33} &= 1 - d_2 + (2 - d_2)D_{15} & A_{34} &= D_{26} + D_{96} \\
 A_{41} &= 2 + D_{103} & A_{42} &= D_{104} + d_3 D_{14} \\
 A_{43} &= -d_3(1 + D_{15}) & A_{44} &= 0
 \end{aligned}$$

Evaluating the three thermodynamic derivatives $c_p = (\partial h / \partial T)_P$, $(\partial v / \partial T)_P$, and $(\partial v / \partial P)_T$ requires the change in the mole fractions y_i due to changes in temperature and pressure. The four independent mole fraction (y_3, y_4, y_5, y_6) derivatives with respect to temperature are

$$\frac{\partial y_3}{\partial T}, \frac{\partial y_4}{\partial T}, \frac{\partial y_5}{\partial T}, \text{ and } \frac{\partial y_6}{\partial T} \quad (\text{E.11})$$

and the remaining derivatives are expressed in terms of this independent set.

$$\begin{aligned}
 \frac{\partial y_7}{\partial T} &= y_6^{1/2} \frac{\partial c_1}{\partial T} + D_{76} \frac{\partial y_6}{\partial T} \\
 \frac{\partial y_8}{\partial T} &= y_4^{1/2} \frac{\partial c_2}{\partial T} + D_{84} \frac{\partial y_4}{\partial T} \\
 \frac{\partial y_9}{\partial T} &= y_4^{1/2} y_6^{1/2} \frac{\partial c_3}{\partial T} + D_{94} \frac{\partial y_4}{\partial T} + D_{96} \frac{\partial y_6}{\partial T} \\
 \frac{\partial y_{10}}{\partial T} &= y_4^{1/2} y_3^{1/2} \frac{\partial c_4}{\partial T} \\
 \frac{\partial y_2}{\partial T} &= y_4^{1/2} y_6 \frac{\partial c_5}{\partial T} + D_{24} \frac{\partial y_4}{\partial T} + D_{26} \frac{\partial y_6}{\partial T} \\
 \frac{\partial y_1}{\partial T} &= y_4^{1/2} y_5 \frac{\partial c_6}{\partial T} + D_{14} \frac{\partial y_4}{\partial T} + D_{15} \frac{\partial y_5}{\partial T}
 \end{aligned}$$

These four independent derivatives are found by solution of the matrix equation that results from differentiating Equation E.8 with respect to T ,

$$\frac{\partial f_j}{\partial T} + \frac{\partial f_j}{\partial y_3} \frac{\partial y_3}{\partial T} + \frac{\partial f_j}{\partial y_4} \frac{\partial y_4}{\partial T} + \frac{\partial f_j}{\partial y_5} \frac{\partial y_5}{\partial T} + \frac{\partial f_j}{\partial y_6} \frac{\partial y_6}{\partial T} = 0 \quad (\text{E.12})$$

$$j = 1, 2, 3, 4$$

In matrix form,

$$[\mathbf{A}] \left[\frac{\partial \mathbf{y}}{\partial T} \right] + \left[\frac{\partial \mathbf{f}}{\partial T} \right] = 0 \quad (\text{E.13})$$

where the matrix \mathbf{A} is identical to that used earlier to solve for the mole fractions. To evaluate $\partial f_j / \partial T$, define

$$\begin{aligned} x_1 &= \frac{y_1}{c_6} \\ x_2 &= \frac{y_2}{c_5} \\ x_k &= \frac{y_k}{c_{k-6}} \quad \text{where } k = 7, 8, 9, 10 \end{aligned} \quad (\text{E.14})$$

Note that the terms x_k are functions of y_3, y_4, y_5 , and y_6 only, so upon substitution of x_k into Equations E.8 followed by differentiation with respect to T yields the $[\partial f / \partial T]$ terms:

$$\begin{aligned} \frac{\partial f_1}{\partial T} &= \frac{\partial c_6}{\partial T} x_1 + \frac{\partial c_5}{\partial T} x_2 + \frac{\partial c_1}{\partial T} x_7 + \frac{\partial c_2}{\partial T} x_8 + \frac{\partial c_3}{\partial T} x_9 + \frac{\partial c_4}{\partial T} x_{10} \\ \frac{\partial f_2}{\partial T} &= 2 \frac{\partial c_5}{\partial T} x_2 + \frac{\partial c_1}{\partial T} x_7 + \frac{\partial c_3}{\partial T} x_9 - d_1 \frac{\partial c_6}{\partial T} x_1 \\ \frac{\partial f_3}{\partial T} &= 2 \frac{\partial c_6}{\partial T} x_1 + \frac{\partial c_5}{\partial T} x_2 + \frac{\partial c_2}{\partial T} x_8 + \frac{\partial c_3}{\partial T} x_9 + \frac{\partial c_4}{\partial T} x_{10} - d_2 \frac{\partial c_6}{\partial T} x_1 \\ \frac{\partial f_4}{\partial T} &= \frac{\partial c_4}{\partial T} x_{10} - d_3 \frac{\partial c_6}{\partial T} x_1 \end{aligned} \quad (\text{E.15})$$

From the definitions of c_i , the $\partial c_i / \partial T$ terms are

$$\begin{aligned} \frac{\partial c_1}{\partial T} &= \frac{1}{P^{1/2}} \frac{dK_1}{dT} & \frac{\partial c_4}{\partial T} &= \frac{dK_4}{dT} \\ \frac{\partial c_2}{\partial T} &= \frac{1}{P^{1/2}} \frac{dK_2}{dT} & \frac{\partial c_5}{\partial T} &= P^{1/2} \frac{dK_5}{dT} \\ \frac{\partial c_3}{\partial T} &= \frac{dK_3}{dT} & \frac{\partial c_6}{\partial T} &= P^{1/2} \frac{dK_6}{dT} \end{aligned} \quad (\text{E.16})$$

As discussed in Chapter 3, the curve-fit equations for the equilibrium coefficients K_i are of the form

$$\log_{10} K_i(T) = A_i \ln(T/1000) + \frac{B_i}{T} + C_i + D_i T + E_i T^2 \quad (\text{E.17})$$

where T is in Kelvin. Differentiation of Equation E.17 with respect to temperature yields

$$\frac{dK_i}{dT} = 2.302585 K_i \left[\frac{A}{T} - \frac{B}{T^2} + D + 2ET \right] \quad (\text{E.18})$$

The evaluation of the mole fraction partial derivatives with respect to pressure parallels the development of the temperature derivatives, with $\partial/\partial P$ replacing $\partial/\partial T$. Note that since neither c_3 nor c_4 depend on pressure, the terms containing $\partial c_3/\partial P$ and $\partial c_4/\partial P$ are zero. The remaining derivatives are

$$\begin{aligned}\frac{\partial c_1}{\partial P} &= -\frac{1}{2} \frac{c_1}{P} & \frac{\partial c_5}{\partial P} &= \frac{1}{2} \frac{c_5}{P} \\ \frac{\partial c_2}{\partial P} &= -\frac{1}{2} \frac{c_2}{P} & \frac{\partial c_6}{\partial P} &= -\frac{1}{2} \frac{c_6}{P}\end{aligned}\quad (\text{E.19})$$

E.3 ISENTROPIC COMPRESSION/EXPANSION WITH KNOWN ΔP

For an isentropic from pressure P_1 to P_2 , such as an exhaust blowdown, it follows that $s_2 = s_1$. To find the unknown final temperature T_2 , an iteration is required. We use an efficient numerical root finding routine, the Newton–Raphson method. First, we define the function f

$$f(T_2) = s_2 - s(T_2, P_2) \quad (\text{E.20})$$

and then find the temperature T_2 where the function $f(T_2) = 0$, since P_2 is known. Denote the correct temperature as T_2^* and let $T_2^{(1)}$ represent a first approximation to T_2^* . The function $f(T_2)$ can be expanded into a Taylor series about T_2^* . Let $\Delta T = T_2^* - T_2^{(1)}$, then neglecting higher order terms, one obtains

$$f + \frac{\partial f}{\partial T} \Delta T = 0 \quad (\text{E.21})$$

The derivative is evaluated at $T_2^{(1)}$ and can be expressed by variables returned by FARG and ECP.

The derivative required in Equation E.21 is

$$\frac{\partial f}{\partial T} = - \left(\frac{\partial s}{\partial T} \right)_P = -\frac{c_p}{T} \quad (\text{E.22})$$

Upon substitution into Equation E.21,

$$\Delta T = \frac{f T_2}{c_{p2}} \quad (\text{E.23})$$

Hence, an improved estimate of the temperature is given by

$$T_2^{(2)} = T_2^{(1)} + \frac{f T_2^{(1)}}{c_{p2}} \quad (\text{E.24})$$

By substituting this second approximation into Equation E.23, an improved estimate of ΔT is obtained. This procedure is repeated until ΔT is less than a specified tolerance. This procedure converges rapidly, and the number of iterations is about 5–10 for the tolerances used in the programs.

E.4 ISENTROPIC COMPRESSION/EXPANSION WITH KNOWN Δv

For an isentropic process such as compression or expansion from specific volume v_1 to v_2 , it also follows that $s_2 = s_1$. We write two equations for the two unknowns T_2 and P_2 :

$$\begin{aligned} s_2 - s(T_2, P_2) &= 0 \\ v_2 - v(T_2, P_2) &= 0 \end{aligned} \quad (\text{E.25})$$

Using Newton–Raphson iteration, we define the following two functions f_1 and f_2 :

$$\begin{aligned} f_1(T_2, P_2) &= s_2 - s(T_2, P_2) \\ f_2(T_2, P_2) &= v_2 - v(T_2, P_2) \end{aligned} \quad (\text{E.26})$$

We denote the temperature T and pressure P where f_1 and f_2 equal zero as T_2^* , and P_2^* . Let $T_2^{(1)}$ represent a first estimate of T_2^* , and $P_2^{(1)}$ represent the first estimate of P_2^* . The functions f_1 and f_2 can be expanded into a Taylor series about T_2^* and P_2^* . If we let $\Delta T = T_2^* - T_2^{(1)}$ and $\Delta P = P_2^* - P_2^{(1)}$, and neglect higher order terms, we obtain

$$\begin{aligned} f_1 + \frac{\partial f_1}{\partial T} \Delta T + \frac{\partial f_1}{\partial P} \Delta P &= 0 \\ f_2 + \frac{\partial f_2}{\partial T} \Delta T + \frac{\partial f_2}{\partial P} \Delta P &= 0 \end{aligned} \quad (\text{E.27})$$

The derivatives in Equation E.27 can be expressed in terms of the three derivatives c_p , $\left(\frac{\partial v}{\partial P}\right)_T$, and $\left(\frac{\partial v}{\partial T}\right)_P$ computed by the programs FARG and ECP:

$$\begin{aligned} \frac{\partial f_1}{\partial T} &= -\left(\frac{\partial s}{\partial T}\right)_P = -\frac{c_p}{T} \\ \frac{\partial f_1}{\partial P} &= -\left(\frac{\partial s}{\partial P}\right)_T = \left(\frac{\partial v}{\partial T}\right)_P \end{aligned} \quad (\text{E.28})$$

$$\begin{aligned} \frac{\partial f_2}{\partial T} &= -\left(\frac{\partial v}{\partial T}\right)_P \\ \frac{\partial f_2}{\partial P} &= -\left(\frac{\partial v}{\partial P}\right)_T \end{aligned} \quad (\text{E.29})$$

Upon substitution into Equation E.27, and solving for ΔT and ΔP ,

$$\Delta T = \frac{(\partial v / \partial P)_T f_1 + (\partial v / \partial T)_P f_2}{c_p / T (\partial v / \partial P)_T + (\partial v / \partial T)_P^2} \quad (\text{E.30})$$

$$\Delta P = \frac{-(\partial v / \partial T)_P f_1 + c_p / T f_2}{c_p / T (\partial v / \partial P)_T + (\partial v / \partial T)_P^2} \quad (\text{E.31})$$

An improved estimate of T_2 and P_2 is

$$\begin{aligned} T_2^{(2)} &= T_2^{(1)} + \Delta T \\ P_2^{(2)} &= P_2^{(1)} + \Delta P \end{aligned} \quad (\text{E.32})$$

By substituting these second approximations into Equation E.30, new values of ΔT and ΔP are obtained. This procedure is repeated until ΔT and ΔP are less than a specified

tolerance. This procedure converges rapidly, and the number of iterations is about 5–10 for the tolerances used in the programs.

E.5 CONSTANT VOLUME COMBUSTION

If the combustion process from state 2 to 3 is assumed to be constant volume and adiabatic, it also follows that $u_3 = u_2$, and the increase in T and P is due to the change in chemical composition from an unburned fuel–air mixture to an equilibrium combustion product mixture. Using the same numerical Newton–Raphson procedure as used in the compression/expansion analyses, but with the constant thermodynamic parameters being u and v instead of s and v , we first write two equations for the two unknowns T_3 and P_3 :

$$\begin{aligned} u_3 - u(T_3, P_3) &= 0 \\ v_3 - v(T_3, P_3) &= 0 \end{aligned} \quad (\text{E.33})$$

We then define the following two functions f_1 and f_2 :

$$\begin{aligned} f_1(T_3, P_3) &= u_3 - u(T_3, P_3) \\ f_2(T_3, P_3) &= v_3 - v(T_3, P_3) \end{aligned} \quad (\text{E.34})$$

To find where f_1 and f_2 are zero, we denote the correct temperature as T_3^* , the correct pressure as P_3^* , let $T_3^{(1)}$ represent a first estimate of T_3^* , and $P_3^{(1)}$ represent the first estimate of P_3^* . The functions f_1 and f_2 can be expanded into a Taylor series about T_3^* and P_3^* . If we let $\Delta T = T_3^* - T_3^{(1)}$ and $\Delta P = P_3^* - P_3^{(1)}$, then neglecting higher order terms, one obtains Equation E.27.

The derivatives in Equation E.27 can be expressed in terms of the three derivatives c_p , $\left(\frac{\partial v}{\partial T}\right)_P$, and $\left(\frac{\partial v}{\partial P}\right)_T$ computed by FARG and ECP:

$$\begin{aligned} \frac{\partial f_1}{\partial T} &= \left(\frac{\partial u}{\partial T}\right)_P = c_p - P \left(\frac{\partial v}{\partial T}\right)_P \\ \frac{\partial f_1}{\partial P} &= - \left(\frac{\partial u}{\partial P}\right)_T = -T \left(\frac{\partial v}{\partial T}\right)_P - P \left(\frac{\partial v}{\partial P}\right)_T \\ \frac{\partial f_2}{\partial T} &= - \left(\frac{\partial v}{\partial T}\right)_P \\ \frac{\partial f_2}{\partial P} &= - \left(\frac{\partial v}{\partial P}\right)_T \end{aligned} \quad (\text{E.35})$$

Upon substitution into Equation E.35, and solving for ΔT and ΔP ,

$$\Delta T = \frac{(-\partial v/\partial P)_T f_1 - [P(\partial v/\partial P)_T + T(\partial v/\partial T)_P] f_2}{c_p(\partial v/\partial P)_T + T(\partial v/\partial T)_P^2} \quad (\text{E.36})$$

$$\Delta P = \frac{(\partial v/\partial T)_P f_1 + [P(\partial v/\partial T)_P - c_p] f_2}{c_p(\partial v/\partial P)_T + T(\partial v/\partial T)_P^2} \quad (\text{E.37})$$

An improved estimate of T_3 and P_3 is

$$\begin{aligned} T_3^{(2)} &= T_3^{(1)} + \Delta T \\ P_3^{(2)} &= P_3^{(1)} + \Delta P \end{aligned} \quad (\text{E.38})$$

By substituting these second approximations into Equations E.36 and E.37, new values of ΔT and ΔP are obtained. This procedure is repeated until ΔT and ΔP are less than a specified tolerance. This procedure converges rapidly, and the number of iterations is about 5–10 for the tolerances used in the programs.

E.6 QUALITY OF EXHAUST PRODUCTS

The exhaust products can include water both in the vapor and in the liquid states. To obtain the equilibrium quality χ_{eq} of the exhaust products, we assume the partial pressure of the water vapor is equal to the saturation pressure corresponding to the mixture temperature, that is,

$$\frac{n_{\text{H}_2\text{O,g}}}{n_g} = \frac{P_{\text{sat}}}{P} \quad (\text{E.39})$$

where n_g is the number of moles of exhaust products in the gas phase. The total number of moles of exhaust products, n is the sum of the gas phase and liquid phase moles,

$$n = n_g + n_{\text{H}_2\text{O,f}} \quad (\text{E.40})$$

and since

$$n_{\text{H}_2\text{O}} = n_{\text{H}_2\text{O,f}} + n_{\text{H}_2\text{O,g}} \quad (\text{E.41})$$

we have

$$n_{\text{H}_2\text{O,g}} = (n - n_{\text{H}_2\text{O}}) \left(\frac{P}{P_{\text{sat}}} - 1 \right)^{-1} \quad (\text{E.42})$$

Therefore, for an equilibrium mixture of products,

$$\begin{aligned} \chi_{\text{eq}} &= \frac{n_{\text{H}_2\text{O,g}}}{n_{\text{H}_2\text{O}}} \\ &= \left(\frac{1}{y_{\text{H}_2\text{O}}} - 1 \right) \left(\frac{P}{P_{\text{sat}}} - 1 \right)^{-1} \end{aligned} \quad (\text{E.43})$$

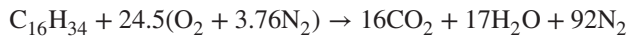
If the combustion is stoichiometric, using the chemical formula of the fuel represented by $\text{C}_a\text{H}_b\text{O}_c\text{N}_d$, the equilibrium quality χ_{eq} can be expressed as

$$\chi_{\text{eq}} = \left(\frac{9.52a + 1.88b - 3.76c + d}{b} \right) \left(\frac{P}{P_{\text{sat}}} - 1 \right)^{-1} \quad (\text{E.44})$$

EXAMPLE E.1: *Quality of Exhaust Products*

Compute the quality χ_{eq} of the water in exhaust products for the stoichiometric combustion of cetane. Assume the exhaust products are at standard reference conditions $P = P_0 = 1$ bar and $T_0 = 298.15$ K.

SOLUTION The stoichiometric combustion equation per mole of cetane ($a = 16$, $b = 34$, $c = 0$, and $d = 0$) is



At 298.15 K, the saturation pressure P_{sat} of water vapor is 3.17 kPa, so upon substitution in Equation E.43, we have

$$\chi_{\text{eq}} = \left(\frac{9.52(16) + 1.88(34) - 0 + 0}{34} \right) \left(\frac{101.3}{3.169} - 1 \right)^{-1} = 0.208$$

E.7 REFERENCES

Bridgman, P. (1914), "A Complete Collection of Thermodynamic Formulas," *Phys. Rev.*, Vol. 3, pp. 273–281.

Appendix F

Computer Programs

The MATLAB® programs contained in this section are listed below. The programs are also available online at the John Wiley web site and at www.engr.colostate.edu/allan/engineers.html.

- Volume.m** Computes and plots the exact and approximate cylinder volume versus crank angle.
- Velocity.m** Computes and plots the piston velocity versus crank angle.
- BurnFraction.m** Computes and plots the burn fraction versus crank angle.
- FiniteHeatRelease.m** Computes pressure profile, work, efficiency, and imep for a given burn profile.
- FiniteHeatMassLoss.m** Computes pressure profile, work, efficiency, and imep, including heat and mass loss.
- FourStrokeOtto.m** Computes volumetric and thermal efficiency, residual fraction, and states for four-stroke Otto engine.
- RunFarg.m** Input/output file for fuel–air–residual gas mixture program farg.m.
- farg.m** Computes mole fractions and thermodynamic properties of a fuel–air–residual gas mixture.
- fuel.m** Fuel property file.
- RunEcp.m** Input/output file for program ecp.m.
- ecp.m** Computes mole fractions and thermodynamic properties for equilibrium combustion of fuel–air mixture.
- AdiabaticFlameTemp.m** Computes constant pressure adiabatic flame temperature of a fuel–air mixture.
- OttoFuel.m** Computes states, work, imep, efficiency of an Otto fuel–air cycle.
- FourStrokeFuelAir.m** Computes states, work, imep, efficiency for a four-stroke Otto fuel–air cycle.
- Homogeneous.m** Computes states, work, imep, efficiency and NO of a two-zone heat release fuel–air cycle.
- Friction.m** Computes component and overall friction mean effective pressure.
- WoschniHeatTransfer.m** Computes pressure profile, work, efficiency, and imep, including Woschni heat and mass loss.

F.1 VOLUME.M

```

function [ ]=Volume( )
clear();
r = 10; % compression ratio
s = 80; % stroke (cm)
len= 120; %connecting rod length (cm)
ep=s/(2*len);
theta=-180:1:180; %crankangle theta vector
ys1=(1-cosd(theta))/2; %approx y/s
ys2= ys1+ (1-(1- ep^2*sind(theta).^2).^(1/2))/(2*ep); %exact y/s
vol1 = 1+(r-1)*ys1; %approx volume
vol2= 1+(r-1)*ys2; % exact volume
%plot results
plot(theta,vol1,'--',theta,vol2,'-','linewidth',2);
set(gca,'Xlim',[-180 180],'Ylim',[0 r],'fontsize',18,'linewidth',2);
xlabel('Crank Angle (deg)', 'fontsize', 18);
ylabel('Dim. Cylinder Volume', 'fontsize', 18);
legend('Approx. Volume', 'Exact Volume', 'Location', 'North');
end

```

F.2 VELOCITY.M

```

function [ ]=Velocity( )
clear();
N=2000; %rev/min
s = 0.080; % stroke (m)
len= 0.120; %connecting rod length (m)
ep=s/(2*len);
theta=0:1:180; %crankangle theta vector
term1=pi/2*sind(theta);
term2= (1+(ep*cosd(theta))./(1 - ep^2*sind(theta).^2)).^(1/2); %exact y/s
Upbar=term1.*term2;
Up=Upbar*2*N*s/60;
%plot results
plot(theta,Up,'linewidth',2);
set(gca,'Xlim',[0 180],'fontsize',18,'linewidth',2);
xlabel('Crank Angle (deg)', 'fontsize', 18);
ylabel(' Piston Velocity (m/s)', 'fontsize', 18);
end

```

F.3 BURNFRACTION.M

```

function [ ]=BurnFraction( )
% this program computes and plots the cumulative burn fraction
% and the instantaneous burnrate
clear();

```

```

a = 5; % Weibe efficiency factor
n = 3; % Weibe form factor
thetas = -20; % start of combustion
thetad = 60; % duration of combustion
theta=linspace(thetas,thetas+thetad,100); %crankangle theta vector
dum=(theta-thetas)/thetad; % theta difference vector
temp=-a*dum.^n;
xb=1.-exp(temp); %burn fraction
dxb=n*a*(1-xb).*dum.^(n-1); %element by element vector multiplication
%plot results
plot(theta,xb,'b','linewidth',2);
set(gca, 'fontsize', 18,'linewidth',2);
xlabel('Crank Angle (deg)', 'fontsize', 18);
ylabel('Cumulative Burn Fraction', 'fontsize', 18);
figure();
plot(theta,dxb,'b','linewidth',2);
set(gca, 'fontsize', 18,'linewidth',2);
xlabel('Crank Angle (deg)', 'fontsize', 18);
ylabel('Burn Rate (1/deg)', 'fontsize', 18);
end

```

F.4 FINITEHEATRELEASE.M

```

function [ ]=FiniteHeatRelease()
% Gas cycle heat release code for two engines
% engine parameters
clear();
thetas(1,1)= -10; % Engine1 start of heat release (deg)
thetas(2,1)= -10; % Engine2 start of heat release (deg)
thetad(1,1) = 40; % Engine1 duration of heat release (deg)
thetad(2,1) = 10; % Engine2 duration of heat release (deg)
r=10; %compression ratio
gamma= 1.4; %gas const
q= 34.8; % dimensionless total heat release Qin/P1V1
a= 5; %weibe parameter a
n= 3; %weibe exponent n
step=1; % crankangle interval for calculation/plot
NN=360/step; % number of data points
% initialize the results data structure
save.theta=zeros(NN,1); % crankangle
save.vol=zeros(NN,1); % volume
save.press=zeros(NN,2); % pressure
save.work=zeros(NN,2); % work
pinit(1) = 1; % Engine 1 initial dimensionless pressure P/P1
pinit(2) = 1; % Engine 2 initial dimensionless pressure P/P1
% for loop for engine1 and engine2
for j=1:2

```

```

theta = -180;           %initial crankangle
thetae = theta + step; %final crankangle in step
fy(1) = pinit(j); % assign initial pressure to working vector
fy(2) = 0.;          % reset work vector
% for loop for pressure and work calculation
for i=1:NN,
    [fy, vol] = integrate(theta,thetae,fy);
    % reset to next interval
    theta = thetae;
    thetae = thetae+step;
    % copy results to output vectors
    save.theta(i)=theta;
    save.vol(i)=vol;
    save.press(i,j)=fy(1);
    save.work(i,j)=fy(2);
end %end of pressure and work iteration loop
end %end of engine iteration loop
[pmax1, id_max1] = max(save.press(:,1)); %Engine 1 max pressure
[pmax2, id_max2] = max(save.press(:,2)); %Engine 2 max pressure
thmax1=save.theta(id_max1);%Engine 1 crank angle
thmax2=save.theta(id_max2);%Engine 2 crank angle
w1=save.work(NN,1);
w2=save.work(NN,2);
eta1= w1/q; % thermal efficiency
eta2= w2/q;
imep1 = eta1*q*(r/(r -1)); %imep
imep2 = eta2*q*(r/(r -1));
eta_rat1 = eta1/(1-r^(1-gamma));
eta_rat2 = eta2/(1-r^(1-gamma));
% output overall results
fprintf('                         Engine 1             Engine 2 \n');
fprintf(' Theta_start   %5.2f   %5.2f \n', thetas(1,1), thetas(2,1));
fprintf(' Theta_dur     %5.2f   %5.2f \n', thetad(1,1), thetad(2,1));
fprintf(' P_max/P_1     %5.2f       %5.2f \n', pmax1, pmax2);
fprintf(' Theta_max     %7.1f       %7.1f \n', thmax1,thmax2);
fprintf(' Net Work/P1V1  %7.2f       %7.2f \n', w1,w2);
fprintf(' Efficiency     %5.3f       %5.3f \n', eta1, eta2);
fprintf(' Eff. Ratio     %5.3f       %5.3f \n', eta_rat1, eta_rat2);
fprintf(' Imep/P1        %5.2f       %5.2f \n', imep1, imep2);
%plot results
plot(save.theta,save.press(:,1),'-','...
      save.theta,save.press(:,2),'--','linewidth',2 )
set(gca, 'fontsize', 18,'linewidth',2);
legend('Engine 1', 'Engine 2','Location','NorthWest')
xlabel('Theta (deg)', 'fontsize', 18)
ylabel('Pressure (bar)', 'fontsize', 18)
print -deps2 heatrelpressure

```

```

figure( );
plot(save.theta,save.work(:,1),'-', ...
      save.theta,save.work(:,2),'--', 'linewidth',2)
set(gca, 'fontsize', 18,'linewidth',2);
legend('Engine 1', 'Engine 2','Location','NorthWest')
xlabel('Theta (deg)', 'fontsize', 18)
ylabel('Work', 'fontsize', 18)
function [fy,vol] = integrate(theta,thetae,fy)
%ode23 integration of the pressure differential equation
%from theta to thetae with current values of fy as initial conditions
[tt, yy] = ode23(@rates, [theta thetae], fy);
for k=1:2
    fy(k) = yy(length(tt),k); %put last element of yy into fy vector
end
%pressure differential equation
function [yprime] = rates(theta,fy)
vol=(1.+ (r -1)/2.* (1-cosd(theta)))/r;
dvol=(r - 1)/2.*sind(theta)/r*pi/180.; %dvol/dtheta
dx=0.; %set heat release to zero
if(theta > thetas(j)) % then heat release dx > 0
    dum1=(theta -thetas(j))/thetad(j);
    x=1.- exp(-(a*dum1^n));
    dx=(1-x)*a*n*dum1^(n-1)/thetad(j); %dx/dtheta
end
term1= -gamma*fj(1)*dvol/vol;
term2= (gamma-1)*q*dx/vol;
yprime(1,1)= term1 + term2;
yprime(2,1)= fy(1)*dvol;
end %end of function rates
end %end of function integrate2
end % heat_release_weibe2

```

F.5 FINITEHEATMASSLOSS.M

```

function [ ] = FiniteHeatMassLoss( )
% Gas cycle heat release code with and w/o heat transfer
% data structure for engine parameters
clear();
thetas = -20; % start of heat release (deg)
thetad = 40; % duration of heat release (deg)
r =10; % compression ratio
gamma = 1.4; % gas const
Q = 20.; % dimensionless total heat release
h = 0.2; % dimensionless ht coefficient
tw = 1.2; % dimensionless cylinder wall temp
beta = 1.5; % dimensionless volume
a = 5; % weibe parameter a

```

```

n = 3;          % weibe exponent n
omega =200.;   % engine speed rad/s
c = 0.8;        % mass loss coeff
step=1;         % crankangle interval for calculation/plot
NN=360/step;   % number of data points
theta = -180;  % initial crankangle
thetae = theta + step; % final crankangle in step
% initialize results data structure
save.theta=zeros(NN,1);
save.vol=zeros(NN,1);    % volume
save.press=zeros(NN,1);  % pressure
save.work=zeros(NN,1);   % work
save.heatloss=zeros(NN,1); % heat loss
save.mass=zeros(NN,1);   % mass left
fy=zeros(4,1); % vector for pressure, work, heat and mass loss
fy(1) = 1; % initial pressure (bar)
fy(4) = 1; % initial mass (-)
%for loop for pressure and work calculation
for i=1:NN,
[fy, vol] = integrate_ht(theta,thetae,fy);
% print values
% fprintf('%7.1f %7.2f %7.2f %7.2f \n', theta,vol,fy(1),fy(2),fy(3));
% reset to next interval
theta = thetae;
thetae = thetae+step;
save.theta(i)=theta; % put results in output vectors
save.vol(i)=vol;
save.press(i)=fy(1);
save.work(i)=fy(2);
save.heatloss(i)=fy(3);
save.mass(i)=fy(4);
end % end of pressure and work for loop
[pmax, id_max] = max(save.press(:,1)); % find max pressure
thmax=save.theta(id_max);           % and crank angle
ptdc=save.press(NN/2)/pmax;
w=save.work(NN,1);      % w is cumulative work
massloss =1- save.mass(NN,1);
eta=w/Q;                % thermal efficiency
imep = eta*Q*(r/(r - 1)); %imep/P1V1
eta_rat = eta/(1-r^(1-gamma));
% output overall results
fprintf(' Weibe Heat Release with Heat and Mass Loss \n');
fprintf(' Theta_start =      %5.2f \n', thetas);
fprintf(' Theta_dur =       %5.2f \n', thetad);
fprintf(' P_max/P1 =       %5.2f \n', pmax);
fprintf(' Theta @P_max =   %7.1f \n',thmax);
fprintf(' P_tdc/P_max =   %5.2f \n', ptdc);

```

```

fprintf(' Net Work/P1V1 = %7.2f \n', w);
fprintf(' Heat Loss/P1V1 = %7.2f \n', save.heatloss(NN,1));
fprintf(' Mass Loss/m = %7.3f \n', massloss );
fprintf(' Efficiency = %5.3f \n', eta);
fprintf(' Eff./Eff. Otto = %5.3f \n', eta_rat);
fprintf(' Imep/P1 = %5.2f \n', imep);

%plot results
plot(save.theta,save.press,'-','linewidth',2 )
set(gca, 'fontsize', 18,'linewidth',1.5);
xlabel('Crank Angle \theta (deg)', 'fontsize', 18)
ylabel('Pressure P (bar)', 'fontsize', 18)
figure();

plot(save.theta,save.work,'-',save.theta,save.heatloss,'--','linewidth',2 )
set(gca, 'Xlim',[ -180 180], 'fontsize', 18,'linewidth',1.5);
hleg1=legend('Work', 'Heat Loss', 'Location', 'NorthWest')
set(hleg1,'Box', 'off')
xlabel('Crank Angle \theta (deg)', 'fontsize', 18)
ylabel('Cumulative Work and Heat Loss', 'fontsize', 18)

function[fy,vol] = integrate_ht(theta,thetae,fy)
% ode23 integration of the pressure differential equation
% from theta to thetae with current values of fy as initial conditions
[tt, yy] = ode23(@rates, [theta thetae], fy);
% put last element of yy into fy vector
for j=1:4
    fy(j) = yy(length(tt),j);
end
% pressure differential equation
function [yprime] = rates(theta,fy)
vol=(1.+ (r -1)/2.* (1-cosd(theta)))/r;
dvol=(r - 1)/2.*sind(theta)/r*pi/180.; %dvol/dtheta
dx=0.;
if(theta>thetas) % heat release >0
    dum1=(theta -thetas)/thetad;
    x=1-exp(- (a*dum1^n));
    dx=(1-x)*a*n*dum1^(n-1)/thetad; %dx/dtheta
end
term1= -gamma*f(1)*dvol/vol;
term3= h*(1. + beta*vol)*(f(1)*vol/f(4) - tw)*pi/180.;
term2= (gamma-1)/vol*(Q*dx - term3);
yprime(1,1)= term1 + term2 - gamma*c/omega*f(1)*pi/180;
yprime(2,1)= f(1)*dvol;
yprime(3,1)= term3;
yprime(4,1)= -c*f(4)/omega*pi/180;
end %end of function rates
end % end of function integrate_ht
end % end of function HeatReleaseHeatTransfer

```

F.6 FOURSTROKEOTTO.M

```
% Four stroke Otto cycle model
% input parameters
Ti = 300; % inlet temperature, K
Pi = 50; % inlet pressure, kPa
Pe = 100; % exhaust pressure, kPa
r = 10; % compression ratio
qin = 2500; % heat input, kJ/kg (mixture)
gamma = 1.3; % ideal gas specific heat ratio
R = 0.287; % gas constant kJ/kg K
cv= R/(gamma-1); %const vol specific heat, kJ/kg K
f=0.05;% guess value of residual fraction f
Tr = 1000; % guess value of exhaust temp, K
tol=0.001; % tolerance for convergence
err = 2*tol; %error initialization
gam=(gamma -1)/gamma;
while (err > tol) %while loop for cycle calc
%intake stroke
T1=(1-f)*Ti + f*(1 - (1- Pi/Pe)*gam)*Te;
P1=Pi;
%isentropic compression
P2=P1*r^gamma;
T2=T1*r^(gamma-1);
%const v heat addition
T3=T2 + qin*(1-f)/cv;
P3=P2*(T3/T2);
%isentropic expansion
P4=P3*(1/r)^gamma;
T4=T3*(1/r)^(gamma-1);
%isentropic blowdown
P5=Pe;
T5=T4*(P4/Pe)^(-gam);
%const p exhaust stroke
Te=T5;
fnew=(1/r)*(Pe/P4)^(1/gamma); %new residual fraction
err=abs(fnew-f)/fnew;
f=fnew;
end
%cycle parameters
eta= 1 - 1/r^(gamma-1);
imep = P1*(qin*(1-f)/(R*T1))/(1-(1/r))*eta;
pmep=Pe-Pi;
etanet= eta*(1-pmep/imep);
imepnet= (imep-pmep)/100.;
voleff=1-(Pe/Pi -1)/(gamma*(r-1));
%output calcs
fprintf(' \nFour Stroke Otto Cycle \n')
```

```

fprintf('State          1          2          3          4 \n');
fprintf('Pressure (kPa): %6.1f %6.1f %6.1f %6.1f \n',P1,P2,P3,P4);
fprintf('Temperature (K): %6.1f %6.1f %6.1f %6.1f \n',T1,T2,T3,T4);
fprintf('Ideal Thermal Eff.= %6.3f      Net Thermal Eff.= %6.3f \n', ...
        eta, etanet);
fprintf('Exhaust Temp. (K)= %6.1f      Volumetric Eff.= %6.2f \n', ...
        Te, voleff);
fprintf('Residual Fraction %6.3f      Net Imep (bar)= %6.2f \n',...
        f, imepnet);

```

F.7 RUNFARG.M

```

%Input-Output program for running farg.m
clear;
T = 500; % enter temperature (K) input
P = 100.; % enter pressure (kPa) input
phi = 0.8; % enter equivalence ratio input
f=0.1; %residual fraction input
fuel_id = 1;
% fuel_id - 1=Methane, 2=Gasoline, 3=Diesel, 4=Methanol, 5=Nitromethane
% call farg function
[Y,h,u,s,v,R,Cp,MW,dvdT,dvdP,dMWdT,dMWdP] = farg( T, P, phi, f, fuel_id );
%echo input
fprintf(' \n Fuel Air Residual Gas \n' );
fprintf(' Pressure (kPa) = %6.1f \n', P );
fprintf(' Temperature (K) = %6.1f \n', T); ...
fprintf(' Fuel Air Equivalence ratio = % 3.1f \n', phi);
fprintf(' Residual Fraction = \t% 3.1f \n ', f);
%print output mole fractions and properties
fprintf(' \n Mole Fractions \n' );
fprintf(' CO2 = \t %6.4f \n', Y(1));
fprintf(' H2O = \t %6.4f \n', Y(2));
fprintf(' N2 = \t %6.4f \n', Y(3));
fprintf(' O2 = \t %6.4f \n', Y(4));
fprintf(' CO = \t %6.4f \n', Y(5));
fprintf(' H2 = \t %6.4f \n', Y(6));
fprintf(' H = \t %6.4f \n', Y(7));
fprintf(' O = \t %6.4f \n', Y(8));
fprintf(' OH = \t %6.4f \n', Y(9));
fprintf(' NO = \t %6.4f \n', Y(10));
fprintf(' \n Mixture Properties \n' );
fprintf(' h(kJ/kg) = \t %6.1f \n', h );
fprintf(' u(kJ/kg) = \t %6.1f \n', u );
fprintf(' s (kJ/Kg K) = \t %6.3f \n', s );
fprintf(' v (m3/kg) = \t %6.3f \n', v );
fprintf(' Cp (kJ/Kg K) =\t %6.3f \n', Cp );
fprintf(' Molecular Mass = %5.2f \n', MW );

```

```
fprintf(' dvdt = %8.2e \n', dvdT );
fprintf(' dvdp = %8.2e \n', dvdP );
```

F.8 FARG.M

```
function [Y,h,u,s,v,R,Cp,MW,dvdT,dvdP]=farg(T,P,phi,f,fuel_id)
% Subroutine for Fuel Air Residual Gas
%
% inputs:
%   T - temperature (K)  [ 300 --> 1000 K ]
%   P - pressure (kPa)
%   phi - equivalence ratio
%   f - residual fraction
%   fuel_id - 1=Methane, 2=Gasoline, 3=Diesel, 4=Methanol, 5=Nitromethane
%
% outputs:
%   y - mole fraction of constituents
%     y(1) : CO2
%     y(2) : H2O
%     y(3) : N2
%     y(4) : O2
%     y(5) : CO
%     y(6) : H2
%   h - specific enthalpy of mixture, kJ/kg
%   u - specific internal energy of mixture, kJ/kg
%   s - specific entropy of mixture, kJ/kgK
%   v - specific volume of mixture, m3/kg
%   r - specific ideal gas constant, kJ/kgK
%   cp - specific heat at constant pressure, kJ/kgK
%   mw - molecular weight of mixture, kg/kmol
%   dvdT - (dv/dT) at const P, m3/kg per K
%   dvdP - (dv/dP) at const T, m3/kg per kPa
% Get fuel composition information
[alpha,beta,gamma,delta,h_fuel,so_fuel,cp_fuel,m_fuel ]=fuel( fuel_id, T );
% Curve fit coefficients for thermodynamic properties
% 300 < T < 1000 K
% Cp/R = a1 + a2*T + a3*T^2 + a4*T^3 + a5*T^4
% h/RT = a1 + a2/2*T + a3/3*T^2 + a4/4*T^3 + a5/5*T^4 + a6/T
% so/R = a1*ln(T) + a2*T + a3/2*T^2 + a4/3*T^3 + a5/4*T^4 + a7
A = [ [ 0.24007797e+1, 0.87350957e-2, -0.66070878e-5, 0.20021861e-8,
0.63274039e-15, -0.48377527e+5, 0.96951457e+1 ]; ... % CO2
      [ 0.40701275e+1, -0.11084499e-2, 0.41521180e-5, -0.29637404e-8,
0.80702103e-12, -0.30279722e+5, -0.32270046 ]; ... % H2O
      [ 0.36748261e+1, -0.12081500e-2, 0.23240102e-5, -0.63217559e-9,
-0.2257725e-12, -0.10611588e+4, 0.23580424e+1 ]; ... % N2
      [ 0.36255985e+1, -0.18782184e-2, 0.70554544e-5, -0.67635137e-8,
0.21555993e-11, -0.10475226e+4, 0.43052778e+1 ]; ... % O2
```

```

[ 0.37100928e+1, -0.16190964e-2,  0.36923594e-5, -0.20319674e-8,
0.23953344e-12, -0.14356310e+5,  0.2955535e+1 ] ; ... % CO
[ 0.30574451e+1,  0.26765200e-2, -0.58099162e-5,  0.55210391e-8,
-0.1812273e-11, -0.98890474e+3, -0.22997056e+1 ] ; % H2
% molar mass of constituents
%      CO2      H2O      N2      O2      CO      H2
Mi = [ 44.01,  18.02,  28.013,  32.00,  28.01,  2.016 ];
% Calculate stoichiometric molar air-fuel ratio
a_s = alpha + beta/4 - gamma/2;
% mole fraction of fuel, O2, N2
y_1 = 1 / (1 + 4.76*a_s/phi); % mole fraction for one mole of reactant
y_fuel = y_1; % assuming 1 mole fuel
y_O2 = a_s/phi * y_1; % a_s/phi moles O2
y_N2 = a_s/phi*3.76 * y_1; % a_s/phi * 3.76 moles N2
% mass of fuel air mixture (M'')
m_fa = y_fuel*m_fuel + y_O2*32.00 + y_N2*28.013;
% default case: no residual gas
Y = zeros(6,1);
m_r = 0; % mass of residual gas
y_r = 0; % mole fraction of residual gas in mixture
n = zeros(6,1);
dcdt = 0;
if ( phi <= 1 )
    % lean combustion
    n(1) = alpha;
    n(2) = beta/2;
    n(3) = delta/2 + 3.76*a_s/phi;
    n(4) = a_s*(1/phi - 1);
else
    % rich combustion
    d1 = 2*a_s*(1-1/phi);
    z = T/1000;
    K = exp( 2.743 - 1.761/z - 1.611/z^2 + 0.2803/z^3 );
    a1 = 1-K;
    b1 = beta/2 + alpha*K - d1*(1-K);
    c1 = -alpha*d1*K;
    n(5) = (-b1 + sqrt(b1^2 - 4*a1*c1))/(2*a1);
    % Required derivatives for Cp calculation of mixture
    % calculate dcdt = dn5/dK * dK/dT
    dkdt = -K*(-1.761+z*(-3.222+z*.8409))/1000;
    dn5dk = -((alpha - n(5))*(n(5) + 2*a_s*(1/phi - 1)))/(beta/2 + n(5)
    + 2*a_s*(1/phi - 1));
    dcdt = dn5dk * dkdt;
    n(1) = alpha - n(5);
    n(2) = beta/2 - d1 + n(5);
    n(3) = delta/2 + 3.76*a_s/phi;
    n(6) = d1 - n(5);

```

```

end
% total moles
N = sum(n);
% calculate mole fractions and mass of residual gas
m_r = 0;
for i=1:6,
    Y(i) = n(i)/N;
    m_r = m_r + Y(i)*Mi(i);
end
% compute residual mole fraction
y_r = 1/(1 + m_r/m_fa * (1/f-1));
% compute total mole fractions in mixture
for i=1:6,
    Y(i) = Y(i)*y_r;
end
% fuel mole fraction based on all moles
y_fuel = y_fuel*(1 - y_r);
% include intake N2 and O2
Y(3) = Y(3) + y_N2*(1 - y_r);
Y(4) = Y(4) + y_O2*(1 - y_r);
% compute properties of mixture
h = h_fuel*y_fuel;
s = (so_fuel-log(max(y_fuel,1e-15)))*y_fuel;
Cp = cp_fuel*y_fuel;
MW = m_fuel*y_fuel;
% compute component properties according to curve fits
cpo = zeros(6,1);
ho = zeros(6,1);
so = zeros(6,1);
for i=1:6
    cpo(i) = A(i,1) + A(i,2)*T + A(i,3)*T^2 + A(i,4)*T^3 + A(i,5)*T^4;
    ho(i) = A(i,1) + A(i,2)/2*T + A(i,3)/3*T^2 + A(i,4)/4*T^3
    +A(i,5)/5*T^4 + A(i,6)/T;
    so(i) = A(i,1)*log(T) + A(i,2)*T + A(i,3)/2*T^2 + A(i,4)/3*T^3
    +A(i,5)/4*T^4 +A(i,7);
end
table = [-1,1,0,0,1,-1];
for i=1:6
    if(Y(i)>1.e-25)
        h = h + ho(i)*Y(i);
        s = s + Y(i)*(so(i)-log(Y(i)));
        Cp = Cp+cpo(i)*Y(i)+ho(i)*T*table(i)*dcdt*y_r/N;
        MW = MW + Y(i)*Mi(i);
    end
end
% compute thermodynamic properties
R = 8.31434/MW; % compute mixture gas constant

```

```

h = R*T*h; % curve fit for h is h/rt
u = h-R*T;
v = R*T/P;
s = R*(-log(P/101.325)+s);
Cp = R*Cp; % curve fit for cp is cp/r
dvdT = v/T; % derivative of volume wrt temp
dvdP = -v/P; % derivative of volume wrt pres

```

F.9 FUEL.M

```

function [alpha,beta,gamma,delta,h,s,cp,mw,Fs,q] = fuel( id, T )
% [ alpha, beta, gamma, delta, h, s, cp, mw, Fs, q ] = fuel( id, T )
%
% Parameters
%   id - 1=Methane, 2=Gasoline, 3=Diesel, 4=Methanol, 5=Nitromethane
%   T - Temperature (K) at which to eval 300<T<1000 K
%
% Outputs
%   alpha - # carbon
%   beta - # hydrogen
%   gamma - # oxygen
%   delta - # nitrogen
%   h     - specific enthalpy (kJ/kg)
%   s     - specific entropy (kJ/kgK)
%   cp    - specific heat (kJ/kgK)
%   mw   - molecular weight (kg/kmol)
%   Fs   - stoichiometric fuel-air ratio
%   q    - heat of combustion (kJ/kg)
%
% Curve fit coefficients for thermodynamic properties of selected fuels
%
%      a1          a2          a3          a6          a7
FuelProps = [ [ 1.971324, 7.871586e-3, -1.048592e-06, -9.930422e+3,
8.873728 ] ; ... % Methane
[ 4.0652, 6.0977e-2, -1.8801e-05, -3.588e+4,
1.545e+1 ] ; ... % Gasoline
[ 7.971, 1.1954e-01, -3.6858e-05, -1.9385e+4,
-1.7879 ] ; ... % Diesel
[ 1.779819, 1.262503e-02, -3.624890e-6, -2.525420e+4,
1.50884e+1 ] ; ... % Methanol
[ 1.412633, 2.0871e-02, -8.14213e-6, -1.02635e+4,
1.917126e+1 ] ]; % Nitromethane
%
% Fuel chemical formula
%
%      C          H          O          N
%      alpha       beta      gamma      delta
FuelInfo = [[ 1          4          0          0 ] ; ... % Methane
[ 7          17         0          0 ] ; ... % Gasoline
[ 14.4       24.9       0          0 ] ; ... % Diesel
[ 1          4          1          0 ] ; ... % Methanol
[ 1          3          2          1 ] ] ; % Nitromethane

```

```
% stoichiometric fuel-air ratio
FSv = [ 0.0584      0.06548      0.06907      0.1555      0.5924 ];
% available energy of combustion ac
ac = [ 52420      47870      45730      22680      12430 ];
% stoichiometric fuel-air ratio
Fs = FSv(id);
% available energy
q = ac(id);
% Get fuel composition
alpha = FuelInfo(id, 1);
beta = FuelInfo(id, 2);
gamma = FuelInfo(id, 3);
delta = FuelInfo(id, 4);
% compute fuel properties
ao = FuelProps(id, 1);
bo = FuelProps(id, 2);
co = FuelProps(id, 3);
do = FuelProps(id, 4);
eo = FuelProps(id, 5);
% compute thermodynamic properties
h = ao + bo/2*T + co/3*T^2 + do/T;
s = ao*log(T) + bo*T + co/2*T^2 + eo;
cp = ao + bo*T + co*T^2;
% Calculate molecular weight of fuel
mw = 12.01*alpha + 1.008*beta + 16.00*gamma + 14.01*delta;
```

F.10 RUNECP.M

```
%Input-Output program for ecp.m
clear;
phi = 0.8; % enter equivalence ratio input
T = 3000; % enter temperature (K) input
P = 5000.; % enter pressure (kPa) input
fuel_id =2;
% fuel_id - 1=Methane, 2=Gasoline, 3=Diesel, 4=Methanol, 5=Nitromethane
% call ecp function
[ierr, Y, h, u, s, v, R, Cp, MW, dvdT, dvdP] = ecp( T, P, phi, fuel_id );
%echo input
fprintf(' \n Equilibrium Combustion Solver \n' );
fprintf(' Pressure (kPa) = \t \t %6.1f \n', P );
fprintf(' Temperature (K) = \t \t %6.1f \n', T); ...
fprintf(' Fuel Air Equivalence ratio = \t% 3.1f \n ', phi);
%print output mole fractions and properties
fprintf(' \n Mole Fractions \n' );
fprintf(' CO2 = \t %6.4f \n', Y(1) );
fprintf(' H2O = \t %6.4f \n', Y(2) );
fprintf(' N2 = \t %6.4f \n', Y(3) );
```

```

fprintf(' O2 = \t %6.4f \n', Y(4) );
fprintf(' CO = \t %6.4f \n', Y(5) );
fprintf(' H2 = \t %6.4f \n', Y(6) );
fprintf(' H = \t %6.4f \n', Y(7) );
fprintf(' O = \t %6.4f \n', Y(8) );
fprintf(' OH = \t %6.4f \n', Y(9) );
fprintf(' NO = \t %6.4f \n', Y(10) );
fprintf(' \n Mixture Properties \n' );
fprintf(' h(kJ/kg) = \t %6.1f \n', h );
fprintf(' u(kJ/kg) = \t %6.1f \n', u );
fprintf(' s (kJ/Kg K) = \t %6.3f \n', s );
fprintf(' v (m3/kg) = \t %6.3f \n', v );
fprintf(' cp (kJ/Kg K) =\t %6.3f \n', Cp );
fprintf(' Molecular Mass = %5.2f \n', MW );
fprintf(' dvdt = %8.2e \n', dvdT );
fprintf(' dvdp = %8.2e \n', dvdP );

```

F.11 ECP.M

```

function [ierr,Y,h,u,s,v,R,Cp,MW,dvdT,dvdP]=ecp(T,P,phi,ifuel )
% Subroutine for Equilibrium Combustion Products
%
% inputs:
%   T - temperature (K)      [ 600 --> 3500 ]
%   P - pressure (kPa)       [ 20 --> 30000 ]
%   phi - equivalence ratio  [ 0.01 --> ~3 ]
%   ifuel - 1=Methane, 2=Gasoline, 3=Diesel, 4=Methanol, 5=Nitromethane
%
% outputs:
%   ierr - Error codes:
%     0 = success
%     1 = singular matrix
%     2 = maximal pivot error in gaussian elimination
%     3 = no solution in maximum number of iterations
%     4 = result failed consistency check sum(Y)=1
%     5 = failure to obtain initial guess for oxygen concentration
%     6 = negative oxygen concentration in initial guess calculation
%     7 = maximum iterations reached in initial guess solution
%     8 = temperature out of range
%     9 = pressure out of range
%    10 = equivalence ratio too lean
% 11 = equivalence ratio too rich, solid carbon will be formed
%
%   y - mole fraction of constituents
%     y(1) : CO2
%     y(2) : H2O
%     y(3) : N2

```

```

%      Y(4)   : O2
%      Y(5)   : CO
%      Y(6)   : H2
%      Y(7)   : H
%      Y(8)   : O
%      Y(9)   : OH
%      Y(10)  : NO
%
%      h - specific enthalpy of mixture, kJ/kg
%      u - specific internal energy of mixture, kJ/kg
%      s - specific entropy of mixture, kJ/kgK
%      v - specific volume of mixture, m3/kg
%      R - specific ideal gas constant, kJ/kgK
%      Cp - specific heat at constant pressure, kJ/kgK
%      MW - molecular weight of mixture, kg/kmol
%      dvdT - (dv/dT) at const P, m3/kg per K
%      dvdP - (dv/dP) at const T, m3/kg per kPa
%
% initialize outputs
Y = zeros(10,1);
h = 0;
u = 0;
s = 0;
v = 0;
R = 0;
Cp = 0;
MW = 0;
dvdT = 0;
dvdP = 0;
%
% solution parameters
prec = 1e-3;
MaxIter = 20;
%
% square root of pressure (used many times below)
PATM = P/101.325;
sqp = sqrt(PATM);
if ( T < 600 || T > 3500 )
    ierr = 8;
    return;
end
if ( P < 20 || P > 30000 )
    ierr = 9;
    return;
end
if ( phi < 0.01 )
    ierr = 10;
    return;
end
%
% Get fuel composition information
[ alpha, beta, gamma, delta ] = fuel( ifuel, T );

```

```
% Equilibrium constant curve fit coefficients.
% Valid in range: 600 K < T < 4000 K
%
%          Ai           Bi           Ci           Di           Ei
Kp = [ [ 0.432168,      -0.112464e+5,   0.267269e+1,  -0.745744e-4,   ...
        0.242484e-8 ] ; ...
        [ 0.310805,      -0.129540e+5,   0.321779e+1,  -0.738336e-4,   ...
        0.344645e-8 ] ; ...
        [ -0.141784,     -0.213308e+4,   0.853461,       0.355015e-4,   ...
        -0.310227e-8 ] ; ...
        [ 0.150879e-1,  -0.470959e+4,   0.646096,       0.272805e-5,   ...
        -0.154444e-8 ] ; ...
        [ -0.752364,      0.124210e+5,  -0.260286e+1,  0.259556e-3,   ...
        -0.162687e-7 ] ; ...
        [ -0.415302e-2,  0.148627e+5,  -0.475746e+1,  0.124699e-3,   ...
        -0.900227e-8 ] ];

K = zeros(6,1);
for i=1:6
log10ki = Kp(i,1)*log(T/1000) + Kp(i,2)/T + Kp(i,3) + Kp(i,4)*T + ...
Kp(i,5)*T*T;
K(i) = 10^log10ki;
end
c1 = K(1)/sqp;
c2 = K(2)/sqp;
c3 = K(3);
c4 = K(4);
c5 = K(5)*sqp;
c6 = K(6)*sqp;
[ierr,y3,y4,y5,y6] = guess( T, phi, alpha, beta, gamma, delta, c5, c6 );
if ( ierr ~= 0 )
    return;
end
a_s = alpha + beta/4 - gamma/2;
D1 = beta/alpha;
D2 = gamma/alpha + 2*a_s/(alpha*phi);
D3 = delta/alpha + 2*3.7619047619*a_s/(alpha*phi);
A = zeros(4,4);
final = 0;
for jj=1:MaxIter,
    sqy6 = sqrt(y6);
    sqy4 = sqrt(y4);
    sqy3 = sqrt(y3);
    y7= c1*sqy6;
    y8= c2*sqy4;
    y9= c3*sqy4*sqy6;
    y10= c4*sqy4*sqy3;
    y2= c5*sqy4*y6;
    y1= c6*sqy4*y5;
```

```

d76 = 0.5*c1/sqy6;
d84 = 0.5*c2/sqy4;
d94 = 0.5*c3*sqy6/sqy4;
d96 = 0.5*c3*sqy4/sqy6;
d103 = 0.5*c4*sqy4/sqy3;
d104 = 0.5*c4*sqy3/sqy4;
d24 = 0.5*c5*y6/sqy4;
d26 = c5*sqy4;
d14 = 0.5*c6*y5/sqy4;
d15 = c6*sqy4;

% form the Jacobian matrix
A = [ [ 1+d103, d14+d24+1+d84+d104+d94, d15+1, d26+1+d76+d96 ] ; ...
[ 0, 2.*d24+d94-D1*d14, -D1*d15-D1, 2*d26+2+d76+d96 ] ; ...
[ d103, 2*d14+d24+2+d84+d94+d104-D2*d14, 2*d15+1-D2*d15-D2, d26+d96 ] ; ...
[ 2+d103, d104-D3*d14, -D3*d15-D3, 0 ] ] ;

if ( final )
    break;
end

B = [ -(y1+y2+y3+y4+y5+y6+y7+y8+y9+y10-1); ...
       -(2.*y2 + 2.*y6 + y7 + y9 -D1*y1 -D1*y5); ...
       -(2.*y1 + y2 +2.*y4 + y5 + y8 + y9 + y10 -D2*y1 -D2*y5); ...
       -(2.*y3 + y10 -D3*y1 -D3*y5) ] ;

[B, ierr] = gauss( A, B );
if ( ierr ~= 0 )
    return;
end

y3 = y3 + B(1);
y4 = y4 + B(2);
y5 = y5 + B(3);
y6 = y6 + B(4);
nck = 0;
if ( abs(B(1)/y3) > prec )
    nck = nck+1;
end
if ( abs(B(2)/y4) > prec )
    nck = nck+1;
end
if ( abs(B(3)/y5) > prec )
    nck = nck+1;
end
if ( abs(B(4)/y6) > prec )
    nck = nck+1;
end
if( nck == 0 )
    % perform top half of loop to update remaining mole fractions
    % and Jacobian matrix

```

```

    final = 1;
    continue;
end
end
if (jj>=MaxIter)
    ierr = 3;
    return;
end
Y = [ y1 y2 y3 y4 y5 y6 y7 y8 y9 y10 ];
% consistency check
if( abs( sum(Y)-1 ) > 0.0000001 )
    ierr = 4;
    return;
end
% constants for partial derivatives of properties
dkdt = zeros(6,1);
for i=1:6,
dkdt(i)=2.302585*K(i)*( Kp(i,1)/T - Kp(i,2)/(T*T) + Kp(i,4)+2*Kp(i,5)*T );
end
dcdt = zeros(6,1);
dcdt(1) = dkdt(1)/sqp;
dcdt(2) = dkdt(2)/sqp;
dcdt(3) = dkdt(3);
dcdt(4) = dkdt(4);
dcdt(5) = dkdt(5)*sqp;
dcdt(6) = dkdt(6)*sqp;
dcdp = zeros(6,1);
dcdp(1) = -0.5*c1/P;
dcdp(2) = -0.5*c2/P;
dcdp(5) = 0.5*c5/P;
dcdp(6) = 0.5*c6/P;
x1 = Y(1)/c6;
x2 = Y(2)/c5;
x7 = Y(7)/c1;
x8 = Y(8)/c2;
x9 = Y(9)/c3;
x10 = Y(10)/c4;
dfdt(1) = dcdt(6)*x1 + dc当地(5)*x2 + dc当地(1)*x7 + dc当地(2)*x8 + dc当地(3)*x9 + ...
dc当地(4)*x10;
dfdt(2) = 2.*dc当地(5)*x2 + dc当地(1)*x7 + dc当地(3)*x9 - D1*dc当地(6)*x1;
dfdt(3) = 2.*dc当地(6)*x1+dc当地(5)*x2+dc当地(2)*x8+dc当地(3)*x9+dc当地(4)*x10 - ...
D2*dc当地(6)*x1;
dfdt(4) = dc当地(4)*x10 -D3*dc当地(6)*x1;
dfdp(1) = dc当地(6)*x1 + dc当地(5)*x2 + dc当地(1)*x7 + dc当地(2)*x8;
dfdp(2) = 2.*dc当地(5)*x2 + dc当地(1)*x7 -D1*dc当地(6)*x1;
dfdp(3) = 2.*dc当地(6)*x1 + dc当地(5)*x2 + dc当地(2)*x8 - D2*dc当地(6)*x1;
dfdp(4) = -D3*dc当地(6)*x1;

```

```

dfdphi(1) = 0;
dfdphi(2) = 0;
dfdphi(3) = 2*a_s/(alpha*phi*phi)*(Y(1)+Y(5));
dfdphi(4) = 2*3.7619047619*a_s/(alpha*phi*phi)*(Y(1)+Y(5));
% solve matrix equations for independent temperature derivatives
b = -1.0 .* dfdt'; %element by element mult.
[b, ierr] = gauss(A,b);% solve for new b with t derivatives
if ( ierr ~= 0 )
    return;
end
dydt(3) = b(1);
dydt(4) = b(2);
dydt(5) = b(3);
dydt(6) = b(4);
dydt(1) = sqrt(Y(4))*Y(5)*dcdt(6) + d14*dydt(4) + d15*dydt(5);
dydt(2) = sqrt(Y(4))*Y(6)*dcdt(5) + d24*dydt(4) + d26*dydt(6);
dydt(7) = sqrt(Y(6))*dcdt(1) + d76*dydt(6);
dydt(8) = sqrt(Y(4))*dcdt(2) + d84*dydt(4);
dydt(9) = sqrt(Y(4)*Y(6))*dcdt(3) + d94*dydt(4) + d96*dydt(6);
dydt(10) = sqrt(Y(4)*Y(3))*dcdt(4) + d104*dydt(4) + d103*dydt(3);
% solve matrix equations for independent pressure derivatives
b = -1.0 .* dfdp'; %element by element mult.
[b,ierr] = gauss(A,b); % solve for new b with p derivatives
if ( ierr~=0 )
    return;
end
dydp(3) = b(1);
dydp(4) = b(2);
dydp(5) = b(3);
dydp(6) = b(4);
dydp(1) = sqrt(Y(4))*Y(5)*dcdp(6) + d14*dydp(4) + d15*dydp(5);
dydp(2) = sqrt(Y(4))*Y(6)*dcdp(5) + d24*dydp(4) + d26*dydp(6);
dydp(7) = sqrt(Y(6))*dcdp(1) + d76*dydp(6);
dydp(8) = sqrt(Y(4))*dcdp(2) + d84*dydp(4);
dydp(9) = d94*dydp(4) + d96*dydp(6);
dydp(10)= d104*dydp(4) + d103*dydp(3);
% molecular weights of constituents (g/mol)
%      CO2      H2O      N2      O2      CO      H2      H      ...
%      O       OH      NO
Mi = [ 44.01,   18.02,   28.013,   32.00,   28.01,   2.016,   1.009,   ...
       16.,   17.009,   30.004];
if ( T > 1000 )
    % high temp curve fit coefficients for thermodynamic properties ...
    1000 < T < 3000 K
    AAC = [ ...
        .446080e+1,.309817e-2,-.123925e-5,.227413e-9, -.155259e-13, ...
        -.489614e+5,-.986359 ];

```

```

[.271676e+1,.294513e-2,-.802243e-6,.102266e-9, -.484721e-14, ...
 -.299058e+5,.663056e+1 ];
[.289631e+1,.151548e-2,-.572352e-6,.998073e-10,-.652235e-14, ...
 -.905861e+3,.616151e+1 ];
[.362195e+1,.736182e-3,-.196522e-6,.362015e-10,-.289456e-14, ...
 -.120198e+4,.361509e+1 ];
[.298406e+1,.148913e-2,-.578996e-6,.103645e-9, -.693535e-14, ...
 -.142452e+5,.634791e+1 ];
[.310019e+1,.511194e-3, .526442e-7,-.349099e-10,.369453e-14, ...
 -.877380e+3,-.196294e+1 ];
[.25e+1,0,0,0,.254716e+5,-.460117 ];
[.254205e+1,-.275506e-4,-.310280e-8,.455106e-11,-.436805e-15, ...
 .292308e+5,.492030e+1 ];
[.291064e+1,.959316e-3,-.194417e-6,.137566e-10,.142245e-15, ...
 .393538e+4,.544234e+1 ];
[.3189e+1 ,.133822e-2,-.528993e-6,.959193e-10,-.648479e-14, ...
 .982832e+4,.674581e+1 ]; ];

elseif ( T <= 1000 )
% low temp curve fit coefficients for thermodynamic properties, ...
300 < T <= 1000 K
AAC = [ ...
[ 0.24007797e+1, 0.87350957e-2, -0.66070878e-5, 0.20021861e-8, ...
 0.63274039e-15, -0.48377527e+5, 0.96951457e+1 ]; % CO2
[ 0.40701275e+1, -0.11084499e-2, 0.41521180e-5, -0.29637404e-8, ...
 0.80702103e-12, -0.30279722e+5, -0.32270046 ]; % H2O
[ 0.36748261e+1, -0.12081500e-2, 0.23240102e-5, -0.63217559e-9, ...
 -0.22577253e-12, -0.10611588e+4, 0.23580424e+1 ]; % N2
[ 0.36255985e+1, -0.18782184e-2, 0.70554544e-5, -0.67635137e-8, ...
 0.21555993e-11, -0.10475226e+4, 0.43052778e+1 ]; % O2
[ 0.37100928e+1, -0.16190964e-2, 0.36923594e-5, -0.20319674e-8, ...
 0.23953344e-12, -0.14356310e+5, 0.29555353e+1 ]; % CO
[ 0.30574451e+1, 0.26765200e-2, -0.58099162e-5, 0.55210391e-8, ...
 -0.18122739e-11, -0.98890474e+3, -0.22997056e+1 ]; % H2
[ 0.25000000e+1, 0, 0, 0, 0, 0.25471627e+5, ...
 -0.46011762e+0 ]; % H
[ 0.29464287e+1, -0.16381665e-2, 0.24210316e-5, -0.16028432e-8, ...
 0.38906964e-12, 0.29147644e+5, 0.29639949e+1 ]; % O
[ 0.38375943e+1, -0.10778858e-2, 0.96830378e-6, 0.18713972e-9, ...
 -0.22571094e-12, 0.36412823e+4, 0.49370009e+0 ]; % OH
[ 0.40459521e+1, -0.34181783e-2, 0.79819190e-5, -0.61139316e-8, ...
 0.15919076e-11, 0.97453934e+4, 0.29974988e+1 ]; % H2
];
end
% Compute cp,h,s
% initialize h, etc to zero
MW = 0;
Cp = 0;

```

```

h = 0;
s = 0;
dMWdT = 0;
dMWdP = 0;
for i=1:10,
    cpo = AAC(i,1) + AAC(i,2)*T + AAC(i,3)*T^2 + AAC(i,4)*T^3 + AAC(i,5)*T^4;
    ho = AAC(i,1) + AAC(i,2)/2*T + AAC(i,3)/3*T^2 + AAC(i,4)/4*T^3 + ...
        AAC(i,5)/5*T^4 + AAC(i,6)/T;
    so = AAC(i,1)*log(T) + AAC(i,2)*T + AAC(i,3)/2*T^2 + AAC(i,4)/3*T^3 + ...
        AAC(i,5)/4*T^4 + AAC(i,7);
    h = h + ho*Y(i); % h is h/rt here
    MW = MW + Mi(i)*Y(i);
    dMWdT = dMWdT + Mi(i)*dydt(i);
    dMWdP = dMWdP + Mi(i)*dydp(i);
    Cp = Cp+Y(i)*cpo + ho*T*dydt(i);
    if (Y(i)> 1.0e-37)
        s = s + Y(i)*(so - log(Y(i)));
    end
end

R = 8.31434/MW;
v = R*T/P;
Cp = R*(Cp - h*T*dMWdT/MW);
h = h*R*T;
s = R*(-log(PATM) + s);
u=h-R*T;
dvdT = v/T*(1 - T*dMWdT/MW);
dvdP = v/P*(-1 + P*dMWdP/MW);
ierr = 0;
return;

function [ierr,y3,y4,y5,y6] = guess(T,phi,alpha,beta,gamma,delta,c5,c6)
    ierr = 0;
    y3 = 0;
    y4 = 0;
    y5 = 0;
    y6 = 0;
    % estimate number of total moles produced, N
    n = zeros(6,1);
    % Calculate stoichiometric molar air-fuel ratio
    a_s = alpha + beta/4 - gamma/2;
    if ( phi <= 1 )
        % lean combustion
        n(1) = alpha;
        n(2) = beta/2;
        n(3) = delta/2 + 3.76*a_s/phi;
        n(4) = a_s*(1/phi - 1);
    end
end

```

```

else
    % rich combustion
    d1 = 2*a_s*(1-1/phi);
    z = T/1000;
    KK = exp( 2.743 - 1.761/z - 1.611/z^2 + 0.2803/z^3 );
    aa = 1-KK;
    bb = beta/2 + alpha*KK - d1*(1-KK);
    cc = -alpha*d1*KK;
    n(5) = (-bb + sqrt(bb^2 - 4*aa*cc)) / (2*aa);
    n(1) = alpha - n(5);
    n(2) = beta/2 - d1 + n(5);
    n(3) = delta/2 + 3.76*a_s/phi;
    n(6) = d1 - n(5);
end
% total product moles per 1 mole fuel
N = sum(n);
% try to get close to a reasonable value of ox mole fraction
% by finding zero crossing of 'f' function
ox = 1;
nIterMax=40;
for ii=1:nIterMax,
    f = 2*N*ox - gamma - (2*a_s)/phi + (alpha*(2*c6*ox^(1/2) + 1))/ ...
        (c6*ox^(1/2) + 1) + (beta*c5*ox^(1/2))/(2*c5*ox^(1/2) + 2);
    if ( f < 0 )
        break;
    else
        ox = ox*0.1;
        if ( ox < 1e-37 )
            ierr = 5;
            return;
        end
    end
end
% now zero in on the ox mole fraction using Newton-Raphson iteration
for ii=1:nIterMax,
    f = 2*N*ox - gamma - (2*a_s)/phi + (alpha*(2*c6*ox^(1/2) + 1))/ ...
        (c6*ox^(1/2) + 1) + (beta*c5*ox^(1/2))/(2*c5*ox^(1/2) + 2);
    df = 2*N - (beta*c5^2)/(2*c5*ox^(1/2) + 2)^2 + (alpha*c6)/ ...
        (ox^(1/2)*(c6*ox^(1/2) + 1)) + (beta*c5)/ ...
        (2*ox^(1/2)*(2*c5*ox^(1/2) + 2)) - (alpha*c6*(2*c6*ox^(1/2) + 1))/ ...
        (2*ox^(1/2)*(c6*ox^(1/2) + 1)^2);
    dox = f/df;
    ox = ox - dox;
    if ( ox < 0.0 )
        ierr = 6;
        return;
    end
end

```

```

        if ( abs(dox/ox) < 0.001 )
            break;
        end
    end
    if( ii == nIterMax )
        ierr = 7;
        return;
    end
    y3 = 0.5*(delta + a_s/phi*2*3.76)/N;
    y4 = ox;
    y5 = alpha/N/(1+c6*sqrt(ox));
    y6 = beta/2/N/(1+c5*sqrt(ox));
end % guess

function [B, IERQ] = gauss( A, B )
% maximum pivot gaussian elimination routine adapted
% from FORTRAN in Olikara & Borman, SAE 750468, 1975
% not using built-in MATLAB® routines because they issue
% lots of warnings for close to singular matrices
% that haven't seemed to cause problems in this application
% routine below does check however for true singularity
IERQ = 0;
for N=1:3,
    NP1=N+1;
    BIG = abs( A(N,N) );
    if ( BIG < 1.0e-05)
        IBIG=N;
        for I=NP1:4,
            if( abs(A(I,N)) <= BIG )
                continue;
            end
            BIG = abs(A(I,N));
            IBIG = I;
        end
        if(BIG <= 0.)
            IERQ=2;
            return;
        end
        if( IBIG ~= N)
            for J=N:4,
                TERM = A(N,J);
                A(N,J) = A(IBIG,J);
                A(IBIG,J) = TERM;
            end
            TERM = B(N);
            B(N) = B(IBIG);
            B(IBIG) = TERM;
        end
    end
end

```

```

        end
    end
    for I=NP1:4,
        TERM = A(I,N)/A(N,N);
        for J=NP1:4,
            A(I,J) = A(I,J)-A(N,J)*TERM;
        end
        B(I) = B(I)-B(N)*TERM;
    end
end
if( abs(A(4,4)) > 0.0 )
    B(4) = B(4)/A(4,4);
    B(3) = (B(3)-A(3,4)*B(4))/A(3,3);
    B(2) = (B(2)-A(2,3)*B(3)-A(2,4)*B(4))/A(2,2);
    B(1) = (B(1)-A(1,2)*B(2)-A(1,3)*B(3)-A(1,4)*B(4))/A(1,1);
else
    IERQ=1; % singular matrix
    return;
end
end % gauss()
end % ecp()

```

F.12 ADIABATICFLAMETEMP.M

```

% Computes const pressure adiabatic flame temperature T2
% from first law: dh = q
% Inputs:
T1 = 600;% initial temperature (K)
P1 = 100; % initial pressure (kPa)
PHI = 1.0; % equivalence ratio
f = .1; % residual fraction
ifuel=2; % 1=Methane, 2=Gasoline, 3=Diesel, 4=Methanol, 5=Nitromethane
% use FARG for initial calc of H1
[~, H1, ~, ~, ~, ~, CP, ~, ~, ~] = farg( T1, P1, PHI, f, ifuel );
fprintf(' Initial Enthalpy H1 = %7.1f Initial CP = %7.3f \n',H1,CP);
P2 = P1;
T2 = 2000; %initial guess of flame temp
MAXITS = 50;
TOL = 0.00001;
for i=1:MAXITS,
    [~,~, H2, ~, ~, ~, ~, CP, ~, ~, ~] = ecp( T2, P2, PHI, ifuel );
    %fprintf(' Iterated Enthalpy H2 = %7.1f Iterated CP = %7.3f \n',H2,CP);
    DELT2 = (H1-H2)/CP;
    T2 = T2 + DELT2;
    fprintf(' Iterated Adiabatic Flame Temp (K) = %8.1f \n',T2);
    if ( abs(DELT2)/T2 < TOL )
        break;

```

```

        end
    end
    fprintf(' Final Adiabatic Flame Temp (K) = %8.1f \n',T2);

```

F.13 OTTOFUEL.M

```

%program OttoFuel - computes const vol fuel air cycle
% first,isentropic compression from v1 to known v2
%establish initial conditions at state 1
clear;
T1 = 350; %Kelvin
P1 = 101.3; %kPa
phi = 0.95; %equivalence ratio
f= .05; %residual fraction,
rc=13.; %compression ratio
fuel_id=3 ; %id:1=Methane,2=Gasoline,3=Diesel,4=Methanol,5=Nitromethane
[ ~, ~, ~, ~, ~, ~, ~, ~, FS, ac ]=fuel(fuel_id, T1);
% FS is stoichiometric fuel/air ratio
% ac is available energy of combustion kJ/kg
maxits = 50;
tol =0.0001;
% call farg to get properties at 1
[y1, h1,u1, s1, v1, r, cp1, mw, dvdT, dvdP]=farg(T1,P1,phi,f,fuel_id);
%initial estimates of T2,P2
v2=v1/rc;
s2=s1;
cv1=cp1+ T1*(dvdT^2)/dvdP;
gam= cp1/cv1;
T2=T1*(v1/v2)^(gam-1.);
P2=P1*(v1/v2)^gam;
%do the iteration to find T2 and P2
for i2 = 1:maxits,
    [y2, h2,u2, s2, v2, r, cp2, mw, dvdT, dvdP]=farg(T2,P2,phi,f,fuel_id);
    f1=s1-s2;
    f2=v1/rc - v2;
    det= cp2*dvdP/T2 + dvdT^2;
    dt=(dvdP*f1 + dvdT*f2)/det;
    dp= (-dvdT*f1 + cp2/T2*f2)/det;
    %update T2 and P2
    T2=T2 + dt;
    P2=P2 + dp;
    %check for convergence
    if ( abs(dt)/T2 < tol && abs(dp)/P2 < tol )
        break;
    end
end
w12=- (u2-u1);% compression work

```

```
%combustion from 2-3 with v and u constant
%initial estimates of T3,P3 at state 3
T3=3000;%Kelvin
P3=7000; % kPa
%do the iteration to find T3 and P3
for i3 = 1:maxits,
    [ierr,y3, h3, u3, s3, v3, r, cp3, mw, dvdT, dvdP]=ecp(T3,P3,phi,fuel_id);
    % fprintf(' \n combustion ierr= %6.2f \n', ierr);
    f1= u2-u3;
    f2= v2-v3;
    det= cp3*dvdP+T3*dvdT^2;
    dt= (-f1*dvdP - f2*(dvdT+dvdP))/det;
    dp= ((P3*dvdT-cp3)*f2 + f1*dvdT)/det;
    %update T3 and P3
    T3=T3 - dt;
    P3=P3 - dp;
    %check for convergence
    if ( abs(dt)/T3 < tol && abs(dp)/P3 < tol )
        break;
    end
end
% isentropic expansion from v3 to known v4
%initial estimates of T4,P4
v4=v1;
cv3=cp3+ T3*(dvdT^2)/dvdP;
gam= cp3/cv3;
T4=T3*(v3/v4)^(gam-1.);
P4=P3*(v3/v4)^gam;
%do the iteration to find T4 and P4
for i4 = 1:maxits,
    [ierr, y4, h4, u4, s4, v4, r, cp4, mw, dvdT, dvdP]=ecp(T4,P4,phi,fuel_id);
    % fprintf(' \n expansion ierr= %6.2f \n', ierr);
    f1=s3-s4;
    f2=rc*v3 - v4;
    det= cp4*dvdP/T4 + dvdT^2;
    dt=(dvdP*f1 + dvdT*f2)/det;
    dp= (-dvdT*f1 + cp4/T4*f2)/det;
    %update T4 and P4
    T4=T4 + dt;
    P4=P4 + dp;
    %check for convergence
    if ( abs(dt)/T4 < tol && abs(dp)/P4 < tol )
        break;
    end
end
%compute cycle parameters
w=u1-u4;% net work
```

```

imep=w/(v1-v2); %imep
eta=w*(1+phi*FS)/phi/FS/(1.-f)/ac;
%output state and cycle parameters
fprintf(' \n Ottofuel input conditions:phi= %6.2f fuel= %4d \n',phi,fuel_id);
fprintf('State \t\t 1 \t\t 2 \t\t 3 \t\t 4 \n')
fprintf('Pressure (kPa)= %7.1f \t %7.1f \t %7.1f \t %7.1f \n',P1,P2,P3,P4);
fprintf('Temperature (K)= %7.1f \t %7.1f \t %7.1f \t %7.1f \n',T1,T2,T3,T4);
fprintf('Enthalpy(kJ/kg)= %7.1f \t %7.1f \t %7.1f \t %7.1f \n',h1,h2,h3,h4);
fprintf('Int.Energy(kJ/kg)= %7.1f \t %7.1f \t %7.1f \t %7.1f \n',u1,u2,u3,u4);
fprintf('Volume (m^3/kg) = %7.3f \t %7.3f \t %7.3f \t %7.3f \n', v1,v2,v3,v4);
fprintf('Cp (kJ/kg K) = %7.3f \t %7.3f \t %7.3f \t %7.3f \n \n', ...
cpl,cp2,cp3,cp4);
fprintf(' Work (kJ/kg)= %7.1f \n', w);
fprintf(' Efficiency= %7.3f \n', eta);
fprintf(' Imep (kPa)= %7.1f \n \n', imep);
fprintf(' Iterations = \t \t %4d \t %4d \t %4d \n', i2,i3,i4);

```

F.14 FOURSTROKEFUELAIR.M

```

%program four stroke ottofuel - computes const vol fuel air cycle
%establish initial conditions for intake stroke
clear;
Ti = 300; % intake temperature (K)
Pi = 52.5; % intake pressure (kPa)
Pe = 105; % exhaust pressure (kPa)
phi = .8; % equivalence ratio
rc = 10.; % compression ratio
%get specific heat input qin and stoichiometric fuel-air ratio FS
fuel_id=2 ; %id: 1=Methane, 2=Gasoline, 3=Diesel, 4=Methanol, 5=Nitromethane
[ ~, ~, ~, ~, ~, ~, ~, FS, qin ] = fuel( fuel_id, Ti );
% find enthalpy hi of intake fuel-air mixture
ff=0; % no residual fraction in intake air
[yi,hi,ui, si, vi, r, cpi, mw, dvdT, dvdP] = farg( Ti, Pi, phi, ff, fuel_id );
maxits = 100;
tol =0.0001;
%initial estimates of residual fraction and initial temp
f= .1; % residual fraction,
T1=350.; % initial temperature
P1=Pi; % no pressure drop in intake
% main iteration loop around cycle to get converged values of f and T1
for imain = 1:maxits,
% isentropic compression from v1 to known v2
% call farg to get properties at 1
[y1,h1,u1, s1, v1, r, cp1, mw, dvdT, dvdP] = farg( T1, P1, phi, f, fuel_id );
%initial estimates of T2,P2
v2=v1/rc;
s2=s1;

```

```

cv1=cp1+ T1*(dvdT^2)/dvdP;
gam= cp1/cv1;
T2=T1*(v1/v2)^(gam-1.);
P2=P1*(v1/v2)^gam;
%do the iteration to get T2 and P2 at end of compression
for i2 = 1:maxits,
[y2, h2,u2, s2, v2, r, cp2, mw, dvdT, dvdP]=farg(T2,P2,phi,f,fuel_id);
f1=s1-s2;
f2=v1/rc - v2;
det= cp2/T2*dvdP + dvdT^2;
dt=(dvdP*f1 + dvdT*f2)/det;
dp= (-dvdT*f1 + cp2/T2*f2)/det;
%update T2 and P2
T2=T2 + dt;
P2=P2 + dp;
%check for convergence
%check for convergence
if ( abs(dt)/T2 < tol && abs(dp)/P2 < tol )
    break;
end
end
w12=- (u2-u1);% compression work
% combustion from 2-3 with v and u constant
%initial estimates of T3,P3 at state 3
T3=3000;%Kelvin
P3=7000; % kPa
%do the iteration to get T3 and P3
for i3 = 1:maxits,
[ierr,y3,h3,u3,s3,v3,r,cp3,mw,dvdT,dvdP] =ecp(T3,P3,phi,fuel_id);
f1= u2-u3;
f2= v2-v3;
det= cp3*dvdP + T3*dvdT^2;
dt= (-f1*dvdP - f2*(dvdT+dvdP))/det;
dp= ((P3*dvdT-cp3)*f2 + f1*dvdT)/det;
%update T3 and P3
T3=T3 - dt;
P3=P3 - dp;
%check for convergence
%check for convergence
if ( abs(dt)/T3 < tol && abs(dp)/P3 < tol )
    break;
end
end
% isentropic expansion of combustion products from v3 to known v4
% initial estimates of T4,P4
v4=v1;
cv3=cp3+ P3*v3/T3*(dvdT^2)/dvdP;

```

```

gam= cp3/cv3;
T4=T3*(v3/v4)^(gam-1.);
P4=P3*(v3/v4)^gam;
%do the iteration to get T4 and P4
for i4 = 1:maxits,
[ierr,y4,h4,u4,s4,v4,r,cp4,mw,dvdT,dvdP]=ecp(T4,P4,phi,fuel_id);
f1=s3-s4;
f2=rc*v3 - v4;
det= cp4*dvdP/T4 + dvdT^2;
dt=(dvdP*f1 + dvdT*f2)/det;
dp= (-dvdT*f1 + cp4/T4*f2)/det;
%update T4 and P4
T4=T4 + dt;
P4=P4 + dp;
%check for convergence
if ( abs(dt)/T4 < tol && abs(dp)/P4 < tol )
    break;
end
end
% isentropic blowdown of control mass to exhaust pressure
P5=Pe;
s5=s4;
%initial estimates of T5
cv4=cp4+ P4*v4/T4*(dvdT^2)/dvdP;
gam= cp4/cv4;
T5=T4*(P5/P4)^((gam-1.)/gam);
% do iteration for T5
for i5 = 1:maxits,
[ierr,y5,h5,u5,s5,v5,r,cp5,mw,dvdT,dvdP]=ecp(T5,P5,phi,fuel_id);
f1=s4-s5;
dt=T5*f1/cp5;
T5=T5 + dt;
%check for convergence
if ( abs(dt)/T5 < tol )
    break;
end
end
% recompute residual fraction
fold = f;
v6=v5;
f=v4/v6/rc;
% constant pressure exhaust stroke
h6=h5;
%recompute h1 with fuel-air mixture and new residual fraction
h1= f*(h6 + (Pi-Pe)*v6) + (1-f)*hi;
T1old=T1;
%recompute T1 with latest f and h1

```

```

for i6 = 1:maxits,
[y1,h1new,u1,s1,v1,r,cp1,mw,dvdT,dvdP]=farg(T1 Pi,phi,f,fuel_id);
g=h1new-h1;
dt=-g/cp1;
T1=T1+dt;
%check for convergence
if ( abs(dt)/T1 < tol )
    break;
end
end
%check for convergence of main iteration loop
dt=T1old - T1;
df=fold - f;
if ( abs(dt)/T1 < tol && abs(df)/f < tol )
    break;
end
end %end of main iteration loop
%compute cycle parameters
w = u1-u4;% net work
imep = w/(v1-v2); %imep
eta = w*(1+phi*FS)/phi/FS/(1.-f)/qin; % thermal efficiency
pmep = Pe -Pi; %pmep
etanet = eta*(1.- pmep/imep); %net thermal efficiency
ev = rc*(1.-f)*vi/(rc-1.)/v1;
%output state and cycle parameters
fprintf(' \n Ottofuel inlet: Temp (K)= %5.1f Pressure (kPa)= %5.1f ...
phi= %6.2f fuel= %3d \n', Ti, Pi, phi, fuel_id );
fprintf(' State \t\1 \t\2 \t\3 \t\4 \t\5 \t\6 \n')
fprintf('Pressure (kPa)= %7.1f \t %7.1f \t %7.1f \t %7.1f \t %7.1f \n',...
P1,P2,P3,P4);
fprintf('Temperature (K)=%7.1f \t %7.1f \t %7.1f \t %7.1f \t %7.1f \n',...
T1,T2,T3,T4);
fprintf('Enthalpy(kJ/kgK)=%7.1f \t %7.1f \t %7.1f \t %7.1f \n',...
h1,h2,h3,h4);
fprintf('Int. Energy(kJ/kg)=%6.1f \t %7.1f \t %7.1f \t %7.1f \n',...
u1,u2,u3,u4);
fprintf('Volume (m^3/kg)= %7.3f \t %7.3f \t %7.3f \t %7.3f \n',...
v1,v2,v3,v4);
fprintf('Entropy(kJ/kgK)= %6.3f \t %7.3f \t %7.3f \t %7.3f \n',...
s1,s2,s3,s4);
fprintf('Cp (kJ/kg K) = %7.3f \t %7.3f \t %7.3f \t %7.3f \n \n',...
cp1,cp2,cp3,cp4);
fprintf('Work (kJ/kg)= %7.1f \t \t Volumetric Efficiency= %7.4f \n', w, ev);
fprintf('Ideal Thermal Efficiency= %7.3f \t Net Thermal Efficiency= %7.4f ...
\n', eta, etanet);
fprintf('Imep (kPa)= %7.1f \t \t Pmep (kPa)= %7.1f \n', imep, pmep);
fprintf('Exhaust Temperature (K)= %7.1f \t Residual Mass Fraction ...

```

```
f =%7.4f \n', T5,f);
fprintf('Iterations = \t %4d\t %4d \t %4d \t %4d \n', imain,i2,i3,i4);
```

F.15 HOMOGENEOUS.M

```
function [ ETA, IMEP, NOX_ppm ] = Homogeneous(varargin)
% Two Zone Arbitrary Heat Release (Fuel Inducted Engine)
%
% Find:
% 1. Indicated thermal efficiency - ETA
% 2. Indicated mean effective pressure - IMEP (kPa)
%
% Note:
% 1. Cosine burning law is employed
% 2. Fuel is gasoline, C7H17
R = 7; % Compression ratio - R
B = .0925; % Bore - B (m)
S = .1143; % Stroke - S (m)
EPS = 0.25; % Half stroke to rod ratio - EPS
RPM = 1200; % Engine speed - RPM
HEAT = 500; % Heat transfer coefficient
BLOWBY = 0.8; % Blowby coefficient
THETAS = -15; % Start of heat release (deg ATDC)
THETAB = 45; % Burn angle (deg)
PHI = 0.88; % Equivalence ratio - PHI
F = 0.05; % Residual fraction - F
TW = 400; % Wall temperature - TW
fuel_type = 2; % gasoline
FS = 0.06548; % stoichiometric fuel-air ratio for gasoline
A0 = 47870; %
T1 = 363; %K
P1 = 100; % kPa
if ( nargin == 3 )
    PHI = varargin{1};
    F = varargin{2};
    RPM = varargin{3};
end
OMEGA = RPM*pi/30;
to_ppm = 10^6; % convert from mass fraction to ppm
MW_NO = 30; % molecular weight of NO, g/mol
THETA = -180;
DTHETA = 1;
THETAE = THETA+DTHETA;
[ VOL, X, EM ] = auxiliary( THETA );
NNOX = THETAB/DTHETA;
NY = 6+NNOX;
Y = zeros(NY,1);
```

```

Y(1) = P1;
Y(2) = nan;
Y(3) = T1;
[~, ~, ~, ~, vU, ~, ~, ~, ~] = farg( Y(3), Y(1), PHI, F, fuel_type );
MN0T = VOL/vU;
M = EM*MN0T;
NN = 36*10;
SAVE.THETA = zeros( NN, 1 );
SAVE.VOL = zeros( NN, 1 );
SAVE.T = zeros(NN, 1 );
SAVE.P = zeros( NN, 1 );
SAVE.MDOTFI = zeros( NN, 1 );
SAVE.NOx = zeros(NN,5);
fprintf( 'THETA VOL BURN FRAC PRESS BURN TEMP UNBURNED T WORK ...
HEAT LOSS MASS H-LEAK NOx\n' );
fprintf( ' deg cm^3 -- kPa K K J ... .
J g J ppm\n' );
fprintf('%7.1f %6.1f %3.3f %6.1f %6.1f %6.1f %5.0f %5.0f %5.3f ...
%5.2f %6.1f\n', THETA, VOL*1000000, X, Y(1), Y(2), Y(3), Y(4)*1000, ...
Y(5)*1000, M*1000, Y(6)*1000, 0.0 );
II = 1;
for III=1:36,
  for JJJ=1:10,
    [ Y ] = integrate( THETA, THETAE, Y );
    [ VOL, X, EM ] = auxiliary( THETA );
    M = EM*MN0T;
    THETA=THETAE;
    THETAE=THETA+DTHETA;
    % save data for plotting later
    SAVE.THETA(II) = THETA;
    SAVE.VOL(II) = VOL;
    SAVE.P(II) = Y(1);
    SAVE.TB(II) = Y(2);
    SAVE.TU(II) = Y(3);
    SAVE.X(II) = X;
    SAVE.NOX(II,:) = [ Y(6+1), Y(round(6+0.25*NNOX)), ...
      Y(round(6+0.5*NNOX)), Y(round(6+0.75*NNOX)), Y(6+NNOX) ]*to_ppm;
    II=II+1;
    if ( THETAS >= THETA && THETAS < THETAE )
      Y(2) = tinitial( Y(1), Y(3), PHI, F );
    end
    if ( THETA > THETAS + THETAB )
      Y(3) = nan;
    end
  end
  fprintf('%7.1f %6.1f %3.3f %6.1f %6.1f %5.0f ... .

```

```

    %5.0f  %5.3f  %5.2f      %6.1f\n', ...
THETA, VOL*1000000, X, Y(1), Y(2), Y(3), Y(4)*1000, Y(5)*1000, ....
M*1000, Y(6)*1000, Y(7)*to_ppm );
end
% integrate total NOx value
NOX_ppm = 0;
for nn=1:NNOX;
    THETA = THETAS + (nn-1)/(NNOX-1)*THETAB;
    dxbdtheta = 0.5*sin(pi*(THETA-THETAS)/THETAB)*pi/THETAB;
    dxb = dxbdtheta*DTHETA;
    NOX_ppm = NOX_ppm + Y(6+nn)*dxb*to_ppm;
end
ETA = Y(4)/MNOT*(1+PHI*FS*(1-F))/PHI/FS/(1-F)/A0;
IMEP = Y(4)/(pi/4*B^2*S);
fprintf('ETA=%1.4f IMEP=%7.3f kPa NOx = %6.1f ppm\n',ETA,IMEP,NOX_ppm );
if ( nargin == 0 )
    % if not called externally with custom PHI, F, and RPM parameters,
    % generate some plots
sTitle = sprintf('Homogenous 2 zone, gasoline, PHI=%2f F=%2f ...
RPM=%1f\nETA=%3f IMEP=%2f kPa NOx=%1f ppm ', PHI, F, ...
RPM, ETA, IMEP, NOX_ppm );
figure;
plot( SAVE.THETA, SAVE.X, 'linewidth',2 );
set(gca,'fontsize',18,'linewidth',2,'Xlim',[-100 100]);
xlabel( '\theta','fontsize',18);
ylabel('burn fraction','fontsize',18);
figure;
plot( SAVE.THETA, SAVE.P,'linewidth',2 );
set(gca,'fontsize',18,'linewidth',2,'Xlim',[-100 100]);
xlabel( '\theta','fontsize',18);
ylabel('pressure (kPa)','fontsize',18);
figure;
plot( SAVE.THETA, SAVE.TU, '--',SAVE.THETA, SAVE.TB,'--','linewidth',2 );
set(gca,'fontsize',18,'linewidth',2,'Xlim',[-100 100]);
xlabel( '\theta','fontsize',18);
ylabel( 'temperature (K)', 'fontsize',18);
legend('Unburned','Burned', 'Location', 'SouthEast');
figure;
plot( SAVE.THETA, SAVE.NOX,'linewidth',2 );
set(gca,'fontsize',18,'linewidth',2,'Xlim',[-100 100]);
xlabel( '\theta','fontsize',18);
ylabel('NOx (ppm)','fontsize',18);
axis( [ THETAS, 110, 0, max(max(SAVE.NOX)*1.1) ] );
%legend( 'X=0', 'X=0.25', 'X=0.5', 'X=0.75', 'X=1', 'Location', ...
'SouthEast' );
%title( sTitle );
end

```

```

function [ TB ] = tinitial( P, TU, PHI, F )
    TB = 2000;
    [~, HU, ~, ~, ~, ~, ~, ~, ~] = farg( TU, P, PHI, F, fuel_type );
    for ITER=1:50,
        [ierr, ~, HB, ~, ~, ~, ~, CP, ~, ~, ~] = ecp( TB, P, PHI, fuel_type );
        if ( ierr ~= 0 )
            fprintf('Error in ECP(%g, %g, %g): %d\n', TB, P, PHI, ierr )
        end
        DELT = +(HU-HB)/CP;
        TB = TB + DELT;
        if ( abs(DELT/TB) < 0.001 )
            break;
        end
    end
end

function [ VOL, X, EM ] = auxiliary( THETA )
    VTDC = pi/4*B^2*S/(R-1); % m3
    VOL = VTDC*(1 + (R-1)/2*(1-cosd(THETA) + 1/EPS*(1-sqrt(1-...
        (EPS*sind(THETA))^2)) );
    X = 0.5*(1-cos(pi*(THETA-THETAS)/THETAB));
    if ( THETA <= THETAS )
        X = 0.;
    end
    if ( THETA >= THETAS+THETAB )
        X = 1.;
    end
    EM = exp(-BLOWBY*(THETA*pi/180 + pi)/OMEGA);
end

function [Y] = integrate( THETA, THETA_E, Y )
    [TT, YY] = ode23( @rates, [ THETA, THETA_E ], Y );
    for J=1:NY,
        Y(J) = YY(length(TT),J);
    end

    function [ YPRIME ] = rates( THETA, Y )
        YPRIME = zeros(NY,1);
        [ VOL, X, EM ] = auxiliary( THETA );
        M = EM*MNOT;
        DUMB = sqrt(1-(EPS*sind(THETA))^2);
        DV = pi/8*B^2*S*sind(THETA)*(1+EPS*cosd(THETA)/DUMB);
        AA = (DV + VOL*BLOWBY/OMEGA)/M;
        C1 = HEAT*(pi*B^2/2 + 4*VOL/B)/OMEGA/M/1000;
        C0 = sqrt(X);
        P = Y(1);
        TB = Y(2);
        TU = Y(3);
        % three different computations are required depending upon the size
        % of the mass fraction burned
    end
end

```

```

if ( X > 0.999 )
    % EXPANSION
[ierr,YB,HL, ~, ~,VB, ~,CP, ~,DVDT,DVDP]=ecp(TB,P,PHI,fuel_type);
    if ( ierr ~= 0 )
        fprintf('Error in ECP(%g, %g, %g): %d\n', TB, P, PHI, ierr );
    end
    BB = C1/CP*DVT*T*B*(1-TW/TB);
    CC = 0;
    DD = 1/CP*T*B*DVT^2 + DVDP;
    EE = 0;
    YPRIME(1) = (AA + BB + CC)/(DD + EE);
    YPRIME(2) = -C1/CP*(TB-TW) + 1/CP*DVT*T*B*YPRIME(1);
    YPRIME(3) = 0;
elseif ( X > 0.001 )
    % COMBUSTION
[~,HU, ~, ~,VU, ~,CPU, ~,DVDTU,DVDPU]=farg(TU,P,PHI,F,fuel_type);
[ierr,YB,HB, ~, ~,VB, ~,CPB, ~,DVDTB,DVDPB]=ecp(TB,P,PHI,fuel_type);
    if ( ierr ~= 0 )
        fprintf('Error in ECP(%g, %g, %g): %d\n', TB, P, PHI, ierr );
    end
    BB = C1*(1/CPB*T*B*DVTB*C0*(1-TW/TB) + 1/CPU*TU*DVTU*(1-C0)* ...
(1-TW/TU));
    DX = 0.5*sin( pi*(THETA-THETAS)/THETAB )*180/THETAB;
    CC = -(VB-VU)*DX - DVDTB*(HU-HB)/CPB*(DX-(X-X^2)*BLOWBY/OMEGA);
    DD = X*(VB^2/CPB/TB*(TB/VB*DVTB)^2 + DVDPB);
    EE = (1-X)*(1/CPU*TU*DVTU^2 + DVDPU);
    HL = (1-X^2)*HU + X^2*HB;
    YPRIME(1) = (AA + BB + CC)/(DD + EE);
    YPRIME(2) = -C1/CPB/C0*(TB-TW) + 1/CPB*T*B*DVTB*YPRIME(1) + ...
(HU-HB)/CPB*(DX/X - (1-X)*BLOWBY/OMEGA);
    YPRIME(3) = -C1/CPU/(1+C0)*(TU-TW) + 1/CPU*TU*DVTU*YPRIME(1);
else
    % COMPRESSION
[~, HL, ~, ~, ~, ~,CP, ~,DVDT,DVDP]=farg(TU,P,PHI,F,fuel_type);
    BB = C1*1/CP*TU*DVT*(1-TW/Y(3));
    CC = 0;
    DD = 0;
    EE = 1/CP*TU*DVT^2 + DVDP;
    YPRIME(1) = ( AA + BB + CC )/(DD + EE);
    YPRIME(2) = 0;
    YPRIME(3) = -C1/CP*(Y(3)-TW) + 1/CP*Y(3)*DVT*YPRIME(1);
end
% common to all cases
YPRIME(4) = Y(1)*DV;
YPRIME(5) = 0;
if ( ~isnan(TB) )
    YPRIME(5) = YPRIME(5) + C1*M*C0*(TB-TW);

```

```

    end
    if ( ~isnan(TU) )
        YPRIME(5) = YPRIME(5) + C1*M*(1-C0)*(TU-TW);
    end
    YPRIME(6) = BLOWBY*M/OMEGA*HL;
    % perform NOx integration for each element burned
    if ( X > 0.001 )
        % COMBUSTION OR EXPANSION
        for k=1:NNOX,
            if ( THETA >= THETAS + (k-1)/(NNOX-1)*THETAB )
                % convert Y(6+k) to [NO] mol/cm^3 from mass fraction
                % and then back
                YPRIME(6+k) = zeldovich( TB, P/100, YB, Y(6+k)/(MW_NO*VB*1000) ) ...
                *MW_NO*VB*1000/OMEGA;
            end
        end
    end
    % 1/omega is s/rad, so convert to s/deg
    for JJ=1:NY,
        YPRIME(JJ) = YPRIME(JJ)*pi/180;
    end
end
function [ dNOdt ] = zeldovich( T, P, y, NO )
    % calculate rate of NO formation d[NO]/dt given
    % inputs:
    %   T [K]           : gas mixture temperature, kelvin
    %   P [bar]          : cylinder pressure, bar
    %   y [...]          : equilibrium mole fraction of constituents
    %   NO [mol/cm^3]   : current NOx concentration
    % outputs:
    %   dNOdt [ (mol/cm^3) / sec ] : rate of NO formation
    % extended zeldovich rate constants from Heywood Table 11.1 (cm^3/mol-s)
    k1 = 7.6*10^13*exp(-38000/T);
    k2r = 1.5*10^9*T*exp(-19500/T);
    k3r = 2*10^14*exp(-23650/T);
    % calculate molar concentration [mol/cm^3]
    N_V = (100000*P)/(8.314*T)*(1/100)^3;
    N2e = y(3)*N_V;
    He = y(7)*N_V;
    Oe = y(8)*N_V;
    NOe = y(10)*N_V;
    R1 = k1*Oe*N2e;
    R2 = k2r*NOe*He;
    R3 = k3r*NOe*He;
    alpha = NO/NOe;
    dNOdt = 2*R1*(1-alpha*alpha)/(1+alpha*R1/(R2+R3));

```

```
end
end
```

F.16 FRICTION.M

```
% program to compute friction mean effective pressure
% fmep units in kPa
% inputs
clear;
N = 3000; %engine speed rpm
b = 86; % bore (mm)
s = 86; % stroke (mm)
nc =4; % # cylinders
pin=101; % intake manifold pressure (kPa)
db = 56; % main bearing diameter (mm)
lb = 21; % main bearing length (mm)
niv = 2; % # intake valves/cyl
nev = 2; % # exhaust valves/cyl
div = 35; % intake valve diameter (mm);
dev= 31; % exhaust valve diameter (mm);
lv = 11; % valve lift (mm)
mu = 100.e-3 ; % dynamic viscosity (Pa s)
pa= 101; %atmospheric pressure (kPa)
Up = 2.* N * s/60; % mean piston speed (mm/s)
denom = nc*b^2*s;
nb= nc+1; %# main crankshaft bearings
nv = (niv+nev)*nc; % # valves (total)
% friction coefficients
c_cb=0.0202; % crankshaft bearing
c_cs=93600; % crankshaft seals
c_pb=0.0202; % piston bearings
c_ps=14; % piston seals
c_pr=2707; % pison ringpack
c_vb=6720; % camshaft bearings
c_vh=0.5; % oscillating hydrodynamic
c_vm=10.7; % oscillating mixed
c_vs=1.2; % seals
c_vf= 207; % flat cam follower
c_vr=0.0151;% roller cam follower
c_1o=1.28; c_2o=0.0079; c_3o=-8.4e-7; %oil pump
c_1w=0.13; c_2w=0.002; c_3w=3.e-7; %water pump
c_1f=1.72; c_2f=0.00069; c_3f=1.2e-7; %fuel injection
c_iv=4.12e-3; % inlet valves (kPa s^2/m^2)
c_ev=c_iv; %exhaust valves (kPa s^2/m^2)
c_es=0.178; % exhaust system (kPa s^2/m^2)
% component fmeps
%crankshaft
```

```

f_cb=c_cb*nb*N.^ (0.6)*db^3*lb/denom;
f_cs=c_cs*db/denom;
f_crank=f_cb+f_cs;
%piston assembly
f_pb=c_pb*nb*N.^ (0.6)*db^3*lb/denom; % bearings
f_ps=c_ps*Up.^ (0.5)/b; % skirt
f_pr=c_pr*Up.^ (0.5)/(b^2); %ringpack
f_piston=f_pb+f_ps+f_pr;
%valvetrain
f_cam=c_vb*nb*N.^ (0.6)/denom; %bearings
f_vh=c_vh*nv*lv^(1.5)*N.^ (0.5)/denom; %oscill hydro
f_vm=c_vm*(2+10./(5+mu.*N))*lv*nv/(nc*s);
f_vs=c_vs; %seals
%cam followers - choose flat or roller
f_ff=c_vf*(2+10./(5+mu.*N))*nv/(nc*s); % flat
%f_rf=c_nv*N/(nc*s); % or roller
f_valve=f_cam+f_vh+f_vm+f_vs+f_ff;
%auxiliary
f_oil= c_1o + c_2o*N + c_3o*N.^2; %oil pump
f_wat= c_1w + c_2w*N + c_3w*N.^2; %water pump
f_fuel= c_1f + c_2f*N + c_3f*N.^2; %fuel pump
f_aux=f_oil+f_wat+f_fuel;
%pumping
dpis= pa-pin;
dpiv=c_iv*(pin/pa.*Up/1000*b^2/niv/div^2).^2;
dpev=c_ev*(pin/pa.*Up/1000*b^2/nev/dev^2).^2;
dpes=c_es*(pin/pa.*Up/1000).^2;
f_pump=dpis+dpiv+dpev+dpes;
%total
f_tot=f_crank+f_piston+f_valve+f_aux+f_pump;
fprintf(' \n fmep crankshaft (kPa)= %7.1f \n',f_crank);
fprintf(' fmep piston (kPa)= %7.1f \n',f_piston);
fprintf(' fmep valvetrain (kPa)= %7.1f \n',f_valve);
fprintf(' fmep auxiliary (kPa)= %7.1f \n',f_aux);
fprintf(' fmep pumping (kPa)= %7.1f \n',f_pump);
fprintf(' fmep total (kPa)= %7.1f \n',f_tot);

```

F.17 WOSCHNIHEATTRANSFER.M

```

function [ ] = WoschniHeatTransfer( )
% Gas cycle heat release code with Woschni heat transfer
clear( );
thetas = -20; % start of heat release (deg)
thetad = 40; % duration of heat release (deg)
r =10; % compression ratio
gamma = 1.3; % gas const
Q = 20; % dimensionless total heat release

```

```

beta = 1.5; % dimensionless volume
a = 5;       % weibe parameter a
n = 3;       % weibe exponent n
omega =200.; % engine speed rad/s
c = 0;       % mass loss coeff
s = 0.1;     % stroke (m)
b = 0.1;     % bore (m)
T_bdc = 300; % temp at bdc (K)
tw = 1.2;    % dimensionless cylinder wall temp
P_bdc = 100; % pressure at bdc (kPa)
Up = s*omega/pi; % mean piston speed (m/s)
step=1;      % crankangle interval for calculation/plot
NN=360/step; % number of data points
theta = -180; % initial crankangle
thetae = theta + step; % final crankangle in step
% initialize results data structure
save.theta=zeros(NN,1);
save.vol=zeros(NN,1);   % volume
save.press=zeros(NN,1); % pressure
save.work=zeros(NN,1); % work
save.heatloss=zeros(NN,1); % heat loss
save.mass=zeros(NN,1); % mass left
save.htcoeff=zeros(NN,1); % heat transfer coeff
save.hflux=zeros(NN,1); % heat flux (W/m^2)
fy=zeros(4,1); % vector for calculated pressure, work, heat and mass loss
fy(1) = 1; % initial pressure (P/P_bdc)
fy(4) = 1; % initial mass (-)
%for loop for pressure and work calculation
for i=1:NN,
[fy, vol, ht,hflux] = integrate_ht(theta,thetae,fy);
% print values
% fprintf('%7.1f %7.2f %7.2f %7.2f \n', theta,vol,fy(1),fy(2),fy(3));

% reset to next interval
theta = thetae;
thetae = theta+step;
save.theta(i)=theta; % put results in output vectors
save.vol(i)=vol;
save.press(i)=fy(1);
save.work(i)=fy(2);
save.heatloss(i)=fy(3);
save.mass(i)=fy(4);
save.htcoeff(i)=ht;
save.hflux(i)=hflux;
end % end of pressure and work for loop
[pmax, id_max] = max(save.press(:,1)); % find max pressure
thmax=save.theta(id_max);           % and crank angle

```

```

ptdc=save.press(NN/2)/pmax;
w=save.work(NN,1);           % w is cumulative work
massloss =1- save.mass(NN,1);
eta=w/Q;                     % thermal efficiency
imep = eta*Q*(r/(r -1)); %imep/P1V1
eta_rat = eta/(1-r^(1-gamma));
% output overall results
fprintf(' Weibe Heat Release with Heat and Mass Loss \n');
fprintf(' Theta_start =      %5.2f \n', thetas);
fprintf(' Theta_dur =        %5.2f \n', thetad);
fprintf(' P_max/P1 =         %5.2f \n', pmax);
fprintf(' Theta @P_max =    %7.1f \n', thmax);
fprintf(' Net Work/P1V1 =   %7.2f \n', w);
fprintf(' Heat Loss/P1V1 =  %7.2f \n', save.heatloss(NN,1));
fprintf(' Mass Loss/m =     %7.3f \n', massloss );
fprintf(' Efficiency =       %5.2f \n', eta);
fprintf(' Eff./Eff. Otto =  %5.2f \n', eta_rat);
fprintf(' Imep/P1 =          %5.2f \n', imep);
%plot results
figure();
plot(save.theta,save.work,'-',save.theta,save.heatloss,'--','linewidth',2 )
set(gca, 'Xlim',[ -180 180], 'fontsize', 18, 'linewidth',1.5);
hleg1=legend('Work', 'Heat Loss', 'Location','NorthWest');
set(hleg1,'Box', 'off')
xlabel('Crank Angle \theta (deg)', 'fontsize', 18)
ylabel('Cumulative Work and Heat Loss', 'fontsize', 18)
plot(save.theta,save.press,'-','linewidth',2 )
set(gca, 'fontsize', 18,'linewidth',1.5,'Xlim', [ -180 180]);
xlabel('Crank Angle (deg)', 'fontsize', 18)
ylabel('Pressure (bar)', 'fontsize', 18)
figure();
plot(save.theta,save.htcoeff,'-','linewidth',2 )
set(gca, 'fontsize', 18,'linewidth',1.5,'Xlim', [ -180 180]);
xlabel('Crank Angle \theta (deg)', 'fontsize', 18)
ylabel('Heat transfer coefficient h (W/m^2-K)', 'fontsize', 18)
figure();
plot(save.theta,save.hflux,'-','linewidth',2 )
set(gca, 'fontsize', 18,'linewidth',1.5,'Xlim', [ -180 180]);
xlabel('Crank Angle \theta (deg)', 'fontsize', 18)
ylabel('Heat flux q{"} (MW/m^2)', 'fontsize', 18)

function[fy,vol,ht, hflux] = integrate_ht(theta,thetae,fy)
% ode23 integration of the pressure differential equation
% from theta to thetae with current values of fy as initial conditions
[tt, yy] = ode23(@rates, [theta thetae], fy);
% put last element of yy into fy vector
for j=1:4

```

```

fy(j) = yy(length(tt),j);
end

% pressure differential equation
function [yprime] = rates(theta,fy)
vol=(1.+ (r -1)/2.* (1-cosd(theta)))/r;
dvol=(r - 1)/2.*sind(theta)/r*pi/180.; %dvol/dtheta
dx=0.;

if(theta>thetas) % heat release >0
dum1=(theta -thetas)/thetad;
x=1-exp(-(a*dum1^n));
dx=(1-x)*a*n*dum1^(n-1)/thetad; %dx/dthetha
end

P=P_bdc*fj(1); %P(theta) (kPa)
T=T_bdc*fj(1)*vol; % T(theta) (K)
term4=T_bdc*(r-1)*(fj(1)-vol^(-gamma))/r; % comb. vel. increase
U=2.28*Up + 0.00324*term4; % Woschni vel (m/s)
ht = 3.26 *P^(0.8)*U^(0.8)*b^(-0.2)*T^(-0.55); %Woschni ht coeff
hflux=ht*T_bdc*(fj(1)*vol/fj(4) - tw)/10^6; %heat flux MW/m^2
h = ht*T_bdc*4/(1000*P_bdc*omega*beta*b); %dimensionless ht coeff
term1= -gamma*fj(1)*dvol/vol;
term3= h*(1. + beta*vol)*(fj(1)*vol/fj(4) - tw)*pi/180.;
term2= (gamma-1)/vol*(Q*dx - term3);
yprime(1,1)= term1 + term2 - gamma*c/omega*fj(1)*pi/180;
yprime(2,1)= fj(1)*dvol;
yprime(3,1)= term3;
yprime(4,1)= -c*fj(4)/omega*pi/180;
end %end of function rates
end % end of function integrate_ht
end % end of function HeatReleaseHeatTransfer

```

Index

A

- Accessory friction, 308
- Adiabatic flame temperature, 100
- Air/fuel ratio
 - definition, 76
 - oxygen sensor, 353
 - stoichiometric, 76
- Alcohol, 265, 279
- Alternative fuels, 274
- Antoine's equation, 75
- Aromatics, 265
- Atmosphere, standard, 68, 158, 402
- Atomization, 163, 173
- Auto-ignition, 7, 197, 215
- Available energy, 99, 104, 372

B

- Balance, 19
- Bearings, 295
- Benz, K., 5
- Biodiesel, 285
- Blowby, 49, 340
- Blowdown, 54, 138
- Brake mean effective pressure (bmep), 12
- Brake specific fuel consumption (bsfc), 14

C

- Carbon monoxide, 85, 243, 358
- Carburetor, 163
- Carnot, S., 32
- Catalytic converter
 - efficiency, 256
 - reactions, 255
- Cetane index, 283
- Cetane number, 219, 280, 284
- Charging efficiency, 185
- Chemical equilibrium, 84
- Choked flow, 133, 155, 165
- Clausius-Clapeyron equation, 75
- Clerk, D., 4
- Combustion analysis, 354
- Combustion diagnostics, 214
- Combustion duration, 43, 207

Combustion visualization, 214

- Complete expansion, 40
- Compression ratio
 - definition, 10
 - effects on performance, 124, 373, 383
 - fuel-air cycle, 108, 128
 - gas cycle, 35, 38, 40
- Compressor map, 155
- Compressors, 150
- Computational fluid dynamics (CFD), 175
- Controls, electronics, 366
- Cooling system, 5, 22, 319
- Cooperative Fuel Research (CFR) engine, 212
- Crevice volume, 246
- Crude oils, 262–266
- Cumulative energy release fraction, 43
- Cycle-to-cycle variations, 198
- Cylinder area, 50
- Cylinder pressure measurement, 354
- Cylinder volume, 17

D

- Daimler, G., 5
- Delivery ratio, 190
- Deposits, 246
- Diesel cycle, 7, 36
- Diesel engines
 - combustion, 215
 - HC emissions, 248
 - numerical models, 225
 - particulate matter (PM) emissions, 249
 - performance, 8, 378
- Diesel fuel, 83, 282
- Diesel, R., 5
- Diffusion coefficient, 390
- Dilution tunnel, 364
- Direct injection, 7
- Discharge coefficient
 - carburetors, 165
 - poppet valves, 134
 - ports, 188
- Displacement volume, 10
- Distillation, 266

- Drag coefficient, 383
- Droplet size, 174
- Dual cycle, 38, 128
- Dynamometer, 10, 347

- E**
- Efficiency
 - compressor, 154
 - mechanical, 11, 372
 - scavenging, 191
 - thermal, 15, 113, 127, 322, 383
 - volumetric, 12, 372
- Electric motors, 27
- Emission regulation, 251
- Emissions testing, 369
- Energy balance, 320
- Energy release
 - combustion measurements, 200, 356
 - compression ignition engines, 222
 - gas cycles, 45
 - modeling, 41, 45, 205, 334, 356
 - spark ignition engines, 204
 - timing, 53
- Engine size, 16, 379
- Engine speed, 16, 124, 376
- Ensemble average, 181
- Enthalpy
 - formation, 74
 - vaporization, 73–75
- Entropy, 69, 99, 269
- Equilibrium
 - composition, 89
 - constants, 79, 90
- Equivalence ratio
 - CFR engine, 124
 - definition, 77
 - fuel-air cycle, 110–127
 - mass fraction burned, 206
 - measurement, 364
- Ethanol, 279
- Exhaust
 - analyzers, 364
 - heat transfer, 338
 - ideal 4 stroke, 55, 113
 - manifold, 189
- Exhaust gas recirculation (EGR), 206, 254, 354

- F**
- Federal driving schedule, 369
- Finite energy release, 41
- Fischer-Tropsch reactions, 285
- Flame ionization detector (FID), 360
- Flame propagation, 201
- Flame quenching, 246

- Flammability limit, 275
- Flow area, 134
- Flow bench, 135, 187
- Flow coefficient, 135
- Flowmeters, 350
- Four stroke cycle
 - definition, 6
 - exhaust stroke, 55
 - intake stroke, 57
 - P-V diagram, 56
- Friction
 - fmep definition, 291
 - journal bearings, 295
 - modeling, 294
 - motoring, 292
 - oil film, 305
 - piston and ring, 298
 - valve train, 306
- Fuel-air ratio, 76, 165, 244, 372
- Fuel cells, 27
- Fuel injection, 166, 353
- Fuels
 - additives, 273
 - properties, 99, 273, 284, 397

- G**
- Gas constants, 67, 388
- Gasoline, 83, 269, 271
- Gas turbine, 28
- Gibbs free energy, 70, 85

- H**
- HCCI engine, 226
- Heat of combustion, 15, 33, 99
- Heat transfer
 - conduction, 327
 - convection, 327
 - modeling, 49, 326
 - measurements, 326
 - radiation, 339
- Helmholtz free energy, 86
- Helmholtz resonator, 149
- Hybrid electric vehicle, 27
- Hydrocarbons
 - emissions, 245
 - fuel components, 263
 - measurement, 359
- Hydrogen, 281

- I**
- Ideal gas, 66, 397
- Ignition, 7, 198, 215
- Ignition delay
 - compression ignition, 220

- spark ignition, 207
- Indicated mean effective pressure (imep)
 - definition, 12
 - finite energy release model, 47
 - fuel-air-cycle, 109, 113, 127
 - Miller cycle, 41
 - Otto cycle, 35
- Indicated specific fuel consumption (ISFC), 14
- Indirect injection (IDI), 7, 376, 382
- Intake manifold, 147, 150
- Intake stroke, 57
- Internal energy, 67
- Isentropic processes, 33, 36, 101, 133

- K**
- Knock
 - measurements, 206, 368
 - modeling, 210

- L**
- Lagrange optimization, 85
- Laminar flame speed, 201
- Laser Dopper Velocimetry (LDV), 174
- Lean NOx trap, 257
- Lenior, J., 4
- Limited pressure cycle, 38, 125
- Low temperature combustion, 225
- Lubrication, 312

- M**
- Mach index, 140
- Mach number, 131
- Mass blowby, 49
- Mass fraction burned, 43, 119
- Maximum work, 103
- MBT timing, 381
- Mean effective pressure
 - accessory, 291
 - brake, 12, 158
 - definitions, 11
 - friction, 12, 291, 311
 - indicated, 12, 47, 109, 113, 127
 - motoring, 292, 380
 - pumping, 59, 113, 310
- Methane, 83, 101
- Methane number, 275
- Methanol, 83, 101, 279
- Microscales
 - integral, 182
 - Kolmogorov, 182
 - Taylor, 182
- Midgley, T., 274
- Mie scattering, 214
- Miller cycle, 39

- Mixture mass fraction, 67
- Molecular mass, 67, 78
- Mole fraction, 67, 389
- Motoring mean effective pressure (mmep), 292

- N**
- Naphthenes, 264
- Natural gas, 277
- Nitrogen oxides
 - chemical reactions, 85, 235
 - measurement, 361, 382
 - rate constants, 236
- Nitromethane, 83
- Non-methane organic gases (NMOG), 245
- Nusselt number, 331, 338

- O**
- Octane
 - combustion, 87
 - number, 5, 212, 280
 - properties, 101
 - requirement, 270
- Oil, 262, 312
- Oil film, 289, 305
- Olefins, 264
- Otto cycle, 6, 33
- Otto, N., 4
- Oxygen sensor, 362

- P**
- Paraffins, 263
- Particle image velocimetry (PIV), 175
- Particulates, 249, 363
- Part-load performance, 376
- PCCI combustion, 227
- Penetration layer, 328
- Performance maps, 376
- Petrov's equation, 297
- Physical constants, 402
- Piston
 - acceleration, 19
 - force balance, 300
 - friction, 298
 - side thrust, 300
 - skirt, 298
 - temperature, 329
 - velocity, 18
 - wrist pin offset, 300
- Piston rings, 298
- Piston speed
 - effect on turbulence, 181
 - geometric similarity, 16
 - instantaneous, 18
 - mean, 10, 376

Poppet valve, 20, 132, 307

Power

- brake, 10, 372
- friction, 11
- indicated, 10
- road load, 383

Prechamber, 179

Pressure transducers, 354

Propane, 276

Pumping work, 310

Purity, 185

Q

Quality, 76, 411

Quenching, 246

R

Radial engine, 17

Rapid compression machine, 209

Rayleigh scattering, 215

RCCI combustion, 228

Reformulated gasoline (RFG), 272

Residual fraction

- fuel-air cycle, 113, 116
- gas cycle, 81
- measurement, 365
- two stroke, 190
- valve timing, 147

Reversion, 341

Reynolds equation, 304

Reynolds number, 173, 180, 331

Ricardo, H., 5

Rings, 298

Roots blower, 150

S

Sampling valve, 366

Saturation vapor pressure, 72

Scavenging

- analysis, 191
- configurations, 186
- definition, 8
- efficiency, 190
- ratio, 190

Second law, 103, 107

Selective catalytic reduction (SCR), 257

Short circuiting, 9, 190

Smoke limit, 249

Soot, 249

Spark ignition

- cycles, 6
- emissions, 246
- performance, 123

Specific fuel consumption, 14, 374

Specific heat

- air, 387
- ideal gas mixtures, 68–71
- motor fuels, 268

Speed of sound, 133, 388

Spray penetration, 173

Squish, 180

Stagnation pressure, 132

Steam engine, 2, 29

Stoichiometry, 76

Stribeck variable, 289

Stroke, 9

Sulphur, 273

Superchargers, 20, 150

Swirl, 175

T

Temperature

- cylinder head, 324
- piston, 324, 330

Thermal conductivity, 387

Thermal efficiency

- Diesel cycle, 36
- finite energy release, 46, 120
- first law, 15
- limited pressure, 38, 127
- Miller cycle, 41
- Otto cycle, 35
- second law, 107

Timing

- CFR engine, 124
- effect on NO_x, 243, 254
- spark, 43, 199, 381
- valve, 143

Torque, 10

Total hydrocarbons (THC), 245

Trapped air-fuel ratio, 189

Trapping efficiency, 190, 373

Tumble, 175

Tuning, 148

Turbocharger, 20, 150

Turbulence, 5, 180, 254

Turbulence models, 184

Turbulent flame regimes, 202

Two-stroke engines, 8, 185, 315

U

Ultra low sulfur diesel (ULSD), 283

Unit conversions, 401

V

Valve

- choked flow, 133
- curtain area, 134

- discharge coefficient, 134
 - overlap, 43
 - poppet, 20, 136
 - timing, 143
 - Valve train, 306
 - Viscosity
 - air, 387
 - combustion gas, 331, 328
 - diesel fuel, 284
 - oil, 314
 - Volatility, 270
 - Volume, 10, 17, 334, 379
 - Volumetric efficiency
 - definition, 12
 - fuel-air cycle, 116
 - gas cycle, 58
 - speed effect, 12, 146, 149
 - valve effect, 140, 144
- W**
- Water-gas reaction, 79
 - Weber number, 173
 - Wiebe function, 43
 - Woschni correlation, 333
- Z**
- Zeldovich mechanism, 235

